
IMPROVING DIE FILLING IN
PHARMACEUTICAL TABLETING
BY EXPERIMENTAL AND NUMERICAL MEANS

DOCTORAL THESIS
SUBMITTED IN THE FULFILLMENT OF THE REQUIREMENTS
FOR THE DEGREE OF DOCTOR IN NATURAL SCIENCES
AT KIEL UNIVERSITY, GERMANY

BY
CLAUDIA HILDEBRANDT

KIEL, 2018

Reviewer:	Prof. Dr. Regina Scherließ
Co-Reviewer:	PD Dr. Nora Anne Urbanetz
Date of exam:	20.11.2018
Accepted for publication:	20.11.2018

sgd. Prof. Dr. Frank Kempken

List of publications

Peer-reviewed articles

Numerical simulation of powder flow in a pharmaceutical tablet press lab-scale gravity feeder

S.R. Gopireddy, [C. Hildebrandt](#), N.A. Urbanetz
Powder Technology, 302:309-327, 2016

Evaluation and prediction of powder flowability in pharmaceutical tableting

[C. Hildebrandt](#), S.R. Gopireddy, A.K. Fritsch, T. Profitlich, R. Scherließ, N.A. Urbanetz
Pharmaceutical Development and Technology, (2017) ahead of print

Simulation of particle size segregation in a pharmaceutical tablet press lab-scale gravity feeder

[C. Hildebrandt](#), S.R. Gopireddy, R. Scherließ, N.A. Urbanetz
Advanced Powder Technology, 29:765-780, 2018

Assessing die filling using high speed camera imaging

[C. Hildebrandt](#), J. Loerzer, S.R. Gopireddy, N.A. Urbanetz
Chemie Ingenieur Technik, 90:472-482, 2018

Numerical analysis of the die filling process within a pharmaceutical tableting machine

[C. Hildebrandt](#), S.R. Gopireddy, R. Scherließ, N.A. Urbanetz
Chemie Ingenieur Technik, 90:483-492, 2018

Investigation of powder flow within a pharmaceutical tablet press force feeder – A DEM approach

[C. Hildebrandt](#), S.R. Gopireddy, R. Scherließ, N.A. Urbanetz
Powder Technology, under revision

Assessment of material and process attributes' influence on tablet quality using a QbD and DEM combined approach

[C. Hildebrandt](#), S.R. Gopireddy, R. Scherließ, N.A. Urbanetz
Powder Technology, under review

A DEM approach to assess the influence of the paddle wheel shape on force feeding during pharmaceutical tableting

[C. Hildebrandt](#), S.R. Gopireddy, R. Scherließ, N.A. Urbanetz
Advanced Powder Technology, under review

Impact of different tableting machines feed frame design on tablet quality: A DEM study of die filling

[C. Hildebrandt](#), S.R. Gopireddy, T. Profitlich, R. Scherließ, N.A. Urbanetz
Advanced Powder Technology, under review

Review articles

Application of numerical simulations in pharmaceutical tableting

C. Hildebrandt, S.R. Gopireddy, N.A. Urbanetz

APV – Ihr Plus an Wissen, 01/2016

Conference contributions

Conference proceedings

Numerical simulation of powder flow in a pharmaceutical tablet press lab-scale gravity feeder

C. Hildebrandt, S.R. Gopireddy, R. Scherließ, N.A. Urbanetz

8. Symposium Produktgestaltung in der Partikeltechnologie, Karlsruhe, June 2017

Assessment of die filling process of powder using high speed camera imaging

J. Loerzer, C. Hildebrandt, S.R. Gopireddy, R. Scherließ, N.A. Urbanetz

8. Symposium Produktgestaltung in der Partikeltechnologie, Karlsruhe, June 2017

Powder flow within a pharmaceutical tablet press – a DEM analysis

C. Hildebrandt, S.R. Gopireddy, R. Scherließ, N.A. Urbanetz

V. International Conference on Particle-based methods, PARTICLES, Hannover, September 2017

Oral presentations

Numerical analysis of the die filling process within a pharmaceutical tableting machine

C. Hildebrandt, S.R. Gopireddy, R. Scherließ, N.A. Urbanetz

8. Symposium Produktgestaltung in der Partikeltechnologie, Karlsruhe, June 2017

Powder flow within a pharmaceutical tablet press – a DEM analysis

C. Hildebrandt, S.R. Gopireddy, R. Scherließ, N.A. Urbanetz

V. International Conference on Particle-based methods, PARTICLES, Hannover, September 2017

Assessment of powder flowability in pharmaceutical tableting

C. Hildebrandt, S.R. Gopireddy, R. Scherließ, N.A. Urbanetz

10th World Congress of Chemical Engineering, Barcelona, October 2017

Understanding Powder Transfer In Force Feeders of Tableting machines: A comparison

C. Hildebrandt, S.R. Gopireddy, R. Scherließ, N.A. Urbanetz

8th World Congress on Particle Technology, Orlando, April 2018

Poster presentations

Application of numerical simulations in pharmaceutical tableting

C. Hildebrandt, S.R. Gopireddy, R. Scherließ, N.A. Urbanetz

DPhG annual meeting, Düsseldorf, September 2015

Numerical analysis of the die filling process within a lab-scale tableting machine

C. Hildebrandt, S.R. Gopireddy, R. Scherließ, N.A. Urbanetz

10th World meeting on Pharmaceutics, Biopharmaceutics and Pharmaceutical Technology, Glasgow, April 2016

Simulation of powder flow within the force feeder of a pharmaceutical tablet press

C. Hildebrandt, S.R. Gopireddy, R. Scherließ, N.A. Urbanetz

International Congress on Particle Technology, PARTEC, Nürnberg, April 2016

Numerical analysis of powder flow in a lab-scale tableting machine

C. Hildebrandt, S.R. Gopireddy, R. Scherließ, N.A. Urbanetz

DPhG annual meeting, München, Oktober 2016

Investigation of powder flowability in a model die filling process

A.K. Fritsch, C. Hildebrandt, S.R. Gopireddy, M. Rackl, N.A. Urbanetz

DPhG annual meeting, München, Oktober 2016

Assessing die filling using high speed camera imaging

J. Loerzer, C. Hildebrandt, S.R. Gopireddy, R. Scherließ, N.A. Urbanetz

8. Symposium Produktgestaltung in der Partikeltechnologie, Karlsruhe, Juni 2017

Influence of paddle wheels shape on tablet quality - A numerical approach

C. Hildebrandt, S.R. Gopireddy, R. Scherließ, N.A. Urbanetz

11th World meeting on Pharmaceutics, Biopharmaceutics and Pharmaceutical Technology, Granada, March 2018

Lack of a specific mark or a reference to a trademark or a patent does not imply that this work or part of it can be used or copied without copyright permission.

Contents

1	Introduction and Objectives	1
1.1	Introduction	1
1.2	Objectives	3
2	Theoretical background	5
2.1	Unit operations and modeling of unit operations involved in tablet manufacturing . . .	5
2.2	Pharmaceutical tableting	9
2.3	Die filling mechanisms	11
2.3.1	Gravity filling	12
2.3.2	Force feeding	12
2.4	Modeling using discrete element method	15
2.4.1	Discrete element classes	15
2.4.2	Governing equations	16
2.4.3	Flowsheet of computational model	16
2.4.4	Contact and non-contact models	19
2.4.4.1	Contact models	19
2.4.4.2	Non-contact models	21
2.4.5	Material properties and their determination	21
2.4.6	Computational considerations in DEM	23
3	Results and Discussion	25
3.1	Gravity filling	27
3.1.1	Evaluation of gravity filling by an experimental model die filling system	27
3.1.2	High speed camera imaging of gravity filling	43
3.1.3	Numerical analysis of mono-disperse sized particles in gravity filling	57
3.1.4	Size-segregation understanding in gravity filling by using the DEM	79
3.2	Force feeding	97
3.2.1	Powder flow in a three-chambered force feeder	97
3.2.2	Extended powder flow evaluation in force feeding	109
3.2.3	Influence of material properties and process parameters on tablet quality in force feeding	137
3.2.4	Influence of paddle wheel shape on powder flow	163
3.2.5	Powder flow comparison in two different force feeders	197
4	Overall findings and future perspectives	221
5	Summary	227
6	Summary (German)	229
	References	231

1 Introduction and Objectives

1.1 Introduction

In contrast to ‘Moore’s law’ which was coined in the context of transistors and is used in a more general way for the exponential improvement of technology over time, pharmaceutical R&D follows the opposite trend. Actually, ‘Eroom’s law’ (backwards of ‘Moore’s law’) was termed for pharmaceutical industry. It reflects the decline of new US Food and Drug Administration (FDA) approved drugs relative to the R&D costs spent in the drug industry over time. Since 1950, this value decreased by 50% every 9 years [1]. Scannell et al. gave different perspectives and described four main root causes for ‘Eroom’s law’. One of them is the ‘cautious regulator’ issue or in other words the risk tolerance decrease of regulatory agencies which raises the bar for new drug approvals and elevates R&D costs [1]. In 2017, solely 46 new drugs were approved in the US by the FDA. Those approvals did not only include new drugs, but also already approved drugs for a new purpose or new patient populations (e.g. children). New formulations, e.g. two extended- and one immediate-release tablet to prevent opioid abuse, or new dosage forms, e.g. higher dose strength tablets to take less tablets daily are other approvals of established drugs [2].

Within R&D, pharmaceutical development showed in the last years an increasing interest in process understanding and process modeling. The impetus has been driven by several factors. First, the ‘Quality by Design’ (QbD) paradigm was introduced and is asking for a clear relationship between process performance and product quality [3]. Second, an accelerated production process development is needed to provide an increased competition-free drug life span within patent expiration [4]. Another factor is the transition trend from batch to continuous manufacturing which itself requires an ameliorated process understanding [5–7]. To summarize, 4-5 years of patent life and 30-35% of R&D expenditures are on average spent by pharmaceutical development [8]. Different target-oriented and advanced possibilities for process modeling have evolved to support the material and time consuming trial and error experiments in pharmaceutical development. Those tools bear the prospect to antagonize the correlation between the reduction of the cost of goods sold and the increase in R&D expenditure by time acceleration, improved efficiency, and cost savings in the pharmaceutical development sector [9].

New technologies should identify the relationship between raw material physical properties and process performance. One of several challenges is the multivariate nature of physical material properties complicating a simple and straightforward determination of product influencing properties [10]. Improved process understanding can be gained by quality risk management [3], statistical tools such as design of experiments (DoE) [11], process analytical technology combining multivariate analysis and experimental tools [12, 13], principal component analysis [14], or artificial neural networks [15].

In the last years, mechanistic modeling emerged to improve process understanding [16, 17]. Process or mechanistic modeling considers the numerical simulation of physical processes for which the physics under consideration can be described by a closed series of mathematical equations. Those equations

are solved using different numerical methods and techniques [18]. In the context of pharmaceutical tableting, computational fluid dynamics (CFD), the finite element method (FEM), and the discrete element method (DEM) are the most important process modeling tools. CFD is an Eulerian method in which the material is treated as continuum. Mass, momentum, and energy balances are solved numerically and CFD can be very accurate for systems consisting of fluids [19, 20]. In FEM a discrete number of degrees of freedom (DOF) at corners of control volumes (nodes) are expressed as the displacements of the nodes. Stress-strain relationships allow to track the DOFs. The DOFs are solved in FEM by converting the governing differential equations in each element into a large discrete set of algebraic equations [21]. In contrast to CFD and FEM, the DEM method is a Lagrangian model that tracks the positions, velocities, and accelerations of each particle individually [20, 22–24].

Tablets still constitute the most important dosage form, though biologics and biosimilars, mostly formulated to be freeze dried or as liquids for injection, are rising fast. Tablets, which are ‘obtained by compressing uniform volumes of particles or by another suitable manufacturing technique (...)’ [25], cover 80% of drug products in the US domestic market [22]. The European Pharmacopoeia groups tablets into the monograph ‘compressi’ including for example uncoated, coated, gastro-resistant, modified-release, effervescent, soluble, dispersible, orodispersible, and chewable tablets or oral lyophilisates [25]. Some of the key advantages of tablets legitimating their importance are for example their ease of handling and administration which increase patient compliance, their production in high quantities at a low cost, and their high storage stability as a solid dosage form [26]. Out of the 46 FDA-approvals in 2017, 37% of the drugs are formulated as a tablet (17 of 46) [2]. Within the 1072 drugs approved in the generic sector, 5 out of the 6 highlighted first generic drug approvals were tablets, too [2]. A survey of the 15 drugs with highest sales in the US in 2017 showed that two drugs out of those 15, Xarelto[®] (no. 9 and \$6.6 billion sales in the US in 2017) and Eliquis[®] (no. 6 and \$7.4 billion sales in the US in 2017) both belonging to the group of blood coagulation inhibitors, are as well formulated as tablets [27].

The brief overview shows, that pharmaceutical development could benefit from process modeling to decrease R&D expenditures particularly in tablet production as tablets are still an extremely important dosage form.

1.2 Objectives

This work aims to demonstrate different mechanistic modeling approaches to shed light on pharmaceutical tableting. Out of the different steps involved in tablet formulation and unit operations, the die filling step in the tablet press was investigated. This step is crucial for the patient's safety as it defines the drug content. Different mechanistic models, namely statistical analysis (partial-least squares method), design of experiments, as well as the numeric DEM were developed.

In the first step, an experimental model die filling system was utilized to quantify and visualize the powder flow from a stationary hopper into a translating die. The model was designed as simple as possible to discern the powder flow mechanisms involved in powder discharge into a die. The main focus was set to the identification of die filling influencing factors supported by high speed camera imaging and to the development of a flowability metric relevant for die filling.

In the second part of the work, a numerical approach, namely the DEM, was utilized to investigate die filling in rotary tablet presses. In principle, models for both die filling mechanisms, gravity filling and force feeding, were developed. For gravity filling, powder was transferred from the gravity feeder, a cylindrical pipe connected to an inclined chute and rectangular box, into the rotating dies of the turret. Firstly, particles of same size were used to identify the powder flow mechanisms in gravity filling and the influence of turret speed and particle properties. Secondly, the same system but poly-disperse sized particles was modeled to ascertain the size segregation mechanisms in the feeding system. Possible levers for formulation optimization via material properties should be identified for an increased process performance in gravity filling.

Force feeding is a more complicated process compared to gravity filling as rotating paddle wheels feed the material actively into the dies. DEM force feeder models were developed for two different pilot-scale tableting machines to simulate a direct compression formulation. The powder transfer within the force feeders was in depth analyzed which would not be possible with classical experiments. Attention was not only given to the common tablet attributes, such as tablet mass and content uniformity, but also to the size segregation mechanisms, the particle rearrangement / mixing, and the particle residence time within the force feeders. One main target was the correlation of the tablet quality attributes and powder flow patterns to the design features of the tablet presses with respect to paddle wheel shapes, number of paddle wheels, and force feeder housings. Additionally, the influence of process parameters as well as material attributes on powder flow within force feeders was determined.

Eventually, the mechanistic models employed in this work may enhance die filling process understanding and provide different possibilities for process improvement in pharmaceutical development.

2 Theoretical background

2.1 Unit operations and modeling of unit operations involved in tablet manufacturing

Classical tablet formulations contain, in addition to the active pharmaceutical ingredient (API), a diluent (inert, to increase bulk volume), a disintegrant (to facilitate tablet disintegration), a binder (for wet granulation or dry granulation), a flow aid (to improve powder flowability), and a lubricant (to decrease friction between formulation and tableting tools) [28].

A typical manufacturing process of tablets includes weighing, milling, mixing, granulation and drying, blending (lubrication), compaction, and coating [26]. Each of them has different underlying physics coming with its own challenges in process modeling. The following description gives a short overview of the unit operations including some examples shown in Tab. 1, in which numerical models help to improve process understanding. Some of the provided examples may not be directly related to pharmaceutical materials though the underlying models and physics could be transferred to pharmaceutical processes. More comprehensive reviews are provided by Ketterhagen [20], Barroso et al. [29], and Kremer et al. [18].

Milling

Milling reduces the particle size of e.g. API particles or excipients by mechanical means for different purposes. The increase of particle surface area improves heat and mass transfer in the following unit operations, the particle size homogenization provides a higher blend uniformity, and a higher API bioavailability can be achieved due to a higher API dissolution rate [28]. Different breakage models in DEM were developed and were used to model the milling process, i.e. the bonded-particle model (BPM) [30], the fast breakage model (FBM) [31], and the particle replacement model (PRM) [32]. Different milling instruments are available, e.g. a ball mill as shown in the study by Metzger et al. using the BPM model [33] (Tab. 1).

Screening

Following the milling process and prior to the mixing step, an in between sieving step may be necessary to ensure a homogeneous powder and powder mixture [28, 34]. An example screening process from the Jafari et al. study is provided in Tab. 1 [34].

Mixing

Mixing intends to process the heterogeneous mixture of the different formulation components, consisting of the API and excipients to a homogeneous mixture. Optimization of the mixing process to ensure a homogeneous mixture is in particular important for formulations which are either further processed by dry granulation or which are directly compacted in the tablet press. The following factors are influencing the mixing efficiency, i.e. particle size distribution, particle density, particle shape, particle surface properties, cohesive forces and particle friability [28]. A range of different mixers are available that differ in terms of their geometry (rotating drum, V-blender, tote blender, mixers with

impellers) as well as their mixing principles (i.e. convection, diffusion, and shearing). Two examples for simulation of powder mixing using the DEM in a turbula mixer [35] and a Bohle container [36] are illustrated in Tab. 1.

Granulation

The blend can either be directly compressed into tablets ((named as ‘direct compression’ (DC), confer section 2.1) or in between granulated. Granulation may be necessary if the compression characteristics of the API in high dose formulations are poor, an inappropriate powder flowability is found, or the mixture tends to segregate [26]. In principle, three different granulation procedures are available [28]. (1) Dry granulation is the ‘controlled crushing of pre-compacted powders densified by either slugging or passing it between two counter-rotating rolls’ [37]. An example for a roll compaction model by a DEM & FEM combined approach is shown in Tab. 1 [38]. In this example, the powder flow in the feeding zone was modeled via the DEM providing time dependent velocity fields which served as input data in the FEM model. The powder compaction between the rolls was then modeled via FEM [38]. (2) Wet granulation is more commonly used compared to dry granulation. It prevents dust formation during the process and generates granules of good flowability. However, the process itself is time, power, and cost consuming. In addition, the API compatibility with the granulating liquid is a prerequisite. A DEM model for high shear wet granulation is provided in Tab. 1 [39]. After the granulation process, the granules have to be dried to evaporate the granulating liquid. The drying step can be performed in a fluidized bed as simulated e.g. by Kafui et al. in a CFD-DEM combined model [40]. (3) The last granulation method is a thermal process utilizing the thermoplastic deformation of low-melting components, e.g. API or excipients at elevated temperatures. This type of granulation is often applied for sustained release formulations [28] which has not yet been numerically modeled.

Blending

An additional mixing step can be necessary to lubricate the formulation, named as ‘blending’, by adding for example magnesium stearate. Powder lubrication can increase powder compaction manufacturability by reducing (1) the die-wall friction, (2) the powder adhesion to metal components of the equipment, and by (3) increasing the powder bulk density [41]. The overall ejection force of the tablet out of the die can be decreased if the material (powder blend) or die are properly lubricated [42]. Same equipment and models as described in ‘mixing’ are used.

Compaction

The granulation step may be omitted and the final blend directly compressed into tablets. DC involves fewer processing stages and eliminates moisture which is necessary in wet granulation [43]. However, the API and excipient properties require a tighter control of material properties [44]. Tableting itself can be split into the three distinct steps, (1) die filling, (2) powder compaction, and (3) tablet ejection. High speed rotary tablet presses are most commonly used to achieve very high outputs (max. 1.6 Mio. tablets/hour) and were first patented in 1904 [45]. Details about the tableting process and a more comprehensive review on the first step in tableting, the die filling, are provided in section 2.2.

The Drucker-Prager Cap model is the most prominent compaction model which was successfully implemented in the FEM. It is able to predict the evolution of local mechanical properties while powder consolidation, as shown by Sinha et al. [46] and Diarra et al. [47] (Tab. 1). So far, the tablet ejection process has not yet been modeled.

Coating

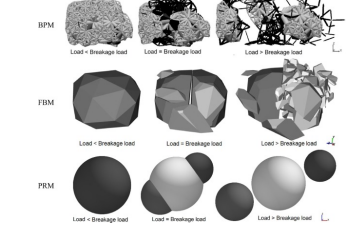
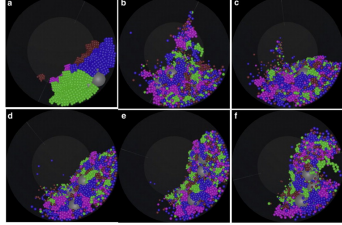
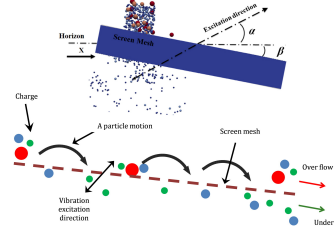
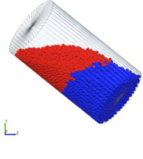
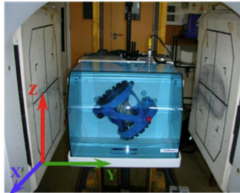
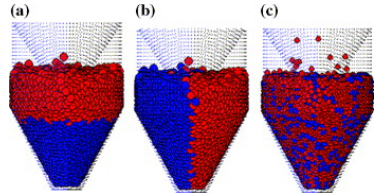
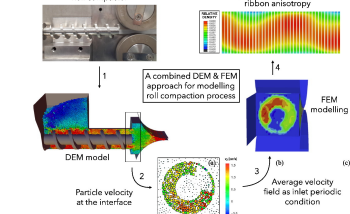
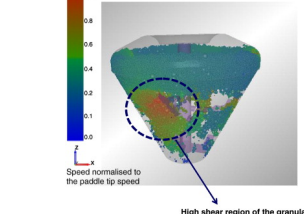
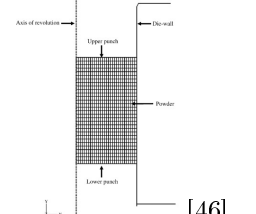
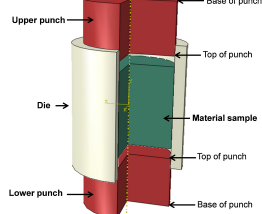
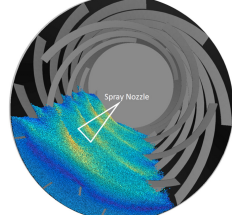
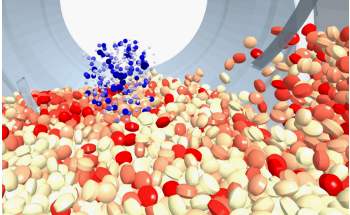
Eventually, tablets may be spray-coated for different purposes, e.g. cosmetic reasons (taste masking, dose differentiation, tablet elegance) or functional reasons implying an API release rate modification.

For the latter, coating polymers with enteric or retard functions can be used to reduce adverse effects, to improve API pharmacokinetics, or to reduce dosing frequency. Toschkoff et al. reviewed different spray models [48] as well as coating models [49] for process modeling. The example given in Tab. 1 evaluated the influence of process parameters (spray rate, number of nozzles, rotation rate, and drum load) on inter-tablet coating variation [50].

Instead of individual unit operation modeling, process simulators follow a different approach and integrate the unit operations into flowsheets. Those simulators collect various types of process models in a single program, such as for example the commercially available gPROMSTM or ASPENTM platforms [5]. These tools can be referred to as ‘equation-oriented’ models with a significantly reduced computational cost compared to the examples given in Tab. 1. A faster computation makes them attractive for continuous process modeling, though at the inherent drawback of a low level of detail.

The examples show that numerical simulations can contribute to a cost effective and robust process development by enhancing process understanding. Those models are consistent with the ICH Q8 guidance on ‘Quality by Design’ [3, 51, 52]. In the next couple of years, numerical models can be able to capture large industrial scale unit operations as computational power scales with Moore’s law. Computational efficiency is also improved by increasing the number of computing cores on a single chip, the Graphical Processor Unit (GPU) [53], as shown in particulate simulations of Radeke et al. [54] and Xu et al. [55].

Tab. 1: Unit operations involved in pharmaceutical tableting and their representation by numerical means (illustrations taken with permission from publishers)

Unit operation	Examples	
Milling	 <p>EPM Load + Breakage load</p> <p>FBM Load + Breakage load</p> <p>PRM Load + Breakage load</p> <p>[56]</p>	 <p>[33]</p>
Screening	 <p>Screen Mesh Vibration excitation direction Particle motion Screen mesh Over flow Under flow</p> <p>[34]</p>	
Mixing	<p>DEM Simulation</p>  <p>PEPT experiment</p>  <p>[35]</p>	 <p>(a) (b) (c)</p> <p>[36]</p>
Granulation	 <p>Roll compactor Experimentally consistent ribbon anisotropy A combined DEM & FEM approach for modelling roll compaction process FEM modelling DEM model Particle velocity at the interface Average velocity field as inlet periodic condition</p> <p>[38]</p>	 <p>Speed normalised to the paddle tip speed High shear region of the granulator</p> <p>[39]</p>
Tableting (compaction)	 <p>Axis of revolution Upper punch Die wall Powder Lower punch</p> <p>[46]</p>	 <p>Upper punch Base of punch Top of punch Die Material sample Top of punch Lower punch Base of punch</p> <p>[47]</p>
Tablet coating	 <p>Spray Nozzle</p> <p>[50]</p>	 <p>[48]</p>

2.2 Pharmaceutical tableting

Tablets have to meet in general the following requirements according to the Ph. Eur. [25]: ‘uniformity of dosage units’ (2.9.40), ‘uniformity of content’ (2.9.6), ‘uniformity of mass’ (2.9.5), and ‘dissolution’ (2.9.3). Those attributes are not only defined by the raw material properties (API and excipients) but also by the tablet manufacturing process. From a patient safety point of view, the ‘uniformity of dosage units’ is the most critical one as it defines the API dose in the drug delivery system.

Most commonly used are high speed rotary tablet presses which are explained in-depth in the following. Details about eccentric feed presses, which differ from rotary tablet presses in terms of, e.g. feeding mechanism, lower and upper punch function, and tablet ejection, can be found elsewhere [28, 45]. The turret is the central part of a rotary tablet press. Different number of tool stations, which are an assembly of lower punch - die - upper punch, are equipped on the turret. During turret rotation, every die passes the same steps as illustrated in Fig. 1.

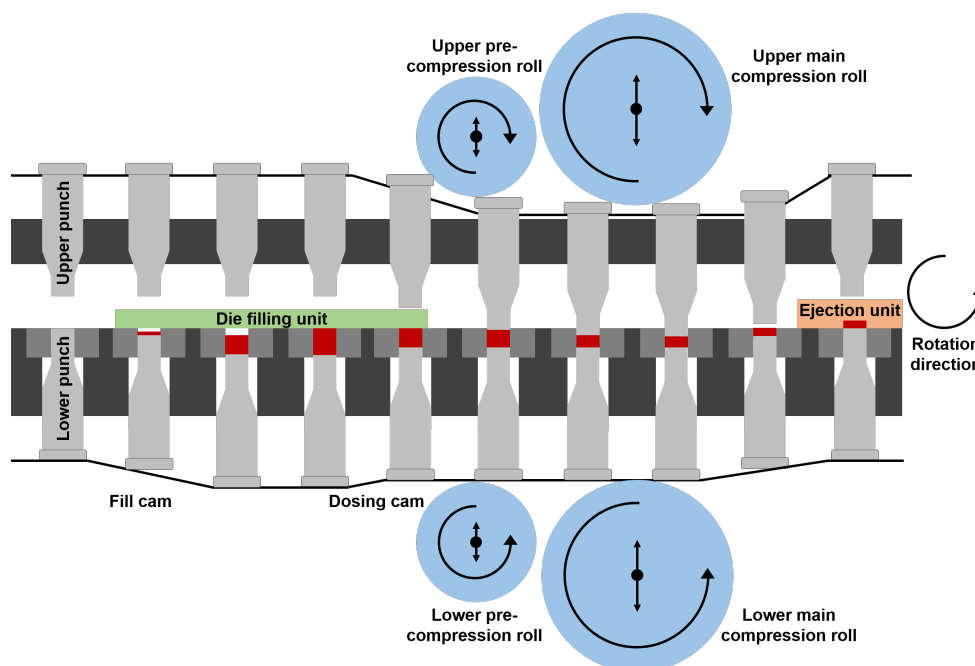


Fig. 1: Schematic illustration of a rotary tablet press.

Die filling

Powder is discharging from a mass flow hopper on top of the tableting machine through a feeding system (confer below (section 2.3)) into the rotating dies. As the die arrives underneath the filling station, the die volume is generated by withdrawing of the lower punch by the fill cam. The movement of the lower punch generates a partial negative pressure, named as ‘suction filling’ and facilitates powder discharge [57]. At the end of the filling station, the lower punch is moving upwards (‘dosing cam’), excess powder is removed by scrapers, and a more confined powder bed in the die is obtained (Fig. 1).

Powder compaction

Most tablet presses are equipped with a two staged compression station, namely pre-compression and main compression. Pre-compression allows the rearrangement of the particles in the die prior to the actual consolidation step. The optimal compression force of the tablets can be adjusted by the

bottom and top pressure rolls for the lower and upper punch, respectively. The following mechanisms are sometimes concurrent while compaction and cannot be distinguished [28]:

- Particle rearrangement (change of particle position, higher packing fraction)
- Elastic deformation of primary particles and granules
- Plastic deformation
- Crack into primary particles of smaller size (increase in contact area)
- Elastic deformation of generated secondary particles
- Plastic deformation of secondary particles

Different factors such as cohesive forces, adhesive forces, solid bridges, liquid bridges, and form-fitting bonds keep the tablets together.

Tablet ejection

The lower punch is moving upwards during the ‘ejection cam’ thereby pushing the tablet out of the die. A scraper transports the tablet via a chute into the storage bin.

The API content is set via the mass delivered into the die (tablet mass) as well as the dose strength of the formulation (relative API content in the blend). Although there are 150 years of tablet production experience (first industrial tablet production in 1877 [28]), nontrivial challenges in die filling still exist. Thus, the first step in the tableting process, the die filling, is still in the research focus as it specifies the mean and range of the tablet mass and API mass, and thus the ‘uniformity of dosage units’ (2.9.40) [25].

2.3 Die filling mechanisms

The powder blend can be delivered from the blending hopper by different mechanisms into the dies of the rotating turret. In the first mechanism, named as gravity filling, the powder blend is passively transported through a chute into the dies of the turret. Force feeding is the second mechanism with a force feeder consisting of one or more paddle wheels which actively feed by rotation the powder into the dies. Thus also materials with a lower powder flowability (confer below) can be transferred into the dies which make force feeding to the most commonly used die filling mechanism. The following aspects are collected from literature and are considered to be some of the most relevant factors in the context of die filling:

- **Powder flowability:**

Different powder flowability indices (Hausner ratio, Carr's index, angle of repose, flow through an orifice, ring shear cell experiments, and indices from custom-designed instruments [58–63]) can help to characterize the powder blend during formulation stage. In general, a direct connection between powder flowability and tableting performance is difficult [64, 65]. Furthermore, several physico-chemical material properties such as particle size, morphology, density, and dispersive surface energy influence powder flowability [66–70]. A good powder flowability is a prerequisite for a high die fill level and a low tablet mass variation [28] and it allows an increase in turret speed which may accelerate the throughput of the tableting process.

- **Feed hopper:**

The geometry of the connection pipe (feed hopper) between the blending hopper and the feeding system (confer section 2.3) should ensure steady mass flow of the material by choosing a sufficiently high wall angle [28] and should prevent segregation during discharge [71]. In addition, the powder at the bottom of the filling system is exerted to the overhead pressure of the material in the blending hopper [64], which is higher at the beginning of the tableting process.

- **API segregation in the filling station:**

Segregation is the 'unintentional de-mixing of one or more components in a mixture of particulates' [72]. Several physical mechanisms, classified by the physical particle properties [73] and by the energy input [74] can cause segregation. Particle size, particle size ratio, particle size distribution, fine particle concentration, particle shape, particle density, and powder flowability are some segregation influencing factors [75]. Vibrations of the turret motor can be transferred to other components of the tableting machine, e.g. the die filling station, and trigger segregation. API particle segregation during tableting can lead to off-target contents which can stem from segregation after homogeneous mixing and during powder flow in the tableting machine. The API segregation risk is much higher for DC formulations and should be carefully considered during formulation and process development. Identification and control of API segregation over process time is a critical issue.

- **Turret speed:**

The turret speed predominantly defines the 'dwell time' which is the time the flat portion of the punch head is in contact with the compression roll. However, the turret speed also influences motor vibrations (confer above), the suction effect, and the centrifugal forces which are higher at higher turret speeds. In addition, the die filling time, or the available time for powder discharge into the die, is defined by the turret speed.

- **Filling station design:**

The different designs of die filling stations differ from tableting machine to tableting machine

and make a simple comparison difficult. Not only the type of feeder and its corresponding design (gravity or force, confer section 2.3) but also the length of the die filling segment, the type of powder re-direction into the feed frame at the dosing cam station, and scrapers on top of the dies and in the filling station to aerate and loosen up the powder, are manufacturer-specific design features.

- **Particle shearing:**

During the powder transfer from the blending hopper into the dies, the powder may undergo additional shear effects which can be higher due to paddle wheel rotation in force feeders (confer section 2.3 [76]). Those effects can lead to particle attrition and over-lubrication which can affect other tablet quality attributes such as dissolution and disintegration [41, 42].

Different approaches have been developed to understand the die filling process in more detail by addressing some of the above mentioned aspects. The studies can be grouped into the type of die filling mechanism (gravity filling or force feeding) and the type of approach (classical experimental, near-infrared spectroscopy (NIR), or numerical). In Tab. 2, a brief chronological overview of published studies in the context of pharmaceutical die filling by different means is provided. Those studies are not discussed in detail at this point as more information is provided in the chapters of the results and discussion part (section 3).

2.3.1 Gravity filling

The first die filling study was published in 2003 by Wu et al. [63]. They developed in the context of ceramic industry a model die filling system to investigate the motion of the powder delivery system on powder discharge into the die. In this model system, powder was filled into a moving shoe which translated over a stationary die having varying geometries. The speed of the shoe could be set to 25 mm/s to 400 mm/s. The powder mass delivered into the die was expressed as a function of shoe speed. Using this system, the effect of humidity [77], vacuum/air [78], die shape [63], and suction filling [79] was studied on die filling. This model system is the most cited one related to gravity filling (Tab. 2). The system can be categorized into gravity filling, though significant differences exist compared to rotary tablet presses. The most dominant difference is the discharge from a translating shoe into a stationary die instead of a stationary feeding system and a rotating die. The study by Yaginuma et al. is the only one which assessed the influence of powder flowability in an actual gravity feeder of a Libra 2 tableting machine [80] (Tab. 2).

In addition to the classical experiments, the same model die filling system or adapted versions were studied by numerical means (e.g. [81–85]). The focus of those numerical studies was the identification of optimal process conditions, the formulation optimization by the adaption of powder flowability, and the evaluation of segregation mechanisms. Comparison of numerical results with experiments allowed an increased process understanding.

This short review shows that most understanding from gravity filling is based on a model die filling system, that lacks some major features that are relevant in rotary tablet presses (confer above and Tab. 2).

2.3.2 Force feeding

The first real comprehensive die filling studies with a force fed-equipped tableting machine started in 2010 by Narang et al. [76] and Mendez et al. [86] (Tab. 2). Narang et al. evaluated the influence of

turret speed and force feeder speed on tablet tensile strength. While the turret speed’s impact was attributed to the dwell time and kinetics of consolidation of granules in the die cavity, the paddle wheel speed influenced the tablet tensile strength via particle shearing and led to particle over-lubrication [76]. Other studies evaluated process variables on tablet weight [86–88], tablet weight variability [87, 88], and powder residence time [89] or the effect of different force feeders on particle attrition [90]. The experimental studies compared what was entered into the system (e.g. powder flowability characterization) to what was coming out of the system (e.g. tablets). The powder flow in between in the force feeder could not be unveiled unless transparent systems were developed as done by Mendez et al. [86].

Another experimental approach, namely NIR spectroscopy, gained very high interest since 2013 in the context of tableting and originally intended to monitor API content in intact tablets [91]. The NIR probe can be located at different positions of the feed frame, e.g. prior to the die filling region [92]. Well developed NIR spectra calibration models are necessary but difficult to obtain to provide valuable content data, e.g. to discriminate API particles from excipient particles. All studies so far focused on NIR method development rather than providing detailed information on the powder flow phenomena within the feed frame, i.e. API segregation. In the next couple of years and with the gain in NIR method understanding, in-line API content measurement within the feed frame might be possible and would add value to force feeder process understanding.

The first reported numerical feed frame study was published in 2014 by Mateo-Ortiz et al. [93]. So far only four studies by other groups have been published. They tested the influence of paddle wheel speed, number of paddle wheel blades, paddle wheel shape, paddle wheel height, and particle cohesion on die filling [41, 93–95]. In addition, first attempts were made to understand particle size segregation mechanisms induced by paddle wheel rotation [93]. In contrast to the classical experimental approaches, the numerical studies allowed to have a detailed look inside the feed frame. Though, the studies can improve process understanding, they are limited by computational power (confer section 2.4.6). Concrete validation of the results was not performed by neither of the studies (Tab. 2).

Tab. 2: Overview of pharmaceutical die filling studies grouped into the type of feeding mechanism (gravity of force feeder) and type of approach (experimental, NIR, numeric). Main studied parameters are provided. * is the same model die filling system reported by Wu et al. [63].

Publication	Year	Gravity feeder	Force feeder	Experimental	NIR	Numeric	Studied parameters	Ref.
Sinka et al.	2004	X*		X			Air, geometry, temperature, relative humidity	[96]
Wu et al.	2006	X*				X	Particle shape, die shape, air (2D model)	[79]
Xie et al.	2006						(Review)	[97]
Jackson et al.	2007	X*		X			Suction	[57]
Schneider et al.	2007	X*		X			Air, scale up	[78]
Yaginuma et al.	2007	X	X	X			Powder flowability, feeding mechanism	[80]
Wu	2008	X*				X	Particle shape, particle size (2D model)	[81]

2.3.2 Force feeding

Tab. 2: Overview of pharmaceutical die filling studies grouped into the type of feeding mechanism (gravity or force feeder) and type of approach (experimental, NIR, numeric). Main studied parameters are provided. * is the same model die filling system reported by Wu et al. [63].

Publication	Year	Gravity feeder	Force feeder	Experimental	NIR	Numeric	Studied parameters	Ref.
Sinka et al.	2009						(Review)	[98]
Mehrotra et al.	2009	X				X	Cohesion (powder compression)	[99]
Narang et al.	2010		X	X			Paddle wheel speed, turret speed, compression force	[76]
Wu et al.	2010	X*		X			Particle velocity during discharge	[100]
Mendez et al.	2010		X	X			Powder properties, paddle wheel speed, turret speed, die diameter	[86]
Guo et al.	2011	X*				X	Size-induced segregation, air	[101]
Nwose et al.	2012	X*				X	Electrostatic charge (2D model)	[83]
Mendez et al.	2012		X	X			Force feeder design, paddle wheel speed, turret speed	[90]
Mendez et al.	2012		X	X			Paddle wheel speed, turret speed	[102]
Wu et al.	2012	X*				X	Suction	[84]
Wu et al.	2012	X*		X			Powder flowability	[103]
Mills et al.	2013	X*		X			Suction, particle size, particle density	[104]
Järvinen et al.	2013		X		X		(NIR method development)	[105]
Ward et al.	2013		X		X		(NIR method development)	[92]
Mateo-Ortiz et al.	2014		X	X		X	Size-induced segregation	[93]
Wahl et al.	2014		X		X		(NIR method development)	[106]
Mateo-Ortiz et al.	2014		X		X		(NIR method development)	[107]
Peeters et al.	2015		X	X			Die fill depth, paddle wheel speed, turret speed	[87]
Ketterhagen	2015		X			X	Paddle wheel speed, paddle shape, particle cohesion	[41]
Sasic et al.	2015		X		X		(NIR method development)	[108]
Tsunazawa et al.	2015	X				X	Arbitrarily shaped dies	[109]
Mateo-Ortiz et al.	2015		X			X	Paddle wheel speed, turret speed	[95]
Mateo-Ortiz et al.	2016		X			X	Paddle wheel speed, number of paddle wheel blades, paddle wheel height	[94]
Peeters et al.	2016		X	X			Paddle wheel speed	[110]
Furukawa et al.	2016	X		X		X	Size-induced segregation	[85]
Durao et al.	2017		X		X		(NIR method development)	[111]
Schiano et al.	2017	X*		X			Powder flowability	[112]
De Leersnyder et al.	2018		X		X		(NIR method development)	[113]
Dülle et al.	2018		X	X			Paddle wheel speed, turret speed	[89]
Dalvi et al.	2018		X		X		(NIR method development)	[114]
Grymonpre et al.	2018		X	X			Paddle wheel speed, turret speed, overflow level, paddle wheel design	[88]

2.4 Modeling using discrete element method

In the next chapters, the DEM background as well as the governing equations, contact models, and non-contact models, micro-mechanical material properties, and numerical considerations for DEM are explained on basis of an example DEM flowsheet (Fig. 4, section 2.4.1 - 2.4.6). The details about the DEM models applied in this work are provided as this is not done in the individual chapters in the results and discussion part (section 3).

2.4.1 Discrete element classes

The DEM belongs to the discrete modelling techniques and includes cellular automata, the Monte Carlo method, the hard-particle approach, the soft-particle approach, and the finite discrete element method [20, 23]. The different models are exemplarily illustrated in Fig. 2.

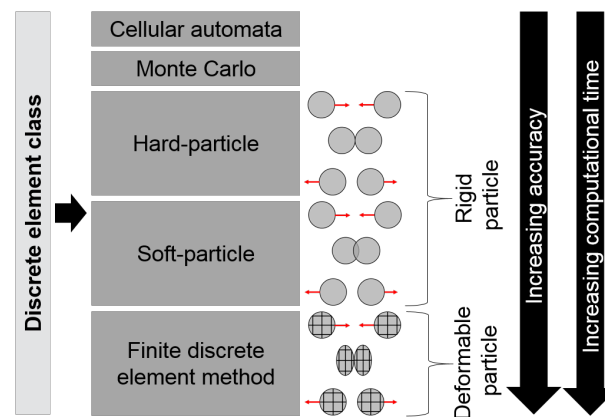


Fig. 2: Overview of different discrete element classes

In cellular automata, the particles are constrained to a lattice. The particle movement is governed by simple equations related from experiments. It can be computed very quickly but allows only qualitative predictions [20]. The probability of random particle arrangement and the energy associated with that arrangements is calculated in the Monte Carlo Method. The model is rather simple to implement and associated with a relatively low computational cost [20]. Computational more complex models are necessary to provide dynamic information such as trajectories and transient forces acting on particles in granular flow. Newton's second law of motion can be used to track the motion of individual particles, and the forces resulting from particle-particle and particle-wall interactions via a distinct approach [18]. In general, the soft-particle and hard-particle DEM approach exist and permit a direct relation between material properties and model parameters [20]. The soft-particle approach was originally developed by Cundall and Strack in 1979 [115] and is usually utilized in particle dynamics with longer particle-particle and particle-wall contacts, i.e. in low-speed, friction-dominated flows of complex particle-particle and particle-wall collisions [18]. Importantly, the model is capable of handling multiple particle contacts as found in quasi-static systems. In contrast, rapid powder flows with instantaneous and binary considered particle-particle and particle-wall collisions are usually modeled via the hard-particle approach. In the finite discrete element approach, particles deform while contact, in contrast to the hard- and soft-particle approach without particle deformation (rigid). The particle deformation is approximated in the soft-particle approach by particle overlap (Fig. 2 and section 2.4.4).

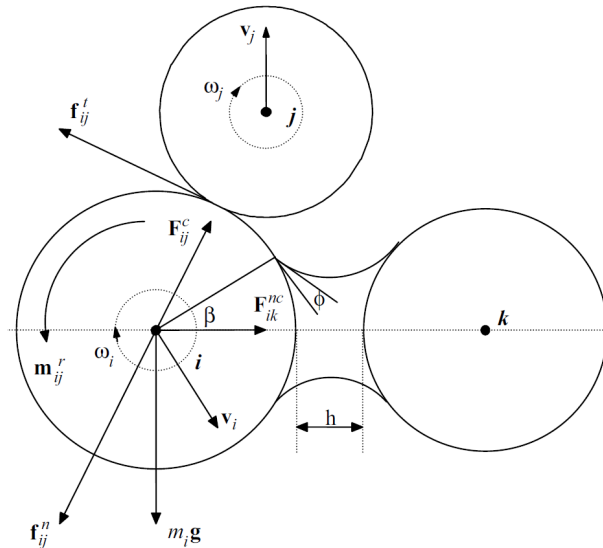


Fig. 3: Forces acting on particle i from contacting particle j and non-contacting particle k via capillary force are schematically shown. Illustration taken from [23].

The increase in model accuracy goes in hand with a significantly longer computation time (Fig. 2). Thus a reasonable assessment of the desired resolution is necessary to select an appropriate model. The dense granular flows with shear and friction in the tablet press have to be represented by the soft-sphere approach which is explained in more detail in the following.

2.4.2 Governing equations

Particulate granular flow may be of translational and / or rotational motion. During particle movement, the particle can interact and exchange momentum and energy with either neighboring particles or walls, or with the surrounding fluid. At all times, the resultant forces on a particle can be determined exclusively [23]. The translational and rotational motion of particle i with mass m_i and moment of inertia I_i can be written as in Eq. 1 and 2, respectively.

$$m_i \frac{d\mathbf{v}_i}{dt} = \sum_j \mathbf{F}_{ij}^c + \sum_k \mathbf{F}_{ik}^{nc} + \mathbf{F}_i^f + \mathbf{F}_i^g \quad (1)$$

$$I_i \frac{d\omega_i}{dt} = \sum_j M_{ij} \quad (2)$$

\mathbf{v}_i and ω_i are the translational and angular velocities of particle i , respectively. \mathbf{F}_{ij}^c and M_{ij} are the contact force and torque acting on particle i by particle j or other sources. The non-contact force acting on particle i by particle k or other sources enter in Eq. 1 via \mathbf{F}_{ik}^{nc} . The particle-fluid interaction force and the gravitational force acting on particle i are given by \mathbf{F}_i^f and \mathbf{F}_i^g , respectively. The forces and torques acting on a particle considered in the DEM are schematically shown in Fig. 3.

2.4.3 Flowsheet of computational model

A flowsheet of a DEM simulation is provided in Fig. 4 and serves as a basis to describe the individual steps. The system initialization and post-processing steps as well as the in between DEM soft-particle algorithm are exemplarily shown for the DEM code ‘LIGGGHTS’ [116], the open source mesh generator ‘Gmsh’ [117], and the post-processing tool ‘Paraview’ [118]. Other DEM codes such as the

commercial EDEM[®] and Rocky DEM[®] and the open-source Yade and ESyS-Particle are available. The soft-particle algorithm shown in the flowsheet of Fig. 4 would be in principle the same, though system initialization and post-processing may differ depending on the software used and its graphical user interface.

System initialization

All necessary parameters for the DEM model are defined in the input file. The most important ‘commands’ are listed below for which a detailed explanation is provided in the next sections. Other necessary parameters are given in e.g. LIGGGHTS documentation [116].

- **Model declaration:**

Before the actual computation, the contact and non-contact models have to be defined. The models are described in detail in section 2.4.4. The selection of an appropriate time step is explained in section 2.4.6.

- **Geometry definition:**

The geometry of the system for particle-wall contacts is imported into the DEM software as finite-element grids, e.g. triangles and can be generated by a meshing tool. Special emphasize may be given to the geometry size and the required resolution of the mesh with more explanation in section 2.4.6.

- **Particle properties definition:**

The powder characteristics of the material(s) have to be defined in terms of their micro-mechanical properties on a particle level as well as their size and size distribution (not shown: other than spherical particle shape). The general properties and how they can be determined is explained in section 2.4.5.

Computation

The actual computation for a soft-sphere algorithm contains the following steps. The particles are inserted into the computational domain by defining their position and velocity. In the next step, all particle-particle and particle-wall contacts are identified. The soft-particle deformation is calculated as an overlap for each contact. By using the overlap values and the force-displacement relations (section 2.4.4.1), the forces acting on each particle are calculated. All forces and momenta acting on each particle are summed up and the translational and rotational accelerations for each particle are determined using Newton’s 2nd law (confer Eq. 1 and 2). The time step is incremented and the accelerations are integrated over time to update particle velocities and positions. The contact detection is repeated until the simulation is completed [20].

Post-processing

The LIGGGHTS DEM code produces for defined increments of the time step an output file. Basically, the output file contains for each particle in the system the actual position, velocity, and force acting on it (additional output styles can be selected [116]). The output file can be further processed into VTK (Visualization ToolKit) files and read with data visualization softwares such as Paraview [118]. In addition, the tabular structure of the output file can be processed with other tools (e.g. C/C++ program or MATLAB) to quickly extract quantitative data.

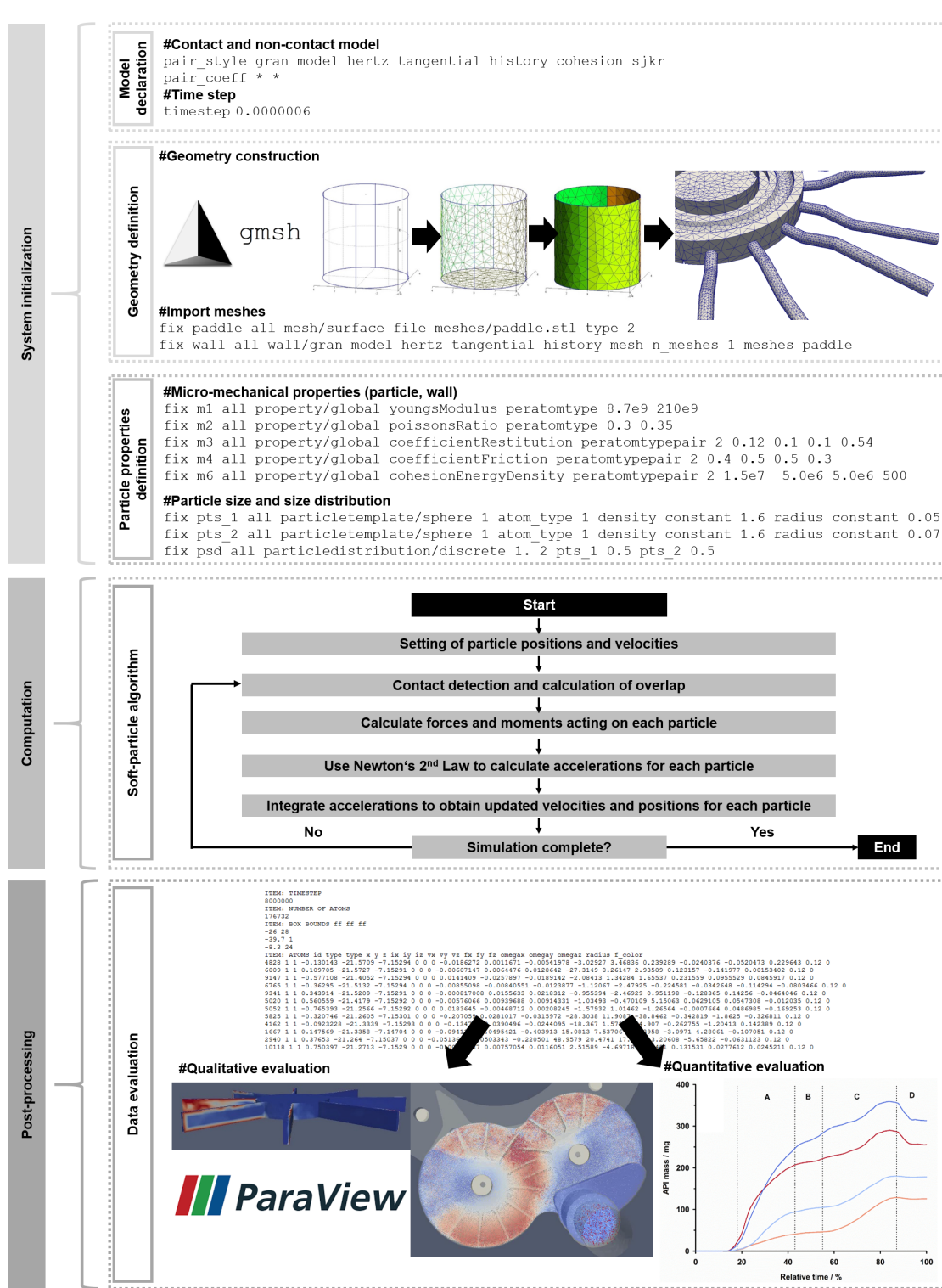


Fig. 4: Example flowsheet for DEM simulation including pre-processing (input file contains only most important commands necessary in LIGGGHTS [116]), computation via soft-particle algorithm (adapted from [20]), and post-processing.

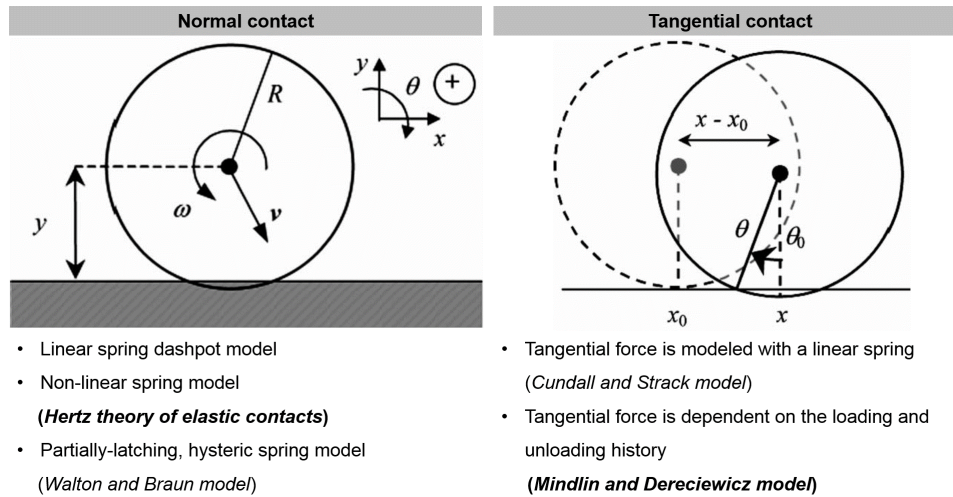


Fig. 5: Normal and tangential particle-wall contact schemes (particle illustration taken from [119]). The most popular models are listed.

2.4.4 Contact and non-contact models

2.4.4.1 Contact models

The heart of the DEM simulation is the particle interaction model. The model calculates the forces acting on particle-particle or particle-wall contacts, which are subdivided into normal and tangential components and which are then used to calculate accelerations (see Eq. 1 and 2). The accelerations are integrated in time for updated particle velocities and positions [20] (section 2.4.3, Fig. 4 ‘computation’). A simple particle-wall normal and tangential contact including the most popular contact models are shown in Fig. 5. More details about the models are provided in the review by Di Renzo et al. [119].

The simplest model to calculate the normal force in normal contacts is the linear spring dashpot model. In this model, the repulsive portion is modeled via a linear spring and the dissipative portion with a viscous dashpot. The Hertz theory of elastic contacts was applied in the current work and has a nonlinear spring in the repulsive portion in contrast to the linear spring dashpot model [120]. Gröger and Katterfeld showed in conveyor belts and transfer chutes the appropriateness of the Hertz model [121].

The Cundall and Strack model is the simplest model for tangential force-displacement [115]. In this model the tangential force is calculated by a linear spring and it is limited by the Coulombic criterion, i.e. the frictional force is proportional to the normal force by the proportionality constant of the coefficient of friction. The Mindlin and Deresiewicz tangential force model considers the dependance of the force-displacement relationship on the whole loading and unloading history [122]. The latter model was applied previously in die filling studies by others, e.g. Mateo-Ortiz and Mendez [94], and is used in the current work.

The equation for contact force calculations used in the current work, derived from the *gran model hertz model* in LIGGGHTS, is given in Eq. 3 [116, 123].

$$\begin{aligned}
 F = & \left(k_n \underbrace{\delta \mathbf{n}_{ij}}_{\substack{\text{normal} \\ \text{overlap}}} - \gamma_n \underbrace{\mathbf{v} \mathbf{n}_{ij}}_{\substack{\text{normal} \\ \text{relative} \\ \text{velocity}}} \right) + \left(k_t \underbrace{\delta \mathbf{t}_{ij}}_{\substack{\text{tangential} \\ \text{overlap}}} - \gamma_t \underbrace{\mathbf{v} \mathbf{t}_{ij}}_{\substack{\text{tangential} \\ \text{relative} \\ \text{velocity}}} \right) \quad (3) \\
 & \underbrace{\hspace{10em}}_{\text{normal force } (F_n)} \quad \underbrace{\hspace{10em}}_{\text{tangential force } (F_t)}
 \end{aligned}$$

The $\delta \mathbf{n}_{ij}$ defines the overlap distance of two particles i and j , when the distance r between the particles with their radii R_i and R_j is less than their contact distance $d = R_i + R_j$. No force between the particles is given if $r > d$. In Eq. 3 the first term is the normal force between two particles with a spring force term and damping force term. Similarly, the second part of Eq. 3 for the tangential force contains two components. The first term is the shear force, the second one the damping force. The tangential displacement or the tangential overlap between particle i and j during the contact duration is included as a ‘history’ effect in the shear force. The tangential overlap ($\delta \mathbf{t}_{ij}$) is calculated by integrating the relative velocity at the contact point over time. The tangential displacement vector is truncated to satisfy the frictional yield criterion as follows. The coefficient of friction (μ) is the upper limit of the tangential force through the Coulomb criterion (Eq. 4), with

$$F_{t\text{spring}} = \mu \cdot F_n \quad (4)$$

The v_n and v_t in Eq. 3 are the normal and tangential component of the relative velocity of the two particles, respectively. The other coefficients such as the k_n (elastic constant for normal contact, Eq. 5), k_t (elastic constant for tangential contact, Eq. 8), γ_n (viscoelastic damping constant for normal contact, Eq. 6), and γ_t (viscoelastic damping constant for tangential contact, Eq. 9) are calculated from material properties. Those properties have to be pre-defined for a given material as described in section 2.4.5 and illustrated in Fig. 4. The effective Young’s modulus (E^*), the effective Shear modulus (G^*), the Poisson’s ratio (ν), and the coefficient of restitution (e), in addition to the particles’ mass (m), enter via the following equations into the contact force calculations (Eq. 5 - 15):

$$k_n = \frac{4}{3} E^* \sqrt{R^* \delta_n} \quad (5)$$

$$\gamma_n = -2 \sqrt{\frac{5}{6}} \beta \sqrt{S_n m^*} \geq 0 \quad (6)$$

$$S_n = 2 E^* \sqrt{R^* \delta_n} \quad (7)$$

$$k_t = 8 G^* \sqrt{R^* \delta_n} \quad (8)$$

$$\gamma_t = -2 \sqrt{\frac{5}{6}} \beta \sqrt{S_t m^*} \geq 0 \quad (9)$$

$$S_t = 8 G^* \sqrt{R^* \delta_n} \quad (10)$$

$$\beta = \frac{\ln(e)}{\sqrt{\ln^2(e) + \pi^2}} \quad (11)$$

$$\frac{1}{E^*} = \frac{(1 - \nu_1^2)}{E_1} + \frac{(1 - \nu_2^2)}{E_2} \quad (12)$$

$$\frac{1}{G^*} = \frac{2(2 - \nu_1)(1 + \nu_1)}{E_1} + \frac{2(2 - \nu_2)(1 + \nu_2)}{E_2} \quad (13)$$

$$\frac{1}{R^*} = \frac{1}{R_1} + \frac{1}{R_2} \quad (14)$$

$$\frac{1}{m^*} = \frac{1}{m_1} + \frac{1}{m_2} \quad (15)$$

2.4.4.2 Non-contact models

In addition to contact forces, non-contact forces can play a detrimental factor in flow dynamics. In Fig. 3 the non-contact capillary force due to surface tension at solid/liquid/gas interfaces is shown. Two additional forces, namely the Van der Waal's attraction and the electrostatic force are included in the fundamental non-contact forces [23]. The Van der Waal's attractive force may be between 'like' bodies (auto-adhesion) and 'unlike' bodies (adhesion). The force arises from the electronic and hydrogen bonding interactions between the molecules of the bodies. Macroscopic charged particles show electrostatic forces due to Coulombic interactions. With decrease in particle size, the influence of the different fundamental forces increases, i.e. cohesive forces show a high impact relative to particle weight. This phenomenon follows the simple rule of the importance of forces relative to the particle diameter (d): Body forces (e.g. weight) $\propto d^3$, surface area based forces (e.g. electrostatic) $\propto d^2$, and interfacial forces (e.g. capillary and Van der Waal's) $\propto d$ [21]. A detailed review on non-contact forces in pharmaceutical powders and their treatment in numerical simulations is provided by Sarkar et al. [21]. Different non-contact models were developed to implement the three fundamental forces individually (e.g. van der Waal's force [124], electrostatic force [125], and capillary force [126]).

For the current study, the simplified Johnson-Kendall-Roberts (JKR) model was applied which does not discriminate between the different non-contact force contributions [127]. It has been used previously in powder flow studies of the tableting machine, e.g. by Ketterhagen [41] and by Mateo-Ortiz et al. [93]. The model adds an additional normal force contribution with A for the particle contact area and k for the cohesion energy density (CED) (Eq. 16).

$$F = k * A \quad (16)$$

The particle contact area (A) is defined through the distance between the particle centers ($dist$) and the particle radii (R_i and R_j) according to Eq. 17 (LIGGGHTS model *gran cohesion sjkr model* [116]).

$$A = \frac{\pi}{4} \frac{(dist - R_i - R_j)(dist + R_i - R_j)(dist - R_i + R_j)(dist + R_i + R_j)}{dist^2} \quad (17)$$

2.4.5 Material properties and their determination

The material properties entering in contact and non-contact force calculations are listed in the previous sections (confer Eq. 3 - 17). The elastic properties of the particles such as the Young's modulus (E), Shear modulus (G), Poisson's ratio (ν), and Coefficient of restitution (e) are necessary to calculate the contact stiffness. Other required properties are the Coefficient of friction (μ) and the Cohesion

Energy Density (CED).

- The Young's modulus (E) is the ratio of stress (σ , ratio of normal force to the applied cross sectional area) to strain (ϵ , change in relative length). Direct measurement techniques are for example nanoindentation (atomic force microscopy) [128–132], four-point beam bending [133], die-in and die-out method [129, 134], uniaxial compression test [135], and diametric compression test [134, 136]. The E of different pharmaceutical excipients (micro-crystalline cellulose, lactose, corn starch etc.) were measured in a size range of 2.9 GPa - 31.3 GPa by nanoindentation in the Govedarica et al. study [128].
- The shear modulus (G) is the ratio of shear stress to shear strain and can be derived from E and ν via Eq. 13.
- The lateral contraction of a material or the change of a material's thickness is specified through the Poisson's ratio (ν) and can be obtained from E and G (Eq. 18 [133, 137]).

$$\nu = \frac{E}{2G} - 1 \quad (18)$$

- Particle drop or free fall tests may be used to measure the coefficient of restitution (e) by the ratio of impact velocity to rebound velocity. The velocities can be captured using a high speed camera. The e for different pharmaceutical materials was determined via this approach by others [138–140]. The e is significantly affected by the impact velocity, particle size and shape, particle surface roughness, the moisture content, the adhesion properties, and the process conditions such as the temperature [141].
- Ai et al. reviewed different rolling resistance models and their assessment in discrete element simulations [142]. In principle, the sliding friction (μ) between two bodies is the ratio of friction force between two bodies (particle-particle or particle-wall) and the force pressing them together. The μ can be assessed via sliding experiments [143–145], atomic force microscopy [146], and a pin-on-disk tribometer [147].
- Different experimental setups exist to evaluate the non-contact force (confer to 2.4.4.2, CED) between particles or between particles and the geometry. Atomic force microscopy allows the quantification of cohesion or adhesion on a single particle level [148, 149]. Other methods apply a centrifuge [150–153], a particle drop test [154], a modified tensiometer [148, 155], or inverse gas chromatography [156].

The previous description shows that for each and every material very unique measurement techniques have to be developed to ascertain the micro-mechanical material properties on a particle level. In case that those techniques are not available, indirect measurements may be applied to calibrate those DEM parameters as described in the review of Coetzee [157]. The 'bulk calibration approach' treats the micro-mechanical material properties as 'adjustment parameters' [157]. Laboratory experiments are performed and repeated numerically in a similar setup. The model parameters are iteratively changed until the laboratory results and numerical results match to a certain accuracy. Most often, particle size and density are measured directly and the other parameters are determined through suitable tests such as a penetration test, direct/ring shear test, uniaxial compression test, static (pile formation) or dynamic (rotating drum) angle of repose, triaxial / biaxial test, and artificial neural networks with angle of repose and shear test [158] (Tab. 1 in [157]).

2.4.6 Computational considerations in DEM

The main advantage of the DEM is the high degree of detail it can provide in complex systems. The internal powder flow dynamics can be unveiled which would not be possible with classical laboratory experiments. Limited by computational power, a main challenge is the choice of a reasonable DEM model. The inherent computational complexity of the DEM model is mainly attributed to the following factors which have to be carefully considered.

Number of particles

The DEM tracks every individual particle in the simulation domain and computational time scales accordingly with the number of particles simulated (N) via $N \log N$ [20]. Furthermore, N is direct proportional to the volume of the system (V) under consideration and the particle diameter (d) according to Eq. 19 [20].

$$N \propto \frac{V}{d^3}. \quad (19)$$

This dependency requires a careful selection of a reasonable particle size and particle size distribution for large systems. One approach artificially increases the size of the particles to reduce N [20] while maintaining the domain size in the model [159] and/or to ignore particles with a size below a certain value [160]. Either particle size scaling laws [161] or size-effect sensitivity studies [162] can help to estimate the maximal possible size enlargement in DEM simulations.

Particle size does not only influence N , but also the time step (Δt) in the DEM model (confer Fig. 4) according to Eq. 20. The time step should be chosen smaller than the particle contact, i.e. 20% of the Rayleigh wave speed through a particle [163]. Δt is increased if the elasticity parameter ($E \propto G$) decreases and particle size (R^*) increases resulting in a faster simulation time. However, the elastic parameters should be chosen carefully if the system under consideration is very dense [163].

$$\Delta t = 0.2 \cdot \frac{\pi R^* \left(\frac{\rho}{G}\right)^{0.5}}{0.1631\nu + 0.8766} \quad (20)$$

Particle shape

Most numerical models consider idealistic spherical particles in DEM simulations facilitating contact detection and contact resolution. However, non-spherical particles may have to be considered in certain cases, in which e.g. particle rotation is not restricted by frictional contacts as in spheres but through mechanical interlocking. Different approaches exist to represent non-spherical particles. The simplest approach ‘glues’ two or more spherical particles in a rigid or flexible manner together to obtain irregular shaped particles. This approach was applied in a numerical tablet coating study to obtain the shape of biconvex round tablets [164]. Another option is the ‘idea of mathematical dilation’ to create spherocylinders. More approaches are found in reviews by Ketterhagen [20] and Coetzee [157].

Powder mixtures

Pharmaceutical materials, in particular direct compression blends, are multi-component mixtures including the API and excipients. All those components have a defined particle size, particle size distribution, particle shape, and particle surface property. The particles interact with particles of the same type and the other components of the mixtures with different forces. Adding the complexity of pharmaceutical mixtures to the computational model requires a time-consuming contact detection [165]. In addition, mixture properties determination on a single particle level are difficult (confer 2.4.5).

Complex geometries

The complexity of a numerical model increases with complicated geometries. Geometries are introduced into the computational domain as a mesh composed of individual triangles. An example mesh is provided in section 2.4.3, Fig. 4. Each triangle of the mesh corresponds to 8 simulated particles. Hence systems of very irregular shape, e.g. round surfaces, have to be resolved by a higher number of triangles to obtain correct particle-wall contact forces. Furthermore, very asymmetric geometries exacerbate the per-processor load or in other words the number of particles and triangles considered per one processor thus some processors having a high load and others a low load. The imbalance increases computational time.

Experimental validation of DEM results

A common concern of numerical simulations is experimental validation of the results. The main advantage of a high resolution within complex industrial systems becomes detriment to experimental validation. Hence, it is either very difficult, expensive, or impossible to verify numerical results experimentally for complex industrial applications. As shown by the following two examples, experimental validation is still limited to small systems. Remy et al. validated their DEM model for powder mixing by an impeller blade utilizing particle image velocimetry (PIV) [166]. The comparison of the particle bed shape and flow in a baffled attrition test and in a rotating drum was used for validation of the DEM model in the study by Marigo and Stitt [167].

Other challenges

- Incorporation of all forces, i.e. adaption of non-contact forces related to larger particles considered
- Determination of micro-mechanical material properties on a particle level (section 2.4.5)
- Long-time scale unit operations (couple of million - billion number of iterations at infinite small time steps (μs range) for computation of a physical time of a few seconds to minutes)
- DEM coupling with fluid effects

3 Results and Discussion

The results and discussion sections is split into two main parts, the first one (chapter 3.1.1-3.1.4) evaluates powder discharge into the die by gravity, the second one the active powder transfer from the feeding system into the rotating dies of the turret (chapter 3.2.1-3.2.5).

For gravity filling at first powder transfer is evaluated by experimental means in a transparent model die filling system made of acrylic glass. The system is designed as simple as possible, i.e. a rectangular hopper serves for powder storage and a die is translating at adjustable speed underneath the former. Several commonly used diluents and disintegrants for direct compression are analyzed with respect to powder flowability in the model system. In chapter 3.1.1 a novel metric is developed to describe a material's die fill ratio in relation to the die filling speed. A correlation is generated between the material's sensitivity to changes in die fill speed and the powder's properties such as particle size. In addition, a comparison is made for the powder flowability quantification via the model die filling system and via the ring shear cell.

Using high-speed camera imaging, the powder discharge into the die in the model die filling system is visualized in chapter 3.1.2. By selecting a very high image framerate, the particle discharge pattern is clearly resolved over die filling time and a material grouping into different flowability classes is provided.

Furthermore to the experimental model die filling system, gravity filling is assessed by numerical means in chapter 3.1.3 and 3.1.4. The feeding system consists of a cylindrical pipe connected to an inclined chute and a rectangular box. In contrast to the experimental system, the turret is not translating but rotating underneath the feeding station. Utilizing this system, the powder flow pattern is evaluated for mono-disperse (chapter 3.1.3) and poly-disperse (chapter 3.1.4) sized particles. Initially, the powder flow pattern through the feeding system is evaluated, i.e. the particle rearrangement and the particle size segregation mechanisms. In a second step, material properties (chapter 3.1.3 and 3.1.4) and process conditions (chapter 3.1.3) are changed to detect their influence on tablet quality.

In the second part of the study, the force feeders of two different tableting machines, a FETTE 1200i and KIKUSUI Virgo, are evaluated by DEM. In chapters 3.2.1-3.2.4, the powder pattern is described for the FETTE 1200i system. Chapter 3.2.1 and 3.2.2 form the basis for the following chapters as the general powder transfer from the feeding hopper through the top wheel (dosing wheel) and the two below located wheels (reverse dosing wheel and filling wheel) into the dies of the turret is described. The analysis includes, in addition to the classical metrics such as tablet weight and tablet weight variation, particle size segregation evaluation and particle tracking for particle residence time measurement / powder mixing quantification within the feed frame. The influence of material properties (particle cohesion, particle-wall friction, and API content in the formulation) and process conditions (turret speed and paddle wheel speed) are assessed applying the QbD approach via a DoE. The influence of the pre-mentioned parameters on tablet weight is described in chapter 3.2.1 with a more extensive evaluation in chapter 3.2.3. The results of the DoE are evaluated in more detail with respect to additional tablet quality attributes (tablet weight variation and content uniformity) and

particle shearing in the latter chapter (3.2.3) to provide potential levers for process optimization. The insights of the DoE results are utilized for comparison of different paddle wheel shape configurations in the FETTE 1200i in chapter 3.2.4. The paddle wheels mainly differ in terms of their particle contact surface area and shape. For two selected combinations of process conditions and material properties which showed highest and lowest tablet quality in the DoE (chapter 3.2.3), the tablet qualities and powder flow patterns are compared with the other paddle wheel shape configuration. Eventually, similar setups (material properties and process conditions combinations) are selected in chapter 3.2.5 for the comparison of the feed frame of the FETTE 1200i with the one of the KIKUSUI Virgo. Significant geometrical differences, e.g. number of paddle wheels, blade dimensions, and housings, are found and related to tablet quality and powder flow pattern (e.g. size segregation) differences.

The following individual chapters are already published (chapters 3.1.1-3.2.1) or in the review process of different scientific journals (chapters 3.2.2-3.2.4) and are marked as such correspondingly.

3.1 Gravity filling

3.1.1 Evaluation of gravity filling by an experimental model die filling system

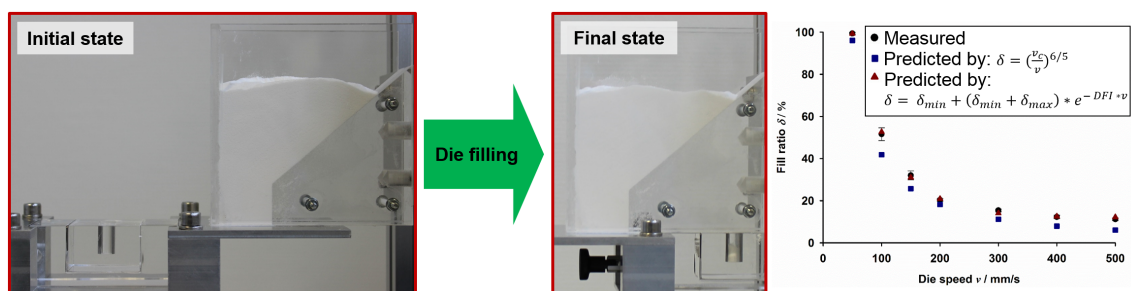
Evaluation and prediction of powder flowability in pharmaceutical tableting

Claudia Hildebrandt¹, Srikanth R. Gopireddy², Alexander K. Fritsch²,
Thomas Profitlich², Regina Scherließ¹, Nora A. Urbanetz²

¹ Department of Pharmaceutics and Biopharmaceutics, Christian-Albrechts-Universität Kiel,
Grasweg 9a, 24118 Kiel, Germany

² Daiichi-Sankyo Europe GmbH, Pharmaceutical Development,
Luitpoldstrasse 1, 85276 Pfaffenhofen, Germany

Pharmaceutical Development and Technology, 2017, ahead of print



Outline

In reality, the geometry of a gravity feeder in a rotary tablet press mainly consists of two portions, an inclined chute and a powder reservoir located on top of the turret. The varying die fill depths during fill and dosing cam as well as the high powder mass in the feeding system (in the order of at least some hundred gram, depending on the machine scale) are just two reasons which complicate die fill measurements in early stage development with limited API amount. Though, keen insight into the relationship between different powder flowability measures and the powder flow into the die are necessary for formulation development. To bridge this gap, a model system is designed. In this system, powder discharges from a storage hopper into a cylindrical die translating underneath the hopper at adjustable speed. The design is intentionally kept as simple as possible to ascertain the die filling with least influence from additional factors, e.g. centrifugal forces by turret rotation. In addition, the system is made of acrylic glass which allows to visualize the die filling process, as described in chapter 3.1.2.

For different pharmaceutical excipients used in direct compression formulations, ring shear cell measurements are performed to assess the '*flow function coefficient*' (*ffc*). In the second step, the die fill ratios (δ) of the materials at increasing die speeds (v) are evaluated using the custom designed model die filling system. A mathematical model is developed to describe the relationship of δ with v and to provide a measure for powder flowability in die filling. Correlations are developed to estimate the flowability measures of the ring shear cell and of the model die filling system from intrinsic particle properties such as particle size. Hence, powder flowability may be derived from particle characteristics.

Eventually, the powder flowability in the context of die filling by gravity is compared between the quasi-static measurement of the ring shear cell and the dynamic measurement of the model die filling system. This comparison is necessary to generate an awareness of the most suitable measurement or equipment to quantify powder flowability in tableting during formulation development, e.g. for optimal excipient selection.

RESEARCH ARTICLE



Evaluation and prediction of powder flowability in pharmaceutical tableting

Claudia Hildebrandt^a, Srikanth R. Gopireddy^b, Alexander K. Fritsch^b, Thomas Profitlich^b, Regina Scherließ^a  and Nora A. Urbanetz^b

^aDepartment of Pharmaceutics and Biopharmaceutics, Kiel University, Kiel, Germany; ^bPharmaceutical Development, Daiichi-Sanyko Europe GmbH, Pfaffenhofen, Germany

ABSTRACT

The focus of this study is to establish a characterization method determining the powder flowability in context of tableting. At first, flowability of different materials is measured using the ring shear tester, and its prediction from particle size is established. Next, the model die-filling system is presented which is a modified version of previous studies. Using this system, flowability of different materials is measured at varying die speeds. A new curve fit to assess die fill ratio vs die speed is suggested improving predictability, and a novel flowability metric, "Die Fill Index" (DFI), is derived. The DFI is appropriate to describe flowability for most of the tested materials, and sensitivity of a material with respect to tableting speed. A correlation is generated predicting DFI from particle size. Additionally, it is shown that model die filling is the preferable method to assess flowability for tableting compared to ring shear tester.

ARTICLE HISTORY

Received 24 August 2017
Revised 18 October 2017
Accepted 28 November 2017

KEYWORDS

Model die filling; die fill index; tableting; flowability prediction; direct compression

1. Introduction

Tablets are the preferred pharmaceutical dosage form and constitute about 80% of all dosage forms mainly due to their ease of manufacturing and high production rate at relatively low cost (Bauer-Brandl and Ritschel 2012). Tablets are produced on high-speed rotary tablet presses in which at first the dies are filled with the blend and consequently compacted to form tablets. On modern tablet machines, it is possible to produce up to 1.6 million tablets per hour (FETTE Compacting GmbH, FE 75 2016). The prerequisite for successful tablet production at such high rates is an adequate powder flow, which ensures that a sufficient amount of powder is filled into the die. Thus the die filling can become one of the rate-limiting factors in tableting. An optimal combination of blend properties, such as cohesion and friction, and process conditions (die diameter and turret speed) can ensure a good pharmaceutical product meeting the specifications (Gopireddy et al. 2016; Ph. Eur. 2016).

One mode of tablet manufacture is the direct compression (DC) of the active pharmaceutical ingredient with a combination of well-chosen excipients requiring fewer processing stages and eliminating effects of added moisture as found for wet granulation (Jivraj et al. 2000). However, direct compression formulations are more prone to segregation, and poor powder flowability can limit their application (Jivraj et al. 2000). In particular, poor powder flow will bear the risk of variations of tablet weight and content uniformity in addition to unsteady tablet strength, disintegration, and dissolution rates (Sun 2010). This gave rise to a thorough characterization of powder flow in the formulation development stage and generation of empirical indices such as Hausner ratio, Carr's index, angle of repose, flow through an orifice (Hausner 1972; Svarovskly 1987; Rios 2006; Zhu et al. 2007; Gentzler et al. 2015; USP), in addition to shear cell experiments (Schwedes 2005; Schulze 2007; Leturia et al. 2014) and custom-designed

instruments (Wu et al. 2003; Sinka et al. 2004; Wu and Cocks 2004; Schneider et al. 2005, 2007; Wu and Cocks 2006; Jackson et al. 2007; Bierwisch et al. 2009a; Sinka et al. 2009; Mills and Sinka 2013).

A short literature review is given in the following sections to provide recent developments in powder flowability determination in the context of pharmaceutical tableting. To facilitate easier understanding, at first different powder flowability characterization methods with a focus on shear cell measurements are presented. Afterwards different model systems that have been specifically designed to get an understanding of the die-filling process are explained and grouped into experimental and numerical approaches.

1.1. Shear cell measurements to assess powder flowability

1.1.1. History of shear cell measurements

One instrument to assess powder flowability is the well-known Jenike Shear Tester (Jenike 1964) that has been developed 50 years ago. Although measurement procedure itself is a quasi-static system, it was originally developed by Jenike (Jenike 1964) to provide design charts determining which flow pattern, mass or funnel flow, can be expected during gravity discharge from a bin or hopper under steady-state flow and finding flow and no-flow condition. Some of the major applications, reviewed by Schwedes (Schwedes 2005), are the design of silos for flow and strength, the calibration of constitutive models, the quality control and the qualitative flowability comparison. One detailed example of how to solve flow problems in bins, hoppers and feeders by good plant design is given by Marinelli and Carson (Marinelli and Carson 2002). Based on Jenike Shear Tester, several shear testers have been developed and one of them is the ring shear tester (RST) (Schwedes 2005; Schulze 2007). Besides the application in

hopper design, shear cell measurements have gained high interest in other processes, such as tableting, due to its simple operating procedure and miniature shear cell sizes, which allow to measure flow characteristics with as little as 30 ml powder (Fitzpatrick et al. 2004; Hou and Sun, 2008). In particular, for shear cell measurements, it is of great importance to use measurement parameters reflecting the stress state in the considered process (Schulze 2007). The reason being, the powder flowability, expressed in the flow function coefficient (*ffc*), defined as the ratio of principle consolidation stress (σ_1) to unconfined yield strength (σ_c), highly depends on the σ_1 . Thus, direct powder flowability comparison is solely allowed at the same σ_1 .

1.1.2. Shear cell measurements in the context of tableting

No distinct definition for powder flowability can be provided as powder flow behavior is multidimensional (Prescott and Barnum 2000). However, many efforts are made to correlate the powder flowability measured using RST to powder flow performance in tableting. For example, Zettler et al. (Zettler et al. 2016) generated different DC blends and characterized powder flowability by the angle of repose, bulk and tapped density, Hausner ratio, Carr's index, mass flowrate, Flodex (flow through an orifice) and RST and compared the results with blend performance during tableting (tablet ejection force, tablet weight variation and material sticking to punches). It was concluded that the Hausner ratio and shear cell measurements are the only methods able to provide a good correlation with respect to tableting performance (Zettler et al. 2016). An additional study (Sun 2010) measured the flowability of different Avicel PH 102 grades using RST and compared them with the tableting performance. It was proposed that the material with the poorest flow can serve as a reference material to judge the adequacy of flow properties of prototype formulations (Sun 2010).

1.1.3. Correlation of powder flowability with physicochemical material properties

In addition to the process performance prediction using powder flowability data assessed by RST, different studies exist to link powder flowability with powder physicochemical properties such as particle size, morphology, density, dispersive surface energy and particle surface silicification (Podczeczek and Mia 1996; Hou and Sun 2008; Leyva and Mullarney 2009; Capece et al. 2015, 2016). Hou and Sun (Hou and Sun 2008) showed in their study with 11 different micro-crystalline cellulose materials, that in general smaller and nonspherical particles result in poorer powder flowability. Moreover, particle density did not reveal a significant impact on flowability. Comparison of powder flowability measured by RST and Carr's index evinced the major drawback of the latter one: the lack of control of the external stress during tapping. In the Podczeczek and Mia study (Podczeczek and Mia 1996), ANOVA analysis of different pharmaceutical excipients and active pharmaceutical ingredients (API) indicated particle shape as the only significant influencing factor for *ffc*. A much larger data set, including 185 different materials grouped into active blends, active granules, APIs and excipients, was applied in the study by Leyva and Mullarney (Leyva and Mullarney 2009). They performed partial-least squares (PLS) regression analysis to compare *ffc* with particle size. The PLS analysis revealed only acceptable results for *ffc* prediction by particle size for the API and excipient groups but failed for the two other ones. In summary, different studies exist to link *ffc* with particle physico-chemical properties but a valid correlation

that can be used on a daily basis in laboratory work is still missing.

1.2. Experimental and numerical studies elucidating the die filling process

1.2.1. Experimental studies using a model die filling system

In 2003, a model die shoe-filling system was developed by Wu et al. (Wu et al. 2003) to investigate the influence of the motion of the powder delivery system on the die filling process. This system comprises a stationary die and a moving shoe filled with powder which translates over the die at a defined speed varying between 25 mm/s and 400 mm/s. When the shoe moves over the die, it gets filled mainly due to gravity. This study introduced a new powder flowability metric, namely, the critical shoe speed v_c , to describe flowability with reference to this special application (Wu et al. 2003). Below the v_c the die will be completely filled by a single pass of the shoe, while above the v_c the die will be only partially filled (Wu et al. 2003; Sinka et al. 2004; Wu et al. 2011). This model die shoe-filling system was extended to investigate the influence of different parameters such as humidity (Sinka et al. 2004), vacuum/air (Schneider et al. 2007), die shape (Wu et al. 2003), suction filling (Wu and Cocks 2006), as well as different materials (Wu et al. 2003; Sinka et al. 2004; Wu and Cocks 2006; Schneider et al. 2007) on the v_c . Some of the major findings of this system are summarized in the following.

By using high-speed camera imaging, details of the flow process as the powder is delivered into the die could be visualized and three major flow types were identified: nose, bulk and intermittent. Nose flow dominated at low shoe speeds, whereas bulk flow controlled die filling at high shoe speeds (Wu et al. 2003). The former occurs if the acceleration of the shoe forces the powder against the back of the die (Schneider et al. 2007). Pharmaceutical powders were more likely to flow intermittently, in other words in a random detachment of individual particles (Schneider et al. 2007).

The system (Wu et al. 2003) was placed into a vacuum chamber to evaluate the effect of air. First, smoother flows were generally observed in vacuum and the filling rate was faster at all shoe speeds. The reason being, for die filling in air the pressure build up caused by entrapped air in the die opposed the flow process thereby instabilities were promoted. Second, significantly higher v_c and fill densities were achieved indicating a better flowability in vacuum (Sinka et al. 2004).

One major feature in actual rotary tablet presses is the so-called 'suction filling'. It is induced by the downwards movement of the lower punch. A fill cam is used to create the die cavity at the feeding position. The Wu et al. (Wu et al. 2003) model die-filling system was also extended to study this effect where the die bottom was lowered as soon as it reached below the shoe thus simulating the suction effect. The v_c in suction filling was improved by a factor of ~ 2.5 compared to gravity filling only (Wu et al. 2003; Wu and Cocks 2006; Wu et al. 2011).

1.2.2. Numerical studies of model die filling system

In parallel to the experimental investigation of the model die-filling system, three years after its invention, numerical simulations using the *discrete element method* were reported (Wu and Cocks 2006). The perspective of these simulation studies included the identification of optimum process conditions, optimization of powder formulation in terms of flowability and segregation and an increased understanding of the process itself (Wu and Cocks 2004, 2006; Wu 2008; Bierwisch et al. 2009a, 2009b;

Guo et al. 2009, 2010, 2011; Nwose et al. 2012; Wu and Guo 2012). Numerical results showed a good accordance with the experimental findings. For example coupling of the *discrete element method* with *computational fluid dynamics* allowed a more detailed understanding of air effects during die filling (Guo et al. 2009; Nwose et al. 2012; Wu and Guo 2012).

In contrast to the experimental system consisting of a moving shoe and stationary die, Wu et al. numerically studied 'active die filling', the flow behavior of powders from a stationary shoe into a moving die (Wu 2008). The influence of particle shape, size and size distribution, the number of particles used in the simulation, the initial height of the powder bed in the shoe, and the die speed on the average mass flow rate and the critical die speed were explored. Unfortunately, no comparison in terms of v_c , either shoe or die speed, was given impeding a quantitative comparison between active and passive die filling. Furukawa et al. (Furukawa et al. 2016) studied a similar system of active die filling to evaluate the segregation behavior of binary particles by using response surface methodology.

1.2.3. Die filling process in rotary tablet presses

Although the model die shoe filling system by Wu et al. (Wu et al. 2003) captures some of the aspects relevant for tableting, including the effect of air back pressure and suction filling, room for improvement still exists with respect to the geometrical/process differences compared to actual rotary tablet presses. First, in reality, the shoe that can be either a filling hopper, force feeder, or gravity feeder, is stationary whereas the die moves underneath it at a defined speed. Second, as the name suggests, in rotary tablet presses the dies move in rotational but not translational motion. These discrepancies hamper the direct transfer of experimental model die shoe filling data to infer the powder fill ratio to rotary tablet presses (Schneider et al. 2007). The rotary tablet presses deliver the powder to the dies either through force feeders or gravity feeders. Typically, a force feeder consists of one or more paddle wheels. Gravity feeders are an alternative to force feeders that are chosen for powder formulations prone to over-lubrication (reducing tablet hardness) and particle attrition. Both are critical side effects in force feeding as paddles exert high shear forces on particles (Ketterhagen 2015). Good powder flowability is prerequisite for gravity feeding. This requires different powder flowability measurements compared to force feeding to characterize the blend prior to tableting (Yaginuma et al. 2007). The numerical study of Gopireddy et al. (Gopireddy et al. 2016) provided a comprehensive insight into the impact of process and material parameters on the performance during the die filling process by gravity feeding.

1.3. Objective of this study

The objective of the current work is to investigate the 'active die filling' process experimentally. The aim of this study is to understand the die-filling process during gravity feeding in the context of the tableting process. Thus, the novelty in comparison to the previous model die filling system is a moving die and a stationary shoe. Therefore, it is one step closer to the actual tableting machine, although some differences still exist, which comprise: (1) the system contains a translational instead of rotational movement, and (2) the effect of suction filling is not included. The latter one (2) implies that air back pressure effects will play a major role.

In this study, first of all the flowability of different materials is analyzed using the RST. The ffc of different pharmaceutical

materials, including DC excipients, placebo and active blends are measured and a correlation to predict the ffc by particle size information is generated. This correlation constitutes a quick tool to assess a static powder flowability index. In the next step, the modified model die-filling system containing a moving die and a stationary shoe is presented. The effect of die speed on the die fill ratio for various pharmaceutical materials that are used in DC formulations, such as excipients and placebo blends, are investigated. First, the v_c of the materials are evaluated and compared followed by a detailed analysis of the curve shapes of the die fill ratio vs die speeds. This curve shape analysis gives rise to introduce an additional metric to the v_c that is able to define a material's sensitivity to die speeds. Eventually a correlation is established to predict this additional flowability metric based on the easily accessible powder physical properties.

2. Materials and methods

This section presents the different materials considered and the physical properties that are measured in this study. The details of the model die-filling experiment is also given along with the analysis procedure of the measured data.

All measurements were performed at constant conditions (25 °C and 40% relative humidity) to make sure that the influence of humidity and moisture is same for all materials. The raw materials have not been pre-conditioned prior to measurement as they are stored under same conditions (25 °C and 40% relative humidity).

All measurements were performed in triplicate to obtain the mean and relative standard deviation (RSD). Results were analyzed and correlations were generated by partial least squares regression analysis with the statistical software tools JMP 13.0.0 (SAS Institute Inc., Cary, NC) and SigmaPlot 12.5 (Systat Software GmbH, Erkrath, Germany).

2.1. Materials

Different DC excipients, placebo and active blends were selected (Table 1) and their physical properties as well as their flowability characteristics were measured. The raw materials, listed in Table 1, can be classified in two different ways (1) based on their functionality as diluents, disintegrants, multipurpose and compound excipients and (2) based on their chemical composition as mannitol, celluloses, starches and their corresponding modifications. The placebo blends are bi-component mixtures with different amounts of SuperTab 24AN (diluent, agglomerated anhydrous lactose, DFE Pharma) and L-HPC NBD-22 (disintegrant, low-substituted hydroxypropylcellulose, Shin-Etsu Chemical Co., Ltd.). The ratio between the diluent and the disintegrant is their theoretical proportion in a typical DC formulation with increasing API dose strengths (5–40% (w/w) and constant (10% (w/w)) disintegrant contents. For example, assuming an API content of 5%, the remaining 95% of the blend are distributed to a constant disintegrant content of 10% and to a diluent content of 90%. This results in a 10.6% (w/w) disintegrant and 89.4% (w/w) diluent content in the bi-component mixture. The active blends belong to different lots of a trademarked DC formulation (Table 1).

2.2. Particle size and size distribution

The particle size and size distribution (PSD) was measured using a Sympatec Helos/Rodos laser diffraction system (Sympatec GmbH, Clausthal-Zellerfeld, Germany) with dry dispersion capability.

3.1.1 Evaluation of gravity filling by an experimental model die filling system

Table 1. Materials and their corresponding properties (mean values out of 3 measurements are given), used to generate Equation (4) or (9) (X), and to prove Equation (4) or (9) (O).

Product name	Vendor	x_{10} μm	x_{50} μm	x_{90} μm	SPAN/-	ρ_p/g ml	TAUC/ Pa	$ff_{measured}/-$	$ff_{predicted}$ (Equation (4))/-	To generate (X) or prove (O) Equation (4)	Fill ratio at 50 mm/s/%	V_c Die(Wu) (by Equation (7))/ mm/s	V_c Die (current) (by Equation (8))/ mm/s	DFI/mm/s ⁻¹	Used to create correlation (X) and used to test correlation (O) (Equation (9))
Ac-Di-Sol	FMC Biopolymer	17.0	37.2	86.8	1.9	0.48	207.3	5.3	6.3	X	14.1	#	#	#	
Carmellose NS-300	Fa. Nichrin Chemical Industries	20.9	56.9	139.9	2.1	0.35	137.9	7.3	8.3	X	16.2	#	#	#	
Ceolus KG-100	Asahi-Kasei Chemicals Corporation	16.2	52.2	125.0	2.1	0.15	297.8	4.0	6.1	X	1.0	#	#	#	
EGG-505	Gotoku Chemical Co., Ltd.	17.3	48.2	106.8	1.9	0.48	134.5	8.0	6.3	O	20.6	#	#	#	X
Lactopress monohydrate	DPE Pharma	54.9	157.8	309.9	1.6	0.58	74.6	14.2	22.4	O	94.3	46.2	46.2	0.0187	X
L-HPC (LH-21)	Shin-Etsu Chemical Co., Ltd.	12.2	50.2	137.0	2.5	0.39	207.4	5.4	4.8	X	12.8	#	#	#	
L-HPC (LH-22)	Shin-Etsu Chemical Co., Ltd.	11.7	42.4	145.1	3.1	0.39	201.6	6.1	5.0	X	11.3	#	#	#	
Ludipress	BASF	59.4	202.1	448.4	1.9	0.49	63.8	19.5	26.4	X	24.6	#	#	#	X
Lycatab C	Roquette Pharma	25.1	82.6	183.2	1.9	0.53	146.0	7.3	9.8	X	34.2	#	#	0.0114	X
Parreck M100	Merck KGaA	25.1	73.3	145.1	1.6	0.38	51.8	19.8	9.1	X	57.0	27.8	19.1	0.0221	X
Parreck M200	Merck KGaA	71.2	181.2	400.2	1.8	0.51	28.4	34.3	31.5	X	99.3	48.4	49.5	0.0153	O
Pearitol 100 SD	Roquette Pharma	66.6	105.7	164.7	0.9	0.48	34.1	27.8	22.1	X	68.2	33.9	25.8	0.0187	X
Prosolv SMCC 90	JRS Pharma	32.3	119.9	240.7	1.7	0.35	120.7	9.0	12.6	X	12.4	#	#	#	
Prosolv SMCC HD 90	JRS Pharma	32.0	118.3	228.2	1.7	0.46	106.5	11.0	12.2	O	14.5	#	#	#	
Spray-dried granules	Coloron	20.0	89.4	235.3	2.4	0.33	148.2	7.9	8.3	X	11.9	#	#	#	
Starch 1500	Coloron	11.8	41.4	134.6	3.0	0.59	188.2	5.7	4.9	O	11.0	#	#	#	
SuperTab 24AN	DPE Pharma	31.0	102.2	229.0	1.9	0.49	63.2	17.2	12.5	X	93.9	44.9	46.2	0.0216	X
Placebo blend 1 (89.4% SuperTab 24AN + 10.6% L-HPC NBD-22)		25.5	103.5	238.1	2.1	0.46	70.0	13.6	10.3	X	49.7	25.9	17.1	0.0245	X
Placebo blend 2 (88.8% SuperTab 24AN + 11.2% L-HPC NBD-22)		25.4	103.2	238.4	2.1	0.45	70.3	13.5	10.2	X	57.5	29.5	20.6	0.0218	O
Placebo blend 3 (86.5% SuperTab 24AN + 13.5% L-HPC NBD-22)		24.4	100.4	239.0	2.1	0.45	81.0	11.8	9.9	X	-	-	-	-	-
Placebo blend 4 (83.1% SuperTab 24AN + 16.9% L-HPC NBD-22)		23.1	94.5	230.9	2.2	0.45	87.7	10.9	9.4	X	-	-	-	-	-
VIVAPUR MCC Spheres 200	JRS Pharma	174.0	236.3	304.7	2.23	0.89	60.7	22.3	-	-	91.0	27.8	19.1	0.0221	X
DC Formulation Lot 1		8.9	101.7	867.5	8.4			5.5	5.6	X	-	-	-	-	-
DC Formulation Lot 2		8.4	102.5	868.4	8.4			5.0	5.2	X	-	-	-	-	-
DC Formulation Lot 3		9.2	109.7	868.4	7.8			5.5	5.6	X	-	-	-	-	-
DC Formulation Lot 4		9.1	99.3	867.6	8.6			5.8	5.8	X	-	-	-	-	-
DC Formulation Lot 5		7.8	111.2	868.8	7.7			4.9	4.6	X	-	-	-	-	-
DC Formulation Lot 6		9.5	106.0	867.9	8.1			6.0	5.9	X	-	-	-	-	-
DC Formulation Lot 7		9.2	103.9	867.6	8.3			6.1	5.7	O	-	-	-	-	-
DC Formulation Lot 8		7.4	107.1	868.7	8.0			4.8	4.4	O	-	-	-	-	-
Mean		28.5	99.4	379.0	4.3	0.5	121.2	10.7	9.9		42.1	40.4	35.5	0.0196	
RSD/%		112.7	46.7	80.2	101.7	29.4	57.7	69.6	69.5		81.9	42.2	56.8	20.8	

(DC: Direct compression). Materials that were tested for the model die filling system but revealed a fill ratio <49.7% at 50 mm/s were not further evaluated (marked with #). The maximum value is given in bold letters, the minimum value in italic letters.

A sample of about 2.5 g was fed into the vibrational feeding system using a spoon. The optimum dispersion pressure for each sample is obtained by varying between 0.5 to 3 bar to break up any loose agglomerates, but not destroying individual particles. The used lens measures particles in the size range of 4.5–875 μm . The cumulative PSD and common PSD statistics were calculated using Sympatec Windox 5 software (Sympatec GmbH, Clausthal-Zellerfeld, Germany). Out of all, of particular interest are the x_{10} , x_{50} , and x_{90} defining the particle sizes that are represented by 10% (w/w), 50% (w/w), and 90% (w/w), respectively, of the cumulative distribution. These particle size parameters define the SPAN value (Equation (1)), which is a measure for the width of the PSD.

$$\text{SPAN} = \frac{x_{90} - x_{10}}{x_{50}} \quad (1)$$

2.3. Bulk density

The bulk density was determined according to Ph. Eur. 8.5, '2.9.34 Bulk density and tapped density of powders' (Ph. Eur. 2016). A constant mass of 100 g material was poured into a vibrating funnel to fill a graduated cylinder of 250 ml volume. The powder volume was read and the bulk density (ρ_b) calculated via the material mass (m) and the loosely filled powder bed volume in the cylinder (V).

2.4. Shear cell analysis

Although shear cell measurements are static, it can be used also for more dynamic processes if, and this is of major importance, the stresses are cleverly chosen. For example, Zettler et al. (2016) tested powder flowability by using shear cell experiments at a preconsolidation stress of 2 kPa that was thought to be in accordance with stresses experienced by the powder during routine manufacturing. The following model calculation is provided as a rationale to support the choice of preconsolidation stress: Neglecting the effects of wall friction, the pressure at the bottom of a bed of powder with bulk density of 0.5 g/cm³ (confer Table 1) and a bed depth of 0.4 m is approximately 2 kPa (Zettler et al. 2016). Thereby the ffc , although it has no direct physical meaning with respect to tableting, can be used for tableting application if measurement is performed at conditions of stresses observed in the tableting machine, that is, during die filling process.

The powder flow behavior of each sample was determined using a Schulze ring shear tester (Model: RST-XS.s, Dietmar Schulze, Wolfenbuettel, Germany). The powder sample was carefully filled into the medium-sized annular cell (volume of 31.37 cm³) and the excess powder was scraped with care to level it with the top of the annulus making sure that an unconsolidated powder bed was established. After determining the filled cell mass, the cell was put on the tester and the lid was placed on top of the cell. The ends of the cell lid were connected to the shear force tie rods (tensile and compression), and the normal loading rod was in hanging position. The powder was first pre-sheared under a normal load of 2 kPa until a critically consolidated state was reached. Each pre-shear step was followed with a shear test under normal stresses of 0.3 kPa, 0.9 kPa and 1.6 kPa, respectively. A yield locus plot was generated by the RST-Xs software (RST-Control 95XS, Dietmar Schulze, Wolfenbuettel, Germany) providing the principle consolidation stress (σ_1) and the unconfined yield strength (σ_c), the ratio of which gives the flow function coefficient (ffc), in other words

flowability, as follows:

$$ffc = \frac{\sigma_1}{\sigma_c} \quad (2)$$

According to Jenike (Jenike 1964) the flowability of the materials can be categorized by their ffc values as following:

- $ffc < 1$ not flowing
- $1 < ffc < 2$ very cohesive
- $2 < ffc < 4$ cohesive
- $4 < ffc < 10$ good flowing
- $10 < ffc$ free flowing

Linear regression of the yield points in the shear stress (τ)-normal stress (σ) plot, i.e. the Mohr diagram gives the linear yield locus. The intercept of the yield locus on the τ -axis is defined as cohesion (TAUC) (Schulze 2007), and it is given for the materials considered in die filling experiment in Table 1. The TAUC can be interpreted as the minimum shear stress required to deform a powder when no normal stress is applied, representing the cohesive forces between the particles.

2.5. Model die-filling system

The custom-designed model die-filling system, which is an extended version of the one proposed by Wu et al. (Wu et al. 2003) is shown in Figure 1. This system consists of a moving die and a stationary shoe to hold the powder above the die. These parts are made of acrylic glass to visualize the powder flow. The shoe consists of a rectangular bottom part and an inclined top part which are joined together. The bottom part has dimensions of 27 mm, 30 mm and 20 mm in length, width and height, respectively. The top part is 45° inclined in the right side, whereas the left side is in line with the bottom part (Figure 1(b,c)). The total shoe size is 100 mm \times 30 mm \times 100 mm. The acrylic glass die is a cylinder with dimensions of 9 mm diameter and 15 mm height providing a volume of $\sim 954 \text{ mm}^3$. The die moves along the guided ramp at an adjustable speed of 50 mm/s to 500 mm/s (Figure 1(a)). The die is constructed in such a way that it can be removed after it passes under the shoe so that the mass of the powder collected in the die can be measured. Using this system, the die-filling behavior of different materials was measured according to a consistent procedure as outlined in the following.

At first, the shoe was filled with the powder up to the top of the inclined part as shown in Figure 1(b,c). Next, the die filling speed was set (a value between 50 mm/s to 500 mm/s was chosen), and upon start the die would move from left to right as indicated in Figure 1(b,c). The powder mass collected in the die was measured by removing the die and it was put back in its position. Following this, the die was re-set to its original position by moving the die in its guided ramp in the backward direction (Figure 1(a)). To minimize the effect of die movement on the powder in the shoe that is in contact with the die, it was moved at lowest possible speed of 50 mm/s. For each set die speed, the above procedure was repeated at least three times (triplicate measurement) before next die speed was chosen. The increasing order of die speeds was considered in the die-filling measurement, that is, at first the measurement was performed with 50 mm/s followed by 100 mm/s, 150 mm/s, 200 mm/s, 300 mm/s, 400 mm/s and 500 mm/s. During the measurement, the amount of powder in the shoe was kept constant by steadily refilling. In addition, all surfaces, in particular the acrylic glass die and shoe, were electrostatically neutralized between every measurement with an anti-static gun (Zerostat 3, Milty Pro, United Kingdom) to eliminate any charge influences. The anti-static gun released a stream of positive ions followed by negative ions.

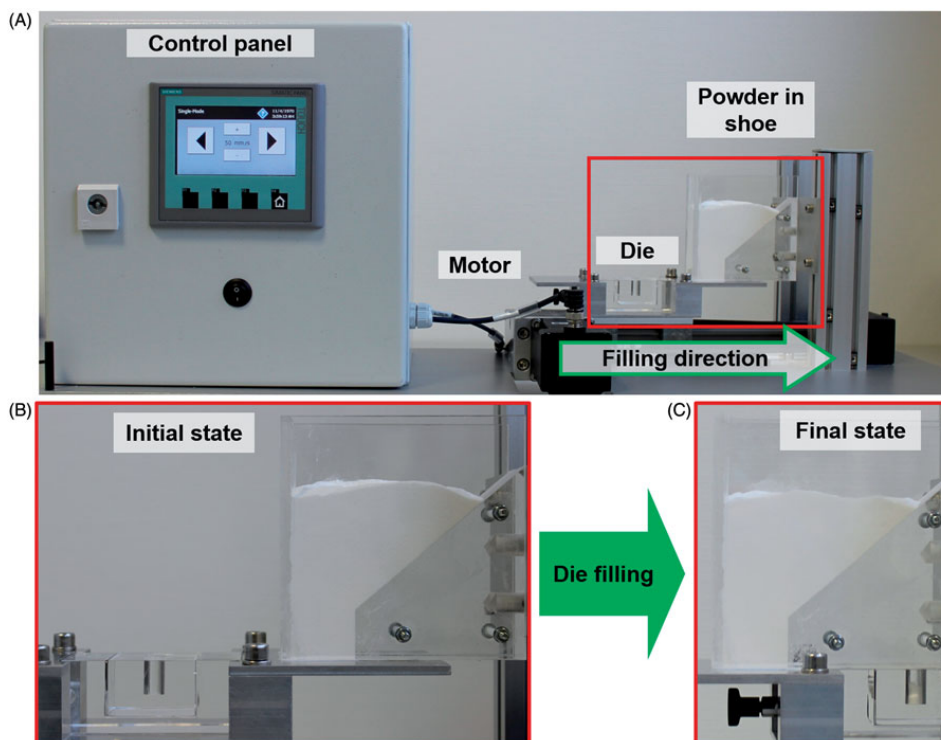


Figure 1. The new model die-filling setup including the complete setup (A) and the shoe and die before (B) and after (C) die filling.

The die fill ratio (δ) of each material was calculated, which is defined as the ratio of the mass collected in the die (m_{die}) and the maximum possible mass that can be filled into the die defined by the powder's bulk density (confer Section 2.3), according to Equation (3).

$$\delta = \frac{m_{die}}{\rho_b \times V_{die}} \quad (3)$$

The complete system was cleaned and completely dried between different materials.

As the new system was not operated under vacuum nor suction filling was considered, the effect of entrapped air in the die as the die was being filled with the powder will have significant influence on the die filling behavior.

3. Results and discussion

The flowability of the materials is assessed using the ring shear tester and the specifically designed and adapted model die filling system. A correlation between ring shear cell measurements and easy accessible physical powder properties is described. The novel model die filling system is used to evaluate (1) the die-filling performance of different materials, and (2) the influence of the die speed on the die fill ratio for the selected materials. A flowability metric in addition to the v_c is derived which can be utilized in assessing the performance of powders in tableting. Also, an attempt is made to predict this newly defined index from the powder physical properties. Eventually, the results obtained using the ring shear tester and the model die filling system are compared.

3.1. Correlation between powder flowability and physical properties

The ratio between principle consolidation stress and unconfined yield stress, in other words the ffc , of materials is a function of different properties such as particle shape (Podczec and Mia 1996; Hou and Sun 2008), size (Podczec and Mia 1996; Hou and Sun 2008; Leyva and Mullarney 2009; Capece et al. 2015, 2016), density (Hou and Sun 2008; Capece et al. 2015, 2016) and chemical nature of the material (Hou and Sun 2008). The ffc is the most prevalent measure, compared to the TAUC (see Section 2.4) and the PHIE (measure of the internal friction at steady-state flow), that can be obtained from shear cell measurements. On a daily basis, it would be of great interest to be able to easily classify a powder, a blend or a formulation into the different flowability categories without actually performing the time- and material-consuming shear cell experiment but through prediction based on other properties that are easier to get. One approach, as proposed by Capece et al. 2015 and 2016, could be to generate a material databank including particle size, particle density, dispersive surface energy of the raw materials and to predict the ffc by an empirical equation that can be applied for raw materials as well as mixtures (Capece et al. 2015, 2016). However, one drawback of the proposed flowability model prediction is the availability of inverse gas chromatography instruments in standard development laboratories. A more convenient way is to exploit the quick, operator-independent, reproducible, and easy particle size measurement via laser diffraction or analytical sieving which is typically available in every formulation

research laboratory. Following a previous study (Leyva and Mullarney 2009), a similar attempt is made to predict the flowability from particle properties. In that, Leyva and Mullarney classified their materials into different groups as excipients, API, active blends, active granules, and for each group one corresponding ffc correlation was proposed. The correlations were developed based on a four-parameter model including the x_{10} , x_{50} , x_{90} and volume mean diameter suggesting a logarithmic relationship with ffc .

In this work, the PSD and ffc of 28 different materials (Table 1), consisting of excipients, placebo and active blends, are measured. The data of 22 materials is used to generate a correlation using partial-least squares (PLS) regression analysis to predict the flowability and the remaining six materials are used for validation. In contrast to previous work (Leyva and Mullarney 2009), the approach in this study generates a single PLS model, which includes all the materials without any grouping. Thus a much wider applicable data range is provided (Table 1) and uni- and multi-modal particle size distributions are included as well. An iterative process is pursued to develop the easiest correlation consisting of least number of variables but at the same time showing best prediction. First of all, all possible particle size variables (x_{10} , x_{50} , x_{90} , and $SPAN$) are included in the PLS model and different linear combinations of them are tested. Best results are obtained for a logarithmic relationship which is in accordance to particle size data of previous studies (Podczeczek and Mia 1996; Leyva and Mullarney 2009) and other powder measurements such as the logarithmic connection between compact tensile strength and solid fraction (Hiestand 2002). The following equation is obtained allowing an 81.6% explanation of the response variation:

$$\ln(ffc) = 0.44 \times \ln\left(\frac{x_{10}}{\mu\text{m}}\right) + 0.53 \times \ln\left(\frac{x_{50}}{\mu\text{m}}\right) + 0.02 \times \ln\left(\frac{x_{90}}{\mu\text{m}}\right) - 0.22 \times \ln(SPAN) - 1.39. \quad (4)$$

Other material properties such as the specific surface area as well as the density (true and bulk) may influence particle flowability, however, including these additional properties in Equation (4) has not shown any improvement in terms of ffc predictability. Applying a non-iterative partial-least squares fitting algorithm (Garthwaite 1994; Wold et al. 2001) suggests the lowest root mean predicted residual sum of squares (PRESS) value including two factors only. Those two most important variables (indicated by their variable importance value (VIP)) are $\ln(x_{10})$ and $\ln(SPAN)$ with VIPs of 1.4 and 1.0, respectively. In the next step, a second PLS model is developed including only those two important variables giving Equation (5):

$$\ln(ffc) = a \times \ln\left(\frac{x_{10}}{\mu\text{m}}\right) + b \times \ln(SPAN) + \text{constant}. \quad (5)$$

The validity of Equation (5) to predict the ffc by x_{10} and $SPAN$ was tested as follows. The normality distribution of the residuals (the delta between measured $\ln(ffc)$ to predicted $\ln(ffc)$ (by Equation (5)) values) by Anderson-Darling normality test (Razali and Wah 2012) gives a p -value of 0.44 ($> \alpha = 0.05$) showing that the residuals are normally distributed. Furthermore, no trend in residuals over ffc can be identified. Next Equation (5) is mathematically transformed into Equation (6) to simplify the logarithmic version of Equation (5) as given below:

$$ffc = \left(\frac{x_{10}}{\mu\text{m}}\right)^a \times SPAN^b \times c. \quad (6)$$

Here the constants a , b and c , are 1.146, 0.422 and 0.185, respectively. The measured and predicted data points of materials to generate and to test the correlation according to Equation (6)

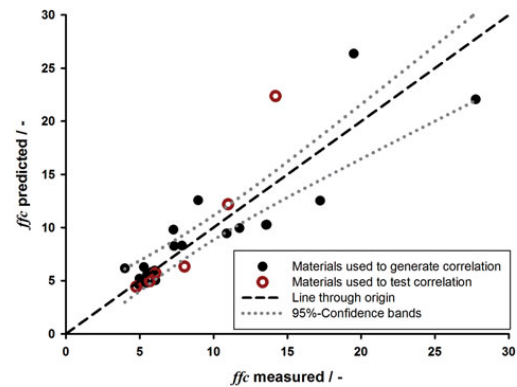


Figure 2. The ffc measured versus ffc predicted for 28 materials. The materials used in generating the correlation (Equation (6)) are indicated in black, filled circles, whereas the materials used for correlation validation are shown in red, unfilled circles.

are plotted in Figure 2. ANOVA analysis of the measured and predicted groups shows that they are statistically not significantly different (p -value = 0.97 at $\alpha = 0.05$). In addition, most of the data are within the 95% confidence band. Importantly, the prediction rate of Equation (6) is highest at low ffc values, in particular in the range of $ffc = 4$ –10 (Jenike 1964, confer Section 2.4)) in which materials are prone to show flowability issues in a given process. Another indicator for goodness of fit is the high correlation coefficient (R^2) between measured and predicted values of 0.75. In addition the mean residual value is 1.9 which is 17.4% relative to the mean measured value. Eventually, 85.7% of all materials are correctly predicted, 7.1% under- and 7.1% over-predicted as per the flowability classification of Jenike (Jenike 1964) (confer Section 2.4). The under-prediction is usually not considered as a critical issue in a given process.

As shown by Equation (6), a decrease in particle size (x_{10}) reduces the flowability (ffc) which is consistent with literature data (Hou and Sun 2008; Leyva and Mullarney 2009; Jager and Bramante 2015). Smaller particles have a higher total contact area which in turn increases the overall particle-particle interactions including van der Waal's force and H-bonding. The stress required to induce particle-particle relative movement (shear failure) is thereby higher. Thus the negative effect of particle size reduction, in particular of smallest size fraction, on flowability is mainly caused by the increased specific surface area (Hou and Sun 2008).

The major benefit of Equation (6) lies in the wide range of particle sizes (x_{10} : 7.4 – 66.6 μm , x_{50} : 37.2 – 202.1 μm , and x_{90} : 88.8 – 868.8 μm) and ffc values (4.0 to 27.8) tested (Table 1) which implies the usability of flowability prediction for a huge set of materials. Overall, the generated correlation is tested and shows a good prediction for all powders in the 'good' and 'free' flowing range (Jenike 1964 Section 2.4, Table 1), however, it is highly suggested to conduct the ring shear tester experiments in case that the predicted flowability of a material falls into the 'cohesive' category ($ffc < 4$). To be able to correctly predict the flowability of 'cohesive' materials as well, further investigation is necessary to include more materials that fall into the 'cohesive' class. Additionally, it may be required to run RST measurements for materials that fall at the boundary/limits of classification. The accuracy of this PLS model prediction can be increased by adding additional measurements. The correlation is generated and validated at 2 kPa pre-shear stress measurement (confer Section 2.4) but different particle size relationships or individual particle size

influence weighting may change at different consolidation stresses. Therefore, adaption of Equation (6) to the stresses found in a given process is required.

In comparison to the approach by Capece et al. 2015 and 2016, Equation (6) is able to predict the full range of ffc values, whereas their proposed approach via the granular Bond number (Capece et al. 2015, 2016) should only be applied to materials with a granular Bond number >1 or in other words for cohesive materials for which powder flowability is mostly affected by the van der Waals force. However, if additional material characteristics, such as dispersive surface energy, are available, the combined approach by Capece et al. 2015 and 2016 might provide more accurate ffc prediction compared to Equation (6) as it takes into account the relationship between the cohesive van der Waals force and the particle weight.

A short application outline of Equation (6) could be for example: In manufacturing, the consistency of flowability between batch to batch can be easily monitored and controlled by two steps: (1) at first establish a standard PLS model for flowability prediction (calculate a , b and c of Equation (6)) based on available batches that work without flowability issues, and (2) then simply predict ffc using Equation (6) for the next batches, and take corrective action if it does not fall into the established working range. Eventually, extensive experience of production operators could be applied and process-dependent flowability limits can be specified (Jenike 1964). This correlation (Equation (6)) of ffc with particle size is a versatile tool and could, if necessary, be improved by including particle shape effects (Johanson 2009; Yu and Muteki 2011). However, it is partly possible to transfer the ffc data to assess die filling performance of a given material (refer Section 3.4 Comparison of die filling metrics with classical ring shear results).

Though the ffc measurement offers a good estimate of powder flowability, its application is validated for flow in hoppers or bins. It is completely understandable that the direct transfer of the ffc to the die filling in tableting may not be possible due to the differences in stress conditions that the powder is subjected to in RST in comparison to die filling. Selecting the pre-consolidation stresses in RST similar to the die filling may enable such data transfer, however such an attempt has not yet been made. The flowability measurements such as angle of repose, Carr's index, etc. also fail to provide direct understanding of the die filling. This gives an impetus to measure the die filling performance using custom-designed devices.

3.2. The flowability assessment using the new model die-filling system

The custom-designed system, which is an extension of the Wu et al. model die-filling system (Wu et al. 2003) (Figure 1) is used to measure the powder flow in the context of die filling (refer to Section 2.5) relevant for gravity feeders. The main difference of this system in comparison to the previous is that powder is delivered from a stationary feeding hopper or shoe into the moving die. This would lead to the following alterations. For example, in the new system, only very little momentum is transferred to the powder in the shoe that is lying just above the die surface due to shear. However, in the Wu et al. system with a moving shoe, the whole powder bed in the shoe gains momentum with some velocity gradient from top to bottom of the shoe. This influences (1) the particle rearrangement within the shoe and (2) the discharge of particles into the die. In addition, the new system has smaller dimensions of the die and the shoe. The former implies that a cylindrical die with dimensions similar as found in tablet presses (diameter of 9 mm and height of 15 mm) was used in contrast to

the cuboid die shapes Wu et al. considered with width \times length dimensions of 5 mm \times 25 mm to 23 mm \times 25 mm, which are relevant for steel or ceramic industry. Furthermore, the shoe of the new system has a smaller cross-sectional area (58.5% less compared to earlier work) that is open to die inlet, and the ratio of shoe opening area to die is 13 and 20 in the new and old system, respectively. The actual filling time at the same speed, calculated by comparing the shoe lengths (new system: 27 mm, previous system: 65 mm) is more than half lower in the new system. The design considerations should allow the results transfer to gravity feeders. All measurements with the new system are performed in air and suction filling is not considered. Thereby the effect of air back pressure as powder is falling into the die will significantly affect the die filling process (Sinka et al. 2004).

In a first set of experiments the die fill ratios (δ), obtained through the maximal possible fill level by the materials' bulk densities, confer Section 2.3) at lowest possible die speed of 50 mm/s for in total 21 materials (Table 1) were tested. In connection with the ffc measurement and prediction given in Section 3.1 (Equation (6)), it can be concluded that only materials with a good powder flowability, namely $ffc > 10$ show sufficient die fill ratios ($> 49.7\%$) at lowest possible speed (50 mm/s). In case that less powder flowability (e.g. as estimated through Equation (6)) is given, the material would not show appropriate die filling in gravity feeding. Since the dimensions of the new system are more close to the actual dimensions of a tablet press compared to the Wu et al. system (Wu et al. 2003), an early decision between 'flow' ($ffc > 10$) and 'no flow' ($ffc \leq 10$) for gravity feeding can be made. As a consequence for the latter case, the die filling for the material should be performed via a force-feeding mechanism or the formulation requires an optimization otherwise it would not be possible to obtain filled dies. In case that a sufficient powder, flowability is provided ($ffc > 10$) the model die filling system can be utilized to further assess the die speed for filled dies and to investigate the influence of tableting speed on tablet mass, as discussed in the following.

The influence of die speed on the die fill ratios for the nine different materials (seven diluents and two placebo blends (Table 1), $ffc > 10$), are shown in Figure 3. For those materials, it is clearly seen that increasing the die speed results in a decreased die fill ratio. This observation is similar to previous work with the moving shoe system (Wu et al. 2003; Sinka et al. 2004; Wu and Cocks 2006; Jackson et al. 2007; Schneider et al. 2007; Mills and Sinka 2013) where the die fill ratio decreased with increasing shoe speed. The die fill ratio shows a sharp decrease between 50 mm/s

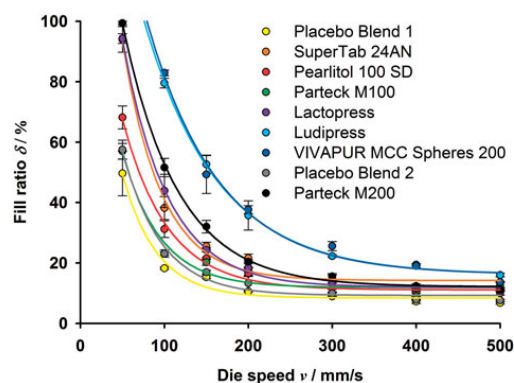


Figure 3. The effect of die speed (v) on the die fill ratio (δ) for different pharmaceutical powders. Lines are generated by applying Equation (8).

to 200 mm/s die speeds, and it reaches a plateau with further increase in die speed assuming an exponential decay profile. The die speed at which this plateau is reached and the value of this constant die fill ratio towards higher speeds is different for different materials (Table 1). This plateau or in other words minimum filling level at high die speeds is also reported for the Wu et al. model die filling system ((Sinka et al. 2009), Figure 3 therein). The minimum die fill ratio is mainly dictated by the particles located at the shear layer between the die table and shoe opening. They form a thin layer on the die holder and fall into the die due to motion and sudden stopping of the moving die. Out of nine materials shown here, only three materials reveal a 100% fill ratio at the lowest possible die speed of 50 mm/s. All other materials cannot reach complete filling even at such a low die speed (see Figure 3), for example, placebo blend 1 can only be filled up to 50% at the lowest die speed. This low die fill ratio or in other words incomplete filling at low die speed for many materials in comparison to the earlier works (Wu et al. 2003; Sinka et al. 2004; Wu and Cocks 2006; Jackson et al. 2007; Schneider et al. 2007; Mills and Sinka 2013) using the moving shoe system can be attributed to the differences in geometrical setups, as discussed. In addition, assuming that the die dimensions are same as the Wu et al. model die filling system (Wu et al. 2003), the reduced cross-sectional area of the new shoe alone would result in a mass flow rate reduction by 33% (calculated by Beverloo equation (Beverloo et al. 1961)). For example, Avicel PH 102, shows a 10% fill ratio at 50 mm/s die speed in the new system (data not shown), whereas it was found to have about 20% fill ratio in the earlier work (Sinka et al. 2004). Furthermore, and as already mentioned, the pressure build up by the entrapped air as powder is entering the die opposes the mass flow rate resulting in a decreased fill ratio (Schneider et al. 2007).

Wu et al. (Wu et al. 2003) proposed that only two tests need to be conducted to determine the v_c : one test at low shoe speed where the die is completely filled; the other at high shoe speed where the die is partially filled (Wu et al. 2003). Their study suggested that from those two tests, the fill ratio at any shoe speed can be obtained by the ratio of v_c to shoe speed, as given in Equation (7) (Wu et al. 2003), Equation (8) therein).

$$\delta = \left(\frac{v_c}{v} \right)^{6/5}. \quad (7)$$

However, this approach cannot be applied to the new system (in this case not critical shoe speed (v_c) but critical die speed ($v_{c, \text{Die}}$) as for most of the materials no complete die filling at the lowest die speed (50 mm/s) is obtained. In addition, it is very difficult to choose a sufficiently low die speed ensuring 100% filling for any desired materials if the powder flow behavior is unknown. As a workaround, the measured fill ratio at a given die speed is plotted versus $(1/v)^{6/5}$ and subsequently the slope is determined, which is nothing but the $(v_{c, \text{Die}})^{6/5}$ (as given by Equation (7)). The $v_{c, \text{Die}}$ for all tested materials are provided in Table 1, and also illustrated in Figure 5. In the next step, the predicted fill levels ($\delta_{\text{predicted, [Wu]}}$) by using the ratio of $v_{c, \text{Die}}$ to die speed following Equation (7) are calculated and plotted in Figure 4 exemplarily for Pearlitol 100 SD and Parateck M200 (see blue color-filled squares). Compared to the measured fill levels (see black color-filled circles), the $\delta_{\text{predicted, [Wu]}}$ are underestimating the fill levels for Pearlitol 100 SD and Parateck M200 over the complete range of die speeds. Furthermore, Equation (7) does not account for the constant fill ratio at sufficiently high die speeds (confer above and Figure 3). Another limitation of Equation (7), which is maybe trivial, is its indefinite form at $v=0$ mm/s and its

application validity for $v > v_{c, \text{Die [Wu]}}$ only. Although it was stated (Wu et al. 2011) that the exponent in Equation (7) ($=6/5$) gave a good fit to the majority of the experimental results reported (Wu et al. 2003; Sinka et al. 2004; Wu and Cocks 2004; Schneider et al. 2005; Wu and Cocks 2006; Wu et al. 2011), it was suggested that an adaption to the material considered could provide more appropriate results. Considering different values for this exponent, ranging from 1.0 to 1.5, the $\delta_{\text{predicted, [Wu]}}$ is calculated (data not shown). It is found that the lower values of the exponent give slightly better fill ratio prediction at lower die speeds, however they still yield lower fill ratios than the experiment. Given those limitations, a new curve fitting of die fill ratio (δ) with die speed (v) is suggested using an exponential decay equation (Equation (8)) as given below (see solid lines in Figure 3):

$$\delta = \delta_{\min} + (\delta_{\max} - \delta_{\min}) \times e^{-b \times v}. \quad (8)$$

Here, δ_{\min} (%) is the minimum die fill ratio (confer above), whereas δ_{\max} (%) is the maximum die fill ratio, and b ($(\text{mm/s})^{-1}$) is the decay rate constant of the curve which will be explained subsequently. The goodness of fit of Equation (8) is shown exemplarily for Pearlitol 100SD and Parateck M200 in Figure 4 (see red color-filled deltas). The predicted fill levels practically overlap with all the measurement points over the complete range of tested die speeds.

Similar to the critical shoe speed (v_c) calculation as defined by Wu et al. (Wu et al. 2003), the "critical die speed" ($v_{c, \text{Die [current]}}$) is calculated by substituting the fill ratio δ with 100% in Equation (8). The $v_{c, \text{Die [current]}}$ is shown for the different materials in Figure 5 and Table 1. The direct proportionality between the $v_{c, \text{Die [current]}}$ and the reciprocal decay rate constant b (DFI in Figure 5), illustrated in Figure 5, exists as per definition of Equation (8). As proposed (Wu et al. 2003), the higher the $v_{c, \text{Die}}$ the better the flowability of the considered material. By comparing the $v_{c, \text{Die [current]}}$ of Parateck M200 and Lactopress only a slight difference, that is, about 6.7% (see Table 1, Figure 5) is observed, however the decay rate constants of the curves (b , DFI) differ quite significantly (Table 1, Figure 5). The fill ratio of Parateck M200 shows less sensitivity to increasing die speeds compared to Lactopress (Figure 3). In conclusion, the $v_{c, \text{Die [current]}}$ alone as given in Equation (8) (Wu et al. 2003) is not appropriate to precisely predict the response of the fill ratio at different die speeds (confer above). However, it is clear from Equation (8) that the decay rate constant b along with $v_{c, \text{Die}}$ is more adequate to capture the influence of the die speed on the die fill ratio. To augment this statement, further explanation is given in the following paragraph.

The response of the fill ratio δ for different values of the decay rate constant b (minimum, maximum, and two intermediate values according to Table 1) keeping δ_{\min} and δ_{\max} values constant (median value of data range) is shown in Figure 6. Overall, it can be clearly seen that increasing the b value results in a steeper decrease of the fill ratio. However, the sensitivity of the die fill ratio to the changes in b value shows dependence on the die speed. For example, at lower speeds, a 10% increase in die speed from 100 to 110 mm/s results in 12% and 9% decrease in fill ratio for $b=0.025$ and $b=0.011$, respectively. Under higher speeds, an increase in die speed from 200 mm/s to 220 mm/s (10% increase) shows a decrease in die fill ratio by 7% and 26% for $b=0.025$ and $b=0.011$, respectively. In summary, for higher b values the die fill ratio of a given material is very sensitive to differences at low die speeds and shows rather resistance to higher speeds. This phenomenon is inverted for lower b values. The $v_{c, \text{Die [current]}}$ values are 29 mm/s, 35 mm/s, 45 mm/s, and 62 mm/s for $b=0.025$ 1/mm/s, 0.020 1/mm/s, 0.016 1/mm/s and 0.011 1/mm/s (Figure 6), respectively. With this model calculation (considering constant

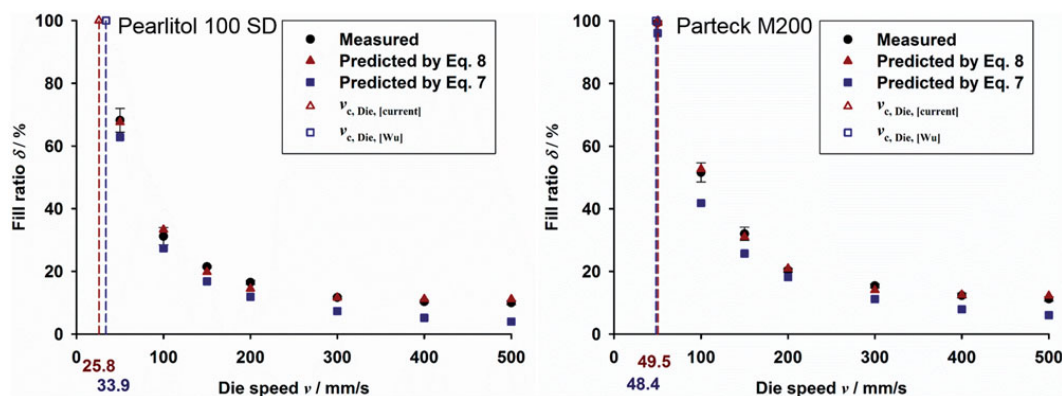


Figure 4. Comparison of fill ratio prediction by power law relationship, proposed by Wu et al. (Equation (7)), and exponential decay rate (Equation (8)). The dotted lines indicate the $v_{c, Die, [Wu]}$ (by Equation (7)) and $v_{c, Die, [current]}$ (by Equation (8)).

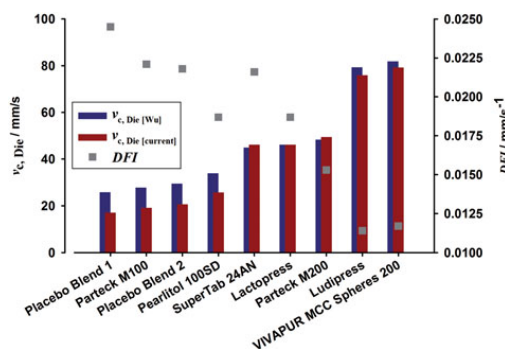


Figure 5. Calculated critical die speeds ($v_{c, Die, [Wu]}$ and $v_{c, Die, [current]}$) and comparison of DFI for different materials in the modified model die filling setup.

δ_{min} and δ_{max} values), it becomes clear that the larger the $v_{c, Die, [current]}$, the lower the b , and the higher the powder sensitivity to high die speeds. As an extension to the definition given by Wu et al. (Wu et al. 2003), powder flowability cannot only be defined by the minimal die speed to obtain complete filling but also by the powder's sensitivity to die speeds. This finding is only possible by using an exponential decay curve fit as given in Equation (8).

The b values of different materials are shown in Figure 5 and tabulated in Table 1. As shown in Figure 3, Lactopress shows a steeper fill ratio decrease at low die speeds due to the high b value ($=0.019$) in comparison to Parteck M200 which shows less decrease in fill ratio as it has a lower b value ($=0.015$, which is about 21% lower than the Lactopress b value). Hence a new flowability metric, termed as 'die fill index' (DFI), which in other words is the b value (refer to Equation (8)), is introduced as an additional metric to the critical die speed providing a starting point for powder sensitivity to tableting speed. Although it is clear that the DFI depends on the die and shoe dimensions (as it is not non-dimensional but has the units of inversed die speed), and the effect of air, with or without suction filling, plays a crucial role during die filling and these effects have not been evaluated for this new system yet, results from the new model die filling system can still serve as a first starting point for understanding the influence of tableting speed on die fill ratio. For example, a similar procedure as proposed by Schneider et al. (2007), who tried to link results

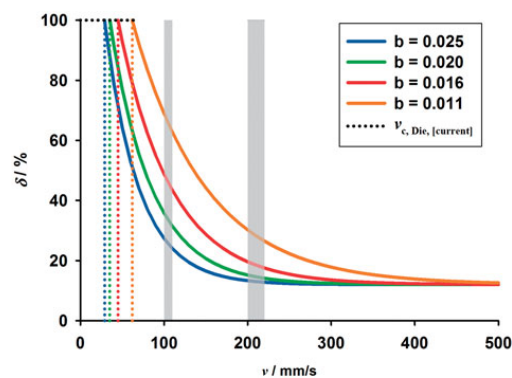


Figure 6. The influence of the DFI or decay rate constant (b) on die fill ratio (δ) at different die speeds (v) under constant δ_{min} (12%) and δ_{max} (178%) values (Equation (8)). The dotted line shows the corresponding $v_{c, Die, [current]}$ at a given DFI (b). Grey zones (100 – 110 mm/s and 200 – 220 mm/s) are marked for comparison purpose, confer text.

from the translational model die filling system (Wu et al. system (Wu et al. 2003), measurement in vacuum) with tableting speed in rotary tablet presses, can be followed. However, experimental verification with a rotational model die filling system and furthermore including the effect of suction filling is necessary.

3.3. Determination of DFI from easily accessible powder properties

From the previous section, it is clear that the DFI and $v_{c, Die, [current]}$ are important flowability measures. However, it is very costly to conduct a model die-filling experiment, which is not a standard method in pharma industries, for each and every material used in tablet formulations to obtain those values. Moreover, in contrast to the proposal of Wu et al. (Wu et al. 2003) (confer also Section 3.2), it is not possible to obtain the $v_{c, Die, [current]}$ by performing die-filling measurements at only two die speeds. On the other hand, knowing the DFI would be a great benefit as it helps to categorize the powders and final blends during the formulation development. To close this gap to a certain extent, an attempt is made to correlate easily available powder properties with the DFI.

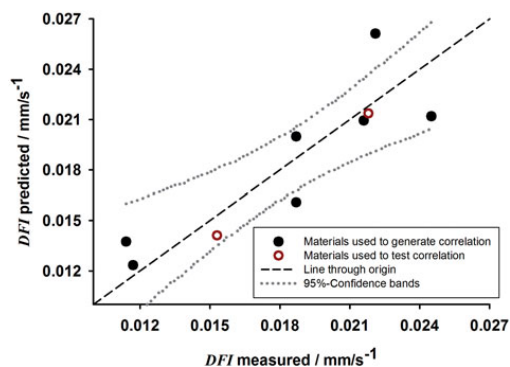


Figure 7. The comparison of measured and predicted (by Equation (9)) values of DFI . The materials used in generating the correlation (Equation (9)) are indicated in black, filled circles whereas the materials used for correlation validation are shown in red, unfilled circles.

The prerequisite for die filling by gravity is a sufficient powder flow with a $ffc > 10$, which can be easily estimated via Equation (6), Section 3.1. Following a similar procedure as described in Section 3.1, different PLS models for the prediction of DFI by intrinsic particle properties have been tested. The basic rule employed in generating such a correlation is to consider only easily accessible material properties so that any additional measurements are not necessary. The best fit for the DFI of 7 out of 9 different materials tested (Table 1) is obtained by a combination with the particle size measures, x_{10} , x_{50} , and x_{90} , (in μm), given in Equation (9):

$$DFI = \left(\frac{x_{10}}{\mu\text{m}}\right)^{-0.147} \times \left(\frac{x_{50}}{\mu\text{m}}\right)^{-0.248} \times \left(\frac{x_{90}}{\mu\text{m}}\right)^{-0.233} \times 0.389. \quad (9)$$

Similar as already described for Equation (6), the applicability of Equation (9) was tested. The goodness of fit of the model is assessed by plotting the calculated DFI values vs the predicted DFI values for all materials (Table 1) according to Equation (9) as shown in Figure 7 along with the 95%-confidence bands. With this PLS model (Equation (9)) 75.5% of the variation of the DFI can be explained. The Anderson-Darling normality test (Razali and Wah 2012) of the residuals (measured vs. predicted DFI by Equation (9)) provided a p -value of 0.99 ($> \alpha = 0.05$) and no trend of the residuals over increasing DFI values can be identified. No statistically significant difference between measured vs. predicted DFI values (ANOVA, p -value = 0.996) is found, and a high correlation coefficient ($R^2 = 0.76$) is obtained. However, the facts that the maximal relative difference of predicted to measured DFI is 20.6% and the data points for Lactopress and Parateck M100 are outside the 95%-confidence bands, gives room for improvement, for example, by including more materials and additional particle properties.

The influence of each factor on the DFI in Equation (9) and the corresponding possible explanation will be given in the following. The x_{10} , x_{50} , and x_{90} are set to a medium value of the data range, to 58 μm , 141 μm , and 275 μm , respectively. From these values, at first each factor is exclusively increased or decreased by 25% by keeping all other factors constant. As the exponents for all variables in Equation (9) are < 0 (negative), their increase results in a decrease in DFI , thereby an increase in $v_{c, \text{Die [current]}}$ and as a result an increase in flowability (confer above). However, the extent of decrease in DFI is different for the individual particle size parameters, with the highest influence by x_{50} , followed by x_{90} and x_{10} .

This model calculation (for a reasonable parameter range in the tested setup) can help to understand which parameter can be changed to reduce/elevate the DFI most significantly thereby the sensitivity of the material to die speeds. Out of all parameters, the x_{50} and x_{90} have the highest influence on the DFI and a thoroughly considered combination of excipients can improve the die filling rate significantly.

It can be recommended to substitute material property data in Equation (9) to check in which range the DFI would fall if the ffc is > 10 , and to get a valuable powder flowability index at an early development stage. However, it is not possible to completely predict the die-filling process as the δ_{max} and δ_{min} , which are also material dependent and necessary to solve Equation (8), are still unknown. With the given correlation (Equation (9)), the DFI could be calculated, and the $v_{c, \text{Die [current]}}$ may be approximated as the reciprocal of DFI . Although the DFI is not non-dimensional and its dependency on the die and shoe dimensions needs further investigation, this approach offers the opportunity to quickly assess whether changes in powder properties (particle size) of a formulation can, and to which extent, positively influence the tableting process.

3.4. Comparison of die filling metrics with classical ring shear results

One of the most accepted powder characterization techniques is shear cell testing in powder handling industries since it can directly provide information for hopper discharge experiments (Schwedes 2005). The basic concept, developed by Jenike (Jenike 1964), was to provide design charts to determine which flow pattern, mass or funnel flow, could be expected during gravity discharge from a bin or hopper under steady-state flow. The obtained information through the material's ffc value is useful to predict the powder behavior in steady-state flow however the link to transient or dynamic flow is unclear (Wu et al. 2011). Depending on the given process for which powder flowability should be predicted, it is well known that the applied powder characterization technique should be carefully chosen (Prescott and Barnum 2000; Leturia et al. 2014). Main considerations are the stress levels and flow conditions the powder is being subjected to during measurement. In the context of die filling, the flow condition consists of three main factors: (1) The flow rate of particles out of the shoe into the die, (2) the interaction between powder flowing into the die and the powder already discharged into the die in particular towards the end of die filling where direct shearing could occur, and (3) lastly, the presence of air in the die slowing down the filling process and potentially altering the particle packing pattern in the die (Wu et al. 2011).

When it comes to tableting and in particular die filling, Wu et al. (Wu et al. 2011) showed for two different grades of microcrystalline cellulose a tendency for correlation of shear cell data with critical shoe speed of the Wu et al. model die shoe-filling system (Wu et al. 2003). As already described in Section 3.2, materials with $ffc > 10$ could provide sufficient δ at lowest die speed and an exponential relationship between δ - v could be identified. In contrast, a low powder flowability indicated by $ffc \leq 10$, would fail to obtain filled dies considering a gravity feeding die filling mechanism.

To evaluate the relationship between flowability of a material measured in terms of ffc and its critical die speed ($v_{c, \text{Die [current]}}$) as well as the DFI , both are plotted in Figure 8 for the set of materials (Table 1) which showed $ffc > 10$. The data clearly shows that there does not exist any correlation between the die filling metrics and their ffc . Though shear cell experiments can add big value to hopper design (Schwedes 2005; Schulze 2007), the difference in methodology in particular flow conditions allows only a 'flow' or 'no flow'

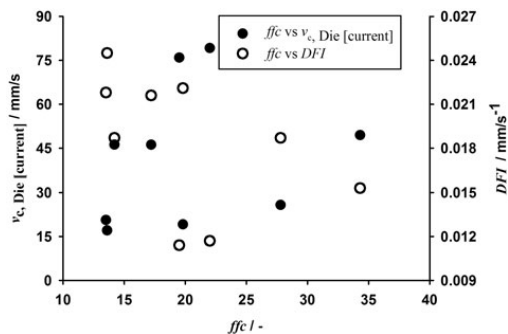


Figure 8. The (1) calculated critical die speed values ($v_{c, Die [current]}$), (2) DFI of different materials, and their corresponding measured ffc value.

discrimination in gravity feeding. Even when the stress states for ffc measurement (confer Section 3.1) are carefully selected to reflect the stress conditions during die filling, the dynamic powder flow into the die can partly be predicted by the steady-state flow principle of the RST, as already explained in Section 3.1. For example Zettler et al. (Zettler et al. 2016) reported a correlation between the collected mass variation in the die and the ffc value. They stated in their study that a stronger powder compact (lower ffc value) would flow more inconsistently into the die causing mass variation. Verification of this hypothesis was not considered in the current study, but could be easily evaluated with the model die filling system. As a conclusion only a 'flow' or 'no flow' discrimination into the die cannot be assessed via ffc but no relation to die filling metrics, for example, powder sensitivity to tableting speed, exists.

4. Conclusions

In this work, a new model die-filling system was introduced to mimic gravity feeding that is capable of assessing the die fill ratio of different powders under various die speeds. In contrast to previous work (Wu et al. 2003), the new system consists of a moving die and a stationary shoe which is one step closer to the actual rotary tablet machines.

The new model die filling system was used to assess the flowability of materials and the results showed similarity in powder discharge behavior with the previous work. The pressure build up due to entrapped air as powder was entering the die reduced the mass flow rate and resulted in incompletely filled dies even at lowest die speed for 18 out of 21 materials. Also similar to the previous system, the critical die speed ($v_{c, Die [current]}$), the die speed at which complete filling of the die is possible, was evaluated for sufficiently flowing materials. The impact of die speed on the fill ratio has been found to be best described by an exponential decay curve. This approach accounted for a minimum die fill ratio at highest die speeds and provided a good curve prediction for the fill ratio over the complete range of tested die speeds. The decay rate constant, that is approximately inversely proportional to the $v_{c, Die [current]}$, strongly correlated with the powder sensitivity to die speeds. It was defined as a new flowability metric, the 'Die Fill Index' (DFI) and could act in tandem with the $v_{c, Die [current]}$ in evaluating die filling performance of powders. Since die-filling experiments are not available in most of the pharmaceutical companies a correlation was established which can predict the DFI from a combination of a material's particle size properties. This correlation provides a first estimate of a material's

sensitivity to different die table speeds, which can be very helpful during formulation and process development.

Additionally, the flowability of different materials was investigated using a ring shear tester. A correlation was generated to predict the flowability from easily accessible particle characteristics.

Furthermore, it was attempted to see the relationship between the die-filling results and the ffc values obtained by classical shear cell measurements. This showed that ffc data can only help to discriminate whether the materials' powder flowability is sufficient for gravity feeding. In case that die filling is possible, no clear correlation between ffc and die-filling metrics could be identified. This is mainly due to the differences in powder flow conditions and the flow regimes in these two methods. As a consequence die-filling measurements, performed to assess the influence of tableting speed on tablet mass cannot be simply replaced by shear cell information.

In conclusion, the generated correlations which predict the ffc and DFI act as a versatile tool to estimate the flowability without the need of extensive, time-consuming laboratory work. Batch-to-batch consistency in pharma production can be monitored using the relationships found, and those relationships can be applied for a quick assessment of quality control. One possibility to even further improve and strengthen these correlations would be to add more data, and to include particle shape information, which is the focus of our future work. In addition, the new model die filling system may be further adapted to finally have a rotational design in hands, suction filling could be included, and last but not least force feeding by paddle wheel rotation instead of gravity feeding could be applied to be able to fully predict die filling in high performance rotary tablet presses.

Disclosure statement

No potential conflict of interest was reported by the authors.

ORCID

Regina Scherließ  <http://orcid.org/0000-0001-8685-5672>

References

- Bauer-Brandl A, Ritschel WA. 2012. Die Tablette, Handbuch der Entwicklung, Herstellung und Qualitätssicherung. 3rd ed. Aulendorf: Cantor-Verlag für Medizin und Naturwissenschaften GmbH.
- Beverloo WA, Leniger HA, van de Velde J. 1961. The flow of granular solids through orifices. Chem Eng Sci. 15:260–269.
- Bierwisch C, Kraft T, Riedel H, Moseler M. 2009a. Three-dimensional discrete element models for the granular statics and dynamics of powders in cavity filling. J Mech Phys Solids. 57:10–31.
- Bierwisch C, Kraft T, Riedel H, Moseler M. 2009b. Die filling optimization using three-dimensional discrete element modeling. Powder Technol. 196:169–179.
- Capece M, Raimundo H, Strong J, Goa P. 2015. Prediction of powder flow performance using a multi-component granular bond number. Powder Technol. 286:561–571.
- Capece M, Ruiz Silva K, Sunkara D, Strong J, Goa P. 2016. On the relationship of inter-particle cohesiveness and bulk powder behaviour: Flowability of pharmaceutical powders. Int J Pharm. 511:178–189.
- FETTE Compacting GmbH, FE 75. 2016. [accessed 2016 December 6]. <http://www.fette-compacting.com/fe75-productivity-redefined/>

- Fitzpatrick JJ, Barringer SA, Iqbal T. 2004. Flow property measurement of food powders and sensitivity of Jenike's hopper design methodology to the measured values. *J Food Eng.* 61:399–405.
- Furukawa R, Shiosaka Y, Kadota K, Takagaki K, Noguchi T, Schimosaka A, Schirakawa Y. 2016. Size-induced segregation during pharmaceutical particle die filling assessed by response surface methodology using discrete element method. *J Drug Deliv Sci Tec.* 35:284–293.
- Garthwaite P. 1994. An interpretation of partial least squares. *J Am Stat Assoc.* 89:122–127.
- Gentzler M, Michaels JN, Tardos GI. 2015. Quantification of segregation potential for polydisperse, cohesive, multi-component powders and prediction of tablet die-filling performance – a methodology for practical testing, re-formulation and process design. *Powder Technol.* 285:96–102.
- Gopireddy SR, Hildebrandt C, Urbanetz NA. 2016. Numerical simulation of powder flow in a pharmaceutical tablet press lab-scale gravity feeder. *Powder Technol.* 302:309–327.
- Guo Y, Kafui KD, Wu CY, Thornton C, Seville JPK. 2009. A coupled DEM/CFD analysis of the effect of air on powder flow during die filling. *AIChE J.* 55:49–62.
- Guo Y, Wu CY, Kafui KD, Thornton C. 2010. Numerical analysis of density-induced segregation during die filling. *Powder Technol.* 197:111–119.
- Guo Y, Wu CY, Kafui KD, Thornton C. 2011. 3D DEM/CFD analysis of size-induced segregation during die filling. *Powder Technol.* 206:177–188.
- Hausner HH. 1972. Effect of quench sintering on the grain structure of sintered metals. *Int J Powder Metall.* 8:159–161.
- Hiestand EN. 2002. *Mechanics and physical principles for powders and compacts: Foundations of pharmaceutical sciences series.* 1st ed. West Lafayette (IN): SSCI Inc.
- Hou H, Sun CC. 2008. Quantifying effects of particulate properties on powder flow properties using a ring shear tester. *J Pharm Sci.* 97:4030–4039.
- Jackson S, Sinka IC, Cocks ACF. 2007. The effect of suction during die fill on a rotary tablet press. *Eur J Pharm Biopharm.* 65:253–256.
- Jager PD, Bramante T. 2015. Assessment of pharmaceutical powder flowability using shear cell-based methods and application of Jenike's Methodology. *J Pharm Sci.* 104:3804–3813.
- Jenike W. 1964. Storage and flow of solids. *Bulletin of the Utah engineering experiment station (Issue 123).* Salt Lake City (Utah): University of Utah.
- Jivraj M, Martini LG, Thomson CM. 2000. An overview of the different excipients useful for the direct compression of tablets. *Pharm Sci Technol. Today.* 3:58–63.
- Johanson K. 2009. Effect of particle shape on unconfined yield strength. *Powder Technol.* 194:246–251.
- Ketterhagen WR. 2015. Simulation of powder flow in a lab-scale tablet press feed frame: effects of design and operating parameters on measures of tablet quality. *Powder Technol.* 275:361–374.
- Leturia M, Benali M, Lagarde S, Ronga I, Saleh K. 2014. Characterization of flow properties of cohesive powders: a comparative study of traditional and new testing methods. *Powder Technol.* 253:406–423.
- Leyva N, Mullarney MP. 2009. Modeling pharmaceutical powder-flow performance using particle-size distribution data. *Pharm Technol.* 33:126–134.
- Marinelli J, Carson JW. 2002. Solve solids flow problems in bins, hoppers, and feeders. *Chem Eng Prog.* 98:24–36.
- Mills LA, Sinka IC. 2013. Effect of particle size and density on the die fill of powders. *Eur J Pharm Biopharm.* 84:642–652.
- Nwose EN, Pei C, Wu CY. 2012. Modelling die filling with charged particles using DEM/CFD. *Particuology.* 10:229–235.
- Ph. Eur. 2016. *European pharmacopoeia.* 8th ed. Strasbourg: Council of Europe.
- Podczec F, Mia Y. 1996. The influence of particle size and shape on the angle of internal friction and the flow factor of unlubricated and lubricated powders. *Int J Pharm.* 144:187–194.
- Prescott JK, Barnum RA. 2000. On powder flowability. *Pharm Technol.* 24:60–85.
- Razali NM, Wah YB. 2012. Power comparisons of shapiro-wilk, kolmogorov-smirnov, lilliefors and anderson-darling tests. *J Stat Modeling Anal.* 2:21–33.
- Rios M. 2006. Developments in powder flow testing. *Pharm Technol.* 30:38–49.
- Schneider LCR, Cocks ACF, Apostolopoulos A. 2005. Ceramic comparison of filling behaviour of metallic, ceramic, hardmetal and magnetic powders. *Powder Metall.* 48:77–84.
- Schneider LCR, Sinka IC, Cocks ACF. 2007. Characterisation of the flow behaviour of pharmaceutical powders using a model die–shoe filling system. *Powder Technol.* 173:59–71.
- Schulze D. 2007. *Powders and bulk solids.* Berlin: Springer-Verlag.
- Schwedes J. 2005. Review on testers for measuring flow properties of bulk solids. *Granul Matter.* 5:1–43.
- Sinka IC, Schneider LCR, Cocks ACF. 2004. Measurement of the flow properties of powders with special reference to die fill. *Int J Pharm.* 280:27–38.
- Sinka IC, Motazedian F, Cocks ACF, Pitt KG. 2009. The effect of processing parameters on pharmaceutical tablet properties. *Powder Technol.* 189:276–284.
- Sun CC. 2010. Setting the bar for powder flow properties in successful high speed tableting. *Powder Technol.* 201:106–108.
- Svarovsky L. 1987. *Powder testing guide, methods of measuring the physical properties of bulk powders.* Netherlands: Springer.
- USP 29-NF 24, US Pharmacopoeial Convention, “<1174> Powder Flow”, p. 3017.
- Wold S, Sjöström M, Eriksson L. 2001. PLS-regression: a basic tool of chemometrics. *Chemometr Intell Lab Syst.* 58:109–130.
- Wu CY, Dihoru L, Cocks ACF. 2003. The flow of powder into simple and stepped dies. *Powder Technol.* 134:24–39.
- Wu CY, Cocks ACF. 2004. Flow behaviour of powders during die filling. *Powder Metall.* 47:127–136.
- Wu CY, Cocks ACF. 2006. Numerical and experimental investigations of the flow of powder into a confined space. *Mech Mater.* 38:304–324.
- Wu CY. 2008. DEM simulations of die filling during pharmaceutical tableting. *Particuology.* 6:412–418.
- Wu CY, Armstrong B, Vlachos N. 2011. Characterization of powder flowability for die filling. *Particul Sci Technol.* 30:378–389.
- Wu CY, Guo Y. 2012. Numerical modelling of suction filling using DEM/CFD. *Chem Eng Sci.* 73:231–238.
- Yaginuma Y, Ozeki Y, Kakizawa M, Gomi SJ, Watanabe Y. 2007. Effects of powder flowability on die-fill properties in rotary compression. *J Drug Deliv Sci Tec.* 17:205–210.
- Yu W, Muteki K. 2011. Prediction of bulk powder flow performance using comprehensive particle size and particle shape distributions. *J Pharm Sci.* 100:284–293.
- Zettler A, Hilden J, Koenig M, Breslin C, Aburub A, Allgeier M, Patel P, Mitra B. 2016. Evaluation of small-scale powder flow characterization tests in the prediction of large-scale process failures. *J Pharm Innov.* 11:189–199.
- Zhu HP, Zhou ZY, Yang RY, Yu AB. 2007. Discrete particle simulation of particulate systems: theoretical developments. *Chem Eng Sci.* 62:3378–3396.

3.1.2 High speed camera imaging of gravity filling

Assessing Die Filling Using High-Speed Camera Imaging

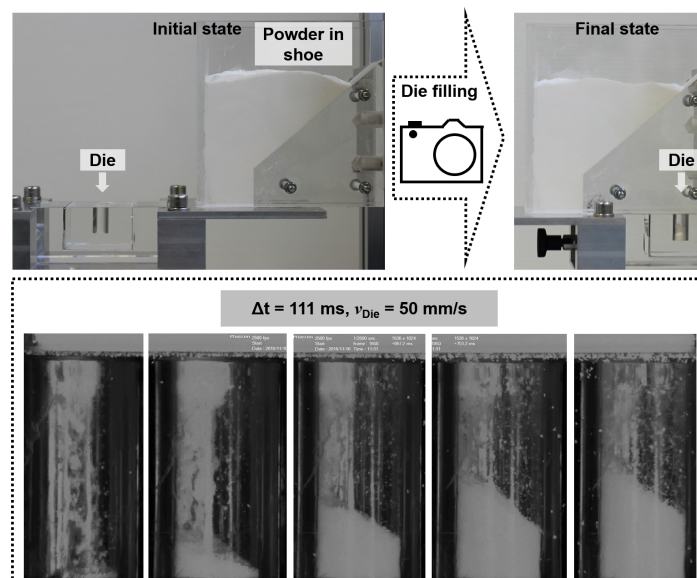
Claudia Hildebrandt¹, Jost Loerzer^{2, 3}, Srikanth R. Gopireddy²,
Nora A. Urbanetz²

¹ Department of Pharmaceutics and Biopharmaceutics, Christian-Albrechts-Universität Kiel,
Grasweg 9a, 24118 Kiel, Germany

² Daiichi-Sankyo Europe GmbH, Pharmaceutical Development,
Luitpoldstrasse 1, 85276 Pfaffenhofen, Germany

³ Clausthal University of Technology,
Adolph-Roemer-Straße 2a, 38678 Clausthal-Zellerfeld, Germany

Chemie Ingenieur Technik, 90:472-482, 2018



Outline

In the previous chapter (3.1.1) the mass discharged into the die to obtain the die fill ratio is measured. This quantification is used to evaluate the powder sensitivity to tableting speed, though it does allow any statement about the actual powder discharge pattern into the die. In the following, high speed camera imaging makes use of the acrylic glass design of the model system to visualize the powder flow pattern.

The visualization of the discharge of different pharmaceutical excipients enables to discern the powder flow pattern and to identify similar characteristics which may be used to categorize the materials into different groups, i.e. ‘good, intermediate, and bad’ flowing. In addition, an image analysis method is developed to estimate the powder volume within the die over filling time, the volume flow rate. The quantification via pixel counts corresponds to the ‘*volume fill ratio*’ and is compared to the mass-based die fill ratio δ described previously (chapter 3.1.1). Hence, differences between the volume fill ratio and mass fill ratio may be used to answer questions that might arise in powder compaction. Similar to the correlations developed to estimate the *DFI* or *ffc* (confer chapter 3.1.1), a mathematical model is established to describe the volume flow rate via particle characteristics. Supported by particle size measurement and scanning electron microscopy, the qualitative powder flow pattern as well as the quantitative volume fill ratio and volume flow rate in gravity filling are described.

Two complementary approaches, simple weighing of the die (confer chapter 3.1.1) as well as more elaborated high speed camera imaging are presented to improve die filling process understanding in gravity feeding.

Assessing Die Filling Using High-Speed Camera Imaging

Claudia Hildebrandt^{1,*}, Jost Loerzer^{2,3}, Srikanth R. Gopireddy³, and Nora Urbanetz³

DOI: 10.1002/cite.201700115

The study presents the die filling process of pharmaceutical powders using high-speed camera imaging. The objectives are to qualitatively visualize and to quantify the powder flow. A model die filling system with a shoe for powder storage and a moving die underneath the shoe was designed. The die filling process is captured through a high-speed camera and the images allow flow type identification and flow rate calculation. Correlations are generated to predict the fill ratios and flow rates based on particle size data, which could help in process understanding and optimization of die filling.

Keywords: Die filling, High-speed camera imaging, Pharmaceutical tableting, Powder flow, Powder characterization

Received: August 31, 2017; *revised:* January 12, 2018; *accepted:* January 24, 2018

1 Introduction

Tablets are the most common type of pharmaceutical dosage forms and are manufactured in high quantities [1]. They are produced on high-speed rotary tablet presses in which at first the dies are filled with the blend and consequently compacted to form tablets. The prerequisite for successful tablet production at such high rates is an adequate powder flow. A model die shoe filling system was developed by Wu et al. [2] to visualize and to quantify the powder flow from a shoe, moving at different velocities, into a stationary die [2–9]. Schneider et al. [4] described three different powder flow types using high-speed camera imaging, which are shown in Fig. 1.

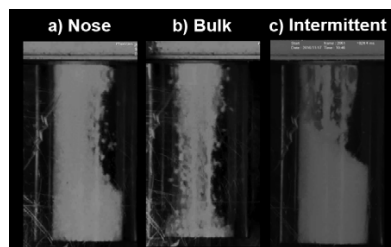


Figure 1. Examples for a) nose, b) bulk, and c) intermittent flow.

Nose flow (a) occurs if the acceleration of the die forces the powder against the back of the die. Bulk flow (b) is defined as the constant flow of powder from the free bottom surface of the powder mass. Eventually some materials show an unsteady flow of particle agglomerates called an intermittent flow (c) [4].

However, in common rotary tablet presses, the cylindrical dies are being filled from a stationary feeding system, either filling hopper, equipped with paddle wheels, or gravity

feeder, whereas the turret moves underneath it at defined speed [10]. These differences impede the direct transfer of the model die filling results [2–9] to powder flow in common tablet presses.

The objective of the current work is to overcome these discrepancies by introducing a novel custom-designed set-up, shown in Fig. 2 [11]. It comprises a die moving with defined speed underneath the stationary shoe. The individual parts are transparent such that the powder flow during the filling process can be seen. Hildebrandt et al. developed an understanding for powder sensitivity to different die speeds by introducing a new metric, the so-called die fill index (DFI). A high DFI would indicate a high fill ratio sensitivity at low and a rather robustness at high die speeds. In extension to this, the current study will visualize the phenomena that are involved in die filling allowing flow type identification of different pharmaceutical materials [4] by using a high-speed camera. In addition and in contrast to the previous mass-based die filling evaluation [2–9, 11], image analysis will allow the quantification of volume fill ratios that has not been done yet. The volume fill ratios during the filling process of one die serve as basis for the calculation of flow rates and represent together with a flow type analysis a new flowability quantification. Furthermore, cor-

¹Claudia Hildebrandt
childebrandt@pharmazie.uni-kiel.de
Kiel University, Department of Pharmaceutics and Biopharmaceutics, Grasweg 9a, 24118 Kiel, Germany.

²Jost Loerzer
Clausthal University of Technology, Adolph-Roemer-Straße 2a, 38678 Clausthal-Zellerfeld, Germany.

³Jost Loerzer, Dr. Srikanth R. Gopireddy, Dr. Nora Urbanetz
Daiichi-Sankyo Europe GmbH, Pharmaceutical Development, Luitpoldstraße 1, 85276 Pfaffenhofen, Germany.

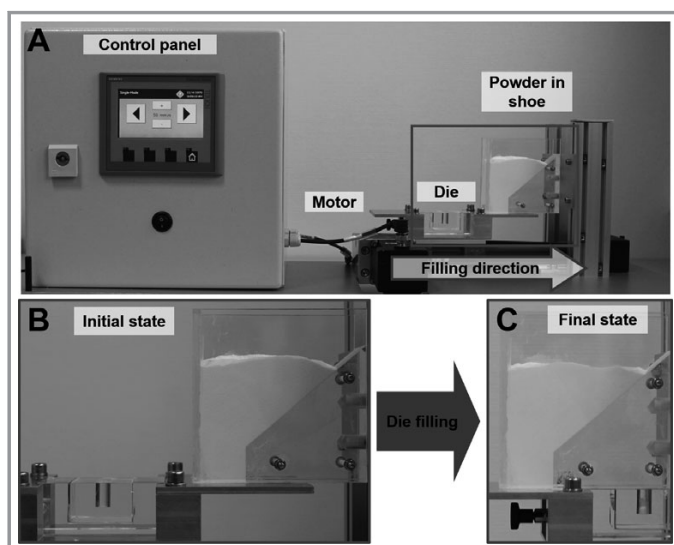


Figure 2. The new model die filling system including the complete setup (top) and the shoe and die before (bottom left) and after (bottom right) die filling [11].

relations are generated to estimate the volume fill ratios and flow rates based on material properties to quickly assess flowability of new materials.

2 Materials and Methods

2.1 Materials

The different pharmaceutical excipients used as diluents for direct compression formulations are listed in Tab. 1. Their

chemical structure, x_{50} , x_{90} , bulk density (ρ_b), maximum volume fill ratio ($V\%_{\max}$), and volume flow rates ($Q\%_t$) are given as well. For the definition of $V\%_{\max}$ and $Q\%_t$, refer to Sect. 3.

2.2 Methods

All measurements were performed at constant conditions (25 °C and 40 % relative humidity) to make sure that the influence of moisture is same for all materials [11]. The raw materials have not been preconditioned prior to measurement as they were stored under the same conditions.

2.2.1 Particle Size and Size Distribution

The particle size and size distribution (PSD) was measured using a Sympatec Helos/Rodos laser diffraction system (Sympatec GmbH, Clausthal-Zellerfeld, Germany) with a dry dispersion capability. The dispersion pressure was optimized to break any loose agglomerates but not to destroy individual particles. In the PSD, the x_{50} and x_{90} defining the particle sizes represented by 50 % and 90 %, respectively, of the cumulative distribution sum are of particular interest (see Tab. 1).

2.2.2 Scanning Electron Microscopy (SEM)

A small sample of each material was fixed on carbon stickers (Plano GmbH, Wetzlar, Germany) and sputter-coated using a Bal-Tec SCP 050 Sputter Coater (Leica Instruments, Wetzlar, Germany) to ensure conductivity of the electrically nonconductive organic materials. Sputtering was conducted

Table 1. Materials.

Material name	Material type	Vendor	x_{50} [μm]	x_{90} [μm]	ρ_b [g cm^{-3}]	$V\%_{\max}$ [%]	$Q\%_t$ [% ms^{-1}]	Used (X) and tested (O) for Eq. (2)
MCC Spheres 350	microcrystalline cellulose	JRS Pharma	463	572	0.97	100	1.16	
Ludipress	93 % lactose + 3.5 % Kollidon 30 + Kollidon CL	BASF	202	448	0.49	100	0.59	X
Parateck M200	mannitol	Merck KGaA	182	400	0.51	100	0.43	O
Lactopress	lactose	DFE Pharma	158	310	0.58	98	0.25	X
FlowLac 90	lactose	Meggle	138	217	0.59	89	0.22	X
Pearlitol 100 SD	mannitol	Roquette Pharma	106	165	0.48	79	0.17	O
SuperTab 24AN	lactose	DFE Pharma	102	229	0.49	73	0.19	X
Lycatab C	cornstarch	Roquette Pharma	83	183	0.53	42	0.11	X
Parateck M100	mannitol	Merck KGaA	73	145	0.58	41	0.10	X

in an evacuated chamber for 65 s at 50 mA with Argon 5.0 (Linde AG, Hamburg, Germany). Coated samples were scanned in the SEM chamber of a Zeiss Ultra 55 Plus (Carl Zeiss NTS GmbH, Oberkochen, Germany) with a working voltage of 2 kV. Images were gained from secondary electrons with the SE-2 detector and are shown at a 100-fold magnification in Fig. 3.

2.2.3 Bulk Density

The bulk density was determined according to Ph. Eur. 9.2 (2.9.34) [12]. A constant mass of 100 g material was poured into a vibrating funnel to fill a graduated cylinder of 250 mL volume. The powder volume was read and the bulk density (ρ_b) was calculated via the material mass (m) and the loosely filled powder bed volume in the cylinder (V) according to Eq. (1). The ρ_b is listed in Tab. 1 for all materials:

$$\rho_b = \frac{m}{V} \quad (1)$$

2.2.4 Model Die Filling System

The custom-designed novel model die filling system is shown in Fig. 2 and described in detail by Hildebrandt et al. [11]. This system consists of a moving die and a stationary shoe to hold the powder as shown in Fig. 2. These parts are made of acrylic glass in order to be able to watch the powder flow. The shoe consists of a rectangular bottom part and

an inclined top part that are joined together. The bottom part has dimensions of 27 mm, 30 mm, and 20 mm in length, width, and height, respectively. The top part is 45° inclined on the right hand side whereas the left side is in line with the bottom part (see Fig. 2). The total shoe size is 100 mm × 30 mm × 100 mm. The acrylic glass die is a cylinder with dimensions of 9 mm diameter and 15 mm height. The die moves along the guided ramp at an adjustable speed (50–500 mm s⁻¹). It accelerates with 600 mm s⁻² and reaches a constant value for the given speed before it arrives underneath the shoe. The die is constructed in such a way that it can be removed after it has passed under the shoe so that the mass of the powder collected in the die can be measured. Using this system, the die filling behavior of different materials (listed in Tab. 1) was measured according to a consistent procedure as outlined in the following.

At first, the shoe was filled with the powder up to the top of the inclined part as shown in Fig. 2. Next, the die filling speed was set to 50 mm s⁻¹ and upon start the die would move from the left hand to the right hand side as indicated in Fig. 2. The mass of the die including the collected powder was weighed and the mass of the die was subtracted. Following this, the die was reset to its original position by moving the die in its guided ramp in the backward direction at the same speed. For each powder the procedure was repeated twice (triplicate measurement). During the measurement, the amount of powder in the shoe was kept constant by steadily refilling. In addition, all surfaces, in particular the acrylic glass die and shoe, were electrostatically neutralized between every measurement with an anti-static gun to eliminate any charge influences. As the system was not operated under vacuum, the effect of entrapped air in the die during powder filling will have significant influence on the die filling behavior [3].

2.2.5 High-Speed Camera Setup

The powder flow behavior during filling of the die was analyzed with the high-speed camera system Photron Fastcam SA2 (Photron Limited, Tokyo, Japan). The focus area of the camera was adjusted at the bottom of the shoe opening recording the powder flow into the moving die. A framerate of 2500 s⁻¹ and a resolution of 1536 × 1024 pixel in the software Photron Fastcam Viewer ver. 352 (Photron Limited, Tokyo, Japan) was chosen to generate images for post processing. As the die enters underneath the shoe, the recording was triggered manually.

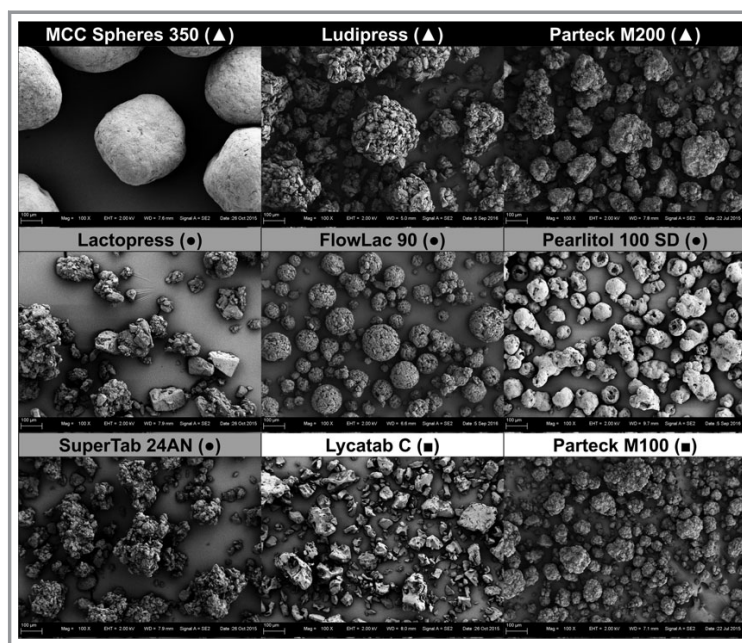


Figure 3. Scanning electron microscope images of the different materials. Same symbols (▲, ●, ■) as in Sect. 3.1 are provided for reference.

2.2.6 Qualitative Analysis, Calculations and Statistics

In total six frames between the beginning and the end of the die filling were selected for further analysis (see Figs. 5–7). Frame no. 1 at t_0 is defined by the first particles entering the die whereas the last frame at t_5 is either the time point when the die is completely filled or, in case of incomplete filling, the time point at which the right hand side walls of die and shoe are overlapping (cf. Figs. 5–7). The remaining four frames were taken at constant time intervals (Δt) between t_0 and t_5 . The frames for t_{1-5} are shown for all materials in Figs. 5–7.

The images were further analyzed with the open source image editor GIMP v. 2.8 (The GIMP Team). The analysis is exemplarily shown in Fig. 4a for Parateck M200. The volume fill ratio ($V\%_i$) at each time point (t_i) is obtained by the pixel quotient of the projected area of the partially or entirely filled and the empty die. This procedure works also in case of uneven powder bed surfaces (cf. Fig. 4b). The final volume fill ratio at the end of the die filling process ($V\%_{\max}$) is given for all materials in Tab. 1.

The local volume flow rate, $Q\%_i$, was estimated via the $V\%-t$ graph (Fig. 4a) and represents the slope between two measurement points with their corresponding $V\%_i$ and $V\%_{i+1}$ at t_i and t_{i+1} values, respectively. Furthermore, the slope (obtained by regression analysis) in the linear part of the $V\%-t$ curve was considered as the total volume flow rate, $Q\%_t$.

Eventually, the mass fill ratio ($M\%_{\max}$), defined as the ratio of the mass collected in the die and the maximum possible mass that can be filled into the die defined by the ρ_b [11], was measured. Comparison of mass and volume fill ratio was performed by checking normality distribution of

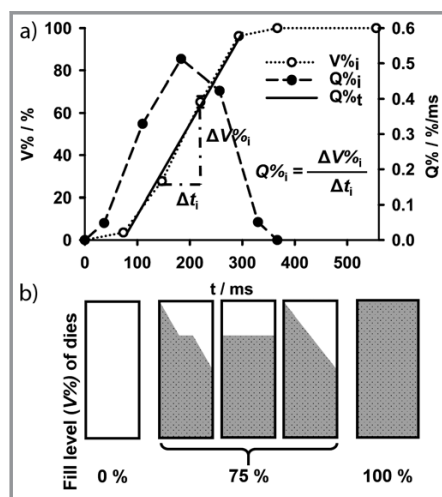


Figure 4. a) Volume fill ratio ($V\%_i$), local volume flow rates ($Q\%_i$) and total volume flow rate ($Q\%_t$) vs time for Parateck M200. b) Schematic illustration of different volume fill ratios of dies.

groups by the Shapiro-Wilk test followed by a t-test at $\alpha=0.05$. For $P<0.05$ a statistical significant difference between the mean values of measured mass and calculated volume fill ratio was assumed.

3 Results and Discussion

First of all, the general process, as powder is being discharged from the rectangular hopper into the cylindrical die, is described for different pharmaceutical materials. They differ in terms of chemical nature, size, shape, and surface roughness as given in Tab. 1 and shown in SEM images (Fig. 3). The qualitative visualization using high-speed camera is supported by a couple of new metrics introduced in this study to quantify the die filling and to generate new insights into powder characterization. Two relationships to describe the volume flow rate and the volume fill ratio are developed that allow a first flowability estimation from particle size information. These analyses can open the door for potentially new applications in pharmaceutical tableting.

3.1 Description of the Die Filling Process and Comparison of Different Materials

High-speed camera images of the die, illustrated in Figs. 5–7, have been taken for the entire die filling process for each and every material (Tab. 1). In comparison to the previously reported model die filling system [2–9], the following differences, in addition to the ones reported by Hildebrandt et al. [11], can be identified. In the new system (Fig. 2), the shoe is completely filled with powder that exerts a high normal pressure on the powder bed at the shearing layer with the die table. Thus, this system is more relevant in the context of pharmaceutical die filling, as similar compared to gravity feeding (see Sect. 1 and [13]), a dense powder bed column is built in the shoe (irrespective of its exact geometry) above the die table, leading to the following phenomenon. It implies that entrained air escaping from the die into the shoe has to find its way through the powder bed in the shoe [14], which is less relevant for the previous system (see to [2–9]). Hence, the powder bed properties, in particular its density and void volume, that are influenced by its absolute particle size and size distribution and inter-particle forces will significantly impact the air stream.

At first a grouping of the nine different materials into *good* (\blacktriangle), *intermediate* (\bullet), and *bad* (\blacksquare) flowing is provided. This grouping is mainly based on the maximum volume fill ratio ($V\%_{\max}$) that is obtained after the complete filling time of 550 ms (cf. Fig. 8) and the flow type [4]. Both are mainly influenced by the mean particle size (Tab. 1, Fig. 3). The quantitative analysis of volume fill ratio over time for all the nine materials is given in Fig. 8. Correspondingly, the high-speed camera images for each and every material at the given time points are shown in Figs. 5–7.

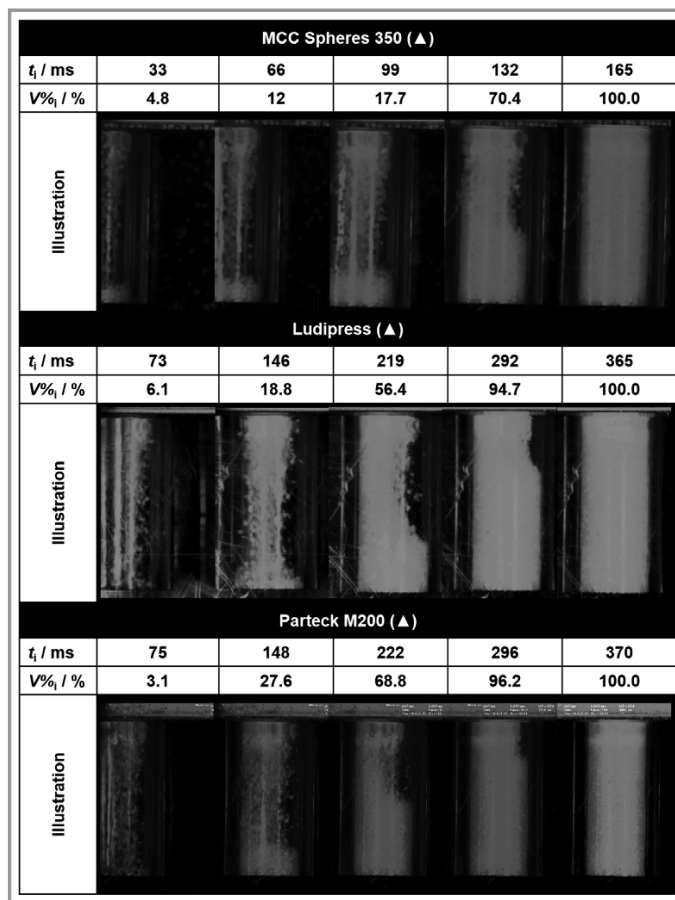


Figure 5. High-speed camera images at different time intervals during die filling of all materials with good flowing (one of the three measurements (Fig. 8)).

The flow behavior of all the measured materials is described in the following as per the groups they fall into.

3.1.1 Good Flowing

Materials that can be categorized into the good flowing group show the following properties. They are able to completely fill the die as the die is moving at 50 mm s^{-1} underneath the shoe ($V\%_{\text{max}} = 100\%$, Fig. 8). The transition from bulk to nose flow type [4] over the filling time results in a high volume flow rate ($Q\%_t \geq 0.43 \text{ \% ms}^{-1}$) which could be even higher if the entrained air as powder is entering the die would not oppose powder discharge [3]. The volume flow rate is lowest in the first intervals (t_{1-3}) since the die opening is only partially open to the powder bed in the hopper but then increases significantly. In the last interval (t_{4-5}) the volume flow rate decreases again attributed to the high powder bed in the left half of the die that is reducing the available die cross-sectional area. MCC Spheres 350,

Ludipress, and Parateck M200 that fall into this category show $x_{50} > 182 \mu\text{m}$ which allows the identification of individual particles in high-speed camera images (Fig. 5). The flow behavior of the individual materials are as follows.

MCC Spheres 350

MCC Spheres are micro-crystalline cellulose particles of spherical shape (Fig. 3) that are not used as diluents in direct compression formulations but constitute a model material for the current study. This material has the largest particle size of all materials under investigation (Tab. 1) and almost perfect spherical shape (Fig. 3). It shows the fastest and complete filling in 165 ms (Fig. 8). Compared to the second best material (Ludipress), just half of the time for complete filling is needed. High-speed camera images reveal a homogeneous powder entering the die indicating least inter-particle cohesion. This observation can be explained by (1) the high gravitational force that is acting on the large particles overcoming non-contact forces and favoring discharge into the die [15]. Furthermore (2) the very smooth surface of the spherical particles (Fig. 3) prevents particle-particle friction and decreases the non-contact forces (van der Waals, capillary, and electrostatic forces) [15]. A high $Q\%_t$ of 1.16 \% ms^{-1} is found which is favoring half filling of the die within the last interval (t_{4-5}).

Ludipress

Ludipress is a multi-component excipient containing a diluent, binding agent, and disintegrant (Tab. 1). The SEM picture (Fig. 3) shows single, large particles of spherical shape composed of individual small particle agglomerates. These properties lead to a good volume flow rate ($Q\%_t = 0.59 \text{ \% ms}^{-1}$) during die filling and a completely filled die in 365 ms (Fig. 8). The flow can be characterized into a steady bulk flow in the first 146 ms (t_{1-2}). However, it changes to a dense nose flow in the third interval ($t_3 = 219 \text{ ms}$, Fig. 5) with an increase in volume flow rate.

Parateck M200

Parateck M200 is a commonly used direct compression excipient as it is, in contrast to lactose, chemically inert. It has a high specific surface area given by the production process as indicated by the particle shape and surface roughness shown in Fig. 3. The type of flow according to [4] and Fig. 1 can be classified as bulk flow at the beginning (t_1) which then changes to nose flow (t_{2-4}). Within the linear part of the $V\%-t$ curve (t_{1-4} , Fig. 4a) a $Q\%_t$ of 0.43 \% ms^{-1} can be obtained.

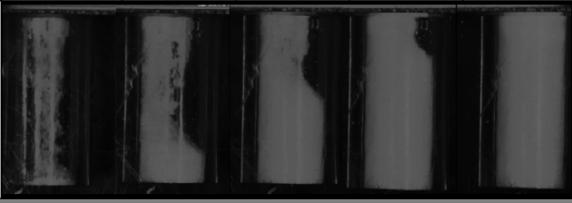
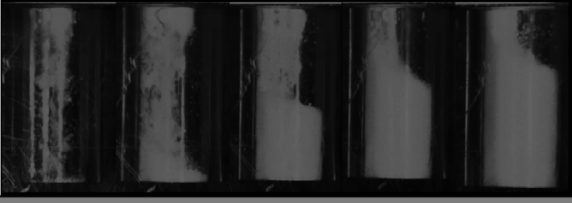
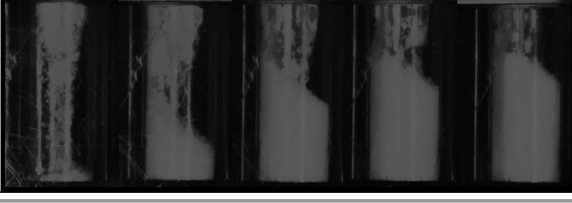
Lactopress (•)						
t_1 / ms	111	222	332	442	553	
$V\%_t$ / %	3.4	33.4	65.4	93.9	100.0	
Illustration						
	FlowLac 90 (•)					
	t_1 / ms	110	220	330	440	550
	$V\%_t$ / %	3.3	21.0	47.1	71.3	85.3
	Illustration					
Pearlitol 100 SD (•)						
t_1 / ms		109	219	328	441	551
$V\%_t$ / %		4.2	26.3	51.2	69.3	89.7
Illustration						
	SuperTab 24AN (•)					
	t_1 / ms	108	206	324	432	540
	$V\%_t$ / %	3.6	34.5	51.4	64.2	71.9
	Illustration					

Figure 6. High-speed camera images at different time intervals during die filling of all materials with intermediate flowing (one of the three measurements (Fig. 8)).

3.1.2 Intermediate Flowing

In comparison to the good, the intermediate flowing materials fill half or more of the die volume but less than 100% in 550 ms of filling time at 50 mm s⁻¹ die speed. A medium volume flow rate ($Q\%_v$, Tab.1) results from the nose and intermittent flow types [4]. All materials that fall into this category (Lactopress, FlowLac 90, Pearlitol 100 SD, Super-

Tab 24AN) have a medium range particle size of $102 \mu\text{m} \leq x_{50} < 182 \mu\text{m}$ (Tab. 1).

Lactopress

Lactopress is produced by granulating crystals of α -lactose monohydrate with water or a lactose solution in a fluid bed process revealing, in contrast to spray-dried lactose, a less spherical but more irregular particle shape as shown in Fig. 3. The mean particle size ($x_{50} = 158 \mu\text{m}$) is only slightly smaller compared to Parreck M200 (Tab.1) and the quantitative (Fig.8) as well as qualitative (Fig.6) high-speed camera image analysis would suggest a grouping between the good and intermediate category with a higher tendency for the latter, as explained in the following. In contrast to the good flowing materials, Lactopress shows almost complete filling ($V\%_{\text{max}} = 98 \pm 3\%$) but requires the complete filling time of 550 ms. Only at the very beginning (t_1) a low volume flow rate of loose agglomerates can be identified which then becomes rather constant with a $Q\%_t$ of $0.25\% \text{ms}^{-1}$ during nose flow (t_{2-5}). In contrast to the good flowing materials, the discharge of Lactopress is characterized by a higher particles' cohesivity, in particular indicated by loose agglomerates at $t_2 = 222 \text{ms}$ (Fig. 6).

FlowLac 90

FlowLac 90 is a spray-dried lactose with a spherical agglomerate shape, consisting of α -lactose monohydrate crystals bound by amorphous lactose (Fig. 3). The discharge behavior of FlowLac 90 into the die right from the beginning (t_1) is characterized by loose but rather large agglomerates (Fig. 6). Only during the first interval (t_{1-2}) the volume flow rate is low, as the complete die cross sectional area is not open to the shoe, but it then increases to a constant value of $0.22\% \text{ms}^{-1}$ for the rest of the filling period (t_{2-5}) during nose flow [4] (Fig. 8). The high-speed camera images show that large agglomerates from the shoe, presumably developed by caking, are separating as soon as the free die volume is available. This can be particularly observed at t_2 in Fig. 6 with a large powder cake in the top portion of die that is cracking. As a result high volume fill ratio standard deviations are obtained for the three individual measurements (Fig. 8). A final volume fill ratio of $89 \pm 3\%$ is obtained.

Pearlitol 100 SD

Although Pearlitol 100 SD is a mannitol, same as Parreck M100 and Parreck M200, the particles resemble more or less spheres that contain holes that are porous (generated

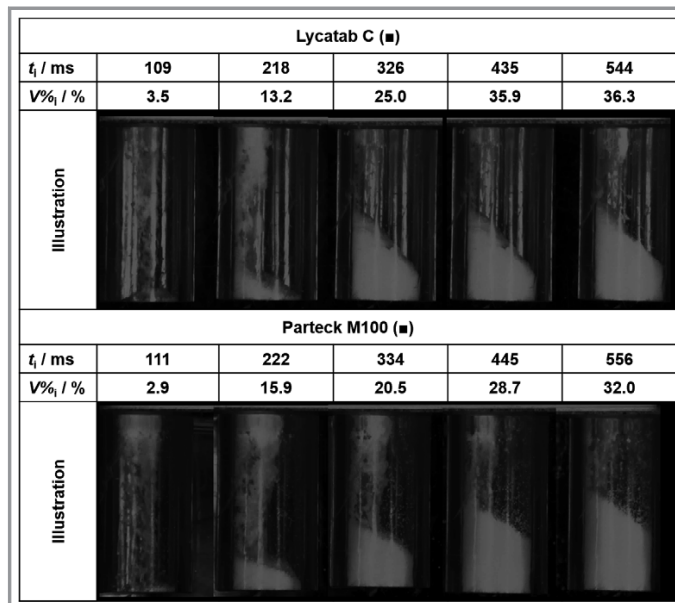


Figure 7. High-speed camera images at different time intervals during die filling of all materials with bad flowing (one of the three measurements (Fig. 8)).

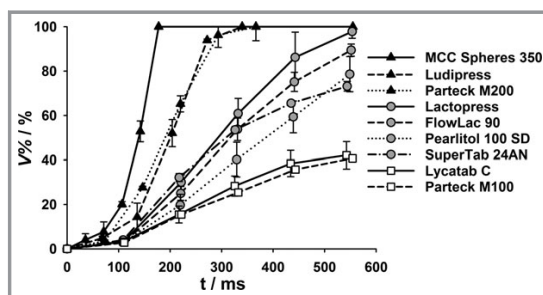


Figure 8. $V\%$ - t plot for all tested materials. Materials with ▲ symbol are grouped into good, ● intermediate, and ■ bad flowing, respectively.

during spray-drying), see Fig. 3. The powder flow of Pearlitol 100 SD differs in several ways compared to FlowLac 90. The high-speed camera images show less agglomerates and a more stream-like powder discharge (Fig. 6). Those observations are attributed to the low particle-particle cohesion although the small particle size ($x_{50} = 106 \mu\text{m}$) might suggest the opposed effect. The smooth surface texture of the particles decreases the contact area for non-contact forces improving powder flowability [16]. The flow type indicates an intermediate between bulk and nose flow that is found to be constant over the filling time. The volume flow rate does not change from the second interval until the end of filling (t_{2-5} , $Q\%_t = 0.17 \text{ \% ms}^{-1}$), which is not found for any other material independent of its group or flow type. This very consistent volume flow rate in addition to a flat and

less steep powder bed angle in the filled die compared to other materials point out the less cohesive nature of the material. A final volume fill ratio of $79 \pm 8 \%$ is obtained.

SuperTab 24AN

The last material in the intermediate flowing group is SuperTab 24AN, an anhydrous lactose generated through roller drying. The particles, as shown in the SEM images (Fig. 3), are of irregular shape and size. The $V\%$ - t curve during die filling shows a clear sigmoidal shape and at the end of the filling time an incompletely filled die ($V\%_{\text{max}} = 73 \pm 2 \%$) is obtained (Fig. 8). Although the particle size is close to Pearlitol 100 SD ($x_{50} = 102 \mu\text{m}$), the significantly differing particle shape increases the powder cohesivity of SuperTab 24AN that can be visualized in terms of the large size, high density, and high frequency of the agglomerates in high-speed camera images (Fig. 6). Those agglomerates give rise to a rather intermittent than nose flow type during t_{2-5} . This inconsistent discharge of large agglomerates prevents entrained air to escape from the die and decreases the volume flow rate already after the third time interval (t_{4-5}) (see

Figs. 6 and 8) [3]. The material is classified into the intermediate and not bad flowing group by the fact that a high $V\%_{\text{max}}$ ($> 50 \%$) is obtained, although high-speed camera images could suggest a grouping located between the intermediate and bad flowing category (see below).

3.1.3 Bad Flowing

The remaining materials, Lycatab C and Pardeck M100, fall into the bad flowing group. This group is characterized by a $V\%_{\text{max}} < 50 \%$ caused by a low volume flow rate that is attributed to the intermittent flow type. The latter is driven by the material's small particle size ($x_{50} \leq 83 \mu\text{m}$).

Lycatab C

Lycatab C, a partially pre-gelatinized maize starch, constitutes of the second smallest particles ($x_{50} = 83 \mu\text{m}$) preventing the identification of individual particles in the high-speed camera images (Fig. 7). The particle shape is least spherical, the particles contain more edges and holes compared to all other materials, and the surface texture is quite smooth. Lycatab C discharges in a bunch of small and low density agglomerates at the beginning (t_1) of die filling. The highest material volume enters the die during t_2 with the highest volume flow rate (Fig. 8). As shown in the high-speed camera images (Fig. 7), large and small clumps fall into the die indicating an intermittent flow type [4]. Subsequently during t_{3-4} only very few agglomerates discharge from the shoe followed by one large agglomerate in t_5 resulting in a $V\%_{\text{max}}$ of $42 \pm 6 \%$. This very inconsistent filling

could be explained by two reasons. First, the very small particle size and the high fines content (Tab. 1 and Fig. 3) increase the cohesive forces which become more important relative to particle weight [15] preventing the discharge from the shoe into the die. Another influence could come from the high particle-particle friction that is given by the large surface asperities increasing the particle interlocking in the shear zone of the moving die table with the particles at the bottom of the powder bed in the shoe. A steep powder heap in the die is developing and it does not change over filling time which is an additional indicator for the high cohesivity.

Parateck M100

Similar observations that are made for Lycatab C hold true for Parateck M100. These are the intermittent flow type characterized by agglomerates, a low volume flow rate ($Q_{\%i} = 0.10\% \text{ ms}^{-1}$), and a low $V\%_{\text{max}}$ of $41 \pm 6\%$. The less steep powder bed angle in the die compared to Lycatab C although the mean particle size is smaller ($x_{50} = 73 \mu\text{m}$) could indicate a slightly improved powder flowability for Parateck M100. This could be explained by a higher particle sphericity as shown in Fig. 3. Although, Parateck M100 has same chemical composition and a comparable production process as Parateck M200, the differences in powder flow that can be identified during die filling (Figs. 5 and 7) arise most presumably from their particle size difference as all other powder flowability influencing factors (e.g., shape, chemical nature, density [11]) are negligible.

3.2 Comparison of Volume and Mass Fill Ratio

The mass filled into the die at 50 mm s^{-1} die speed was measured for all the materials and the mass fill ratio ($M\%_{\text{max}}$) according to Hildebrandt et al. [11] was determined. The comparison of $M\%_{\text{max}}$ and $V\%_{\text{max}}$ for all the materials (Fig. 9) shows, that for MCC Spheres 350, Ludipress, FlowLac 90, SuperTab 24AN, and Parateck M100 a significant difference is obtained (t-test, $P < 0.05$, indicated with *).

For the two good flowing materials MCC Spheres 350 and Ludipress, which are showing almost constant bulk flow during die filling (see Sect. 3.1), the $V\%_{\text{max}}$ values are higher than $M\%_{\text{max}}$ indicating that the filled densities are lower than the powders' bulk densities. In other words, completely filled dies are shown in high-speed camera images (confer Fig. 5) in contrast to their mass-based analysis (via their bulk densities). Since those materials show a very good powder flow, entrained air has less time to escape from the die [3] increasing the air volume in the powder bed, and thus, decreasing the fill densities.

It is the other way round for FlowLac 90, SuperTab 24AN, and Parateck M100. For these materials, the significant difference between $M\%_{\text{max}} > V\%_{\text{max}}$ may arise from the observations that can be made during die filling. In particular, those materials discharge from the shoe into the die

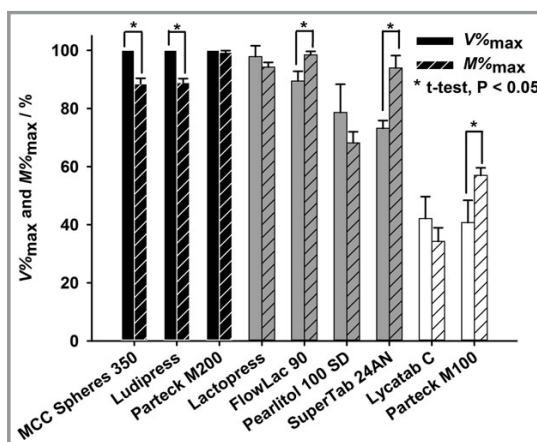


Figure 9. Comparison of maximal fill ratio obtained through image analysis ($V\%_{\text{max}}$) and weighing of collected mass ($M\%_{\text{max}}$).

rather as agglomerates (Figs. 6 and 7) that have been formed in the shoe due to different mechanisms like caking. Although those agglomerates are rather small but indeed they show a high density resulting in higher mass fill ratios.

The remaining materials (Parateck M200, Lactopress, Pearlitol 100 SD, and Lycatab C) show slightly higher but not significant volume compared to the mass fill ratio differences. This observation might arise due to the less accurate volume than mass fill ratio determination. The powder bed projection area in the images that is used for volume fill ratio assessment might not be constant over the breadth of the die giving a volume overestimation (Fig. 4b).

In summary, the detailed visualization of the die filling process by using high-speed camera imaging gives several opportunities. (1) The incremental analysis allows the flow type identification and its possible transition over filling time [4]. (2) Local and volume flow rates constitute new measures for powder flowability in the context of pharmaceutical tableting that have not been reported for the previously used system [2–9]. (3) Last but not least, a quantitative comparison of final mass and volume fill ratio can indicate enclosed air in the powder bed, and high density particle agglomerates in the filled dies. The latter could provide an explanation for possible peculiarities during subsequent compaction in the tablet press [17].

3.3 Relationship Between Volume Flow Rate and Particle Size

From the previous sections, it is clear that high-speed camera analyses are valuable to provide insights in the die filling mechanisms. However, it is very costly to conduct these experiments and they are not a standard method in pharmaceutical industries. To close this gap, an attempt is made to correlate

the easily available particle size information with the volume flow rate results from the image analysis. Particle size is one of the main powder flow influencing factors in die filling (see above and as shown in [11]) which gave rise to include only this material property in the fit. MCC Spheres 350 have not been included and tested in the correlation as they served as a model material with significantly differing properties in terms of shape and size compared to the other classical direct compression excipients (Tab. 1 and Fig. 3). Out of the eight remaining materials in this study, six have been used to generate (indicated with an X in Tab. 1) an exponential dependency between $Q\%_t$, x_{50} , and x_{90} via non-linear least squares regression analysis (see Eq. (2)). Other particle size data (x_{10} , and the particle size distribution factor SPAN [11]) and mathematical correlations have been tested as well but did not improve the goodness of fit.

$$Q\%_t = 0.00047 \frac{\%}{\text{ms}} \exp\left(\frac{0.0089 x_{50} + 0.0018 x_{90}}{\mu\text{m}}\right) \quad (2)$$

This correlation (Eq. (2)) allows a first estimate of powder flow rate into the die using x_{50} and x_{90} data. In general, a decreased mass flow rate for increased particle size is observed by the Beverloo correlation at constant orifice diameter in hopper discharge studies [18–20]. This holds true if the ratio between the orifice diameter (D) and the particle diameter (d) is small, i.e., $D/d < 20$, whereas the Beverloo correlation shows no influence of particle size on the flow rate when $D/d > 20$ [18]. In this study, the materials considered (d corresponds to x_{50}) and the system used (D corresponds to die diameter) show D/d in the range of 44.6–123.3 (Tab. 1) which impedes the application of the Beverloo correlation. Thus, a contrasting behavior with an increase in flow rate for larger particles is found. This observation is explained by the fact that for this system the relationship between gravitational and non-contact forces, e.g., van der Waals and electrostatic forces, is the driving force in discharge rate. In case of small particles, the non-contact forces can exceed the gravitational force thereby hindering powder discharge from the shoe into the die [15], resulting in a decreased $Q\%_t$. In addition, this leads to an intermittent [4] and non-constant flow of agglomerates, i.e., similar to the one found in case of Parateck M100.

The validity of the relationship between $Q\%_t$ and the particle size (Eq. (2)) is tested by comparing measured and calculated $Q\%_t$ values in Fig. 10 (●). The linear regression line through the data points shows a very high correlation coefficient ($R^2 = 0.975$), slope (1.0677) and y -intercept (0.0001) that are close to a line through the origin (indicating 100% agreement). Five data points are within the 95%-confidence band (one exception) and no trend of the residuals is found. Finally, Eq. (2) was applied for the remaining two materials which were not included to generate the relationship (O in Tab. 1). Those materials show very good agreement between the measured and calculated flow rates as well (■, Fig. 10). More materials could be evaluated and included in Eq. (2)

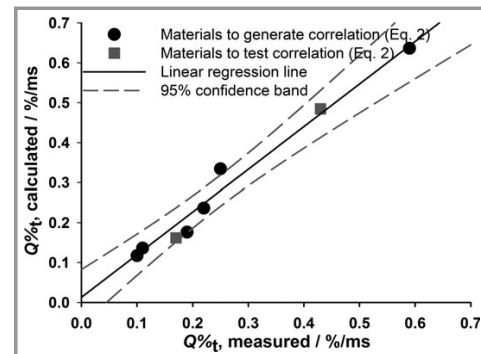


Figure 10. Verification of validity of Eq. (2) by comparing $Q\%_t$ measured with $Q\%_t$ calculated.

in the future to strengthen its applicability and validity. The generated correlation holds true for similar material properties in terms of particle size, shape, and surface roughness as given in Tab. 1 (O and X) and Fig. 3. As already described by Beverloo [18] and for the previous model die filling system [2–9], the volume flow rate depends on the shoe and die dimensions, hence, adaption of the constants in Eq. (2) for other setups would be necessary. Finally other die speeds than 50 mm s^{-1} have to be tested to evaluate its influence on $Q\%_t$ and in turn on its relationship with the material's particle size.

3.4 Relationship Between Flow Rate and Fill Ratio

In the next step, it is tested how the volume flow rate during die filling influences the final fill ratio. The $V\%_{\text{max}}$ vs $Q\%_t$ plot, as depicted in Fig. 11a, shows that materials with $Q\%_t < 0.241 \text{ % ms}^{-1}$ yield incompletely filled dies. In other words, by using Eq. (2) it can be easily estimated whether a material of specific particle size would get completely filled at the die speed of 50 mm s^{-1} . In addition, a linear relationship between $V\%_{\text{max}}$ and $Q\%_t$ is found for $Q\%_t < 0.241 \text{ % ms}^{-1}$ (gray background in Fig. 11a). The relationship between the two measures in this zone is given in Eq. (3) and provides a very good correlation ($R^2 = 0.9956$, linear regression line in Fig. 11a).

$$V\%_{\text{max}} = 404.63 \text{ms } Q\%_t \quad (3)$$

With the help of Eq. (3) the maximal fill ratio of a material can be assessed by utilizing either (1) measured flow rates, or (2) estimated flow rates via particle size information according to Eq. (2). The $V\%_{\text{max}}$ values for the materials are calculated by using Eq. (2) and plotted vs the measured data points in Fig. 11b. In case that $V\%_{\text{max}} > 100\%$, a reasonable value of 100% is assigned. Even though one data point is lying beyond the 95%-confidence band, the estimation of $V\%_{\text{max}}$ via particle size information and $Q\%_t$ (Eqs. (2) and (3)) provides very good results ($R^2 = 0.90411$).

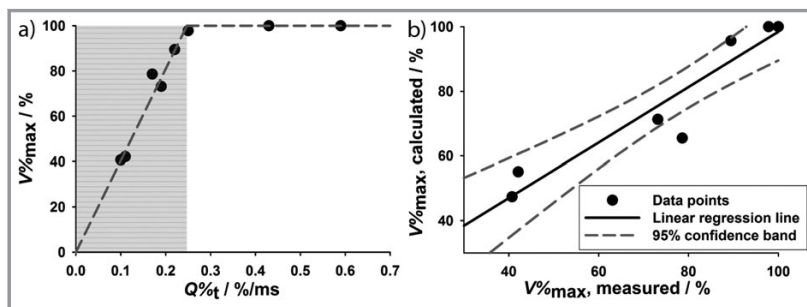


Figure 11. a) $V\%_{\max}$ vs $Q\%_t$ data points. The gray-line inked zone highlights data points with $V\%_{\max} < 100\%$. Dashed lines are linear regression lines for $V\%_{\max} < 100\%$ and $V\%_{\max} \geq 100\%$, respectively. b) $V\%_{\max}$ calculated via $Q\%_t$ calculated (obtained through particle size information (Eq. (2) and Eq. (3)) vs $V\%_{\max}$ measured.

Thereby, the filling ratio of a material at the tested die speed can be evaluated by using just the particle size information.

4 Summary and Conclusion

In this study a new setup was introduced to evaluate powder discharge from a stationary shoe into a moving die. High-speed camera imaging provided a clear insight into the transfer of the particles from the shoe into the die over filling time. Furthermore, the image analysis constituted a novel approach to quantify powder flowability in the context of tableting. Different pharmaceutical materials could thereby be discriminated into good, intermediate, and bad flowing materials according to their flow type and maximal die fill ratio. The comparison of mass vs volume fill ratios identified the influence of entrapped air in the die that could counteract high powder flow rates. For those materials a very loose powder bed with a high void fraction in the die was obtained. In contrast more cohesive materials that showed a high frequency of agglomerates in the high-speed camera images revealed a dense powder bed after die filling.

As this model die filling system in conjunction with the high-speed camera setup is not commonly available, an attempt was made to correlate easily accessible material properties, such as particle size, with the volume fill rate. Thus, not only a minimum fill rate to obtain completely filled dies could be identified but also a relationship between fill rate and ratio. Consequently with the given relationships the powder fill ratio for unknown materials with similar materials properties as the ones tested in this study can be estimated. It can serve as a basis to optimize materials with respect to particle size, i.e., through sieving to obtain the minimal required flow rate to ensure completely filled dies at the given die speed.

In conclusion, this study helps in understanding the die filling process in a qualitative and quantitative manner. Pharmaceutical development can exploit those findings and use the new system to optimize formulation design. However, in a next step, more materials including mixtures

should be tested. Furthermore, the elaborated relationships hold true at the tested die speed, but in order to transfer to different speeds, further experiments are required. Last but not least, instead of a translational system, a similar setup with a rotational motion will be used in the future to be able to include the effect of centrifugal forces that are found in rotary tablet presses.

Symbols used

d	[μm]	particle diameter (x_{50})
D	[μm]	orifice diameter / die diameter
ρ_b	[g cm^{-3}]	bulk density
m	[g]	mass
$M\%_{\max}$	[%]	mass fill ratio
$Q\%_i$	[$\% \text{ms}^{-1}$]	volume fill rate at time point t_i
$Q\%_t$	[$\% \text{ms}^{-1}$]	volume fill rate at linear part of the $V\%-t$ curve
t_i	[ms]	time point
V	[cm^3]	volume
$V\%_i$	[%]	volume fill ratio at time point t_i
$V\%_{\max}$	[%]	volume fill ratio at end of filling process
x_{10}	[μm]	particle size of 10% of the cumulative distribution sum
x_{50}	[μm]	particle size of 50% of the cumulative distribution sum
x_{90}	[μm]	particle size of 90% of the cumulative distribution sum

References

- [1] A. Bauer-Brandl, W. A. Ritschel, *Die Tablette, Handbuch der Entwicklung, Herstellung und Qualitätssicherung*, 3rd ed., Cantor-Verlag für Medizin und Naturwissenschaften GmbH, Aulendorf 2012.
- [2] C.-Y. Wu, L. Dihoru, A. C. F. Cocks, *Powder Technol.* **2003**, *134* (1–2), 24–39. DOI: 10.1016/S0032-5910(03)00130-X
- [3] I. C. Sinka, L. C. R. Schneider, A. C. F. Cocks, *Int. J. Pharm.* **2004**, *280* (1–2), 27–38. DOI: 10.1016/j.ijpharm.2004.04.021

- [4] L. C. R. Schneider, I. C. Sinka, A. C. F. Cocks, *Powder Technol.* **2007**, *173* (1), 59 – 71. DOI: 10.1016/j.powtec.2006.11.015
- [5] L. A. Mills, I. C. Sinka, *Eur. J. Pharm. Biopharm.* **2003**, *84* (3), 652 – 652. DOI: 10.1016/j.ejpb.2013.01.012
- [6] C.-Y. Wu, A. C. F. Cocks, *Mech. Mater.* **2006**, *38* (4), 304 – 324. DOI: 10.1016/j.mechmat.2005.08.001
- [7] S. Jackson, I. C. Sinka, A. C. F. Cocks, *Eur. J. Pharm. Biopharm.* **2007**, *62* (2), 253 – 256. DOI: 10.1016/j.ejpb.2006.10.008
- [8] C. Bierwisch, T. Kraft, H. Riedel, M. Moseler, *J. Mech. Phys. Solids* **2009**, *57* (1), 10 – 31. DOI: 10.1016/j.jmps.2008.10.006
- [9] C.-Y. Wu, A. Brian, N. Vlachos, *Part. Sci. Technol.* **2011**, *30* (4), 378 – 389. DOI: 10.1080/02726351.2011.588302
- [10] E. Peeters, T. De Beerm, C. Vervaeet, J.-P. Remon, *Drug Dev. Ind. Pharm.* **2015**, *41* (4), 530 – 539. DOI: 10.3109/03639045.2014.884121
- [11] C. Hildebrandt, S. R. Gopireddy, A. K. Fritsch, T. Profitlich, R. Scherliess, N. A. Urbanetz, *Pharm. Dev. Technol.* **2017**. DOI: 10.1080/10837450.2017.1412462
- [12] *European Pharmacopoeia (Ph. Eur.)*, 9th ed., EDQM – Council of Europe, Strasbourg **2017**.
- [13] Y. Yaginuma, Y. Ozeki, M. Kakizawa, S. I. Gomi, Y. Watanabe, *J. Drug Deliv. Sci. Technol.* **2007**, *17* (3), 205 – 210. DOI: 10.1016/S1773-2247(07)50037-7
- [14] Y. Guo, K. D. Kafui, C.-Y. Wu, C. Thornton, J. P. K. Seville, *AIChE J.* **2009**, *55* (1), 49 – 62. DOI: 10.1002/aic.11734
- [15] S. Sarkar, R. Mukherjee, B. Chaudhuri, *Int. J. Pharm.* **2017**, *526* (1–2), 516 – 537. DOI: 10.1016/j.ijpharm.2017.05.003
- [16] U. Zafar, C. Hare, A. Hassanpour, M. Ghadiri, *Powder Technol.* **2014**, *264*, 236 – 241. DOI: 10.1016/j.powtec.2014.04.022
- [17] I. C. Sinka, F. Motazedian, A. C. F. Cocks, K. G. Pitt, *Powder Technol.* **2009**, *189* (2), 276 – 284. DOI: 10.1016/j.powtec.2008.04.020
- [18] W. A. Beverloo, H. A. Leniger, J. van de Velde, *Chem. Eng. Sci.* **1961**, *15*, 260 – 269. DOI: 10.1016/0009-2509(61)85030-6
- [19] R. M. Neddermann, *Statics and Kinematics of Granular Materials*, Cambridge University Press, New York **1992**.
- [20] A. Anand, J. S. Curtis, C. R. Wassgren, B. C. Hancock, W. R. Ketterhagen, *Chem. Eng. Sci.* **2008**, *63* (24), 5821 – 5830. DOI: 10.1016/j.ces.2008.08.015

3.1.3 Numerical analysis of mono-disperse sized particles in gravity filling

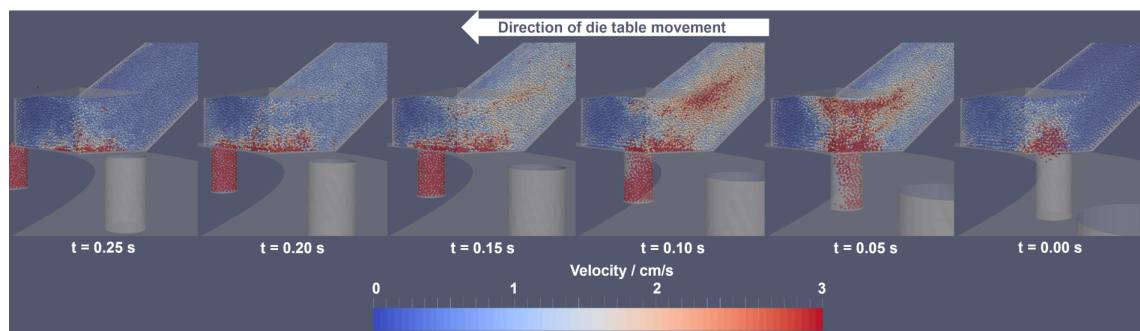
Numerical simulation of powder flow in a pharmaceutical tablet press lab-scale gravity feeder

Claudia Hildebrandt¹, Srikanth R. Gopireddy², Nora A. Urbanetz²

¹ Department of Pharmaceutics and Biopharmaceutics, Christian-Albrechts-Universität Kiel, Grasweg 9a, 24118 Kiel, Germany

² Daiichi-Sankyo Europe GmbH, Pharmaceutical Development, Luitpoldstrasse 1, 85276 Pfaffenhofen, Germany

Powder Technology, 302:309-327, 2016



Outline

The previous chapters (3.1.1 & 3.1.2) evaluated the die filling by gravity in a translational model system. In contrast, gravity feeding in high speed tableting involves the rotation of the turret and a slightly modified geometry of the feeding system, i.e. an inclined chute and powder reservoir located on top of the turret. In the next two chapters (3.1.3 & 3.1.4), those dissimilarities are considered by applying a numerical approach.

Using the DEM instead of an experimental approach is driven by two main reasons. First, the DEM gives the opportunity to look into closed systems which is only possible in experiments by using transparent housings (confer to chapter (3.1.2)). Thus the powder flow pattern not only from the feeding system into the die but also within the feeding system, i.e. the rearrangement of particles by filling up the void space as particles discharge into the die, may be visualized.

The second reason is driven by the inherent connection of individual material properties with each other as found in real powders. Thus discriminating the influence of individual factors is hardly possible without affecting another factor. For example, a change in particle size usually goes in hand with a change of inter-particle cohesion (confer to chapter 2.4.4.2). In the DEM, the material properties on a particle level may be independently changed (confer Fig. 4) and thus a single material property influence on the die filling process can be unveiled.

The following two chapters focus on the gravity feeder of a lab-scale tableting machine. The material is discharging from a feeding system consisting of a cylindrical pipe, inclined chute, and rectangular box into the rotating dies of the turret. First of all, particles of same size are used to provide a general understanding of the powder flow within the gravity feeder. The influence of individual material properties that are considered to affect powder flowability is studied. Those properties are the inter-particle cohesion, the coefficient of friction, and the coefficient of restitution. This analysis should help to understand which property is the most influencing one in die filling and should provide a starting point for formulation optimization. In addition, process parameters such as the turret speed and the die diameter are evaluated.

The approach of using mono-disperse particles creates the basis for the size segregation analysis of poly-disperse particles in chapter 3.1.3.



Contents lists available at ScienceDirect

Powder Technology

journal homepage: www.elsevier.com/locate/powtec

Numerical simulation of powder flow in a pharmaceutical tablet press lab-scale gravity feeder

Srikanth R. Gopireddy^{a,*}, Claudia Hildebrandt^b, Nora A. Urbanetz^a^a Daiichi-Sankyo Europe GmbH, Pharmaceutical Development, Luitpoldstrasse 1, 85276 Pfaffenhofen, Germany^b Department of Pharmaceutics and Biopharmaceutics, Christian-Albrechts-Universität Kiel, Grasweg 9a, 24118 Kiel, Germany

ARTICLE INFO

Article history:

Received in revised form 23 August 2016

Accepted 27 August 2016

Available online 28 August 2016

Keywords:

Die filling

Gravity feeder

Discrete element method

Tableting

ABSTRACT

The die filling process within a lab-scale rotary tablet press is simulated using the Discrete Element Method (DEM). The particle motion is captured as particles travel from the gravity feeder consisting of a chute connected to the shoe represented by a rectangular box to the dies/cavities of the turret. The particles fill the dies mostly due to gravity. The process conditions such as die table speed, die diameter as well as the material characteristics e.g. cohesion, coefficient of friction, coefficient of restitution, etc. influence the die filling process. The process conditions and material characteristics are systematically investigated by varying one of those parameters at a time while keeping other conditions constant. Eventually process conditions as well as material properties were changed simultaneously to analyze interaction relationships. The results give both qualitative (powder flow pattern from the feeder to the dies) and quantitative (tablet mass variation, mass flow rate etc.) insights into the die filling process. The numerical results indicate that faster die table speeds and smaller die diameters give rise to lower tablet mass with a significantly increased mass variation, which would eventually increase the challenges in meeting the specifications. On the other hand, cohesion between the particles significantly reduces the tablet mass and increases the mass variation. The influence of particle-wall friction coefficient on the particle rearrangement is analyzed both qualitatively and quantitatively, which shows that increasing the particle-wall friction reduces the dead zones within the shoe. The coefficient of restitution does not exhibit any influence on the die filling which may be attributed to the very confined space of the feeding system. Eventually this study emphasizes the importance of tablet blend characterization prior to tableting and provides operators with optimal process parameters and material attributes to ensure a high tableting process performance.

© 2016 Elsevier B.V. All rights reserved.

1. Introduction

The first industrial production of tablets dates back in 1877 and today this dosage form covers 80% of all available drug delivery systems [1]. Over almost 150 years of tablet production and process development, nontrivial challenges still remain to ensure product quality. One major challenge in tablet production and from a patient safety point of view is the accurate content and content uniformity of the active pharmaceutical ingredient (API). Tablets are produced in current age on high speed rotary tablet presses in which the process is generally divided into three distinct stages: die filling, compaction and ejection. Out of these three stages, the die filling represents the most crucial step since it is the last stage to control and specify the mean and range of both the tablet mass as well as the API content.

Owing to the importance of the die filling process on the final product quality, in 2004 the first experimental study of the die filling process of pharmaceutical powders was conducted [2]. The work considered a

model die-shoe filling system, which was similar to the one introduced in cement and steel industry [3]. The model system contained a stationary die and a moving delivery system (shoe) which were made transparent to facilitate the visualization of the filling process. The shoe, a rectangular box, was filled with powder and translated over a transparent die with a constant velocity between 33 and 1000 mm/s. This approach provides an opportunity to determine flowability and the amount of powder collected in the die as a function of the shoe velocity [3]. Qualitative results include high-speed camera images which provide details of the flow process as the powder is delivered into the die. Three major types of flow have been identified: nose, bulk and intermittent flow. It was shown that pharmaceutical powders are more likely to flow intermittently which is illustrated by a random detachment of individual particles [4]. There are several works with this model die-shoe filling system and the latest study was in 2013 by Mills et al. [5] with the focus on the effect of particle size and density of microcrystalline cellulose. The flowability is quantified using the concept of the “critical velocity” which describes the maximum velocity of the shoe for which a given die is still completely filled with powder after one pass [3]. The critical velocity is correlated with the particle size, which results

* Corresponding author.

E-mail address: srikanth.gopireddy@daiichi-sankyo.eu (S.R. Gopireddy).

in a higher critical velocity for larger particles [5]. This model-die system was further extended to find the influence of air and vacuum as well as gravity and suction filling [2–8].

In parallel to experimental studies, numerical simulations mainly using the *discrete element method* (DEM) started in 2006 with the calculation of different flowability metrics [6]. Those studies with the same model die-shoe filling system aimed at the identification of optimum process conditions and the optimization of powder formulation in terms of flowability and segregation through increased process understanding [6,8–15]. The initial numerical model was limited to two-dimensional analysis and only a very low number of particles (3000) were simulated [9]. With increasing computational capabilities more realistic simulations in terms of including the effect of air [11–13] and different particle sizes as well as a higher number of particles (120,000) [14] were considered. It was shown that suction filling, which is achieved by moving the lower punch in a rotary tablet press downward, significantly increases the critical shoe velocity compared to gravity filling in air due to the development of a pressure gradient across the powder bed which augments the flow into the die [15]. However, most of these experimental and numerical studies investigated a moving-shoe-static-die setup rather than a setup present in today's modern rotary tablet presses where the dies are moving below the shoe.

The interest in die filling has further grown and recently shifted to investigate the feed frame of a rotary tablet press which is a closed box with inlet and outlet, and contains one or more paddle wheels. Different designs of feed frames exist in terms of number, dimensions and shapes of the paddles and the number of chambers and heights [16], which are specific to every commercial tablet machine. Recent experimental works [16,17] investigated the effect of process parameters within the feed frame. It was reported that the powder weight in the dies increased for faster paddle wheel speeds and decreased for higher turret speeds [16]. However, a higher turret and paddle wheel speed reduced the tablet tensile strength and the tableability. Numerical studies also supported the experimental data in which the particle velocities and residence time distributions were calculated to measure the work done on the particles and the resulting effects such as particle attrition and powder lubrication were shown [18,19]. In particular, Ketterhagen [18] studied the impact of paddle wheel shape, speed and direction on the tablet weight, mixing, and lubrication for a lab-scale tablet press. Furthermore, particles' segregation for low paddle wheel speeds was calculated [19].

In contrary to the published work [18,19], which focused on the influence of force feeders on tableting, the current study presents numerical simulations of the powder flow from a gravity feeder to the dies within a lab-scale rotary tablet press. The simulations are performed using a three-dimensional DEM. The objectives of this work include the investigation of the effect of (1) tableting machine operating conditions, mainly the die table speed and the die dimensions, and (2) material attributes on the powder flow within this gravity feeder. This study is the first of its kind which would give a comprehensive understanding of powder flow in the tableting unit operation under several material and process conditions. Through this study it is aimed to find the critical process parameters as well as the decisive material attributes which impact the tablet quality.

2. Methodology

This section presents the details about the mathematical approach, geometrical configuration as well as the numerical simulations performed.

2.1. Discrete element method

The DEM is a well-known approach in the particle technology, and it has been used for more than three decades after its introduction by Cundall and Strack [20]. The DEM has evolved over the years and has

found applications in several industries including pharmaceutical technology to predict the powder flow in tableting unit operations [21]. The advantage of the DEM over the continuum approach is that it is able to capture the trajectory of each and every particle in the system through Newton's equation of motion. The forces acting on each particle which may be due to particle-particle or particle-wall contacts or the non-contact forces such as gravity, cohesion etc. enter as source terms in the equation of motion [22]. The theory behind the DEM, including a comprehensive literature review, is given by Zhu et al. [22], whereas Hermann and Luding [23] present the different models relevant to particulate simulations. The details of DEM models and numerical algorithms of computing the particle flow dynamics is beyond the scope of this study and those details can be found elsewhere [21,22]. Instead, the current study aims at using the well-developed models of DEM to capture the particle flow in a tableting unit operation under different material and process attributes.

There are several ways to solve DEM transport equations such as using commercial software, open source packages or in-house programming. In this work all the computations were performed using the open source DEM software known as LIGGGHTS [24]. LIGGGHTS is developed based on the molecular dynamic simulation tool known as LAMMPS developed by Sandia National Laboratories [25], and in this study LIGGGHTS version 3.2.1 is used. The models chosen in this study include Hertz and Mindlin & Deresiewicz theories for the calculation of normal and tangential forces, respectively [26]. The cohesion is included through the simplified Johnson-Kendall-Roberts model [27] which adds an additional normal force contribution and this is successfully implemented in [18] and in [19]. The other non-contact force considered includes gravity. The implementation of all the above mentioned models as well as their validation within LIGGGHTS is given by Kloss et al. [24].

The impact of fluid presence on the particle motion is ignored in this study, which can be modeled by coupling the DEM with the conservation of mass, momentum and energy equations of fluid. Most of the tablet machines apply suction filling i.e. the lower punch moves downwards to create a negative pressure within the die so that the particles fall from the shoe into the die under suction. The study of Wu and Guo [15] showed that the mass flow rate observed with gravity filling under vacuum, which is considered in this study, is equivalent to suction filling in presence of air.

2.2. Computational setup

The model die-shoe filling system found in earlier studies considered a rectangular box as shoe, which moves linearly over a fixed die [6,9]. Following this, in the current study a similar rectangular box to represent the shoe was chosen. But unlike the previous studies, the shoe here is connected to a feeding pipe like in an actual lab-scale tablet press with a rotating die table. The complete geometrical configuration considered in this study is shown in Fig. 1. Such a configuration of the shoe and feeding pipe is commonly found in lab-scale tablet presses e.g. RoTab T (Luxner Tablet Presses, Germany) and Pressima AX (IMA Pharma, Italy) and is referred to as gravity feeder, see Fig. 2. The main difference among these gravity feeders is the extension of the shoe to the right side (compare Figs. 1 and 2). By choosing a rectangular box to represent the shoe rather than the original geometry it is possible to generalize the results obtained here to other systems having similar design. The dimensions of the feeding pipe and die table shown in Fig. 1 correspond to RoTab T.

In those tableting machines, the powder enters the feeding pipe from a hopper (not shown here) and fills the shoe. From the shoe, when the die table is rotated, the dies get filled as soon as they reach the bottom of the shoe, mainly due to gravity so as the name gravity feeder. After the die filling, the powder within these dies is compacted to yield tablets. The compaction process is neither displayed nor modeled here. This whole process is called tableting. The die filling

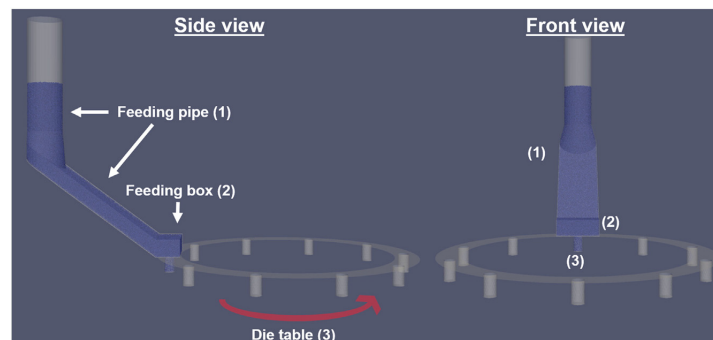


Fig. 1. Computational setup of the open feeder in a rotary tablet press filled with mono-disperse particles of 1 mm diameter (blue color). (Left) Side view with the cylindrical and inclined feeding pipe (1), the rectangular feeding box (2) and die table with 10 dies (3). (Right) Front view. (For interpretation of the references to color in this figure legend, the reader is referred to the web version of this article.)

unit consists of a feeding pipe, a shoe and a die table with 10 cylindrical shaped dies, see Fig. 1, and the blue region in this figure indicates the powder bed. The feeding pipe consists of two parts (1) a cylinder with 3 cm diameter and 10 cm height, and (2) a rectangular inclined part which has an angle of 45° with the horizontal axis and length of 10.6 cm. The inclined part of the feeding pipe is connected to the shoe with the dimensions of length, width and height 4, 2 and 1.5 cm, respectively. The shoe acts as a powder storage unit before it is discharged into the dies. Each die is a cylinder which has a height of 1.5 cm and a diameter of 0.9 cm unless otherwise specified, and the die table which holds the dies is a circular plate with a diameter of 10 cm. All these geometries were constructed with the open source finite element mesh tool known as Gmsh [28], and later imported to LIGGGHTS as physical boundaries to powder flow.

2.3. Material properties and process conditions

All the numerical simulations presented in this study correspond to mono-disperse granules having a particle diameter of 1 mm and a density of 1.6 g/cm^3 . The different material properties of these granules considered in DEM simulations are listed in Table 1, which are within the range of corresponding data reported in literature [13,19,29,30]. The parameters which are varied extensively to investigate their influence on powder flow are coefficient of friction (particle-particle and particle-wall), restitution coefficient (particle-particle and particle-wall), and

cohesion energy density. The latter quantity is a measure of cohesion between the particles and has units of J/m^3 , see Table 1.

The process conditions which are varied include die table speed and die diameter. The values considered in these two parameters are given in Table 2, which are within the range of general tableting machine operating conditions. The different numerical setups generated through variation of the material and process conditions are described in the next section.

2.4. Initialization and numerical setups

Similar to the tableting unit operation, described in Section 2.2, at first the particles are filled into the feeding system without discharging them to the dies. The time step considered in all the calculations is $0.5 \mu\text{s}$, which is well below the Rayleigh- and Hertz-time [24,31].

The particles filling is done through a step-by-step procedure where around 20,000 to 40,000 particles are inserted randomly for every 2 s into the feeding pipe, and were allowed to settle before the next set of particles are inserted. By this way, around 130,000 mono-disperse particles are filled in a total time of 9 s. The status of the particles after filling and settling under gravity in the gravity feeder is visualized in Fig. 1. During the whole filling process the temporal development of mass holdup in the shoe is calculated and reaches a constant value of 11.2 g within 2 s of insertion, however the discharge of powder only starts after 9 s during which the whole feeder system gets filled to attain a total mass of 128 g.

Following the filling and settling, the die table is rotated at a constant speed to enable the die filling process. During the die filling, particles are added to the feeding pipe at a rate approximately equal to the rate of particles leaving the simulation domain due to filled dies. In this way, the filling level in the feeding pipe is kept constant to ensure a constant normal force acting on the particles. In reality, several tablets are discarded at the beginning of the tableting process due to several reasons. These include (1) lubrication of the moving parts such as punches,



Fig. 2. Pictures of Rotab T (left) and Pressima AX (right). Top: Complete tablet press illustration. Bottom: Open feeder.

Table 1
DEM parameters.

Parameter	Property of	Value
Young's modulus (GPa)	Particle	8.7
	Wall	210
Poisson's ratio (–)	Particle	0.3
	Wall	0.35
Coefficient of friction (–)	Particle-particle contact (μ_{PP})	0.35–0.9
	Particle-wall contact (μ_{PW})	0.3–0.9
Coefficient of restitution (–)	Particle-particle contact (e_{PP})	0.15–0.3
	Particle-wall contact (e_{PW})	0.15–0.3
Cohesion energy density (CED) (MJ/m^3)	Particle	0–3.0

Table 2
Process parameters.

Parameter	Value
Die table speed (rpm)	20, 30 and 40
Die diameter (mm)	6, 9 and 12

and (2) machine settings adjustment to produce tablets as per the specifications such as weight, hardness etc. Additionally, the machine vibrations could also influence the tableting process [2,4,7,32,33]. However, this study focuses mainly on the die filling process alone to get a detailed understanding on the development of flow pattern within the feeder during the initial tableting time before a steady flow is achieved and on identifying the process and material attributes that would influence in establishing a steady flow. With this objective, for a given die table speed in total 70 dies are filled which corresponds to 7 complete rotations of the die table, after which the simulation is stopped. This corresponds to a physical tableting time of 21 s, 14 s, and 10.5 s for 20 rpm, 30 rpm, and 40 rpm die table speed, respectively.

The filled dies are analyzed over the complete discharge time and the corresponding mean tablet mass and relative standard deviation (RSD) are calculated. In parallel, the particle mass remaining in the shoe as the dies are filled is computed. Similarly, the rate at which the dies are filled or in other words mass flow rate, explicitly for the 10th die is also analyzed and it corresponds to time points of 2.89, 1.92 and 1.45 s for 20, 30 and 40 rpm, respectively. Moreover, the box was split into four equally sized zones, and the particles in these zones are colored to visualize the particles' movement and their rearrangement within the shoe.

The numerical simulations are performed with different process conditions (Table 2) and the material characteristics are given in Table 1. In order to gain clear understanding towards the impact of each and every parameter on the powder flow within the gravity feeder, different numerical setups are created by altering one parameter at a time, and additional setups where two-parameters are changed at once. An overview of all these simulation setups is given in Table 3. The first setup is referred as the *basic setup* throughout the reminder sections, corresponding to a die table speed of 20 rpm and a die diameter of 9 mm. The material properties such as cohesion between the particles, the coefficients of friction and coefficients of restitution are at a minimum value compared to all other setups, see Table 3. The

differences among these setups and their influence on powder flow is analyzed extensively and they are described in the next section.

In addition to the single parameter influence on the flowability metrics, the interaction effects of process conditions and material properties are also evaluated. This interaction effects calculation is performed by choosing a 2^2 full factorial design in which the categorical factors of the lowest and highest chosen value are assigned to coded values of -1 and $+1$, respectively. Such coded value assignment procedure is well described, and for more details refer to Leardi [34], Andersson [35], and Kleppmann [36]. Following these works, in this study the process condition is referred to as A, the material property as B, and the interaction between process condition and material property as AB, respectively, see Table 4. The interaction is coded by multiplying the coded values of column A with column B.

Main factor effects (A or B) and interaction effects (AB) are computed as follows: at first the sum of the row product of the coded value with the response (X_i) is evaluated, followed by computing its mean of absolute values. Higher values are considered as major effects.

3. Results and discussion

The simulations are performed to evaluate the influence of (a) process conditions, and (b) material properties of a given formulation on the powder flow from a gravity feeder, commonly known as open feeder, to the dies of a lab scale rotary tablet press. The process conditions investigated are (1) the die table speed, and (2) the die diameter. The results analyzed include the total mass in dies which corresponds to tablet mass, the flow rate into the dies, the variation of mass holdup with time as well as the particle flow pattern within the feeding box.

To understand the basic process of die filling within a rotary tablet press the results are elaborated for the 20 rpm die table speed with a die diameter of 9 mm. The respective material properties are given in Table 3, setup number 1. This numerical configuration is considered as the *basic setup* whereas all other setups are generated by changing one single parameter either material property or process condition to capture its effect on the die filling process as described in Section 2.4. All these numerical cases are given in Table 3. The results corresponding to the basic setup (setup no. 1, Table 3) are explained in the next section whereas the effect of process conditions and material properties are given in the following sections, respectively.

Table 3
Simulation setups showing different process conditions and formulation properties.

Setup number	Process conditions		Material characteristics				Changed parameter	
	Die table speed/rpm	Die dia-meter/mm	CED/MJ/m ³	Coefficient of friction		Coefficient of restitution		
				$\mu_{pp}/-$	$\mu_{pw}/-$	$e_{pp}/-$		$e_{pw}/-$
1	20	9	0.0	0.35	0.3	0.15	0.15	–
2	30	9	0.0	0.35	0.3	0.15	0.15	Die table speed
3	40	9	0.0	0.35	0.3	0.15	0.15	Die table speed
4	40	6	0.0	0.35	0.3	0.15	0.15	Die diameter
5	40	12	0.0	0.35	0.3	0.15	0.15	Die diameter
6	20	9	1.5	0.35	0.3	0.15	0.15	CED
7	20	9	3.0	0.35	0.3	0.15	0.15	CED
8	20	9	0.0	0.70	0.3	0.15	0.15	μ_{pp}
9	20	9	0.0	0.90	0.3	0.15	0.15	μ_{pp}
10	20	9	0.0	0.35	0.6	0.15	0.15	μ_{pw}
11	20	9	0.0	0.35	0.9	0.15	0.15	μ_{pw}
12	20	9	0.0	0.70	0.6	0.15	0.15	μ_{pp} and μ_{pw}
13	40	9	0.0	0.35	0.3	0.30	0.15	e_{pp}
14	40	9	0.0	0.35	0.3	0.15	0.30	e_{pw}
15	40	9	0.0	0.35	0.3	0.30	0.30	e_{pp} and e_{pw}
16	40	9	1.5	0.35	0.3	0.15	0.15	Die table speed and CED
17	40	9	3.0	0.35	0.3	0.15	0.15	Die table speed and CED, die diameter and CED
18	40	6	3.0	0.35	0.3	0.15	0.15	Die diameter and CED
19	40	12	3.0	0.35	0.3	0.15	0.15	Die diameter and CED

Table 4
Full factorial design matrix (2^2) of process conditions (A) and material properties (B).

A	B	AB	Response
-1	-1	+1	X_1
-1	+1	-1	X_2
+1	-1	-1	X_3
+1	+1	+1	X_4

3.1. Die filling process description

3.1.1. Particle flow pattern within the shoe and the die

In Fig. 3, the typical powder flow during the die filling in the basic configuration (setup 1, see Table 3) is exemplarily shown for the 10th die out of 70 filled dies. The die table consisting of 10 dies moves with a constant rotational speed of 20 rpm in the anti-clockwise direction, whereby each die spends about 0.23 s underneath the feeding box. The particles shown in Fig. 3 are colored according to their velocity where red colored particles move with the highest velocity (>3 cm/s) and the blue colored ones remain stationary. As soon as the die opening enters the bottom of the shoe the powder starts to slowly enter the die mainly due to gravity and it accelerates with time. Within 0.1 s more than half of the die volume is filled and after 0.15 s the die is completely filled, see Fig. 3. During the filling process, the top right corner of the box (the portion of the shoe in which particles move with highest velocity) is getting emptied, which implies that the powder filled into the die is mostly composed of the particles that lie within the right hand side of the shoe. Simultaneously, the particles in the inclined chute above the shoe move slowly to refill the empty space within the shoe which is more prevalent in the right side as indicated by the particles velocity in Fig. 3. The particles in the left side of the shoe remain mostly stagnant throughout the die filling process. Also, the particle rearrangement pattern shown in Fig. 6 (Section 3.1.4) further strengthens this observation. This confinement of particles on one side of the shoe and empty space on the other side may lead to segregation within the feeding system in case of non-cohesive free flowing poly-disperse powders [37,38]. Most of the particles in the shoe are stationary as seen by their velocity magnitude whereas the particles in the bottom part of the shoe are moving at about 20 cm/s which is equivalent to the die table speed of 20 rpm.

3.1.2. Tablet mass and mass holdup in the feeding box

Fig. 4 shows the mass collected in the dies (or tablet mass) for the basic numerical configuration (setup 1, Table 3). The mean tablet mass is 834 mg with a standard deviation of 4.8 mg. It is apparent that the tablet mass fluctuates around this mean within the range of two

standard deviations excluding one value. This mean and fluctuations are significantly influenced by the material and process conditions as explained in the Sections 3.2–3.4. This result indicates that with the selected process and material attributes (setup 1, Table 3) a constant tablet mass will be achieved and will remain constant throughout the whole process.

In parallel, the variation in mass holdup of the feeding box throughout the die filling process is shown in Fig. 5 which corresponds to 21 s of tableting with 20 rpm die table speed. Before the die filling begins the feeding box is completely filled (see also Fig. 1) and contains a maximum mass holdup of about 11.3 g. When the die filling process begins the mass holdup starts to decrease as the particles leave the feeding box. The mass decreases by almost 10% until the 5th die (1.39 s) is filled and then increases again up to a constant level from about die 10 (2.89 s) on. Eventually, the mass in the feeding box is ranging within a constant zone having a void volume of around 5% compared to the initial filling level. The results indicate that there is always a decreasing followed by an increasing trend in the mass holdup which corresponds to the mass flow rate into the dies and particles entering the shoe to refill the void space from the feeding pipe, respectively. This trend implies that even though the particles enter the shoe continuously to fill its void space, the rate at which particles are drawn to fill the dies is higher than the rate they enter the shoe from the connecting pipe or feeding hopper, so there is always a wave like behavior in mass holdup. This void volume helps in particle rearrangement within the box which could give rise to segregation within the whole feeding system in case of non-cohesive, free flowing particles having poly-dispersity in size [37,38].

Moreover, this analysis points out that in order to distinguish the time at which equilibrium has been achieved in the die filling process, it is not sufficient to evaluate the mass in the dies alone but also an analysis of mass holdup within the feeding box is recommended.

3.1.3. Mass flow rate into the dies

Besides the mass which is collected in the die and the mass holdup in the feeding box, the mass flow rate into the dies is also an important parameter for tableting. The mass collected in the die with time for the 10th die with basic configuration is shown in Fig. 9 (see blue line, refer to Section 3.3.1). The graph indicates that the powder starts to fill the die slowly, then accelerates with time and steadies up to 0.15 s. Within this time period, the die gets almost filled, confer Fig. 3, due to which the mass flow rate starts to decelerate. An estimate of mass flow rate is computed following the linear zone of the mass discharge period. Even though the mass flow rate of the basic setup is as high as 6400 mg/s, only about 834 mg of powder is collected in the die since the die volume is already completely filled before it leaves the shoe.

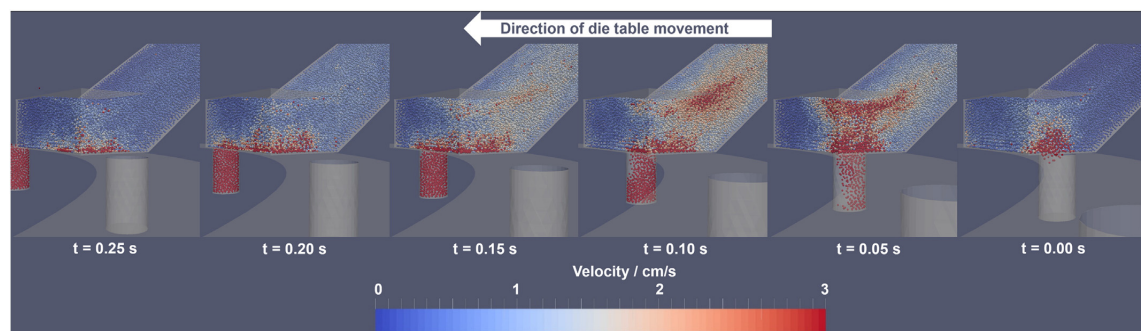


Fig. 3. Particle discharge from the feeding box into the 10th die. The die table moves with a constant rotational speed of 20 rpm in the anti-clockwise direction (indicated by the arrow). Particles are colored according to their velocity (red >3 cm/s and blue 0 cm/s). The interval between each image is 0.05 s. (For interpretation of the references to color in this figure legend, the reader is referred to the web version of this article.)

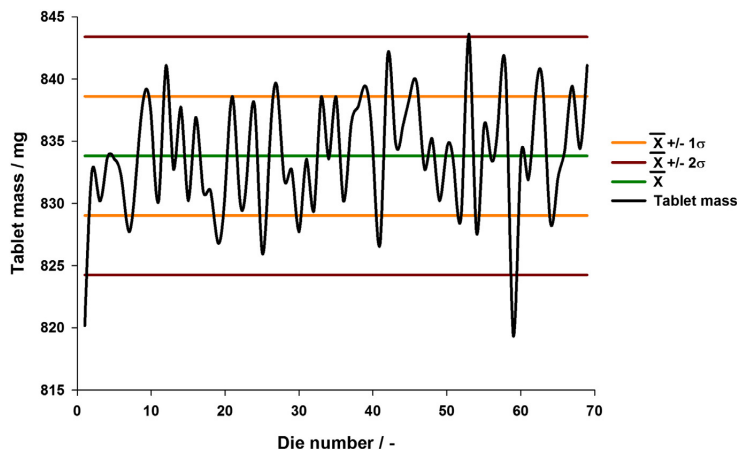


Fig. 4. Tablet mass obtained in the basic configuration for 70 filled dies. Lines indicate the mean, and one and twofold standard deviations.

3.1.4. Particle rearrangement in the feeding box

To find out how the particles move and rearrange within the feeding box as they discharge, the shoe is divided into four equal sized zones across its length. Each section has the dimensions of $1\text{ cm} \times 2\text{ cm} \times 1.5\text{ cm}$. The particles in these four sections are assigned four different colors (light blue, white, orange and red), refer to Fig. 6 (die no. 1) and the freshly added particles from the feeding pipe are represented by dark blue color. An illustration of these colored particles in the feeding box after the first, fifth, tenth, and seventieth dies have been filled is given in Fig. 6, where the left side images are the front view and right side ones correspond to the top view. Accordingly, the ratio of different colored particles filled into the first 10 dies for the basic configuration is shown in Fig. 11 (see zero cohesion case, refer to Section 3.3.1). As the die enters the feeding box from the right hand side (red zone), initially the red colored particles are found to be highest in proportion within the die. This corresponds to the powder state in the feeding box which shows that the particles filled in the die stems from the right hand side of the box and there is void space developing on this side of the shoe, see Figs. 3 and 6. Due to this empty space on the top right hand side of the box (Fig. 6 (front view)), immediate neighbor particles i.e., orange colored particles start to cross over to the initially red zone followed by the grey colored particles (see Fig. 6 (front view),

die 10) causing an inter mixing in the feeding box. The amount of orange colored particles in the die starts with 37% in die 1 and contributes only 9% in die 10 (Fig. 11 (zero cohesion case), Section 3.3.1). With time, the proportion of newly added particles represented by the dark blue color increases and shows an inflection point between dies 5 and 6 with a contribution of 88% in the 10th die (Fig. 11 (zero cohesion case), Section 3.3.1). The steadily slightly decreasing trend of red, orange, white and light blue colored particles and the steadily increasing trend of dark blue particles starts after 6th die and this observation is also supported by data from the mass holdup shown in Fig. 5 displaying an equilibrium is almost reached after die 6. This means under equilibrium, the new particles roll directly from the feeding pipe to the back-side of the feeding box from where they enter the dies whereas 'old' particles remain in the front portion of the feeding box, shown in the right bottom side of the shoe in Fig. 6 (top view). Moreover, the colored particles state in the shoe shown after the seventieth die filling reveals that the particles which remain in the left front corner (Fig. 6 (front view)) of the feeding box remain there during the whole process and may consolidate over time. Also, the proportion of "old particles" in the shoe with time decreases, more rapidly during the first 10 dies filling and slowly afterwards, i.e., the percentage of old particles in the shoe is about 43% and 24% after 10 and 70 dies filling, respectively. This means that the particle rearrangement and colored particles ratio in the die after the first 10 dies would stay more or less unchanged throughout the tableting, so in the next sections this color pattern analysis is only carried out for the first 10 dies. This coloring study in the feeder helps to determine the die number at which a steady flow can be obtained and to estimate how long particles from the initial filling remain in the shoe through the flow pattern.

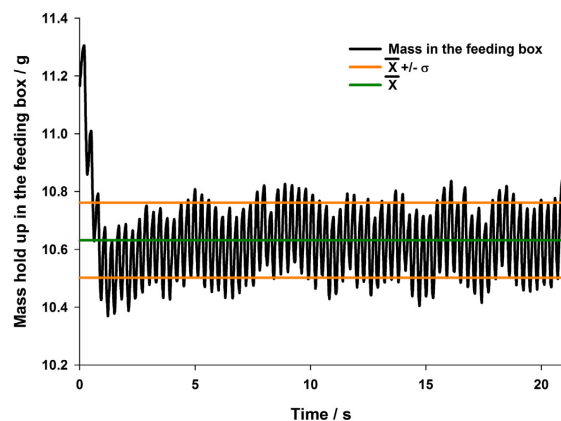


Fig. 5. Mass holdup obtained in the feeding box in the basic configuration over the complete discharge time (21 s). Lines indicate the mean and standard deviation.

3.2. Influence of process conditions

Process conditions considered in this study include die table speed and die diameter. Different numerical setups were configured by varying these conditions (each at a time). The different values of die table speeds and die diameters investigated in comparison to the basic configuration are given in Table 3, see setup no. 2 to 5. In the following sections, the effects of these process conditions on each and every parameter of flowability metrics mentioned previously are elaborated.

3.2.1. Die table speed

The first studied parameter is the die table speed which mainly influences the acceleration and outcome of the tableting unit operation.

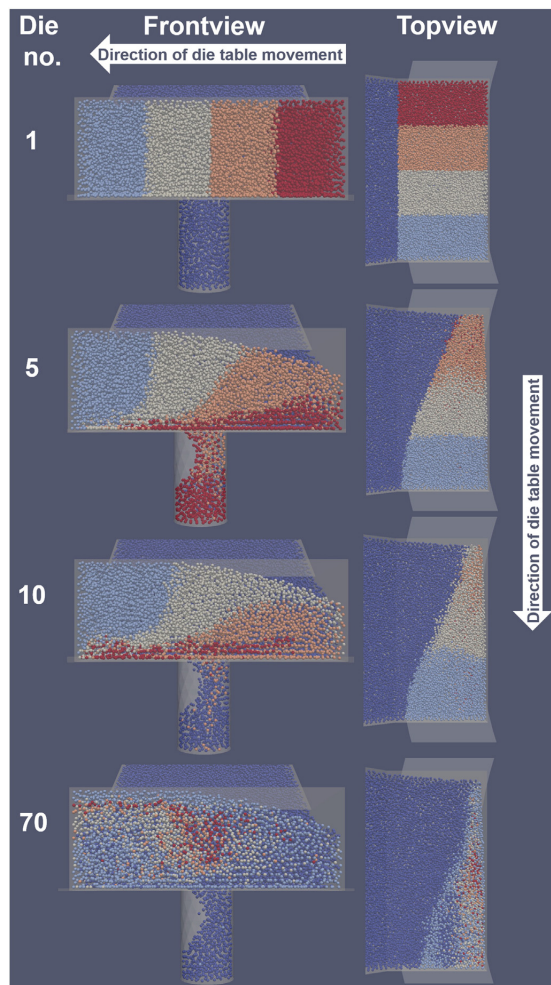


Fig. 6. Particle rearrangement in the feeding box visualized by initial coloring of the particles (die no. 1) The front view (left) and top view (right) of the shoe after filling the 1st, 5th, 10th, and 70th die.

The particle characteristics were the same as in the basic setup (see Table 3) but the die table speed was varied from 20 rpm (basic setup, 1) to 30 rpm (setup no. 2) and 40 rpm (setup no. 3). An increased turret speed leads to a decreased final tablet mass from 834 mg to 666 mg and 474 mg with 20 rpm, 30 rpm and 40 rpm, respectively. With increased speed the die dwells shorter time under the shoe implying that the particles have less time to discharge into the die. Each die spends only 0.15 s with 30 rpm and 0.1 s with 40 rpm underneath the shoe. Furthermore, the RSD of the tablet mass is 0.6%, 1.5% and 1.6% with 20 rpm, 30 rpm and 40 rpm, respectively, indicating that the RSD is three-fold higher for faster die table speeds (30 and 40 rpm) compared to 20 rpm. This fluctuation may be due to the incompletely filled dies with higher speeds. The results also indicate that increasing the die table speed decreases the mass flow rate. The mass flow rate with 30 rpm die table speed corresponds to approximately 84% of the mass flow rate observed with 20 rpm and similarly with 40 rpm it corresponds to 81% relative to 20 rpm. This is due to the decreased die dwell time under the shoe.

Similar to the basic setup the particle motion and rearrangement within the feeding box and the variation of the ratio of colored particles in the dies is evaluated. The results indicate that the die table rotational speed influences the particle flow pattern in the shoe. With increased speed, the colored particles in the shoe reveal that intermixing is delayed. However the ratio of the colored particles in the dies shows similar results which indicate that the inflection point of the newly added particles (dark blue particles) is observed at a later time with increased die table speed. The dark blue color particles start to increase after die 6 for 30 rpm and after die 8 for 40 rpm whereas with 20 rpm the same occurs after die 5. The inflection point is shifted to a higher number of dies which is due to the less discharged mass per die for faster die table speeds but can be generally observed at a total discharged mass of 4.6 g in all setups irrespective of die table speed. On the other hand, colored particles ratio in the dies indicates that the contribution of particles from the left side of shoe (light blue color) is quite insignificant with increased die table speed. This shows that the powder consolidation in this part of the shoe still exists and it is not influenced by the die table speed which can be confirmed by the mass holdup in the shoe.

The temporal development of the mass holdup in the shoe is shown in Fig. 7 for the three die table speeds. The results show that there is a fluctuation or oscillating behavior as explained in Section 3.1.2 (Fig. 5). This fluctuation/wave behavior is greater in case of slower die table speed, i.e. with 20 rpm the mean mass holdup is 10.63 mg with RSD of 1.22% whereas with 30 and 40 rpm this corresponds to $10.66 \pm 1.05\%$ and $10.66 \pm 1.00\%$, respectively. The lower the die table speed, the more the particles are drawn to fill the die. This leads to more void space in the shoe that could potentially be filled with the new particles, thereby yielding a higher RSD in mass holdup for lower die table speed. The interval between the peaks is shorter for higher die table speed since the die spends less time underneath the shoe.

Such a simulation setup shows that incompletely filled dies, which is the case for higher die table speeds, will cause significantly higher fluctuations in the tablet mass thereby potentially increasing the challenges in meeting the specifications of mass variation.

3.2.2. Die diameter

Another process parameter analyzed in this study is the die diameter which is varied from 6 mm to 9 mm and to 12 mm. The die table speed is kept constant at 40 rpm and the material attributes are considered the same in all three setups to evaluate the effect of the die diameter on different flowability metrics. The setup numbers for these configurations include 4, 3 and 5 for 6 mm, 9 mm and 12 mm respectively, see Table 3.

The mean tablet mass of 70 filled dies with the die diameter of 6 mm, 9 mm and 12 mm is 174 mg, 474 mg and 968 mg, respectively. The

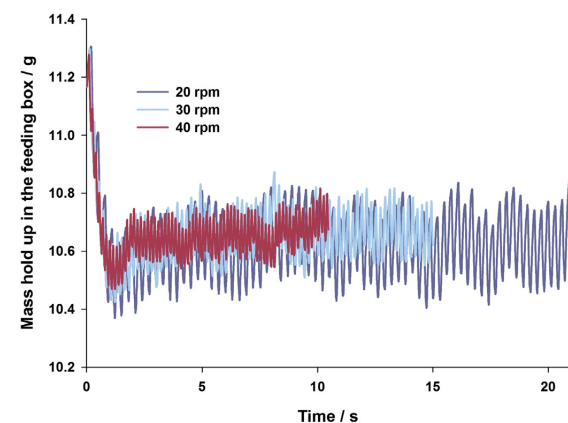


Fig. 7. Mass holdup in the feeding box for 20 rpm, 30 rpm, and 40 rpm die table speeds.

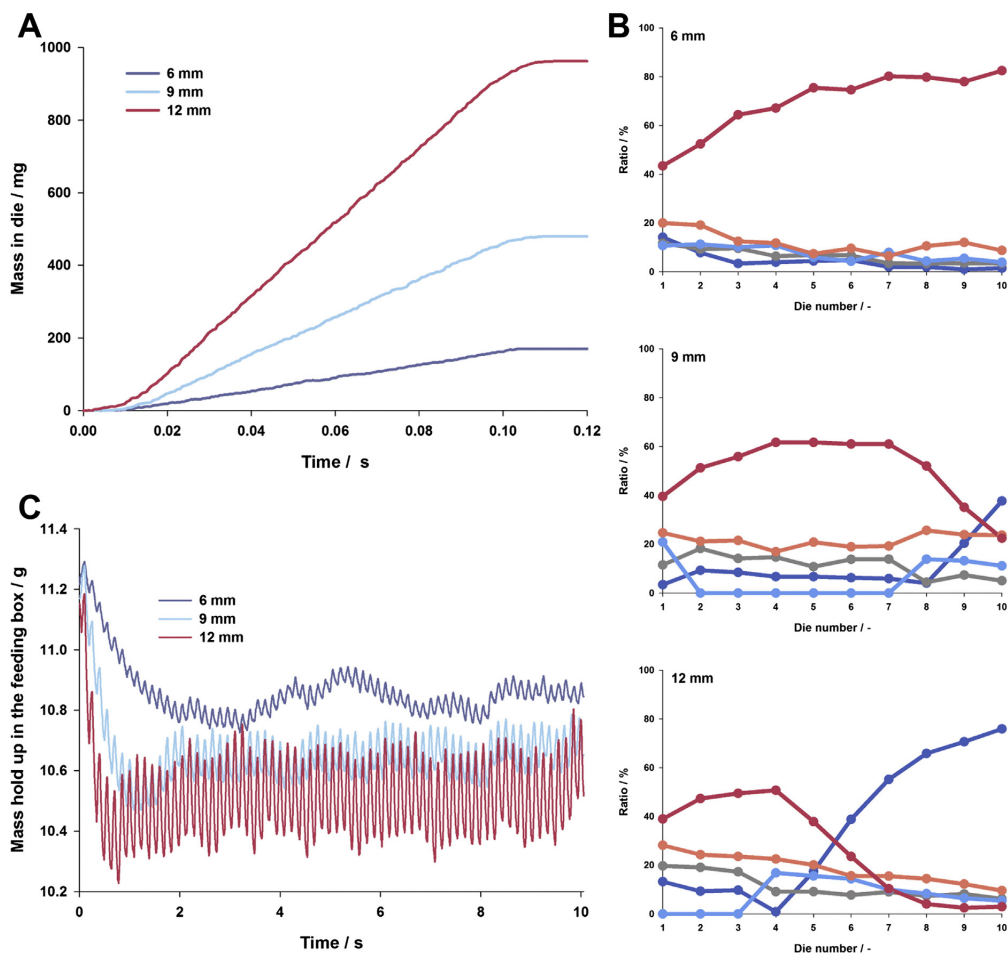


Fig. 8. (A) Mass collected in the die no. 10 with time for the die diameters of 6 mm, 9 mm, and 12 mm; (B) Distribution of the colored particles in the first 10 dies for 6 mm, 9 mm, and 12 mm die diameters as per their initial coloring within the feeding box; (C) Mass holdup in the feeding box for 6 mm, 9 mm, and 12 mm die diameters.

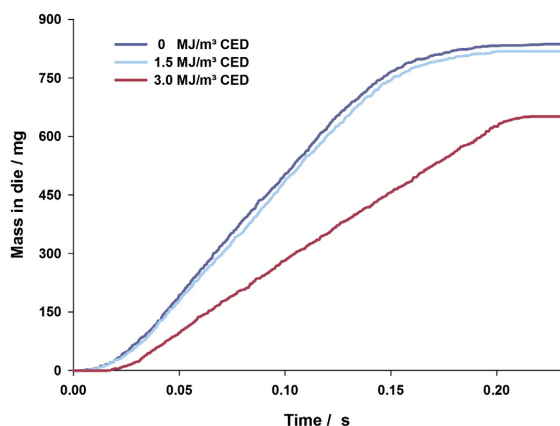


Fig. 9. Mass collected in die no. 10 with time for 0 MJ/m³, 1.5 MJ/m³, and 3.0 MJ/m³ cohesion energy densities.

increase in the die diameter leads to an increase in the die volume, i.e. the die volume rises approximately by 44% when the diameter is enlarged from 6 mm to 9 mm and similarly increases by 56% when the diameter is changed from 9 mm to 12 mm, respectively. This augmented die volume causes an increased tablet mass. On the other hand, the RSD of the tablet mass for 70 filled dies for 6 mm, 9 mm and 12 mm die diameters is 3.3%, 1.6% and 0.9%, respectively. This indicates that with smaller die diameter not only less particles are collected but its variation also rises, i.e., the RSD is increased by about 3.7 fold for the 6 mm diameter compared to the 12 mm.

Moreover, with increased die diameter the mass flow rate is also found to be higher as shown in Fig. 8 (A). As the die cross section increases with larger diameter more particles can enter the die and hence a higher mass flow rate can be observed, i.e. mass flow rate increases by approximately 37% when the die diameter is increased from 6 mm to 9 mm and by 49% for the increase from 9 mm to 12 mm.

The temporal development of colored particles proportion filled into dies for the first 10 dies is shown in Fig. 8 (B) for the three die diameter conditions. The comparison of these profiles shows that there is a significant difference which can be attributed to the unequal discharged mass for these three die diameters. Due to the higher rotational speed, the particles in the shoe move along with the die plate thereby causing

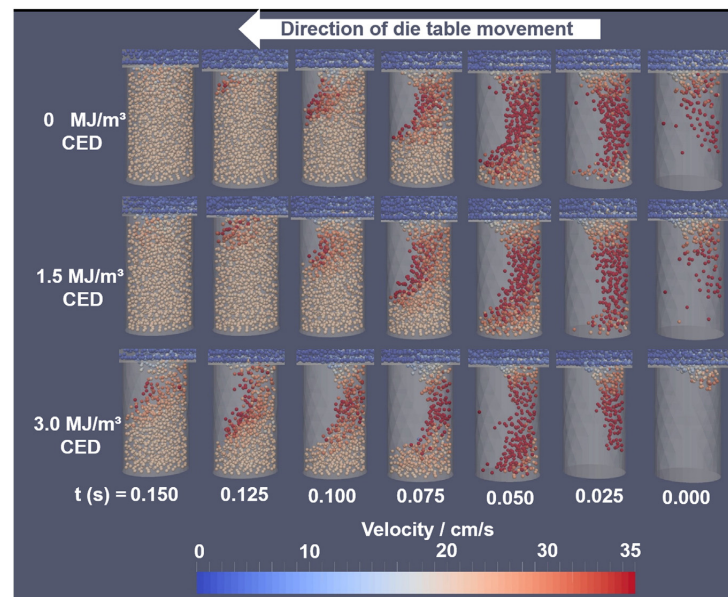


Fig. 10. Particles' velocities and their filling pattern for the 10th die under 0 MJ/m^3 , 1.5 MJ/m^3 , and 3.0 MJ/m^3 cohesion energy densities.

the red particles to spread all over the shoe bottom. This effect is more pronounced for the lower die diameter which requires less amount of particles to fill the die, which explains the increasing proportion of red particles with 6 mm die diameter. A similar trend is observed with 9 mm die diameter which shows a decreasing amount in red particles proportion after the 7th die whereas in case of 12 mm diameter more number of particles are discharged leading to less increase in red particles proportion and earlier observation of decreasing red particles proportion in the dies after the 4th die (see Fig. 8 (B)). This observation is also supported by the temporal development of the mass holdup which is shown in Fig. 8 (C) for the three die diameters. A higher die diameter causes a significantly higher amount of powder discharged from the shoe thereby causing an increased void volume in the shoe. The void space is 5.7% for 12 mm in comparison to initial filled state and it is 4.5% for 9 mm and 2.7% for 6 mm die diameter. The mass holdup profile has the similar trend of decreasing followed by increasing or in other words fluctuation as seen in case of different die table speeds (confer Fig. 7). This fluctuation tends to increase with increased die diameter, see Fig. 8 (C), which is in agreement with the total mass discharged and mass flow rate.

Hence, it is noticed that a small die diameter to produce tablets with a very low weight may bear the drawback of a high standard deviation in the tablet mass which can cause regulatory issues.

3.3. Influence of material properties

The final blend properties of solid formulations depend on the characteristics of the APIs as well as the excipients. Most of the APIs show highly cohesive behavior and the formulation properties are significantly influenced by the API proportion in the final blend. In this study the effect of three different materials characteristics on the flow behavior is investigated. In the following sub-sections the properties considered are briefly defined to give a clear picture of their physical meaning and then their influence on the powder flow properties and quality attributes in the gravity feeder are elaborated. This is the first time such a detailed investigation of the effect of material characteristics on powder flow in a gravity feeder is carried out. The results could serve as a

reference to elucidate the impact of material properties on the powder flow in tableting.

3.3.1. Cohesion

The most important material characteristic grouped into the non-contact forces is the cohesion which may affect the packing fraction and flow behavior of particles significantly. In the past and even to date, the flow characteristics of powders are often evaluated by empirical indexes such as Hausner ratio, Carr's index, angle of repose etc. [22, 39,40]. The non-contact forces involve a combination of three fundamental forces, namely, (1) the van der Waals attraction, (2) the capillary force and (3) the electrostatic force. These forces can act concurrently or successively to different extents [41]. In the recent development of DEM, these forces can be combined into one force term called cohesion and represented by a single quantity known as cohesion energy density (CED) [18,19]. From a computational point of view, the CED enters as a contribution to the normal force. If two particles are in contact, the CED adds an additional normal force tending to maintain the contact [24]. In this numerical study, the CED is computed following the simplified JKR (Johnson, Kendall and Roberts) model [27] which was developed to improve the classical Hertz contact theory [22]. The JKR model recognizes that both the tensile and compressive interactions contribute to the total contact radius, and more details of this model can be found in [22,27].

The influence of the CED between the particles is captured by selecting zero cohesion or no attractive forces, see setup 1, and two different values of cohesion energy densities which are 1.5 MJ/m^3 (setup 6) and 3.0 MJ/m^3 (setup 7) for a constant die table speed of 20 rpm (Table 3). The values of CED chosen here are based on the in-house DEM input parameters calibration data for several powders which consists of two steps. At first, powder properties like angle of repose, flowability, bulk density etc. are measured as per the standard measurement procedure of Ph. Eur. [42]. In the second step, these measured properties are reproduced by changing the DEM input parameters through simulations. The mean tablet mass of all 70 dies filled for the three setups is evaluated, which shows that in comparison to zero cohesion, there is only little difference in the total mass collected within the

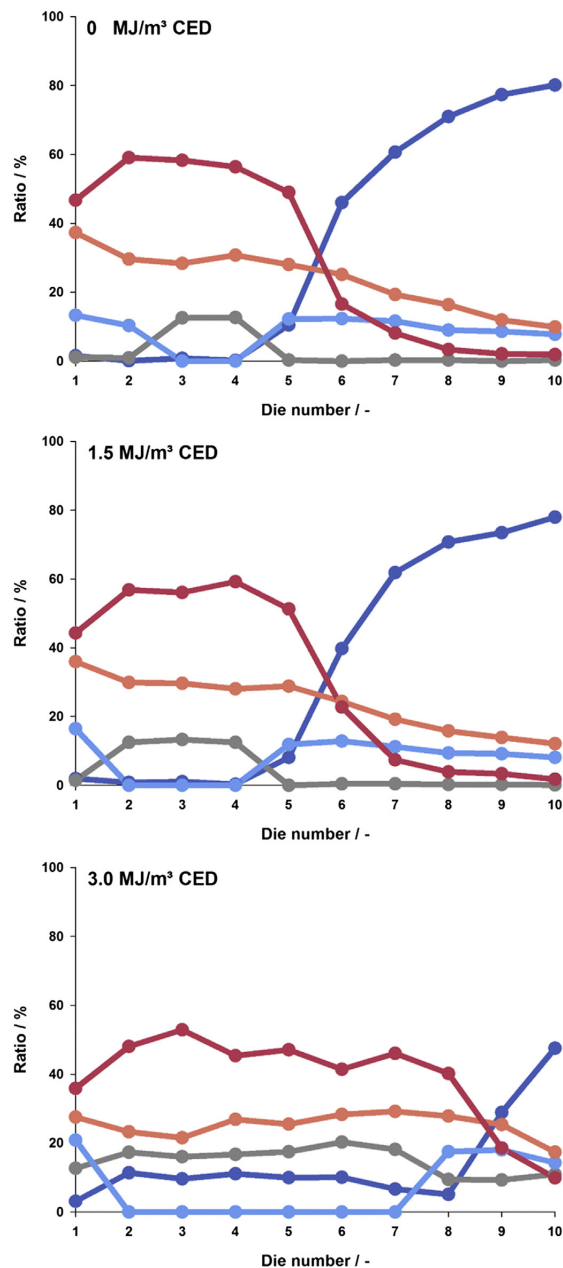


Fig. 11. Distribution of the colored particles in the first 10 dies for cohesion energy densities of 0 MJ/m^3 , 1.5 MJ/m^3 , and 3.0 MJ/m^3 as per their initial coloring within the feeding box.

dies in case of low CED (1.5 MJ/m^3) (834 mg vs 828 mg). However, when the CED is increased by two-fold (3.0 MJ/m^3) the dies are incompletely filled so the final mass in the die is 22% lower than with zero cohesion (651 mg). This can be attributed to the lower mass flow rate which is shown in Fig. 9. The flow rate in case of higher cohesion is 40% less than the zero cohesion case. Also, with higher cohesion, the RSD of the tablet mass is increased to 2.4% which is 0.6% in case of

zero cohesion. The lowering of flow rate is induced by the cohesion and the normal force acting on the bottom of the box. The average of the total force acting on the bottom of the box is about 0.134 N and 0.109 N in case of no cohesion (0 MJ/m^3) and high cohesion (3 MJ/m^3), respectively. This measure of the total force is influenced by (1) mass holdup in the shoe, and (2) particle motion (velocity). Though the difference in mass holdup between the zero cohesion (10.6 g) and high cohesion (9.3 g) is about 12% but the velocity difference is higher as the particles are less mobile due to cohesion. This leads to a higher difference in total force acting on the bottom of the box, which corresponds to about 19%. Less force at the bottom of the box explains the observation of less mass flow rate.

The visualization of the die filling in all three cases is depicted in Fig. 10. The coloring in this figure is done based on the particles' velocities. The temporal development of the particle discharge visualizes that with increased cohesion the particles fall into the die more as clumps or aggregates (see Fig. 10 for $\text{CED} = 3.0 \text{ MJ/m}^3$ at $t = 0.025 \text{ s}$) than as individual particles which is observed in case of zero cohesion. The comparison of zero or low cohesion case with that of higher cohesion shows that dies are incompletely filled with increased cohesion due to the enhanced attractive interparticle force. This hampers the free particle flow into the die, and moreover leads to increase in fluctuation of the total tablet mass.

A previous study about the powder flow in a force feeder of a lab-scale tableting machine, which is quite different from the current study also showed a similar trend [18], where reduced fill weights and an increased weight variability for increased cohesion is reported [18].

The proportion of colored particles in the die which indicates their origin from the shoe is shown in Fig. 11 for all three setups. The ratio pattern looks similar for zero and lower cohesion ($\text{CED} = 0$ and 1.50 MJ/m^3) along with the inflection point of newly added particles which is consistent with the above observations. However, under higher cohesion ($\text{CED} = 3.0 \text{ MJ/m}^3$) the ratio is quite different than the lower cohesion cases. The comparison shows that with increased cohesion there is not only less amount of freshly added particles in the die but also there is no change in the amount of red/orange/grey/light blue color particles, which start to decrease at a later time point than the lower cohesion cases. The proportion of freshly added particles represented by dark blue color starts to rise after the 5th die in case of zero and low cohesion whereas with higher CED the same happens only after the 8th die, see Fig. 11, as the particles' motion from the chute as well as in the shoe is hampered due to the increased attractive interparticle forces. The variation of the mass holdup in the shoe with time also showed similar trend found in the above results.

In conclusion, the non-contact forces have a significant impact on the flow characteristics of a tablet formulation which should be evaluated prior to the tableting process.

3.3.2. Coefficient of friction

The next property on a particle level which has enormous influence on flowability is friction. Particularly, in the design of hoppers or bins friction is considered as a main parameter within the calculations among others. As it is hard to experimentally determine the friction between single particles, i.e. on the *microscopic* scale, it is typically measured as a bulk property or in other words *macroscopic* property using shear cells [43–45]. Several different measurements, both experimentally and numerically, have been performed so far to explore the link between microscopic and macroscopic friction relations [46–48]. On the *macroscopic* scale, the friction can be classified into two categories, namely, (1) *internal friction* which acts within a bulk material, and (2) *wall friction* which is present between a bulk powder and the wall of a processing equipment [49]. In contrast to these *macroscopic* friction parameters, the DEM requires the *microscopic* friction coefficients in contact force calculations. These micro-mechanical friction coefficients describe the Coulombic frictional characteristics between two bodies touching in binary contact [49]. They are differentiated into particle-

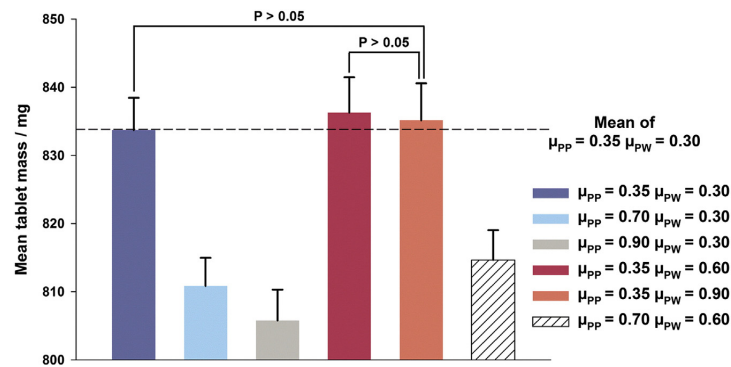


Fig. 12. Mean tablet mass over 70 filled dies for different particle-particle (μ_{PP}) and particle-wall (μ_{PW}) friction coefficients. Statistical analysis: One way ANOVA and Bonferroni's post t-test ($\alpha = 0.05$). Pairs having P values >0.05 are indicated.

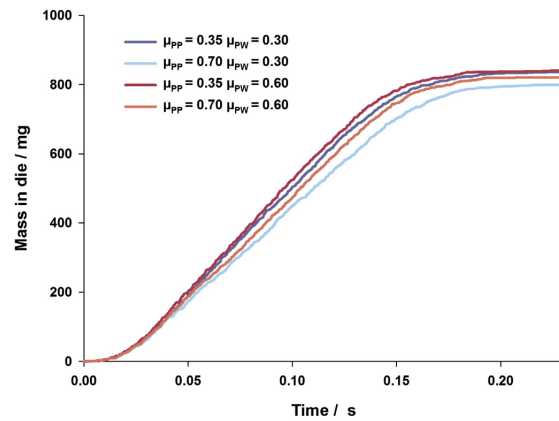


Fig. 13. Mass collected in die no. 10 with time for different particle-particle (μ_{PP}) and particle-wall (μ_{PW}) friction coefficients.

particle (μ_{PP}) and particle-wall (μ_{PW}) coefficient of friction similar to the macroscopic scale.

In this section, the effect of these two friction coefficients on powder flow is thoroughly studied by varying the values of friction from 0.35 to 0.9 in case of μ_{PP} and from 0.3 to 0.9 with respect to μ_{PW} . In total six configurations are set up, which include (1) low $\mu_{PP} = 0.35$ and low $\mu_{PW} = 0.30$ (setup 1), (2) medium $\mu_{PP} = 0.70$ and low $\mu_{PW} = 0.30$ (setup 8), (3) high $\mu_{PP} = 0.90$ and low $\mu_{PW} = 0.30$ (setup 9), (4) low $\mu_{PP} = 0.35$ and medium $\mu_{PW} = 0.60$ (setup 10), (5) low $\mu_{PP} = 0.35$ and high $\mu_{PW} = 0.90$ (setup 11), and (6) medium $\mu_{PP} = 0.70$ and medium $\mu_{PW} = 0.60$ (setup 12). In these configurations other attributes (material and process) remain the same, see Table 3. The first configuration is the basic setup and the results of this setup have been described in Section 3.1. The chosen friction coefficients are within the limits of reported literature and range between 0.1 and 1.0 [11,18,29,49].

The mean tablet mass of all the 70 filled dies along with the RSD is given in Fig. 12 for all these six configurations. A two-fold increase in μ_{PP} (0.70, light blue bar) under constant μ_{PW} leads to a decrease in mean tablet mass by about 2.8%. This can be attributed to the increase in resistance offered to the particle motion due to increased μ_{PP} , and it is also confirmed by the mass flow rate observed in the 10th die shown in Fig. 13. To estimate the significance of tablet mass decrease,

Table 5
One-way ANOVA test results (SEM = standard error of the mean, DF = degrees of freedom, SS = sum of squares, MS = mean squares, F = F statistic, P = P value).

Coefficient of friction		Color in the graph	N/-	Mean/g	Standard deviation/g	SEM
μ_{PP}	μ_{PW}					
0.35	0.30		68	833.7	4.7	0.575
0.70	0.30		68	810.9	4.1	0.498
0.90	0.30		68	805.8	4.5	0.551
0.35	0.60		68	836.3	5.2	0.629
0.35	0.90		68	835.1	5.4	0.659
0.70	0.60		68	814.7	4.4	0.530

Source of variation	DF	SS	MS	F	P
Between Groups	5	64777.4	12955.5	573.8	< 0.001
Residual	402	9077.1	22.6		
Total	407	73854.5			

a one-sided ANOVA test with Bonferroni's post *t*-test (significance level 0.05) is performed. The ANOVA test results along with the mean tablet mass and its standard deviation for all the six configurations are summarized in Table 5. The *P*-values (probability value) of <0.05 correspond to a statistical significant difference. The ANOVA test finds that the differences in the mean tablet mass among these six configurations is statistically significant, which is confirmed by the *P* value <0.001 (see Table 5). To identify the pairs which exhibit statistical difference among these six configurations, Bonferroni's post *t*-test is performed. As per this *t*-test, a decrease by 2.8% in mean tablet mass observed for two-fold increase in μ_{pp} (see light blue bar, Fig. 12) is found to be a statistically significant difference. The tendency of a significant decrease in tablet mass is observed in case of further increase in μ_{pp} (0.90, grey bar) which corresponds to about 3.4% in comparison to basic setup. This is mainly because particle motion hindrance due to increased μ_{pp} is compensated by the low die table speed (20 rpm) which allows the die to spend sufficient time underneath the shoe thereby small influence on the tablet mass is observed. The influence of a two-fold (0.60, red bar) and three-fold (0.90, orange bar) increase in μ_{pw} from the basic setup under constant μ_{pp} on mean tablet mass given in Fig. 12. The results indicate that there is a change in mean tablet mass which increases (by about 0.3%) for two-fold increase and then decreases for three-fold increase in μ_{pw} . However, there is a slight increase in RSD although very small (see Table 5). This slight increase and then decrease in mean tablet mass with increased μ_{pw} reveals that there is a certain maximum value of μ_{pw} beyond which there is no influence on the tablet mass how little it may be. It is also confirmed by the statistical significance test, which failed to identify any statistical significant difference in all the setups where μ_{pw} is changed as the computed *P* values are >0.05 except one setup. This exceptional setup corresponds to the configuration where μ_{pw} is increased by two-fold from the basic setup exhibiting a *P* value of 0.027, and it is the same setup in which a slight increase in mean tablet mass is observed (see red bar, Fig. 12). When the μ_{pw} and μ_{pp} are simultaneously increased by two-fold from the basic setup, the mean tablet mass decreases significantly (see dashed bar, Fig. 12), and this decrease is similar to the case where μ_{pp} is alone increased (see Fig. 12 and Table 5). The *t*-test also confirms that there is a statistical significant difference in mean tablet mass between the basic setup and the setup in which the μ_{pw} and μ_{pp} are simultaneously increased. The mass flow rate in to the 10th die under different friction coefficients is given in Fig. 13. A two-fold increase in μ_{pp} ($\mu_{pp} = 0.70$ and $\mu_{pw} = 0.30$, light blue) compared to the basic setup (dark blue) reduces the mean tablet mass by 2.8% (Fig. 12) whereas the mass flow rate is decreased by about 16% (see Fig. 13). The particle motion is hampered by the increase in μ_{pp} whereby the reduction of the flow rate is observed. Similarly, a two-fold increase in μ_{pw} ($\mu_{pp} = 0.35$ and $\mu_{pw} = 0.60$, red) from the basic setup indicates that it has no effect on the mass flow rate (Fig. 13). Moreover, the simultaneous two-fold increase in μ_{pp} and in μ_{pw} ($\mu_{pp} = 0.70$ and $\mu_{pw} = 0.60$, orange) shows that the mass flow is slightly affected, similar to the two-fold increase only in μ_{pp} (confer Figs. 12 and 13). These results are in accordance with the observations made in powder flow from a bin or hopper where μ_{pp} was shown to influence the flow rate [29]. To understand clearly, what happens in the shoe with respect to particle motion and rearrangement inside the shoe in these six configurations it is visualized in Fig. 14 after the 10th die filling. An increase in μ_{pp} (compare Fig. 14 (A), (B) and (C)) under constant μ_{pw} has little effect on the particle rearrangement after filling ten dies whereas increase in μ_{pw} shows significantly different patterns in both the cases, see Fig. 14 (D) and (E), at the same time point. It is interesting to note that increasing the μ_{pp} and μ_{pw} simultaneously has the similar rearrangement pattern as in case of μ_{pw} increased alone (compare Fig. 14 (A) with (F) and (A) with (D)). It is clear that the μ_{pp} influences the flow rate whereas μ_{pw} has no influence on the flowrate but the particle reorganization pattern is affected under higher values of μ_{pw} .

To get more clarification on this qualitative observation which could explain the effect of μ_{pw} , the particle rearrangement pattern in the shoe

for the basic setup, for two-fold, and for three-fold increase in μ_{pw} from basic setup is shown in Fig. 15 (A), (B) and (C), respectively, during filling of the first 10 dies. The temporal development of the particles' pattern in the shoe for the basic setup shown in Fig. 15 indicate that the particles tend to move along the die table surface as red particles from right (Fig. 15 (A)) slowly reach the left bottom of the shoe. The particles in extreme left side of the shoe ((Fig. 15 (A)) remain there throughout the die filling thus making this end of the shoe as a dead zone. Doubling the μ_{pw} from basic setup shows that the particles from the right side start to cross over to the left side and initiate a mixing within the shoe thus decreasing the dead space (compare Fig. 15 (A) with (B)). With increased μ_{pw} this tendency is more pronounced as higher μ_{pw} reduces the particles' motion on the wall thereby allowing the particles to move along the die table. Particles rise from the bottom left side of the shoe to the top as observed in Figs. 15 (B) and (C). The red colored particles are therefore moving a longer distance in the feeding box before they are discharged into the die. A similar observation is also reflected in the proportion of colored particles contribution in the die shown in Fig. 16, which further elucidates the effect of friction coefficients on the particle motion. Increasing the μ_{pp} shows that there is no influence on colored particles ratio (compare Fig. 16 (A) with (B)). The comparison of Fig. 16 (A) or (B) with (C) indicates that under high μ_{pp} values the

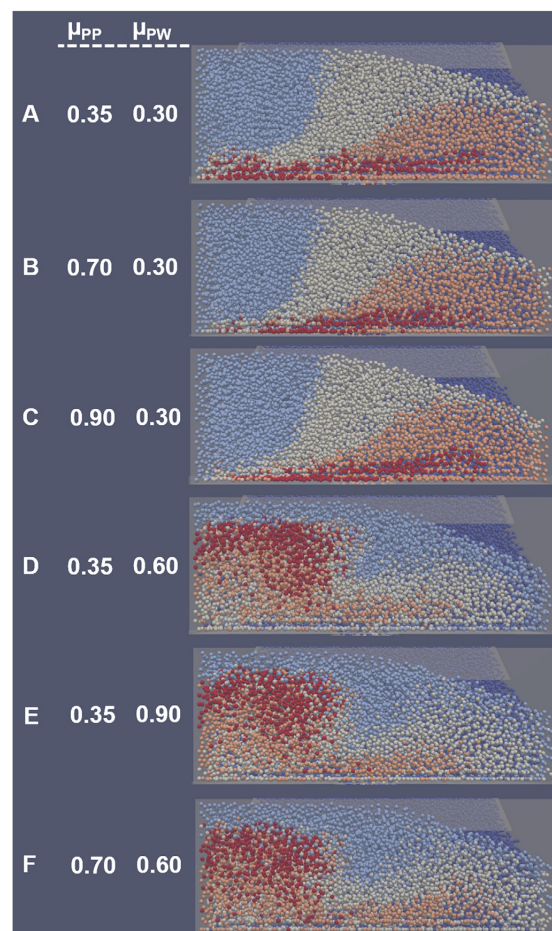


Fig. 14. Particle rearrangement in the feeding box during filling of the 10th die for different particle-particle (μ_{pp}) and particle-wall (μ_{pw}) friction coefficients.

time point at which the newly added particles appear within the die is similar to the lower μ_{pp} case. However, the grey and light blue colored particles (located in the left side of shoe) ratio is changing, especially between 2nd to 5th die as the μ_{pp} values are changed but their ratio sum remains constant. On the other hand, increasing the μ_{pw} shows that there is almost no contribution of red colored particles in the die after the 6th die in case of higher μ_{pw} whereas the same is discerned after the 8th die in case of lower μ_{pw} (compare Fig. 16 (A, B, and C) with (D and E)). This profile also indicates that with higher μ_{pw} the orange particles' contribution increases at the same time point when the red particles start to deplete in the die as they follow the red particles to reach the bottom right side of the shoe (Fig. 15). Also, it is interesting to note that increasing the μ_{pp} and μ_{pw} simultaneously has the similar color particles ratio as in case of μ_{pw} increased alone (compare Fig. 16 (D) with (F)), which is in agreement with the observation of particle rearrangement within the shoe (confer Fig. 14 (D) with (F)). Overall, in comparison to the basic configuration, the increased particle-wall friction allows particles in the shoe to move all over the shoe thus preventing dead zones. However, this movement may increase the shear stresses thereby particles could face attrition and over lubrication in pharmaceutical tablet blends. Moreover, there may be less chance for particle segregation due to percolation [48–51] with the increased particle motion, because the percolated particles will always be carried

upward due to higher μ_{pw} . An additional flowability parameter is computed to get a quantitative understanding of the particle motion in the feeding system. This is achieved through splitting the shoe and pipe into different sections, shown in Fig. 17 (A), and calculating the mean particles' velocity in these sections. Figs. 17 (B), (C) and (D) show the variation in particle mean velocity in all sections (B: Feeding box, horizontal sections, C: Feeding pipe, horizontal sections, and D: Feeding pipe, vertical sections) for three values of μ_{pw} i.e., 0.3 (basic setup 1), 0.6 (setup 10), and 0.9 (setup 11) under constant μ_{pp} of 0.35. The mean velocity of the basic setup in the shoe indicates that the red colored particles are moving with the highest velocity whereas the light blue particles move with the minimum velocity (see Fig. 17 (B)). The comparison of the basic setup with higher μ_{pw} ($=0.6$) reveals that on an average particles in all four sections of the shoe move with 1.5 – fold higher velocity (Fig. 17 (B)). This is in accordance with the qualitative observation made in Fig. 15. Further increase in μ_{pw} ($=0.9$) shows that the particles in the light blue, grey and orange sections exhibit an increase in mean particles' velocity though the most significant influence is observed for particles in the light blue section (Fig. 17 (B)). The particles in the red section show no change in velocity for increasing μ_{pw} from 0.6 to 0.9 indicating that they are moving at maximum velocity that could be achieved in this confined space. Overall, the μ_{pw} has a significant impact on the dead space within the shoe which decreases

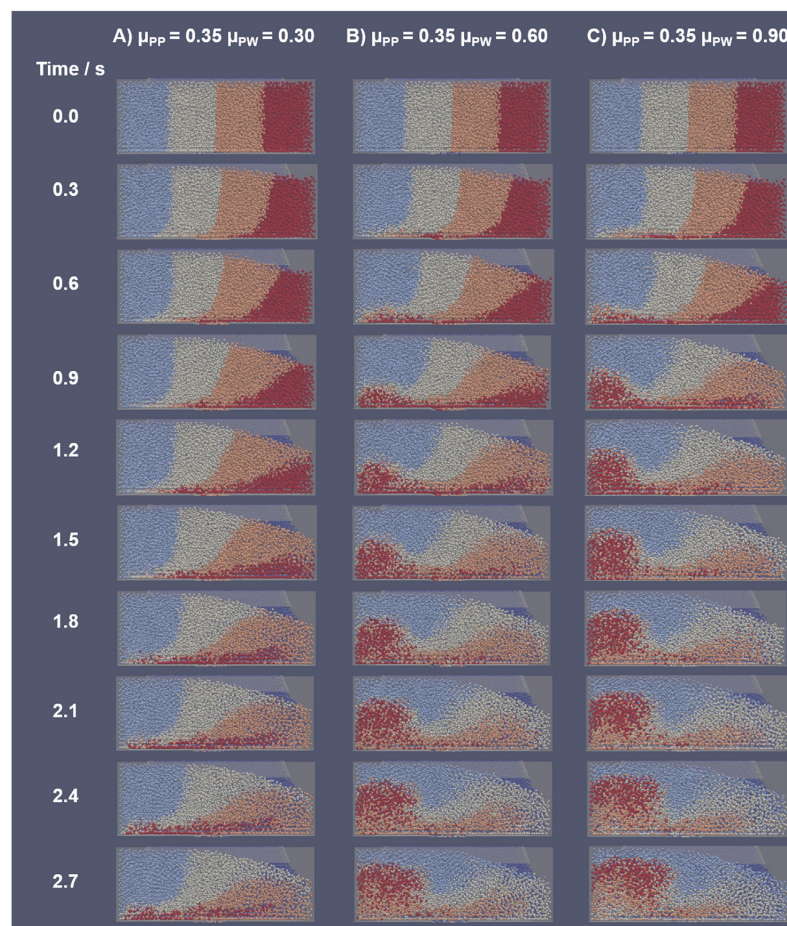


Fig. 15. Effect of particle-wall friction coefficient on particle rearrangement during the 10th die filling for different values of μ_{pw} .

with increasing μ_{PW} (confer Fig. 14). On the other hand, the mean velocity of particles within the feeding pipe shown in Fig. 17 (C and D) indicates the particles move at much lower rate (less than half) compared to the particles in the shoe (Fig. 17 (B)). Also, the particles in the red and orange sections show higher velocity than the grey and light blue sections (Fig. 17 (C)) implying that the majority of the contribution in refilling the shoe is from red and orange sections, which is in accordance with the available void space in the shoe. Moreover, there is hardly any difference in mean particle velocity in the feeding pipe between the basic setup and the higher μ_{PW} cases (Fig. 17 (C and D)). This means that even though there is a higher movement of particles inside the shoe with increased μ_{PW} , due to the confinement of the particles in the feeding pipe there is less space for particle movement in the light blue/grey sections within feeding pipe, so the particles mean velocity is not affected by μ_{PW} in this region. Similarly, the effect of μ_{PW} on

particles velocity within the pipe divided into vertical sections shown Fig. 17 (D), indicates that in case of basic setup all the particles move with same mean velocity except the ones in the bottom section. In comparison to the basic setup, increasing the μ_{PW} slightly increases the particle velocity in the regions where there is no contact or less contact with the walls (purple, light and dark green). On the other hand, increasing the μ_{PW} to 0.6 shows a slight decrease in particle velocity within the bottom section, shown in pink color (Fig. 17 (D)), which can be attributed to the higher hindrance offered by the walls with increased friction. Further increase in μ_{PW} to 0.9, does not show any influence on the particles velocity within this vertical section in the feeding pipe, demonstrating that for such confined regions a saturation effect is achieved.

In summary, the higher μ_{PW} in combination with the moving walls (here die table surface) shows the highest impact on the particle motion

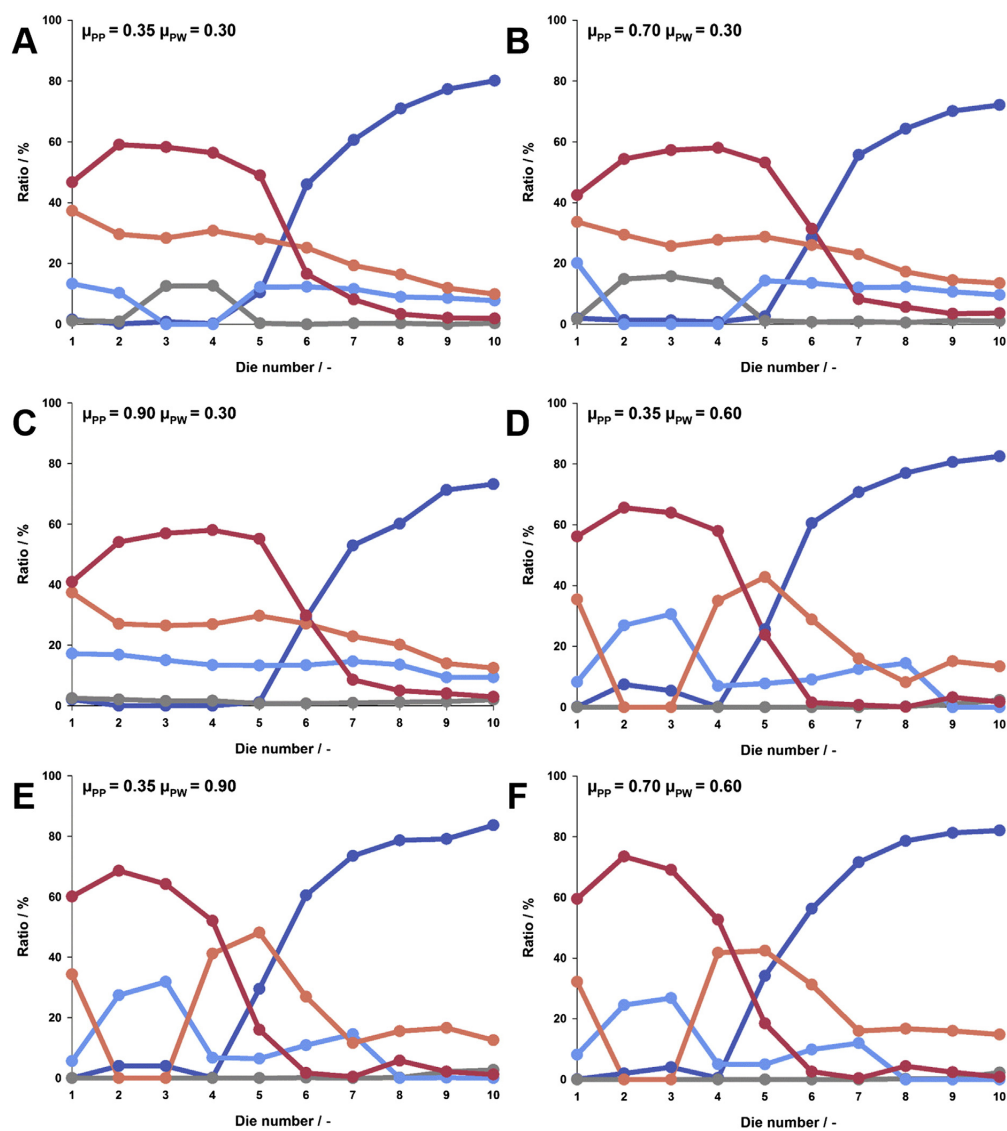


Fig. 16. Distribution of the colored particles in the first 10 dies under different friction coefficients (μ_{PP} and μ_{PW}) as per their initial coloring within the feeding box.

compared to the stationary walls where a slight reduction in particle velocity is observed as higher μ_{PW} hampers the motion over a stationary wall.

The temporal development of the mass holdup in the shoe for four configurations, ((1) low μ_{PP} and low μ_{PW} (setup 1), (2) medium μ_{PP} and low μ_{PW} (setup 8), (3) low μ_{PP} and medium μ_{PW} (setup 10), and (4) medium μ_{PP} and medium μ_{PW}) (setup 12)), is shown in Fig. 18. An increase in μ_{PP} by two-fold reduces the mass holdup by approximately 3.2% which is mainly due to the increased friction leading to a reduction of particle mobility thus causing less particles entering the shoe, which is in accordance with the mass flow rate, confer Fig. 13. On the other hand increasing μ_{PW} shows hardly any effect on the mass holdup, which is also consistent with the mass flow rate (Figs. 13 and 18). Moreover, increasing both μ_{PP} and μ_{PW} simultaneously causes a similar effect as the increased μ_{PP} alone, which is in agreement with the other results presented in this section. Similarly, increasing μ_{PP} (=0.90, setup 9) and μ_{PW} (=0.90, setup 11) further did not show any impact on the mass holdup and its variation (results are not shown here). All these results conform to the particle behavior within hoppers or bins reported in literature stating that μ_{PW} affects the flow behavior or type (funnel or mass flow) and μ_{PP} influences the flow rate [43].

Summing up, the powder flow within and out of the shoe is influenced by two different friction factors. The tablet mass and mass flow rate are mainly influenced by the inter-particle friction whereas the rearrangement in a confined space with a moving geometry is affected by the particle-wall friction. Furthermore, it should be noticed that the mixing in the feeding box caused by a higher particle-wall friction may decrease the chances of segregation due to percolation in case of a free flowing formulation with poly-disperse particle size distribution

[50–53]. In addition, the shearing action with higher particle-wall friction can bear the risk of over lubrication which can affect the dissolution profile of the produced tablet over time [18,54–57].

3.3.3. Coefficient of restitution

The last material property which is evaluated is the coefficient of restitution (e). It is a measure of the fraction of kinetic energy recovered after a collision. This coefficient is a function of the geometry of the colliding bodies and their relative velocities. It is an important collisional parameter that is for example used in some granular flow models in order to predict the velocities and positions of the particles in fluidized beds [58,59]. There are several experimental methods existing to determine e , and one of them is based on the free fall test in which e is calculated by the ratio of the height from which the ball has been dropped and the one that it regains after the impact [60]. Several factors such as the impact velocity, the material behavior of impacted bodies, the particle size and shape, the roughness, moisture content and adhesion properties influence the e values [30,60]. Reported e values of pharmaceutical excipients are within the range of 0.1–1.0 [30,61]. In general, particles with higher e values cannot be contained within the small dies as they would jump out of the geometry due to higher kinetic energy, whereas the particles with low e values would normally have less influence on the particle motion.

In this study two different e values are investigated, i.e. 0.15 and 0.3. The selected values are lower than the values used in literature within DEM simulations of particle flow in feeders and die filling [6,9,18,19], which are in the range of 0.4 to 0.9. However, such high e values may not be observed in real pharmaceutical powders, which depends on the impact velocity, particle size and surface energy, adhesion

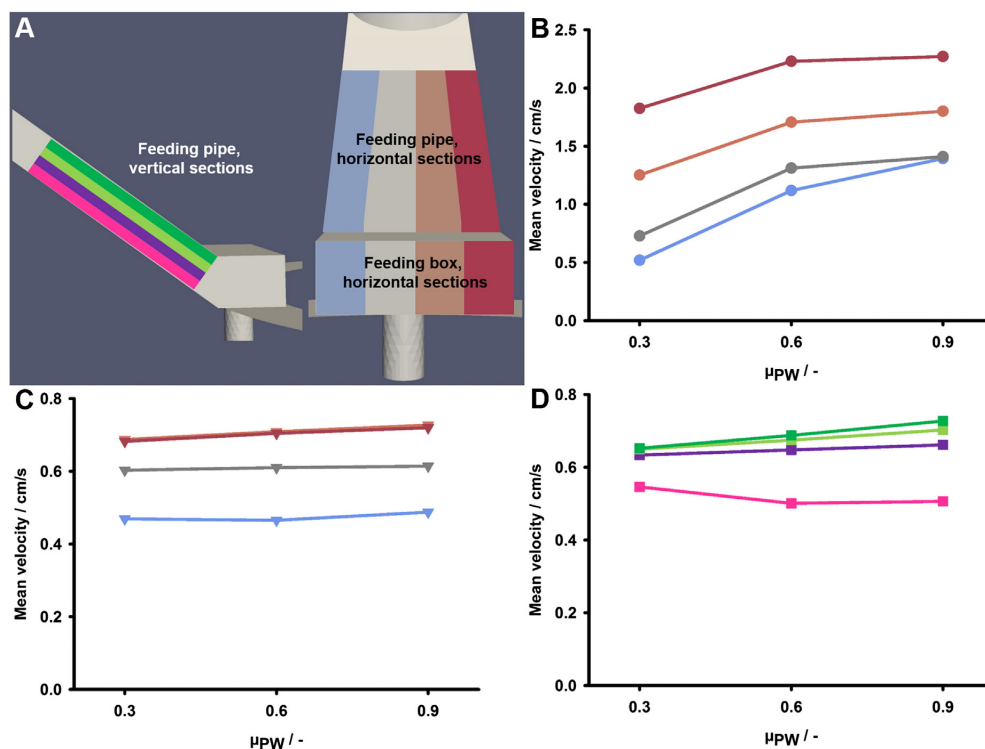


Fig. 17. (A) Different sections in the feeding system based on which the mean velocity over time has been calculated. (Left) Side view of the vertical sections in the feeding pipe, (right) front view of the vertical slices in the feeding pipe and feeding box. Quantitative comparison of the particles' mean velocities in the feeding system observed in (B) feeding box, horizontal sections, (C) feeding pipe, horizontal sections and (D) feeding pipe, vertical sections.

properties etc. Moreover, in confined geometries the e values were found to have no influence on the flowability metrics [29,62,63]. The e values in this study are considered between the particles (e_{pp}) and between the particle and the geometry (e_{pw}). The corresponding configurations include (1) low $e_{pp} = 0.15$ and low $e_{pw} = 0.15$ (basic setup 3), (2) high $e_{pp} = 0.30$ and low $e_{pw} = 0.15$ (setup 13), (3) low $e_{pp} = 0.15$ and high $e_{pw} = 0.30$ (setup 14), and (4) high $e_{pp} = 0.30$ and high $e_{pw} = 0.30$ (setup 15). In these configurations, the die table speed is fixed as 40 rpm whereas all other material and process attributes are kept the same (Table 3).

The mean tablet mass \pm standard deviation over all dies in all these four configurations are 474 ± 7.6 mg, 479 ± 8.1 mg, 475 ± 8.0 mg and 478 mg \pm 7.6 mg, respectively. The mass flow rate in case of the 10th die for all these four configurations is 5.2 g/s, 5.2 g/s, 5.3 g/s and 4.9 g/s, respectively. These results indicate that there is hardly any difference in the mean tablet mass, mass variability and mass flow rate among these four configurations. Furthermore, the variation in the shoe mass holdup with time for these four configurations is 10.66 g, 10.68 g, 10.67 g, and 10.69 g, which also implies that there is no significant difference. As these results show quantitatively no variation among these configurations, the particle rearrangement pattern is visualized in Fig. 19. The comparison of these color profiles indicate there is no difference between them which is in agreement with the quantitative observations presented so far.

The very confined space of the feeding system with close contact between the particles leads to a relatively low overall particle motion thus particles gaining low kinetic energy thereby less energy to dissipate. The particles falling into the die show high velocity in the whole gravity feeder system however there is less space they could jump or move around. This would mean the flowability metrics are not influenced by the e values and it does not constitute as a critical material characteristic within the tableting unit operation. This observation is in agreement with the previous works, which show that coefficient of restitution has negligible influence on flow rate in confined environment [29,62, 63].

3.4. Influence of the combination of process conditions and material properties

The previous sections show that the tableting process performance can be influenced by process conditions as well as material properties. Hence, in this section, the impact of changing material properties and at the same time process conditions will be discussed. The chosen factors include cohesion and die table speed as well as die diameter. The rationale in selecting these parameters is driven by the previous section results, which show that the cohesion has a significant impact on the particle flow, and both the die table speed and die diameter are shown to be equally important with respect to all the flowability metrics. The combined effect of (1) cohesion with die table speed, and (2) cohesion with die diameter are analyzed, and the results will be discussed in the following sections. The analysis of the interaction effect is carried out following the procedure described in Section 2.4.

3.4.1. Die table speed and cohesion

The die table speed considered include 20 rpm and 40 rpm. Similarly, the cohesion values investigated include 0, 1.5, and 3.0 MJ/m³, and corresponding setup numbers of these simulations are 1, 6, 7 (20 rpm), and 3, 16, 17 (40 rpm).

Fig. 20 shows the variation in mean tablet mass (Fig. 20 (A)) as well as the mass holdup in the shoe (Fig. 20 (B)) in all these configurations. The results show that with low die table speed (20 rpm) the mean tablet mass decreases by 0.7% when the cohesion is increased from zero to 1.5 MJ/m³, and decreases by 22.0% when cohesion is increased from zero to 3.0 MJ/m³. However, this reduction is more prominent for 40 rpm die table speed, where the mean tablet mass is reduced by 3.6% and 33.0%, when cohesion is increased from 0 to 1.5 MJ/m³ and 0

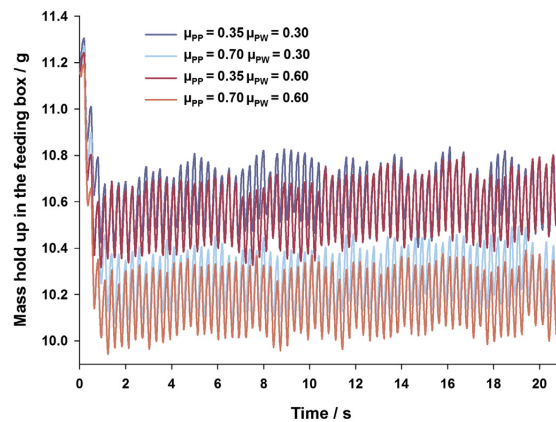


Fig. 18. Variation in shoe mass holdup under different coefficients of friction.

to 3.0 MJ/m³, respectively (see Fig. 20 (A)). The interaction effect is computed by assigning a coded value of -1 for 20 rpm and $+1$ for 40 rpm. Similarly, the no cohesion is given a coded value of -1 , and $+1$ for high cohesion ($CEd = 3.0$ MJ/m³). The mean tablet mass and its standard deviation are considered as the responses. This interaction effect calculation shows that the mean tablet mass is influenced by the die table speed, and the cohesion. However, the influence of die table speed on the mean tablet mass is two times more than the influence of cohesion, and the mean tablet mass to a small extent is also influenced by both, die table speed and cohesion together. Moreover, the tablet mass variation is most significantly affected by the cohesion. The die table speed as well as both, cohesion and die table speed together had less influence on the tablet mass variation compared to cohesion.

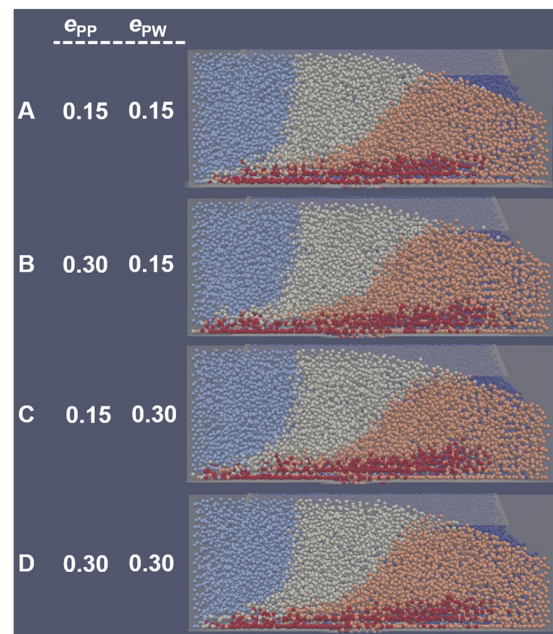


Fig. 19. Particle rearrangement in the feeding box during filling of the 10th die for different particle-particle (e_{pp}) and particle-wall (e_{pw}) restitution coefficients.

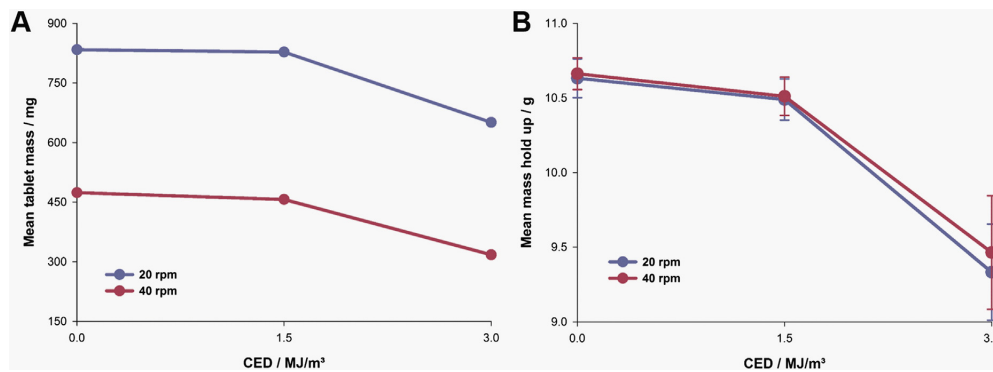


Fig. 20. Effect of the combination of different die table speeds (20 and 40 rpm) with CED values (0–3.0 MJ/m³) on (A) mean tablet mass, and (B) mass holdup in the feeding box.

The mass holdup in the shoe shown in Fig. 20 (B) indicates that it is independent of the die table speed for the considered CED values (confer Sections 3.2.1 and 3.3.1). In addition, the particle rearrangement which is mainly influenced by the void space in the feeding box is found to be similar with 20 and 40 rpm die table speeds (data not shown).

In conclusion, the interaction effect calculation suggests that the mean tablet mass is mainly influenced by the die table speed and to a lower extent by the CED whereas the particle rearrangement and void space in the system are mainly dependent on the tablet blend cohesion.

3.4.2. Die diameter and cohesion

The die diameter considered include 6 mm, 9 mm, and 12 mm. Similarly, the cohesion values investigated include 0, and 3.0 MJ/m³, and corresponding setup numbers of these simulations are 4, 3, 5, and 17–19, see Table 3. The mean tablet mass as well as the mass hold up in the feeding box are shown in Fig. 21 (A) and (B), respectively, for all these setups.

In Section 3.2.2, it was shown that an increase in die diameter from 6 mm to 9 mm would lead to an increase in mean tablet mass by 63%, whereas increasing the die diameter further from 9 mm to 12 mm increases the mean tablet mass further by 51% under no cohesion. Similarly, under cohesion (CED = 3.0 MJ/m³, setup 18, 17 and 19) the mean tablet mass decreases by 24.6%, 33.0% and 35.7% for 6, 9 and 12 mm die diameter, respectively, relative to the no cohesion cases. The interaction effect of the die diameter and the cohesion is computed by assigning a coded value of –1 for 6 mm and +1 for 12 mm. Similarly, the no cohesion is given coded value of –1 and +1 for high cohesion

(CED = 3.0 MJ/m³). The mean tablet mass and its standard deviation are considered as the responses. This calculation shows that the mean tablet mass is affected by the die diameter, and the cohesion. However, comparing the influence of these individual factors on the mean tablet mass indicates that the die diameter alone is found to have a higher impact than the cohesion alone or cohesion and die diameter together. The RSD of the tablet mass is found to be decreased for increasing die diameters under zero cohesion (confer Section 3.2.2). Under cohesion, the RSD values in tablet mass are 4.1%, 2.9% and 2.0% for 6 mm, 9 mm and 12 mm. The cohesion as well as both the cohesion and die diameter together have less impact on the tablet mass variation compared to the die diameter alone.

The same trend can be shown for the mass holdup in the feeding system. A high CED causes a decrease in mean mass holdup by ~9% for 6 mm, ~11% for 9 mm and ~13% for 12 mm die diameter (see Fig. 21 (B)).

Summing up, an analog effect of the process parameter (die diameter) on tablet characteristics, e.g. tablet mass, observed in the previous section (Section 3.4.1) could be shown. The die diameter predominantly determines the tablet mass followed by the CED and to a small extent by the interaction effect. On the other hand, the CED predominantly influences the tablet mass variation and the mass holdup in the feeding box.

Finally, the cohesion, as one of the evaluated material properties, has a high impact on the quality attribute of the final product, the mass variation of the tablet irrespective of the considered process parameter. Hence, the importance of final blend characterization should be emphasized as a standard procedure before tableting to pre-evaluate its impact on the tablet quality. Moreover, the proper selection of process

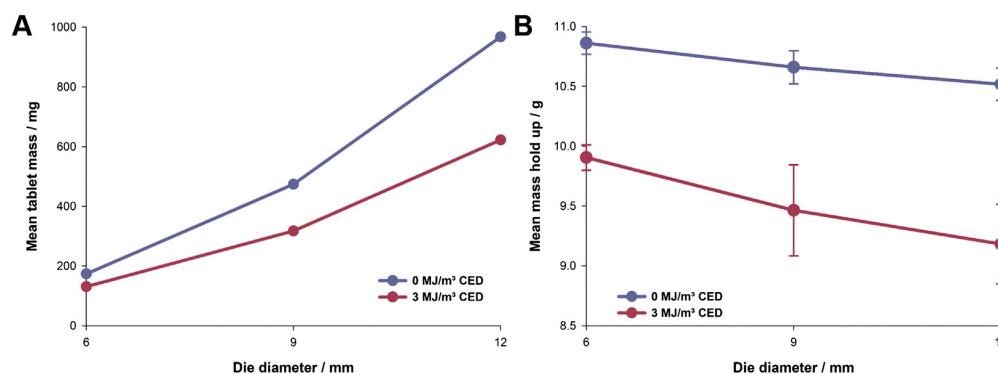


Fig. 21. Effect of the combination of different die diameters (6 mm, 9 mm, and 12 mm) with CED values (0 and 3.0 MJ/m³) on (A) mean tablet mass, and (B) mass holdup in the feeding box.

parameters such as die table speed and die diameter help in optimizing the tablet mass range.

This work can support the process development by suggesting the optimal manufacturing conditions, e.g. in case of very cohesive powders ($CED = 3.0 \text{ MJ/m}^3$), there are two options available to produce tablets with a mass of 620 mg to 650 mg. The first option is to choose a die table speed of 20 rpm and die diameter of 9 mm (setup 7, Section 3.4.1), and the second one is to select 40 rpm die table speed with 12 mm die diameter (setup 19, Section 3.4.2). Both of them have a comparable mass variation of around 2%, however the second option offers the benefit of producing the same number of tablets in half the time.

4. Conclusion

The die filling process within a tablet press constitutes an important step in the tablet production since it is decisive regarding content uniformity of the drug and mass variation of the tablets. In this study, a three-dimensional discrete element method is used to simulate the powder flow from a gravity feeder to the moving dies of a lab-scale rotary tablet press. It is the first study providing an in depth analysis of the powder flow in a gravity feeder of a tableting machine, and besides it also offers a comprehensive insight into the impact of critical process and material attributes on the performance of the die filling process.

The die filling performance parameters include the tablet mass and its variation, mass holdup in the feeding box, mass flow rate from the feeding box into the dies and the particle motion and rearrangement within the feeding box. All of them, potentially impact the final tablet quality.

The selection of the different values of process and material attributes is driven by literature data and practical operating conditions. From the process conditions perspective, it is shown that for higher die table speeds the mean tablet mass is reduced and the mass variation is increased. On the other hand, the die table speed does not influence the dead zones formation within the shoe. A small die diameter reduces the tablet mass dramatically but it is unfavorable due to higher variation in mass, which could pose problems to meet the requirements of the regulatory authorities. The optimal setup to establish good powder flow under a high tablet production rate for a given tablet mass is an increased die diameter. This numerical study can help to define the operating ranges as well as optimal process parameters to ensure a high tableting process performance.

The micro-mechanical properties of the tablet blend cause different phenomena when it comes to die filling. For example, very sticky material, which is in other words cohesive powder, will not flow so properly leading to a decreased tablet mass and an increased variation in mass. The tablet press should also be operated under low die table speed to achieve the specified tablet mass and reduce the risk of tablet weight variation. The second very important material property is the coefficient of friction between particles and the wall. The spherical particles with rough surface or geometry having surface apertures exhibit no influence on the mass flow rate into the dies and tablet mass but enhance their motion or flow pattern within the shoe thereby decrease the dead zones. However, the coefficient of restitution showed no effect on any of the flowability characteristics.

Changing process parameters and material attributes (mainly cohesion) at a time has significant effect on the flowability metrics compared to changing one parameter, and conclusions drawn based on the single parameter change hold true.

Even though this work emphasizes the importance of understanding the effect of material and process attributes, the particles considered are still equal sized granules, i.e. mono-disperse particle size. The actual solid formulations are generally a mixture of several powders, which show poly-disperse particle size distribution, and this will be the focus of future work.

References

- [1] A. Bauer-Brandl, W.A. Ritschel, Die Tablette, Handbuch der Entwicklung, Herstellung und Qualitätssicherung, Third ed Cantor-Verlag für Medizin und Naturwissenschaften GmbH, Aulendorf, 2012.
- [2] I.C. Sinka, L.C.R. Schneider, A.C.F. Cocks, Measurement of the flow properties of powders with special reference to die fill, *Int. J. Pharm.* 280 (2004) 27–38.
- [3] C.-Y. Wu, L. Dihoru, A.C.F. Cocks, The flow of powder into simple and stepped dies, *Powder Technol.* 134 (2003) 24–39.
- [4] L.C.R. Schneider, I.C. Sinka, A.C.F. Cocks, Characterisation of the flow behaviour of pharmaceutical powders using a model die–shoe filling system, *Powder Technol.* 173 (2007) 59–71.
- [5] L.A. Mills, I.C. Sinka, Effect of particle size and density on the die fill of powders, *Eur. J. Pharm. Biopharm.* 84 (2013) 642–652.
- [6] C.-Y. Wu, A.C.F. Cocks, Numerical and experimental investigations of the flow of powder into a confined space, *Mech. Mater.* 38 (2006) 304–324.
- [7] S. Jackson, I.C. Sinka, A.C.F. Cocks, The effect of suction during die fill on a rotary tablet press, *Eur. J. Pharm. Biopharm.* 65 (2007) 253–256.
- [8] C. Bierwisch, T. Kraft, H. Riedel, M. Moseler, Three-dimensional discrete element models for the granular statics and dynamics of powders in cavity filling, *J. Mech. Phys. Solids* 57 (2009) 10–31.
- [9] C.-Y. Wu, DEM simulations of die filling during pharmaceutical tableting, *Particuology* 6 (2008) 412–418.
- [10] C. Bierwisch, T. Kraft, H. Riedel, M. Moseler, Die filling optimization using three-dimensional discrete element modeling, *Powder Technol.* 196 (2009) 169–179.
- [11] E.N. Nwose, C. Pei, C.-Y. Wu, Modelling die filling with charged particles using DEM/CFD, *Particuology* 10 (2012) 229–235.
- [12] Y. Guo, C.-Y. Wu, K.D. Kafui, C. Thornton, Numerical analysis of density-induced segregation during die filling, *Powder Technol.* 197 (2010) 111–119.
- [13] Y. Guo, K.D. Kafui, C.-Y. Wu, C. Thornton, J.P.K. Seville, A coupled DEM/CFD analysis of the effect of air on powder flow during die filling, *AIChE J.* 55 (2009) 49–62.
- [14] Y. Guo, C.-Y. Wu, K.D. Kafui, C. Thornton, 3D DEM/CFD analysis of size-induced segregation during die filling, *Powder Technol.* 206 (2011) 177–188.
- [15] C.-Y. Wu, Y. Guo, Numerical modelling of suction filling using DEM/CFD, *Chem. Eng. Sci.* 73 (2012) 231–238.
- [16] R. Méndez, F. Muzzio, C. Velázquez, Study of the effects of feed frames on powder blend properties during the filling of tablet press dies, *Powder Technol.* 200 (2010) 105–116.
- [17] R. Méndez, F.J. Muzzio, C. Velázquez, Powder hydrophobicity and flow properties: effect of feed frame design and operating parameters, *AIChE J.* 58 (2012) 697–706.
- [18] W.R. Ketterhagen, Simulation of powder flow in a lab-scale tablet press feed frame: effects of design and operating parameters on measures of tablet quality, *Powder Technol.* 275 (2015) 361–374.
- [19] D. Mateo-Ortiz, F.J. Muzzio, R. Méndez, Particle size segregation promoted by powder flow in confined space: the die filling process case, *Powder Technol.* 262 (2014) 215–222.
- [20] P.A. Cundall, O.D.L. Strack, A discrete numerical model for granular assemblies, *Geotechnique* 29 (1979) 47–65.
- [21] W.R. Ketterhagen, M.T.a. Ende, B.C. Hancock, Process modeling in the pharmaceutical industry using the discrete element method, *J. Pharm. Sci.* 98 (2009) 442–470.
- [22] H.P. Zhu, Z.Y. Zhou, R.Y. Yang, A.B. Yu, Discrete particle simulation of particulate systems: theoretical developments, *Chem. Eng. Sci.* 62 (2007) 3378–3396.
- [23] H.J. Herrmann, S. Luding, Modeling granular media on the computer, *Contin. Mech. Thermodyn.* 10 (1998) 189–231.
- [24] C. Kloss, C. Goniva, A. Hager, S. Amberger, S. Pirker, Models, algorithms and validation for opensource DEM and CFD-DEM, *Prog. Comput. Fluid Dy. An Int. J.* 12 (2012) 140–152.
- [25] S. Plimpton, Fast parallel algorithms for short-range molecular dynamics, *J. Comput. Phys.* 117 (1995) 1–19.
- [26] A. Di Renzo, F.P. Di Maio, Comparison of contact-force models for the simulation of collisions in DEM-based granular flow codes, *Chem. Eng. Sci.* 59 (2004) 525–541.
- [27] K.L. Johnson, K. Kendall, A.D. Roberts, Surface energy and the contact of elastic solids, *P. Roy. Soc. Lond. A Mat.* 324 (1971) 301–313.
- [28] C. Geuzaine, J.-F. Remacle, Gmsh: a 3-D finite element mesh generator with built-in pre- and post-processing facilities, *Int. J. Numer. Methods Eng.* 79 (2009) 1309–1331.
- [29] A. Anand, J.S. Curtis, C.R. Wassgren, B.C. Hancock, W.R. Ketterhagen, Predicting discharge dynamics from a rectangular hopper using the discrete element method (DEM), *Chem. Eng. Sci.* 63 (2008) 5821–5830.
- [30] D. Antypov, J.A. Elliott, B.C. Hancock, Effect of particle size on energy dissipation in viscoelastic granular collisions, *Phys. Rev. E* 84 (2011) 021303–021311.
- [31] C. Kloss, LIGGGHTS – Manual, <http://www.cfdem.com2015> (accessed 12-02-2015).
- [32] I.C. Sinka, F. Motazedian, A.C.F. Cocks, K.G. Pitt, The effect of processing parameters on pharmaceutical tablet properties, *Powder Technol.* 189 (2009) 276–284.
- [33] E. Peeters, T. De Beer, C. Vervae, J.-P. Remon, Reduction of tablet weight variability by optimizing paddle speed in the forced feeder of a high-speed rotary tablet press, *Drug Dev. Ind. Pharm.* 41 (2015) 530–539.
- [34] R. Leardi, Experimental design in chemistry: a tutorial, *Anal. Chim. Acta* 652 (2009) 161–172.
- [35] Ö. Andersson, Experiment! Planning, Implementing and Interpreting, First edn Wiley, 2012.
- [36] W. Kleppmann, Versuchsplanung: Produkte und Prozesse optimieren, Eighth edn Hanser, 2013.
- [37] J.M. Ottino, D.V. Khakar, Mixing and segregation of granular materials, *Annu. Rev. Fluid Mech.* 32 (2000) 55–91.

- [38] S. Wiederseiner, N. Andreini, G. Épely-Chauvin, G. Moser, Experimental investigation into segregating granular flows down chutes, *Phys. Fluids* 23 (2011) 1–10, 013301.
- [39] H.H. Hausner, Effect of quench sintering on the grain structure of sintered metals, *Int. J. Powder Metall.* 8 (1972) 159–161.
- [40] L. Svarovsky, Powder testing guide, *Methods of Measuring the Physical Properties of Bulk Powders*, Springer, Netherlands, 1987.
- [41] H. Rumpf, The strength of granules and agglomerates, in: W.A. Knepper (Ed.), *Agglomeration*, Wiley Interscience, New York 1962, pp. 379–413.
- [42] Ph. Eur., *European Pharmacopoeia*, 8th edn, 2016.
- [43] D. Schulze, *Powders and Bulk Solids*, Springer-Verlag, Berlin, 2007.
- [44] J. Schwedes, Review on testers for measuring flow properties of bulk solids, *Granul. Matter* 5 (2005) 1–43.
- [45] M. Leturia, M. Benali, S. Lagarde, I. Ronga, K. Saleh, Characterization of flow properties of cohesive powders: a comparative study of traditional and new testing methods, *Powder Technol.* 253 (2014) 406–423.
- [46] S. Masson, J. Martinez, Effect of particle mechanical properties on silo flow and stresses from distinct element simulations, *Powder Technol.* 109 (2000) 164–178.
- [47] A.S.J. Suiker, N.A. Fleck, Frictional collapse of granular assemblies, *J. Appl. Mech.* 71 (2004) 350–358.
- [48] C. Thornton, Numerical simulations of deviatoric shear deformation of granular media, *Geotechnique* 50 (2000) 43–53.
- [49] W.R. Ketterhagen, J.S. Curtis, C.R. Wassgren, B.C. Hancock, Predicting the flow mode from hoppers using the discrete element method, *Powder Technol.* 195 (2009) 1–10.
- [50] P. Tang, V.M. Puri, Methods for minimizing segregation: a review, *Particul. Sci. Technol.* 22 (2004) 321–337.
- [51] D. McGlinchey, Assessment of segregation in industrial processes, *J. Powder. Bulk Solids. Technol.* 22 (1998) 54–56.
- [52] J. Mosby, Investigations of the Segregation of Particulate Solids With Emphasis on the Use of Segregation Testers Ph. D. diss. Telemark College, Department of Technology, 1996.
- [53] S.R. de Silva, A. Dyroy, G.G. Enstad, Segregation mechanisms and their quantification using segregation testers, in: A.D. Rosato, D.L. Blackmore (Eds.), *IUTAM Symposium on Segregation in Granular Flows*, Kluwer Academic Publishers, Boston 2000, pp. 11–29.
- [54] J. Wang, H. Wen, D. Desai, Lubrication in tablet formulations, *Eur. J. Pharm. Biopharm.* 75 (2010) 1–15.
- [55] J. Kushner IV, F. Moore, Scale-up model describing the impact of lubrication on tablet tensile strength, *Int. J. Pharm.* 399 (2010) 19–30.
- [56] D.S. Desai, B.A. Rubitski, S.A. Varia, A.W. Newman, Physical interactions of magnesium stearate with starch-derived disintegrants and their effects on capsule and tablet dissolution, *Int. J. Pharm.* 91 (1993) 217–226.
- [57] A.C. Shah, A.R. Mlodozieniec, Mechanism of surface lubrication: influence of duration of lubricant-excipient mixing on processing characteristics of powders and properties of compressed tablets, *J. Pharm. Sci.* 66 (1977) 1377–1382.
- [58] F. Taghipour, N. Ellis, C. Wong, Experimental and computational study of gas-solid fluidized bed hydrodynamics, *Chem. Eng. Sci.* 60 (2005) 6857–6867.
- [59] C. Mangwandi, Y.S. Cheong, M.J. Adams, M.J. Hounslow, A.D. Salman, The coefficient of restitution of different representative types of granules, *Chem. Eng. Sci.* 62 (2007) 437–450.
- [60] S. Antonyuk, S. Heinrich, J. Tomas, N.G. Deen, M.S. van Buijtenen, J.A.M. Kuipers, Energy absorption during compression and impact of dry elastic-plastic spherical granules, *Granul. Matter* 12 (2010) 15–47.
- [61] R. Šibanc, T. Kitak, B. Govedarica, S. Srčić, R. Dreu, Physical properties of pharmaceutical pellets, *Chem. Eng. Sci.* 86 (2013) 50–60.
- [62] G.H. Ristow, Outflow rate and wall stress for two-dimensional hoppers, *Phys. A* 235 (1997) 319–326.
- [63] V. Vidyapati, S. Subramaniam, Granular flow in silo discharge: discrete element method simulations and model assessment, *Ind. Eng. Chem. Res.* 52 (2013) 13171–13182.

3.1.4 Size-segregation understanding in gravity filling by using the DEM

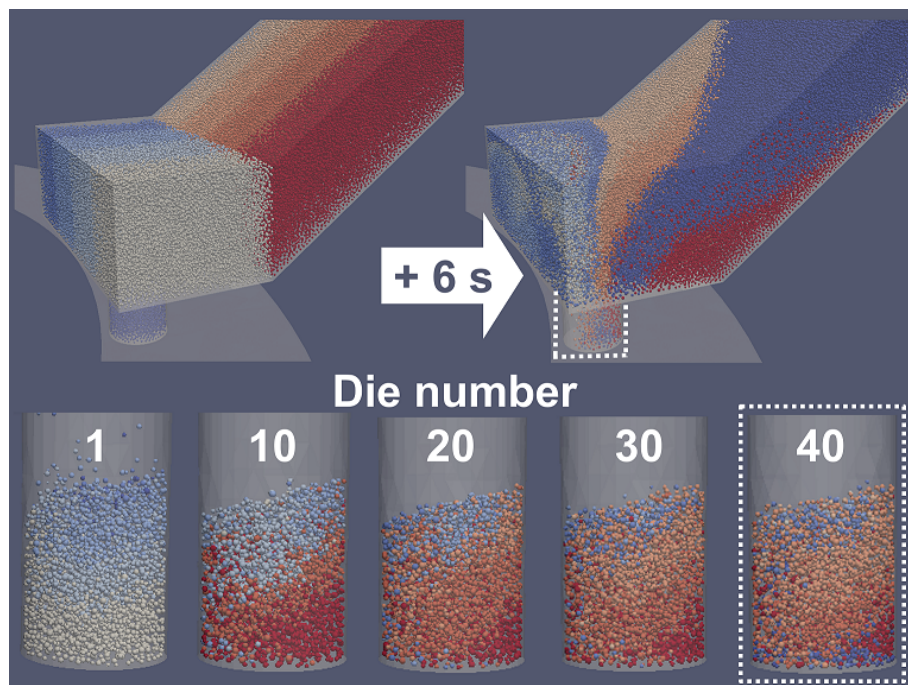
Simulation of particle size segregation in a pharmaceutical tablet press lab-scale gravity feeder

Claudia Hildebrandt¹, Srikanth R. Gopireddy², Regina Scherließ¹,
Nora A. Urbanetz²

¹ Department of Pharmaceutics and Biopharmaceutics, Christian-Albrechts-Universität Kiel,
Grasweg 9a, 24118 Kiel, Germany

² Daiichi-Sankyo Europe GmbH, Pharmaceutical Development,
Luitpoldstrasse 1, 85276 Pfaffenhofen, Germany

Advanced Powder Technology, 29:765-780, 2018



Outline

On the basis of the results presented in the previous chapter (3.1.3), the same system but particles of different size were studied and thus the particle size segregation in the gravity feeder may be identified. The material properties (micro-mechanical properties and particle size distribution) correspond to micro-crystalline cellulose particles (VIVAPUR MCC Spheres 500). The poly-disperse approach is one step closer to real formulations which are of different components and differently sized particles. On the first hand, the die filling is compared for mono- and poly-disperse particles. An understanding of the size segregation mechanisms at different locations of the gravity feeder is developed and helps to evaluate its influence on tablet quality, i.e. content uniformity.

The mono-disperse study showed with respect to material properties a significant influence on die filling of the inter-particle cohesion and of the coefficient of friction (confer chapter 3.1.3). Hence those properties are evaluated in the poly-disperse setup, too. The effect of the material properties on classical tablet quality attributes, such as tablet weight, tablet weight variation, content uniformity, as well as the powder flow in the gravity feeder including the underlying size segregation mechanisms are evaluated. By generating a risk assessment, the material property with highest influence on quality attributes is identified. This approach may be helpful in formulation development as it provides potential levers for gravity filling optimization.



Contents lists available at ScienceDirect

Advanced Powder Technology

journal homepage: www.elsevier.com/locate/apt

Original Research Paper

Simulation of particle size segregation in a pharmaceutical tablet press lab-scale gravity feeder

Claudia Hildebrandt^{a,*}, Srikanth R. Gopireddy^b, Regina Scherließ^a, Nora A. Urbanetz^b^a Department of Pharmaceutics and Biopharmaceutics, Kiel University, Grasweg 9a, 24118 Kiel, Germany^b Daiichi-Sankyo Europe GmbH, Pharmaceutical Development, Luitpoldstrasse 1, 85276 Pfaffenhofen, Germany

ARTICLE INFO

Article history:

Received 4 August 2017

Accepted 21 December 2017

Available online 30 December 2017

Keywords:

Die filling

Gravity feeder

Particle size segregation

Discrete element method

Tableting

ABSTRACT

The die filling process within a lab-scale rotary tablet press is simulated using the Discrete Element Method (DEM). Powder is transferred from a gravity feeder (comprising of a cylindrical pipe, an inclined chute, and a rectangular box) into rotating dies. Spherical shape micro-crystalline cellulose particles serve as an experimental pendant to measure the particle size distribution (PSD) and to calibrate the micro-mechanical material properties entering in the DEM calculations. At first, the die filling process of the particles having poly-dispersity in size is explored by analyzing the basic metrics such as tablet mass, tablet mass variation, and mass flow rate. Particle size segregation is investigated by computing the PSD development in different locations of the feeding system and in the filled dies. In addition, particles' velocity and coloring analysis (both qualitative and quantitative) are performed. Results show that different zones of the system are involved in various powder flow phenomena constituting varying particle size segregation causes. Next, the micro-mechanical properties, namely inter-particle cohesion, particle-particle and particle-wall friction, are varied one at a time to shed light on their influence on the particle size segregation and tablet quality. Finally, the influence of different material properties on various metrics are compared with each other providing a guide towards formulation optimization resulting in optimal tableting process performance.

© 2017 The Society of Powder Technology Japan. Published by Elsevier B.V. and The Society of Powder Technology Japan. All rights reserved.

1. Introduction

Today solid dosage formulations constitute the most frequent administration route of drug substances arising from outstanding advantages of tablets as dosage forms. Some of them are for instance the ease of handling, high production rates at low cost, and self-administration providing patient compliance [1]. Tablets are produced in industrial scale on high speed rotary tablet presses with a productivity of e.g. max. 1.6 million tablets per hour [2]. The production process can be divided into three distinct stages comprising die filling, compaction, and ejection. Each of them represents various challenges when it comes to tablet product quality according to the Ph. Eur. [3]. Those requirements are the “friability of uncoated tablets” [2.9.7], the “resistance to crushing of tablets” [2.9.8], the “disintegration of tablets and capsules” [2.9.1], the “uniformity of dosage units” [2.9.40], and eventually the “dissolution test for solid dosage forms” [2.9.3] [3]. However, all of the distinct process stages are intertwined with each other as well as with

the product quality requirements. Hence in 2009 the International Council for Harmonisation (ICH) adopted the Quality by Design (QbD) paradigm for process development by introducing the ICH guideline Q8 to “build quality into products by design” using pharmaceutical development [4]. There are several options on how to implement the QbD approach into science-based manufacturing of pharmaceuticals such as process analytical tools, design of experiments, and implementation of risk management strategies but also process modeling and control via numerical simulations, see also [5].

As the die filling stage during manufacturing defines the accurate mass as well as content and content uniformity of the active pharmaceutical ingredient (API) it has been focused by experimental [6] and more recently by numerical research. In 2003 the first experimental system was mentioned to describe die filling in a model setup [7]. This system contained a stationary die and a moving delivery system (shoe) providing the opportunity to determine flowability and the amount of powder collected in the die as a function of the shoe velocity [7]. It has also been used and further developed by others [8] supporting process understanding of powder delivery into a confined space with respect to the influence

* Corresponding author.

E-mail address: childebrandt@pharmazie.uni-kiel.de (C. Hildebrandt).<https://doi.org/10.1016/j.apt.2017.12.019>

0921-8831/© 2017 The Society of Powder Technology Japan. Published by Elsevier B.V. and The Society of Powder Technology Japan. All rights reserved.

of particle size and density, of air and vacuum, and of gravity and suction filling [7–14]. In parallel to experimental studies the same system or adapted versions have been used as a framework for numerical simulations [11,15,13,16–23]. The geometry of these systems rather resembles an eccentric feed press [24] limiting its transfer to the pharmaceutical process. In high speed tableting the dies are moving underneath the delivery system which can be either shoe, hopper, or feed frame [25]. This shortcoming has been eliminated by [26,27] in which the powder is delivered in either a translating [26] or rotating [27] die. Recently much more complex systems found in rotary tablet presses with a closed feed frame system consisting of one or more paddle wheels which force incoming powder to pass into the dies of the rotating turret were developed [28–31].

Besides the limitations of the geometrical configurations, the numerical setups constitute additional restrictions that impede process understanding. Those include the much larger particle size (e.g. [27–31]) and the significantly differing material properties [28] considered compared to pharmaceutical powders. In addition, the powder stress level in some of the studies is either not including the normal stress exerted by powder mass in the feeding hopper (e.g. [26]) or lacks the re-filling of particles as mass is being discharged into the dies (e.g. [29]).

Even though the poly-disperse particle size nature of pharmaceutical powders significantly affects the product quality [32,33] it has only been taken into account by very few numerical studies [23,26,29–31] due to high computational effort. For the model-die filling system proposed by Wu et al. [11] Guo et al. [19] showed that the mass flow rate is higher in case of poly-disperse particles compared to mono-disperse particles. In addition, different fines concentrations were identified along the die width and height [20]. In a similar geometrical setup, Furukawa et al. [26] showed that the percolation of small particles which progressed in the feed shoe before particles were discharged into the die influenced segregation to a greater extent than die velocity. Mateo-Ortiz et al. [29] detected particle size segregation at low paddle wheel speeds in the feed frame of a Manesty Beta Press. Size segregation occurred between the different paddle wheel zones of a Fette tablet press impairing tablet quality [30].

Particle segregation, e.g. defined as the “unintentional demixing of one or more components in a mixture of particulates” [34], could be triggered by different physical mechanisms that can be classified by the physical particle properties [35] as well as the energy input [36]. For the former absolute particle size, particle size ratio, particle size distribution, fine particle concentration, particle shape, particle density, and particle flowability can be named [37]. Furthermore different means to avoid, or control/limit segregation, e.g. choosing an optimal interparticle cohesion, have been suggested [38]. However, only very little is known about particle size segregation during the tableting process impairing API content and uniformity [30,39].

Numerical simulation of powder flow from a gravity feeder to the dies within a lab-scale rotary tablet press [27] provided a comprehensive insight into the impact of process and material attributes on the performance of the die filling process. The micro-mechanical material properties such as cohesion, friction, and the coefficient of restitution were systematically investigated and their influence on different performance parameters analyzed. Even though this work emphasized the importance of understanding the effect of material and process attributes, the particles considered were still equal sized granules. Reference is missing when it comes to the awareness of particle size segregation of materials having a poly-disperse particle size distribution under differing material properties. Consequently, the objectives of this work using three-dimensional discrete element method (DEM) simulations include a detailed investigation of particle size distribution

in the system of Gopireddy et al. [27]. Moreover this study is the first of its kind investigating comprehensively the influence of particle properties on size segregation within an actual pharmaceutical application system.

2. Methodology

This section presents the details about the mathematical approach, geometrical configuration as well as the numerical simulations performed.

2.1. Discrete element method

After the introduction of the DEM in 1979 [40] it has evolved over almost 40 years to a well-known approach in particle technology and it is being used for different applications. This numerical model captures the trajectories of each and every particle in the system through Newton's equation of motion offering the main advantage, compared to the continuum approach, of high resolution in particulate flows. The details about the theory and algorithms are not the scope of this work but are well described in literature [41–43].

All computations in this study were performed using the open source DEM software known as LIGGGHTS [44], version 3.2.1. The normal and tangential forces were modeled by the Hertz and the Mindlin & Deresiewicz theories, respectively [45]. The non-contact inter-particle force other than gravity was included through the simplified Johnson-Kendall-Roberts (JKR) model [46]. All the force models as well as their implementation in LIGGGHTS are given by Kloss et al. [47] and the same models given by Gopireddy et al. [27] were used in this study.

The impact of air on the particles was assumed to be negligible due to the dense particle packing and the closed system (tableting machine). This assumption was shown to be valid in the earlier studies [21,27].

2.2. Geometrical setup

The geometrical configuration consisted of a rectangular shoe, which was connected to a feeding system similar to actual tablet presses, and a rotating die table. This system is shown in Fig. 1, and it is identical to Gopireddy et al. [27], so detailed dimensions can be found in the same. The geometry was constructed with the open source finite element mesh tool known as Gmsh [48] and later imported as physical boundaries into LIGGGHTS.

2.3. Material properties

As mentioned in the introduction, powder flow of a poly-disperse particle size distribution (PSD) was simulated. The PSD of VIVAPUR MCC Spheres 500 (JRS Pharma GmbH & Co. KG, Rosenberg, Germany), spherical particles of purely microcrystalline cellulose, was measured by laser diffraction (HELOS, Sympatec GmbH, Clausthal-Zellerfeld, Germany). The sizes and their corresponding density distribution (q_3) of the VIVAPUR MCC Spheres 500 were used to obtain the PSD in the simulation, as illustrated in Fig. 2. In total six different particle size fractions were modeled ranging up to 402.5 μm out of which one particle size fraction (200–237.5 μm) with a proportion of 8.5% (w/w) served as the model “API”, confer Section 3.1.2.4. The micro-mechanical properties (Table 1) as well as the particle density (1.6 g/cm³) were set constant for all particle sizes. No individual value for different particle sizes have been set, rather the total bulk property was considered that is usually also assessed in powder flowability experiments. This implies that a given particle property, i.e. the cohesion energy density in which

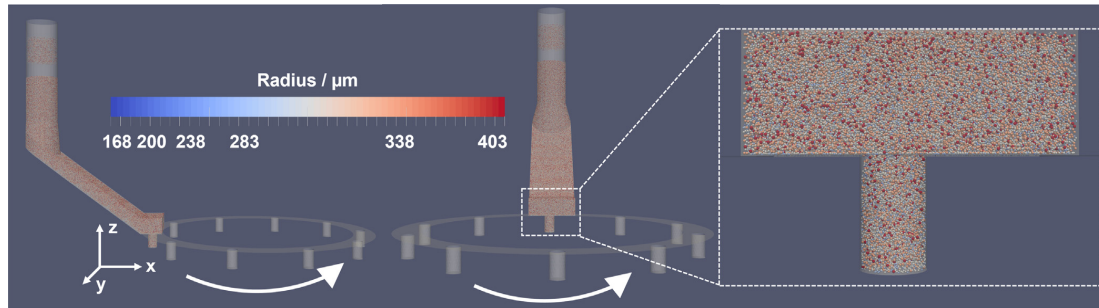


Fig. 1. Illustration of the geometrical setup after filling the system with particles. (Left and middle) Side and front view of the complete system. (Right) In addition, zoom into the feeding box is given. The arrow indicates the turret rotation direction.

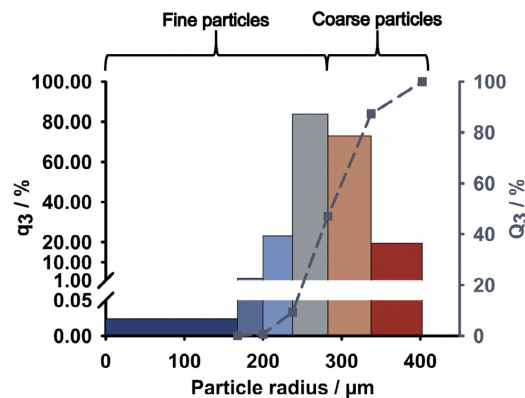


Fig. 2. Particle size distribution of the VIVAPUR MCC Spheres determined by laser diffraction. The bar colors of the individual sizes are subsequently used in illustrations.

Table 1
DEM parameters (varied properties are indicated in italic).

Parameter	Property of	Value(s)
Young's modulus/GPa	Particle	8.7
	Wall	210
Poisson's ratio/-	Particle	0.3
	Wall	0.35
Coefficient of friction/-	Particle-particle contact (μ_{PP})	0.2–0.6
	Particle-wall contact (μ_{PW})	0.25–0.75
Coefficient of restitution/-	Particle-particle contact (e_{PP})	0.12
	Particle-wall contact (e_{PW})	0.10
Cohesion energy density (CED)/MJ/m ³	Particle	0.0–3.0

the contact area is a function of the particle radii, will have a different, particle size dependent, influence in contact force calculations. According to Table 1, three material properties indicated in italic letters were systematically changed to evaluate their influence on the die filling process. Detailed explanation is given in Section 2.5.

2.4. Initialization and die filling process

According to the tableting unit operation, particles were first filled into the feeding system before the discharge into the dies

started. A time step of 0.1 μ s for particles' filling and 0.2 μ s for discharge was considered which are both well below the Rayleigh and Hertz-time [44,47]. The filling followed a step-by-step procedure with a particle insertion rate of 10,000–100,000 particles every 0.4 s into the feeding pipe until 5.75 s. In total around 650,000 particles with a mass of 121.3 g were filled and settled in the system. The properties were set corresponding to setup no. 1 (default) in Table 2.

Afterwards the turret was rotated at a constant speed of 40 rpm thereby particles were discharged into the die. The particles in the filled dies were leaving the simulation domain. To ensure a constant fill level in the feeding pipe, new particles were added at an equal rate providing a constant normal force acting on the particles, thereby eliminating the fill level effect on die filling. For discharge, the material properties were systematically changed (setup no. 1–7, Table 2) as described in Section 2.5. This sequence allowed a homogeneous packing structure at the beginning of all setups and ensured that observations during discharge were related to material features [23,27].

The process parameters were evaluated directly from the beginning of discharge. Thereby a detailed understanding of the flow pattern development in tableting in reaching the steady state and beyond could be provided. However, it should be mentioned at this point that during real tableting the first tablets are discarded. During this phase an adjustment of machine settings to debug optimal conditions for tablet production within the specifications of tablet weight, hardness etc. is performed [8,9,12,25,49].

The turret was rotated for in total 4 complete revolutions resulting in 40 filled dies corresponding to a physical time of 6 s, sufficiently long enough to uncover the influence of the different material properties (confer Section 3.3). The computation for one

Table 2
Selected values for assessing the influence of the different material properties. Bold values indicate the property that has been changed compared to the default setup (setup no. 1, italic letters).

Setup number	Material property		Evaluated material property	
	CED / MJ/m ³	Coefficient of friction		
		μ_{PP} / -		μ_{PW} / -
1	1.5	0.4	0.5	-
2	0.0	0.4	0.5	CED
3	3.0	0.4	0.5	-
4	1.5	0.2	0.5	μ_{PP}
5	1.5	0.6	0.5	-
6	1.5	0.4	0.25	μ_{PW}
7	1.5	0.4	0.75	-

setup (Table 2) on 72 parallel running processors took more than two weeks attributed to the high number of particles considered.

2.5. Numerical setups and statistical analysis

Seven different numerical setups, given in Table 2, were created to gain clear understanding of the impact of different material properties in the die filling process by changing one parameter at a time [27]. The material properties were chosen within the range of corresponding literature data [19,27,29,50,51] and in-house calibration experiments [27,52]. The calibration procedure was divided into two steps starting with the measurement of the VIVA-PUR MCC Spheres 500 powder properties like angle of repose, flowability, and bulk density according to standard procedures of Ph. Eur. [3]. Afterwards these measured properties were reproduced by changing the DEM input parameters through simulations. The parameters which were varied extensively by choosing three different values ranging from low, medium, and high (Table 2) were derived from Gopireddy et al. [27]. In particular, the influence on powder flow was investigated for cohesion energy density and the coefficients of friction (particle-particle and particle-wall). The values for the different setups are given in Table 2.

Statistical analysis included one-sided ANOVA tests at $\alpha = 0.05$ and for multiple group comparisons Bonferroni's *t*-test or Turkey's test (if normality test failed the Kruskal-Wallis one way analysis of variance on ranks was used) were performed (SigmaPlot 12.5, Systat Software GmbH, Erkrath, Germany). The content uniformity of the model "API" particles was assessed according to the monograph 2.9.40 in Ph. Eur. [3]. Briefly, 30 tablet samples were randomly picked during the process and the API content determined. Initially, from 10 samples the measured to specified API content was assessed and the "Acceptance Value" (AV) calculated by a formula including the mean and standard deviation. If $AV > 15$, the specification could not be met and the API content of the remaining 20 samples was assessed giving a new AV value. This AV value had to be ≤ 15 again and, in addition, none of the 30 samples might have a very extreme relative API content ($\pm 25\%$ of specification) so that content uniformity was met.

3. Results and discussion

The die filling of mono-sized granules in a lab-scale gravity feeder has been extensively described by Gopireddy et al. [27]. In extension to [27] the focus of this study was the evaluation of the die filling in case of particles having a poly-disperse PSD. Therefore microcrystalline cellulose particles (Section 2.3) were used as an experimental pendant to numerical simulations. Same PSD and micro-mechanical properties (obtained through calibration as described in Section 2.4) served as basis for the numerical setups (Tables 1 and 2).

First of all the die filling will be in-depth described by using calibrated MCC spheres micro-mechanical properties. Same metrics as outlined by Gopireddy et al. [27], such as powder flow pattern, mass flow rate, tablet mass, mass hold up, and particle rearrangement in the feeding box will be evaluated. In addition to those, the PSD in the system will be intensively studied by introducing new measures. A detailed explanation of the distribution of the different particle sizes supported by particles' velocity analysis will provide an understanding for particle size segregation in the tableting machine.

Afterwards the influence of three different material properties within the afore-mentioned framework will be studied and all relevant metrics are listed in Table 3 for easy reference. The inter-particle cohesion, the particle-particle, and the particle-wall friction were changed one at a time. The value of the property

was kept in the medium range for the default setup (setup no. 1, Table 2) and additionally two setups with one minimum and one maximum property value were created. For each material property first the general and PSD metrics with focus on particle size segregation will be determined followed by a ranking of the values with respect to the influence on the most important quality attributes of the product. At the end all the material properties will be compared with each other to unveil the most superior/critical one.

3.1. Description of the die filling process

3.1.1. Powder flow pattern

The die filling of the particles with the properties corresponding to the default configuration (setup no. 1, Table 2) is shown in Fig. 3. The powder flow was visualized in Fig. 3A by coloring the particles according to their velocity (red color: high velocity, blue color: particles remain stationary) as the die was moving at 40 rpm in anti-clockwise direction. In parallel, the mass in the die and the relative die fill level are illustrated in Fig. 3B. The latter one was determined via the material's bulk density and the die volume giving a maximal possible tablet mass of 924 mg. As the die opening entered underneath the feeding box, the particles slowly started to fall into the die mainly due to gravity and accelerated with time. During the die filling process, the top right corner of the box got emptied, implied by a high particles velocity (Fig. 3A and Fig. 4A). Simultaneously, the box was re-filled by particles from the inclined chute above which was most prevalent in the right hand side (Fig. 3A). At the bottom of the box, particles were dragged by the turret motion gaining velocity whereas particles at the top left of the feeding box remained stationary over the complete filling time. Those observations are similar to mono-sized granules reported by Gopireddy et al. [27].

The relative die fill level as the die was located in the middle of the feeding box ($t = 0.05$ s, Fig. 3B) was 29% and it only reached 59% after 0.10 s resulting in a mean tablet mass of 545 mg (Fig. 3C). The high turret motion of 40 rpm resulting in the low filling time caused an incompletely filled die (confer Fig. 3A, $t = 0.13$ s). Though the mass flow rate was 5912 mg/s, estimated by the linear zone of the mass discharge period, slightly less than the theoretical tablet mass of 591 mg was obtained as the mass flow rate is lower at the beginning ($t = 0.0-0.015$ s) and end ($t = 0.085-0.10$ s) of the die filling period.

After die no. 4, the mass collected in the die fluctuated around the mean and roughly one standard deviation resulting in a low RSD (0.7%, confer Fig. 3C). In parallel, the determined mass hold up in the feeding box decreased by around 1 g from initial value of 11.3 g after die no. 8. In particular, the time point at which constant mass hold up in the feeding box was reached is considered as "steady state" (ss) (confer Table 3). The void volume of 9% enabled a particle rearrangement in the feeding box (see Section 3.1.3).

In Fig. 4A the qualitative particles' velocity is shown as the feeding box was split into four equal sized sections (Fig. 4B). It can be observed that the sections on the right hand side, namely sections 2 and 4, had a 99% higher mean particles' velocity than on left hand side (section 1 and 3) of the box (Table 3). This difference mainly arose from the particles' re-filling in section 2 and the momentum particles obtained as the die opening was approaching in section 4. Particles in the top left of the box (section 1) showed the lowest velocity, confer also Fig. 3A. The detailed particles' velocity analysis per particle size for the different sections (Fig. 4B), shown in Fig. 4C, indicated that only for section 4, in which particles mainly discharge into the die, a particle size dependent velocity could be identified. More precisely, the particles' velocity increased with particle size attributed to the higher gravitational force of the larger particles favoring the discharge into the die.

Table 3

List of results for the basic metrics. The location within the text for definition or generation of the metrics is given under “Metric explanation”. Default setup properties are listed in Table 2, setup no. 1. “Quality numbers” correspond to quality attributes described in Table 4.

Metric	Quality no.	Metric explanation	Unit	Material property changed compared to default (setup no.)						
				Default (1)	CED/0.0 MJ/m ³ (2)	CED/3.0 MJ/m ³ (3)	$\mu_{PP}/0.2$ (4)	$\mu_{PP}/0.6$ (5)	$\mu_{PW}/0.25$ (6)	$\mu_{PW}/0.75$ (7)
Mean tablet mass	1	Section 3.1.1, Fig. 3C	mg	545.24	564.27	364.32	605.79	527.90	480.94	551.19
Tablet mass variation (RSD)	2	Section 3.1.1, Fig. 3C	%	0.65	0.77	1.42	0.58	0.68	0.74	0.56
Mass flow rate		Section 3.1.1, Fig. 3B	mg/s	5917.47	6047.07	N/A	6532.87	5715.10	5104.83	5977.27
Mean mass hold up in feeding box		Section 3.1.1, Fig. 3C	g	10.36	10.52	9.08	10.85	10.10	10.45	10.23
Mean particles' velocity in section 1		Section 3.1.1, Fig. 4A	cm/s	0.80	0.55	0.36	0.70	0.85	0.30	0.95
Mean particles' velocity in section 2		Section 3.1.1, Fig. 4A	cm/s	2.25	1.23	0.70	2.03	2.40	1.27	2.54
Mean particles' velocity in section 3		Section 3.1.1, Fig. 4A	cm/s	1.98	2.30	1.83	1.54	2.10	0.52	2.24
Mean particles' velocity in section 4		Section 3.1.1, Fig. 4A	cm/s	3.27	2.71	1.89	2.98	3.44	1.92	3.45
Mean particles' velocity in complete feeding box		Section 3.1.1, Fig. 3C	cm/s	2.05	1.73	1.22	1.80	2.15	0.98	2.25
Die no. after reaching of steady state (ss)		Section 3.1.1, Fig. 3C	–	8	7	11	8	8	17	8
Mean fines content in dies during steady state (fines Q_3 , dies, ss)		Section 3.1.2.2, Fig. 5A	%	44.65	44.56	44.84	45.11	44.28	46.69	43.92
RSD of fines content in dies during steady state (RSD _{dies, ss})	4	Section 3.1.2.2, Fig. 5A	%	3.05	3.07	3.36	2.75	3.27	3.16	2.68
RQT of fines in dies during steady state in dies (RQT _{dies, ss})	5	Section 3.1.2.2, Fig. 5A	%	0.18	0.16	0.19	0.13	0.22	-0.03	0.13
API acceptance value (AV) in dies	3	Section 3.1.2.4	–	21.24	21.55	20.99	17.39	23.95	13.29	24.22
Mean API content in dies		Section 3.1.2.4	%	7.88	7.80	7.97	8.07	7.70	8.69	7.62
API content variation in dies (RSD)		Section 3.1.2.4	%	7.83	7.91	8.34	7.03	8.25	6.82	8.02
Mean fines content in box during steady state (fines' Q_3 , box, ss)		Section 3.1.2.3, Fig. 5A	%	45.08	45.04	44.72	44.53	45.28	43.29	45.25
RSD of fines content in box during steady state (RSD _{box, ss})	6	Section 3.1.2.3, Fig. 5A	%	0.90	0.85	0.55	0.66	0.88	0.91	1.08
RQT of fines in dies during steady state in box (RQT _{box, ss})	7	Section 3.1.2.3, Fig. 5A	%	0.54	0.48	0.14	0.32	0.53	-0.60	0.71
Ratio of old particles in feeding box after 6 s		Section 3.1.3, Fig. 6B	%	45.68	44.89	51.17	38.15	51.48	28.18	48.43
Appearance of color 1 particles in section 4	8	Section 3.1.3, Fig. 6B	s	2.40	2.25	2.40	3.15	2.25	6.00	1.95

In addition, the absolute x-, y-, and z-direction components of the velocity vector were separately evaluated and are illustrated in Fig. 4D (for clarification of the x-, y-, and z- directions confer Fig. 1). In general, the particles in the right half of the box (sections 2 and 4), influenced by particles re-filling and die filling, showed high x- and z-direction velocity vector components. The highest x-direction velocity vector component was found for particles entering the box from the pipe (section 2). The particles' shearing by turret rotation was indicated by the high y-velocity vector component for sections 3 (1.75 cm/s) and 4 (1.82 cm/s). In contrast, particles in section 1 had the lowest velocity in all directions though the highest contribution came from y-direction resulting from the particle movement from left to right in the feeding box (from section 1 into 2, detailed explanation given in Section 3.1.3).

3.1.2. Particle size distribution in the system and its change over time

3.1.2.1. During feeding system filling. The filling process (Section 2.4) of the feeding system (pipe and box) itself caused a top to bottom particle size segregation leading to a decreased ratio of particle radii $\leq 282.5 \mu\text{m}$ and accumulation of larger particles (radius $> 282.5 \mu\text{m}$) in the top of the box (section 1 & 2). However, the mean particle radius was found to be not much different as it was $324 \mu\text{m}$ and $318 \mu\text{m}$ in the top and bottom sections, respectively.

This difference in particle sizes between top and bottom occurred during the filling of the feeding system. As particles were

inserted in the feeding pipe (see Fig. 1, Section 2.4), they traversed through the vertical pipe to the inclined chute and then into the feeding box. During this particle motion larger particles were rolling and sliding down the chute surface acting as a “non-blinding screen” through which the smaller particles percolated [53]. This segregation mechanism, also known as sieving, caused an accumulation of larger particles on the top and smaller ones at the bottom [53–55]. In general this type of mechanism can take place when there is a sufficient amount of large particles forming a moving layer in addition to an adequately low fines content (particles $\leq 200 \mu\text{m}$, $<1\%$ (w/w), refer Fig. 2) [53,56,57].

As particle size segregation with a cut-off size at $282.5 \mu\text{m}$ was already found during the feeding system filling process (confer above), this gave rise to separate the PSD into two groups for the following die filling explanation. Fine particles with radii $\leq 282.5 \mu\text{m}$ and coarse particles with radii $> 282.5 \mu\text{m}$ were defined (Fig. 2). In the complete system (feeding box and feeding pipe) the initial content of fines was 46.3% and of coarse 53.7% (Fig. 2), respectively. The sieving mechanism during filling caused a fines concentration of 42.6% in the top (section 1 + 2) and 47.0% in the bottom (section 3 + 4) of the feeding box, respectively. This PSD grouping (fines/coarse) is remained throughout the rest of the manuscript.

3.1.2.2. In the filled dies. Small particles can enter the voids during the compaction process resulting in a closer particle packing [32].

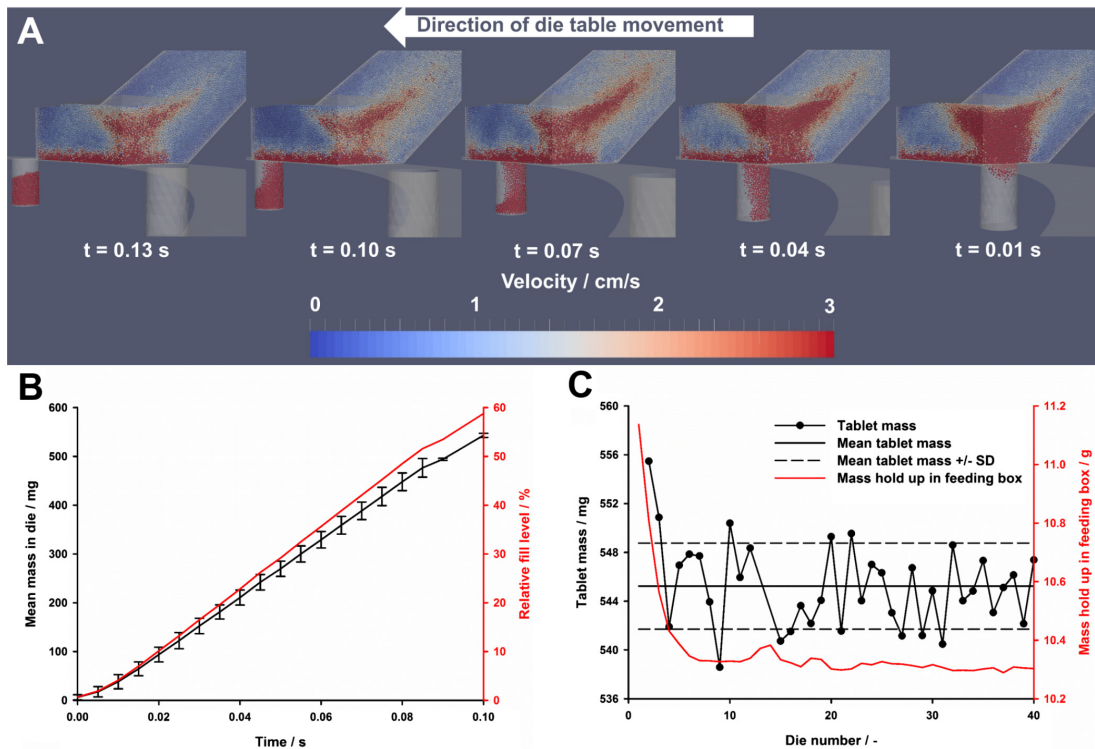


Fig. 3. (A) Qualitative illustration of die filling by coloring the particles according to their velocity (red: 3 cm/s, blue: 0 cm/s). (B) Absolute and relative mass flow rate into the die. The relative fill level was obtained by comparing the actual mass to the max. possible mass in the die at the given bulk density of the material. (C) Tablet mass and mass hold up in the feeding box. For the tablet mass, the mean mass is indicated by a solid line, the mean plus and minus one standard deviation by the dotted lines, respectively. (For interpretation of the references to color in this figure legend, the reader is referred to the web version of this article.)

Thereby they can lead to an increased tablet hardness as their higher surface area forms increased interparticulate bonds [32,58–64]. However, no simple rule regarding the impact of granule size on tablet strength exists [33,65–70]. It is of main importance to understand the PSD evolution during the die filling process as it might influence particle compression characteristics, tablet hardness and in turn the dissolution profile. Although PSD metrics of the fines were focused on in the following chapters, it should be kept in mind that the fines content shows per definition opposite trends compared to the coarse particles.

First of all, the fines content in the dies over time will be discussed followed by a thorough explanation of the PSD development within the feeding box (see Section 3.1.2.3). For clarification the corresponding data is depicted in Fig. 5A. All data belonging to the dies are colored in red, those belonging to the feeding box in blue (confer Fig. 5A, left). Solid lines connect the individual data points, dashed lines the mean fines q_3 content during steady state (die no. 8–40, for definition of steady state confer Section 3.1.1). The linear regression lines through the raw data points during steady state are marked as dotted lines.

During the first filled dies, the fines content was decreasing from initially 49% to 42% in die no. 8 until a steady mass hold up in the box (confer Fig. 3C) has been established. This initial decrease was characterized by the discharge of the higher fines content that was found after the filling process at the bottom of the feeding box (confer Section 3.1.2.1). As soon as steady mass hold up in the box was reached, the fines content was steadily

increasing to 46% in the last filled die. A linear regression line through the fines content data points from die 8 till last filled die (40) showed a slope of 0.082%. Normalization of the slope to the averaged data points was defined as a new segregation index, the “Relative q_3 trend” ($RQT_{\text{initial die no.} - \text{last die no.}}$ [%]), and will be explained in the following. The mean fines q_3 , 8–40 content in the dies during steady state (the subscript indicates the considered range of die numbers, dashed line in Fig. 5A) was found to be 44.7%. Normalizing the increasing trend over time (slope of the regression trend line (0.082%), dotted line in Fig. 5A) to the mean q_3 , 8–40 content (44.7%) gave a RQT_{8-40} value of 0.18%. This RQT value was able to describe whether an accumulation or depletion of fines during steady state die filling over time was found. A positive RQT sign indicated a relative increase in fines q_3 content over time whereas a negative RQT sign a depletion. The absolute RQT value could serve as an indicator for the extent of long-term segregation. From a quality point of view, a low absolute RQT value is desirable as low PSD differences between initially produced tablets and the tablets at the end of the production process are obtained.

In addition, the fluctuation of the fines content could be measured by the relative standard deviation ($RSD_{\text{first die no.} - \text{last die no.}}$ [%]) of the q_3 data points. A low RSD quantified a low tablet-to-tablet variation of the fines q_3 content. In this setup the fines q_3 RSD_{8-40} in the dies was found to be 3.05%.

Both measures, the RQT and RSD of the fines q_3 content in the dies (Table 3) could be utilized to quantify the PSD development

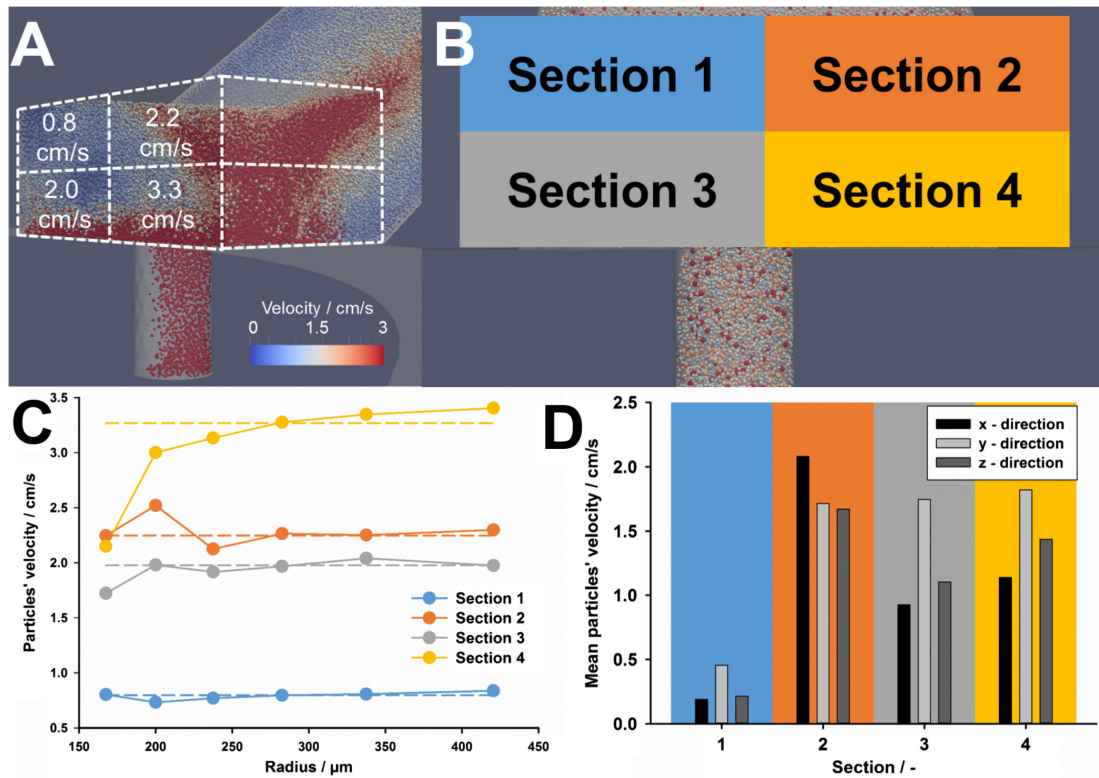


Fig. 4. (A) Mean particles' velocity in 4 sections of the feeding box that are defined in (B). (C) Mean particles' velocity per individual particle size in the 4 cross-sections of the feeding box and the complete box. The mean velocity over all sizes is given in dotted lines for the different locations, respectively. (D) Mean particles' velocity per x-, y-, and z-direction in the 4 cross-sections (confer Fig. 1 for directions).

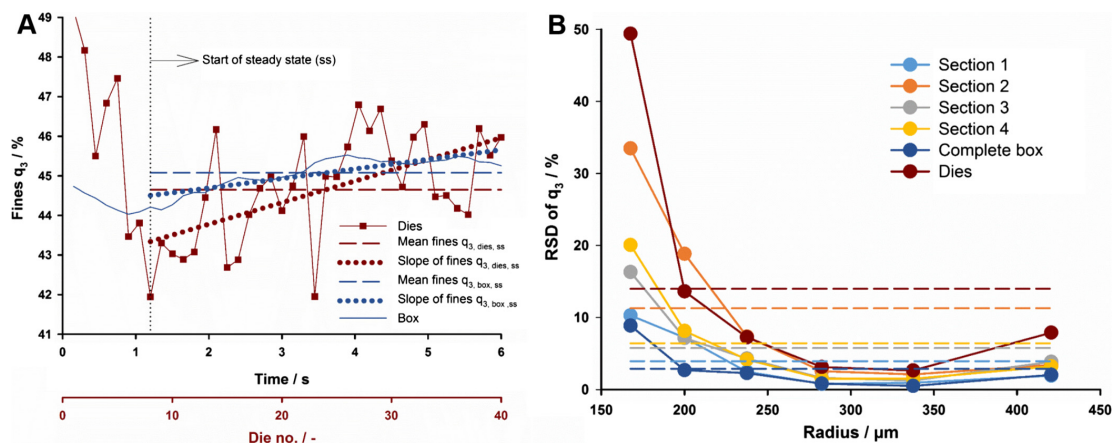


Fig. 5. (A) Explanation of the fines q₃ content development for default setup (setup no. 1, Table 2). Data corresponding to dies is shown in red, for complete feeding box in dark blue. Solid lines show raw data points. After steady state (ss, die no. 8 or t = 1.2 s), the mean fines q₃ content is indicated in dashed lines, the linear regression line through the raw data points of the fines q₃ after steady state in dotted lines. (B) Overview of q₃ RSD of the different particle sizes in the four cross sections of the box, the complete box, and the dies. (For interpretation of the references to color in this figure legend, the reader is referred to the web version of this article.)

during the tableting process thereby providing indices for tablet hardness and dissolution.

3.1.2.3. In the feeding box. During filling of the dies by turret rotation, the concurrent processes of particles leaving the feeding box to the dies and particles being re-filled into the box through the inclined chute resulted in a PSD fluctuation. During the time between one die leaving the box to the next die entering the box, the particles in the box, particularly in the bottom part which were in contact with the turret, were forming a shearing layer due to the turret rotation (Fig. 3A). Therefore, each cross-section of the box, confer Fig. 4B, was involved in a different sub-process bearing the possibility for PSD variation due to different segregation mechanisms. The particles' flow within the system and the particularities at all those sections are separately explained in the following.

Particles were re-filled from the feeding pipe into the right half of the feeding box as this part was mainly involved in particle discharge (section 2, see Section 3.1.1 and Fig. 3A). Again a top (section 2) to bottom (section 4) segregation in the box with an initially higher fines content at the bottom was found. The difference in fines q_3 content between top (section 2) to bottom (section 4) of around 6% (40.6% and 46.5% in section 2 and 4, respectively) remained constant throughout the die filling process. Over time, at the back side of the feeding box small particles accumulated. This accumulation evolved as a cause of particles' velocity gradient over the horizontal sections of the inclined feeding pipe [27] and the particles' discharge in the front half of the box. Particles in direct contact with the bottom of the inclined pipe moved with lower velocity compared to particles on top (see [27] for detailed explanation and [71]). During this movement in the pipe, large particles rose to the top whereas small ones could percolate through them. At the entrance of pipe to box, coarse particles (radius > 282.5 μm) on top gained increased velocity due to their higher mass and rolled/slid down on the particles' surface bed to enter the die. As particles were either re-filled from the feeding pipe (section 2) or discharged into the die (section 4), the velocity component for vertical movement (z) was highest compared to the rest of the feeding box (confer Section 3.1.1 and Fig. 4D).

Particles either entered the die on the right hand side of the feeding box (section 4) or were sheared on top of the turret from right to left into section 3. Hence the bottom left section of the box (section 3) was involved in at least three different processes. (1) The turret rotation caused a shearing of the particles at the bottom of the box whereby voids were generated. Small particles could percolate through those voids [34,72]. The shear rate, defining the voids size and percolation extent was influenced by the turret speed and the particle-wall friction. (2) As particles were discharged into the die, they were re-filled from the rotating shearing layer originating from right hand side of the box. Hence the PSD in section 3 was mutually influenced by the PSD in section 4 and the ratio of particles being discharged into the die and being held back in the box. (3) As the shearing layer was reaching the left wall of the box, the particles dodged the flow by moving upwards into section 1 [27]. This upwards movement was visualized by the particles' coloring described in Section 3.1.3. In addition, the z -component of the particles' velocity vector was significantly decreased from 1.44 cm/s in section 4 to 1.11 cm/s in section 3 as shown in Fig. 4D.

The largest particles (radius of $\geq 420.5 \mu\text{m}$) with very high mass couldn't follow this upwards motion as gravitational force was counteracting. Hence they showed a depletion over time in the top left of the box (section 1). During the overall upwards movement of the powder bed, small particles could fall through the particles' voids thereby partly resisting the opposed flow. However within the width of section 1, different powder flow layers evolved

over time (confer Fig. 6C). These layers were generated as the back side of the box was influenced in particles' re-filling from the pipe, the middle part was majorly involved in die filling and showed highest particles' velocity/turnover (orange colored particles in Fig. 6C, right), and the front of the box was primarily sheared. At the borders where high and low particles' velocity/turnover were encountered an increased fines content was found.

Particles which were pushed upwards in the left half of the feeding box (section 1) rolled/slid down on top to the right half of the box (section 2) causing a particles' recirculation within the box. This rearrangement was visualized by the particles' coloring (confer Section 3.1.3) and could be quantified by a y -direction velocity vector component of 0.46 cm/s (Fig. 4D).

Independent of the analyzed region, the fluctuation of the q_3 (RSD) was directly dependent on the particle size and its q_3 value. Fig. 5B shows the q_3 RSD for each particle size in all the analyzed sections. An exponential decrease in q_3 RSD was observed for particle sizes up to 282.5 μm (fine particles). Between 282.5 μm and 337.5 μm a plateau and for particles >337.5 μm there was a slight increasing trend (see Fig. 5B) identified. Regions with a high particles' turnover rate and particles' velocity (Fig. 4 and Table 3) turned out to have on an average higher RSDs, i.e. dies, section 2, and 4 showed the largest fluctuation in PSD. Apart from dies, the highest mean RSD over all particle sizes was found in section 2 (11.3%) and the lowest in section 1 (3.9%) (Fig. 5B, dashed lines).

In summary, over the complete feeding box (Fig. 5A), the fines q_3 content initially decreased from 44.7% to 44.2% until steady mass hold up was reached ($t = 1.2 \text{ s}$, corresponds to die no. 8) and then increased by a RQT_{3-40} of 0.54% until a final fines q_3 content of 45.3% ($t = 6 \text{ s}$). Although the complete box showed a relatively constant variation in tablet-to-tablet fines content (measured in terms of $q_3 \text{ RSD}_{\text{box, ss}}$) of 0.90%, the consistency in the dies was decreased significantly ($\text{RSD}_{\text{dies, ss}}$ of 3.05%, confer above). This discrepancy was attributed to the different powder flow phenomena within the feeding box during the die filling process. For this given setup the overall fines q_3 pattern over time within the dies and the complete feeding box were highly similar (Fig. 5A). Hence a thorough understanding of the powder flow phenomena within the feeding box could help in understanding particle size segregation in the filled dies.

3.1.2.4. Ph. Eur. content uniformity. Last but not least one major tablet quality requirement, "content uniformity" was evaluated. Therefore one particle size out of the distribution served exemplarily as the model "API" and its uniformity over time was evaluated. The particles of size 200–237.5 μm and an initial q_3 of 8.5% (Fig. 2) were selected and tracked in the box as well as in the dies over time. This size range out of the PSD has been selected as it could reflect a low dose direct compression formulation [73] with a reasonable particle size of model "API" relative to excipient particles. Our experience from direct compression formulations shows that usually API particles are in the particle size range of the disintegrant which is much smaller compared to the diluent.

Over 40 filled dies, the model "API" particles were slightly accumulating in the feeding box (API particles $RQT_{\text{box, 1-40}} = 1.2\%$) and depleting in the dies (API particles $RQT_{\text{dies, 1-40}} = -0.4\%$). These observations were differing compared to the fines content analysis in the feeding box and dies (fine particles $RQT_{\text{box, 1-40}} = 0.5\%$, $RQT_{\text{dies, 1-40}} = 0.1$). This discrepancy could be explained by the wider range of particle sizes defined as fines compared to "API" particles (Fig. 2). Hence other particle sizes in the fines group showed opposite trends compared to "API" particles counteracting the "API" particle size trend. A high "API" content variation in the filled dies of 8% (RSD) was found thereby resulting in an AV of >15 which did not meet the criteria for content uniformity according to the Ph. Eur. [3] (confer Section 2.5, Table 3).

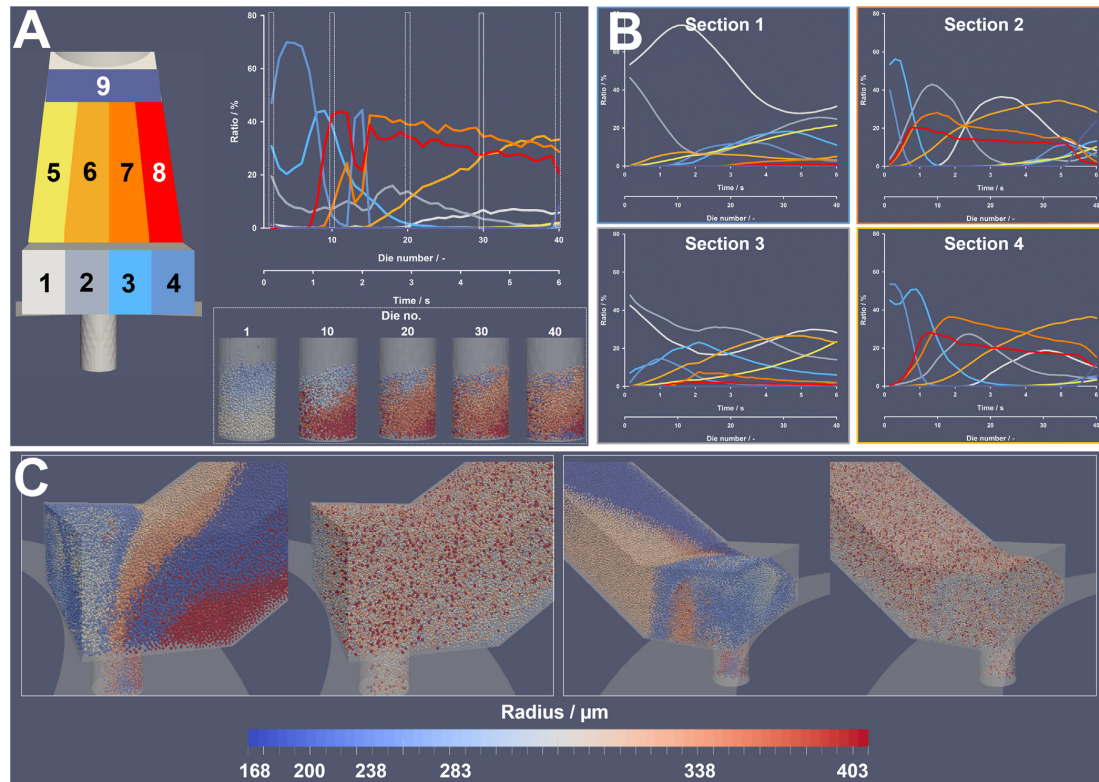


Fig. 6. (A) 8 vertical zones in the feeding box and feeding pipe assigning particles in total 9 different colors as per their initial position. Colors 1–4 were assigned in the feeding box, colors 5–8 in the feeding pipe, and the rest of the particles in the pipe were assigned as color 9. The graph shows the frequency (number based) of the colored particles in the dies. Exemplarily the filled dies for the first, 10th, 20th, 30th, and last (40th) filled die are shown. (B) Distribution of the colored particles in the 4 sections (confer Fig. 4B) of the feeding box over time. (C) Visualization of the feeding box by the initially colored particles as well as by their radius after 6 s of die filling. (For interpretation of the references to color in this figure legend, the reader is referred to the web version of this article.)

In conclusion, this detailed analysis of poly-disperse die filling showed that the PSD development in the system was influenced by mainly two phenomena. First, the box cross-sections were involved in different sub-processes during the die filling thereby influencing the particles turnover and particles' velocity to a dissimilar extent. These sub-processes generated different particle size segregation phenomena. Second, the absolute particle size and the relative contribution of gravitational to the net force determined whether particles were rather discharged into the die or remained in the box. Thereby a well-chosen PSD in terms of absolute and relative particle sizes as well as their distribution could significantly influence the tablet product with respect to content uniformity, dissolution, and hardness.

3.1.3. Particle rearrangement in the feeding box

In Sections 3.1.1 and 3.1.2 the particle flow pattern in the box was qualitatively described by the particles' velocity (Fig. 4), and its influence on the PSD (Fig. 5) was determined. To further strengthen these observations the particles in the feeding system were colored by their initial position, in analogy to [27]. In extension of four-equal volume zones split along the width of the feeding box, the lower half of the feeding pipe or inclined chute was split into 4 additional zones where the particles were colored in these zones. These were in line with the zones of the feeding box

so that in total 9 different zones were obtained, and the schematic of all these zones as per the assigned colors is depicted in Fig. 6A. The contribution of these colored particles in the die was analyzed both quantitatively and qualitatively. The graph in Fig. 6A shows the percentage of different colored particles in the die, i.e. the contribution of particles from individual zones that were filled into dies 1–40 is presented.

During the initial period the particles entering the die originated from the very right hand side of the box as the die arrived underneath the box at the right hand side (Fig. 6A (top right), color 4 and 3), followed by particles from the middle of the box (color 2). No particles from the very left side of the feeding box (color 1) were entering the die until the 20th die for which they already have been traveled from the upper half of the feeding box to the re-filling zone on the right side of the box (see below). Re-filled or fresh particles (color 5–9) appeared after die no. 8 (see Fig. 6A, color 8) and mainly originated from the right hand side of the feeding pipe. After 6 s of discharge, which comprised filling of 40 dies, the first particles from the upper half of the feeding pipe started falling into the die (see Fig. 6A, color 9).

To visualize these colored particles in the die as part of a qualitative analysis, the contents of the 1st, 10th, 20th, 30th and 40th dies are exemplarily shown in Fig. 6A (bottom right). This visualization

supported the quantitative analysis shown in Fig. 6A (top right). Additionally, it illustrated that there was not only a top to bottom but also a horizontal difference of colored particles in the filled dies. Over the die width non-uniform coloring layers were developed indicating a mixture of (1) “old particles” (white – blue color), which stayed in the feeding box for certain time experiencing high shear, and (2) “fresh particles” (yellow – orange color), which directly entered the die thereby these particles were subjected to less shear force. As “fresh” particles traveled less distance within the feeding system and were exerted to less shearing forces compared to “old” particles, different compressive properties over the height and width of the tablet might be obtained [74]. This may lead to capping with an increasing tendency over production time. Also, these differences may not pose a major problem in round tablets however could cause issues in other tablet shapes, e.g. oblong tablets.

Similar analysis was performed to study the temporal rearrangement of particles within the feeding box (Fig. 6B), which helps in identifying the high mixing and dead zones. This was achieved by splitting the feeding box into four-sized sections (as shown in Fig. 4B and for PSD and particles' velocity analysis). Fig. 6B shows the percentage of different colored particles within these four sections of the feeding box and their development over time. By definition color 1 and 2 particles were initially positioned in section 1 and 3 whereas color 3 and 4 particles in sections 2 and 4, and were constituting each ~50% of initial number of particles, respectively (confer Figs. 4B and 6A (left)). At the beginning of the die filling color 1 particles located at the very left of the box, were not falling into the die (confer Fig. 6A). Due to (1) the overall particle motion, and (2) additional space created as a result of less mass hold up in the box, the particles from section 1 moved to section 2 at which they appeared after die no. 10 and then in section 4 after die 18, respectively (see Fig. 6B, section 2 and 4). Color 2 particles entered the dies to a low extent (<20%, confer Fig. 6A), hence their contribution in section 3 was decreasing at a slow rate and they were, similar to color 1 particles, moving from the left to the right hand side of the feeding box into section 2. In this given setup, it can be clearly seen that particles originally located on the right hand side of the box (color 3 and 4), were significantly decreasing in section 2 and 4 since they mainly entered the die (Fig. 6A and B), and the rest of them was being moved by the turret into section 3 and then into section 1 due to the pushing of particles as a result of the moving turret. The different particle flow patterns within the box and from the pipe into the box revealed an intriguing distribution of colored particles within the system after 6 s of die filling, as depicted in Fig. 6C. There the side view from the right and left side and coloring as per the zones and as per the particle size is shown. Eventually, at 6 s 54% of 'fresh' particles (color 5–9, Fig. 6A) from the pipe contributed to the overall particles in the box. Fresh particles (color 5–9) constituted about 93% in the last die and 31%, 66%, 50%, and 77% in sections 1, 2, 3, and 4, respectively, resulting in the highest intermixing in the zones which were involved in particles discharge and re-filling. Overall, the particles in section 1 remained under no or low moving status (confer velocity analysis in Fig. 4, Section 3.1.1 and Table 3) whereas the sections 2 and 4 were constantly intermixed/rearranged, which is in agreement with the mono-sized granules data [27]. Thereby section dependent PSD evolution within the box resulted, which was in agreement with the observations that have been made in Section 3.1.2.3.

This coloring analysis supported the understanding of particles rearrangement and flow within the box thereby helped in understanding the shear forces acting on the particles. A high particle residence time in the box might bear the risk of over lubrication affecting the dissolution profile of the tablets over time [28,74–77].

3.2. Influence of material properties

In this section, the influence of inter-particle cohesion, particle-particle friction and particle-wall friction on the different metrics defined in Section 3.1 will be described.

3.2.1. Influence of inter-particle cohesion

One of the most annoying particle properties during powder handling that every formulation researcher experiences is the powder “stickiness” generated by inter-particle cohesion. Different non-contact forces acting on particles such as van der Waals, electrostatic, and liquid/solid bridge forces contribute to the material's “stickiness” [78]. The different forces can act concurrently or successively to different extents [79]. In this study, the influence of the inter-particle cohesion was tested by introducing it as a single quantity known as cohesion energy density (CED) [23,27–30] via the simplified JKR model [46]. The main focus was to gauge the influence of this material property on the die filling as well as on the PSD of the model spheres by varying the CED value between 0, 1.5 MJ/m³, and 3.0 MJ/m³ (setup no. 2, 1 (default), and 3, respectively in Table 2). The rationale behind the selection of these CED values is given by Gopireddy et al. [27].

In general, only minor differences with respect to mass flow rate, mass hold up, tablet mass, and mass variation could be identified between zero and medium (1.5 MJ/m³) CED setups (confer Table 3). However, a higher particle-particle stickiness (CED = 3.0 MJ/m³) caused significantly different results. Most intriguing, in contrast to the constant mass flow rate over the complete discharge time for the medium CED setup (1.5 MJ/m³, confer Fig. 3B), a tri-phasic profile for CED = 3.0 MJ/m³ was found, shown in Fig. 7A. The high mass flow rate (3912 mg/s) in the first third was attributed to the steep powder bed angle in the right half of the box enhancing the particles' transfer from the pipe through the box into the die. The steeper powder bed angle is visualized in Fig. 7B with side view on the right half of the feeding box for medium (1.5 MJ/m³) and high (3.0 MJ/m³) cohesion setups. The low mass hold up in the feeding box (confer Table 3) reduced the normal force exerted on the particles, confer [27], reducing the mass flow rate in the middle die filling period (0.04–0.06 s, Fig. 7B). For the last third, the mass flow rate increased again due to the higher powder bed height in the box. Overall, a mean tablet mass reduction of 33% compared to medium cohesion setup (Table 3) was obtained.

For a CED of 3.0 MJ/m³ mainly clotted particles entered in an unsteady manner (data not shown) from the right half of the feeding box into the die (confer above) leading to a significantly higher tablet mass fluctuation and a higher long-term (RQT_{dies, ss}) and tablet-to-tablet (RSD_{dies, ss}) PSD variation (Table 3). In contrast, the PSD consistency in the feeding box was improved (RSD_{box, ss} and RQT_{box, ss}) demonstrating the discrepancy between PSD development in the box and the die. The reduced segregation tendency in the box for more sticky material was consistent with Gentzler et al. [39]. However, the general assumption of increased cohesion results in decreased segregation could not be confirmed since the highest segregative effect in the feeding box (RQT_{box, ss}) was found for the medium cohesion setup (CED = 1.5 MJ/m³, Table 3), an observation also reported by others [38,80].

Particles' coloring analysis revealed that, again, low and medium CED setups showed similar patterns, unlike to the high CED setup. For the latter, particles remained a longer time in the feeding box (51% “old” particles (color 1–4) after 6 s, Table 3), due to less discharged mass into the die. In parallel, the reduced mass hold up in the feeding box was favoring a higher particles' traveling distance (maximum frequency of color 1 particles in section 4 (confer Section 3.1.3) of 26% and 19% for CEDs of 3.0 MJ/m³ and 1.5

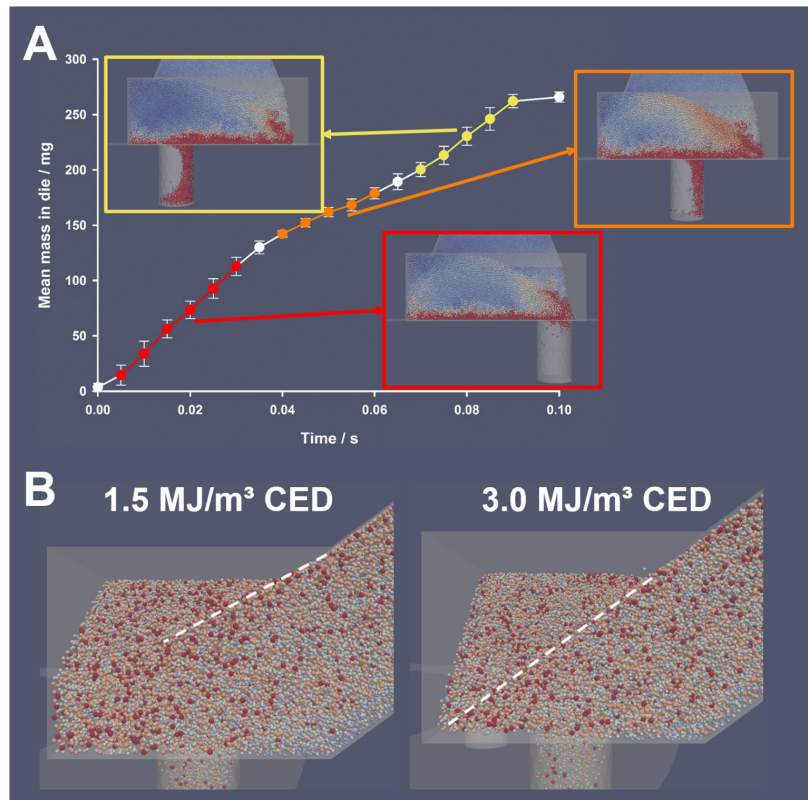


Fig. 7. (A) Mass flow rate into the die for highest CED setup (3.0 MJ/m^3). Additionally, the snapshots of the qualitative illustration of particles' velocity in the box is given at three different time points (beginning, middle, and end). (B) Side view of the feeding box (sections 2 and 4) for medium (1.5 MJ/m^3) and high (3.0 MJ/m^3) cohesion setups. The dotted line indicates the particles' heap in contact with the box boundary to highlight the difference of particles' filling.

MJ/m^3 , respectively). Overall, these effects might enhance the risk for particle attrition and over lubrication by a higher particles' shearing rate [28,30,74].

In summary, it could be clearly stated that for highly cohesive formulations the advantage of a reduced particle size segregation in the gravity feeder was opposite to the drawback of PSD inconsistency in the dies caused by clotted particles filling. This also resulted in a high tablet mass variation. In addition powder flow blockage in the feeding pipe and particle attrition in the box as well as over lubrication might occur. Hence it is advised to generate medium sticky formulations by a clever choice of excipients and lubricant content.

3.2.2. Influence of particle-particle friction

The microscopic particle-particle friction (μ_{pp}), that is entering in DEM contact force calculations [43], was shown to influence significantly the tablet mass due to an increased resistance of particle motion at high μ_{pp} values [23,27,81–83]. This is consistent with a reduced discharge rate found in hoppers [50]. Only few experimental and numerical studies have evaluated the influence of the inter-particle friction on the segregation behavior and most of them used two different friction parameters for particles of same size [84–89]. To our knowledge, only one group investigated the influence of the μ_{pp} on particle size segregation [90,91]. They found that the rate of segregation intensity was nonmonotonous, being high at low μ_{pp}

values, decreasing to a minimum value at $\mu_{pp} \sim 0.1$, and increasing again with increasing μ_{pp} indicated by the presence of competing segregation mechanisms. Different patterns of collective flow of the granular material were identified with dominating local mixing at low μ_{pp} compared to a cyclic motion of the total bulk at high μ_{pp} [90,91]. In this study the influence of the μ_{pp} in a poly-disperse gravity die filling setup was studied by setting the μ_{pp} to three different values, 0.2, 0.4, and 0.6 (setup nos. 4, 1, and 5 in Table 2).

Consistent with literature findings [23,27,81–83], an increase in μ_{pp} caused a significant decrease in tablet mass, mass flow rate, and mass hold up in the feeding box (Table 3). At higher μ_{pp} , the energy dissipation during particle-particle contact is reduced. Hence particles in the shearing layer with the turret transferred their momentum to particles above them resulting in an overall mean particles' velocity increase in the complete feeding box by 19% for μ_{pp} of 0.6 compared to 0.2 (Table 3). With increasing μ_{pp} the mean fines content in the dies during steady state ($q_3, \text{dies}, \text{ss}$) decreased and the tablet-to-tablet ($\text{RSD}_{\text{dies}, \text{ss}}$) as well as long-term content consistency ($\text{RQT}_{\text{dies}, \text{ss}}$) were deteriorating (Table 3). No explanation for those observations can be given at this moment. In addition the mean content in the dies of the model "API" particles was further away from the label claim of 8.5% (Fig. 2, q_3 of API particles = 8.1%, 7.8%, and 7.7% for μ_{pp} of 0.2, 0.4, and 0.6, respectively), and their uniformity was lowest ($\text{AV} = 17.4$ and 24.0 for μ_{pp} of 0.2 and 0.6, respectively [3], Table 3). The fines content seg-

regation indices in the feeding box showed highest segregation tendency ($RQT_{\text{box, ss}}$ and $RSD_{\text{box, ss}}$) for a μ_{pp} of 0.6 (consistent with Dziugys and Navakas [90,91]) and which is similar to the filled dies. This segregation similarity in the feeding box and in the filled dies is opposite to the observations made for the influence of the inter-particle cohesion (confer Section 3.2.2). In case of higher cohesion ($CED = 3.0 \text{ MJ/m}^3$) the discharge of clotted particles into the dies counteracted the low segregation tendency in the feeding box. Particles coloring analysis showed no distinctive differences between medium (0.4) and high (0.6) μ_{pp} setups, compared to a significant different pattern at low μ_{pp} (0.2). For the latter, first the higher mass flow rate (confer above, Table 3) provided a more uniform filling over the length of the feeding box indicated by a higher contribution of color 1 and 2 particles in the dies. Second, the reduced particles' velocity (Table 3) could also be reflected by a decreased intermixing of particles in the feeding box from section 1 to 2, and to 4. As a result of the higher mass throughput by increased tablet mass, less "old" particles (color 1–4) remained in the feeding box (38% at 6 s). In sum, particle attrition and over lubrication [27,28,30,74] might be prevented with low μ_{pp} . Furthermore tablet weight RSD, API content RSD, and PSD variation in the filled dies were reduced constituting the best product quality over production time.

These significant differences between the μ_{pp} setups highlight the importance of flowability experiments, e.g. by using a ring shear tester. Thus the effective angle of internal friction [92] ("PHIE", a macroscopic particle-particle friction measure) of the powder bulk can be determined and this might significantly help to classify materials into critical (high μ_{pp} /PHIE) or not, and subsequently aid formulation optimization aiming to reduce the μ_{pp} .

3.2.3. Influence of particle-wall friction

The surfaces of different materials contain a unique distribution of peaks and valleys depending upon the structure or the type of processing used [93]. The degree of surface roughness of the geometry, e.g. a hopper, can significantly impact the material discharge [50]. Though its influence on particle size segregation was so far only tested in rotating drums [94,95] and an inclined base [71]. Reference to the tableting unit operation, in particular the die filling is missing so far. The influence of the particle-wall friction on the die filling behavior of particles having poly-dispersity in size within the lab-scale gravity feeder was evaluated considering three different particle-wall friction coefficients (μ_{pw}) of 0.25, 0.50, and 0.75 (confer Table 2, setup 6, 1, and 7).

Gopireddy et al. [27] showed that a higher geometry surface roughness (high μ_{pw}) could enhance particle motion within the feeding system. Similar to the mono-disperse die filling, poly-disperse particles with high μ_{pw} revealed significantly increased particles' motion. However, the differences of powder flow pattern between a μ_{pw} of 0.50 and 0.75 were only small (Table 3) indicating a non-linear μ_{pw} effect. As the turret was rotating underneath the feeding box, the particles in the shearing layer, showing highest effect by friction with the geometry, transferred their momentum to particles above them. Hence for the highest particle-wall friction ($\mu_{\text{pw}} = 0.75$) an increased particles' velocity was found in comparison to the lowest particle-wall friction ($\mu_{\text{pw}} = 0.25$) (Table 3). This resulted in an increased mass flow rate thereby higher collected mass and mass consistency in the die (Table 3). The higher turnover rate in the feeding box led to an increased particle mixing indicated by earlier appearance of color 1 particles in section 4 (confer Section 3.1.3) at $t = 1.95 \text{ s}$ for $\mu_{\text{pw}} = 0.75$ and 2.40 s for $\mu_{\text{pw}} = 0.5$, consistent with [27].

In contrast, significantly different powder flow phenomena could be identified at low (0.25) compared to high μ_{pw} (≥ 0.50). Those differences mainly arose due to a significantly reduced particles' velocity at low particle-wall friction ($\mu_{\text{pw}} = 0.25$) and led to a

decreased mass flow rate and tablet mass in addition to an increased tablet mass fluctuation (Table 3). The reduced particles' shearing by turret rotation for $\mu_{\text{pw}} = 0.25$ led to three phenomena. (1) The particles impacted with reduced velocity on the left wall of the feeding box hence less momentum was transferred to the particles above (section 1). As a result no particles from the box bottom were transported upwards into section 1 favoring size segregation by "brazil-nut-effect" (BNE) [96]. The disturbances in the powder bed caused by time intervals of high (during die filling) and low (shearing during inter-dies) particles' velocity led to a rise and accumulation of coarse particles on top of the box. (2) The lack of re-circulation from left to right (section 1–2) on top of the box (confer Fig. 8) significantly reduced the particles' residence time and as a result the potential risk of particle attrition and over lubrication [27,28,30,74]. (3) Only one interface over the width of the left half of the feeding box at which "old" particles (blue color, box) and "fresh" particles (orange color, pipe) were coinciding (Fig. 8) has been developed during 6 s of die filing (compare to Fig. 6C for $\mu_{\text{pw}} = 0.50$). In contrast to higher μ_{pw} values, an "API" particles depletion over the complete box ($RQT_{\text{box, ss}} = -0.60\%$) was found. The mean "API" content in the dies was higher in comparison to higher values of μ_{pw} and was most close to the label claim (Fig. 2) and a low tablet-to-tablet content variation gave an AV value of 13.3, constituting the only setup out of all meeting the requirements for content uniformity [3]. However at this moment an explanation for all those observations cannot be provided.

The comparison of the three different μ_{pw} setups showed that with respect to tablet weight variation and particle size consistency from tablet-to-tablet ($RSD_{\text{dies, ss}}$) a high μ_{pw} was beneficial. In contrast, the quality of formulations that show issues with content uniformity (AV) and long term PSD consistency ($RQT_{\text{dies, ss}}$) might be improved by smoothing the geometry surface, thus a reduction of μ_{pw} . It should be mentioned that the findings and drawn conclusions hold only true for the tested turret speed. Altered particles' velocity due to a modified turret speed could lead to different particle size segregation phenomena. In particular the particle shearing layer and the generated voids that are influencing the percolation extent [34,72] (confer Section 3.1.2.3) could change.

3.3. Comparison of all tested material properties

Eventually, a comparison of the influence of all tested material properties (setup no. 1–7) on the quality of the final product and segregation tendency is given in Table 4 to generate a material dependent risk assessment [97]. First of all a short description of the different quality attributes followed by their evaluation with respect to the material properties is provided. The different setups were compared for each and every quality attribute separately assigning the coded value "6" for the setup showing the best result and in descending order to "0" for the worst result. At the end all values were averaged for the individual setups thereby a conclusive comparison between them was generated (confer below).

As the turret was rotating with very high speed (40 rpm), no complete die filling could be obtained (Fig. 3A). However in general, during installation of the process parameters (e.g. pre- and main compression force), the position of the lower punch and turret speed are set to obtain the anticipated tablet mass at completely filled dies. Here, the highest mass in the filled dies was defined as best ("6") since it could also serve as a measure of powder flowability [7,8]. It was shown that out of all setups, the highest mass was 606 mg at a μ_{pp} of 0.2 assigning the coded value of "6" (confer Table 3) and it was almost halved at a CED of 3.0 MJ/m^3 (coded value of "0", confer Table 3). All other setups showed moderate tablet masses between 481 and 564 mg.

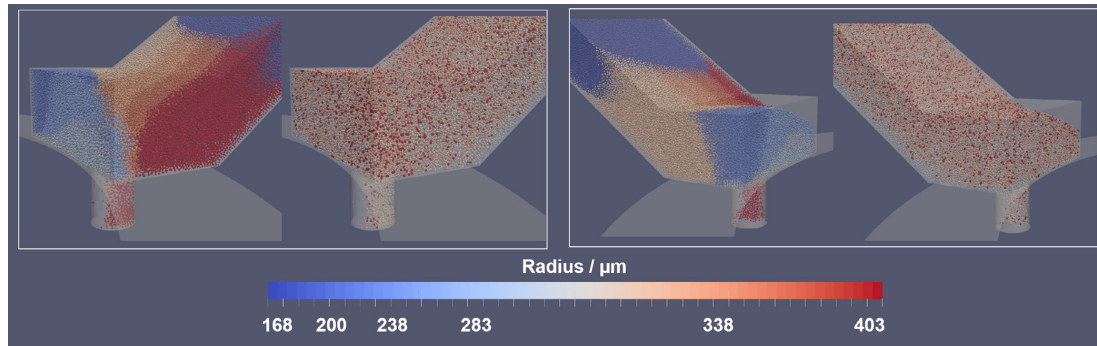


Fig. 8. Visualization of the feeding box by the initially colored particles as well as by their radius after 6 s of die filling for a μ_{PW} of 0.25. (For interpretation of the references to color in this figure legend, the reader is referred to the web version of this article.)

Table 4

Comparison of performance of all tested material properties. A coded value of “0” corresponds to worst, “6” to best performance, respectively. The default setup (setup no. 1, Table 2) has a CED of 1.5 MJ/m³, μ_{PP} of 0.4, and μ_{PW} of 0.50. Cells are marked in ■ if performance is worst (“0”), ■ second worst (“1”), ■ second best (“5”), and ■ best (“6”).

No.	Quality attribute	Measured via	Target value	Material property changed compared to default (setup no.)						
				Default (1)	CED / 0.0 MJ/m ³ (2)	CED / 3.0 MJ/m ³ (3)	μ_{PP} / 0.2 (4)	μ_{PP} / 0.6 (5)	μ_{PW} / 0.25 (6)	μ_{PW} / 0.75 (7)
1	Tablet weight	Mean	High	3	5	0	6	2	1	4
2	Tablet weight uniformity	RSD	Low	4	1	0	5	3	2	6
3	Content uniformity	AV	Low	3	2	4	5	1	6	0
4	Intra-tablet mean particle size consistency	RSD _{dies, ss}	Low	4	3	0	5	1	2	6
5	Long term mean particle size consistency in dies	RQT _{dies, ss}	Low	2	3	1	4	0	6	5
6	Particle size consistency in feeding box	RSD _{box, ss}	Low	2	4	6	5	3	1	0
7	Segregation trend in feeding box	RQT _{box, ss}	Low	2	4	6	5	3	1	0
8	Remixing within feeding box	Onset time	High	3	2	4	5	1	6	0
Average				2.9	3.0	2.6	5.0	1.8	3.1	2.6
Ranking (based on average)				3	4	2	6	1	5	2
No. of extreme low performance (■ and/or ■)				0	1	4	0	4	3	4
No. of extreme high performance (■ and/or ■)				0	1	2	7	0	3	3

The fluctuation of the tablet mass (RSD) entering the calculations for tablet weight uniformity [3] was for all setups, as anticipated, very low (RSD < 1%) with one exception found at highest cohesion (RSD = 1.4% for CED of 3.0 MJ/m³). A similar setup ranking as for the mean tablets mass (confer above) was found for its RSD although no inter-particle interaction (0.0 MJ/m³) revealed a good performance for tablet mass (“5”) but inferiority for its uniformity (“1”).

The third criteria was the calculation of the content uniformity according to Ph. Eur. [3] by selecting one particle size out of the distribution as the model “API” particles. The target value of the AV is ≤ 15 and could only be fulfilled for lowest particle-wall friction ($\mu_{PW} = 0.25$, “6”) setup. All other setups could not meet this criteria thus closest proximity to 15 was considered as second best (“5”) for $\mu_{PP} = 0.2$). The highest particle-wall friction setup ($\mu_{PW} = 0.75$) with highest AV value of 24 (“0”, Table 3) revealed least content uniformity. Surprisingly, the same setup ranking as for content uniformity was found for particles’ remixing within the feeding system (confer below).

The tablet-to-tablet consistency of the PSD was measured in terms of fines q_3 RSD (RSD_{dies, ss}) (confer Section 3.1.2.2). A low fluctuation (low RSD_{dies, ss}) could prevent intermediate differences

in compaction force and dissolution [32,33,58–70]. Content uniformity and the tablets’ PSD consistency were showing comparable rankings over the tested material properties. However, for most extreme particle-wall friction setups ($\mu_{PW} = 0.25$ and 0.75) this relationship could not be confirmed, i.e. highest μ_{PW} setup showed least content uniformity (“0”) although the intra-tablet fines q_3 content consistency was superior compared to other setups (“6”). Long-term PSD consistency, measured via the fines relative q_3 trend over time to mean q_3 (RQT_{dies, ss}), should be as low as possible to obtain tablets of the same properties produced at the beginning and end of the batch. The highest consistency could be obtained at very smooth geometry surfaces, namely at μ_{PW} of 0.25 (“6”).

PSD metrics for the feeding box revealed different setup rankings compared to dies. Though within the box the setups’ ranking for short-term (RSD_{box, ss}) and long-term (RQT_{box, ss}) consistency were same. Hence the most uniform PSD was found in the feeding box at highest particle cohesion (“6”), however this consistency could not be transferred to the dies (confer Section 3.2.1, coded value of “0” and “1” for RSD_{dies, ss} and RQT_{dies, ss}, respectively) as mainly clotted particles discharged in an uncontrollable manner

into the die. The segregation trend ($RQT_{\text{box, ss}}$) within the box was highest at very extreme geometry surface roughness (“1” and “0” for $\mu_{\text{PW}} = 0.25$ and 0.75 , respectively).

Last but not least, the intermixing within the feeding box that might cause particle attrition, over lubrication, and dissolution differences, was analyzed. Since for some setups, the ratio of “old” to “fresh” particles after 6 s in the box did not fully capture the intermixing (confer Section 3.2.3, $\mu_{\text{PW}} = 0.25$ has lowest ratio of “old” particles) so the time point at which color 1 particles appeared in section 4 was used (Table 3). An earlier time point was considered as faster intermixing and should be avoided to reduce particles’ shearing. As shown in Table 4, the highest influence on the residence time/intermixing has the particle-wall friction (“0” for $\mu_{\text{PW}} = 0.75$ and “6” for $\mu_{\text{PW}} = 0.25$) followed by the particle-particle friction. Very low friction values, either between particles or between particles and the geometry were favorable (“6” for $\mu_{\text{PW}} = 0.25$ and “5” for $\mu_{\text{PP}} = 0.2$).

The coded values were averaged for each and every setup individually assigning the coded value “6” for highest and “0” for lowest performance. This average value provided a basic judgment or advice for this setup. In principle, a high average value and less “low” and more “high” performance results would indicate a formulation that could be handled with low caution when it comes to tableting. The best performance out of all could be expected for lowest particle-particle friction setup ($\mu_{\text{PP}} = 0.2$, average “5.0”), the least for highest particle-particle friction ($\mu_{\text{PP}} = 0.6$, average “1.8”). Although some setups obtained quite high average values (“2.6” for CED of 3.0 MJ/m^3 and “3.1” for μ_{PW} of 0.25), they should be handled with medium caution. Namely these two setups showed at least in 3 out of 8 criteria extremely low (“0” or “1”) performance. For highest μ_{PW} ($=0.75$) the most extreme results (best and worst) were found, i.e. in 7 ($4 \times$ “low” and $3 \times$ “high”) out of 8 quality criteria. Hence this setup should be handled with high caution as the superiority with respect to some quality attributes might bear high failure risk for others. Only the setup at medium range parameters (default setup) for cohesion and friction (particle-particle and particle-wall) could provide a good balance as extreme performances are lacking. Formulation design towards a low particle-particle friction ($\mu_{\text{PP}} = 0.2$) should be preferably aimed (average coded value of “5.0”).

The strength of Table 4 lies in the guide provision which property has highest influence on a particular quality attribute. However, all 8 quality attributes obtained the same weighting and adaption might be required if one of them is considered as more critical. This risk assessment could serve as a basis for formulation scientists to control and direct blend properties to highest product quality. Although it should be kept in mind that in reality, compared to numerical simulations, neither of the attributes can be modified independent of each other. In addition, changing two properties at a time, e.g. increasing cohesion and particle-particle friction, could erase the merit or drawback of either of them. Last but not least, it should be mentioned that the ranking provided in Table 4 holds only true at the tested process setup, particularly turret speed (confer influence of turret speed on particles’ velocity and shearing rate, Section 3.2.3).

4. Conclusion

Die filling constitutes a critical step during tablet manufacturing which influences the product quality with respect to tablet weight, content uniformity, and to a lower extent tablet hardness and dissolution by defining its particles’ content. In this study powder flow of a poly-disperse particle size distribution with a real pharmaceutical material pendant from a gravity feeder into the dies of a rotating turret was evaluated. First of all, the die filling

itself has been described with respect to basic metrics such as tablet mass, mass flow rate, mass hold up, and particles’ velocity in the feeding system. In extension to this, novel measures have been introduced to capture the effects of poly-dispersity in size. These, including the individual particles’ size velocity and velocity direction, the mean fines content, its fluctuation and its trend over time, were analyzed within the filled dies and different cross-sections of the feeding box. One out of the six particle size fractions was selected as the model “API” for which the Ph. Eur. requirement for content uniformity has been determined. Lastly, the particle mixing in the system could be assessed by tracking initially colored particles providing reference for particles’ residence time and intermixing indicating the risk for particle attrition and over lubrication. Not only the initial filling of the system caused size segregation but also during discharge different sub-processes within the system revealed location specific segregation differences. As main segregation influencing factors the particles’ velocity, the relative particle mass to size and the shearing forces could be identified.

Additionally to the detailed description of poly-disperse die filling, the influence of three different material properties has been systematically investigated.

The first tested material property was the inter-particle cohesion, a measure for the material cohesiveness. Even though more cohesive particles showed least segregation tendency within the feeding system, they could pose the risk for tablet-to-tablet fluctuations in terms of fines content and tablet mass. Hence an optimal range for blend cohesiveness during formulation development should be complied.

The particle-particle friction turned out to result, within the chosen values of 0.2 – 0.6 , in most extreme performances compared to the other material properties. More clearly, a low particle-particle friction had the most restricted particles’ mobility thereby the die filling was most uniform. Not only the “classic” die filling metrics showed superiority but also segregation tendency was lowest. In contrast, a high particle-particle friction should be strictly avoided as the performance in most of the quality attributes was inferior.

Similar to the mono-disperse die filling, poly-disperse particles with high μ_{PW} revealed significantly increased particles’ motion although it turned out to be least favorable for content uniformity of the model “API” particles.

This study is the first one providing an actual reference for pharmaceutical die filling of a poly-disperse material using calibrated material input parameters. In addition and more importantly, it can serve as a framework for formulation scientists as it sheds light on the influence of material properties on segregation. Thereby product design and quality can be improved.

Although it should be mentioned that the consideration of binary, ternary, etc. mixtures of individual particle sizes, size distributions, and material properties etc. is required to be able to truly predict powder flow in the tableting process.

References

- [1] B.R. Conway, *Pharmaceutical Manufacturing Handbook*, John Wiley & Sons Inc, Solid Dosage Forms, 2007.
- [2] FETTE Compacting GmbH, FE 75. <<http://www.fette-compacting.com/fe75-productivity-redefined/>> (accessed 06.12.2016).
- [3] Ph. Eur., *European Pharmacopoeia*, 8th ed, 2016.
- [4] ICH, *Guidance for Industry Q8 (R2) Pharmaceutical Development*, 2009.
- [5] J. Rantanen, J. Khinast, *The future of pharmaceutical sciences*, *J. Pharm. Sci.* 104 (2015) 3612–3638.
- [6] X. Xie, V.M. Puri, *Uniformity of powder die filling using a feed shoe: a review*, *Part. Sci. Technol.* 24 (2006) 411–426.
- [7] C.-Y. Wu, L. Dihoru, A.C.F. Cocks, *The flow of powder into simple and stepped dies*, *Powder Technol.* 134 (2003) 24–39.
- [8] C. Hildebrandt, S.R. Gopireddy, A.K. Fritsch, T. Profitlich, R. Scherließ, N.A. Urbanetz, *Evaluation and prediction of powder flowability in pharmaceutical*

- tableting, *Pharm Dev Technol* (2017) 1–13, <https://doi.org/10.1080/10837450.2017.1412462>.
- [9] L.C.R. Schneider, I.C. Sinka, A.C.F. Cocks, Characterisation of the flow behaviour of pharmaceutical powders using a model die-shoe filling system, *Powder Technol.* 173 (2007) 59–71.
 - [10] L.A. Mills, I.C. Sinka, Effect of particle size and density on the die fill of powders, *Eur. J. Pharm. Biopharm.* 84 (2013) 642–652.
 - [11] C.-Y. Wu, A.C.F. Cocks, Numerical and experimental investigations of the flow of powder into a confined space, *Mech. Mater.* 38 (2006) 304–324.
 - [12] S. Jackson, I.C. Sinka, A.C.F. Cocks, The effect of suction during die fill on a rotary tablet press, *Eur. J. Pharm. Biopharm.* 65 (2007) 253–256.
 - [13] C. Bierwisch, T. Kraft, H. Riedel, M. Moseler, Three-dimensional discrete element models for the granular statics and dynamics of powders in cavity filling, *J. Mech. Phys. Solids* 57 (2009) 10–31.
 - [14] C.-Y. Wu, A. Brian, N. Vlachos, Characterization of powder flowability for die filling, *Part. Sci. Technol.* 30 (2011) 378–389.
 - [15] C.-Y. Wu, DEM simulations of die filling during pharmaceutical tableting, *Particology* 6 (2008) 412–418.
 - [16] C. Bierwisch, T. Kraft, H. Riedel, M. Moseler, Die filling optimization using three-dimensional discrete element modeling, *Powder Technol.* 196 (2009) 169–179.
 - [17] E.N. Nwose, C. Pei, C.-Y. Wu, Modelling die filling with charged particles using DEM/CFD, *Particology* 10 (2012) 229–235.
 - [18] Y. Guo, C.-Y. Wu, K.D. Kafui, C. Thornton, Numerical analysis of density-induced segregation during die filling, *Powder Technol.* 197 (2010) 111–119.
 - [19] Y. Guo, K.D. Kafui, C.-Y. Wu, C. Thornton, J.P.K. Seville, A coupled DEM/CFD analysis of the effect of air on powder flow during die filling, *AIChE J.* 55 (2009) 49–62.
 - [20] Y. Guo, C.-Y. Wu, K.D. Kafui, C. Thornton, 3D DEM/CFD analysis of size-induced segregation during die filling, *Powder Technol.* 206 (2011) 177–188.
 - [21] C.-Y. Wu, Y. Guo, Numerical modelling of suction filling using DEM/CFD, *Chem. Eng. Sci.* 73 (2012) 231–238.
 - [22] Y. Tsunazawa, Y. Shigeto, C. Tokoro, M. Sakai, Numerical simulation of industrial die filling using the discrete element method, *Chem. Eng. Sci.* 138 (2015) 791–809.
 - [23] O.I. Imole, D. Krijgsman, T. Weinhart, V. Magnanimo, B.E. Chávez Montes, M. Ramaioli, S. Luding, Experiments and discrete element simulation of the dosing of cohesive powders in a simplified geometry, *Powder Technol.* 287 (2016) 108–210.
 - [24] L. Martínez-Martínez, E. Sainz-García, J. Muro-Hernández, F. Alba-Eliás, A. González Marcos, Project Management and Engineering, Segregation of a Binary Granular Mixture in a Feed Shoe of a Single Punch Press Using DEM, Springer International Publishing, 2015.
 - [25] E. Peeters, T. De Beer, C. Vervae, J.-P. Remon, Reduction of tablet weight variability by optimizing paddle speed in the forced feeder of a high-speed rotary tablet press, *Drug Dev. Ind. Pharm.* 41 (2015) 530–539.
 - [26] R. Furukawa, Y. Shiosaka, K. Kadota, K. Takagaki, T. Noguchi, A. Schimosaka, Y. Shirakawa, Size-induced segregation during pharmaceutical particle die filling assessed by response surface methodology using discrete element method, *J. Drug Deliv. Sci. Technol.* 35 (2016) 284–293.
 - [27] S.R. Gopireddy, C. Hildebrandt, N.A. Urbanetz, Numerical simulation of powder flow in a pharmaceutical tablet press lab-scale gravity feeder, *Powder Technol.* 302 (2016) 309–327.
 - [28] W.R. Ketterhagen, Simulation of powder flow in a lab-scale tablet press feed frame: effects of design and operating parameters on measures of tablet quality, *Powder Technol.* 275 (2015) 361–374.
 - [29] D. Mateo-Ortiz, F.J. Muzzio, R. Méndez, Particle size segregation promoted by powder flow in confined space: the die filling process case, *Powder Technol.* 262 (2014) 215–222.
 - [30] C. Hildebrandt, S.R. Gopireddy, R. Scherließ, N.A. Urbanetz, Investigation of powder flow within a pharmaceutical tablet press force feeder - A DEM approach, *Powder Technol.* (2017), under review.
 - [31] D. Mateo-Ortiz, R. Méndez, Microdynamic analysis of particle flow in a confined space using DEM: the feed frame case, *Adv. Powder Technol.* 27 (2016) 1597–1606.
 - [32] S. Lakio, S. Siirä, H. Rääkkönen, S. Airaksinen, T. Närviäinen, O. Antikainen, J. Yliruusi, New insights into segregation during tableting, *Int. J. Pharm.* 397 (2010) 19–26.
 - [33] M. Santl, I. Ilic, F. Vrečer, S. Baumgartner, A compressibility and compactability study of real tableting mixtures: the effect of granule particle size, *Acta Pharm.* 62 (2012) 325–340.
 - [34] N. Kholá, C. Wassgren, Correlations for shear-induced percolation segregation in granular shear flows, *Powder Technol.* 288 (2016) 441–452.
 - [35] H.J. Venables, J.I. Wells, Powder mixing, *Drug Dev. Ind. Pharm.* 27 (2001) 599–612.
 - [36] A.D. Rosato, D.L. Blackmore, N. Zhang, Y. Lan, A perspective on vibration-induced size segregation of granular materials, *Chem. Eng. Sci.* 57 (2002) 265–275.
 - [37] P. Tang, V.M. Puri, Methods for minimizing segregation: a review, *Particul. Sci. Technol.* 22 (2004) 321–337.
 - [38] J.J. McCarthy, Turning the corner in segregation, *Powder Technol.* 192 (2009) 137–142.
 - [39] M. Gentzler, J.N. Michaels, G.L. Tardos, Quantification of segregation potential for polydisperse, cohesive, multi-component powders and prediction of tablet die-filling performance - a methodology for practical testing, re-formulation and process design, *Powder Technol.* 285 (2015) 96–102.
 - [40] P.A. Cundall, O.D.L. Strack, A discrete numerical model for granular assemblies, *Geotechnique* 29 (1979) 47–65.
 - [41] H.P. Zhu, Z.Y. Zhou, R.Y. Yang, A.B. Yu, Discrete particle simulation of particulate systems: theoretical developments, *Chem. Eng. Sci.* 62 (2007) 3378–3396.
 - [42] H.J. Herrmann, S. Luding, Modeling granular media on the computer, *Continuum. Mech. Therm.* 10 (1998) 189–231.
 - [43] W.R. Ketterhagen, M.T. am Ende, B.C. Hancock, Process modeling in the pharmaceutical industry using the discrete element method, *J. Pharm. Sci.* 98 (2009) 442–470.
 - [44] C. Kloss, LIGGGHTS - Manual, 2015. <<http://www.cfdem.com/>> (accessed 12-02-2015).
 - [45] A. Di Renzo, F.P. Di Maio, Comparison of contact-force models for the simulation of collisions in DEM-based granular flow codes, *Chem. Eng. Sci.* 59 (2004) 525–541.
 - [46] K.L. Johnson, K. Kendall, A.D. Roberts, Surface energy and the contact of elastic solids, *Proc. Roy. Soc. Lond. A. Mat.* 324 (1971) 301–313.
 - [47] C. Kloss, C. Goniva, A. Hager, S. Amberger, S. Pirker, Models, algorithms and validation for opensource DEM and CFD-DEM, *Prog. Comput. Fluid Dy. An Int. J.* 12 (2012) 140–152.
 - [48] C. Geuzaine, J.F. Remacle, Gmsh: a 3-D finite element mesh generator with built-in pre- and post-processing facility, *Int. J. Numer. Methods Eng.* 79 (2009) 1309–1331.
 - [49] I.C. Sinka, F. Motazedian, A.C.F. Cocks, K.G. Pitt, The effect of processing parameters on pharmaceutical tablet properties, *Powder Technol.* 189 (2009) 276–284.
 - [50] A. Anand, J.S. Curtis, C.R. Wassgren, B.C. Hancock, W.R. Ketterhagen, Predicting discharge dynamics from a rectangular hopper using the discrete element method (DEM), *Chem. Eng. Sci.* 63 (2008) 5821–5830.
 - [51] D. Antypov, J.A. Elliott, B.C. Hancock, Effect of particle size on energy dissipation in viscoelastic granular collisions, *Phys. Rev. E.* 84 (2011) 021303–021311.
 - [52] C.J. Coetzee, Review: Calibration of the discrete element method, *Powder Technol.* 310 (2017) 104–142.
 - [53] J. Mosby, S.R. de Silva, G.G. Enstad, Segregation of Particulate Materials - Mechanisms and Testers, *KONA Powder Part. J.* 14 (1996) 31–43.
 - [54] Holmes: Colliery Engr., 1934, pp. 11.
 - [55] L.R. Lawrence, J.K. Meddow, Powder segregation during die filling, *Powder Technol.* 2 (1968/69) 253–259.
 - [56] J.W. Carson, R.A. Royal, D.A. Goodwill, Understanding and eliminating particle segregation problems, *Bulk Solids Handling* 6 (1986) 139–144.
 - [57] J.R. Johanson, Solids segregation - causes and solutions, *Powder Bulk Eng.* (1988) 13–19.
 - [58] C. Nyström, G. Alderborn, M. Duberg, Bonding surface area and bonding mechanism - two important factors for the understanding of powder compactibility, *Drug Dev. Ind. Pharm.* 19 (1993) 2143–2196.
 - [59] F. Fichtner, A. Rasmuson, G. Alderborn, Particle size distribution and evolution in tablet structure during and after compaction, *Int. J. Pharm.* 292 (2005) 211–225.
 - [60] S. Patel, A.M. Kaushal, A.K. Bensal, Effect of particle size and compression force on compaction behavior and derived mathematical parameters of compressibility, *Pharm. Res.* 111–124 (2007).
 - [61] T. Lee, C.S. Kuo, Effects of initial average particle size on tableting: evaluating predictive tools for crystal engineers and formulators, *Pharm. Technol.* 30 (2006).
 - [62] J.A. Hersey, G. Bayraktar, E. Shotton, The effect of particle size on the strength of sodium chloride tablets, *J. Pharm. Pharmacol.* 19 (1967) 245–305.
 - [63] T. Yajima, S. Itai, H. Hayashi, K. Takayama, T. Nagai, Optimization of size distribution of granules for tablet compression, *Chem. Pharm. Bull.* 44 (1996) 1056–1060.
 - [64] C. Sun, D.J.W. Grant, Effect of initial particle size on the tableting properties of L-lysine monohydrochloride dehydrate powder, *Int. J. Pharm.* 215 (2001) 221–228.
 - [65] B. Johansson, F. Nicklasson, G. Alderborn, Effect of pellet size on degree of deformation and densification during compression and on compactability of microcrystalline cellulose pellets, *Int. J. Pharm.* 163 (1998) 35–48.
 - [66] M. Wikberg, G. Alderborn, Compression characteristics of granulated materials. II. Evaluation of granule fragmentation during compression by tablet permeability and porosity measurements, *Int. J. Pharm.* 62 (1990) 229–241.
 - [67] K. Zuurman, K.A. Riepma, G.A. Bolhuis, H. Vormans, C.F. Lerk, The relationship between bulk density and compactability of lactose granulations, *Int. J. Pharm.* 102 (1994) 1–9.
 - [68] K.A. Riepma, H. Vormans, K. Zuurman, C.F. Lerk, The effect of dry granulation on the consolidation and compaction of crystalline cellulose, *Int. J. Pharm.* 97 (1993) 29–38.
 - [69] A.B. Bangudu, O.F. Akande, V.T. Adewuyi, The effect of interacting variables on the compaction performance of paracetamol/millet starch tablets, *Pharm. World J.* 8 (1991) 87–90.
 - [70] M. Rehula, The effect of granule size on dissolution of drugs from tablets, *Folia Pharmacol.* 8 (1985) 101–107.
 - [71] W. Zhou, Z. Lai, G. Ma, L. Yang, Y. Chen, Effect of base roughness on size segregation in dry granular flows, *Granul. Matter* 18 (2016) 83.
 - [72] Y. Fan, C.P. Schlick, P.B. Umbanhowar, J.M. Ottino, R.M. Lueptow, Modelling size segregation of granular materials: the roles of segregation, advection and diffusion, *J. Fluid Mech.* 741 (2014) 252–279.

- [73] M. Jivray, L.G. Martini, C.M. Thomson, An overview of the different excipients useful for the direct compression of tablets, *Pharm. Sci. Technol. Today* 3 (2000) 58–63.
- [74] J. Wang, H. Wen, D. Desai, Lubrication in tablet formulations, *Eur. J. Pharm. Biopharm.* 75 (2010) 1–15.
- [75] J. Kushner IV, F. Moore, Scale-up model describing the impact of lubrication on tablet tensile strength, *Int. J. Pharm.* 399 (2010) 19–30.
- [76] D.S. Desai, B.A. Rubitski, S.A. Varia, A.W. Newman, Physical interactions of magnesium stearate with starch-derived disintegrants and their effects on capsule and tablet dissolution, *Int. J. Pharm.* 91 (1993) 217–226.
- [77] A.C. Shah, A.R. Mlodozienec, Mechanism of surface lubrication: Influence of duration of lubricant–excipient mixing on processing characteristics of powders and properties of compressed tablets, *J. Pharm. Sci.* 66 (1977) 1377–1382.
- [78] U.V. Shah, V. Karde, C. Ghoroi, J.Y.Y. Heng, Influence of particle properties on powder bulk behaviour and processability, *Int. J. Pharm.* 518 (2017) 138–154.
- [79] H. Rumpf, *The Strength of Granules and Agglomerates*, in: W.A. Knepper (Ed.), *Agglomeration*, Wiley Interscience, New York, 1962, pp. 379–413.
- [80] D. Geromichalos, M.M. Kohonen, F. Mugele, S. Herminghaus, Mixing and condensation in a wet granular medium, *Phys. Rev. Lett.* 90 (2003) 168702.
- [81] O.I. Imole, M.B. Wojtkowski, V. Magnanimo, S. Luding, Micro-macro correlations and anisotropy in granular assemblies under uniaxial loading and unloading, *Phys. Rev. E* 89 (2014) 042210.
- [82] T. Gröger, A. Ketterfeld, On the numerical calibration of discrete element models for the simulation of bulk solids, *Comput. Aided Chem. Eng.* 21 (2006) 533–538.
- [83] A. Singh, V. Magnanimo, S. Luding, Effect of friction and cohesion on anisotropy in quasi-static granular materials under shear, *AIP Conf. Proc.* 1542 (1) (2013) 682–685.
- [84] K.A. Gillemot, E. Somjai, T. Börzsönyi, Shear-driven segregation of dry granular materials with different friction coefficients, *Soft Matter* 13 (2017) 415–420.
- [85] M.P. Ciamarra, M.D. De Vizia, A. Fierro, M. Tarzia, A. Coniglio, M. Nicodemi, Granular species segregation under vertical tapping: effects of size, density, friction and shaking amplitude, *Phys. Rev. Lett.* 96 (2006) 058001.
- [86] G. Plantard, H. Saadaoui, P. Snabre, B. Pouligny, Surface-roughness-driven segregation in a granular slurry under shear, *Europhys. Lett.* 75 (2006) 335–341.
- [87] C.-C. Liao, S.-S. Hsiau, C.-S. Wu, Combined effects of internal friction and bed height on the Brazil-nut problem in a shaker, *Powder Technol.* 253 (2014) 561–567.
- [88] M. Combarros, H.J. Feise, H. Zetzener, A. Kwade, Segregation of particulate solids: Experiments and DEM simulations, *Particuology* 12 (2014) 25–32.
- [89] S.H. Chou, H.J. Hu, S.S. Hsiau, Investigation of friction effect on granular dynamic behavior in a rotating drum, *Adv. Powder Technol.* 27 (2016) 1912–1921.
- [90] A. Dziugys, R. Navakas, The role of friction on size segregation of granular material, *Mechanika* 4 (2007) 59–68.
- [91] A. Dziugys, R. Navakas, The role of friction in mixing and segregation of granular material, *Granul. Matter* 11 (2009) 403.
- [92] D. Schulze, *Powders and Bulk Solids*, Springer-Verlag, Berlin, 2007.
- [93] P. Narayan, B.C. Hancock, The relationship between the particle properties, mechanical behavior, and surface roughness of some pharmaceutical excipient compacts, *Mater. Sci. Eng.* 355 (2003) 24–36.
- [94] A.C. Santomaso, R. Artoni, P. Canu, Controlling axial segregation in drum mixers through wall friction: cellular automata simulations and experiments, *Chem. Eng. Sci.* 90 (2013) 151–160.
- [95] C.-F. Lee, H.-T. Chou, H. Capart, Granular segregation in narrow rotational drums with different wall roughness: symmetrical and asymmetrical patterns, *Powder Technol.* 233 (2013) 103–115.
- [96] M.E. Möbius, B.E. Lauderdale, S.R. Nagel, H.M. Jaeger, Brazil-nut effect: size separation of granular particles, *Nature* 414 (2001) 270.
- [97] A. Selen, P.A. Dickinson, J.R. Crison, H.B. Mistry, M.T. Cruanes, M.N. Martinez, H. Lennernäs, T.L. Wigal, D.C. Swinney, J.E. Polli, A.T.M. Serajuddin, J.A. Cook, J.B. Dressman, The biopharmaceutics risk assessment roadmap for optimizing clinical drug product performance, *J. Pharm. Sci.* 103 (2014) 3377–3397.

3.2 Force feeding

3.2.1 Powder flow in a three-chambered force feeder

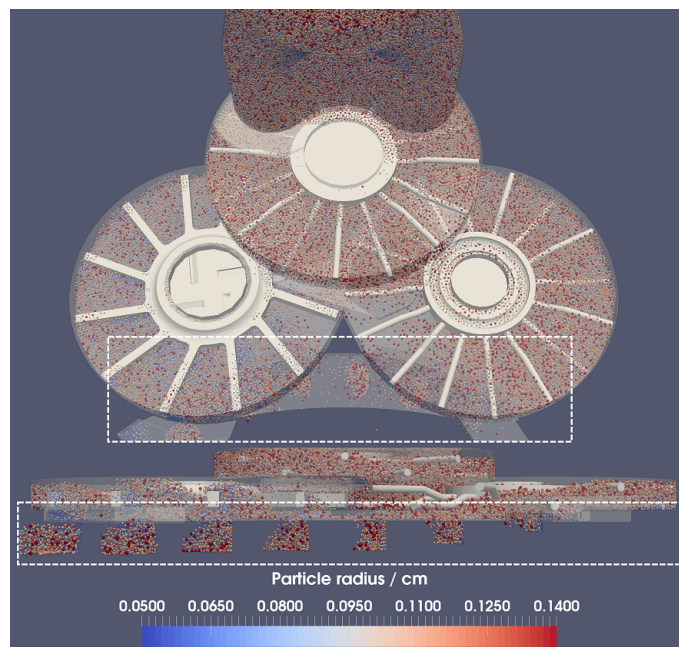
Numerical Analysis of the Die Filling Process Within a Pharmaceutical Tableting Machine

Claudia Hildebrandt¹, Srikanth R. Gopireddy², Regina Scherließ¹,
Nora A. Urbanetz²

¹ Department of Pharmaceutics and Biopharmaceutics, Christian-Albrechts-Universität Kiel,
Grasweg 9a, 24118 Kiel, Germany

² Daiichi-Sankyo Europe GmbH, Pharmaceutical Development,
Luitpoldstrasse 1, 85276 Pfaffenhofen, Germany

Chemie Ingenieur Technik, 90:483-492, 2018



Outline

In contrast to gravity filling described in the previous chapters by an experimental die filling system (chapter 3.1.1 & 3.1.2) and a numerical lab-scale gravity feeder (chapter 3.1.3 & 3.1.4), force feeding for a FETTE 1200i tableting machine is evaluated in the following using the DEM. In force feeding, the powder is actively transported by rotating paddle wheels into the dies of the turret and thus adds complexity to the die filling process. For example, the force feeder of the FETTE 1200i consists of three counter-rotating paddle wheels, a dosing wheel, a filling wheel, and a reverse dosing wheel.

For the numerical gravity feeding studies a two step approach is described with at first mono-disperse (chapter 3.1.3) and then poly-disperse (chapter 3.1.4) sized particles. For force feeding, directly poly-disperse particles are utilized to evaluate the size segregation within the feeding system. Though the size distribution does not have an experimental pendant as in chapter 3.1.4, a PSD is developed which contains several differently sized particles referred as ‘excipients’ and one particle size fraction referred as ‘API’. This PSD is artificially designed to mimic a direct compression formulation within the computational capabilities of the DEM. Lacking an experimental counterpart, direct calibration of the material properties for this model formulation is not possible. The material properties of the complete mixture are adapted in such a way that bulk density, mass flow rate, and angle of repose would fall into the group of good flowing pharmaceutical diluents.

In the following chapter, reference is given to the first process step, the filling of the force feeder during process setup, as well as to the high speed tableting process. The mass hold up, mass flow rate, and tablet mass are studied. A first evaluation of the size segregation mechanisms within this force feeder is given and is further intensified in chapter 3.2.2 with additional measures.

Furthermore, results from a DoE, which are in more detail explained in chapter 3.2.3, are presented. The gravity feeder studies in chapters 3.1.3 & 3.1.4 show a significant influence on die filling from inter-particle cohesion and the coefficient of friction. As more particle-wall contacts are found in the force feeder due to the rotating paddle wheels compared to the static walls in the gravity feeder, the particle-wall instead of the particle-particle coefficient of friction is selected as variable factor in the DoE. In addition to the inter-particle cohesion and particle-wall coefficient of friction as micro-mechanical material properties, the API content of the model formulation is varied. Similar as in the first gravity feeder study (chapter 3.1.3), the turret speed and moreover, the paddle wheel speed are included as factors in the DoE. In the current study, the influence of the different material properties and process conditions on the tablet mass is evaluated. As already mentioned, results of the DoE are more extensively studied in chapter 3.2.3 for more tablet quality attributes.

This first chapter in force feeding serves as a basis for the following ones (chapters 3.2.2- 3.2.5) as it introduces additional measures to describe the higher complexity of die filling by force feeding.

Numerical Analysis of the Die Filling Process Within a Pharmaceutical Tableting Machine

Claudia Hildebrandt^{1,*}, Srikanth R. Gopireddy², Regina Scherließ¹, and Nora Urbanetz²

DOI: 10.1002/cite.201700114

One of the main benefits of numerical simulations is the ability to shed light on the underlying physics in unit operations. This advantage was exploited in this work to study the die filling process in a lab-scale pharmaceutical rotary tablet press. The die filling process with emphasis on mass holdup, mass flow rate, tablet mass, and API content in the dies is described in detail. Eventually a design of experiments provides a clear picture on the influence of process conditions and material properties on the tablet mass to improve the process understanding.

Keywords: Discrete element method, Material properties, Pharmaceutical tableting, Powder flow, Process parameters

Received: August 29, 2017; *accepted:* January 09, 2018

1 Introduction

Tablets, the most important application form to deliver active pharmaceutical ingredients (API) to patients, are mostly produced at high throughput on rotary tablet presses. Tableting consists of three distinct stages: First powder is filled into dies, followed by powder compaction, and finally the compressed tablets are ejected. To achieve high output, rotary tablet presses usually contain a feeding system with rotating paddles that force the powder into the dies of the rotating turret. Various geometries, differing in terms of number of paddle wheels and paddle wheel shapes, exist. Although material transfer from the feeding system to the dies plays a crucial role during tablet manufacturing as it defines product quality attributes, only very little is known about the powder flow pattern within feeders.

The first study reported in this field focused on a model die filling system consisting of a stationary die and a moving shoe [1]. This system was extensively studied experimentally as well as numerically by means of the discrete element method (DEM) [2]. More recently die filling into rotating dies by gravity [3, 4] and force feeding containing one [5] and two [6] paddle wheels were studied numerically. The major benefit of numerical simulations by DEM lies in the highly detailed results since each and every particle can be tracked within the system [7]. However, this benefit comes along with a high computational cost. Thereby most numerical studies either focused on the effect of geometry design, process parameters, or micro-mechanical material properties [3, 5, 6]. Only very few considered the fundamental inheritance of differently sized particles within pharmaceutical blends [4, 6].

One mode of tablet manufacture is direct compression (DC) of the blend without prior granulation [8]. In DC blends API particles are mixed together with different excipients such as disintegrants, flow aids, and diluents. This

results in a characteristic particle size distribution (PSD) and different particle properties such as shape, density, and surface roughness of the blend, which influence as a whole powder flowability [9].

In this study, the limitations of previous studies have been addressed by shedding light on powder flowability in the context of a lab-scale rotary tablet press consisting of a force feeder with three paddle wheels. Additionally, particles of different sizes mimicking a DC formulation have been applied. A detailed design of experiments has been generated to ascertain the influence of different process conditions and material properties on the tablet mass. Eventually this study helps understanding the die filling process in tableting by using a realistic system and it provides different means of process optimization.

2 Methodology

2.1 Discrete Element Method

After introduction of the DEM in 1979 it has evolved to a well-known approach in particle technology. This numerical model captures the trajectories of every individual particle in the system through Newton's equation of motion. Details about theory and algorithms are described in [7, 10, 11]. All computations were performed using the open

¹Claudia Hildebrandt, Prof. Dr. Regina Scherließ
childebrandt@pharmazie.uni-kiel.de

Kiel University, Department of Pharmaceutics and Biopharmaceutics, Grasweg 9a, 24118 Kiel, Germany.

²Dr. Srikanth R. Gopireddy, Dr. Nora Urbanetz
Daiichi-Sankyo Europe GmbH, Pharmaceutical Development,
Luitpoldstraße 1, 85276 Pfaffenhofen, Germany.

source DEM software LIGGGHTS [12], version 3.4.1. Same models to calculate normal, tangential, and non-contact forces as in [3, 4] have been used.

2.2 Geometrical Setup

The geometrical configuration and dimensions correspond to the "Fill-O-Matic" of a lab-scale Fette 1200i rotary tablet press (Fette Compacting GmbH, Schwarzenbek, Germany) and are illustrated in Fig. 1. It consists of a feeding hopper ((1) in Fig. 1) and a feeding plate comprising three differently shaped paddle wheels. The dosing wheel ((2) in Fig. 1), reverse dosing wheel ((4) in Fig. 1), and turret ((5) in Fig. 1) are rotating in anti-clockwise, the filling wheel ((3) in Fig. 1) in clockwise direction. The die height is changing according to the die position during filling. Initially, at the positioning of the filling wheel (position B in Fig. 5), the lower punch is lowered during *fill cam* to create a maximal die height of 1.5 cm which remains constant during position C and D in Fig. 5. At the end of filling, during *dosing cam*, the lower punch is moving upwards by 0.2 cm at to remove excess powder and to create a more confined powder bed (position E in Fig. 5). A large die diameter of 2.4 cm was selected to ensure least influence of particle size (see Section 2.2) on the powder flow [13].

2.3 Material Properties

As mentioned in the introduction, a PSD, shown in Fig. 2, reflecting a blend consisting of API and excipient particles was defined. For excipients, six different particle sizes ranging up to 2800 μm diameter at a mean diameter of 2201 μm were selected. In DC formulations, the API particles' flowability and compressive properties limit its maximal content

[8]. A reasonable content (w/w) of 5 % and 30 % and size ratio of 1:2 to the excipients' mean diameter (API particle diameter of 1000–1129 μm) [14] were chosen. Although absolute particle sizes are much higher compared to realistic DC blends, the total number of simulated particles ($\sim 286\,000$ for 5 % and $\sim 622\,000$ for 30 % API, Tab. 3) is already at the computational limit.

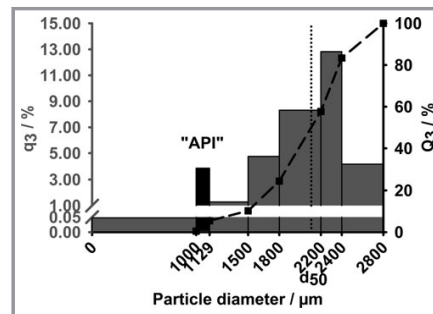


Figure 2. Particle size distribution consisting of seven different sizes, out of which one particle size reflects API particles and the remaining are excipient particles.

Bulk density, angle of repose, and mass flow rate according to Ph. Eur. [15] of different pharmaceutical diluents (different grades of lactose, mannitol, and micro-crystalline cellulose used in DC formulations) have been measured. Values obtained through experiments have been compared to numerical results, and micro-mechanical properties, especially non-contact force (cohesion energy density (CED)) and friction between particles and geometry (coefficient of friction, particle-wall) have been adapted iteratively to obtain good results accordance. The adapted micro-mechanical properties used during filling and discharge are

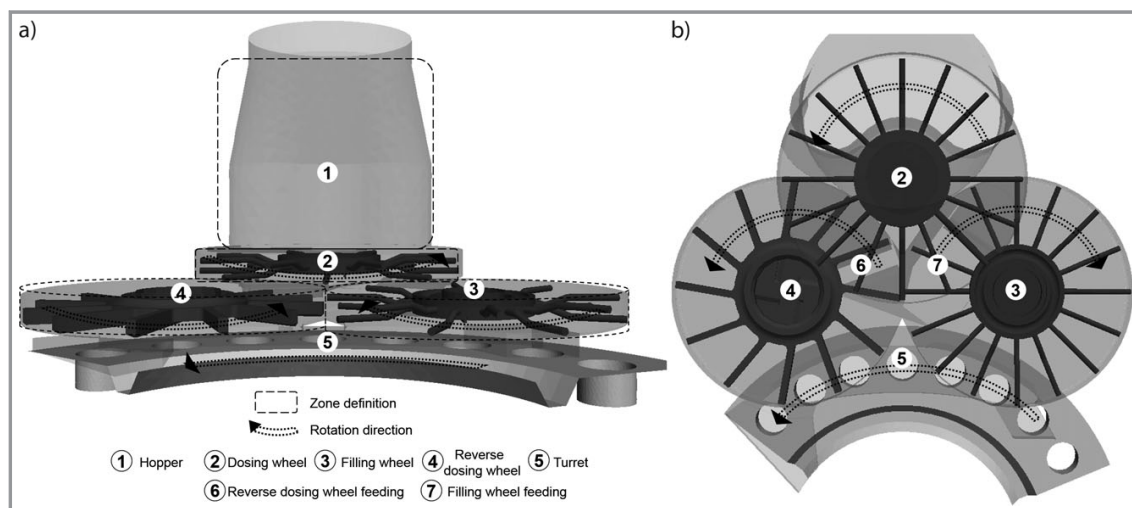


Figure 1. Illustration of the geometrical setup in a) front- and b) top view.

within the range of literature data [2–6, 16, 20, 21] and listed in Tab. 1.

Table 1. Material properties, the numbers in parenthesis correspond to computation step in Tab. 2.

Parameter / Unit	Property of	Value during filling (1–3)	Value during discharge (4) (setup no. 9, Tab. 3)
Young's modulus [GPa]	particle	8.7	8.7
	wall	210	210
Poisson's ratio [-]	particle	0.30	0.30
	wall	0.35	0.35
Coefficient of restitution [-]	particle-particle	0.15	0.15
	particle-wall	0.15	0.15
Coefficient of friction [-]	particle-particle	0.35	0.40
	particle-wall	0.30	0.25
Cohesion energy density (CED) [MJ m ⁻³]	particle-particle	1.5	1.0

2.4 Initialization and Die Filling Process

The system was filled with particles (with the PSD for 5% and 30% API content) mimicking the real process by a stepwise procedure, listed in Tab. 2. At the very beginning, powder was filled from the blending container into the feeding system hopper (step no. 1, Tab. 2). Subsequently, powder was distributed evenly within the Fill-O-Matic by slow paddle wheel rotations (step 2, Tab. 2). Afterwards, the complete tableting machine was filled with powder by one turret rotation at low speed (step 3, Tab. 2). Eventually after a physical time of 15.8 s, the system was completely filled with particles (illustrated in Fig. 3 for 5% API content).

This filling procedure ensured a constant filling level independent of subsequent process parameters and material properties (Tab. 1). Powder discharge, meaning the actual die filling process, started by high-speed tableting at increased paddle wheel speed (e.g., 30 rpm, setup no. 9 in Tab. 3) and turret speed (e.g., 75 rpm, setup no. 9 in Tab. 3) to generate a maximal output of 108 000 tablets per hour with 24 punch stations. To get an understanding of die filling during high-speed tableting, ten turret revolutions to fill in total 240 dies have been simulated. As particles filled in dies left the simulation domain, continuous particles' refill-

Table 2. Process parameters at different computation steps (setup no. 9 in Tab. 3 during discharge).

No.	Description	Physical time [s]	Turret speed [rpm]	No. of turret rotations [-]	Paddle wheel speed [rpm]	No. of paddle wheel rotations [-]
1	Filling of hopper	0.8	0	0	0	0
2	Filling of Fill-O-Matic	9	0	0	15	2.26
3	Filling of turret	6	10	1	15	1.5
4	Discharge	8	75	10	30	4

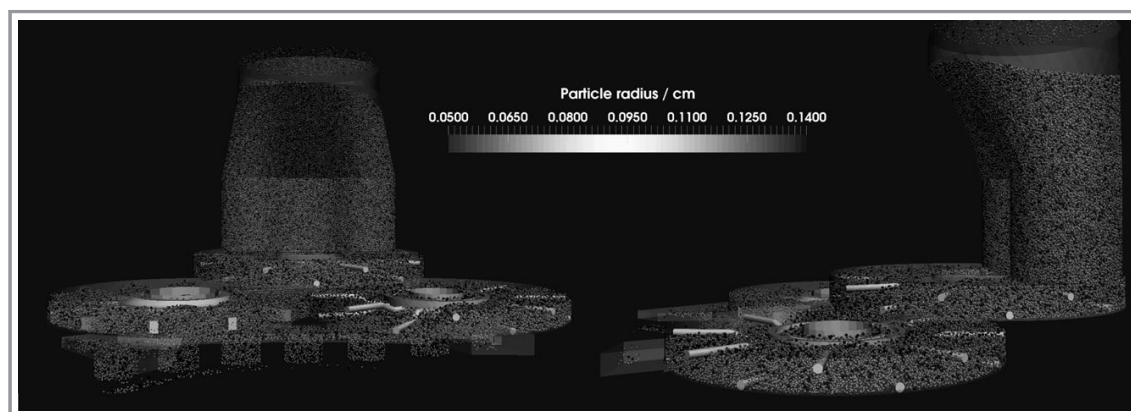


Figure 3. System at the end of filling (3) and before discharge (4) (Tab. 2); left: front view, right: side view.

Table 3. Overview of the changed parameters in the setups for the DoE (setup no. 1–16) and verification (setup no. 17).

No.	Pattern	Process conditions		Material properties			Mean tablet mass [g]
		Turret speed [rpm]	Paddle wheel speed [rpm]	API content [%]	CED [MJ m^{-3}]	μ_{PW} [-]	
1	----+	40	30	5	1.0	0.75	4.7
2	---+-	40	30	5	3.5	0.25	4.8
3	--+-	40	30	30	1.0	0.25	5.3
4	---++	40	30	30	3.5	0.75	4.7
5	-+---	40	60	5	1.0	0.25	5.1
6	-++--	40	60	5	3.5	0.75	4.7
7	-+++-	40	60	30	1.0	0.75	5.2
8	-+++-	40	60	30	3.5	0.25	5.1
9	+----	75	30	5	1.0	0.25	3.6
10	+---+	75	30	5	3.5	0.75	2.7
11	+---+	75	30	30	1.0	0.75	3.2
12	+---+	75	30	30	3.5	0.25	3.6
13	++++	75	60	5	1.0	0.75	3.6
14	++++	75	60	5	3.5	0.25	4.1
15	+++--	75	60	30	1.0	0.25	4.7
16	+++++	75	60	30	3.5	0.75	3.7
17	-+---	40	60	30	1.0	0.25	5.3

ing in the feeding hopper ensured constant mass in the system.

2.5 Design of Experiments

To perform simulation, a fractional factorial design of experiments (DoE) including five factors at two levels, with a resolution of V, and D-optimality was generated (JMP 13.0.0, SAS Institute). In total 16 different experiments have been performed (2^{5-1} , Tab. 3) as per the DoE. From a process parameters point of view, the two most important parameters turret speed and paddle wheel speed were selected. Their factor levels were set at a reasonable operating range of 40 and 75 rpm for turret speed and 30 and 60 rpm for paddle wheel speed.

In addition, three different material properties have been included. They were identified by previous data analysis, pharmaceutical development batches, and numerical results [3, 4]. First, the impact of API content, namely high or low dose strength formulations have been considered by selecting an API content of 5% and 30%, respectively [8]. Second, the inter-particle cohesion or powder stickiness that is in reality a combination of different non-contact forces, such as van der Waals, electrostatic, and capillary forces,

was set at a low (1.0 MJ m^{-3}) and high (3.5 MJ m^{-3}) level (see Tab. 3) [3, 4]. Third, the friction between the particles and the geometry (μ_{PW}) that is mainly attributed to the degree of surface roughness was varied between 0.25 and 0.75 [3, 4, 15]. The results, in particular tablet mass, have been evaluated with JMP (JMP 13.0.0, SAS Institute) in terms of effect analysis.

3 Results and Discussion

The die filling process in an actual lab-scale pharmaceutical tablet press (Fette 1200i) has been studied with a PSD found in DC formulations and calibrated material properties. First of all, the filling of the Fill-O-Matic, following the standard procedure in experiments, will be described exemplarily for a low dose strength formulation (5% API content). Afterwards die filling in high-speed tableting at one selected combination (setup no. 9 in Tab. 3) of process parameters (paddle wheel and turret speed) and material properties (API content, cohesion, and particle-wall friction) will be extensively discussed focusing on mass and API distribution. Finally the influence of different process conditions and material attributes on the tablet mass will be explained based on the DoE.

3.1 Filling of System

The filling of the system with the PSD for 5% API content (cf. Fig. 2) was performed according to the respective experimental procedure and is in detail described in Section 2.4 and Tab. 2. In interval (1) the hopper is filled with particles causing a steep increase in mass holdup in this section (Fig. 4a). Under constant refilling, the first particles arrive in the dosing wheel zone and as soon as the dosing wheel is rotating at 15 rpm, first particles enter the reverse dosing wheel zone followed by the filling wheel zone attributed to the feeding zones location and the dosing wheel rotation direction (cf. Fig. 4a (2), and Fig. 1 (6) and (7)). As soon as the dies start being filled by turret rotation (10 rpm, Tab. 2, step (3)), the mass holdup in the filling wheel zone decreases as dies are majorly filled at the very beginning of the fill zone (see below). In contrast, mass holdup in the reverse dosing wheel zone steadily increases until maximum at

$t = 15.8$ s is reached. Before discharge starts ((4) in Tab. 2 and Fig. 4a), the mass holdup within the force feeder is highest in the dosing wheel zone, followed by filling and reverse dosing wheel zones.

API content analysis reveals non-uniform distribution of API particles within the Fill-O-Matic. Although the API content is constant and corresponds to the label claim (5%) in the hopper (Fig. 4b), it is significantly increased in the reverse dosing wheel zone (maximum API content of 11% at $t = 16.5$ s) and decreased in the filling wheel zone. During filling of the Fill-O-Matic particle size segregation with an accumulation of small particles (particle diameter ≤ 1800 μm) in the dosing wheel and the reverse dosing wheel zones occurs, whereas the opposite (depletion of small particles) is found in the filling wheel zone. Particles are fed from the hopper first into the dosing wheel zone where a top-to-bottom segregation of particles is found. At the bottom smaller particles (particle diameter ≤ 1800 μm)

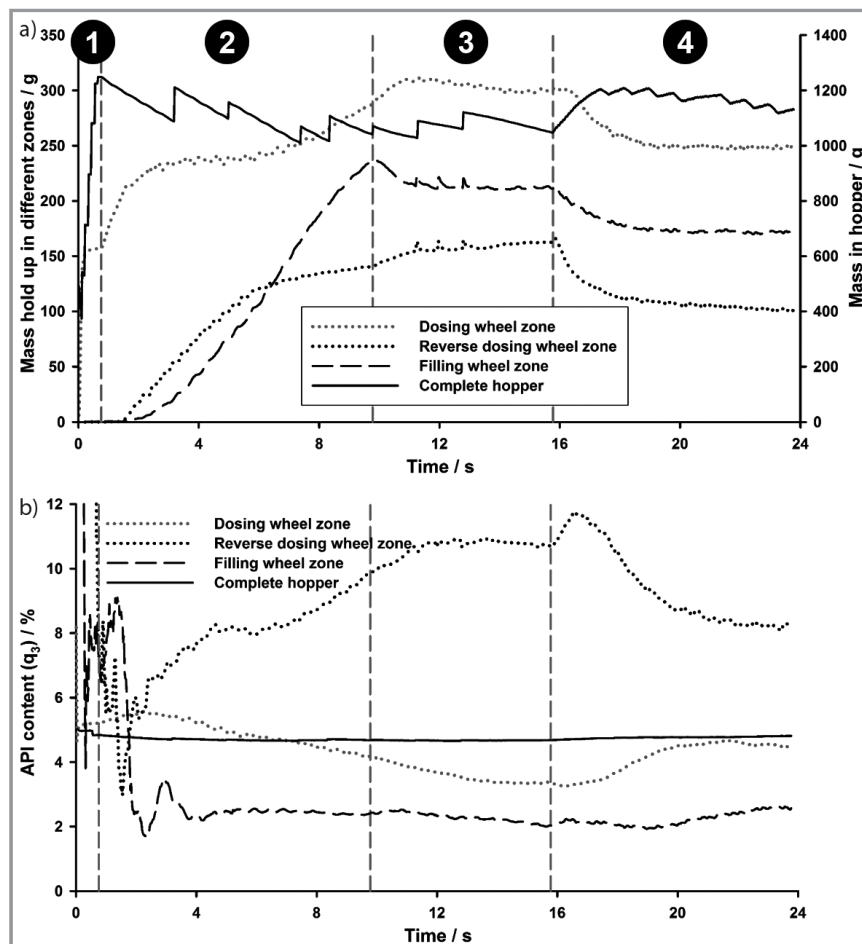


Figure 4. Mass holdup (a) and API content (b) in different locations of Fill-O-Matic over time. Same time intervals as listed in Tab. 2 are indicated.

are located whereas large particles rise on the top of the zone. During anti-clockwise rotation of the dosing wheel (cf. Fig. 1, (2)), particles are first fed into the reverse dosing wheel zone (Fig. 1, (6)). Hence more small particles from the bottom of the dosing wheel zone are falling into the reverse dosing wheel zone transferring particle size segregation. During subsequent dosing wheel rotation the remaining particles fall through the filling wheel feeding hole (Fig. 1, (7)) and enter the filling wheel zone (Fig. 1, (3)). Since less small particles are found after reverse dosing wheel feeding, a decreased API content in the filling wheel zone is identified. At the end of the filling procedure (Fig. 4b, $t = 15.8$ s, (3)) the following order of API content in different locations of the Fill-O-Matic has been established: filling wheel zone 2.0 % < dosing wheel zone 3.4 % < hopper 4.7 % < reverse dosing wheel zone 10.7 %.

3.2 Die Filling Process

After filling of the system, which allowed a homogeneous packing structure at the beginning of all setups and ensured that observations during discharge were related to process condition and material features, the actual die filling and tableting process is initiated by setting the process parameters, especially paddle wheel and turret speed to operating conditions (Tab. 2, step 4, setup no. 9 in Tab. 3). In addition, material properties with respect to particle-wall friction and non-contact force have been changed (Tab. 1). To facilitate the understanding of tablet properties, in particular the two quality attributes tablet mass and API content, which are majorly influenced by the die filling step, mass flow rate, mass holdup, and API content are explained in detail.

3.2.1 Mass Flow Rate

Die filling occurs as the turret is rotating in anti-clockwise direction underneath the Fill-O-Matic. As soon as the die is entering the Fill-O-Matic (position A to B in Fig. 5), the lower punch is moving downwards to form the die volume. A die height of 1.5 cm is created by downwards movement of the lower punch (cf. Fig. 6b, interval B). As the die volume increases, particles are forced into the die by rotation of the filling wheel. Over time in interval B, a mass flow rate of $28.6 \pm 4.8 \text{ g s}^{-1}$ is found (Fig. 6a, B). Between filling and reverse dosing wheel, the mass flow rate is decreasing to $9.8 \pm 2.8 \text{ g s}^{-1}$ as particles on top of the turret are entering the die through gravity (C in Fig. 6a). Subsequently opposed to turret rotation direction, the reverse dosing wheel pushes particles into the die causing again an increase in mass flow rate ($20.3 \pm 2.9 \text{ g s}^{-1}$). Eventually in

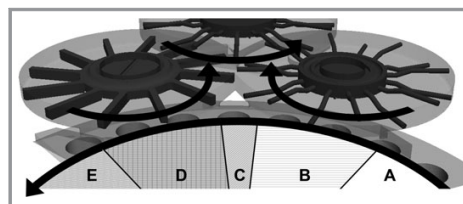


Figure 5. Illustration of die filling positions within Fill-O-Matic. Letters are chosen according to sections of Fig. 6. Arrows indicate rotation direction of turret and paddle wheels.

interval E (*dosing cam*, Fig. 5) and after the dies have left the Fill-O-Matic, the die height is decreasing by 0.2 cm by upwards movement of the lower punch, thereby 74 mg or 2 % of die mass are scraped. Particles removed from the dies during *dosing cam* are transported in the turret gutter and subsequently re-enter the Fill-O-Matic during interval A (Fig. 5).

In total, during interval B 50 %, interval C 14 %, and interval D 36 % of the maximum die mass (before *dosing cam*) are filled into the die (Fig. 6a). In other words, half of the die is filled by particles originating from the filling wheel zone and only a little more than one third by the reverse dosing wheel zone. Those differences do not only influence the mass collected in the die but also the API content, as follows.

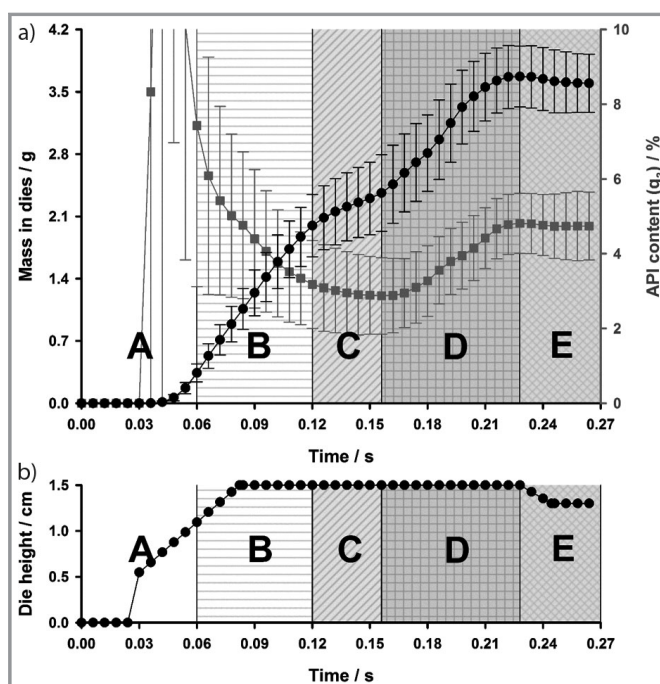


Figure 6. a) Mass collected in dies and API content during die filling. Letters and sections indicate corresponding positions within the Fill-O-Matic as shown in Fig. 5. b) Die height as it changes over filling time.

Parallel to mass in die, API content over time in the filled die is plotted in Fig. 6a. Particles from the gutter enter the Fill-O-Matic in an unsteady manner, indicated by a high API content fluctuation during interval A (Fig. 6). In the following, API content decreases from interval B to C to a mean content of 3.3%. Since API content in the filling wheel zone is on average 2.2% (cf. Fig. 4b, (4)) only a low content blend is transferred to the dies. Afterwards API content in the dies increases significantly during interval D as the API content in the reverse dosing wheel zone is 9.4% (cf. Fig. 4b, (4)). Although over the filling time for each die the API content in the die is changing dramatically, the API content differences between filling and reverse dosing wheel zone taken together result in a final mean die API content of 4.8% (Fig. 6a and 7).

3.2.2 Mass Holdup and API Content in Fill-O-Matic

After system filling, operation parameters are changed to 75 rpm turret and 30 rpm paddle wheel speed (interval 4 in Tab. 2, setup no. 9 in Tab. 3). As the dies leave the simulation domain, particles are constantly refilled at the same iteration rate into the feeding hopper (Fig. 4a, (4)) to ensure constant normal pressure exerted on particles within the Fill-O-Matic. Although the fill level in the hopper is constant, the mass holdup in different paddle wheel zones initially shows a steep decrease until $t \approx 19$ s followed by a constant fill level. Two different mechanisms may explain this observation.

- 1) Every second around 108 g are leaving the simulation domain in filled dies (per second: 1.25 turret rotations, i.e., 24 filled dies with 3.6 g mean tablet mass). Initially the paddle wheel rotation and mass redistribution within the Fill-O-Matic cannot catch up mass decrease.
- 2) Increased paddle wheel rotation speed, from 15 rpm at interval 3 to 30 rpm in interval 4 (Tab. 2), leads to a ra-

dial distribution of particles by centrifugal force towards the border of the paddle wheel zone. Thereby less mass is located in the center of paddle wheels compared to the zone margin.

In comparison to the differences in API content distribution within the Fill-O-Matic during system setup (Fig. 4b, $t < 15.8$ s), the API content increases both in the dosing and filling wheel zone whereas the opposite trend, a constant decrease (after a short maximal peak) in the reverse dosing wheel zone is found during tableting (Fig. 4b, (4)). This trend is not only found for API particles but also for particles of diameter $\leq 1800 \mu\text{m}$. In sum, the content deviations of API and excipient particles that have evolved during system filling are inverted and a converging trend towards the set PSD (cf. Fig. 2) can be identified.

3.2.3 Tablet Mass and API Content

Tablet mass and API content in the dies is shown in Fig. 7. The first 18 dies have already been filled during slow turret rotation in interval 3 (Tab. 2), hence, they contain the highest mass and API content. Subsequently tablet mass is decreasing until die no. 120 followed by a constant tablet mass. Over all filled dies during discharge (Tab. 2, interval 4), an average tablet mass of $3.6 \text{ g} \pm 0.3 \text{ g}$ is obtained. The mean API content ($4.8 \% \pm 0.8 \%$) is significantly lower than the specified label claim of 5% (Fig. 2). However, it is found to be constantly fluctuating within the range of mean ± 2 standard deviations after die no. 18 (Fig. 7). With the provided insight in mass flow rate it is clear how the API content in the dies can be constant although API contents in filling wheel and reverse dosing wheel zones (Fig. 4b, (4)) are showing dissimilar trends. As soon as the API content in the filling wheel zone increases, the opposite trend is found for the reverse dosing wheel. Those counteracting tendencies finally result in a constant API content in the dies.

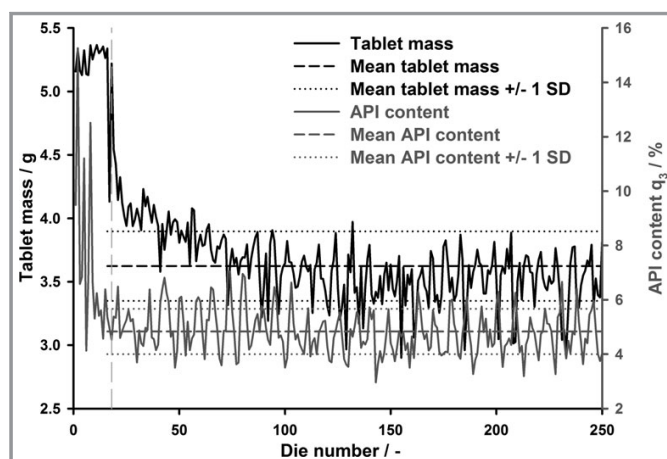


Figure 7. Tablet mass and API content during 10 turret rotations and 240 filled dies.

3.3 Effect of Process Conditions and Material Properties on Tablet Mass

In order to evaluate the influence of different process conditions (turret speed and paddle wheel speed) and material properties (API content, cohesion, and particle-wall friction) on the tablet mass, a set of simulations was performed according to a fractional factorial design of experiment as explained in Section 2.5 (see Tab. 3). The mean tablet masses of all 16 simulations are given in Tab. 3. The statistical evaluation shows that out of the five factors varied, the most significant effect on the tablet mass is found for turret speed, μ_{PW} , and paddle wheel speed (see sorted effect estimates in Tab. 4). The prediction profiler given in Fig. 8a displays the change in

Table 4. Sorted effect estimates for the tablet mass model (* for $p < 0.05$, significant effect).

Term	Estimate	Std error	t ratio	Prob > t
Turret speed	-0.65	0.009553	-68.24	< 0.0001*
μ_{PW}	-0.22	0.009553	-23.51	< 0.0001*
Paddle wheel speed	0.22	0.009553	22.99	< 0.0001*
Turret speed \times paddle wheel speed	0.14	0.009553	14.47	< 0.0001*
Cohesion	-0.13	0.009553	-13.40	< 0.0001*
Turret speed $\times \mu_{PW}$	-0.13	0.009553	-13.37	< 0.0001*
API content	0.12	0.009553	12.94	< 0.0001*
Cohesion \times API content	-0.04	0.009553	-4.01	0.0051*

the response when a factor varies from its low level to its high level, with all other factors kept constant at their average [17, 18]. The slopes for the factors are also specified in Tab. 4 (“Estimate”). In addition to the influence of single factors, the significant two-factor interactions (turret speed \times paddle wheel speed, turret speed $\times \mu_{PW}$, cohesion \times API content) are shown in the interactions plots in Fig. 8b.

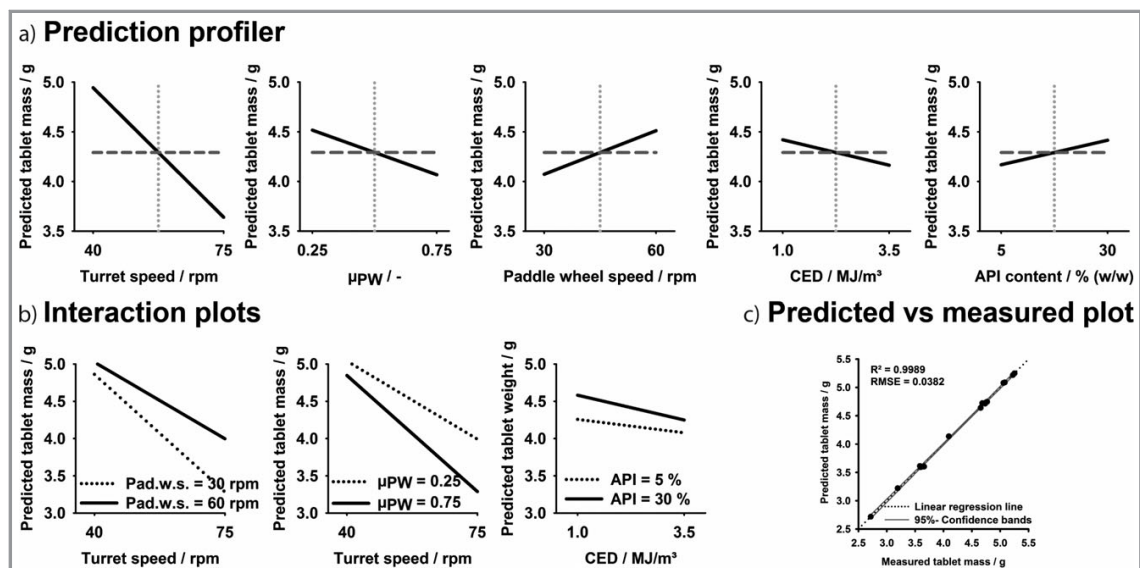
A negative effect on tablet mass is observed for an increase in turret speed from 40 rpm to 75 rpm with a significant decrease in tablet mass. At higher tableting speed, the die spends less time underneath the force feeder allowing a shorter filling time (at 40 rpm: 0.36 s, at 75 rpm: 0.19 s), thus less tablet mass is obtained. This observation is consistent with literature [3, 17, 19, 20].

The second highest factor influence is found for μ_{PW} . Previously, this factor was shown to increase the mass flow rate

during gravity filling [3, 4]. During gravity filling, the powder bed laid on top of the rotating turret whereby particles in direct contact with the turret transferred their momentum to particles above. As a result of the overall increase in particles’ velocity an accelerated mass flow rate and consequently a higher tablet mass were found [3, 4]. In contrast, those observations do not hold true to force feeding due to the difference in the filling mechanism. A decreased mass holdup in the filling wheel zone is found at a higher μ_{PW} (7.2 % less mass holdup for μ_{PW} of 0.75 compared to 0.25), which in turn decreases the mass flow rate from filling wheel zone. Consequently, a lower tablet mass at higher μ_{PW} is obtained.

The third factor with significant influence on tablet mass is the paddle wheel speed (Tab. 4). The particles’ velocity increases at higher paddle wheel speeds (mean particles’ velocity in filling wheel zone of 40.6 cm s^{-1} at 60 rpm compared to 19.3 cm s^{-1} at 30 rpm paddle wheel speed (data not shown)). The higher particles’ velocity can increase the re-feeding rate in the force feeder as particles are filled into the die. This is shown by a mass holdup increase in the filling wheel zone from 167.5 g to 174.5 g for 30 rpm compared to 60 rpm paddle wheel speed. Consequently, a higher tablet mass is obtained at a higher paddle wheel speed.

Associated with the paddle wheel speed, an interactive effect with the turret speed is identified (turret speed \times paddle wheel speed, cf. Fig. 8b). This interaction shows that at a low turret speed (40 rpm), the particles filled into the dies and leaving the system can be refilled likewise with a low or high

**Figure 8.** Prediction profiler (a), interaction plots (b), and predicted vs measured plot (c) of the tablet mass model.

paddle wheel speed resulting in a negligible tablet mass difference. In contrast, the higher mass throughput at high turret speeds (75 rpm, see above) requires an increased refilling rate that can only be compensated by a high paddle wheel speed (60 rpm). This observation is consistent with [21] though it was not described explicitly. Hence, an optimal combination of process parameters (turret speed and paddle wheel speed) to obtain highest possible mass is provided.

The stickiness of the material, introduced by different CED values (1.0 MJ m^{-3} and 3.5 MJ m^{-3} , Tab. 3) shows a negative effect on tablet mass, as expected and reported in [3–5]. Higher particle cohesion leads to reduced mean tablet mass since powder less readily flows into the dies [5]. This observation was also made in experiments [19, 20].

The significant interactive effect between turret speed and μ_{PW} (Tab. 4, Fig. 8b) indicates that the effect of the μ_{PW} on tablet mass is negligible at a low turret speed. In contrast at high turret speeds, only a low μ_{PW} can ensure a high tablet mass (see above).

The formulation strength, given by different API contents, shows the influence of particle packing during filling of the die. In case of the higher fines content, given by an increase in q_3 of the API particle size (second smallest size fraction, cf. Fig. 2) from 5% to 30%, the particles can rearrange in the filled dies more effectively. This results in a higher packing fraction and mean tablet mass (Fig. 8a).

The last effect on tablet mass is found for the interaction between cohesion and API content. Only at a high API content changing the cohesion value from low to high shows a considerable tablet mass decrease. Hence, powder flowability is more affected by cohesion at higher fines content.

A final model fit for the tablet mass response is performed after insignificant model terms were removed and the statistics are summarized in Tabs. 5 and 6. Evaluative statistics indicate a very good model fit with a R^2 value of 0.9989 and the model is significant with a p -value < 0.0001 . The predicted vs measured tablet masses are plotted in Fig. 8c, showing no outliers and all data points are within the 95% confidence bands. This model allows the tablet mass prediction and is most suitable for the given factor levels (Tab. 3). One additional simulation was performed (setup no. 17, Tab. 3) to verify the predictability of the model for tablet mass. The predicted mass was 5.4 g indicating the model's usability as the computed value was 5.3 g.

Table 5. ANOVA and model fit statistics for tablet mass: summary of fit.

Term	Value
R^2	0.9989
R^2 adjusted	0.9977
Root mean square error	0.04
Mean of response	4.29
Observations (or sum wghts)	16

Table 6. ANOVA and model fit statistics for tablet mass: analysis of variance (* for $p < 0.05$, significant).

Source	DF	Sum of squares	Mean square	F ratio
Model	8	9.48	1.18	811.19
Error	7	0.01	0.01	Prob $> F$
Corrected total	15	9.49		$< 0.0001^*$

4 Summary and Conclusion

This is the first study evaluating the die filling process within the dimensions of an actual lab-scale rotary tablet press. Furthermore material properties, in particular particle size distribution, were adapted to model a direct compression formulation of low and high API content. Through an iterative calibration procedure, powder flowability was compared between different DC grade diluents and material properties defined in the numerical setup.

Already during filling of the Fill-O-Matic, the filling system of a Fette 1200i rotary tablet press, particle size segregation was identified, leading to different API contents within the force feeder. Subsequently actual die filling was simulated at a given set of realistic process parameters (turret and paddle wheel speed). The first half of the mass in the dies is filled with particles from the filling wheel zone, whereas only roughly one third of mass originates from the reverse dosing wheel zone. Although those two paddle wheel zones show different API contents (higher content in reverse dosing wheel zone), an overall constant API content in the dies can be obtained, though it is lower than the label claim. This clear tracking of particles in the dies and their corresponding origin from the force feeder can be used to

- 1) optimize the feeding system geometry,
- 2) optimize the amount and type of ingredients,
- 3) evaluate the influence of the paddle wheel shape on the force exerted on particles, and
- 4) evaluate particles' residence time in the system.

It can give a hint towards particle attrition and over-lubrication [5] and will be subject of further research.

At this given parameter set, particle size segregation and mass holdup in different locations of the system were shown. Additional setups have been performed according to a DoE. They provided a clear picture on the influence of material properties in combination with process parameters on tablet quality such as tablet mass. The highest influence was found for turret speed and particle-wall friction, followed by paddle wheel speed. In the next step, the DoE will be analyzed with respect to other tablet quality parameters such as tablet mass variation and content uniformity. Eventually, a better understanding in pharmaceutical tableting can be generated by means of numerical simulation.

The authors would like to thank and acknowledge Mr. Thomas Heinrich (Fette Compacting GmbH, Schwarzenbek, Germany) and his team for generously providing the Fette 1200i Fill-O-Matic CAD files. Dr. Wolfgang Schmid's support (Daiichi-Sankyo Europe GmbH) in DoE generation and analysis is highly appreciated.

References

- [1] C.-Y. Wu, L. D. A. C. F. Cocks, *Powder Technol.* **2003**, *134* (1–2), 24–39. DOI: 10.1016/S0032-5910(03)00130-X
- [2] C.-Y. Wu, A. C. F. Cocks, O. T. Gillia, D. A. Thompson, *Powder Technol.* **2003**, *138* (2–3), 216–228. DOI: 10.1016/j.powtec.2003.09.011
- [3] S. R. Gopireddy, C. Hildebrandt, N. A. Urbanetz, *Powder Technol.* **2016**, *302*, 309–327. DOI: 10.1016/j.powtec.2016.08.065
- [4] C. Hildebrandt, S. R. Gopireddy, R. Scherliess, N. A. Urbanetz, *Adv. Powder Technol.* **2017**, in press. DOI: 10.1016/j.appt.2017.12.019
- [5] W. R. Ketterhagen, *Powder Technol.* **2015**, *275*, 361–374. DOI: 10.1016/j.powtec.2015.01.073
- [6] D. Mateo-Ortiz, R. Mendez, *Powder Technol.* **2015**, *278*, 111–117. DOI: 10.1016/j.powtec.2015.03.015
- [7] H. P. Zhu, Z. Y. Zhou, R. Y. Yang, A. B. Yu, *Chem. Eng. Sci.* **2007**, *62* (13), 3378–3396. DOI: 10.1016/j.ces.2006.12.089
- [8] M. Jivray, L. G. Martini, C. M. Thomson, *Pharm. Sci. Technol. Today* **2000**, *3*, 58–63. DOI: 10.1016/S1461-5347(99)00237-0
- [9] C. Hildebrandt, S. R. Gopireddy, A. K. Fritsch, T. Profitlich, R. Scherliess, N. A. Urbanetz, *Pharm. Dev. Technol.* **2017**, in press. DOI: 10.1080/10837450.2017.1412462
- [10] H. J. Herrmann, S. Luding, *Continuum. Mech. Therm.* **1998**, *10* (4), 189–231. DOI: 10.1007/s001610050089
- [11] W. R. Ketterhagen, M. T. am Ende, B. C. Hancock, *J. Pharm. Sci.* **2007**, *98* (2), 442–470. DOI: 10.1002/jps.21466
- [12] C. Kloss, C. Goniva, A. Hager, S. Amberger, S. Pirker, *Prog. Comput. Fluid Dyn.* **2012**, *12* (2/3), 140–152. DOI: 10.1504/PCFD.2012.047457
- [13] W. A. Beverloo, H. A. Leniger, J. van de Velde, *Chem. Eng. Sci.* **1961**, *15*, 260–269. DOI: 10.1016/0009-2509(61)85030-6
- [14] P. Tang, V. M. Puri, *Part. Sci. Technol.* **2004**, *22* (4), 321–337. DOI: 10.1080/02726350490501420
- [15] *European Pharmacopoeia (Ph. Eur.)*, 9th ed., EDQM – Council of Europe, Strasbourg **2017**.
- [16] A. Anand, J. S. Curtis, C. R. Wassgren, B. C. Hancock, W. R. Ketterhagen, *Chem. Eng. Sci.* **2008**, *63* (24), 5821–5830. DOI: 10.1016/j.ces.2008.08.015
- [17] E. Peeters, T. De Beer, C. Vervaeke, J.-P. Remon, *Drug Dev. Ind. Pharm.* **2015**, *41* (4), 530–539. DOI: 10.3109/03639045.2014.884121
- [18] E. Johannson, N. Kettaneh-Wold, C. Wikstrom, S. Wold, L. Ericksson, *Design of Experiments – Principles and Applications*, 1st ed., Umetrics Academy, Umeå **2000**.
- [19] Y. Yaginuma, Y. Ozeki, M. Kakizawa, S. I. Gomi, Y. Watanabe, *J. Drug Deliv. Sci. Technol.* **2007**, *17* (3), 205–210. DOI: 10.1016/S1773-2247(07)50037-7
- [20] R. Mendez, F. J. Muzzio, C. Velazquez, *Powder Technol.* **2010**, *200* (3), 105–116. DOI: 10.1016/j.powtec.2010.02.010
- [21] D. Mateo-Ortiz, F. J. M. R. Mendez, *Powder Technol.* **2014**, *262*, 215–222. DOI: 10.1016/j.powtec.2014.04.023

3.2.2 Extended powder flow evaluation in force feeding

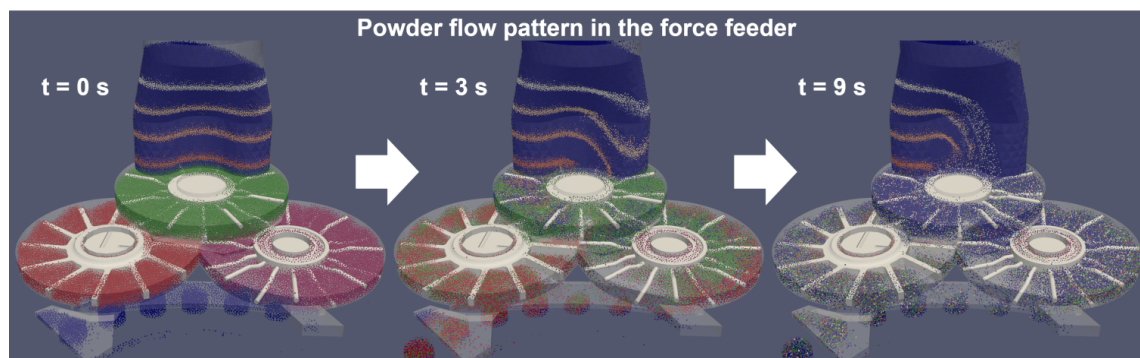
Investigation of powder flow within a pharmaceutical tablet press force feeder - A DEM approach

Claudia Hildebrandt^{1, 2}, Srikanth R. Gopireddy², Regina Scherließ¹,
Nora A. Urbanetz²

¹ Department of Pharmaceutics and Biopharmaceutics, Christian-Albrechts-Universität Kiel,
Grasweg 9a, 24118 Kiel, Germany

² Daiichi-Sankyo Europe GmbH, Pharmaceutical Development,
Luitpoldstrasse 1, 85276 Pfaffenhofen, Germany

Submitted to Powder Technology, under revision



Outline

The following chapter is a continuation of the previous chapter (3.2.1) as it adds additional information to the powder flow pattern in the force feeder of the FETTE 1200i. More detailed information of the underlying size segregation mechanisms are provided and supported by particle velocity analysis. Using a classical spot sample analysis which is usually applied in mixing studies, the size segregation is quantified for different locations of the force feeder. The analysis explains the unintentional demixing of the differently sized particles of the model formulation in the feeding system. Furthermore, the particle rearrangement over the feeding hopper and within the paddle wheel zones is visualized by assigning the particles position specific colors. The approach of particle coloring is already utilized in the numerical gravity feeder studies (chapter 3.1.3 & 3.1.4). The particles are tracked over tableting time which allows a quantitative description of the powder mixing in the different locations. Eventually, selected particles within the feeding hopper are tracked while discharge and the residence time is calculated.

The following and previous chapter (3.2.1) constitute the basis for the remaining force feeder chapters. In chapters 3.2.3-3.2.5 the principle powder flow patterns within the FETTE 1200i are not repeated for the sake of brevity again, though emphasize will be given to the DoE (chapter 3.2.3), the paddle wheel shape configuration (chapter 3.2.4), and the force feeder type (chapter 3.2.5).

1 Introduction

Although more than 150 years of expertise are existing in pharmaceutical tableting [28], it is still in the focus of scientific research. This is attributed to the significance of tablets as one of the most convenient drug administration routes. The main challenges in pharmaceutical tableting are related to the tablet quality requirements according to the regulatory authorities [25]. Out of the three processing stages, namely die filling, powder compaction, and tablet ejection, the die filling step has been investigated by different means. Those include classical tableting experiments, Process Analytical Technology (PAT), and numerical simulations. The die filling in the tableting machine comprises the powder flow from the blending hopper through the feeding system into the rotating dies. It defines the amount and composition of powder to be compacted thereby specifying the tablet mass and the content. Two main feeding mechanisms exist, namely gravity feeding and force feeding. Gravity feeding was studied by our group by numerical means to identify the influence of process conditions and material attributes of mono- and poly-disperse particle size distributions on tablet quality [168, 169]. Force feeding is more popular and consists of one or more rotating paddle wheels which force the powder into the dies. The powder flow in force feeders is highly depending on the unique geometry of the tableting machine, i.e. the shape and the arrangement of the paddle wheels. A real scientific rationale for the design of a force feeder is lacking and thus is usually based on long-time experience of design engineers and operators. The following approaches exist to study the performance of force feeders in high speed rotary tablet presses.

Classical experimental approaches subject a blend with a characterized powder flowability to the tableting process and evaluate the tablet properties. The influence of process variables on tablet weight [86, 87], tablet weight variability [87], and tablet tensile strength [76, 110] were studied by using this approach. Different force feeder designs showed an effect on particle attrition which could be attributed to varying powder residence times and to applied total shear forces [95, 102]. The experimental approach does not make any assumptions / simplifications (see below) that could impact the obtained results which is a main benefit. However, it can only be compared what is being entered into the system (powder blend) to what is coming out of the system (tablet). The powder flow in between remains uncertain unless transparent custom designed housings are developed [86]. In addition, for new formulations it is time consuming and expensive to perform experiments, especially if the availability of the new molecular entity is limited in quantity.

Another approach uses PAT such as Near-infrared Spectroscopy (NIRS) to look into the system and allows, e.g. the evaluation of mass hold up in the system thus mass steady state [107]. In addition to mass based analysis, the powder blend potency was studied in a two-paddled feed frame with the NIR probe located prior to the die filling [92]. This approach could help in the future to understand powder mixing dynamics occurring within the feed frame. NIR in combination with other imaging techniques (light-induced fluorescence spectroscopy, color imaging (red, green, and blue)) allowed the evaluation of multicomponent flow dynamics [111]. The drawback of the NIRS technique is the focus of a small area in the feed frame which is defined by the size of the NIRS probe. In addition, the powder wave behavior promoted by paddle wheel movement results in different distances between the powder and the detector leading to changes in spectra baselines [107]. Another challenge constitutes the careful development of NIR spectra calibration models to be able to obtain valuable content data.

Recently numerical techniques, in particular the discrete element method (DEM), gained significant interest. It is the only method that allows an understanding of flow dynamics on a particle level over the complete scale of the system under investigation. The powder flow was investigated in one-paddled

[41][94] and two-paddled [93, 95] feed frames of tablet presses. For the former it was shown that faster paddle wheel speeds generally led to a more uniform tablet mass compared to slower paddle wheel speeds [41, 94]. However, a slower paddle wheel movement decreased the risk for particle attrition and over lubrication [41]. Changing the number of blades of the paddle wheel, the blade shape, or the diameter of the inner hub influenced the powder flow significantly and provided different means for feed frame design optimization, i.e. more blades could decrease tablet weight variation [41, 94]. Particle size segregation in a two-paddle equipped feed frame showed that the percolation phenomenon was the most significant segregation phenomenon [93]. Residence time distribution analysis showed that smaller sized particles were leaving the feed frame faster [95]. Although these studies provided a good basis for powder flow understanding in the feed frame, several limitations or disadvantages still exist. The advantage of a high resolution on a particle level of the DEM goes in hand with a high computational cost. It limits the number of particles simulated and usually requires particle size enlargement [157, 161]. Micro-mechanical material properties did not correspond to pharmaceutical materials but e.g. to glass beads [41]. Other limitations are in general the long calculation times for poly-disperse size distributions, irregular shaped particles, and multi-component mixtures. Multi-component mixtures imply that a lot of different interparticle interaction forces have to be discerned and computed. Although computational power has increased significantly in the last decade, it is still not possible to reflect the complete tableting production process lasting for more than a couple of hours, though less than 60 s of physical time have been computed using the DEM.

The current study aims to investigate the powder flow in a feed frame of a pilot-scale FETTE 1200i tableting machine consisting of three paddle wheels. It is an extension of our previous work [170, 171] to assess this particular process using the DEM. A poly-disperse particle size distribution of large particles is developed and mimics a good flowing direct compression formulation. The absolute particle sizes and their distribution are larger compared to reality limited by computational power impeding a one-to-one transfer of the numerical results to reality. However, the general powder flow dynamics in the force feeder can be assessed. The analysis includes different means, i.e. the detailed dynamics during system filling and subsequent high speed tableting until mass steady state is reached. Different quantitative as well as qualitative approaches provide a thorough system understanding which serve as a basis for follow-up studies. At a defined set of process conditions (turret speed and paddle wheel speed) and material properties, the powder flow is simulated and is explained. The study will be extended to a design of experiments to elucidate the influence of process conditions and material attributes on, e.g. tablet quality [170].

2 Materials and Methods

2.1 Discrete Element Method

The DEM was developed in 1979 by Cundall and Strack [115] and gained increasing attention in the pharmaceutical industry in the last decade [20, 47, 172–177]. The basic concept of capturing the trajectories of each particle in the system through Newton’s second law of motion is well described in literature [20, 24, 178]. All computations were performed using the open source DEM software ‘LIGGGHTS’ [116]. The Hertz and the Mindlin & Deresiewicz theories were used to model the normal and tangential forces, respectively [119]. In this study, the cohesion is included using the simplified Johnson-Kendall-Roberts (JKR) model implemented in LIGGGHTS [127]. According to this model, the cohesion between two particles or particle-wall is calculated by adding an additional normal force contribution with $F = k * A$ which tends to maintain the contact. Here, A is the particle contact area and k is the cohesion energy density (CED) in J/m^3 [116]. The same model has been used previously by Ketterhagen [41] and Mateo-Ortiz et al. [93] in force feeder simulations, and also in open/gravity feeder simulations [168, 169]. At the selected particle size and Young’s modulus (section 2.2 and Tab. 1), a time step of $0.6 \mu\text{s}$ was chosen that is well below the Rayleigh- and Hertz-time [116, 123]. The force models and their implementation in LIGGGHTS are given by Kloss et al. [123]. The dense particle packing in the closed system (tableting machine) and the large particle sizes considered (section 2.4) allowed to neglect the air impact [84, 168, 169].

2.2 Geometrical setup

The geometrical setup (Fig. 1), as already described by Hildebrandt et al. [170], corresponds to a pilot-scale tableting machine, the FETTE 1200i (Fette Compacting GmbH, Schwarzenbek, Germany) with 24 punch stations. Its so-called ‘Fill-O-Matic’ is a three stage controlled feeding system consisting of a feeding hopper (1, Fig. 1) and three differently shaped paddle wheels (2-4, Fig. 1). The dosing wheel (2, Fig. 1), reverse dosing wheel (4, Fig. 1), and turret (5, Fig. 1) are rotating in anti-clockwise, the filling wheel (3, Fig. 1) in clockwise direction. A large die diameter of 24 mm was selected to ensure least influence of the rather large particles on powder flow [179] (confer section 2.3, Fig. 2). The die height was changing over filling time to reflect the fill and dosing cam as found in conventional rotary tablet presses. In other words, the die volume was generated by a decrease of the lower punch as soon as the die was approaching the filling wheel zone. It reached its maximum volume at a die height of 15 mm after 0.216 s (at 40 rpm turret speed) and remained constant during gravity filling and underneath the reverse dosing wheel zone. After the die left the feeding station, the lower punch was moved upwards for 0.031 s (at 40 rpm turret speed) by 2 mm to scrape excess powder and to create a more confined powder bed (Fig. 6). Since the focus of the current study is the die filling process, the subsequent powder compaction and tablet ejection processes are not examined.

2.3 Material properties

A poly-disperse particle size distribution was considered in simulations to mimic a direct compression (DC) blend (Fig. 2). The general concept of particle size enlargement was considered given by the complexity of the geometrical system [157, 161]. Although the particle size was larger compared to real pharmaceutical powders, the D/d ratio, with D as the paddle wheel zone diameter and d as the mean particle diameter, was selected larger (79, confer below) than the recommendation of 20-50 of Dubey [161]. In addition, Hassanpour et al. showed in a paddle mixer study, that the average particle velocity was only slightly sensitive to the particle size and the effect was not very significant [162]. A similar observation was made by Boonkanokwong et al. [180]. Thus, the concept of particle size

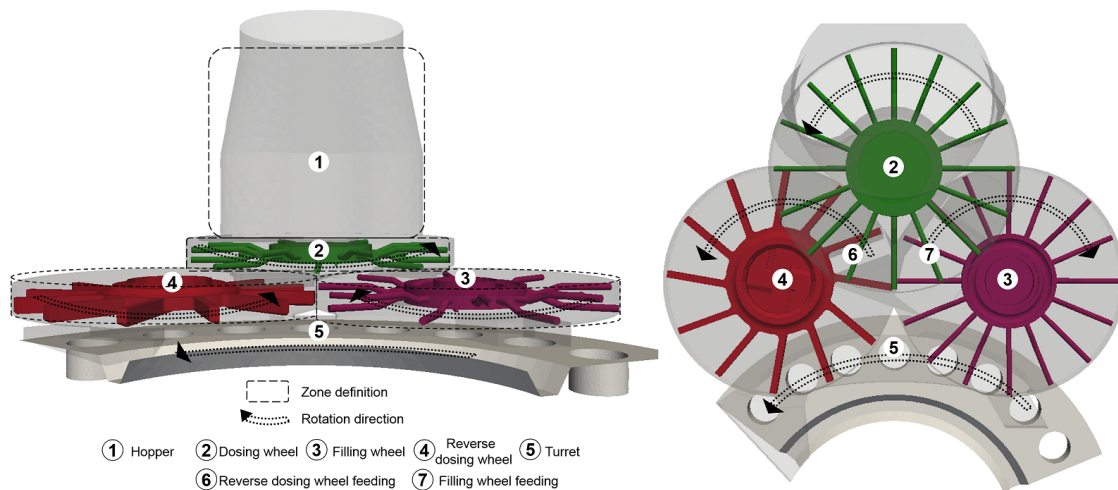


Fig. 1: Illustration of the geometrical setup in front- (left) and top- (right) view taken from our previous work [170] with permission from John Wiley and Sons.

enlargement to provide an acceptable computation time was considered valid to assess the general powder flow dynamics in the force feeder. In this study in total seven size fractions were included ranging up to 2800 μm diameter. At first the distribution corresponding to the ‘excipients’ phase with a mean diameter of 2173 μm was considered. The width of the PSD, although it is not as wide as found in real formulations, already results in a large number of particles in simulations. In addition to the excipients phase, one size fraction (1000 – 1129 μm) was considered with a size ratio of 1:2 to the mean excipients diameter and reflected the ‘API’ particles. This size ratio would allow size segregation through sieving mechanism to occur [181, 182]. A reasonable API content of 5% (w/w) was considered [43]. The mean particle size of the PSD was 2107 μm (d) giving a D/d ratio for the reverse dosing wheel zone or filling wheel zone ($D = 166 \text{ mm}$) of 79.

The segregation analysis described in section 3 showed a cut-off between particles with $x \leq 1800 \mu\text{m}$ and $x > 1800 \mu\text{m}$. The former are referred as fines (24.5% (w/w)), the latter as coarse particles (75.5% (w/w)) in the current study although the definition of fines is different compared to pharmaceutical powders ($x < 10 \mu\text{m}$). The PSD resulted in a total of 268,000 particles after filling the complete system (section 2.4). The computational time for system filling (section 3.1) and high speed tableting (section 3.2) took 3 months on a workstation with 72 parallel running processors. The high computation time is attributed to the large number of particles considered and the complexity of the geometry in terms of the curvature resolution and the asymmetry complicating the per-processor load balancing.

Not only the poly-disperse size nature of DC formulations was taken into account, but also their powder flowability. Thus, the bulk density, angle of repose, and mass flow rate according to the Ph. Eur. [25] were determined for different pharmaceutical diluents used for DC (different grades of lactose, mannitol, and micro-crystalline cellulose). Similar to experiments, the powder flowability of the model DC blend (Fig. 2) was assessed in simulations. The DEM input parameters were adapted accordingly to achieve good agreement with the powder flowability results of the pharmaceutical diluents. Especially, the non-contact force (cohesion energy density (CED)) and the friction between the particles and the geometry (particle-wall coefficient of friction (μ_{PW})) were iteratively adapted. One μ_{PW} was defined for the entire geometry (walls) though in reality anodized aluminum and special bronze are used for the force feeder housing and the paddle wheels, respectively. Thereby the effect of the friction between the particles and the whole geometry is considered in a follow up study using

two different μ_{PW} values [170] rather than identifying the effect of individual zones. The final micro-mechanical particle properties considered and corresponding to a free flowing powder are listed in Tab. 1. The values are within the range of literature data [93, 168, 169, 183–185].

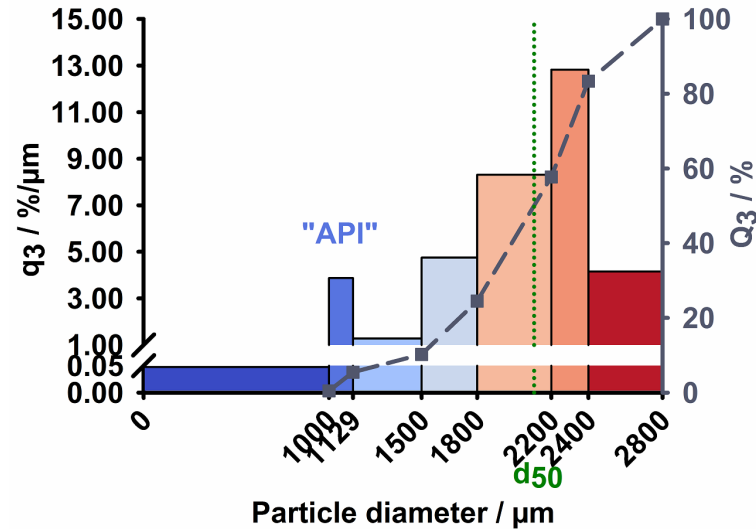


Fig. 2: Particle size distribution of the model DC formulation (from our previous work [170] with permission from John Wiley and Sons).

Tab. 1: Material properties, the numbers in parenthesis correspond to step in Tab. 2.

Parameter / Unit	Property of	Value during filling (❶-❸)	Value during discharge (❹)
Young's modulus / GPa	Particle	0.87	0.87
	Wall	21	21
Poisson's ratio / -	Particle	0.30	0.30
	Wall	0.35	0.35
Coefficient of restitution / -	Particle-particle	0.15	0.15
	Particle-wall	0.15	0.15
Coefficient of friction / -	Particle-particle	0.35	0.40
	Particle-wall	0.30	0.75
Cohesion energy density (CED) / MJ/m ³	Particle	1.5	1.0

2.4 Initialization and die filling process

The system was filled with particles mimicking the real process according to a step-wise procedure as depicted in Fig. 3A. (1) The powder was filled into the feeding hopper resembling in reality the opening of the blending hopper (❶, Tab. 2). (2) The force feeder was then evenly filled with particles by slow paddle wheel rotations (15 rpm, ❷, Tab. 2). (3) System initialization was completed by one complete rotation of the turret at a low speed (10 rpm, ❸, Tab. 2). For actual high speed tableting the throughput was increased to 57,600 tablets / hour (40 rpm turret and 30 rpm paddle wheel speeds, ❹, Tab. 2). During high speed tableting equal amount of powder was refilled into the feeding hopper as material was leaving in the filled dies.

In this study the die filling process is in general explained at a fixed set of material properties and process conditions during high speed tableting (Tab. 1 and 2). However this setup stems from a

design of experiments in which material attributes and process conditions have been varied and their influence on the die filling is evaluated. Those results are presented in a follow-up paper [186]. For this purpose the system filling process was same for all the setups. It allows a homogeneous packing structure at the beginning and ensures that the observations during high speed tableting are related to the altered parameters [168, 169, 187].

Tab. 2: Process parameters at different computation steps.

No.	Description	Physical time / s	Turret speed / rpm	No. of turret rotations / -	Paddle wheel speed / rpm	No. of paddle wheel rotations / -
①	Filling of hopper	0.8	0	0	0	0
②	Filling of Fill-O-Matic	9	0	0	15	2.26
③	Filling of turret	6	10	1	15	1.5
④	Discharge	15	40	10	30	4

2.5 Quantification of particle size segregation

In general, particle segregation can be defined as the ‘unintentional de-mixing of one or more components in a mixture of particulates’ [72] that can be triggered by physical particle properties [73] and by energy input [74]. In a lab-scale gravity feeder, it could be shown that the interparticle forces and the friction coefficients (particle-particle and particle-wall) influence segregation of micro-crystalline cellulose particles of varying size to a different extent [169]. In the current study, an attempt is made to evaluate size segregation of the poly-disperse particle size distribution (Fig. 2) in the force feeder through mixing analysis (section 3.2.3).

The most common mixing approach extensively described in literature includes a traditional sampling method that yields a couple of different mixing indices that basically have the following concept: take a number of samples, analyze them, and determine the spread of the composition [188]. Usually the spread is expressed through the sample variance (σ_s^2) which is subsequently compared to the variance that would reflect a perfect random mixture (σ_r^2) [189, 190]. In contrast, a particle-scale mixing index, developed for mixing through impeller blades, uses the particles’ coordination number to define the particle fraction p_i of one type of particles in the immediate neighbor of particle i in a binary mixture. A particle-scale mixing index is obtained that is similar to the Lacey’s mixing index [191, 192]. In addition to these spot sampling approaches via statistical interpretation and coordination or contact number analysis, a different strategy is considered for continuous operations. As reviewed by Pernenkil and Cooney [193] the variance reduction ratio (VRR) assesses the ratio of the variance of the concentration fluctuation at the inlet with that at the outlet. The individual components enter separately the mixing system and get continuously mixed giving best mixing for highest VRR . The tableting process is from a mixing point of view a continuous system as mass continuously enters and leaves the system. However, the VRR cannot be applied in the current setup as the blend enters the hopper as a random mixture during continuous refilling. On the contrary, the components enter completely de-mixed in continuous mixing [193].

For the current study the general approach via spot sampling analysis was applied using the ‘Poole Index’ according to Eq. 1 [188]:

$$PI_{i,location} = \frac{\sigma_{s,i,location}}{\sigma_{r,i,location}} = \frac{\sqrt{\frac{\sum(q_{3,i,location} - \overline{q_{3,i,location}})^2}{n}}}{\sqrt{\frac{q_{3,i,spec} * (100 - q_{3,i,spec})}{n_{location}}}} \quad (1)$$

With

$PI_{i,location}$	Poole index of particle size fraction i in a defined location
$\sigma_{s,i,location}$	measured standard deviation of particle size fraction i in defined location
$\sigma_{r,i,location}$	standard deviation for random mixture of particle size fraction i in defined location
$q_{3,i,location}$	instantaneous measured content (% w/w) of particle size fraction i in defined location
$\overline{q_{3,i,location}}$	mean content (% w/w) of particle size fraction i in defined location
$q_{3,i,spec}$	content (% w/w) of particle size fraction i specified according to particle size distribution (Fig. 2)
$\overline{n_{location}}$	mean number of particles in location

The variance $\sigma_{s,i,location}$ during mass steady state ($t = 6.1 - 15.0$ s, in detail explained in section 3.2) will be considered for the segregation analysis in the system. A $PI_{i,location} > 1$ indicates a segregated system, < 1 a more than random mixture, and $= 1$ a random mixture. The $PI_{i,location}$ was assessed at different locations of the system and for different particle size fractions. In particular the denominator, $\sigma_{r,i,location}$, depends on the total number of particles considered and the content of the analyzed particle size fraction. For this purpose the mean number of particles per location are provided in Tab. 5 for reference.

In addition to the $PI_{i,location}$ for individual particle size fractions, a combined segregation index was computed that would take into account the complete blend. Although, the classical segregation indices [188–190] have been developed for bi-disperse mixtures and particles of same size, it was necessary to generate a single value that would be able to easily identify and characterize the segregation of a multi-component mixture, i.e. in this case of differently sized particles. The approach using the particle coordination number, as proposed by Cho et al. [194] and Chandratilleke et al. [191], could not be applied in this study due to technical limitations. An alternative is suggested by computing a single value that quantifies the segregative effect of all particles, the $PI_{location}$ (Eq. 2):

$$PI_{location} = \sum PI_{i,location} * \frac{\overline{q_{3,i,location}}}{100\%} \quad (2)$$

The mean content of the individual particle size fractions i is used ($\frac{\overline{q_{3,i,location}}}{100\%}$) for Eq. 2 to account for their actual contribution in the defined region. In case that neither of the particle size fractions are segregated ($PI_{i,location} = 1$, Eq. 1) the sum of the product with ($\frac{\overline{q_{3,i,location}}}{100\%}$) would result in a $PI_{location}$ of 1. However, same ($PI_{location} = 1$) would be obtained if high and low segregated particle size fractions would compensate each other. Thus, it has to be kept in mind that a $PI_{location}$ close to 1 does not necessarily indicate, unlike the $PI_{i,location}$, that a random mixture over all particle size fractions is obtained, however some size fractions might show a higher, others a lower segregation tendency.

3 Results and Discussion

In the following, different quantitative and qualitative analysis will help to evaluate the die filling process within the force feeder of a pilot-scale rotary tablet press. First the filling of the system, comprising different steps, will be briefly explained for the sake of completeness. More details can be found in our previous study [170]. Subsequently the actual high speed die filling process will be evaluated by introducing different metrics that are directly and in-directly linked to different tablet quality attributes.

3.1 Filling of system

A detailed description of the filling process of the system is given by Hildebrandt et al. [170] and is only briefly repeated to later emphasize the differences that are found between system filling and high speed tableting (section 3.2).

The filling of the system was divided into three separate steps including filling of the feeding hopper (❶), filling of the force feeder (❷), and filling of the turret (❸) (confer section 2.2, Tab. 2, Fig. 3). The powder mass and the API content that is found during these intervals in different zones of the system are given in Fig. 4.

In general, the powder is moving from the feeding hopper to the dosing wheel zone. The latter rotates in anti-clockwise direction and the powder first falls through the refilling hole (6, Fig. 1) into the reverse dosing wheel zone. The fines content (size $\leq 1800 \mu\text{m}$) during system filling is plotted for three horizontal zones (bottom, middle, top) in the dosing wheel zone in Fig. 3B. At the beginning of system filling, no significant difference between the horizontal zones can be identified and similar contents as the specified content are obtained. However, the fines contents in the horizontal zones significantly change during filling time by a mechanism named as sieving segregation [181, 195]. The smaller particles have enough time to get sieved through the voids of the larger ones as the powder bed is moving at rather low particle velocities given by the low paddle wheel speed of 15 rpm. A higher content of small particles is discharged through the hole located above the reverse dosing wheel zone (fines content of 35.9%, orange line in Fig. 3). As a consequence a higher content of fines is developing in the reverse dosing wheel zone (Fig. 4B exemplarily for API size fraction (1000 – 1129 μm)). The particles in the dosing wheel zone after refilling of the reverse dosing wheel zone consist of less small particles therefore a different PSD is transferred during refilling of the filling wheel zone (fines content of 19.5%, yellow line in Fig. 3B). In summary the size segregation through sieving in the dosing wheel zone in combination with the location of the refilling holes (Fig. 1, 3, and 4) are fostering the size segregation in the complete force feeder [170]. At the end of the filling process, different fines contents, i.e. 3.4%, 2.0%, and 10.7% API content have been developed in the dosing wheel zone, filling wheel zone, and reverse dosing wheel zone, respectively, as shown Fig. 4 [170].

3.2 Die filling process

The actual high speed tableting process of the completely filled system started by increasing the turret speed from 10 rpm to 40 rpm and the paddle wheel speed from 15 rpm to 30 rpm (❹ Tab. 2). The beginning ($t = 15 \text{ s}$) of the die filling process is captured however, not the complete tableting process that may take several hours, could be mapped considering the high computational cost (section 2.3). Several different metrics are evaluated for the die filling process including the mass based (tablet mass and API content, mass flow rate, mass hold up), particles' velocity, particle size segregation, particles' tracking through coloring, and finally particles' residence time analysis.

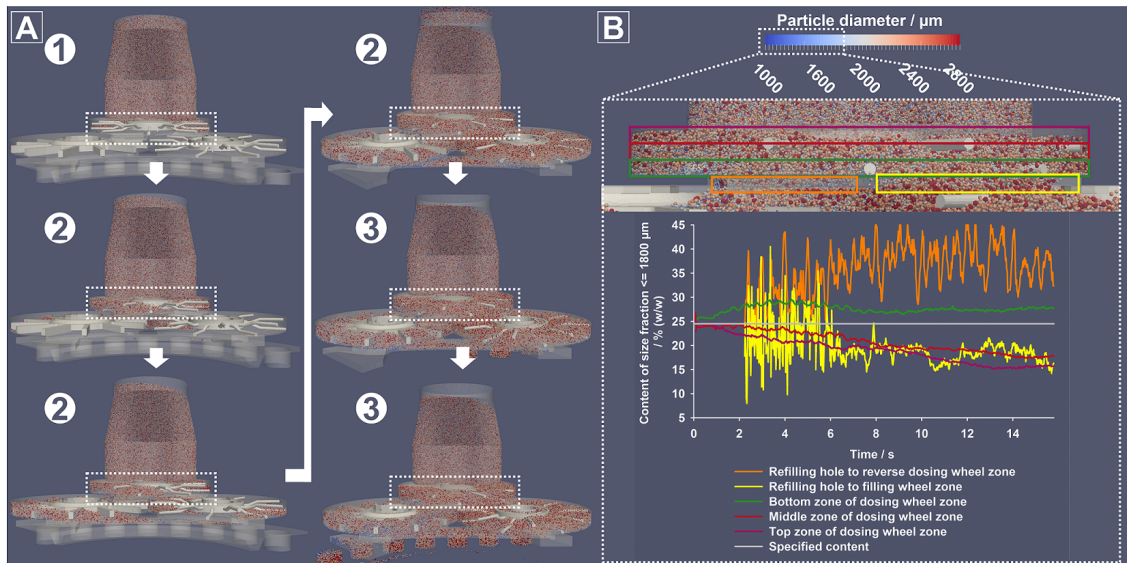


Fig. 3: Illustration of the system during filling (A), numbers correspond to steps in Tab. 2). (B) Content of particles $\leq 1800 \mu\text{m}$ in three horizontal zones of the dosing wheel zone and in the refilling regions of the reverse dosing wheel zone and the filling wheel zone during system filling (A).

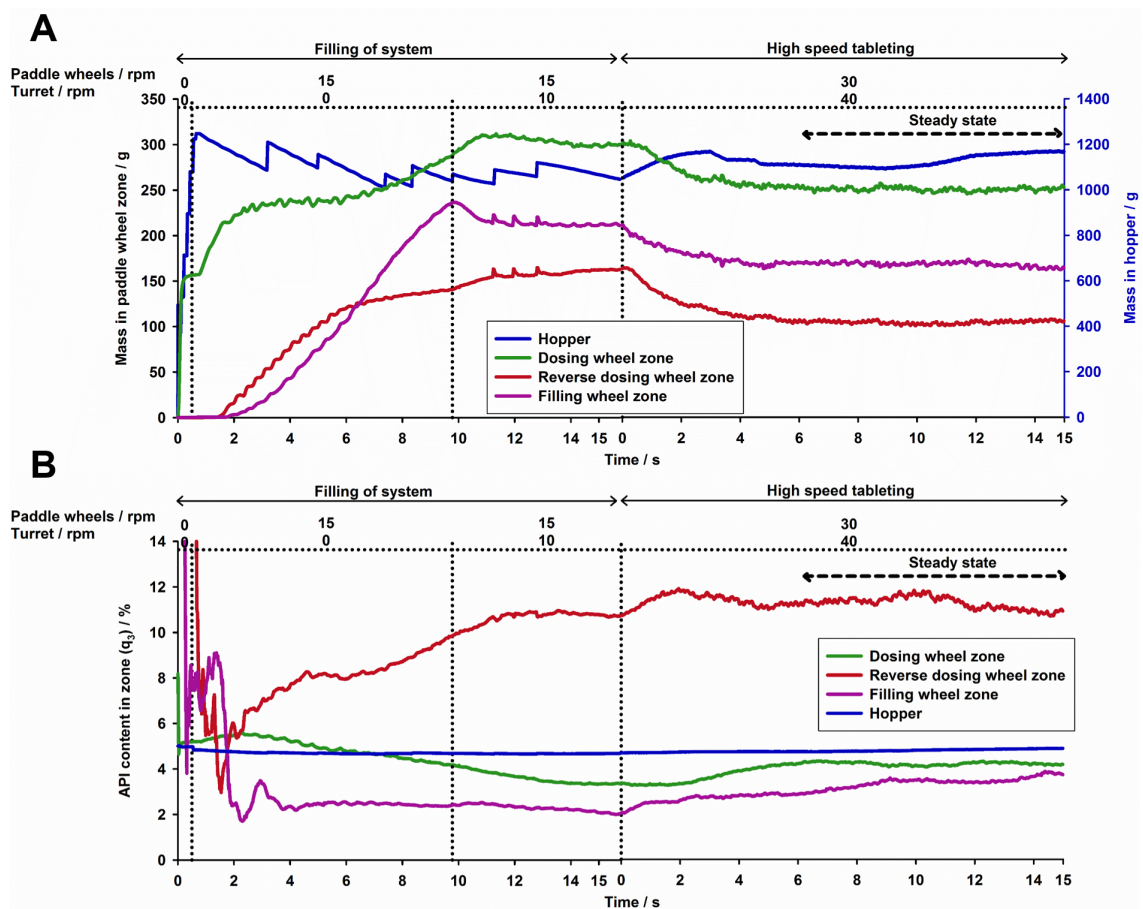


Fig. 4: Mass hold up (A) and API content (B) in different locations of the Fill-O-Matic over time during system filling (taken from our previous work [170] with permission from John Wiley and Sons) and high speed tableting.

Tab. 3: Summary of metrics

Quality measure	Unit	Value
Mean tablet mass	g	4.7
Mean API content in dies	%	4.6
Tablet weight variation (RSD)	%	3.7
$Tablet\ mass_{change}$	g	-0.4
PI_{dies}	-	1.4
$PI_{hopper\ left}$	-	0.9
$PI_{hopper\ right}$	-	1.0
$PI_{dosing\ wheel\ zone}$	-	0.9
$PI_{reverse\ dosing\ wheel\ zone}$	-	1.4
$PI_{filling\ wheel\ zone}$	-	1.0
PI_{feeder}	-	16.8
Mean residence time	s	12.6

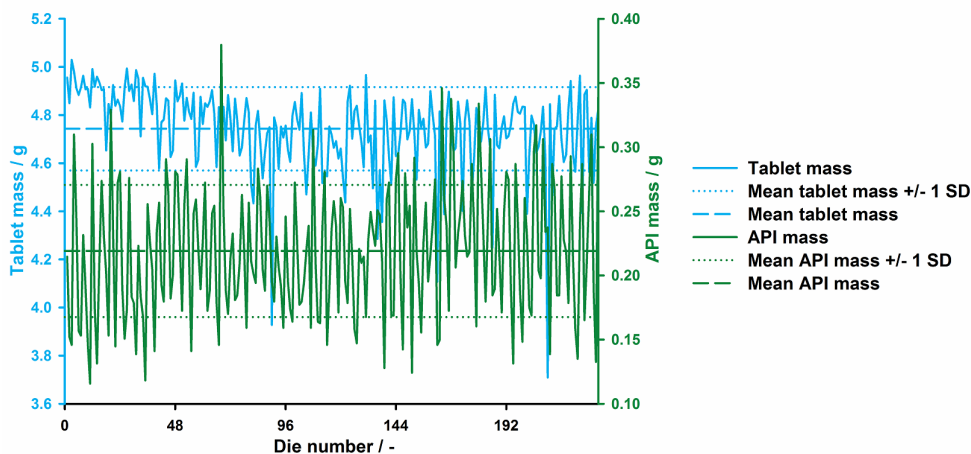


Fig. 5: Tablet mass and API content during 10 turret revolutions and 232 filled dies. The ranges between mean and mean \pm standard deviation are indicated in dashed and dotted lines, respectively.

3.2.1 Mass based analysis

Tablet mass

The first 8 tablets were filled during the last third of the system filling process, in which the turret rotated at 10 rpm (⊖ Tab. 2, section 3.1) and contain a mean tablet mass of 5.2 g (data not shown). In contrast, during high speed tableting a significantly decreased mean tablet mass of 4.7 ± 0.2 g is obtained (Fig. 5). The tablet mass is slightly higher at the beginning and evens out as soon as the mass hold up in the force feeder is in equilibrium (Fig. 4) resulting in a steady supply of powder mass to the dies. The high tablet mass fluctuation of 3.7% (RSD) can impede the uniformity of dosage units [25] and thus constitutes an important tablet quality attribute (Tab. 3). Die no. 90, 162, and 210 reveal tablet mass outliers (tablet mass < 4.1 g) that might originate from an unfavorable combination of mass hold up / refeeding rate in the force feeder and particles' velocity. Several factors that can cause tablet weight variation are discussed in the following sections.

API mass / content

A detailed analysis of API content fluctuation, as shown in Fig. 5, is discussed under section 3.2.3 via mixing analysis.

In addition to API content consistency, correct dosing is playing a crucial role for the patients' safety. The dose strength of the tablet is defined by the tablet mass and the API content in the formulation. The mean API mass in the filled dies is 219 mg which is 4.6% (w/w) relative to mean tablet mass (Fig. 5). This relative content is significantly lower than the defined content of 5.0% (236 mg at given tablet mass) in the formulation (Fig. 2 and Tab. 5). This discrepancy is quantified by the *Tablet mass_{change}* given in Eq. 3.

$$Tablet\ mass_{change} = \bar{x} * \left(\frac{\overline{q_{3,API,dies}} - q_{3,API,spec}}{q_{3,API,spec}} \right) \quad (3)$$

At the mean tablet mass of 4.7 g (\bar{x}), the relative difference of measured API content ($\overline{q_{3,API,dies}}$) to specified API content ($q_{3,API,spec}$) results in a *Tablet mass_{change}* of - 0.4 g (Tab. 3, Eq. 3). If less API mass than specified is obtained, a negative (< 0) *Tablet mass_{change}* value is found (Eq. 3). It indicates that the tablets contain at the given tablet mass less API mass than expected. Hence the tablet mass has to be increased by 0.4 g, e.g. by decreasing the turret speed or increasing the die height to obtain correct API dosing. The particle size segregation and de-mixing within the force feeder in section 3.2.3 explain the API false dosing.

Mass flow rate

The mass filled into one single die as it moves underneath the filling station is evaluated. The die height is changing over filling time according to actual rotary tablet presses (section 2.2) [28]. The die height (purple line) and the corresponding mass relative to the maximal mass filled into the die (green line) are shown in Fig. 6. Similar to findings in our previous study for a different combination of turret speed (75 rpm) and paddle wheel speed (30 rpm) [170], the mass flow rate (MFR) is higher during filling through force feeding underneath the filling wheel zone ($t = 0.06 - 0.22$ s, 25.7 g/s) and reverse dosing wheel zone ($t = 0.30 - 0.43$ s, 17.6 g/s) compared to the one in between, in which only gravity filling is found ($t = 0.22 - 0.30$ s, 5.3 g/s). A total mass of 492 mg (9% of maximum mass) is scrapped during dosing cam as the die height is decreased from 15 mm to 13 mm. In total 59%, 7%, and 34% of the maximal tablet mass (before dosing cam) originate from filling wheel zone, inter-wheel zone, and reverse dosing wheel zone, respectively.

The MFR from the different paddle wheel zones and of the individual particle size fractions given in Tab. 4 and Fig. 6 show diverging observations. A MFR ratio of filling wheel zone to reverse dosing wheel zone is calculated. A MFR ratio of > 1 indicates a higher filling in the first part of the die filling process, i.e. from the filling wheel zone, and a MFR ratio of < 1 means filling predominantly from the reverse dosing wheel zone. The MFR ratios are < 1 for particles size fractions ≤ 1500 μm indicating that they are mainly filled from reverse dosing wheel zone. Larger particles (size fractions > 1500 μm) originate mainly from the filling wheel zone and enter the die first. As a consequence larger particles are located at the bottom of the die, followed by small particles on top entering from reverse dosing wheel zone. The relative mass to maximum mass filled into the die per size fraction and over time shown in Fig. 6 support these observations. Since the higher mass of larger particles contributes to a higher extent to the total mass, the overall MFR from filling compared to reverse dosing wheel zone is higher (green line in Fig. 6, confer above). In section 3.2.3, the particle size distribution in the different paddle wheel zones is evaluated and an explanation for the different MFRs per particle size fraction is provided. In summary, over the die height different particle size fractions are found as they originate from different locations of the force feeder.

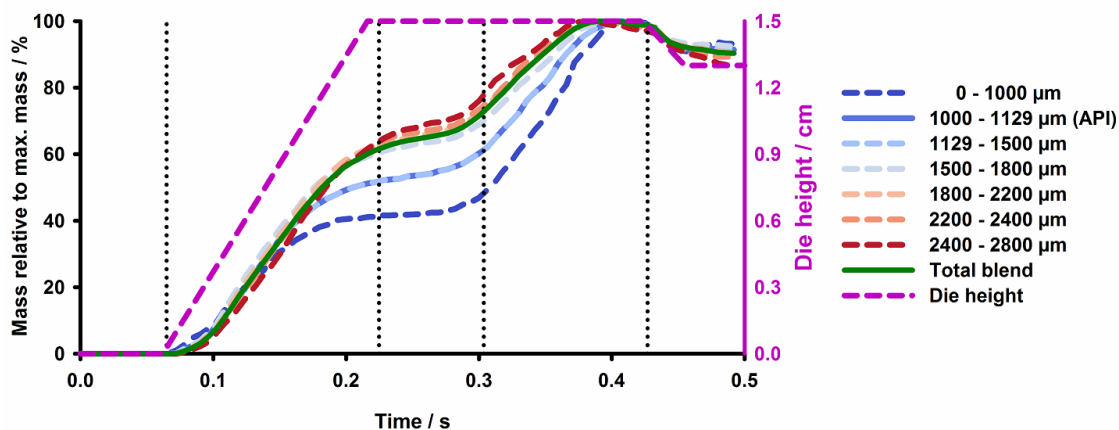


Fig. 6: Corresponding die height during filling of one die (pink). Relative mass to maximal mass (before dosing cam) that is obtained for each individual size fraction.

Tab. 4: MFR from filling wheel zone and reverse dosing wheel zone for the different particle size fractions.

Particle size fraction / μm	MFR from filling wheel zone / mg/s	MFR from reverse dosing wheel zone / mg/s	Ratio MFR of filling to reverse dosing wheel zone
0 - 1000	59 ± 33	104 ± 45	0.57
1000 - 1129 (API)	608 ± 230	1099 ± 275	0.55
1129 - 1500	907 ± 271	938 ± 265	0.97
1500 - 1800	3378 ± 785	2524 ± 777	1.34
1800 - 2200	8817 ± 2930	5746 ± 2019	1.53
2200 - 2400	6968 ± 2583	4416 ± 1570	1.58
2400 - 2800	5006 ± 2383	2806 ± 1185	1.78

Mass hold up in the force feeder

The mass hold up in different locations of the force feeder during high speed tableting are shown in Fig. 4 and are in detail described in our previous study [170]. The steady refilling of a random mixture of the particles into the feeding hopper at the same iteration rate as particles are leaving the system in the filled dies ensures a constant mass of 1.1 ± 0.03 kg in the hopper. In contrast, the initial filling level in the three paddle wheel zones decreases until about 6.1 s whereupon a constant mass hold up is obtained. The initial decrease can be explained by the following phenomenon [170]. More particles are leaving the system in the form of filled dies due to faster turret rotation during high speed tableting (increase from 10 rpm to 40 rpm, Tab. 2) which cannot be replaced in time by particles flowing from the hopper into the three paddle wheel zones. The concept of steady state, as already described by others [94, 168, 169], is introduced and defined as the time interval of constant mass hold up in the paddle wheel zones from $t = 6.1 - 15.0$ s during high speed tableting. The reason being is that the basic machine settings, e.g. pre- and main-compression forces to obtain the specified tablet hardness, are assumed to be already debugged during the first turret rotations [57, 78, 87, 98]. Thus the computed metrics in the following sections 3.2.2 – 3.2.3 are evaluated for a system in mass equilibrium. In Fig. 7 it is visualized that areas of different densities are found within the paddle wheel zones. Regions with a higher void fraction are found in the front portion of the dosing wheel zone where the refeeding holes are located and in the right hand half and the left hand half after the die filling region of the reverse dosing wheel zone and the filling wheel zone, respectively.

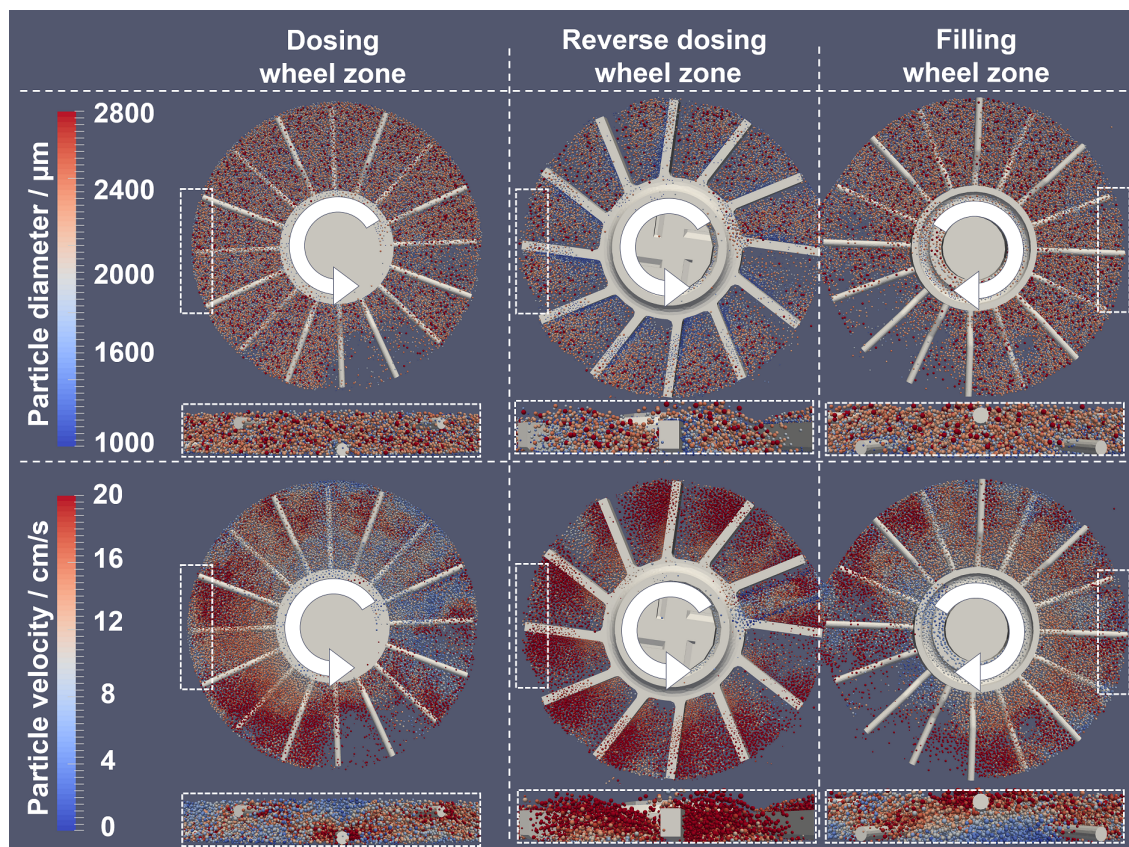


Fig. 7: Top and side view of the three individual paddle wheel zones with particles colored according to their size (top) and their velocity (bottom).

3.2.2 Particles' velocity

Several groups have studied particle flow in vertical, cylindrical mixers with impeller blades either through experiments (e.g. particle image velocimetry, particle emission particle tracking, high speed camera imaging) or numerical simulations using the DEM [180, 196–204]. These studies are extensively describing different aspects of powder flow over a rotating blade by different means, e.g. particles' velocity analysis or force networks. However, the current work does not intend to get into such detail, but rather aims to provide a basic powder flow understanding by force feeding in the context of pharmaceutical tableting. The powder flow by particles' velocity analysis is subsequently described for the dosing wheel zone and filling wheel zone together as their paddle wheel shape show similar powder flow patterns. Afterwards the powder flow is analyzed in the reverse dosing wheel zone.

Particles' velocity in the dosing wheel zone and filling wheel zone

The dosing wheel and filling wheel have almost similar paddle wheel shape that only differs in terms of dimensions (Fig. 1). Both of them contain 16 round / cylindrical shaped blades with a diameter of 4 mm that are bent at half of their length with an angle of 14° (Fig. 1). The paddles rotate through a powder bed height of 15.5 mm and 17.5 mm out of which only 23% and 26% are in direct contact with the blades in the filling wheel zone and dosing wheel zone, respectively. This leads to the following qualitative (Fig. 7) as well as quantitative (Fig. 8) observations. First, the side views of the paddle wheel zones show that only half of the powder bed height, which in particular is in contact with the blade, is being put into motion by paddle wheel rotation. Second, a small radial particles' velocity gradient in the two paddle wheel zones can be identified in the top view illustrations (Fig. 7).

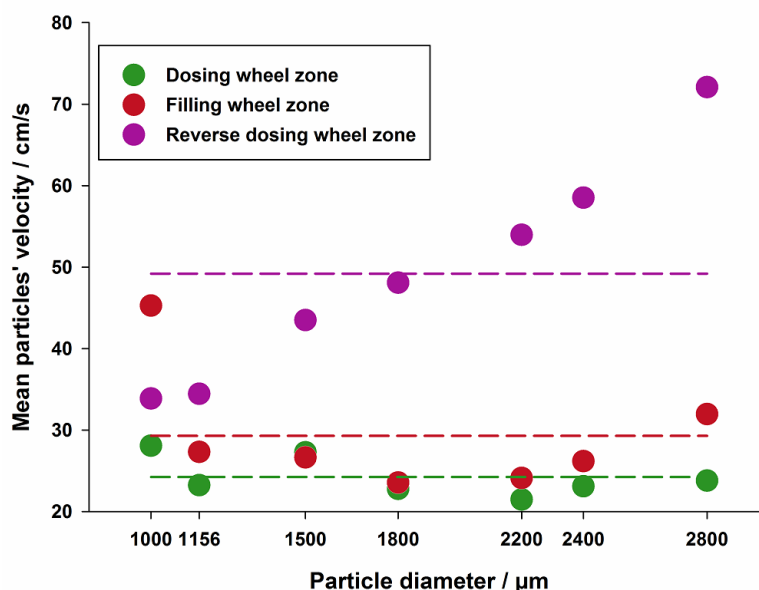


Fig. 8: Particles' velocity for the individual size fractions in the different paddle wheel zones during steady state. The dashed lines indicate the mean particles' velocity per zone.

Particles' with higher velocities are located at the periphery due to higher centrifugal forces. Third, in the dosing wheel zone, regions with higher particles' velocities are found in the refilling regions (into reverse dosing wheel zone and filling wheel zone). In case of the filling wheel zone, regions with higher particles' velocities are located underneath the hole of the dosing wheel zone and in the front, the die filling region. Thus particles can gain increased velocity in regions of higher void space (confer section 3.2.1) where they can follow their trajectories.

Collectively similar mean particles' velocities of 21 cm/s and 23 cm/s for dosing wheel zone and filling wheel zone are obtained (Fig. 8), which are slightly lower than the angular velocities at the blade tips (26 cm/s and 28 cm/s). No distinctive trend over individual particle sizes are found (except smallest size fraction in filling wheel zone). However, larger particles in the filling wheel zone are gaining slightly higher velocities due to their kinetic energy increase as they are about to discharge into the die in the front portion of the filling wheel zone. The cylindrical shaped blades, which constitute only a low contact area with the particles and a low powder bed penetration depth, transfer less momentum to the particles thus decreasing the particles' velocity and shearing. This could prevent particle attrition and powder over lubrication. Both factors can influence tablet tensile strength and dissolution rate [41, 42, 76, 102, 205–208].

Particles' velocity in the reverse dosing wheel zone

In contrast to the very unique blade shape of the dosing wheel and filling wheel, which lack any literature reference, the powder flow in the reverse dosing wheel zone could be partially compared to vertical mixers with impellers [180, 196–204] or to the force feeder of a Manesty Beta Press [94]. The cuboid shaped blades of the reverse dosing wheel are comparable to the impeller shape reported by others [94, 196, 198, 200–203]. Gaps are found between the blade corpus and the feeder housing with clearances of 0.7 mm at the bottom and 6.3 mm at the top. The high depth of immersion of 55%, which is the blade height relative to the powder bed height as described by Bagster and Bridgwater [209–211], significantly alters the powder flow pattern [94] compared to the cylindrical shaped blades of

the two other paddle wheels. A powder wave behavior between two blades of the reverse dosing wheel can be identified in side view of Fig. 7, which is consistent to experiments [107] and simulations [94]. When the blade is pushing into the powder bed, a heap is formed and some particles are going over the blade [196] enabled by the small free volume above the blade (confer above) which is producing recirculation [204]. This recirculation is majorly found for larger particles that are located on top of the powder bed / heap. A turbulent powder flow, indicated by a high particles' velocity (red, Fig. 7), is found near the blade, given by the high applied forces by blade rotation. Particles farther from the blade move with a lower velocity due to energy dissipation and a less confined powder bed is obtained [94]. The paddle is moving with 30 rpm or 26 cm/s at the blade tip, however the overall mean particles' velocity is 1.9-fold higher (49 cm/s, Fig. 8). This observation can be explained by the following mechanisms. (1) The shape of the rectangular blade offers a large contact area that causes a high momentum transfer to the particles. (2) The high void volume between the blades allows the larger particles to travel their trajectories without hurdles before they come to stop, which supports trajectory segregation (confer section 3.2.3) [181, 195, 212, 213]. Thus the mean particle velocity vs particle size plot in Fig. 8 indicates that the particles' velocity linearly increases with particle size. Furthermore larger particles traverse from one inter-blade zone into the one following (recirculation), increasing kinetic energy [202]. As a consequence, the smallest particles move only at slightly higher mean velocity (34 cm/s) than the blade tip (26 cm/s) in comparison to a more than 2.8-fold increase for largest particles (72 cm/s). (3) The overall mean velocity is determined by the particle size distribution (Fig. 2) and thus major contribution comes from the higher velocities of the larger particles.

The top view of the particles' velocity in the reverse dosing wheel shows a clear radial distribution (Fig. 7). Particles closer to the rotation axis move with a lower velocity and remain in this zone for more time compared to particles farther from the axis. This observation is consistent with results from Mateo-Ortiz et al. [93, 94] and can be confirmed by particles coloring analysis (section 3.2.4).

To sum up, particles in the reverse dosing wheel zone are experiencing higher shear forces (higher particles' velocities) and have a longer residence time (confer section 3.2.4) at the increased shear rate that could collectively alter the particle properties. The first particles entering and settling at the bottom of the die originate from the filling wheel zone where they have experienced less shearing than the successively discharging particles from reverse dosing wheel zone. Thus over the die height different particle properties (in addition to size segregation, section 3.2.1), might evolve, consistent with observations made in the experimental Mendez et al. studies [86, 90, 102]. This variation could increase the risk of, e.g. capping of the produced tablets.

The PSD does not reflect, with respect to absolute particle size and size distribution, a direct compression formulation (confer section 2.3 and Fig. 2). However, the general understanding of particles' velocity and mixing in the force feeder could be transferred to smaller particles sizes as well. For example Boonkanokwong et al. showed for mixing by an impeller blade that different ratios of mixer dimensions to particle diameter showed insignificant effects on powder transport mechanisms [180]. For a deeper understanding of powder mixing by the different paddle wheel shapes further metrics, e.g. calculation of a dimensionless shear rate as done by Radl et al. [202], could be computed. Though the basic particles' velocity analysis already describes the different powder flow mechanisms induced by varying blade shapes thus improves process understanding and the influence on product quality.

3.2.3 Particle size segregation

In section 2.5 a brief summary of different mixing quantification approaches are presented that help to assess particle size segregation. In this chapter the following particle size segregation analysis are discussed:

- Quantification of API particle segregation in the filled dies that finally define the patients' safety.
- Assessment of PSD variation in the filled dies to estimate its effect on the powder blend's compressive properties [214–220].
- Determination of the PSD within the hopper and the different paddle wheel zones to evaluate segregation induced by paddle wheel movement during mass steady state.
- Calculation of the overall segregative / mixing effect in the force feeder (between the three paddle wheels zones) during mass steady state.

API distribution in the dies

As defined by the authorities [25], content uniformity has to be assessed through the monograph 2.9.40 ('Uniformity of dosage units'). An 'Acceptance Value' (AV) is calculated for a set of samples (10 - 30) based on the relative ratio of measured to label claim content, its standard deviation, and a statistical constant. This approach, if applied to the current system, reveals an un-proportionally high AV value (data not shown). The high AV value can be attributed to the large particle sizes considered in relation to the rather small die dimensions (section 2.2 and 2.3).

A classical statistical, sampling based mixing index, the 'Poole Index' [188] is used in the following. The $PI_{API,dies}$ is calculated according to Eq. 2 (section 2.5) during high speed tableting (die no. 1 - 232, Fig. 5). The complete die content is used for analysis to unify the effect of sample size and sampling technique [188]. At a mean no. of 746 particles filled per die ($\overline{n_{dies}}$), a $q_{3,i,spec}$ of 5%, a $\sigma_{r,API,dies}$ of 0.64%, and a $\sigma_{s,API,dies}$ of 1.11%, a $PI_{API,dies}$ of 1.40 is obtained (Tab. 5). The $PI_{API,dies} > 1.0$ indicates that not a random but segregated API distribution in the filled dies is obtained [188] which is also shown in the high API mass fluctuation in Fig. 5. Practically a high $PI_{API,dies}$ indicates that the API distribution over time in the filled dies is not constant.

DC blend size segregation in the dies

In analogy to the $PI_{API,dies}$, $PI_{i,dies}$ of the other excipient particle size fractions (according to Eq. 2) are measured for the dies and are given in Tab. 5. A slight influence of particle size on the $PI_{i,dies}$ with a slight increase of the $PI_{i,dies}$ for larger particles can be found which could stem from their higher $\sigma_{s,i,dies}$. The higher fluctuations could be attributed to the relationship between the small die sample volume of 7 cm³ and the large particle volume (59-fold smaller). It implies an influence of sample size on the segregation quantification, as reported in literature [188]. However it should be noted that the size fractions are unevenly distributed and have varying contents (Fig. 2) which impede to draw a clear conclusion.

From a practical point of view the $PI_{i,dies}$ should be low for all size fractions. It is important to obtain a low $PI_{i,dies}$ for larger particles as these particles contribute to highest extent to the mass filled into the die. They predominantly define the tablet mass variation. In addition, a low segregation index is also desirable for smaller particles since they can enter the voids during compaction and can result in a close particle packing [221]. Smaller particles can lead to an increased tablet hardness as their surface area forms increased interparticle bonds [221–228].

A combined segregation index for the complete DC blend is calculated according to Eq. 2 resulting in a PI_{dies} of 1.4 (Tab. 3). The $PI_{dies} > 1.0$ indicates that the content in the filled dies over time is not constant and individual $PI_{i,dies}$ in combination with their content ($\frac{q_{3,i,location}}{100\%}$) do not compensate

each other (for detailed explanation see section 2.5).

In addition to size segregation, or in other words PSD fluctuation analysis, the measured content in the filled dies ($\overline{q_{3,i,dies}}$) can be compared to the label claim content ($q_{3,i,dies}$). It is shown that at a cut-off diameter between 1800 - 2200 μm , a lower than specified content is found for particles $\leq 1800 \mu\text{m}$, whereas the opposite is true for particles $\geq 2200 \mu\text{m}$ (Tab. 5). As a consequence the powder blend compaction properties may differ from expectations of the defined PSD (Fig. 2) and could be compensated by, e.g. adjusting the compression force. This observation is a consequence of the particle size segregation in the feeding system which is explained in the following.

Segregation in hopper

Size segregation is evaluated in the hopper and in the different paddle wheel zones of the force feeder during mass steady state in high speed tableting (Fig. 4). Pre-empt, in section 3.2.4 the particles' refilling from the hopper into the dosing wheel zone is described by particles' coloring analysis. Since the refilling is not consistent over the complete hopper width (Fig. 9A), the bottom zone of the hopper (height of 25 mm) in direct connection with the dosing wheel zone is cut half over the hopper width and the PSD over discharge time extracted. The PSD and segregation metrics are given for the left hand half and right hand half of the bottom zone of the hopper in Tab. 5. The most significant difference in PSD content is found for the API particle size fraction with a $\overline{q_{3,API,hopper\ left}}$ of 3.6% and a $\overline{q_{3,API,hopper\ right}}$ of 4.7%. Since the right hand half is showing a higher mass throughput (section confer section 3.2.4, Fig. 9 and 10), higher $\sigma_{s,i,hopper(left\ or\ right)}$ and thus higher $PI_{i,hopper(left\ or\ right)}$ (Eq. 1) values are found. As a consequence, the overall PI_{hopper} (Eq. 2) is 16% higher in the right hand half compared to left hand half of the hopper (Tab. 3).

Segregation in dosing wheel zone

In the dosing wheel zone, the zone connecting the feeding hopper with the two paddle wheel zones below, a clear particle size segregation is found after system filling (confer section 3.2). In particular smaller particles are moving to the bottom of the zone (side view, Fig. 7) by sieving mechanism [181, 195] once they enter from the right hand half of the hopper. This kind of mechanism was already found during system filling (confer section 3.2) [170]. In contrast to system filling, less small particles move through the voids of the larger ones as particles move with higher velocities during high speed tableting (increase in paddle wheel speed from 15 rpm to 30 rpm, Tab. 2). The resultant is a reduced sieving mechanism in the dosing wheel zone [170]. It explains the increase of fines in the dosing wheel zone and filling wheel zone and their decrease in the reverse dosing wheel zone (confer below) in comparison to system filling (Fig. 4). Consequently, during high speed tableting less small particles are found at the bottom of the dosing wheel zone. Less fines are transferred to the reverse dosing wheel zone, and more remain within the dosing wheel zone which can refill the filling wheel zone.

During high speed tableting, a minimal radial size segregation with larger particles located farther to the rotation axis is found, as shown in Fig. 7. This can be explained by the increased centrifugal force (by higher rotational speed) pushing them towards the periphery.

The $PI_{i,dosing\ wheel\ zone}$ ranging between 0.3 and 1.1 (Tab. 5) and a $PI_{dosing\ wheel\ zone}$ (Tab. 3) of 0.9 indicate a constant PSD during mass steady state in high speed tableting.

Segregation in reverse dosing wheel zone

As already described in section 3.1, the particles first fall from the dosing wheel zone into the reverse dosing wheel zone. An accumulation of fines and depletion of coarse particles relative to their specified contents after system filling is obtained in reverse dosing wheel zone (Fig. 4). Although this size

segregation is maintained during high speed tableting, the relative content differences to specification are decreasing (confer above, Tab. 5) [170]. A unique powder flow pattern is found in the reverse dosing wheel zone which is majorly attributed to the paddle wheel shape as already discussed in section 3.2.2 Consistent with experiments [197], coarse (red) particles segregate from finer (blue) particles radially to the outer wall and vertically to the free surface on the top, as shown in top and side view (Fig. 7 top). The underlying mechanism is trajectory segregation, in which the larger particles and their resultant higher kinetic energies show longer trajectories before they come to stop [181, 195, 212, 213]. The small particles are getting ‘trapped’ in front of the rotating blade (Fig. 7) as their reduced particles’ velocity prevents recirculation between the inter-blade zones (section 3.2.2). Furthermore, and described by Conway et al. [197], larger particles have the ability to flow over a rough granular surface more readily than smaller particles. Thus coarse particles are rolling preferentially to the outer wall, which is also influenced by centrifugal force. The $\sigma_{s,i,reverse\ dosing\ wheel\ zone}$ are significantly higher for almost all particle size fractions compared to the dosing wheel zone and filling wheel zone. This can be attributed to the higher particles’ velocity (confer section 3.2.2) that increases the content fluctuation. As a result, the individual $PI_{i,reverse\ dosing\ wheel\ zone}$ are higher for most of the particle size fractions (Tab. 5) leading to the highest overall paddle wheel zone segregation index ($PI_{reverse\ dosing\ wheel\ zone}$) of 1.4 (Tab. 3).

Segregation in filling wheel zone

The filling wheel zone has similar PSD patterns and size segregation mechanisms as already described for dosing wheel zone, e.g. the top-to-bottom segregation of fines. These similarities are illustrated in Fig. 7 and can be traced back to the comparable paddle wheel shape as described in section 3.2.2. The initial $q_{3,i,filling\ wheel\ zone}$ of the individual particle sizes that are found directly after system filling are approaching towards the specified contents during high speed tableting (Fig. 4) [170]. The high mass turnover rate (section 3.2.4) causes higher content variations ($\sigma_{s,i,filling\ wheel\ zone}$) compared to the dosing wheel zone. They can be attributed to the particles’ discharge into the dies and the refilling from the dosing wheel zone which is transferring content fluctuations from dosing wheel zone into filling wheel zone. The $PI_{i,filling\ wheel\ zone}$ are for most of the particle sizes comparable to the dosing wheel zone (attributed to the decreased number of particles for filling wheel zone in the denominator of Eq. 1) resulting in a $PI_{filling\ wheel\ zone}$ of 1.0.

Influence of segregation in paddle wheel zones to segregation in filled dies

In section 3.2.1 an explanation for the collected mass and the individual particle size fractions in the die originating from the filling wheel zone and reverse dosing wheel zone is provided (Tab. 4). As a direct consequence, the segregation indices of fines in the dies are predominantly influenced by the PSD in the reverse dosing wheel zone and for coarse particles by the PSD in the filling wheel zone. Thus the detailed mass flow rate, particles’ origin, and PSD in the force feeder analysis allows a direct understanding of tablet quality in terms of particle size consistency.

Segregation over the complete force feeder

It has been described already that within the three paddle wheel zones small content fluctuations during high speed tableting could be identified. Furthermore the PSD entering from the hopper into the force feeder ($\overline{q_{3,i,hopper\ right}}$) is close to the specified PSD (Fig. 2, Tab. 5). However sieving segregation in the dosing wheel zone causes a de-mixing of the blend which is subsequently transferred into the reverse dosing zone and filling wheel zone. These resulting PSD differences, as exemplarily shown for API particle size fraction in Fig. 4, indicate that the force feeder causes a de-mixing. This de-mixing is quantified by calculating the content deviations between the three paddle wheel zones

according to Eq. 4:

$$\sigma_{s,i,feeder} = \left(\frac{1}{3} \left((q_{3,i,dosing\ wheel\ zone} - \overline{q_{3,i,feeder}})^2 + (q_{3,i,reverse\ dosing\ wheel\ zone} - \overline{q_{3,i,feeder}})^2 + (q_{3,i,filling\ wheel\ zone} - \overline{q_{3,i,feeder}})^2 \right) \right)^{\frac{1}{2}} \quad (4)$$

Basically, the mean content of each particle size fraction over the complete three paddle wheel zones is determined ($\overline{q_{3,i,feeder}}$). Subsequently the difference found in the three individual paddle wheel zones is computed and finally gives the $\sigma_{s,i,feeder}$. In case that no de-mixing is found, the contents in the different paddle wheel zones are same and a $\sigma_{s,i,feeder} = 0$ are obtained. The $\sigma_{r,i,feeder}$ and the $PI_{i,feeder}$ is then calculated according to Eq. 1. For the API particle size fraction an example calculation is provided to thoroughly explain the concept of the $PI_{i,feeder}$:

API contents of 4.2%, 11.3%, and 3.4% are found during steady state in the dosing wheel zone ($q_{3,API,dosing\ wheel\ zone}$), reverse dosing wheel zone ($q_{3,API,reverse\ dosing\ wheel\ zone}$), and filling wheel zone ($q_{3,API,filling\ wheel\ zone}$) (Tab. 5, Fig. 4B), respectively. The mean content within the complete feeder, or in other words over all three paddle wheel zones is 6.3% ($\overline{q_{3,API,feeder}}$). This results in a $\sigma_{s,API,feeder}$ of 3.5% (Eq. 4) which is a measure to quantify the content deviation of the individual zones to the mean content in the feeder. This deviation is 48-fold higher ($PI_{API,feeder}$) than the deviation assuming a random mixture ($\sigma_{r,API,feeder}$). Furthermore, for all particle size fractions a segregation index is calculated which results in a combined value of 16.1 (PI_{feeder}) (Eq. 2). This very high value indicates that significant different PSDs in the three paddle wheel zones of the force feeder are found. Thus the force feeder causes the undesired side effect of material de-mixing. The absolute size segregation extent is higher compared to reality given by the larger particle sizes considered, though a general understanding of size segregation in the force feeder is provided.

The gained process insight allows different means of improvement, e.g. modification of the size and the position of the refilling holes at the bottom of the dosing wheel zone to decrease the size segregation and de-mixing in the force feeder. Other options could be for example a change of the paddle wheel shape or, more drastically, the transfer from a three to a two paddled system.

Tab. 5: Segregation indices during steady state (for explanation confer section 2.5)

Quantity	Location (η_{location}) / -	Particle size fraction / μm							
		0-1000	1000- 1129	1129- 1500	1500- 1800	1800- 2200	2200- 2400	2400- 2800	2800
$\beta_{3,i,\text{spec}}$ / %		0.1	5.0	4.8	14.3	33.3	25.7	16.6	
$\sigma_{s,i,\text{dies}}$ / %	Dies (746)	0.1	1.1	0.9	1.7	2.1	2.3	2.9	
$\beta_{3,i,\text{dies}}$ / %		0.4	4.6	4.5	13.9	33.3	26.1	17.1	
$PI_{i,\text{dies}}$ / -		0.5	1.4	1.1	1.3	1.2	1.5	2.2	
$\sigma_{s,i,\text{hopper left}}$ / %	Hopper bottom left (14271)	0.0083	0.0270	0.0660	0.1200	0.4600	0.2500	0.2200	
$\beta_{3,i,\text{hopper left}}$ / %		0.3	3.6	4.7	14.6	34.6	26.1	16.2	
$PI_{i,\text{hopper left}}$ / -		3.4	0.8	2.8	1.8	3.6	2.3	3.0	
$\sigma_{s,i,\text{hopper right}}$ / %	Hopper bottom right (14898)	0.0170	0.0900	0.1300	0.2000	0.3200	0.400	0.3200	
$\beta_{3,i,\text{hopper right}}$ / %		0.4	4.7	4.7	14.3	33.4	26.0	16.5	
$PI_{i,\text{hopper right}}$ / -		0.4	0.5	0.9	0.8	0.9	1.2	1.2	
$\sigma_{s,i,\text{dosing wheel zone}}$ / %	Dosing wheel zone (38229)	0.0130	0.0660	0.0370	0.2000	0.1800	0.2500	0.2100	
$\beta_{3,i,\text{dosing wheel zone}}$ / %		0.4	4.2	4.3	13.8	33.6	26.3	17.5	
$PI_{i,\text{dosing wheel zone}}$ / -		0.4	0.6	0.3	1.1	0.8	1.1	1.1	
$\sigma_{s,i,\text{reverse dosing wheel zone}}$ / %	Reverse dosing wheel zone (23718)	0.0440	0.2700	0.1600	0.4800	0.2300	0.2500	0.5800	
$\beta_{3,i,\text{reverse dosing wheel zone}}$ / %		1.3	11.3	7.3	16.8	30.7	21.3	11.5	
$PI_{i,\text{reverse dosing wheel zone}}$ / -		1.0	1.9	1.2	2.1	0.8	0.9	2.4	
$\sigma_{s,i,\text{filling wheel zone}}$ / %	Filling wheel zone (24425)	0.0190	0.2200	0.1200	0.2300	0.1700	0.3700	0.3500	
$\beta_{3,i,\text{filling wheel zone}}$ / %		0.3	3.4	4.1	13.8	34.2	27.3	17.0	
$PI_{i,\text{filling wheel zone}}$ / -		0.4	1.6	0.9	1.0	0.6	1.3	1.5	
$\sigma_{s,i,\text{feeder}}$ / %	Feeder (86372)	0.4	3.5	1.4	1.4	1.5	2.7	2.7	
$\beta_{3,i,\text{feeder}}$ / %		0.6	6.3	5.2	14.8	32.8	25.0	15.3	
$PI_{i,\text{feeder}}$ / -		18.9	47.7	19.9	12.0	9.6	17.8	21.3	

3.2.4 Particles' coloring analysis

Usually experiments do not allow to look inside a closed system unless a transparent housing is used, i.e. as reported by Mendez et al. [86]. The DEM gives the opportunity to look into a closed system. By coloring the particles at their initial location, the powder flow can be visualized and the colored particles tracked over time [41, 168, 171]. Some of the key findings of our pre-communication [171] are provided for the sake of completeness.

At the time point of high speed tableting, different zones in the Fill-O-Matic are assigned different colors, as shown in Fig. 9 ($t = 0$ s). Particles in green, pink, and red are initially located in the dosing wheel zone, filling wheel zone, and reverse dosing wheel zone, respectively. In addition to the paddle wheel zones, four additional horizontal zones in the feeding hopper with a height of 5 mm in grey, yellow, light orange, and dark orange color separated by non-colored particles (blue, height of 25 mm) were assigned. Particles below the force feeder (in the initially filled dies and between turret and force feeder) were non-colored as well (blue). Five different metrics / powder flow phenomena that can be observed by coloring analysis as shown in Fig. 9 are discussed in the following and have been described partly by Hildebrandt et al. [171].

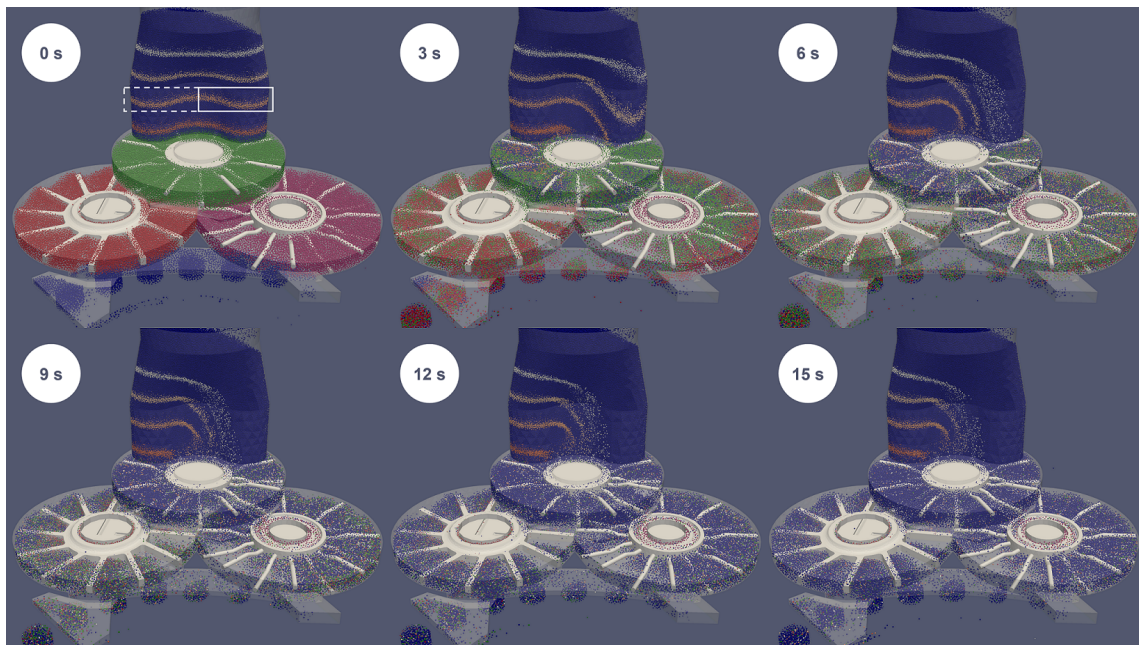


Fig. 9: Tracking of particles, colored by their initial position during high speed tableting at intervals of 3 s.

Powder flow in the feeding hopper

Fig. 9 shows that particles are non-uniformly fed from the hopper into the dosing wheel zone since a gradient across the hopper width is found. Thereby particles that are initially located in the left hand half of the hopper tend to remain there throughout the complete discharge period. Solely particles from the right hand half enter and refill the dosing wheel zone. This phenomenon is quantitatively shown in Fig. 10A in which the hopper is split into a left hand half (dashed lines, Fig. 9, $t = 0$) and right hand half (solid lines, Fig. 9, $t = 0$) and the number frequencies of colored particles appearing in this zone are plotted over discharge time. Light orange colored particles in the left hand half only slowly deplete from initially 16% to 12% after 15 s. In contrast in the right hand half of the hopper they show a very steep decrease after 1.3 s and completely disappear after 7.1 s. Furthermore, in the latter, light orange and grey colored particles from zones above show up with maximum frequencies

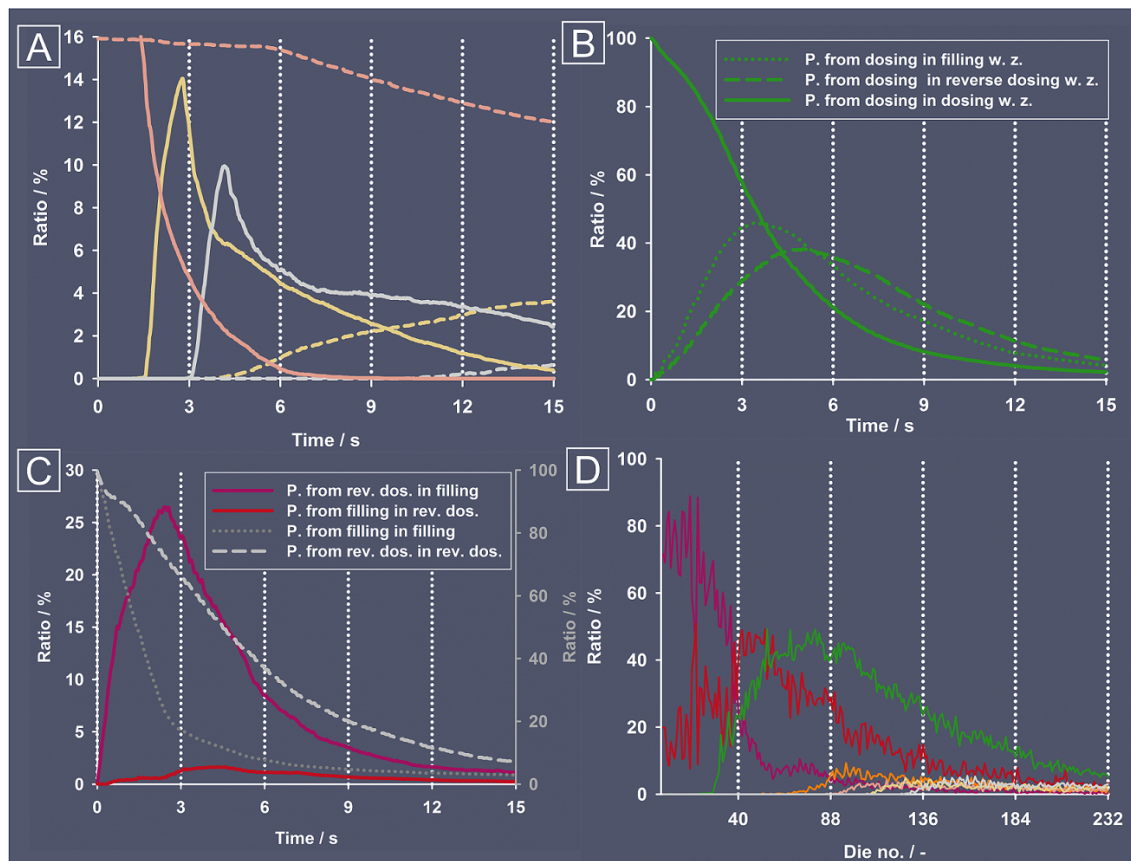


Fig. 10: Quantitative analysis of colored particles during discharge (for initial position of colors confer Fig. 9). (A) Ratio of colored particles in the hopper left hand half and right hand half (zones shown in Fig. 9, $t = 0$ s) and travel path of green (B) and red and pink (C) colored particles. (D) Colored particles in the filled dies.

of 13% at 2.9 s and 9% at 4.3 s, respectively. Particles in the left hand half of the hopper constitute a dead zone and may get consolidated over production time as a result of the pressure exerted by the overlying powder bed in the feeding hopper and blending container. In addition, the higher mass throughput in the right hand half of the hopper is also apparent in the increased segregation indices (confer section 3.2.3 and Tab. 5 and 3).

Powder refilling

The geometrical configuration of the Fill-O-Matic (Fig. 1) shows that the material from the dosing wheel zone refills the reverse dosing wheel zone and the filling wheel zone. As already described in section 3.2.3, this configuration transfers particle size segregation. Green colored particles from the dosing wheel zone are illustrated in Fig. 9 and plotted in Fig. 10B. The larger refilling hole into the filling wheel zone (Fig. 1) promotes an earlier onset and an initially higher contribution of green particles in this zone compared to the reverse dosing wheel zone (Fig. 9 and 10B) [171]. However the total frequencies (area under the curve) of green colored particles in the filling wheel zone and reverse dosing wheel zones are almost the same with 21% and 20%, respectively. More small particles discharge from the dosing wheel zone into the reverse dosing wheel zone, confer section 3.2.3, which results in the high number frequency (20%) although the mass based analysis reveals higher frequencies for the filling wheel zone (data not shown).

Mixing in the reverse dosing wheel zone and filling wheel zone

The high mass throughput in the filling wheel zone can be characterized by a very steep number frequency decrease of initially located particles (grey dotted line, Fig. 10C) in this zone in contrast to the curve profile of the red particles in the reverse dosing wheel zone (grey dashed line, Fig. 10C) [171]. An additional observation, enabled by coloring analysis, indicates that particles remain a longer residence time in the reverse dosing wheel zone. Over time 40.2% of all particles found in the reverse dosing wheel zone were originally located there (area under the curve, grey dashed line Fig. 10C). In contrast, 2.6-fold less particles from filling wheel zone were found in the same over time (15.4%, area under the curve, grey dotted line, Fig. 10C). The higher particles' velocity (section 3.2.3, Fig. 7 and 8) / shearing rate and longer residence time in the reverse dosing wheel increase the risk of particle attrition and over lubrication [41, 42, 76, 102, 205–208].

Particles from the reverse dosing wheel zone are mixed, enabled by an unclosed intersection of 46 mm width (Fig. 1), into the filling wheel zone to catch up the mass decrease in the filling wheel zone. During the complete high speed tableting time, 8.7% and 0.7% of initially located particles were mixed from reverse dosing into filling wheel zone and vice versa (area under the curve for pink and red lines in Fig. 10C). Consequently, a predominant intermixing from reverse dosing wheel zone into filling wheel zone is found [171].

Colored particles in dies

The colored particles as they appear in the dies are shown in Fig. 10D [171]. Initially the highest contribution in the filled dies comes from the filling wheel zone given by the pink colored particles. The pink colored particles show a steep decrease right from the beginning in contrast to particles from reverse dosing wheel (red) which show only a slow decrease, attributed to their higher residence time in the reverse dosing wheel zone (confer above). As soon as the pink colored particles start to deplete, particles that originate from the dosing wheel (green) zone appear from die no. 20 onwards up to their maximum in die no. 55. In die no. 60, 86, 107, and 125 the first colored particles from the hopper (orange, light orange, yellow, and grey) appear.

The first particles entering the die have traveled less distance in the force feeder compared to the particles in the later filled dies. Thus not only over the die height (confer section 3.2.1) but also over production time differences in particle properties might be found which could lead to varying tablet tensile strengths and dissolution rates.

Colored particles in system

At the end of discharge, only a few colored particles that were initially located in the different paddle wheel zones have remained in the system, namely 3%, 8%, and 6% of the pink, green, and red particles (Fig. 9). Thus almost the complete initial mass in the paddle wheel zones have been discharged into the dies during 15 s of high speed tableting.

3.2.5 Particles' residence time

In chemical engineering and related fields, the 'Residence Time Distribution' (RTD) is defined as the 'probability distribution of time that solid or fluid materials stay inside one or more unit operations in a continuous flow system' [229]. In the context of powder flow in a pharmaceutical tablet press, the RTD has been linked to forces applied by paddles causing particle attrition [95] and has been compared to operation parameters and powder cohesion [41].

For the current study, particles at a height of 10 mm in the hopper left hand half and right hand half (Fig. 11) are tracked over discharge time (Ⓓ, Tab. 2) and their time point of leaving the system is computed (Fig. 11, right). A clear difference between the left hand half and right hand half of the

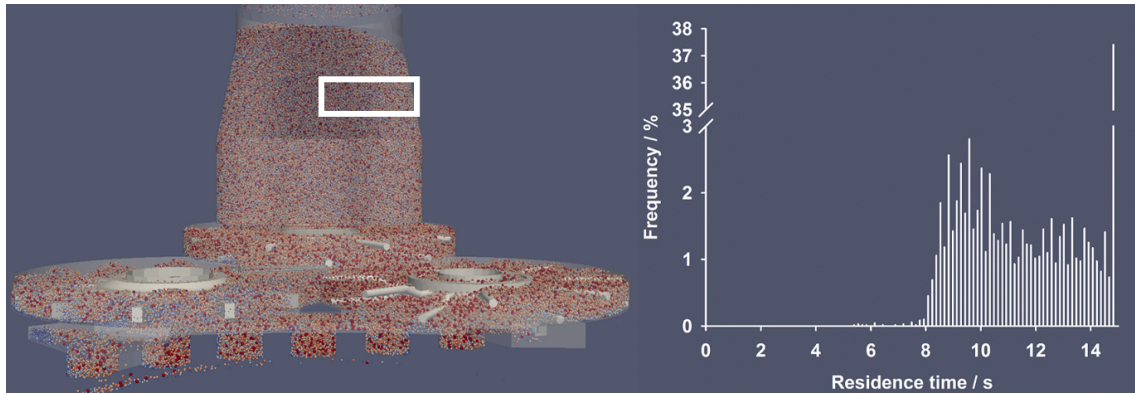


Fig. 11: Residence time distribution of all particles that were initially located in the top right hand half of the hopper (box, left).

hopper could be identified. More than 99% of all particles that were initially located in the left hand half of the hopper are still within the system after 10 turret revolutions (data not shown), which is consistent with the particles coloring analysis (confer section 3.2.4, Fig. 9 and 10A). In contrast, more than 60% of the particles from the right hand half of the hopper have been discharged into the dies (Fig. 10E). No difference between the particle size fractions can be identified, i.e. all of them start to leave the system after $t = 7.1$ s (Fig. 11) and the frequency plots have comparable shapes (data not shown). This means, that particles take more than 7.1 s and on an average 12.6 s (Tab. 3, Fig. 11) to travel from the right top portion of the hopper to the dosing wheel zone and then through the two paddle wheels below until they leave the system in the filled dies. Furthermore no particle size fraction is held back in the complete system which would be indicated by a different area under the curve (data not shown), in contrast to observations made by Mateo-Ortiz et al. [93]. No particle size segregation over the complete system is found although de-mixing within individual zones of the force feeder (section 3.2.3) is prominent. The RTD function does not, in contrast to previously reported force feeder studies (experiments and simulations) [41, 95], resemble to the shape of a continuous stirred tank reactor [229], showing a sharp peak and a tail, since the computation time of 15 s (⚡, Tab. 2) is too short and would have to be further extended.

The RTD analysis (1) supports the coloring observations, i.e. the dead zone in the left hand half of the hopper, (2) indicates that over the complete system no particle size fraction is held back, and finally (3) particles remain on an average 12.6 s in the force feeder until they discharge into the dies. During this time period particle de-mixing / size segregation in different zones of the force feeder is found and an alteration of particle properties by particles' shearing might be indicated.

4 Conclusion

The powder flow in the force feeder of a pilot-scale tableting machine containing three paddle wheels of different shapes was investigated through numerical simulations. An attempt was made to reflect the reality as well as possible by (1) using a model direct compression formulation containing particles of different sizes and calibrated material properties. (2) The process in terms of system filling and high speed tableting was adapted to the general procedure used in experiments. Different means, e.g. mass based analysis, particles' velocity comparison, particle size segregation quantification through mixing indices, particles' tracking through particles' coloring, and particles' residence time calculation, were developed to provide a thorough powder flow understanding. The key findings can be summarized as follows:

- (1) The design of the geometry in terms of the housing, in particular the arrangement of the paddle wheel zones and their connection through holes, in addition to paddle wheel shape favored particle size segregation and de-mixing within the force feeder.
- (2) In addition to size segregation, the blade shape influenced the particles' velocity and thus the forces acting on the particles and the shear rates.
- (3) A dead zone in the hopper could be identified that may lead to powder consolidation.

It was shown that the force feeder design has a clear influence on the tablet quality, as follows:

- (1) Particle size segregation developed in the force feeder was transferred into the dies. Thus first larger particles, which experienced less shear forces, entered the die first. Smaller particles followed on top, which were exposed to significantly higher shear forces. As a consequence, the intra-die PSD and particle properties variations may lead to differences in compaction properties over the die height and thus capping may occur.
- (2) Over production time, API segregation was quantified which could constitute an issue for content uniformity. In addition, API false dosing was identified that could be remedied by tablet mass adaption.
- (3) Furthermore an inter-tablet variation might be found over process time as a consequence of the different distances particles traveled in the force feeder before they discharged into the dies. Through their path in the force feeder their particle properties might have changed by particle attrition and / or over lubrication.

In conclusion this study provides a thorough understanding of powder flow in the force feeder and its direct influence on tablet quality attributes. It serves as a starting point for follow-up studies that will include more setups combined in a design of experiments. The powder dynamics in the force feeder were identified for a free flowing model DC formulation, though limited by computational power, the particle sizes had to be enlarged and the process time reduced in comparison to reality. Hence a one-to-one prediction of the tableting process was not intended. Experimental validation of the numerical results using a custom-designed model force feeder system is currently ongoing and the results will be shared in our future work.

Acknowledgments

The authors would like to thank and acknowledge Mr. Thomas Heinrich (Fette Compacting GmbH, Schwarzenbek, Germany) and his team for generously providing the FETTE 1200i Fill-O-Matic CAD files. Dr. Thomas Profitlich's and Dr. Wolfgang Bauer's support (Daiichi-Sankyo Europe GmbH) in supporting the project are highly appreciated.

3.2.3 Influence of material properties and process parameters on tablet quality in force feeding

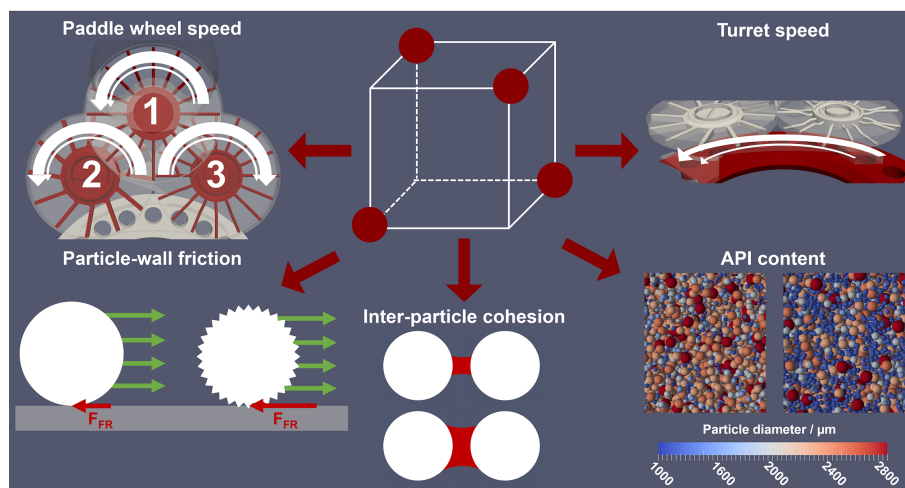
Assessment of material and process attributes' influence on tablet quality using a QbD and DEM combined approach

Claudia Hildebrandt^{1, 2}, Srikanth R. Gopireddy², Regina Scherließ¹,
Nora A. Urbanetz²

¹ Department of Pharmaceutics and Biopharmaceutics, Christian-Albrechts-Universität Kiel,
Grasweg 9a, 24118 Kiel, Germany

² Daiichi-Sankyo Europe GmbH, Pharmaceutical Development,
Luitpoldstrasse 1, 85276 Pfaffenhofen, Germany

Submitted to Powder Technology, under review



Outline

In chapter 3.2.1 the influence of the material properties inter-particle cohesion, particle-wall coefficient of friction, and API content and the process conditions turret speed and paddle wheel speed on tablet mass is ascertained using a DoE. Other than tablet mass, additional critical quality attributes (CQAs) of tablets are defined through the die filling step, i.e. the tablet mass variation and the content uniformity. Those CQAs are addressed in the following chapter by applying the Quality by Design (QbD) approach. The influence of the different parameters (= factors) on those CQAs is assessed using the same DoE as in chapter 3.2.1. As shown in the previous chapter (3.2.2), the paddle wheels exert different stresses on the particles which may lead to particle attrition and over lubrication. The particle shearing at different factor combinations is assessed through the DoE by (1) measuring the particle's origin within the force feeder and by (2) the shear rate the particles may have experienced.

The DoE design targets the factor screening or the identification of the most significant factor effects. It provides first details on factor combinations which result in highest or lowest tablet quality. Thus the combination of the DEM with the QbD may be utilized in formulation and process development for an enhanced understanding of the connection between force feeding and tablet quality.

1 Introduction

1.1 Quality by design and process modeling in pharmaceutical development

The quality by design (QbD) approach was introduced into the pharmaceutical development in 2009 by the International Conference on Harmonisation (ICH) via the guideline ‘Pharmaceutical Development Q8(R2)’ [3]. Drug product development based on the QbD approach is a step-wise procedure as follows. First, the ‘Quality Target Product Profile’ (QTPP) is defined which is the ‘summary of the quality characteristics of a drug product that ideally will be achieved to ensure the desired quality, taking into account safety and efficacy of the drug product’ [3]. Thus the characteristics that make up the QTPP should be ‘designed into the product’ via a science-based process [230] in contrast to quality testing into the product [3]. After developing the lead formulation and the manufacturing process, the process understanding is generated by determining the critical quality attributes (CQA). According to the guideline, ‘the CQAs of a solid oral dosage form are typically those aspects affecting product purity, strength, drug release, and stability’ [3]. The QbD core objectives are to identify the most important CQAs, namely the formulation (critical material attributes, CMA) and process parameters (critical process parameters, CPP) that significantly affect the QTPP and to get an understanding of their relationship to product performance. The design space is generated which is a ‘multidimensional combination and interaction of input variables (e.g. material attributes) and process parameters that have been demonstrated to provide assurance of quality’ [3].

Eventually, the QbD approach gives the opportunity to develop more flexible regulatory approaches if the applicant can demonstrate an enhanced knowledge of product performance [3]. Several possibilities exist to develop a valuable science-based process such as risk management [3, 231] including multivariate analysis, risk filtering, fishbone diagram, and failure mode and effect analysis (FMEA) [232]. An increased process understanding can be gained by ‘application of, e.g. formal experimental designs, process analytical technology (PAT), and/or prior knowledge’ [3]. However science-based manufacturing may not only involve PAT but also other fundamental tools such as first-principle based process modeling and control [16]. Such numerical tools for *in silico* experimentation include multiphase computational fluid dynamics (CFD), lattice Boltzmann methods, or the discrete element method (DEM) [233]. In the context of QbD, the pharmaceutical tablet coating [234] and powder blending [235] process have been numerically studied. Though numerical studies are referred to as analysis tools, they are still not straightforward implemented in QbD and have not been fully adopted by regulatory authorities [233].

1.2 Modeling of powder flow in the force feeder of rotary tablet presses

Tablets are the most prominent drug product and are produced in high quantities using rotary tablet presses [28]. Tableting involves three distinctive stages, namely die filling, powder compaction, and tablet ejection. The first step constitutes the powder transfer from the blending hopper through the feeding system into the rotating dies of the turret. The powder flow within the tablet press shows a significant impact on tablet quality in terms of tablet weight, tablet weight variation, content uniformity, and tablet tensile strength [76, 87] and thus gave rise to evaluate the die filling process in gravity [168, 169] and force feeders [41, 93–95, 236] by numerical means.

The following summarized key observations for powder flow in the three paddled force feeder of a FETTE 1200i were made in our previous study by using DEM [170]. The design of the geometry, consisting of a dosing wheel (1, Fig. 1), reverse dosing wheel (2, Fig. 1), and filling wheel (3, Fig. 1),

in particular the arrangement of the paddle wheel zones favored particle size segregation or de-mixing within the force feeder. A non-uniform powder flow with a dead zone within the feeding hopper could be identified that might lead to powder consolidation and segregation [171].

The characteristic of powder transfer from the feeding hopper to the dosing wheel zone (1, Fig. 1), then to the reverse dosing wheel zone (2, Fig. 1), and the filling wheel zone (3, Fig. 1) from where the particles start to enter the dies of the rotating turret, was linked with tablet quality, e.g. in terms of tablet mass variation and content uniformity. Since in the former study only the influence of process conditions and material attributes on tablet mass was studied [170], the current work provides a more thorough understanding of their impact on additional tablet quality attributes.

1.3 Objectives

The essential objective of the current study is the evaluation of the influence of selected process conditions and material attributes on tablet quality. A model direct compression (DC) formulation is developed considering a poly-disperse particle size distribution. However, the absolute particle sizes and their distribution are larger compared to experiments given by the computational complexity impeding a one-to-one transfer of the numerical results to reality. Part of this study was already published in our previous work [170] and is extended in the current. Hence some of the results with respect to tablet mass may be taken over for the sake of explanation.

In comparison to our previous work [170], the current study adds value on the following points:

- Extensive analysis of different CQAs (tablet mass variation, and ‘uniformity of dosage units’ [2.9.40 and 2.9.47] [25]) instead of one (tablet mass)
- Evaluation of particle flow and shearing within force feeder that might affect tablet disintegration [2.9.19] and API dissolution [2.9.3] [25] though the actual powder compaction step is not simulated
- Assessment of DoE results and verification
- Design space evaluation to find optimum process conditions and material attributes

A fractional factorial screening design, developed previously [170], helps to discern the individual factor and two-factor effects on tablet quality in a FETTE 1200i tableting machine. The numerical work is embedded in the QbD framework [3] to identify the most important CPPs and CMAs affecting the CQAs. The main target is the generation of a general science-based tableting process understanding using a combined approach of QbD and DEM which has not been reported previously.

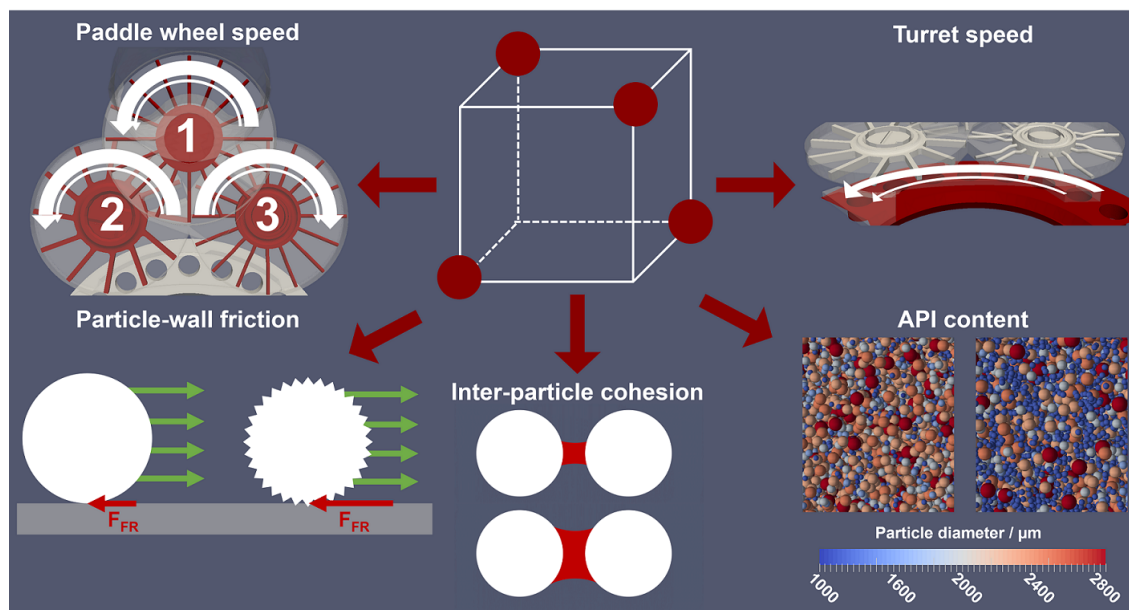


Fig. 1: Schematic illustration of the screening design and the included factors.

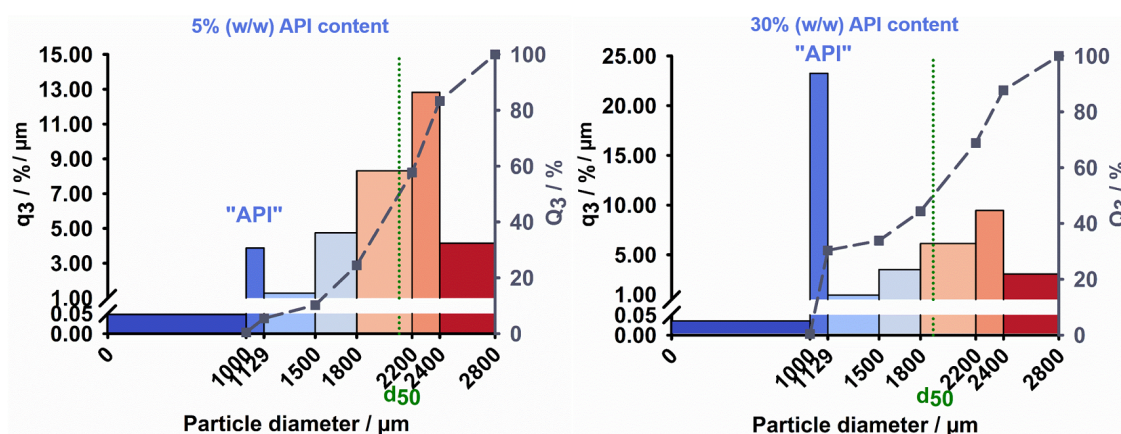


Fig. 2: Particle size distribution of the low (5% (w/w)) and high (30% (w/w)) API dose strength formulations.

2 Materials and Methods

2.1 DEM and geometrical setup

All details about the different models used in DEM utilizing the open source code LIGGGHTS [123] and the geometrical setup are given in our previous studies [168–170, 236]. The complexity of the geometrical setup is increased mainly by three factors, (1) the large size of the system defining the simulation domain volume, (2) the bent paddle wheel shapes and housing (Fig. 1) that require a compromise between curvature resolution and number of geometry triangles to be computed, and (3) the agitation of the components (turret and paddle wheels rotation, Fig. 1). This complexity limits the number of particles simulated and requires particle size enlargement [157] as shown in Fig. 1 & 2.

2.2 Design of Experiments (DoE)

The main target of the DoE is to identify the CPPs and CMAs affecting the CQAs. This poses the fundamental problem of studying too many possible variables prolonging the study versus studying

too few variables risking an insufficient process understanding. The same DoE as given in our previous study [170] was chosen. A compromise was made by selecting a fractional factorial screening design to first identify the most significant CPPs and CMAs using JMP software (JMP 13.0.0, SAS Institute) [11]. Five factors at two levels were defined and they are schematically illustrated in Fig. 1. The two process conditions, turret speed and paddle wheels speed, and the three material attributes, API content (dose strength, particle size distribution for formulations with 5% (w/w) and 30% (w/w) API content in Fig. 2), inter-particle cohesion (cohesion energy density (CED)), and particle-wall coefficient of friction (μ_{PW}) were included. Details about their choice and factor levels (low (–) and high (+)) are given in our previous study [170] and in Tab. 1. A resolution of V and D-optimality was decided resulting in total in 2^{5-1} (= 16) different experiments (Tab. 1) [237]. This design is widely used for the identification of ‘main factors’ at a limited number of experiments needed [11]. However, only two-factor interactions can be resolved as higher order interactions are confounded. The current model allows to identify single factors and two-factor interactions with linear relationships. The model would have to be extended by additional experiments, to e.g. central composite design including axial points and center points (response surface design [238]), to be able to resolve non-linear (higher order) relationships [238–241].

Tab. 1: Overview of factor combinations for CPPs and CMA and the measured responses (CQAs and the measured responses (CQAs are red shaded). **Bold** and *italic* values indicate the highest and lowest result for a given parameter though the font doesn't account for a good or bad result, respectively. Data for mean tablet mass was already given in our previous work [170] and is added in the current study with permission from John Wiley and Sons for the sake of completeness.

Setup number	CPP			CMA		CQA			Standard deviation of relative content (s) / %	Mean mass contribution from filling wheel zone / %	Mean particles' velocity filling wheel zone / cm/s	Mean mass contribution from reverse dosing wheel zone / %	Mean particles' velocity reverse dosing wheel zone / cm/s	Mean mass hold up in force feeder / g	Desired CQAs / -	Predicted CQAs / -
	Pattern	Turret speed / rpm	Paddle wheels speed / rpm	API content / % (w/w)	Inter-particle cohesion (CED) / MJ/m ³	MPW / -	Mean tablet mass / g	Tablet mass variation (RSD) / %								
1	-	40	30	5	1	0.75	4.7	3.7	56.3	92.6	22.3	52.6	23.0	40.1	31.0	0.45
2	-	40	30	5	3.5	0.25	4.8	1.8	61.8	98.1	27.8	61.5	21.1	29.8	41.0	0.43
3	-	40	30	30	1	0.25	5.3	1.2	36.9	99.5	16.7	66.7	19.1	24.2	35.8	0.47
4	-	40	30	30	35	0.75	4.7	3.6	32.4	99.1	14.7	57.0	21.3	36.3	28.7	0.73
5	-	40	60	5	1	0.25	5.1	1.1	26.6	100.1	12.0	81.7	44.3	9.1	40.8	0.63
6	-	40	60	5	3.5	0.75	4.7	1.8	31.3	100.4	14.2	73.3	50.9	17.0	588	0.79
7	-	40	60	30	1	0.75	5.2	1.1	<i>16.4</i>	99.5	<i>7.4</i>	83.3	43.2	6.0	493	0.72
8	-	40	60	30	3.5	0.25	5.1	1.0	35.8	104.3	14.9	86.0	39.5	4.1	574	0.88
9	-	75	30	5	1	0.25	3.6	7.6	38.6	96.7	16.7	46.3	<i>16.3</i>	72.0	582	0.72
10	-	75	30	5	3.5	0.75	<i>2.7</i>	<i>14.8</i>	41.0	<i>91.2</i>	15.3	<i>42.4</i>	18.0	<i>46.6</i>	525	0.45
11	-	75	30	30	1	0.75	3.2	12.0	24.3	95.7	9.7	48.2	16.4	38.4	<i>48.3</i>	0.15
12	-	75	30	30	3.5	0.25	3.6	9.3	25.4	100.6	11.5	49.9	18.8	37.4	32.3	0.22
13	-	75	60	5	1	0.75	3.6	10.5	40.2	96.9	17.5	54.3	43.2	32.4	29.4	0.36
14	-	75	60	5	3.5	0.25	4.1	4.7	53.9	103.0	23.4	61.3	35.8	26.9	85.8	0.37
15	-	75	60	30	1	0.25	4.7	3.6	27.1	101.7	12.2	61.0	32.7	23.1	89.5	0.41
16	-	75	60	30	3.5	0.75	3.7	9.2	25.8	99.5	11.7	56.5	35.3	25.9	568	0.71
verification measured	-	40	60	30	1	0.25	5.3	0.9	24.8	101.5	11.2	87.3	40.3	2.7	69.0	0.83
verification predicted	-	40	60	30	1	0.25	5.4	0.0	24.6	102.2	10.4	86.2	39.0	3.1	27.5	0.90

2.3 Filling and high speed tableting procedure

The system filling and high speed tableting procedure is in detail described in [170, 171] and is here mentioned very briefly for the sake of completeness. The initialization includes the filling of the feeding hopper, the paddle wheels zones, and finally the turret. This comprised a physical time of 15.8 s. Since two different model formulations in terms of API content are included in the DoE (confer section 2.2), the system filling was performed separately for the PSD of the 5% (w/w) and 30% (w/w) API content model formulations (Fig. 2) at same micro-mechanical material properties, given by Hildebrandt et al. [170, 171].

For actual high speed tableting, the process conditions and material attributes have been changed according to the DoE (Tab. 1). Thus all setups containing either 5% (w/w) or 30% (w/w) API content showed same homogeneous packing structure at the beginning of tableting (data not shown). This ensured that the observations during high speed tableting were related to the changed factors in the DoE [168, 170, 171, 187]. For all setups in total 10 turret rotations were computed including the filling of 232 dies (24 punch stations, 8 dies were located underneath the feeder and have already been filled during system initialization) implying a physical time of 15 s at 40 rpm and 8 s at 75 rpm turret speed, respectively. This period allowed for all setups to have achieved and to be operated at mass steady state [168, 169, 236]. This was considered as constant mass hold up in the paddle wheels zones and is in detail described by Hildebrandt et al. [170]. During high speed tableting, equal amount of powder was refilled into the feeding hopper as material was leaving the system in the form of filled dies [170, 171]. At the given number of particles simulated ($\sim 622,000$ particles, section 2.2) and the system complexity (section 2.1), performing complete simulations of the DoE took > 9 months on 4 workstations each of them having 72 processors running in parallel.

2.4 Statistical analysis of DoE results

For all CQAs and other responses (section 3.1 and 3.2) the same procedure was followed for the statistical analysis of the DoE. All single factors and two factor interactions were included to generate the statistical model. A significant factor influence was considered if the p -value was < 0.05 . This was supported by a half normal plot (plot over the absolute values of the estimates against the normal quantiles for the absolute value normal distribution [242]) in which the non-significant effects tend to fall on a straight line through the origin, while significant effects deviate from this [242, 243]. The final model fit for the response was generated after the insignificant model terms were removed to make the model more parsimonious [232]. The most important ANOVA and model fit statistics are summarized in Tab. 2. An adjusted R^2 value close to 1 showed a good model fit. A p -value < 0.05 for the analysis of variance indicated the model's significance [242]. If a lack of fit was identified, a high p -value (≥ 0.05) showed its insignificance. The final estimates for significant factors (p -value < 0.05) are summarized in Tab. 2.

For each model the prediction profilers are provided in Fig. 3 in white and green plots for single and two-factor effects, respectively. They display the change in the response when a factor varies from its low ($-$) to its high level ($+$), with all other factors kept constant at their average [87, 244]. The slopes for the factors in the prediction profiler are also specified in Tab. 2 as 'estimate'.

The final model fit allowed the prediction of the response according to Eq. 1:

$$R_{pred.} = I + \left[\sum E_X * \left(\frac{L_X - \left(\frac{L_{X(+)} - L_{X(-)}}{2} \right) + L_{X(-)}}{\frac{L_{X(+)} + L_{X(-)}}{2}} \right) \right] + \left[\sum E_{X*Y} * \left(\frac{L_X - \left(\frac{L_{X(+)} - L_{X(-)}}{2} \right) + L_{X(-)}}{\frac{L_{X(+)} + L_{X(-)}}{2}} \right) * \left(\frac{L_Y - \left(\frac{L_{Y(+)} - L_{Y(-)}}{2} \right) + L_{Y(-)}}{\frac{L_{Y(+)} + L_{Y(-)}}{2}} \right) \right] \quad (1)$$

With

$R_{pred.}$	predicted response
I	intercept of response model (Tab. 2)
E_X	estimate of factor X (Tab. 2)
E_{X*Y}	estimate of factor interaction $X * Y$ (Tab. 2)
L_X, L_Y	level of factor X and Y
$L_{X(+)}, L_{Y(+)}$	max. level of factor X and Y according to Tab. 1
$L_{X(-)}, L_{Y(-)}$	min. level of factor X and Y according to Tab. 1

For each individual factor the factor levels according to the model ($L_{X(+)}, L_{X(-)}$, (+) and (-) in Tab. 1) and the factor level of interest (L_X) enter with the respective E_X (Tab. 2) into the model. For two-factor interactions ($X * Y$) the single factor contributions enter as a product with the E_{X*Y} (Tab. 2) into the model.

The model was verified by performing one additional setup at a factor level combination that has not been included in the screening DoE (Tab. 1, ‘verification measured’).

The impact of potential CPPs and CMAs on overall blend quality (all CQAs) was evaluated by combining the individual CQA models through a standard least squares model. For each CQA a desirability function was generated which transforms the response variable to a scale from 0 to 1 (Fig. 3, blue plots) [245]. The individual CQA desirability functions were defined as linear functions with 0 as completely undesirable and 1 as most desirable response [242]. The response limits are set within the range of the setups’ results (Tab. 1) and are in more detail described in section 3.4. The overall setup’s desirability including all CQAs was combined through the geometrical mean of the individual CQA desirability functions.

Tab. 2: Statistical overview for the different CQAs (red shaded) and other response models including only significant factor effects (p -value < 0.05). Not significant factors ($p \geq 0.05$, indicated with *) are included into the model to improve the predictability due to their interaction effect with another factor. Tablet mass data is adopted from [170] with permission from John Wiley and Sons.

	CQA			Standard deviation of relative content (s) / %	Mean mass contribution from filling wheel zone / %	Mean particles' velocity filling wheel zone / cm/s	Mean mass contribution from reverse dosing wheel zone / %	Mean particles' velocity reverse dosing wheel zone / cm/s	Mean mass hold up in force feeder / g
	Mean tablet mass / g	Tablet mass variation (RSD) / %	AV / -						
Two-factor interactions	API content *	-0.04							
	CED								
	API content * μ PW								
	CED * μ PW								
R ² adjusted of summary of fit	0.997	0.929	0.663	0.750	0.971	0.984	0.961	0.965	0.900
p -value of Analysis of Variance	<0.0001	<0.0001	0.002	0.001	<0.0001	<0.0001	<0.0001	<0.0001	<0.0001
Lack of fit p -value	-	0.086	0.177	-	-	-	-	-	-
Desirability	Maximize	Minimize	Minimize	Minimize	-	Minimize	-	Minimize	-

3 Results and Discussion

According to the QbD approach [3] first the CQAs are defined. These are in other words the performance attributes designed into the tablet to meet the performance aims [230] and are the tablet mass, tablet mass variation, and content uniformity in this study. In addition, the powder flow in the force feeder is in detail assessed with respect to the particles' shearing. It provides an understanding of the force feeder's effect on over-lubrication and particle attrition. After giving a brief explanation of the individual CQAs and particles' shearing, they are separately analyzed to identify the most important CMAs and CPPs. The potential CPPs (turret speed and paddle wheels speed) and CMAs (API dose strength, inter-particle cohesion (CED), and particle-wall friction (μ_{PW})) are tested via a screening design. Eventually, all responses are combined in a standard least square model to define the best factor combination of 'input variables (e.g. material attributes and process parameters) that have been demonstrated to provide assurance of quality' [3].

3.1 Critical quality attributes (CQAs)

3.1.1 Tablet mass

The mass filled into the die substantially influences the compression force and is in many modern rotary tablet presses connected, e.g. through the principle of 'force measurement under fixed thickness' [246]. Calibration of compression force with tablet mass allows tablet mass control during batch manufacturing through a compression force metering system. A detected fluctuation in compression force is traced back to an alteration in fill weight. The latter is then being changed by readjusting the fill and dosing cam, or in other words the die volume [28]. In this and our previous study [170], the fill / dosing cam configuration (more details are given by [170, 236]) is same for all setups and helps to discern the relationship between tablet mass and process conditions / material attributes. We reported previously that a significant influence on tablet mass was identified (in descending order) for turret speed, μ_{PW} , paddle wheels speed, the interaction turret speed * paddle wheels speed, cohesion, the interaction turret speed * μ_{PW} , API content, and the interaction cohesion * API content (Tab. 2, Fig. 3) [170]. The explanation of the factor influences are already described by Hildebrandt et al. [170] and are not repeated for the sake of brevity in the current study. The factor influences will be included in section 3.4 for design space evaluation.

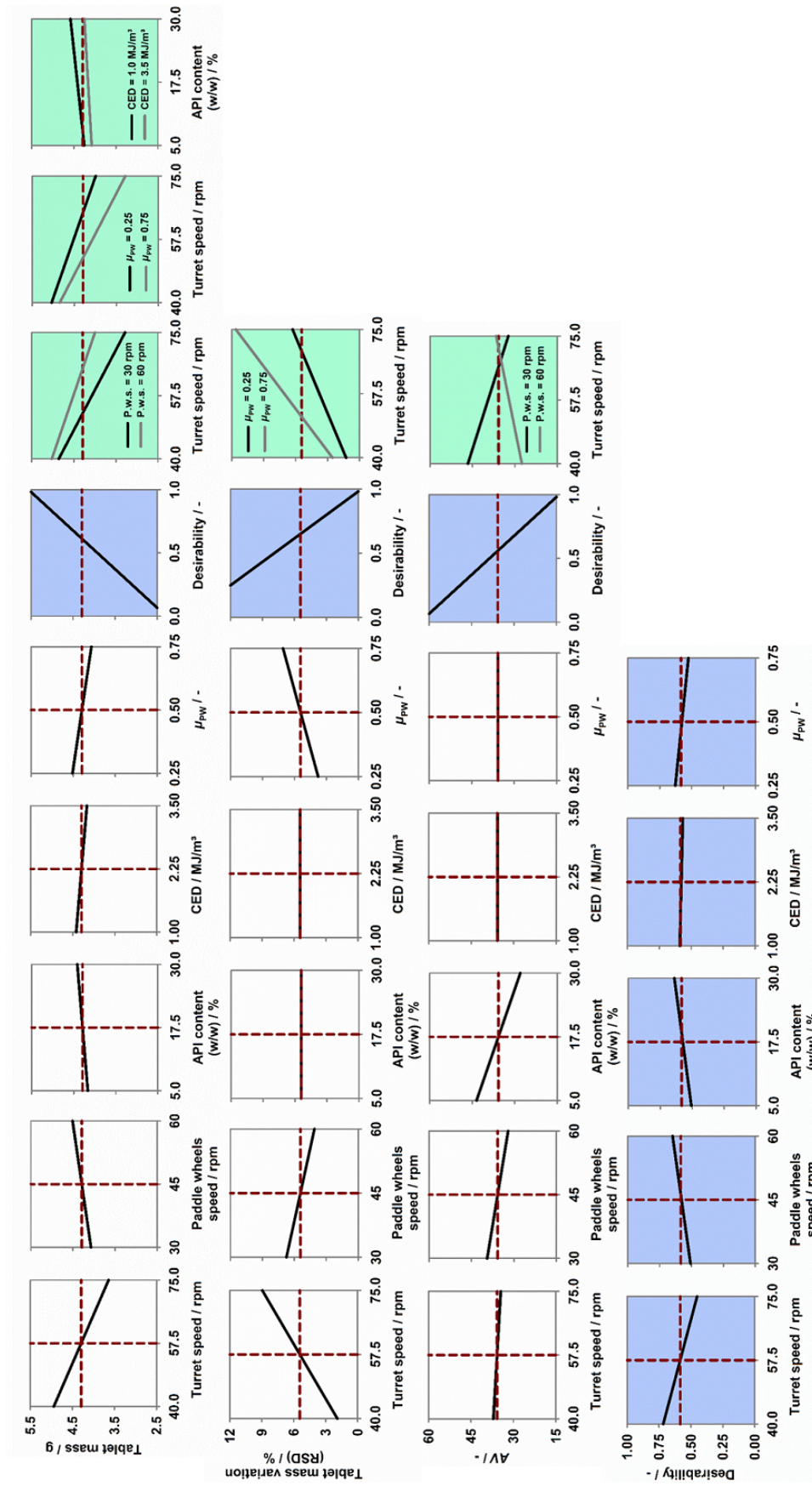


Fig. 3: Prediction profiles for single factor (white plots), two factor interactions (green plots), and desirability functions (blue plots) for the three CQAs for factors at intermediate levels. Profiles of tablet mass are taken from our previous work [170] with permission from John Wiley and Sons.

3.1.2 Tablet mass variation

The second CQA is tablet mass variation, which is a consequence of several factors including the tableting operational parameters, the die diameter, and the powder flowability [41]. The tablet mass variation is calculated as the relative tablet mass standard deviation and is predominantly influenced by the turret speed, μ_{PW} , paddle wheels speed, and the interaction turret speed * μ_{PW} (Fig. 3, Tab. 2). In comparison to reality, the numerical experiments reveal significantly higher absolute tablet mass RSD values (Tab. 1) which can be attributed to the large particle sizes compared to the relatively small die dimensions (Figs. 2 and 4, confer section 2.2). In reality, the ratio of the die diameter (D) to the mean particle size (d) of the formulation would be in the range of 90 to 180 assuming a die diameter of 9 mm and a mean particle size of 50 – 100 μm . In simulations, the mean particle size of the two model formulations is significantly higher (confer section 2.2) resulting in D/d ratios of 11.4 – 12.7. However, general dependencies could be found and explained from simulation results.

A less uniform die filling is found in case of a higher turret speed and a higher μ_{PW} value (Tab. 2, Fig. 3). For the former, the higher mass variability at higher tableting speeds could be linked to the lower tablet mass (confer section 3.1.1, Fig. 4). The reason being is the lower fill density or incompletely filled dies at higher tableting speeds as found in literature [80, 86, 87, 168]. The mean tablet mass vs tablet mass variation plot in Fig. 4 clearly highlights the importance of a high die fill density and complete die filling to ensure a constant fill ratio. In Fig. 4 exemplarily three filled dies are shown for setup no. 10, 14, and 3 at the top, middle, and bottom, respectively, to visualize the different die fill densities and incomplete die fillings. Furthermore, the linear relationship between tablet mass and tablet mass variation ($R^2 = 0.96$, Fig. 4) implies that these quality profiles cannot be independently optimized which was also not expected.

Similar effect is found for μ_{PW} , that may, in addition to die fill density and filling level, also be linked to powder flowability as reported by Peeters et al. [87]. However the factor interaction (Fig. 3) turret speed * μ_{PW} also indicates that the combination of a high μ_{PW} value and a high turret speed causes most inconsistent mass filled into the dies. In contrast, at a low turret speed the effect of the μ_{PW} value is rather negligible. As a consequence, it can be supposed that an a priori determination of the particle-wall friction coefficient, e.g. by using a ring shear tester [62], is beneficial to identify the risk of tablet mass variation at higher turret speeds.

A high paddle wheels speed increases the mass hold up in the force feeder (4% relative increase for 60 rpm compared to 30 rpm, Tab. 2) and thus enables a more constant discharge into the dies resulting in lower tablet mass variation, which is consistent with previous observations [41, 86, 94].

In contrast to the mean tablet mass model (Tab. 2 and [170]), the other factors such as API content, CED, turret speed * paddle wheels speed, turret speed * μ_{PW} show no significant impact ($p \geq 0.05$) in the tablet mass variation model. Although it was shown previously for gravity feeding that the inter-particle cohesion significantly influenced the tablet mass RSD [168, 169], this could not be confirmed at this given set of process conditions and material attributes for force feeding. Though the relative mass hold up decrease in the force feeder of 8% for a CED of 3.5 MJ/m^3 compared to 1.0 MJ/m^3 is significant (Tab. 2, $p < 0.05$), it doesn't affect neither mean tablet mass nor tablet mass variation (Tab. 2, Fig. 3).

Adjustment of the tablet press settings, e.g. turret speed and paddle wheels speed, for a given tablet ridge height (die height) to ensure high die fill densities could provide low tablet mass fluctuations. This could be further improved by considering the formulation's powder flowability in terms of the particle-wall friction coefficient.

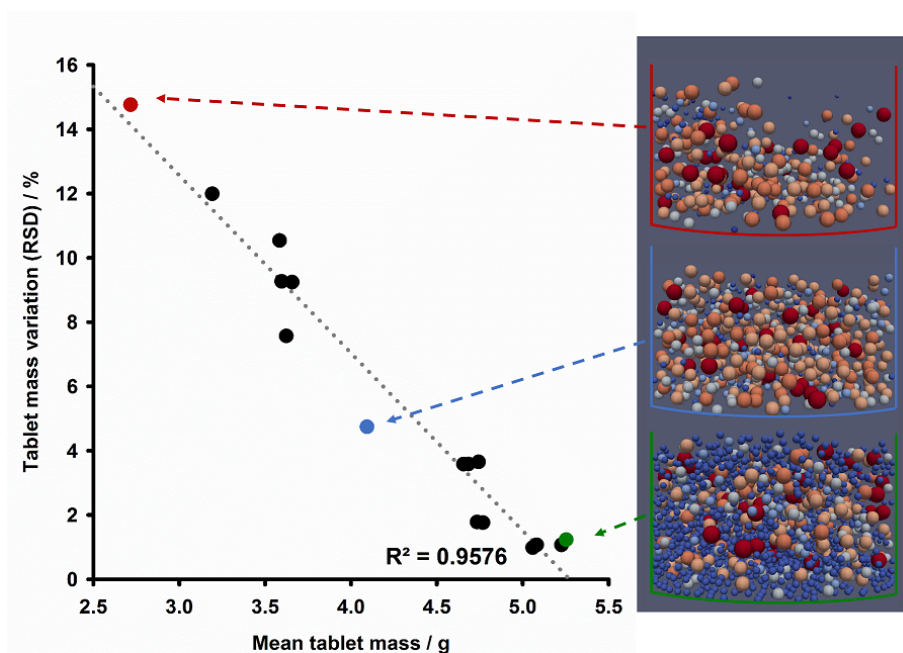


Fig. 4: Tablet mass variation vs tablet mass; for setup nos. 10 (top, red), 14 (middle, blue), and 3 (bottom, green) exemplary dies are shown.

3.1.3 Content uniformity

Content uniformity (CU) of tablets is an essential tablet quality criteria, since it determines the safety and efficacy of the pharmaceutical product. The Ph. Eur. stipulates that ‘to ensure the consistency of dosage units, each unit in a batch should have an active substance within a narrow range around the label claim’ [25]. In the context of DC formulations, it is still a great challenge and needs to be well controlled [247]. It is considered that for low dose formulations, a low tablet mass variation does not necessarily ensure a high content uniformity, whereas a large mass variation precludes a high content uniformity [248]. The regulatory authorities ask for the content uniformity test according to monograph 2.9.40 in Ph. Eur. or < 905 > in USP [25, 249]. The Ph. Eur. 2.9.40 content uniformity test contains the calculation of an ‘Acceptance Value’ according to the following formula (Eq. 2) [25]:

$$AV = |M - \bar{X}| + k * s \quad (2)$$

With

AV	acceptance value
M	reference value
	if $98.5\% \leq \bar{X} \leq 101.5\%$ then $M = \bar{X}$
	if $98.5\% > \bar{X} \geq 95\%$ then $M = 98.5\%$
	if $101.5\% < \bar{X} \leq 105\%$ then $M = 101.5\%$
\bar{X}	mean of individual contents (x_1, x_2, \dots, x_n)
k	acceptability constant
	if $n = 10$ then $k = 2.4$
	if $n = 30$ then $k = 2.0$
n	number of samples
s	sample standard deviation
$L1$	maximum allowed acceptance value, $L1 = 15.0$

<i>L2</i>	<p>maximum allowed range for deviation of each dosage unit tested from the calculated value of M:</p> <p>on the low side, no dosage unit result can be less than $0.75M$ while on the high side, no dosage unit result can be greater than $1.25M$ ($L2 = 25.0$)</p>
-----------	--

The requirements for dosage uniformity are met if the AV value for $n = 10$ is $\leq L1\%$. If the AV value is $> L1\%$, the next 20 dosage units are tested. The requirements are met if the final AV value ($n = 30$) is $\leq L1$ and no individual content of the dosage unit is $< (1 - L2 * 0.01)M$ or $> (1 + L2 * 0.01)M$. For formulations containing a high API content (≥ 25 mg or 25%) instead of the content uniformity test, the mass variation can be determined [25]. The CU test takes into account the sample mean as it applies a stricter standard deviation requirement if the \bar{X} is more than 1.5% off-target.

With the introduction of the QbD concept, the drug product can be more tightly controlled compared to traditional analytical methods, e.g. by PAT [106, 250]. The increased batch control through PAT is reflected in the new chapter 2.9.47 in Ph. Eur. entitled ‘demonstration of uniformity of dosage units using large sample sizes’. In contrast to the general chapter 2.9.40, the larger number of samples increases the probability to detect units that deviate from the $\pm L2$ criteria therefore, e.g. for $176 \leq n < 270$, one sample may deviate from the $L2$ criteria (2.9.47-1. alternative (parametric) [25]). In addition, a sample size-dependent value for k is defined. The 2.9.47 is an alternative means to demonstrate compliance with the 2.9.40 criteria [250] and does not constitute a mandatory requirement [25].

The \bar{X} , s and AV (with $k = 2.21$) values according to Ph. Eur. 2.9.47 have been calculated for the 232 dies of the different setups in the DoE and are given in Tab. 1. The API content was measured and corrected by tablet mass given by the significant differences in tablet mass (Tab. 1). Thus the \bar{X} is the API content at the mean tablet mass relative to the specified API content according to the formulation (either 5% (w/w) or 30% (w/w), Tab. 1) and is given in Eq. 3.

$$\bar{X} = \frac{\frac{\text{mean API mass}}{\text{mean tablet mass}}}{\text{specified API content}} \quad [\%] \quad (3)$$

To get a better understanding of the AV value, first the contributions in the formula (Eq. 2) resulting from the \bar{X} and the s are discussed individually.

Mean relative content (\bar{X})

The correct API dosing in the tablets is detrimental for the patient’s safety and both, under- and overdosing constitute a severe risk for the patient. Off-target contents in the tablets can either stem from (1) a non-uniform mixture, e.g. blending causes an inherent segregation due to differences in powder properties between API and excipient particles, or from (2) segregation after homogeneous mixing during powder flow in the handling instrument and equipment [248]. In this study a random mixture is continuously filled into the system (section 2.3, [170, 236]) to exclude the first but rather to evaluate the second effect. It was shown for the FETTE 1200i that the random mixture segregated remarkably during its path in the force feeder [236] (the reader is referred to the reference for a detailed analysis and explanation).

The mean relative content (\bar{X}) over the 232 filled dies for the 16 different setups reveals that only 7 setups show the $\bar{X} \pm 1.5\%$ target whereas 6 show under- ($\bar{X} < 98.5\%$) and 3 over- ($\bar{X} > 101.5\%$) dosing (Tab. 1). Although it would be possible to generate a model fit for \bar{X} , it is unreasonable as

the \bar{X} is a complex interplay from the powder flow in the force feeder. First, the API content in the filled dies may originate from either filling or reverse dosing wheel zone, depending on the process conditions combination (confer section 3.2). In those paddle wheels zones different API contents are obtained. As described by Hildebrandt et al. [236] for setup no. 1 (Tab. 1), during the powder flow from the feeding hopper to the dosing wheel zone, from which the particles first enter the reverse dosing wheel zone and then the filling wheel zone, size segregation is found. It results in an increase of fines (particle size $\leq 1800 \mu\text{m}$) in the reverse dosing wheel zone and an accumulation of coarse grains (particle size $> 1800 \mu\text{m}$) in the filling wheel zone. This size segregation is found for all setups as shown in Fig. 5 but the extent differs depending on the factor combinations. Second, within the different paddle wheel zones the predominant particle size segregation mechanisms, i.e. sieving/percolation [181, 195] in dosing and filling wheel zone in contrast to trajectory [181, 195, 212, 213] in reverse dosing wheel zone (in detail described in Hildebrandt et al. [170, 236]), are influenced both by the material properties (in particular the μ_{PW} as described for s , confer below) and the paddle wheels speed. Images of the bottom of the filling and reverse dosing wheel of the different setups are given in Fig. 5 highlighting their significant dissimilarities. An extensive analysis for each and every setup would be necessary as there are no general rules applicable. This is not done at this moment for the sake of brevity.

This study only evaluates the size segregation during mass steady state (confer section 2.3) however, size segregation might be more enhanced towards the end of the process when refilling from the hopper into the force feeder is diminishing [106].

Standard deviation of relative content (s)

The second parameter in the AV calculation (Eq. 2) is the standard deviation of the relative content (s) which is given for all setups in Tab. 1. The final model fit for s in Tab. 2 suggests that highest influence stems from API content followed by the interaction turret speed * paddle wheels speed and the μ_{PW} .

The influence of API content on s follows the common understanding that low dose formulations are more likely to suffer from content variations [247]. The following model calculation helps to explain this observation. The number frequency (q_0) of API particles in the low dose and the high dose formulations are 27.5% and 73.8%, respectively. For example in setup nos. 5 and 8 similar tablet mass and API content variations (s) are obtained for different API contents of 5% (w/w) and 30% (w/w), respectively (Tab. 1). Given by the large particle sizes considered in the model formulations (confer section 2.2, Fig. 2), the mean total number of particles collected in the dies for setup 5 and 8 are 819 and 1753 out of which 211 and 1313 particles belong to API particle size fraction, respectively. Assuming a theoretical increase of 10 API particles collected in the dies, a relative API content difference of 5.2% and 0.5% is obtained for setup no. 5 and 8, respectively. Thus, marginal variations in API particles filled in the dies have a higher effect on the API content at a low compared to a high number frequency of API particles. Furthermore, the total number of particles collected in the dies (< 1800) is significantly lower than in reality given by the large particle sizes considered (confer section 2.2, Fig. 2) and provides an explanation for the generally very high content variations in the numerical model ($\geq 7.4\%$, Tab. 1).

In Fig. 5 the relative API contents between die nos. 180 to 204 (one turret rotation) for the setups with turret / paddle wheels speed combinations 40 rpm / 30 rpm, 40 rpm / 60 rpm, 75 rpm / 30 rpm, and 75 rpm / 60 rpm are shown. In addition, images depicting the bottom of the filling wheel zone (left) and reverse dosing wheel zone (right) are given for the individual setups. The factor interaction

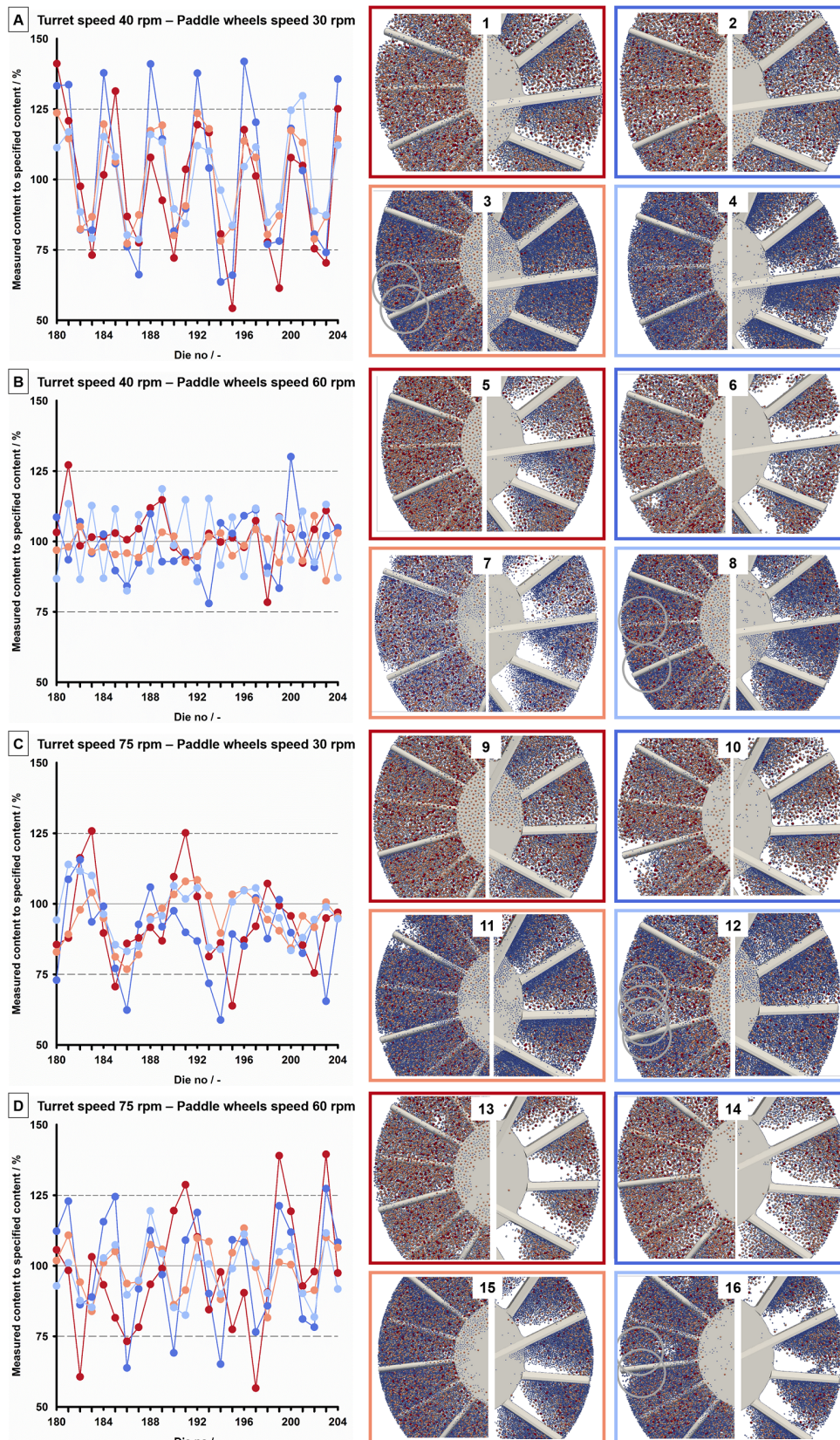


Fig. 5: Relative API content over tableting time and instantaneous images of the bottom of the filling wheel (left) and reverse dosing (right) wheel zone (particles are colored by their size, confer as legend to Fig. 1 & 2):

- A) 40 rpm turret / 30 rpm paddle wheels speed (setup nos. 1 – 4, Tab. 1)
- B) 40 rpm turret / 60 rpm paddle wheels speed (setup nos. 5 – 8, Tab. 1)
- C) 75 rpm turret / 30 rpm paddle wheels speed (setup nos. 9 – 12, Tab. 1)
- D) 75 rpm turret / 60 rpm paddle wheels speed (setup nos. 13 – 16, Tab. 1)

turret speed * paddle wheels speed demonstrates highest s for the combinations (turret speed / paddle wheels speed) 40 rpm / 30 rpm (20.4%), following 75 rpm / 60 rpm (16.2%), 75 rpm / 60 rpm (13.3%), and finally lowest for 40 rpm / 60 rpm (12.1%) (data not shown). Calculation of the time intervals for the turret speeds of 40 rpm and 75 rpm shows that for the former every 0.0625 s and for the latter every 0.0333 s a new die is arriving underneath the force feeder. Given by the number of blades in the filling wheel zone, at 30 rpm and 60 rpm every 0.1250 s and 0.0625 s the next blade is approaching the front portion of the filling station, respectively. The ratio of those time increments for a new die arrival and a blade change in the filling wheel are (turret speed / paddle wheels speed) 2.000 (40 rpm / 30 rpm), 1.000 (40 rpm / 60 rpm), 3.750 (75 rpm / 30 rpm), and 1.875 (75 rpm / 60 rpm). This ratio tells the number of dies that are being filled by one inter-blade of the filling wheel. Exemplarily for the different factor combinations grey circles indicate the dies to be filled by the filling wheel zone in Fig. 5A-D.

In particular the two worst turret speed / paddle wheels speed combinations (40 rpm / 30 rpm and 75 rpm / 60 rpm) show constant API content fluctuation patterns at a frequency of ~ 2 dies (Fig. 5A & D). Thus most of the setups show every two dies low and then high API contents. Exemplarily for setup nos. 3 (Fig. 5A) and 16 (Fig. 5D) those two dies to be filled from the filling wheel zone are illustrated as grey circles. The unique shape of the filling wheel consisting of cylindrical blades which are alternately bent leads to size segregation by sieving mechanism. In particular the smaller particles (particle size $\leq 1800 \mu\text{m}$) are accumulating at the bottom of the zone and in front of the blades which are bent downwards (Fig. 1 & 5, [236]). As illustrated in Fig. 5A (setup no. 3) the API content is non-uniformly distributed at the bottom of the filling wheel zone. Consequently for those factor combinations two dies are filled with the high followed by two dies with low API contents. For factor combination 40 rpm turret speed and 60 rpm paddle wheels speed always one die is being filled with the alternated bended blade of the filling wheel, as illustrated in Fig. 5B exemplarily for setup no. 8 showing an API content fluctuation for every other die. In contrast to those patterns, Fig. 5C shows that the 3.750 dies being filled from one inter-blade zone of the filling wheel at the factor combination 75 rpm turret speed and 60 rpm paddle wheels speed does not result in any constant API content fluctuation.

The amplitude of the fluctuation depends on the segregation extent in front of the lower bended blades of the filling wheel which is higher at a low μ_{PW} (Tab. 2). This effect can be well described by comparing setup nos. 7 and 8 in Fig. 5B with s values of 7.4% and 14.9% (Tab. 1), respectively. A reduced size segregation of fines (particle size $\leq 1800 \mu\text{m}$) to the bottom of the filling wheel zone by sieving segregation is favored by the higher disturbance of the powder bed at a high μ_{PW} (setup no. 8). Similar observation was described by Zhou et al. investigating a horizontal mixer with impeller blades. They found that an increase in μ_{PW} promoted the internal vortexing and enhanced the mixing kinetics [200] which is reducing the extent of size segregation by sieving/percolation mechanism.

This comparison shows that the content variation is predominantly influenced by the API strength of the formulation as it defines the probability of API particles fluctuation in the filled dies. Furthermore the extent of inter-blade size segregation can negatively impact the content variation if it coincides with the die filling increment.

Only the analysis of each and every die allowed to discern the API content fluctuation pattern which is usually missed by taking only a few samples over the batch as proposed by the Ph. Eur. test 2.9.40 [25]. From a process development point of view, it is worth to quickly estimate the die filling increment at a given turret speed and paddle wheels speed and take action if a disadvantageous combination is obtained.

Acceptance value (*AV*)

In all setups of the DoE, the *AV* value is predominantly influenced by the very high content variations (relative contribution of *s* compared to \bar{X} on *AV* is at least 82.3%). Thus it is not surprising that similar influence of the factors from *s* are obtained for *AV*, too (Tab. 2). The *L1* criteria ($AV \leq 15$) cannot be met by either of the setups. Only the factor combination of setup no. 7 is closest to the requirement with an *AV* value of 16.4 (Tab. 1). All of the setups result in more than one die having an API content of either $< 75\%$ or $> 125\%$ (confer reference lines in Fig. 5). The numerical model may not adequately predict the content uniformity (*AV*) owed to the very high *s* value given by the low number of particles filled into the die (confer above). However, it provides potential levers how size segregation in the force feeder may be diminished and how high content fluctuations can be avoided (confer above).

3.2 Particle shearing in the force feeder

The tablet tensile strength and therefore the disintegration and dissolution profile, important quality parameters asked by the authorities (monograph [2.9.19] and [2.9.3] [25]), are predominantly defined in the second step of the tableting process, the powder compaction. It was shown that the particles' shearing in the feed frame highly depends on the paddle wheels shape and speed [76, 199, 236, 251, 252] and could increase the risk for particle attrition and over-lubrication. It is reported in literature that the powder flow phenomena in the force feeder during the die filling process can influence the tablet tensile strength and disintegration / dissolution rate for a given formulation [41, 42, 76, 102, 206–208, 253]. Thus tablet tensile strength is not only influenced by the functionality of the excipients and the particle properties of the API. Although the actual powder compaction step is not simulated in the current study, the powder flow in the feed frame is evaluated with respect to its potential influence on over-lubrication and particle attrition.

On the first hand, it will be evaluated from where the particles in the filled dies originate, whether filling wheel zone or reverse dosing wheel zone, and then the shearing they might have experienced in those locations before they discharge into the die.

Relative mass contribution from filling and reverse dosing wheel zone

Given by the geometrical arrangement of the feed frame, the particles first discharge from the filling wheel zone into the rotating dies (Fig. 1). The die volume is created underneath the filling wheel zone by lowering the lower punch up to a maximal die height of 1.5 cm ('A' in Fig. 6). After a short period of gravity filling ('B'), the die arrives underneath the reverse dosing wheel zone ('C') followed by an upwards movement of the lower punch by 0.2 cm ('D') to generate a more confined powder bed [170, 236]. In Fig. 6, exemplary images of one die and the mass relative to the maximal mass over filling time are shown for setup no. 8 and 10 (Tab. 1). The plot in Fig. 6 emphasizes qualitatively and quantitatively that different mass contributions from filling and reverse dosing wheel zone are found. Different trends for the individual particle size fractions can be identified originating from the size segregation in the force feeder. The higher fines content (particle size $\leq 1800 \mu\text{m}$) in the reverse dosing wheel zone compared to the filling wheel zone (confer Fig. 6) results in their higher relative mass contribution from the latter ('C' in Fig. 6) and is in detail described in [236].

For setup no. 8, the die gets mainly filled from the filling wheel zone (88.1% of total blend), very little mass for the small particle size fractions enters the die from the reverse dosing wheel zone, and for largest size fractions even a small amount is being scraped by the reverse dosing wheel. On an average over all particle sizes only 4.1% of the maximal mass in the die is originating from the reverse

dosing wheel zone (interval ‘C’ and table in Fig. 6).

The opposite phenomenon is shown for setup no. 10. For this setup, on an average almost half of the maximal mass filled in the dies originates from the filling wheel zone (42.4%), the other half from the reverse dosing wheel zone (46.6%). Thus the particles’ compositions in the dies for setup no. 8 and 10 show significantly different traveling paths, force feeder origins, and thus might have experienced different shear forces.

The final model for the mean mass contribution in the filled dies from filling wheel zone includes the following significant factors: turret speed, paddle wheels speed, μ_{PW} , turret speed * paddle wheels speed, and API content. Similar significant factors but at inversed effects are obtained for the mean mass contribution from reverse dosing wheel zone (Tab. 2). To understand the influence of the different factors, the direct relationship between the die filling from the filling and the reverse dosing wheel zone must be explained. In case that less mass enters from the filling wheel zone into the die, e.g. setup no. 10 (Fig. 6), the free die volume may be filled from the reverse dosing wheel zone. The opposite is found when the die is already almost completely filled as it arrives underneath the reverse dosing wheel zone, as e.g. shown for setup no. 8 (Fig. 6). Thus the factor influence for the mean mass contribution from filling wheel zone is opposite to the one from the reverse dosing wheel zone. At a high turret speed, less mass from filling wheel zone can enter the die which can then generate a higher mean mass contribution from reverse dosing wheel zone. A high paddle wheels speed can cause a higher force feeding effect by an increased mass hold up (Tab. 1), which leads to a higher die filling from the filling wheel zone and thus less mass contribution from the reverse dosing wheel zone. For a lower API content and higher μ_{PW} slightly less die mass contribution from the filling wheel zone is found. The paddle wheels speed * turret speed interaction predicts a higher effect of the paddle wheels speed at a low turret speed.

Particles’ velocity in filling and reverse dosing wheel zone

The mean particles’ velocity is on an average almost doubled (1.95) in the reverse dosing wheel zone compared to the filling wheel zone, irrespective of the factor combination (Tab. 1 confer [236]). This is attributed to the higher contact area of the angular shaped blades of the reverse dosing wheel with the particles which allows a higher momentum transfer (Fig. 1, [236]). Thus the reverse dosing wheel may alter the material properties by particles’ shearing to a higher extent compared to the filling wheel. The mean particles’ velocity serves as a measure to estimate the shear rate [41, 94] and is computed over the complete filling wheel and reverse dosing wheel zone (Tab. 1). The mean particles’ velocity in filling and reverse dosing wheel zone are 39.5 cm/s and 72.0 cm/s for setup no. 8 and 18.0 cm/s and 32.3 cm/s for setup no. 10, respectively (Tab. 1). An illustration of the particles’ velocities, exemplarily for those two setups, is shown in Fig. 7 highlighting their differences. The models for the mean particles’ velocities in the filling and reverse dosing wheel zones suggest most important effect from paddle wheels speed (Tab. 2). The higher blade speed transfers more momentum on the particles which significantly increases the particles’ velocity, similar to observations made by [41]. Slightly less particles’ shearing is obtained at a higher turret speed as reported by Mendez et al. [86].

In general, if a high mean particles’ velocity in a paddle wheel zone is obtained in combination with a high mean relative mass contribution from this zone filled into the die, then it is possible that it might affect the tablet quality. In particular the particle properties could have changed due to shearing in this paddle wheel zone and the over-lubrication could affect the tablet tensile strength and the disintegration / dissolution profile. The risk for those setups are orange shaded in the mean relative mass contribution versus mean particles’ velocities plot in Fig. 7. For the exemplary setup nos. 8 and 10 only the relatively high mean particles’ velocity in the filling wheel zone of setup no.

8 in combination with the high mean relative mass contribution could constitute a risk for a particle properties change. In contrast, the significantly higher mean particles' velocity in reverse dosing wheel zone may not dramatically affect the tablet quality as only very little mass originates from this paddle wheel zone. For setup no. 10, neither of the paddle wheels zones might cause over-lubrication or particle attrition as they both reveal rather low particles' velocities.

This detailed analysis of powder flow in the force feeder in terms of the particles' origin in combination with the particles' velocity may allow an estimation of the risk for over-lubrication, and particle attrition during the die filling step which could influence tablet tensile strength, disintegration, and dissolution [41, 42, 76, 102, 206–208, 253]. Furthermore differences in powder properties over the die height might be identified which may cause axial failure / capping of the tablets and was already mentioned in the experimental study of Mendez et al. with a two-paddled feed frame [86]. The risk for over-lubrication may be attenuated in formulations without lubricant and for lubricant containing formulations it could be influenced by the blending procedure (shear rate and time) prior to the tableting step [110]. The approach of quantifying the particles' shearing via their velocity could be combined with residence time analysis to make it more accurate. Though the model does not consider any change in particle properties which makes experimental verification of those observations inevitable.

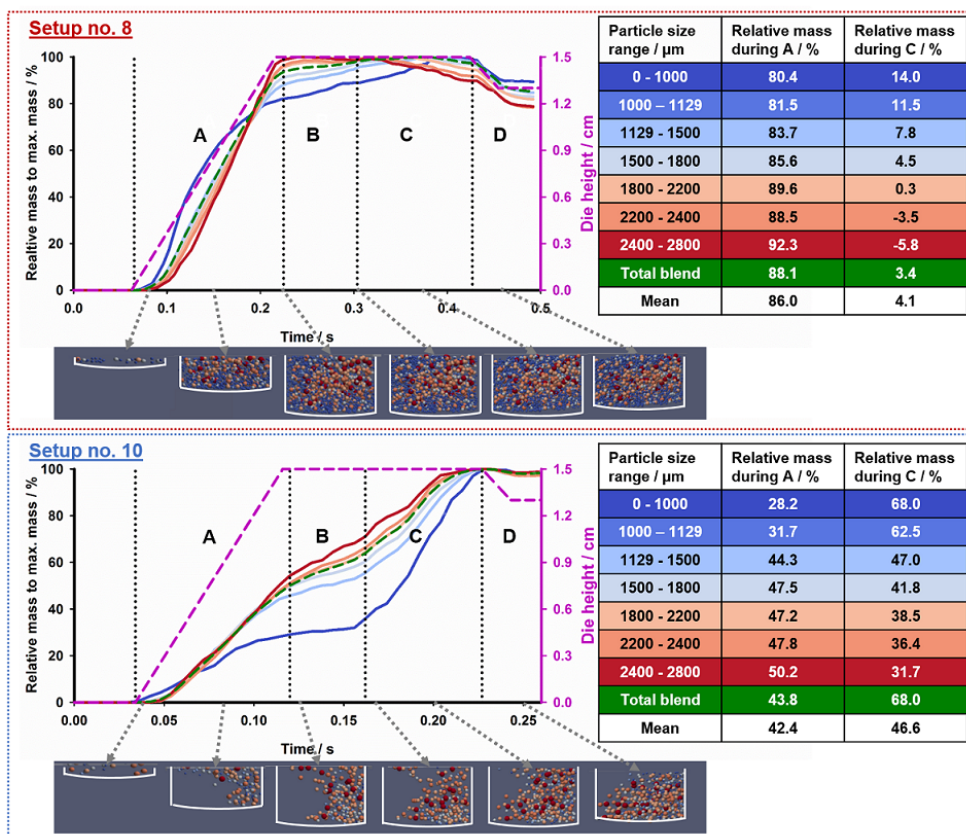


Fig. 6: Relative mass to maximal mass for individual particle size fractions and die height over filling of one die are shown. The die is located under the filling wheel ('A'), inter-wheel ('B'), reverse dosing wheel ('C'), and dosing cam ('D') zone.

Bottom: Exemplary images of one die being filled over time. The table provides the relative mass during 'A' and 'C' to maximal mass of every particle size fraction, of the complete blend ('total blend') and averaged over the individual size fractions ('mean'). Setup no. 8 (top) and 10 (bottom) are shown (Tab. 1).

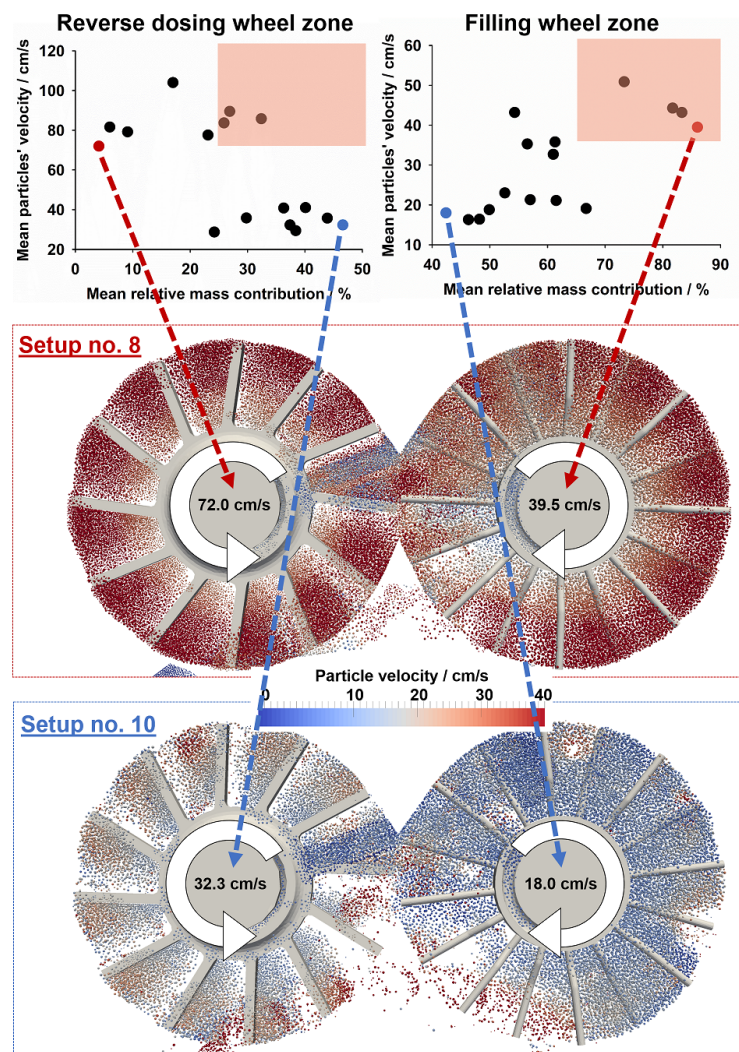


Fig. 7: Mean particles' velocity vs mean relative mass contribution (Fig. 6) for reverse dosing wheel (left) and filling wheel (right) zone (top) with exemplarily images for setup no. 8 and 10 (bottom, Tab. 1).

3.3 Model verification

In addition to the 16 experiments of the DoE, one extra setup was performed to verify the different generated models predicting the CQAs and the particles' shearing (Tab. 1) at a factor combination not mapped in the screening DoE. In Tab. 1 the measured and predicted values for the verification setup are listed and provide a very high match. A minor discrepancy is obtained for tablet mass variation with a value of 0.9% in the measurement compared to 0.0% in the model prediction. However in relation to the other setups going up to 40.8% (Tab. 1) it is the lowest measured as well as predicted value. Another dissimilarity in prediction is the mean relative API content (\bar{X}) that is predicted to be off-target ($> 101.5\%$) which would involve a higher reference value (M) in Eq. 2.

Thus the individual models allow the prediction of tablet quality and powder flow in the force feeder for factor levels identical or close to the ones chosen in the DoE. However, the chance for non-linear factor effects may prevent the prediction over a wider range of factor levels and would require the extension of the screening design by adding additional factor levels.

3.4 Design space evaluation for CQAs

The individual models for every CQA (tablet mass, tablet mass variation, and content uniformity, Tab. 2) are combined in a standard least squares model to identify the CPPs and CMAs and to draw generalized conclusions. The approach searches along the model for an optimal range of input variables to obtain maximized / minimized / targeted response variables [232, 240, 254, 255]. The objective of optimization in this study is to maximize tablet quality (CQAs) through the prediction profilers of the potential CPPs and CMAs in Fig. 3. In the column next to the prediction profilers (Fig. 3), for each CQA the desirability function is given (blue plot). Tablet mass should be maximized whereas tablet mass variation and content uniformity are to be minimized. Since neither of the setups meet the *AV* target value of $L1 \leq 15.0$ (Tab. 1), the *L1* is set as highest desirability (1). At the bottom row additional profilers for the individual factors are provided. They illustrate the factor level that would result in the best result for all CQAs and the slopes imply the factors' leverage on total product quality. The tablet quality attributes are assigned equal weighing in the desirability model (section 2.4).

Process conditions

The process conditions turret speed and paddle wheels speed constitute, compared to the material properties, the factors with highest leverage on final product quality (Fig. 3). Setting all other factors at a medium value, a low turret speed (40 rpm) results in a desirability value of 0.70 with a good result for all CQAs, except for content uniformity (*AV* value of 37 at 40 rpm and 34 at 75 rpm), in contrast to a desirability value of 0.45 for a high turret speed (75 rpm). The paddle wheels speed has a less leverage effect compared to the turret speed. The desirability is 0.51 for 30 rpm vs 0.66 for 60 rpm with solely a difference of 0.15. Thus higher paddle wheels speeds are beneficial for all defined CQAs. The interaction of turret speed * paddle wheels speed for mean tablet mass and *AV* value (Tab. 2), results in the following desirability values (descending order): 40 – 60 (0.82), 40 – 30 (0.58), 75 – 60 (0.50), and least quality for 75 – 30 (0.35). The turret speed and paddle wheels speed may not be independently optimized and should be thoroughly combined. Those findings are strictly applicable for the tableting machine considered under tested process conditions.

Material attributes

The powder flowability is influenced by several factors, though in this study the screening design considers only the particle size distribution (via API content), the blend cohesivity, and the particle-wall friction (section 2.2). Usually those factors are difficult to adapt independently during formulation development, however theoretically the following advice can be given:

For the API content a distinct choice for a high dose strength can be provided as the desirability value is 0.14 higher compared to the low dose formulation. Having a deeper look at the individual CQAs, the API content has highest influence on the content uniformity, whereas for the others it plays a minor role. This conclusion is true for the given model formulations' PSDs and requires further analysis and experimental validation for different PSDs. In particular the size segregation effect in the force feeder might be attenuated or elevated at different PSDs which would in turn significantly affect content uniformity.

The particle-wall friction often increases with wall surface roughness [256, 257] and including this factor in the DoE was motivated by literature showing an influence on the particle flow in bladed mixers at a moderate change in μ_{PW} [166, 202, 251, 252]. A low μ_{PW} is beneficial for tablet mass and tablet mass variation though the μ_{PW} does not influence content uniformity (*AV*). The desirability values are 0.64 and 0.53 for μ_{PW} 0.25 and 0.75, respectively. In reality, the μ_{PW} on a particle level might be only decreased by wet granulation generating spherical particles. This suggests that the

tablet quality may differ between DC and wet granulation formulations. Polishing of the force feeder housing (bottom plate) and the blades of the paddle wheels could be a worth effort for tablet manufacturers to improve tablet quality without considerable design changes. The influence of the μ_{PW} on CQAs might be assessed during early development by measuring the wall friction of the formulation via, e.g. a ring shear tester [256].

The last material attribute, the inter-particle cohesion only affects tablet mass. Consequently for the given DoE, the inter-particle cohesion doesn't show any substantial influence on total tablet quality with a decrease in desirability of 0.03 for a change from 1.0 MJ/m³ to 3.5 MJ/m³. This finding is contrasting the empirical understanding that highly cohesive formulations could cause troubles during tableting. The effect of the cohesion should be further evaluated in simulations considering different values and validated in experiments to cross-check with the current observations.

Optimal combination of CPPs and CMAs

This model would predict the CQAs desirability of 0.58 if all factors are set to their medium factor level, whereas for 40 rpm turret speed, 60 rpm paddle wheels speed, 30% (w/w) API content, 0.25 μ_{PW} , and 1.0 MJ/m³ CED the highest possible desirability of 0.90 is obtained (Tab. 1). This factor combination corresponds to the verification setup which indeed shows very good or even best performance for all CQAs (Tab. 1) and indicates the corridor for optimal design space. The screening DoE included two potential CPPs and three CMAs. The desirability value differences by changing the factor levels show that the highest influence on CQAs could be expected from turret speed (0.25), paddle wheels speed (0.15), API content (0.14), μ_{PW} (0.11), and least from inter-particle cohesion (0.03). Consequently, both process conditions tested constitute CPPs and only API content and μ_{PW} are CMAs.

However, this model only considers linear factor effects within a defined range of tested factor levels and would have to be extended by including axial and center points to elucidate non-linear / higher order factor effects. The current model is biased by the chosen absolute particle sizes and their distribution (confer section 2.2) and would require additional experiments for generalized conclusions which will be focus of future work. As the tablet press is in reality a closed system it can be only compared what is being entered into the force feeder to what is coming out in form of a compressed tablet. Consequently the detailed particle size segregation mechanisms, mass based comparisons, and particles' velocity analysis by means of the DEM cannot be easily verified in reality. This impedes a holistic validation of the numerical model.

4 Conclusion

The current work is the first of its kind applying the QbD approach in combination with the DEM for pharmaceutical tableting, in particular the die filling step. A fractional factorial screening design was generated including different process conditions and material attributes to link the potential CPPs and CMAs to the CQAs. Individual models for the CQAs tablet mass, tablet mass variation, and content uniformity identified linear effects of single factors and two-factor interactions. Those models allowed good predictability of the product quality for the given factor levels. However, higher order relationships would require the design extension to a response surface design.

As already described in our previous study [236], the powder flow phenomena, such as particle size segregation within the paddle wheels zones due to their geometrical arrangement and blade shapes, are directly interconnected with tablet quality. The DEM allows to fully characterize the system as it gives a detailed understanding on a particle level, which is not possible in reality. This major advantage provided a quantitative and qualitative explanation for, e.g. the size segregation in the force feeders and its influence on content uniformity and fluctuation. In general it could be shown that the CQAs are most significantly affected by the interplay between the two process conditions turret speed and paddle wheels speed. Low dose formulations are more susceptible to content variations in the filled dies. Furthermore the API content analysis of each and every die allowed the identification of content fluctuation patterns for different increments of dies being filled from inter-blades of the filling wheel. The particle-wall friction showed a significant influence on the powder flow in the force feeder, in particular in terms of the mass hold up and the size segregation, thus affecting the CQAs. Least influence on the defined CQAs was found for inter-particle cohesion.

In addition to the defined CQAs, the particles' origin from either filling wheel or reverse dosing wheel zone and the shear the particles' may have experienced in those two zones via particles' velocity analysis was assessed. The tablet tensile strength and in turn the disintegration and dissolution might be affected if a process condition combination is chosen that shows a high particles' shearing.

This QbD study could serve as a basis for understanding the die filling process as it allows a clear insight into the closed system of a force feeder thus could add value in process development.

Acknowledgment

The authors would like to thank Thomas Heinrich and the company (Fette Compacting GmbH, Schwarzenbek, Germany) for providing the FETTE 1200i Fill-O-Matic CAD files. The authors would also like to thank Dr. Wolfgang Schmid for his support in generating and analyzing the design of experiments and Dr. Thomas Profitlich for his comments on powder flowability.

3.2.4 Influence of paddle wheel shape on powder flow

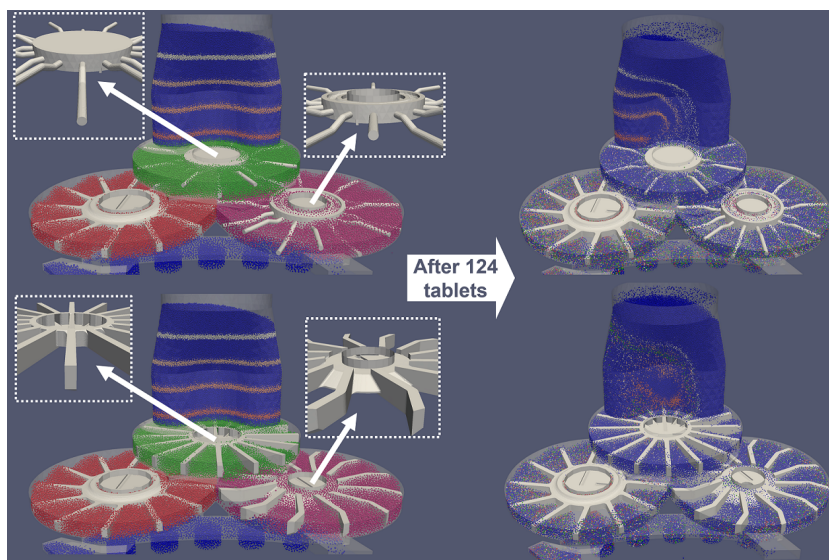
A DEM approach to assess the influence of the paddle wheel shape on force feeding during pharmaceutical tableting

Claudia Hildebrandt^{1, 2}, Srikanth R. Gopireddy², Regina Scherließ¹,
Nora A. Urbanetz²

¹ Department of Pharmaceutics and Biopharmaceutics, Christian-Albrechts-Universität Kiel,
Grasweg 9a, 24118 Kiel, Germany

² Daiichi-Sankyo Europe GmbH, Pharmaceutical Development,
Luitpoldstrasse 1, 85276 Pfaffenhofen, Germany

Submitted to *Advanced Powder Technology*, under review



Outline

Specifications in the regulatory documents impede formulation modifications at a later development stage and thus require process optimization without approval from the authorities. One possibility to improve product quality without a change of the formulation, may be the adaption of the tableting machine as described in chapter 3.2.5 or the paddle wheel shape as described in the following.

Two different paddle wheel shape configurations are available for the FETTE 1200i, more precisely in addition to the cylindrical shaped (evaluated in chapters 3.2.1-3.2.3), a cuboid shaped dosing wheel and filling wheel are offered. However, operator experience or the general approach of ‘doing it as always’ usually decide the selection of the paddle wheel shape configuration. In the following, a more profound understanding of the influence of the paddle wheel shape on the powder flow within the force feeder as well as on the tablet quality (CQAs as in chapter 3.2.3) is developed. The system filling is directly compared between the cylindrical and cuboid shaped configuration to assess the different onsets, i.e. size segregation extents, for high speed tableting. From the DoE developed previously (chapter 3.2.3), the two factor combinations with highest and lowest tablet quality for the cylindrical shaped paddle wheel configuration are selected and additional simulations performed with the cuboid shaped paddle wheel configuration. Thus it may be evaluated if tablet quality worsens or improves for different paddle wheel shapes. In addition, an in-depth comparison of the powder flow within the force feeder, e.g. particle shearing and particle residence time, is performed.

This study does not intend to entirely predict tablet quality for both paddle wheel shape configurations as only a very limited number of setups are compared, though it aims to raise the awareness for process improvement by a simple change of the paddle wheel shape.

1 Introduction

1.1 Powder flow in pharmaceutical tableting

Pharmaceutical tablets are produced on rotary tablet presses in which the powder is transferred from the blending hopper through a feeding system into the rotating dies of the turret. The feeding system may either consist of a chute transferring the powder due to gravity or a force feeder with one or more paddle wheels that force feed the material by paddle rotation into the dies. The latter system was evaluated for different tableting machines (e.g. FETTE 102i [89], FETTE 1200i [170, 171, 186, 236], FETTE 3090 [93, 102, 258], Korsch PH106 [76], Korsch XL-100 [41], Korsch XL-400 [76], GEA Modul P [87, 110, 113], Manesty Beta Press [76, 86, 90, 107], Kilian T-100 [92], Manesty Novapress [111, 114]) that varied e.g. in terms of the force feeder housing, the number of paddle wheels, the paddle wheel shapes, and the number of punch stations. The studies include classical experiments that evaluated the powder that is being entered compared to the tablets that are coming out of the tableting machine [76, 87, 95, 102]. Other studies used Process Analytical Technology (PAT) applying Near-infrared spectroscopy [92, 107, 111, 114, 258], e.g. allowing the assessment of powder blend potency within the feed frame [92, 113, 114, 258], and numerical methods, especially by means of the discrete element method (DEM) [41, 93, 95, 170, 171, 186, 236]. The DEM provides the main advantage of being able to have a detailed look into the system under consideration. The system is resolved on a single particle level thus a very comprehensive powder flow understanding can be developed.

1.2 Powder flow with impeller blades

In addition to powder flow in the tablet press, a significant number of studies investigated the powder flow induced by impeller blades relevant e.g. in granular mixing. A literature review in Tab. 1 for the last more than 15 years summarizes the most important differences between the analyzed systems and the key findings. The different systems considered are illustrated in Fig. 1 for reference and understanding. The powder flow was studied by Positron-Emission-Particle-Tracking (PEPT), Particle-Image-Velocimetry (PIV), and numerical methods (especially using the DEM). The granular matter was agitated either by translational or rotational motion of a single or of multiple blades, respectively. The influence of the blade shape, more precisely in terms of the blade rake angle and the blade curvature, on the particle velocity, particle-particle contact forces, granular temperature, particle size segregation, and powder mixing was assessed. Significantly differing powder flow patterns have been identified for low and high blade speeds. The majority of the experimental and numerical studies tested glass beads or made use of their corresponding micro-mechanical properties. The influence of the particle size, the particle size distribution (mono-, bi-, and poly-disperse), the particle-particle and particle-wall friction, and the particle density have been assessed.

Several tablet machine vendors offer the possibility to purchase different paddle wheel shapes for a given force feeder. However a real scientific rationale for a proper design choice is missing. The influence of the paddle wheel shape has been partially investigated for the mixers with impeller blades (Tab. 1) [196, 197, 201–203, 251, 259], though the systems exhibit significant differences that impede a direct comparison with pharmaceutical tablet machines. For example, the mixer studies investigated a closed system [180, 196–198, 200–204, 251, 252, 259, 260] in contrast to the continuous system of the force feeders in which powder is continuously added into the force feeder from the blending hopper and is leaving in filled dies [171, 186, 236]. Moreover, the impeller blade studies considered the granular motion of glass beads [166, 180, 196, 197, 199, 202–204, 251, 252, 260] unlike pharmaceutical powder blends used in tableting differing in terms of e.g. particle size, particle size

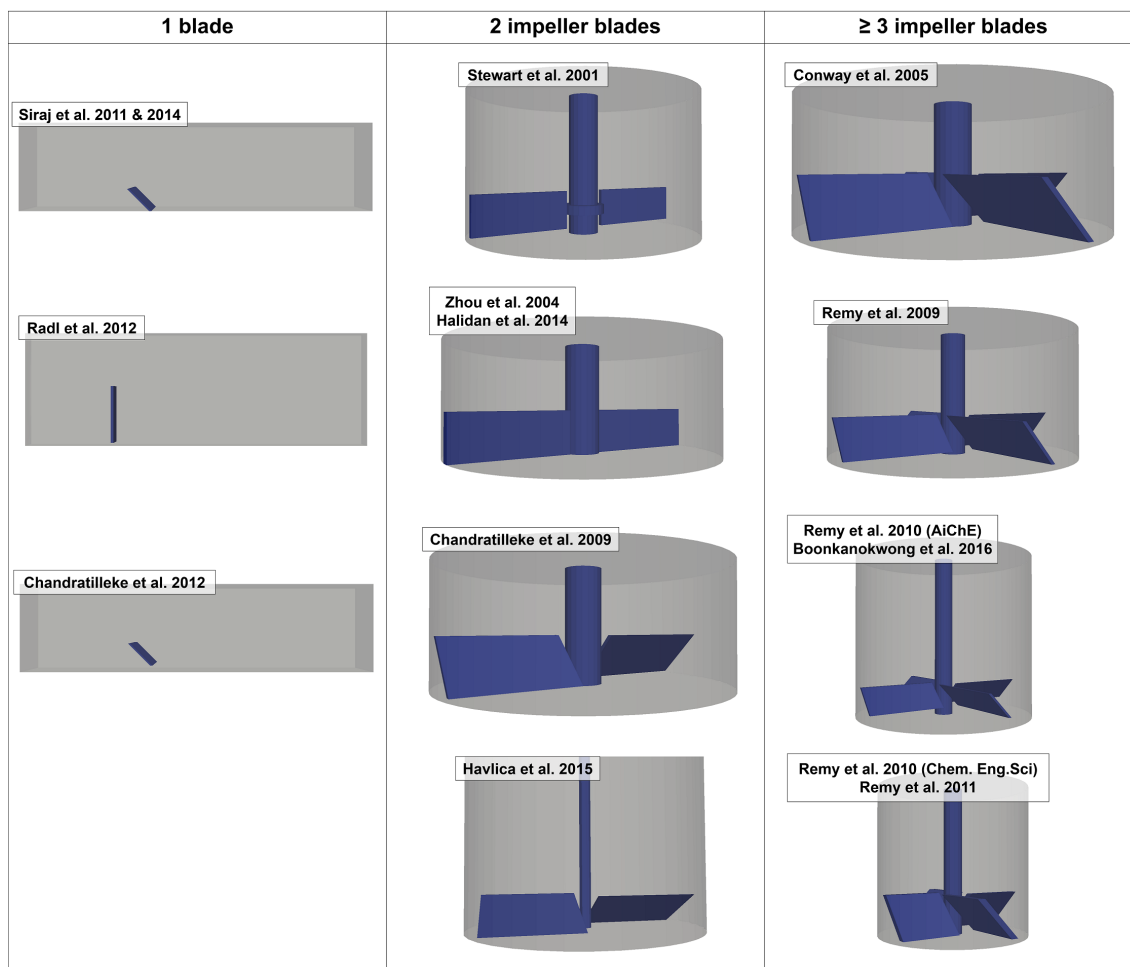


Fig. 1: Systematic illustration (reconstructed from original) of the different impeller blade studies ordered by their number of impeller blades (different scales).

distribution, and micro-mechanical particle properties.

1.3 Objectives of the current work

Our previous studies evaluated the powder flow in a FETTE 1200i with a force feeder consisting of three paddle wheels providing a general system understanding [170, 171, 236]. In addition, the influence of process conditions and material attributes on tablet quality was assessed [186]. In continuation of those studies, the current study evaluates the effect of the paddle wheel shape for the same system on the powder flow. Special emphasis will be given towards the powder bulk behavior and its influence on the micro-scale processes, in particular particle velocity and particle size segregation. The detailed process analysis within the force feeder will help to discern the influence of the paddle wheel shape on the tablet quality which is of major importance for pharmaceutical development. More precisely, it will be evaluated which paddle wheel shape configuration provides optimal tablet quality in terms of tablet mass, tablet mass variation, and content uniformity.

Tab. 1: Literature review on powder mixing by impeller blades, illustrations in Fig. 1. Number of blades consider translational (blade no. = 1) or rotational blade motion (blade no. ≥ 2). Studies performing experiments and simulations compared the results with each other.

Reference	Year	Type of work	No. of blades	Blade angle and shape	Particle properties	Blade speed	Effect studied of	Analyzed data	Key findings (relevant for current study)
Stewart et al. [204]	2001	Experimental (PEPT)	2	90°	Glass beads (mono-disperse, ~ 2 mm)	10, 20, 40, 80, 160 rpm	<ul style="list-style-type: none"> Fill level Blade speed 	<ul style="list-style-type: none"> Particle velocity Residence time Bed surface shape 	<ul style="list-style-type: none"> Higher fill level showed smaller heaps in front of the blade and recirculation regions Particle velocities varied linearly with blade speed throughout the powder bed apart from the falling zone behind the blade Decreased recirculation at higher blade speeds
Zhou et al. [200]	2004	Numerical (DEM)	2	90°	Mono-sized (5 mm)	19 rpm	Particle-particle and particle-wall sliding (μ_s) and rolling (μ_r) friction	<ul style="list-style-type: none"> Spatial and statistical velocity distribution Flow structure (porosity and coordination number) Mixing kinetics Force structure Particle-blade interaction (force distribution, kinetic vs. potential energy) 	<p>At higher μ_s and μ_r:</p> <ul style="list-style-type: none"> increase of bed porosity, potential energy of particles, torque required to drive the system decrease of mean coordination number no influence on kinetic energy
Conway et al. [197]	2005	Experimental (PIV)	4	45°, 135°	<ul style="list-style-type: none"> Near mono-disperse dry art sand (355 μm - 425 μm) Poly-disperse glass beads (A: mixture of 0.9, 1.6, and 4 mm; B: mixture of 0.125 and 0.450 mm) 	3, 50, 100, 200, 300 rpm	<ul style="list-style-type: none"> Particle size distribution Blade speed Blade rake angle 	<p>2D particle velocity fields (instantaneous, average, and fluctuation)</p>	<ul style="list-style-type: none"> Recirculation patterns indicative of avalanching and bed penetration Low shear: <ul style="list-style-type: none"> Complex lobe and striation size segregation patterns through stretching and folding due to surface avalanching → enhanced initial mixing rates High shear: <ul style="list-style-type: none"> Size segregation controlled by rotation of blades → coarse particles migrated both to the free surface and to the outer wall
Chantratillek et al. [201]	2009	Numerical (DEM)	4	45°, 90°, 60°, 120°, 135°	Mono-disperse (5 mm)	20 rpm	<ul style="list-style-type: none"> Blade rake angle Blade gap at the vessel bottom (1.5 and 2.5 x particle diameter) 	<ul style="list-style-type: none"> Velocity fields Lacey's mixing index Particle-particle contact forces Applied torque on blade Force networks 	<ul style="list-style-type: none"> 90° blade rake angle: <ul style="list-style-type: none"> highest deformation of the particle bed in front of the blade, highest heap height which caused a re-circulating flow in front of the particle heap, increased particle velocities highest mixing rate, highest forces exerted on the particles Good mixing at reduced forces imparted to the particles at blade rake angles 120° and 135° Torque required to turn the blades and inter-particle forces reduced when rake angle increased from 45° to 135° and at a larger blade gap

Tab. 1: Literature review on powder mixing by impeller blades, illustrations in Fig. 1. Number of blades consider translational (blade no. = 1) or rotational blade motion (blade no. ≥ 2). Studies performing experiments and simulations compared the results with each other.

Ref-er-ence	Year	Type of work	No. of blades	Blade angle and shape	Particle properties	Blade speed	Effect studied of	Analyzed data	Key findings (relevant for current study)
Reny et al. [251]	2009	Numerical (DEM)	4	45°, 135°	Mono-disperse particles corresponding to glass beads (5 and 10 mm)	10, 30 rpm	<ul style="list-style-type: none"> Blade rake angle Microscopic friction (μ_{pp} of 0.1, 0.3, and 0.5) 	<ul style="list-style-type: none"> Particle velocity Granular temperature Mixing (by particle coloring) Shear and normal stress profiles 	<ul style="list-style-type: none"> Effect of blade rake angle: 45°: no recirculation zone in front of the blade, particles moved mainly in tangential direction with little radial and vertical mixing, lower granular temperature in the particle bed → decrease in particle diffusivity → hindered diffusive mixing → higher bulk density → increase of pressure Effect of μ_{pp}: low μ_{pp}: no 3D recirculation in front of the blade → reduced convective mixing high μ_{pp}: increase in diffusive mixing, higher shear stresses Shear stresses independent of shear rate → granular flow in the quasi-static regime thus momentum transfer governed by inter-particle contacts
Reny et al. [252]	2010	Numerical (DEM)	4	45°	Mono-disperse particles corresponding to glass beads (10 mm)	10, 20 rpm	<ul style="list-style-type: none"> Fill level Particle-wall and particle-particle friction (μ_{pp} 0.5 and 0.1, μ_{pw} 0.5 and 0.1) Blade position (change of mixer diameter (D) at constant particle diameter (d), 31.5, 63.0 94.5) 	<ul style="list-style-type: none"> Particle velocity Granular temperature Mixing (by particle coloring) Shear and normal stress profiles 	<ul style="list-style-type: none"> Effect of fill level: <ul style="list-style-type: none"> lower fill level: higher convective and diffusive mixing, best mixing performance when height of particle bed just covered the top of the blade above a certain fill level: bed dilation, convective and diffusive mixing independent of fill level linear increase of impeller torque with fill level pressure profile: at low fill level linear relationship; at high fill levels two different regimes Effect of μ_{pw}: <ul style="list-style-type: none"> high μ_{pw}: secondary flow structures in front of the blades, increase in particle diffusivity and diffusive mixing low μ_{pw}: no secondary flow structures in front of the blades, reduced convective mixing, decreased shear stresses inside the particle bed Effect of D/d (scale-up): <ul style="list-style-type: none"> low D/d ratios showed lower convective and diffusive mixing linear increase of normal and shear stress profiles with mixer size above a critical system size, the effect of wall friction minimized and granular behavior could be predicted based on simple scaling relationships particle velocities and diffusivities varied linearly with tip speed of the blade normal and shear stresses scaled linearly with the total mass of the system

Tab. 1: Literature review on powder mixing by impeller blades, illustrations in Fig. 1. Number of blades consider translational (blade no. = 1) or rotational blade motion (blade no. ≥ 2). Studies performing experiments and simulations compared the results with each other.

Reference	Year	Type of work	No. of blades	Blade angle and shape	Particle properties	Blade speed	Effect studied of	Analyzed data	Key findings (relevant for current study)
Renny et al. [166]	2010	Experimental (image analysis and PIV) and numerical (DEM)	4	45°	<ul style="list-style-type: none"> Glass beads with coating to obtain different surface roughness Mono-disperse (2 mm and 10 mm) 	3, 20, 55, 120 rpm	<ul style="list-style-type: none"> Particle surface roughness (μpp 0.3 and 0.5) Cylinder wall roughness (μPW 0.3 and 0.5) Blade speed 	<ul style="list-style-type: none"> Particle velocity Granular temperature Mixing (by particle coloring) 	<ul style="list-style-type: none"> Effect of particle surface roughness (μpp): high μpp: increase of velocity fluctuation amplitude, bed dilation, granular temperature, contribution of the diffusive mechanism in the momentum transport process Effect of cylinder wall surface roughness (μPW): Similar effect as μpp, influence expected to be scale dependent Effect of blade speed: > 50 rpm: particle flow in the bumping regime; characterized by particle velocities and diffusivities linearly proportional to blade tip speed < 50 rpm: particle flow in the roping regime; characterized by radial and vertical velocities which increased with blade speed but not proportional to blade tip speed \rightarrow enhanced mixing kinetics
Renny et al. [199]	2011	Experimental (image analysis and PIV) and numerical (DEM)	4	45°	<ul style="list-style-type: none"> Glass beads Comparison exp. and simulations with 1:1 mixture of 2 mm and 4 mm Poly-disperse ranging from 2-10 mm including 2, 3, 5, and 11 different particle sizes 	25 rpm	<ul style="list-style-type: none"> Polydispersity (increasing the amount of intermediate particle sizes while keeping the small to large particle size ratio the same) 	<ul style="list-style-type: none"> Particle velocity Granular temperature Normalized particle diffusivities (Pelet number) Void fraction Mixing index Normal and shear stress profiles Normalized pressure inside the particle bed Normal contact force network 	<ul style="list-style-type: none"> At a size ratio of 2:1 and equal contents segregation by size occurred by blade rotation due to sieving mechanism Extent of segregation reduced at increased degree of polydispersity Stress differences reduced at increased polydispersity leading to a reduction in the segregation driving force
Sirej et al. [203]	2011	Numerical (DEM)	1	40-15° (at 10° increments)	<ul style="list-style-type: none"> Mono- and bi-disperse glass beads (6 mm, 8 mm, and 10 mm at different ratios) 	0.5 m/s	<ul style="list-style-type: none"> Particle size ratios Blade rake angle Particle-wall friction (0.0 and 0.5) 	<ul style="list-style-type: none"> Particle velocity Particle-particle contact forces Modified Generalized Mean Mixing Index (MGMMI) 	<ul style="list-style-type: none"> Improved mixing when larger particles were filled first (located at the bottom) Particles of uniform size flowed differently than particles with size variation At smaller blade rake angles ($< 90^\circ$), particles trapped in front of the blade increasing the contact force Wall friction needed to transmit energy into the particle bed, leading to increased mixing

Tab. 1: Literature review on powder mixing by impeller blades, illustrations in Fig. 1. Number of blades consider translational (blade no. = 1) or rotational blade motion (blade no. ≥ 2). Studies performing experiments and simulations compared the results with each other.

Reference	Year	Type of work	No. of blades	Blade angle and shape	Particle properties	Blade speed	Effect studied of	Analyzed data	Key findings (relevant for current study)
Radl et al. [202]	2012	1	Experimental (high-speed imaging and PIV)	90°, 45°, 135°	<ul style="list-style-type: none"> Mono-disperse glass beads (0.5 - 6 mm) Dry and wet particle bed (with and without cohesion) 	0.060, 0.15, 0.28, 0.50 m/s	<ul style="list-style-type: none"> Particle size (mono-disperse) Bed height Distance between blade and bottom of container Blade rake angle 	<ul style="list-style-type: none"> Velocity profiles Particles' coloring by initial location Dispersion coefficient to quantify mixing 	<ul style="list-style-type: none"> No significant change of flow for different blade angles More intense mixing near the free surface of the particle bed → small, dry glass beads mixed the slowest → wet particles mixed faster
Chandra-Illeke et al. [196]	2012	Numerical (DEM)	1	45°, 60°, 90°, 135°	<ul style="list-style-type: none"> Mono-disperse particles, corresponding to glass beads (3 mm and 5 mm) 	0.2-0.6 m/s	<ul style="list-style-type: none"> Blade rake angle Blade speed System scale-down Single-blade model vs cylindrical mixer 	<ul style="list-style-type: none"> Mass flow rates Mixing (by coloring, particle scale mixing index) Velocity fields Force on blade Contact forces on the particles Particle dispersion 	<ul style="list-style-type: none"> Blade rake angle: <ol style="list-style-type: none"> 90°: high heap in front of the blade with very slow particle velocities, stagnant region in front of the blade, less suitable for mixing > 90°: reduced heap length and height, increased particle flow over the blade, no stagnant region in front of the blade, more suitable for mixing influences on recirculating flow but only limited role in mixing (small as a convective flow) Large dispersion near the free surface and bed base but moderate in the middle of the bed Slightly better mixing for side-by-side than top-to-bottom arrangement Decreased horizontal force on the blade for rake angle in the range of 45-135° Inter-particle forces increased with increase of blade speed and decreased for blade rake angle from < 90° to > 90° Scaling-down showed dynamic similarity for macroscopic quantities but not for particle-scale quantities Single-blade cell model could predict mixing behavior of cylindrical mixer with a difference of 10%
Siraj et al. [259]	2014	Numerical (DEM)	1	<ul style="list-style-type: none"> 40-150° (at 10° increments) Straight, concave, convex 	<ul style="list-style-type: none"> Mono-disperse glass beads with 2 mm and 10 mm 	0.05, 0.5 m/s	<ul style="list-style-type: none"> Particle size (mono-disperse) Blade rake angle Blade shape Particle-wall friction (0.0 and 0.5) Box width (referred as 2D- and 3D) Blade speed 	<ul style="list-style-type: none"> Particle velocity Blade force Particle-particle contact forces Modified Mean Mixing Index (MGMMI) 	<ul style="list-style-type: none"> Maximal blade force in descending order: concave, straight, convex Particle-particle forces depended inversely on blade-rake angle and decreased from concave to straight, and convex blade shapes 2D and 3D setups revealed partly different mixing effect (degree of freedom) Particle size had an effect on the blade force and the particle-particle force Best mixing performance of convex blades at angles < 90°, concave and straight blades at higher angles

Tab. 1: Literature review on powder mixing by impeller blades, illustrations in Fig. 1. Number of blades consider translational (blade no. = 1) or rotational blade motion (blade no. ≥ 2). Studies performing experiments and simulations compared the results with each other.

Reference	Year	Type of work	No. of blades	Blade angle and shape	Particle properties	Blade speed	Effect studied of	Analyzed data	Key findings (relevant for current study)
Haldan et al. [198]	2014	Numerical (DEM)	2	90°	Bi-disperse in terms of: a) size 4 – 9 mm at different ratios b) density c) volume fraction of large particles	20 rpm	<ul style="list-style-type: none"> Particle size Density Volume fraction 	<ul style="list-style-type: none"> Velocity fields Inter-particle forces Particle-scale mixing index (FSMI) 	<ul style="list-style-type: none"> No linear relationship between size, density, and volume fraction ratios on mixing index Simultaneous size and density differences in a binary mixtures might improve mixing Derived empirical equation to predict mixing of binary particles in a wide range of size and density ratios and volume fractions at constant blade speed
Haylican et al. [200]	2015	Numerical (DEM)	2	45°	Mono-disperse particles (2 mm) corresponding to glass beads	0.1-960 rpm	Blade speed	<ul style="list-style-type: none"> Individual particle trajectories Axial, radial, and tangential velocity profiles Volume fraction 	<ul style="list-style-type: none"> Identification of 6 flow regimes based on the blade rotation speed Best transport in the tangential direction for blade rotation speeds (7.5, 60 rpm) and (90, 150 rpm) (mixing efficiency)
Boonkangwong et al. [180]	2016	Numerical	1, 2, 3, 4	45°	Mono-disperse particles (5 mm) properties to glass beads	20 rpm	<ul style="list-style-type: none"> Number of impeller blades D/d ratio (change of mixer diameter (D) at constant particle diameter (d), 63 and 90) 	<ul style="list-style-type: none"> Velocity fields and velocity frequency distributions Granular temperature Mixing (by coloring, Lacey index) Particle diffusivities Void fraction 	<ul style="list-style-type: none"> Particles velocities: 1 and 2 blades: higher radial and vertical velocities 3 and 4 blades: higher tangential velocity components Better mixing for 2 and 3 blades Significant effect on the behavior of particulate flows for increasing the system size (D/d ratio)

2 Materials and Methods

Owing to the limitations of the DEM which include (1) the number of particles in simulations [157] and (2) the total computation time, the aim of this paper is to look at basic powder flow differences for different paddle wheel shapes considering a limited number of particles and simulating up to a certain physical time. The number of particles was reduced by considering a larger particle size and a narrower particle size distribution in comparison to actual pharmaceutical blends (section 2.3). Similarly, the computations were performed until the mass steady state, e.g. constant mass hold up in the force feeder, was achieved, in contrast to a few hours of the actual tableting operation (section 2.2).

2.1 Discrete Element Method

All computations were performed with the open source DEM code LIGGGHTS [123]. The details about the force models and calculations are given in our previous studies [170, 171, 186, 236].

2.2 Geometrical setup

The system under consideration is the force feeder of a FETTE 1200i (Fette Compacting GmbH, Schwarzenbek, Germany) (Fig. 2A). It contains a feeding hopper, a counter-clockwise rotating dosing wheel (green, DW), a counter-clockwise rotating reverse dosing wheel (red, RW), a clockwise rotating filing wheel (pink, FW), and a counter-clockwise rotating turret with 24 punch stations. The dosing wheel zone (DW-Z) is connected with the reverse dosing wheel zone (RW-Z) and filling wheel zone (FW-Z) via two openings at the bottom (yellow). The RW and FW are not interlocking, however the zones are connected by an unclosed intersection of 4.6 cm. The turret rotates underneath the FW-Z and RW-Z.

Two different paddle wheel shaped configurations for the DW and FW exist. The different paddle wheels are illustrated in Fig. 2 with the detailed dimensions in Tab. 2 corresponding to numbers in Fig. 2 B&C. One configuration is called ‘cylindrical’ (referred as ●, marked as solid lines in figures throughout the article, and blue color code) and contains cylindrical shaped blades that are arranged alternating for the DW-● and FW-● (Fig. 2). For this configuration the powder flow pattern and the influence of process parameters and material attributes on tablet quality were described by Hildebrandt et al. in [170, 171, 236] and [186], respectively.

The second configuration is called ‘cuboid’ (referred as ■, marked as dotted lines in figures throughout the article, and red/orange color code) and has cuboid shaped blades. In contrast to the straight blades of the DW-■, the FW-■ has two units of differing lengths connected at an angle of 167° (Fig. 2). Furthermore, the DW-■ is tangentially attached to the cylindrical shaft, in contrast to the FW-■ which is joined with the cylindrical shaft at an angle of 79.3°.

The RW is kept the same for both the ● and ■ configuration (Fig. 2). A powder ‘scraper’ or in other words an inclined surface is found at the bottom of the blades of all ■ paddle wheels (DW-■, FW-■) and the RW (Tab. 2, Fig. 2).

The powder bed penetration of the blades was calculated via the ‘depth of immersion’ (Tab. 2, adapted from [209–211]) which is the ratio of the blade height to the paddle wheel zone height.

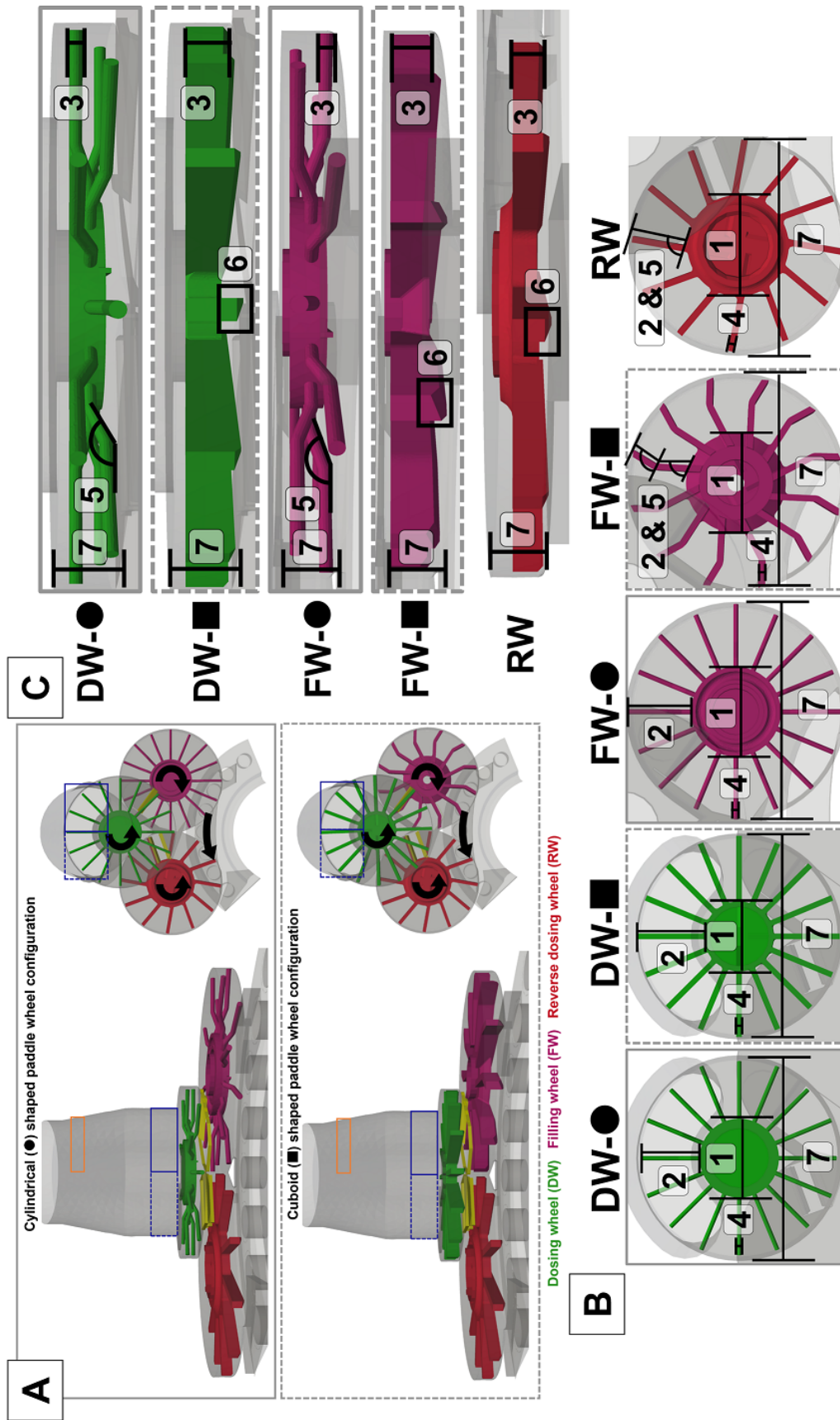


Fig. 2: System overview for the ● and ■ shaped paddle wheel configurations. The color code of the different paddle wheels are kept throughout the study. ● and ■ shaped paddle wheels are referred with solid and dashed lines, respectively. The letters in B and C refer to Tab. 2.

Tab. 2: Blade shape dimensions (in mm), corresponding numbers are given in Fig. 2B&C.

Paddle wheel	No. in Fig. 2	DW-●	DW-■	FW-●	FW-■	RW
Size of inner shaft (radius x height)	1	35.0 x 10.8	30.5 x 10.8	35.0 x 10.8	40.0 (outer max) 29.2 x 7.3	40.0 x 6.8
Blade shape		Cylindrical, alternated bended (vertical)	Cuboid	Cylindrical, alternated bended (vertical)	Cuboid, two-bended (horizontal)	Cuboid
Blade length	2	53.0 (total) segment 1: 7.3 segment 2: 10.4 segment 3: 32.6	58.6	49.0 (total) segment 1: 7.3 segment 2: 10.4 segment 3: 28.6	long part: 35.5 short part: 19.9 (from center: 90.3)	42.9
Blade height	3	2.0 radius	11.0	2.0 radius	8.7	7.0
Blade width	4	2.0 radius	5.0	2.0 radius	5.7	5.0
(Connection to shaft) Blade angle	5	(tangential to shaft) between segments: 161.1°	(tangential to shaft)	(tangential to shaft) between segments: 161.1°	shaft and blade: 79.3° between long and short part of blade: 165.7°	8.5 (incl. scrapper) blade and shaft: 63.3°
Scrapper at bottom of blade	6	no	yes	no	yes	yes
Number of blades		16	16	16	12	12
Dimension of paddle wheel zone (radius x height)	7	90 x 17.3	90 x 17.3	83 x 15.5	83 x 15.5	83 x 15.5
Blade depth of immersion / %		23	72	26	84	32
Rotation direction		counter-clockwise	counter-clockwise	clockwise	clockwise	counter-clockwise

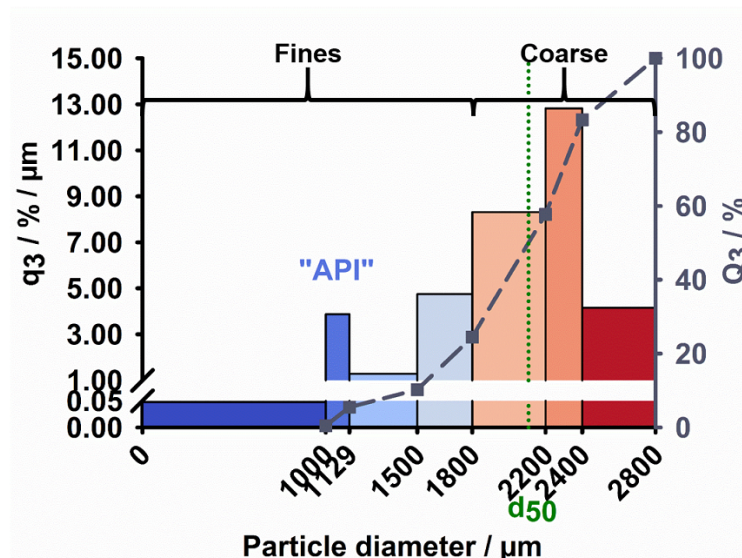


Fig. 3: Particle size distribution of the simulated DC formulation.

2.3 Material properties

A poly-disperse particle size distribution (PSD) was generated to represent a direct compression (DC) formulation consisting of 7 different particle size fractions. One size fraction simulated the active pharmaceutical ingredient (API) at a content of 5% (w/w) and $1000 \mu\text{m} < x \leq 1129 \mu\text{m}$ (Fig. 3). Details on the rationale to select this PSD can be found in our previous studies [170, 171, 186, 236]. Particles with diameter $\leq 1800 \mu\text{m}$ are referred as ‘fines’, particles with diameter $> 1800 \mu\text{m}$ as ‘coarse’ particles as particle size segregation at this cut-off size was identified in the previous studies [170, 171, 186, 236]. Throughout the article, size segregation will be evaluated for all size fractions, however reference will be only given for the API size fraction which is of most importance in pharmaceutical industry. Since the API size fraction was in the range of the fines, the results indicating a decrease of API particles was always linked with a decrease of fines and vice versa, although this will not be explicitly mentioned for the sake of brevity.

The absolute particle sizes were significantly larger and the distribution was narrower than in real pharmaceutical formulations, though the complexity of the system was at the computational limit. The particle properties during system filling and high speed tableting are given in Tab. 3. The properties were selected by comparing the powder flowability of commonly used DC excipients with the numerical model DC formulation (Fig. 3), described by Hildebrandt et al. [170, 171, 186, 236]. The color code of Tab. 3 with dark colors for condition 1 and pale colors for condition 2 are kept throughout the article.

Tab. 3: Process conditions and material properties during system filling (* if changed for high speed tableting) and high speed tableting. Condition 1 and 2 have respectively same factor combinations according to [186]. ● (data taken from [186]) and ■ correspond to the cylindrical and cuboid shaped paddle wheel configuration, respectively (Fig. 2). API contents in different paddle wheels zones are given for mass steady state in high speed tableting [236].

Micro-mechanical material properties				
Young's modulus / GPa	0.87			
Poisson's Ratio / -	0.3			
Particle-particle coefficient of restitution (e_{PP}) / -	0.15			
Particle-wall coefficient of restitution (e_{PW}) / -	0.15			
Particle-particle coefficient of friction (μ_{PP}) / -	0.35			
Particle-wall coefficient of friction (μ_{PW}) / -	0.30*			
Inter-particle cohesion (CED) / MJ/m ³	1.5*			
High speed tableting				
Condition no. / -	1		2	
Turret speed / rpm	40		75	
Paddle wheel speed / rpm	60		30	
Inter-particle cohesion (CED) / MJ/m ³	1.0		3.5	
Particle-wall coefficient of friction (μ_{PW}) / -	0.25		0.75	
Paddle wheel shape configuration	● ([186])	■	● ([186])	■
Setup	1●	1■	2●	2■
Mean tablet mass / g (= 232) (CQA)	5.1	5.1	2.7	3.0
Tablet mass variation (RSD) / % (CQA)	1.1	1.0	14.8	8.2
Mean API content in dies (w/w) / %	5.0	6.2	4.6	5.7
Mean relative API content to label claim content in dies (\bar{X}) / %	100.1	124.7	91.2	114.0
Mean API mass / mg	254.3	317.9	124.1	172.2
Mean relative API content (\bar{X}) standard deviation (s) / %	12.0	13.8	15.3	15.1
AV / - (CQA)	26.6	53.8	41.0	45.8
CQA desirability value / -	0.79	0.32	0.15	0.51
API mass filled in die after interval 'A' (FW-Z) / mg	206.1	244.9	42.6	97.0
Mean residence time / s	11.4	10.3	> 8.0	7.4

3 Results and Discussion

The powder flow pattern in the force feeder of a FETTE 1200i consisting of three paddle wheels is discussed for two different paddle wheels shape configurations (Fig. 2). The blades of the DW and FW are either cylindrical (●) or cuboid (■) shaped. The two configurations have the same RW (Fig. 2, Tab. 2). First of all, the powder filling into the system is described for the two different configurations followed by high speed tableting at two different process conditions and material properties (referred as ‘conditions’). The tablet quality for the different conditions is compared and then explained by the powder flow analysis in the force feeder. It comprises the analysis of the particle trajectories in the force feeder, the particle velocities, and the particle size segregation. Eventually, this evaluation provides the basis to discern the best configuration for an optimal tablet quality.

3.1 System filling comparison

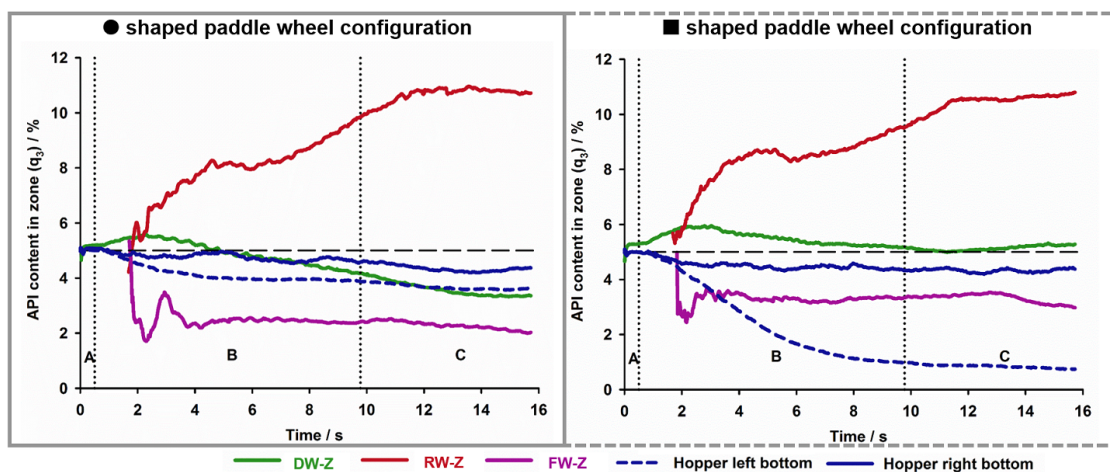


Fig. 4: API content (dashed line corresponds to target value) in different zones during system filling: (A) hopper filling, (B) paddle wheel rotation, and (C) paddle wheel and turret rotation (API content given in FW-Z and RW-Z once > 0.1 g total mass is filled in the zone).

The system filling procedure was performed similarly for the ■ configuration as already described by Hildebrandt et al. [170, 236] for the ● configuration. For the sake of completeness and for easy comparison, parts of the previous study [170] are repeated and are clearly indicated where applicable. The filling sequence consists of three steps: (A) filling of the feeding hopper (until $t = 0.8$ s), (B) filling of the force feeder by paddle wheel rotation at 15 rpm (until $t = 9.8$ s), and (C) filling of the turret at 10 rpm turret speed and 15 rpm paddle wheel speed (until $t = 15.8$ s). During this stepwise filling, the temporal development of the API content in different zones is given in Fig. 4, the respective filling steps are denoted by the letters A, B, and C in Fig. 4. At the end of the filling sequence ($t = 15.8$ s), API contents (w/w) of 3.4%, 2.0%, and 10.7% for the ● [170] and 5.3%, 3.0%, and 10.8% for the ■ configuration in the DW-Z, FW-Z, and RW-Z are obtained, respectively (Fig. 4). The most significant difference in API content between the configurations is found for the DW-Z. The powder flow through the force feeder is exemplarily shown for one particle in Fig. 5. In general, the powder is fed from the feeding hopper into the DW-Z (green). The powder gets filled from the DW-Z through two openings at the bottom of the zone (yellow) either into the RW-Z (red) or the FW-Z (pink). Hence the powder that is located at the bottom of the DW-Z determines the content that is discharged into the two below paddle wheel zones. In accordance to Fig. 4 showing the API

content development over time, the powder flow pattern in the individual zones (feeding hopper left bottom, DW-Z, RW-Z, and FW-Z) for the ● and ■ configuration is briefly summarized in Fig. 5. The API content at the end of system filling is given (confer above) in addition to the API content ratios between the bottom and the top of the paddle wheel zones for easy reference (Fig. 5). The explanations in Fig. 5 are supported by Fig. 6A showing the particle trajectories (arrows) colored according to the particle velocity in the feeding hopper. The qualitative particle velocity and the particle size distribution in the paddle wheel zones at the end of system filling are shown in Fig. 6B and Fig. 7, respectively. Percolation / sieving is identified in all paddle wheel zones as the predominant size segregation mechanism (Fig. 5) [181, 195]. The size segregation speed is influenced by the depth of immersion of the blades and by the blade shapes (Tab. 2). This implies that if the system would be closed (no particles are leaving in filled dies) and operated for a sufficiently long time ($\gg 15.8$ s), similar API content ratios between the bottom and top (= size segregation extent) in the individual paddle wheel zones would be expected.

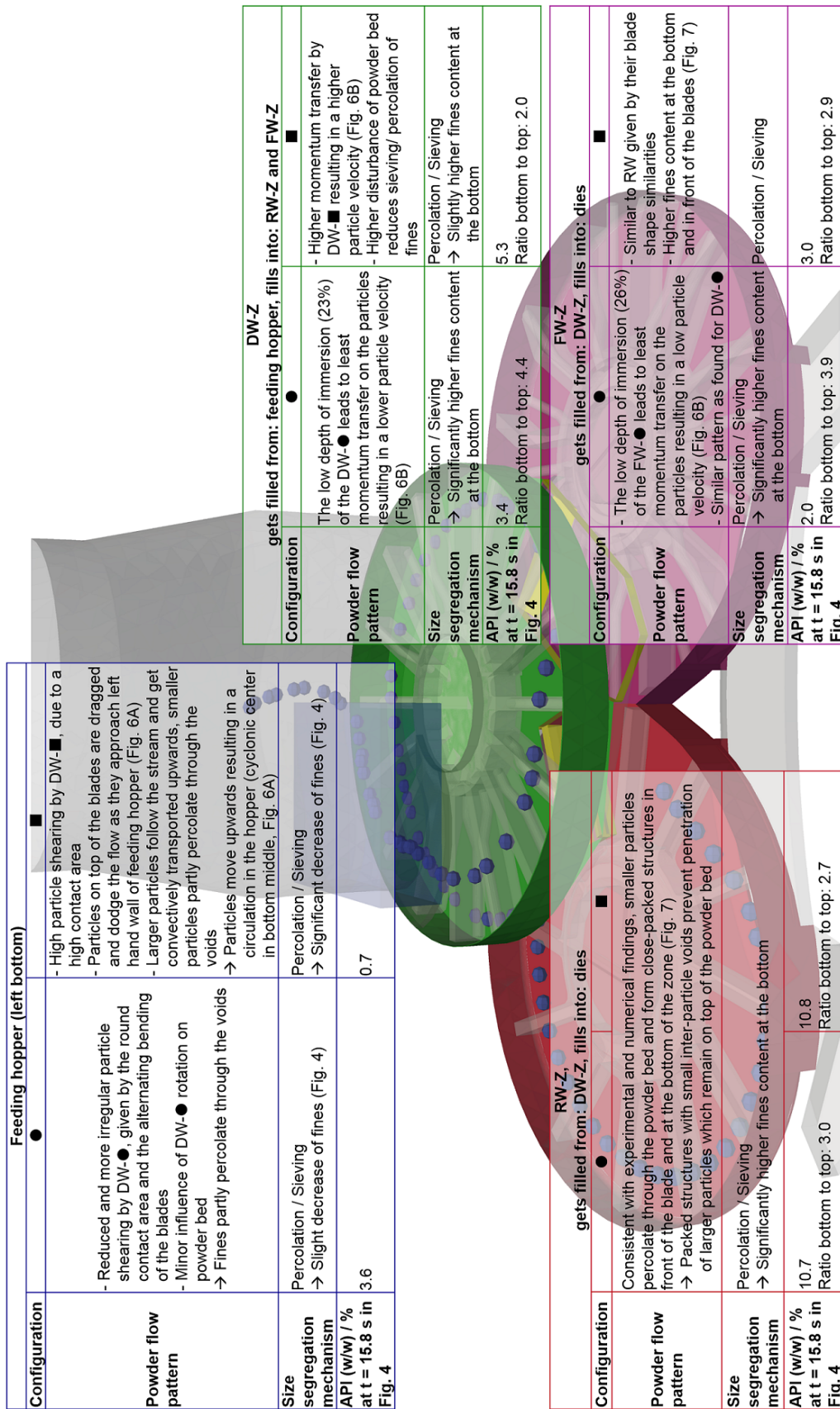


Fig. 5: Powder flow pattern in different locations of the force feeder during system filling for the ● (refer to [170]) and ■ configuration. The trajectory of one particle (scaled in size) is exemplarily shown.

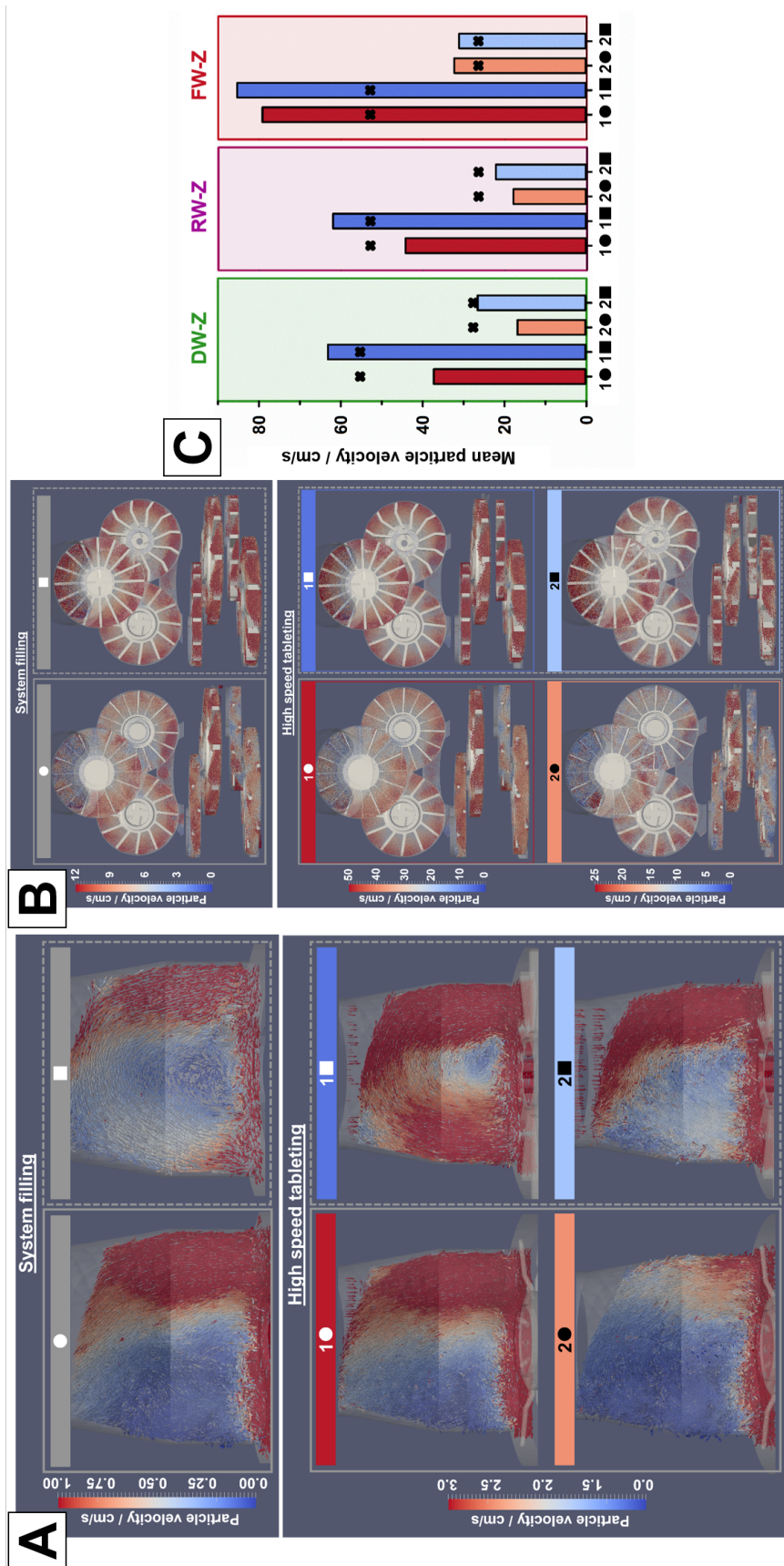


Fig. 6: (A) Particle trajectories (arrow) and velocity (color) during system filling and high speed tableting in the feeding hopper, (B) qualitative particle velocity during system filling and high speed tableting (check different legends), (C) and mean particle velocity during high speed tableting alongside with maximal blade tip speed in different paddle wheel zones (cross).

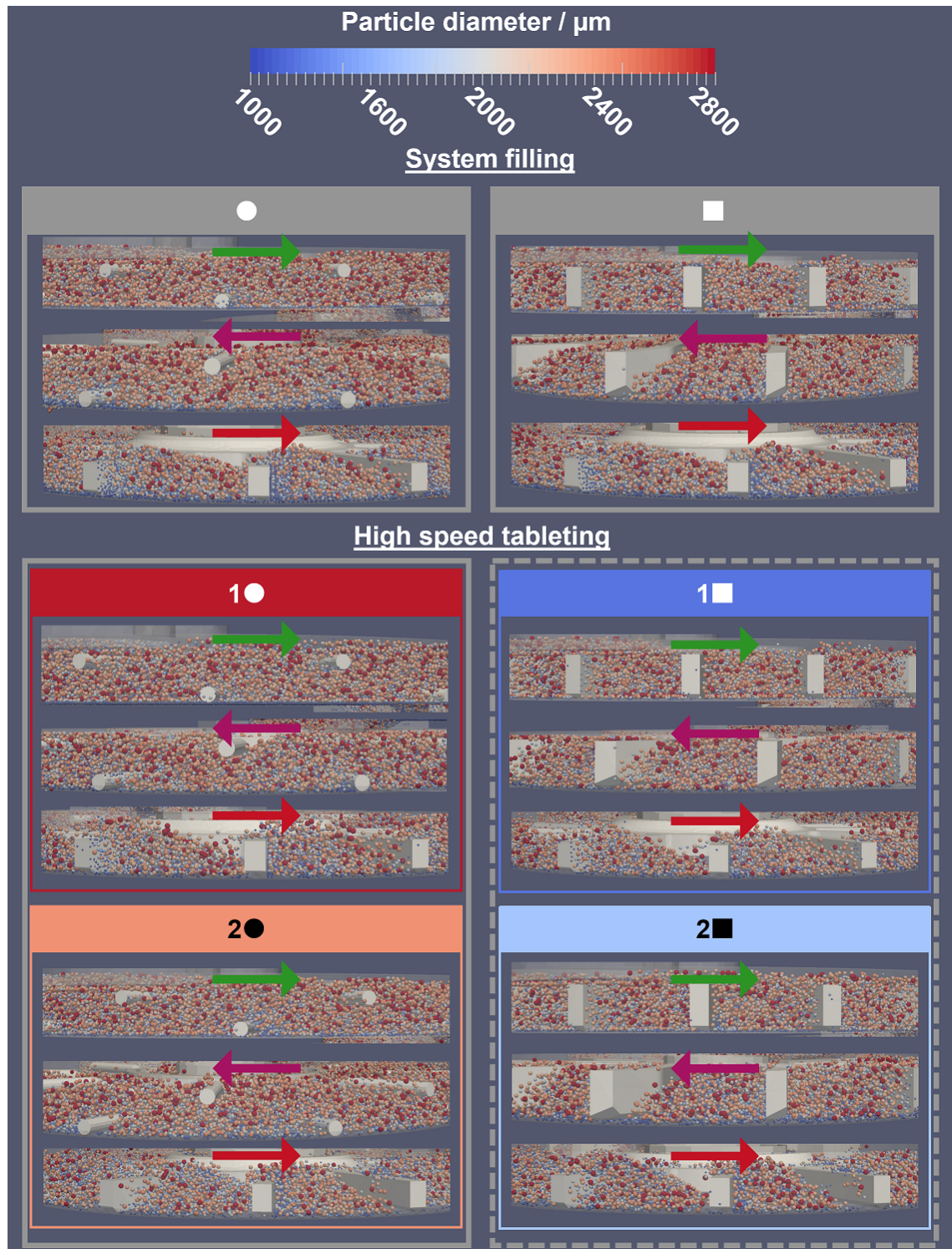


Fig. 7: Particle size distribution during system filling and at the end of high speed tableting. The arrows (color code refers to paddle wheels Fig. 2) indicate the rotation direction.

3.2 High speed tableting comparison

Following the system filling, actual high speed tableting was initiated by increasing the turret speed and paddle wheel speed in addition to an adaption of the material properties in terms of inter-particle cohesion (CED) and particle-wall friction (μ_{PW}) (Tab. 3). We previously evaluated the influence of process conditions and material attributes ('factors' in a design of experiments) on tablet quality in terms of tablet mass, tablet mass variation, and content uniformity for the ● configuration [186]. The following two conditions with opposite factor levels revealed significantly different product qualities, as explained in [186]:

Good tablet quality: 40 rpm turret speed, 60 rpm paddle wheel speed, 1.0 MJ/m³ CED, and 0.25 μ_{PW} (corresponding to setup no. 5 in [186]) (referred as condition 1, Tab. 3);

Bad tablet quality: 75 rpm turret speed, 30 rpm paddle wheel speed, 3.5 MJ/m³ CED, and 0.75 μ_{PW} (corresponding to setup no. 10 in [186]) (referred as condition 2, Tab. 3).

These conditions with extreme product qualities were selected for high speed tableting until mass steady state (measured in terms of constant mass hold up in the paddle wheel zones) was reached to compare the different configurations (Tab. 3). For all the setups, mass steady state is achieved before 10 turret rotations (data not shown).

First, the tablet quality is evaluated before the powder flow differences for the ● and ■ configuration are ascertained. The macroscopic powder flow pattern is elucidated through particle coloring and residence time analysis to identify the dead zones following a detailed microscopic analysis based on the particle velocity and its influence on particle size segregation. Those descriptions help to identify the shearing action in the force feeder. Although for condition 1 and 2, the process conditions as well as the material properties are changed simultaneously (Tab. 3), for the sake of brevity, the identified differences between the configurations are predominately referred to process conditions.

3.2.1 Tablet quality comparison

The tablet quality obtained for the different setups (1●, 1■, 2●, and 2■) is compared (Tab. 3) to provide a general understanding for process development. The details about the quantification and meaning of the defined critical quality attributes (CQA) according to the quality by design approach (QbD) are described in [186]. The best and worst results of the individual CQAs for the 4 different setups are indicated in green and red letters in Tab. 3, respectively.

1.A) Tablet mass and tablet mass variation

The ■ configuration provides significantly higher tablet masses compared to the ● configuration for both conditions (*t*-test, $p < 0.005$ at $\alpha = 0.05$, Fig. 8A), although the difference between 1■ and 1● is only minor (5.08 g for 1● and 5.10 g for 1■). The differences are more pronounced for condition 2 (Tab. 3). The increase in turret speed from 40 rpm (condition 1) to 75 rpm (condition 2) decreases the time the die spends underneath the filling station of the force feeder and shows a high influence on tablet mass, similar to findings from [80, 86, 87, 186, 261]. It leads to incompletely filled dies in both configurations for condition 2 (2● and 2■), as illustrated in the exemplary die images in Fig. 8A. In reality, the die fill height would be adjusted to counteract the incomplete die filling. Though general dependencies for the configurations can be identified in this study. An increased force feeding effect by the ■ compared to the ● configuration results in a higher mass contribution from FW-Z which will be explained in section 1.C) (Fig. 8A, Tab. 3). In turn, the FW-■ increases the mean tablet mass, which is most prominent at a high turret speed (condition 2).

In addition, the ■ configuration gives a reduced tablet mass variation in both conditions (1■ and

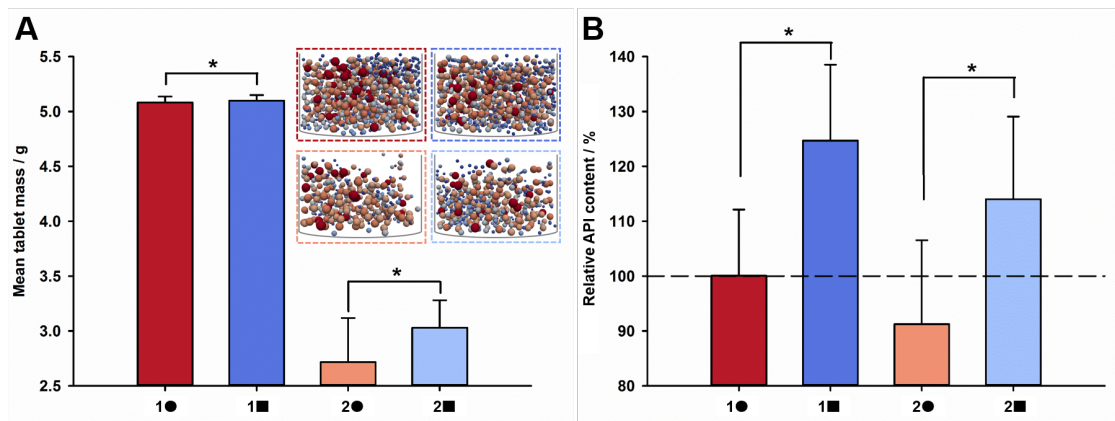


Fig. 8: (A) Mean tablet mass and (B) API content relative to label claim (* significant difference in *t*-test). Exemplary screenshots of filled dies are given in Fig. 8A (confer to Fig. 3 for particle size legend).

2■, Tab. 3) which can be explained by a more uniform force feeding effect and indirectly through higher die fill densities, as similarly reported by [80, 86, 87, 168, 169].

1.B) Content uniformity

Content uniformity (CU) was assessed according to monograph 2.9.47 in Ph. Eur. considering the mean relative API content in the filled dies (\bar{X}), expressed as percentage to the label claim of 5% (section 2.3) and the standard deviation of the relative content (s) [25]. Both measures enter into the calculation of the acceptance value (AV) that has to meet two criteria to ensure CU [25]. More background information and details on the calculation can be found in our previous study [186].

Though the same model DC formulation with a specified API content of 5% (w/w) (Fig. 3) was filled into the feeding hopper of all setups, only the dies filled by setup 1● contain the mean API content of 5.0% whereas the others either show under- (4.6% for 2●) or significantly over- (6.2% for 1■ and 5.7% for 2■) dosing (Tab. 3). The mean relative API contents to the label content (\bar{X}) are given in Fig. 8B. Those values correspond to the API content corrected to the respective mean tablet mass [186]. The absolute API mass filled into the dies and thus the actual API dosing differs more significantly between the setups with 254.3 mg, 317.9 mg, 124.1 mg, and 172.2 mg for setup 1●, 1■, 2●, and 2■, respectively (Tab. 3). The incomplete die filling (confer above and Fig. 8A) contributes to these differences. For instance, using the same process parameters and tablet formulation (condition), a drastic API dose increase of 25% and 39% for condition 1 and 2, respectively, using the ■ instead of the ● configuration are obtained. These observations give an impetus to assess the API mass flow rate into the die, explained in section 1.C).

The API content fluctuations (s) obtained are much higher compared to reality (Tab. 3, Fig. 8B) given by the large particle sizes considered (Fig. 3) and the low total number of particles collected in the dies (Fig. 8A) [186]. Though general dependencies can be identified, e.g. the API content fluctuations, expressed as the standard deviation of \bar{X} (s), are reduced for condition 1 when the ● instead of the ■ configuration is used. No differences for s are found between the configurations for condition 2 (Tab. 3).

The time increments, providing the number of dies that are filled by one inter-blade of the FW at a given turret speed and paddle wheel speed combination, are calculated for the different configurations and conditions. 1.0 die and 1.3 dies for condition 1 and 3.8 dies and 5.0 dies for condition 2 are filled by the inter-blades of the FW-● and the FW-■, respectively. Neither of the conditions coincides

with the size segregation patterns thus the API content does not reveal any constantly fluctuating pattern (data not shown). However it is worth to check the inter-blade time increments during process development at different turret speed and paddle wheel speed combinations than the ones tested in this study (Tab. 3) to prevent API content fluctuations due to size segregation in the paddle wheel zones [186].

CU cannot be met by either of the setups since all of them show AV values > 25.0 [25], though the ● configuration shows for both conditions lower AV values compared to the ■ configuration. However the AV value is dominated by the API content fluctuation (s , contribution $> 82\%$) in the ● configuration whereas a contribution from \bar{X} on AV of at least 27% is obtained in the ■ configuration (Tab. 3). Consequently, the ● and ■ configurations have different levers for CU optimization. Though for both configurations a decrease of s would improve CU, a higher effect through an optimization of \bar{X} would be expected for the ■ configuration.

1.C) Mass flow from the force feeder into the die

The influence of size segregation in the force feeder on the particles entering the die is studied by tracking the die as it is rotating underneath the force feeder [186, 236, 262]. This helps to identify the root causes for the significant API content differences filled into the dies described in section 1.B) and shown in Fig. 8B. The total mass and API mass collected over time in the die are shown in Fig. 9A & B, respectively. The die filling time is normalized for easier comparison of condition 1 (40 rpm turret speed, 0.492 s) with condition 2 (75 rpm turret speed, 0.264 s). During interval ‘A’ the die volume is generated by lowering the lower punch to a maximal die height of 1.5 cm while the die is rotating underneath the FW-Z, called ‘fill cam’. During interval ‘B’ solely gravity filling is possible, before the die can get filled in ‘C’ from the RW-Z. The die leaves the force feeder after the lower punch was moved up by 13% during ‘dosing cam’ in ‘D’. More details about the die height during fill and dosing cam can be found elsewhere [236]. In general, discrepancies between the mass flow rate (MFR) of the complete blend (Fig. 9A) and individual particle size fractions, e.g. as shown for the API particles in Fig. 9B, indicate size segregation in the force feeder [236]. Differences in MFR between the FW-● and FW-■ exist if a change in the slope during interval ‘A’ is identified (Fig. 9). The following observations for total mass filled into the die are made (Fig. 9A):

Condition 1: 1■ vs. 1●:

- The low turret speed (40 rpm) in combination with the high paddle wheel speed (60 rpm) enables almost similar blend MFR from FW-Z, irrespective of the configuration.
- No clear differences between 1■ and 1● are found, consistent with Fig. 8A.

Condition 2: 2■ vs. 2●:

- The increased force feeding effect of the FW-■ compared to the FW-● is most distinctive at very high turret speeds (75 rpm) with a relative total blend MFR increase of 27% during interval ‘A’.
- A similar mass contribution during die filling from RW-Z (similar slope during interval ‘C’) for 2■ and 2● is found.

In contrast to total mass, more significant differences between the configurations are obtained for API mass. Those differences are most prominent for API mass filled into the die during interval ‘A’ (FW-Z, Fig. 9B) whereas no significant differences in the API-MFR slopes during interval ‘C’ (RW-Z) are found.

Condition 1: 1■ vs. 1●:

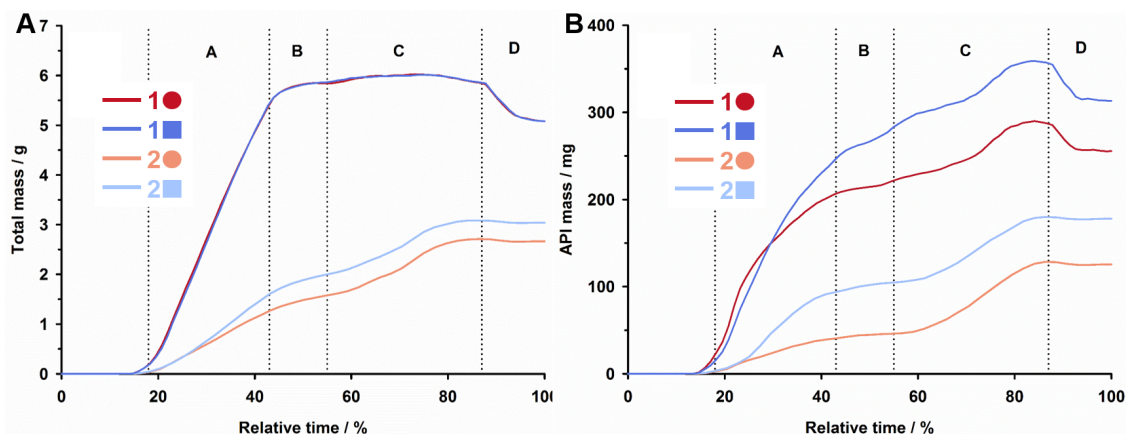


Fig. 9: (A) Total and (B) API mass filled into the die over time (confer for letters to text).

- The 1.4-fold higher API content in the FW-Z-■ compared to FW-Z-● (Tab. 3, detailed explanation in section 2.C)) results in a 1.2-fold higher API mass filled into the die after interval ‘A’. This gives the explanation for the 1.3-fold higher API mass filled into the die after die filling for setup 1■ compared to 1● (Fig. 8B, section 1.B), Tab. 3).

Condition 2: 2■ vs. 2●:

- The 1.8-fold higher API content in the FW-Z-■ compared to FW-Z-● (Tab. 3, detailed explanation in section 2.C)) results in a 2.3-fold higher API mass filled into the die after interval ‘A’. The API ratio differences (1.8- vs. 2.3-fold) for setup 2■ can be attributed to inter-blade segregation pattern for the FW-■. A detailed explanation is given in section 2.C).
- On average a 1.4-fold higher API mass filled into the dies is obtained for setup 2■ vs. 2● (Fig. 8B, section 1.B), Tab. 3).

The particle size segregation having occurred in the force feeder for the different configurations and conditions is transferred into the dies and results in different particle size distributions in the dies and over the die height. The detailed MFR analysis gives reference for the API dose filled into the dies (confer section 1.B)) and emphasizes the differences between the FW-■ and FW-●. In addition, the particles have experienced different shear forces (confer section 2.C)) which may alter particle properties (particle attrition, over-lubrication) and may affect the risk for capping of the produced tablets [86, 90, 102].

3.2.2 Powder flow comparison in the force feeder

2.A) Coloring profile and residence time

The powder flow in the force feeder is ascertained by (A) coloring the particles according to their initial position and by (B) calculating the residence time.

(A) The powder flow in the force feeder is visualized by coloring the particles according to their position when high speed tableting is started (confer to [171, 236]). As illustrated in Fig. 10, at the beginning particles are colored in the individual paddle wheel zones and in 4 different heights of the feeding hopper with each colored layer having equal height of 5 mm. These 4 layers in the feeding hopper are separated by 25 mm height powder bed. In addition to the qualitative representation in Fig. 10, the mass throughput is quantitatively shown in Fig. 11. For this purpose, the cumulative mass discharged into the dies was calculated for all setups. Setup 2● has the lowest mass filled in dies (630 g in 232 filled dies, 8 s, 10 turret revolutions). The same discharged mass is found after 8.2 s for

1● and 1■, and after 7.2 s for 2■. The mass ratio of colored particles that were initially located in the respective paddle wheel zones and that are found at those time points of same discharged mass are computed, given in Fig. 11, and illustrated in Fig. 10 (right).

(B) The particle residence time is calculated by tracking the particles that are at the beginning of high speed tableting located in the top right hand half of the feeding hopper, as indicated in the orange box in Fig. 2A. The tracking of those particles allows the assessment of (1) the time point at which the first particles discharge into the die (Tab. 3), (2) the mean residence time in the system, and (3) the ratio of the tracked particles in the system after 10 turret rotations compared to the beginning for individual size fractions (Fig. 12).

The following observations for the ● and ■ configurations are made using the qualitative (Fig. 10) and quantitative (Fig. 11) particle coloring by their initial position analysis and the residence time evaluation (Fig. 12):

● configuration, 1● and 2●:

- Only the right hand half of the feeding hopper is involved in the refilling of the DW-Z, whereas the left hand half is stationary indicating a dead zone (similar to [171, 236]) whereby the powder bed may consolidated over time (Fig. 10).
- A higher mass throughput from RW-Z is found for setup 2● compared to 1● (Fig. 11) given by the higher MFR into the die from RW-Z (interval ‘C’ in Fig. 9A).

■ configuration, 1■ and 2■:

- The right hand half of feeding hopper is likewise refilling the DW-Z as found for the ● configuration, though particles in the left hand half are being pushed upwards and recirculate within the hopper to the right hand half (Fig. 10). Particles from the DW-Z (green) move up in the left hand half of the hopper. For example, maximal 14% (w/w) of green colored particles are found in the feeding hopper for setup 2■ (data not shown).
- A higher mass throughput for ■ compared to ● configuration is found, as shown by:
 - After 2.5 turret revolutions more green colored particles have been refilled from DW-Z into FW-Z. Hardly any particles initially located in FW-Z (pink) and RW-Z (red) can be identified after 10 turret revolutions (Fig. 10, 2■)
 - Particles show on average a lower residence time in the force feeder (Tab. 3) for the ■ compared to the ● setups.
- As a consequence of the recirculating powder flow in the feeding hopper, not all particles that refill the DW-Z from the right hand half of the feeding hopper are subsequently force fed into the dies. Thus particles partly recirculate in the feeding hopper leading to an overall higher ratio of particles that remain in the system for setup 1■ compared to 1● (Fig. 12). Less mass from the hopper is refilling the DW-Z as particles are recirculation and thus more initially located particles from DW-Z have to refill the RW-Z and FW-Z. This results in a lower ratio of particles remaining in the DW-Z for setup 1■ compared to 1● (Fig. 11).
- Setup 1■: Interestingly, the ratio of particles remaining in the system (Fig. 12) shows a significant trend over the individual particle size fractions. The results indicate that 27% of the API particle size fraction ($1000 \mu\text{m} < x \leq 1129 \mu\text{m}$) in contrast to 55% of the largest particles ($x \geq 2800 \mu\text{m}$) are still located in the force feeder, emphasizing particle size segregation within the system. This observation will be explained in section 2.B).
- A higher mass turnover is found in the two paddle wheel zones involved in die filling (FW-Z and RW-Z) for the ■ compared to the ● setups (irrespective of condition 1 or 2) though same mass is filled into the dies (Fig. 10).

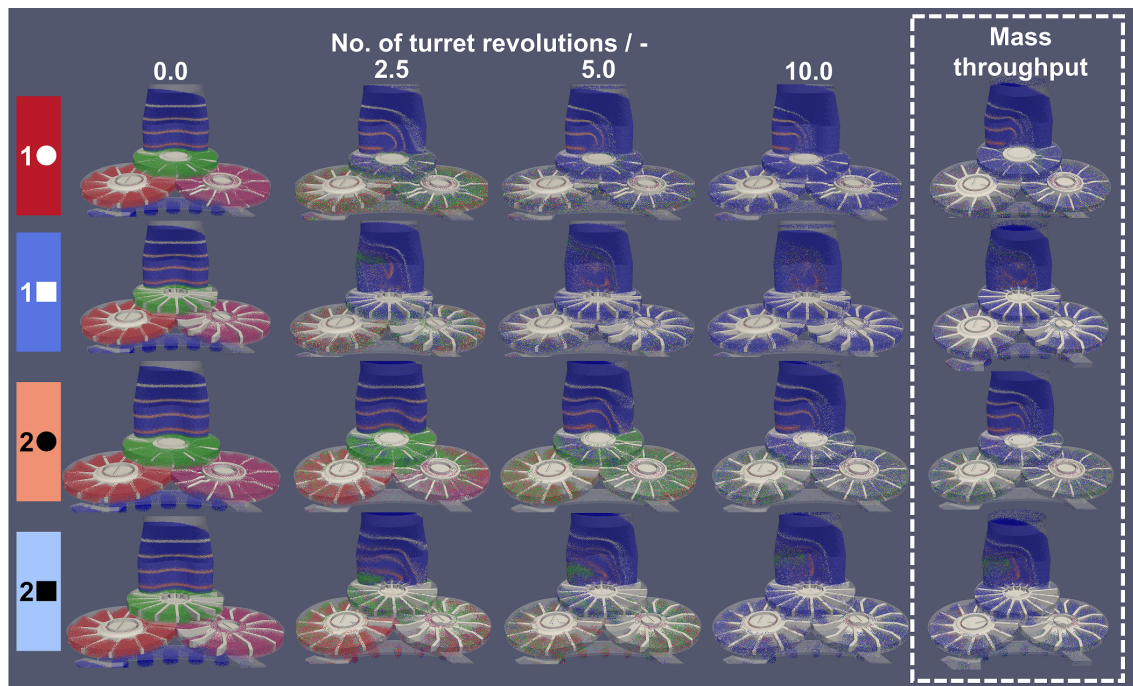


Fig. 10: Qualitative visualization of the traveling path of initially colored particles during high speed tableting and at the time point of same mass filled in the dies (quantitative in Fig. 11).

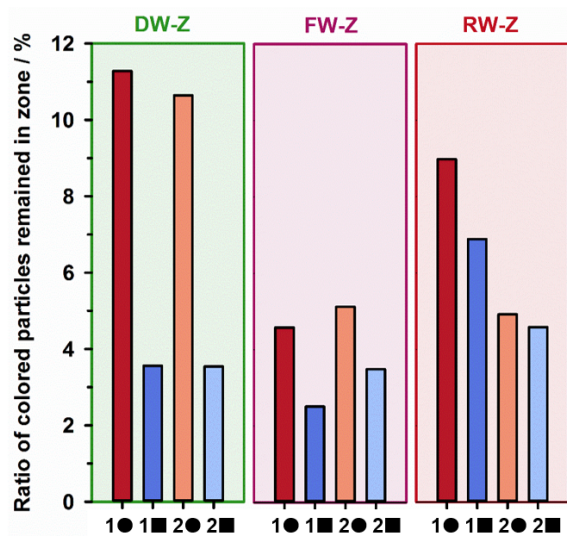


Fig. 11: Ratio of colored particles remaining (after same mass filled into the dies) compared to initially located in the paddle wheel zones (qualitative in Fig. 10)

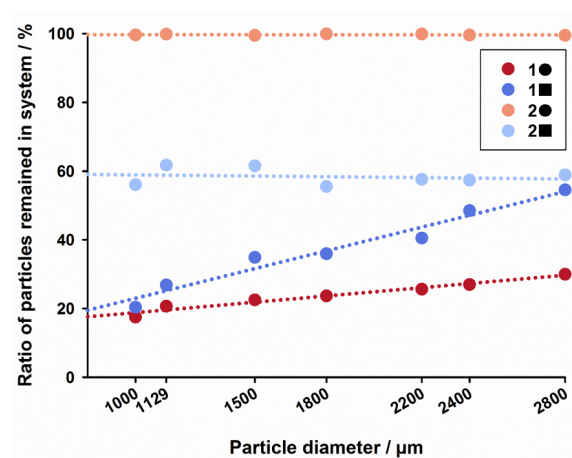


Fig. 12: Ratio of particles remaining after high speed tableting compared to initially located in the right top half of the feeding hopper (Fig. 2A, orange box) for different particle size fractions.

2.B) Particle velocity and its influence on particle size segregation

In the first place, a particle velocity analysis helps to discern the underlying powder flow pattern which subsequently supports the understanding of potential particle size segregation.

A qualitative illustration of the particle velocity is given for the feeding hopper in Fig. 6A and for the different paddle wheel zones in Fig. 6B (in top and side view). In addition, Fig. 6C gives the mean particle velocity in the different paddle wheel zones along with the maximal tip speed of the paddle wheel at the given rotation speed (cross).

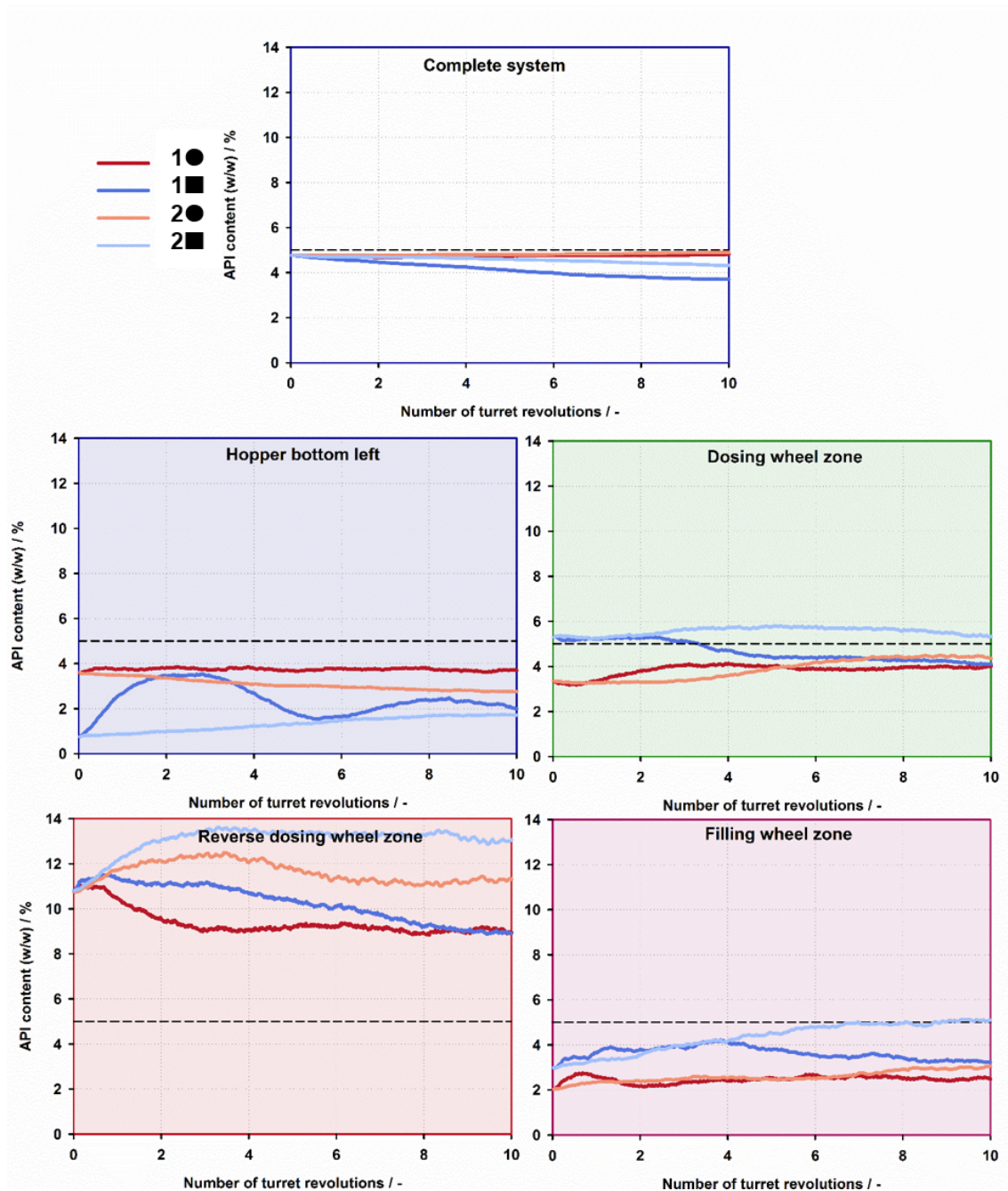


Fig. 13: API content during high speed tableting in different locations of the system (normalized to no. of turret revolutions for condition 1 and 2).

Fig. 13 depicts the API content during high speed tableting in the complete system, hopper bottom left, DW-Z, FW-Z, and RW-Z for the different setups (Tab. 3). The side view of the paddle wheel zones at the end of high speed tableting is shown in Fig. 7. (The reader is referred to the supplementary videos supporting the following descriptions (section 5).

In general, the powder flow pattern and the particle size segregation in the DW-Z are predominantly influenced by the shear zone between the DW and the bottom of the feeding hopper. The shear zone is mutually affected by the blade shape of the DW and by the paddle wheel speed.

The ■ compared to the ● configuration increases the radial velocity gradient (particles at the blade tip move with significantly increased velocity compared to the blade center (Fig. 6B) which is more prominent at a higher paddle wheel speed (condition 2, Fig. 6C). The powder flow pattern in the RW-Z is comparable for the ● and ■ configuration and only differs between 60 rpm and 30 rpm paddle wheel speed. More details can be found elsewhere [186].

The following particular observations can be made by comparing the ● with the ■ configuration. Similar as for system filling (section 3.1), the powder flow pattern in the feeding hopper, more precisely in the bottom left hand half, and the paddle wheel zones are described separately.

Condition 1, 1■ and 1●:

Bottom left hand half of feeding hopper

- 1■:
 - The higher convective powder motion in the feeding hopper compared to system filling reduces the extent of size segregation by percolation mechanism in the left hand half of the feeding hopper (Fig. 6A). Consequently an increase of fines including API particles in the bottom left hand half of the feeding hopper is found (Fig. 13).
 - The recirculating powder flow (confer section 2.A), Fig. 10) leads to a wave like API content fluctuation in the hopper bottom left at a frequency of 9 paddle wheel revolutions (= 6 turret revolution in Fig. 13).
 - The complete feeding hopper, making up > 64% of the mass in the force feeder, reveals during high speed tableting a depletion of fines and an accumulation of coarse particles (data not shown). The coarse particles can follow the convective motion more easily as shown in the hopper image at the end of high speed tableting in Fig. 14. This finding gives the explanation for the increase in the ratio of particles remaining in the system with particle size identified for setup 1■ during residence time analysis (Fig. 12, section 2.A)).
- 1●:
 - A steady state in the diffusive shear zone between the hopper bottom left and the DW (Fig. 6A) is found. The counterbalance of particles moving slightly downward (by gravitational force, sieving / percolation) and upwards (by momentum transfer of the blades) gives a constant API content (Fig. 13).

Paddle wheel zones:

- 1■:
 - Over the complete height of every paddle wheel zone no particle velocity gradient is found (Fig. 6B). In radial direction, the particles move at equal velocity with the respective blade speed (lower towards the center, higher at the blade tip, Fig. 6B). This indicates that the particles are transferred as a ‘complete inter-blade bulk’ by paddle wheel rotation preventing

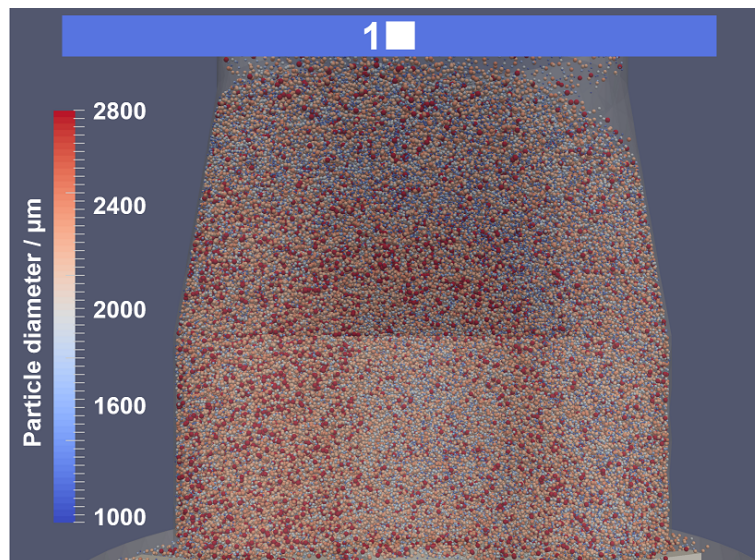


Fig. 14: Particle size distribution in the feeding hopper at the end of high speed tableting for setup 1■.

size segregation either by percolation / sieving [181, 195] or trajectory mechanism [181, 195, 212, 213].

- In return, whatever enters into the inter-blades of the DW-Z is transferred and discharged into the RW-Z zone and into the FW-Z.
- The absence of top to bottom size segregation during rotation of the DW reduces the fines content discharge into the RW-Z (Fig. 7). Consequently a steady decrease of API particles from initially 10.8% (after system filling) to 8.9%, in the RW-Z zone is obtained (Fig. 13).
- Similar to DW-Z, no top to bottom size segregation in the FW-Z can be identified (Fig. 7).
- 1●:
 - Compared to system filling, the higher DW-Z speed causes less sieving / percolation segregation of fines (Fig. 7), thus less fines discharge into the RW-Z. The fines content, as shown for API particles, decreases in RW-Z (Fig. 13).

Condition 2, 2■ and 2●:

Bottom left hand half of feeding hopper

- 2■:
 - A convective powder flow is found, though the higher paddle wheel speed of 30 rpm compared to system filling (15 rpm, section 3.1) causes a more disturbed shear zone preventing the downward motion of fines due to gravitational force. This leads to a slight increase of fines as shown for API particles in Fig. 13 (confer also to 1■).
- 2●:
 - The reduced particle velocity in the diffusive powder flow region at the low DW speed (30 rpm) increases the percolation of fines as shown by a decrease of API particles (Fig. 13) which in turn results in a higher API content in DW-Z.

Paddle wheel zones

- 2■:
 - In the DW-Z a clear radial and a minor horizontal particle velocity gradient can be identified (Fig. 6B).

- The low paddle wheel speed favors the fine particle percolation to the bottom in the DW-Z from where they discharge into RW-Z causing a relative content increase in the latter (Fig. 13).
- In the FW-Z, in addition to the radial particle velocity gradient, a distinctive horizontal gradient is found (Fig. 6B). The reduced packing fraction in the inter-blades (qualitatively shown in Fig. 6B & 7) enables a wave like behavior of the particles. Momentum is transferred from the blade to the particles in direct contact developing a particle heap. Coarse particles on top of the heap avalanche more readily than small particles and come to stop behind the next blade. This phenomenon was already described by Conway et al. [197] in an experimental system applying PIV technology (Tab. 1). This kind of segregation mechanism is also known as trajectory segregation [181, 195]. The coarse particles get picked up by the rotating blade leading to a recirculation between the inter-blade zones. Fines partly resist this recirculation, get trapped directly in front of the rotating blade and at the bottom of the zone (Fig. 7), and thus cause a slight content increase over time (Fig. 13). The API particles at the bottom of the FW-Z and in front of the blade increase the API MFR into the die, as explained in section 1.C) (Fig. 9B).
- 2●:
 - The low paddle wheel speed increases the horizontal particle velocity gradient (Fig.6B). The reduced interference of the powder bed enhances the extent of fines sieving / percolation in the DW-Z (Fig. 7) which increases the fines content in the RW-Z (Fig. 13).
 - Similarly to DW-Z, the low depth of immersion of the FW-● leads to a higher top to bottom segregation in the FW-Z (Fig. 7).

The size segregation during the particle travel path (section 2.A)) leads to different API contents in the paddle wheel zones (Fig. 13). In turn the size segregation in the force feeder significantly influences the API dose filled into the die, as explained in section 1.B) and 1.C).

2.C) Particle shearing in the force feeder

Narang et al. [76] identified an approximately linear correlation of $\log(\text{tableability})$ with $\log(\text{shear number})$ across different rotary tablet presses differing in terms of number of paddle wheels, number of blades per wheel, blade geometries, and blade and housing dimensions. Tableability was estimated as the ratio of tablet tensile strength to the applied compression pressure (through the initial, linear portion of the compression profile). The shear number (dimensionless) was calculated via an empirical correlation including the shear rate, the shear frequency, and the residence time. Those included blade diameter, paddle wheel speed, clearance between the blades and the housing bottom, number of spokes, powder mass in the force feeder at equilibrium, tablet weight, turret speed, and punch number. Above a critical point of shear, the effect of the force feeder on tablet tensile strength became significant with a decrease in tableability at higher shear numbers. The limitations and assumptions of the shear number were the negligence of the curvature shape, the gravitational pressure on the powder blend given by the filled hopper, and the clearance between the blade and the housing top [76].

The relationship between tableability and shear number indicates that the tablet tensile strength is not solely influenced by the compression step during tableting, but also through the shearing action by the rotation of the paddle wheels in the force feeder [76, 102]. The shearing action of the two configurations in this study is assessed via, first, the mean particle velocity in the different paddle wheel zones (Fig. 6C) as an estimate for the forces acting on the particles [41, 94, 95]. Secondly, the particle coloring analysis helps to discern the residence time in the individual paddle wheel zones at

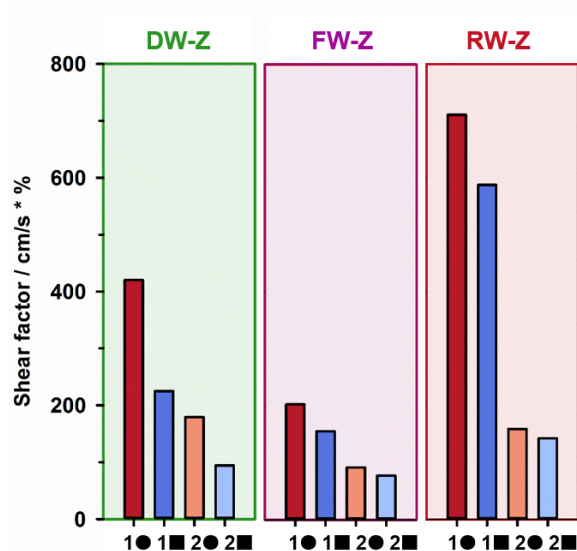


Fig. 15: Shear factor in the different paddle wheel zones according to Eq. 1.

same mass filled into the die (Fig. 11). This serves as an estimate to evaluate the time the particles have been exposed to a given shear rate. *Shear factors* are computed for the individual paddle wheel zones according to Eq. 1 and are plotted in Fig. 15:

$$Shear\ factor_{paddle\ wheel\ zone} = Mean\ particle\ velocity_{paddle\ wheel\ zone} \left[\frac{cm}{s} \right] * \quad (1)$$

$$Ratio\ of\ particles\ remained\ compared\ to\ initial_{paddle\ wheel\ zone} [\%]$$

The *Shear factor* (Fig. 15) indicates that over the different paddle wheel zones as well as for the different setups the particles are exerted to significantly different shearing. For example in the setup 1 the particles experience highest shearing in the RW-Z as less mass is filled from the RW-Z into the die (Fig. 9A, section 1.C)). The increased mass throughput (Fig. 10 & 11) for the ■ configuration (1■ & 2■) can counteract the increased particle velocity (Fig. 6C) in particular in the DW-Z and FW-Z. This in returns reduces the shearing extent (Fig. 15) in the force feeder for the ■ compared to the ● setups.

This kind of approach serves only as a first estimate for comparison purposes and could provide an indication for powder over-lubrication and particle attrition induced by the paddles in the force feeder in lab experiments [42, 76, 102, 205–208]. However, to accurately predict the shear extent, complex force and residence time calculations on a single particle level are necessary. It could be interesting to quantify the shearing during the powder motion in the feeding hopper, especially for the ■ configuration which could potentially affect particle properties, too. In addition, the actual powder compaction step has to be performed or computed to directly relate it to the tablet tensile strength, as done by [76].

Overall paddle wheel shape comparison

The ■ configuration compared to the ● configuration can provide an increased tablet mass and a reduced tablet mass variation, at the cost of a lower content uniformity (higher *AV* value, Tab. 3). The size segregation in the force feeder, in particular in the FW-Z determines the API dose filled

into the dies which is significantly higher for the ■ compared to the ● configuration. All CQAs (tablet mass, tablet mass variation, and AV) are combined at equal weighing in a desirability model [232, 240, 254, 255] (detailed explanation is given in [186]). For condition 1, the best product quality (desirability close to 1) can be obtained for the ● configuration (1● of 0.79) hence it is advised to choose the cylindrical paddle wheels to achieve highest tablet quality. The relatively high AV value for 1■ reduces the desirability compared to 1● by 59% to 0.32 (Tab. 3). The opposite is found for condition 2 in which it is favorable to choose the ■ configuration (desirability of 0.51 for 2■ and 0.15 for 2●, Tab. 3). Thus depending on the process conditions and the formulation, this study suggests to choose different paddle wheel shapes to obtain a high tablet quality with regard to a high tablet mass, a low tablet mass variation, in addition to a high CU. The powder flow patterns in the feed frame significantly differed for the configurations at the given numerical conditions. If an unfavorable turret speed (high) and paddle wheel speed (low) combination is chosen (more details given in [186]), it is indicated that the ■ configuration may improve the tablet quality (condition 2). If the ● configuration already provides a good tablet quality (1●), further improvement by changing the paddle wheel shape is not indicated. Hence it is worth to check different paddle wheel shape configurations, if a low tablet quality is obtained during process development. However to draw a more general conclusion, more different conditions would have to be compared. The results were predominantly related to the paddle wheel speed and turret speed although the micro-mechanical material properties of the particles have been changed between condition 1 and 2, too (Tab. 3). Additional experiments have to be performed, e.g. by generating a design of experiments as done in our previous study for the ● configuration [186], to elucidate the influence of the material properties, e.g. of the inter-particle cohesion and the particle-wall friction, on the powder flow with different paddle wheel shapes.

Although not directly measurable without performing the actual compaction step, the current numerical setup indicates that the higher shearing by the blades of the ■ paddle wheels (measured via particle velocity) is compensated by a decreased particle residence time in the force feeder. The validity of this finding could be tested in experiments by comparing the shear sensitivity of different lubricant containing formulations [110]. The recirculation for the ■ vs the dead zone for the ● configuration in the left hand half of the feeding hopper is compared in terms of their effect on particle size segregation. An influence on particle shearing might be possible but has not been evaluated yet. The intriguing powder flow patterns in the feeding hopper were not expected and reported previously due to the limitation of a closed experimental system. It gives an impetus for further numerical studies, e.g. combining the DW-■ with the FW-■ and vice versa, as well as experimental validation by developing custom-designed equipment.

4 Summary and conclusion

This study evaluated the influence of different paddle wheel shape configurations (dosing (DW) and filling (FW) wheel) on the powder flow pattern for the same force feeder in a pharmaceutical tablet press. Although different shapes are in use, the selection of these is rather by experience than by rationale. The differences in the paddle wheel shapes are related to the blade design which are either cylindrical (●) or cuboid (■) shaped and result in different depth of immersions and contact area shapes / sizes with the particles.

First of all, the differences in system filling showed that predominantly the altered shearing of the blades of the DW-■ influenced the size segregation in the feeding hopper that was then transferred into the other paddle wheel zones.

Two conditions (turret speed, paddle wheel speed, and particle properties) were chosen to assess the powder flow pattern during high speed tableting. The higher force feeding effect of the FW-■ compared to the FW-● increased the tablet mass and in turn reduced the tablet mass variation. Significantly differing API dose strengths in the tablets have been obtained that showed a lower content uniformity for the ■ compared to the ● configuration. Depending on the process parameters and material properties, the paddle wheel shapes may alter the critical quality attributes of the produced tablets. In particular, it is worth to check a different paddle wheel configuration in case that the combination of the process conditions yields a low tablet quality. The higher mass throughput by the ■ configuration could counteract the increased particle shearing in the force feeder. In addition to the tablet quality, the powder flow in the force feeder was assessed through particle coloring, residence time, particle velocity, and particle size segregation analysis. Similarly as for system filling, most significant differences in powder flow were identified in the feeding hopper. More precisely, a cyclic motion due to the particle shearing by the DW-■ caused an accumulation of coarse particles in the feeding hopper which was most prominent at a high paddle wheel speed. In contrast, for the DW-● the powder bed might get consolidated in the feeding hopper lacking any powder motion. The dominant particle size segregation mechanism in the paddle wheel zones was trajectory for the ■ in contrast to sieving / percolation for the ● paddle wheels, respectively. Size segregation in the force feeder was transferred into the dies resulting in significantly different API contents.

For process development it is helpful to know that and how product quality can be changed by simply changing the paddle wheel configuration. This opens new process adaption possibilities, e.g. for lubrication sensitive or size segregation prone formulations.

This study shows the benefit of numerical simulations to provide a highly detailed look into complex systems which would not be possible in lab experiments. However, the DEM study was limited by the computational power in terms of particle size and particle size distribution. Additional numerical conditions have to be tested and corresponding experiments need to be performed to validate the conclusions drawn here.

5 Supplementary videos

Videos of high speed tableting for the four setups (Tab. 3):

Complete discharge and coloring via particle size:



Complete discharge and coloring via initial position:



Zoom into filling wheel zone, coloring via particle size:



Acknowledgments

The authors would like to thank Mr. Heinrich from Fette Compacting GmbH for providing the CAD files of the tablet machine.

3.2.5 Powder flow comparison in two different force feeders

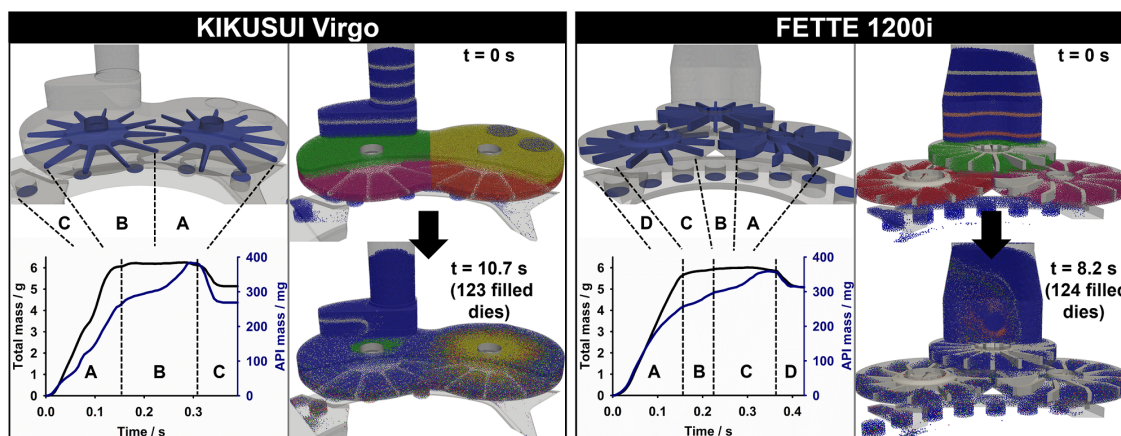
Impact of different tableting machines feed frame design on tablet quality: A DEM study of die filling

Claudia Hildebrandt^{1, 2}, Srikanth R. Gopireddy², Thomas Profitlich²,
Regina Scherließ¹, Nora A. Urbanetz²

¹ Department of Pharmaceutics and Biopharmaceutics, Christian-Albrechts-Universität Kiel,
Grasweg 9a, 24118 Kiel, Germany

² Daiichi-Sankyo Europe GmbH, Pharmaceutical Development,
Luitpoldstrasse 1, 85276 Pfaffenhofen, Germany

Submitted to *Advanced Powder Technology*, under review



Outline

During pharmaceutical development of a drug candidate, the tableting machine may change for different reasons, e.g. due to a limited lab capacity, and a technical transfer is required. Force feeding is in-depth studied in chapters 3.2.1-3.2.4 for the three-chambered force feeder of the FETTE 1200i. In the following, the FETTE 1200i is directly compared with the KIKUSUI Virgo, a two-chambered force feeder. The comparison aims to point out the differences in powder flow between the force feeders which may impact tablet quality.

At first, the powder flow is described in the KIKUSUI Virgo based on the measures previously introduced for the FETTE 1200i (chapters 3.2.1-3.2.4). Those measures include for example the particle size segregation mechanisms and the particle mixing within the feed frame. Secondly, the tablet quality is compared between the two force feeders (including different paddle wheel shape configurations for the FETTE 1200i). Tablet quality differences, e.g. in terms of content uniformity, are related to the geometries of the feed frames and emphasize the necessity of powder flow understanding in die filling.

Similar as in the comparison of the paddle wheel shape configurations in the FETTE 1200i (chapter 3.2.4), only selected combinations of material properties and process parameters are evaluated. The force feeder comparison points out the differences between the machines, though extensive and accurate tablet quality prediction is not intended.

1 Introduction

Typical batch sizes for drug product development of ‘new chemical entities’ are categorized into laboratory-, pilot-, and production-scale by the European Medicines Agency’s guidance for Process Validation [263, 264]. Batch sizes continuously grow from formulation design to Phase I and subsequently to Phase II & III clinical trials followed by commercialization after marketing authorization. Process equipment for laboratory-, pilot-, and production-scale batches changes to account for the produced number of units, e.g. the available amount of the active pharmaceutical ingredient (API) at the given development stage. Different approaches applying the ‘Quality by Design’ (QbD) concept [3] are available for process optimization and scale-up, e.g. (1) a minimal approach ensuring quality by end-product testing, (2) full design of experiments, and (3) hybrid method combining elements of both approaches (1 and 2) [263].

Tablets cover more than 80% of all available drug delivery systems, given by several advantages. From an economical and industrial perspective, they can be produced at a low cost in high quantities. Patients can easily handle and administer tablets themselves assuring a very high patient compliance [26]. The tableting process can be subdivided into three steps, die filling, powder compaction, and tablet ejection. All of these steps show their own challenges when it comes to tablet quality which is defined by the ‘disintegration of tablets’ (2.9.1), ‘dissolution test for solid dosage forms’ (2.9.3), ‘friability of uncoated tablets’ (2.9.7), ‘resistance to crushing of tablets’ (2.9.8), and ‘uniformity of dosage units’ (2.9.40) according to the regulatory authorities [25]. The uniformity of dosage units, considers the uniformity of the tablet mass as well as the API. Both the tablet mass and the dose strength are defined for a given formulation during the die filling step.

In the context of process optimization and scale-up for tableting, different die filling mechanisms may be applied, e.g. gravity feeding or force feeding. As the name suggests, in gravity feeding the material is fed from the hopper through a vertical chute into the dies of the rotating turret. It was shown by numerical means that the material’s cohesiveness, particle-particle friction, and particle-wall friction significantly influenced tablet quality [168, 169]. Different experimental model systems, e.g. considering a die translating underneath a stationary hopper [183, 262], were developed to provide a deeper understanding of powder flowability related to gravity feeding [57, 63, 78, 79, 103, 104, 183, 262, 265]. For the second mechanism, force feeding, the material is transferred from the hopper through a force feeder, consisting of one or more rotating paddle wheels, into the dies. Applying different methodologies such as classical experiments [76, 86, 87, 89, 95, 102, 110], Process Analytical Technology [92, 105, 107, 108, 111, 113, 114, 258, 266], or numerical models, e.g. the discrete element method (DEM) [41, 93, 94, 170, 186, 236, 267], supported force feeding mechanism understanding. For example, the paddle wheel speed influenced the tablet mass [41, 87, 94, 186], the tablet mass variation [41, 87, 94, 186], and the risk for particle attrition and over lubrication [41, 94, 186]. Most of those studies (irrespective of the applied approach) focused on one single force feeder / tableting machine and evaluated the influence of process conditions and material attributes on tablet quality [186].

An in depth understanding of the process and its relation to the specific force feeder geometry features are essential for process development [236, 267]. However, the very unique force feeder designs of different tablet press manufacturers, e.g. consisting of different number of paddle wheels, may impede a direct tableting process transfer from one tableting machine to other one during process development and scale-up.

The current study aims to evaluate the powder flow in the force feeders of two different pilot-scale tableting machines using DEM. The numerical results are related to tablet quality differences among

these two machines. The force feeders of the two tableting machines mainly differ in terms of (1) the number of paddle wheels, (2) the paddle wheel shapes, (3) the positioning of the paddle wheels, and (4) the housing geometry. The first machine is a FETTE 1200i, for which the general powder flow [170, 171, 236], the influence of the process conditions and material attributes on tablet quality applying the QbD approach [186], and the effect of the paddle wheel shapes [267] were reported in our previous studies. For the second machine, a KIKUSUI Virgo, first the powder flow is explained in this study. A comparison of the tablet quality in these two machines is presented by considering different conditions with regard to process parameters and powder flowability. The in depth analysis of the two force feeder systems allows an improved relation of the different geometry design features to tablet quality which has not been reported yet.

2 Methods and Materials

2.1 Numerical methods

LIGGGHTS, an open source DEM code, was used for computations [123]. Same force models as described in previous work were applied [168–170, 186, 236]. Normal and tangential forces were modeled using the Hertz and the Mindlin & Deresiewicz theories, respectively [119]. The non-contact inter-particle force was included through the simplified Johanson-Kendall-Roberts model [127]. A time step of 0.6 μs was chosen for the selected material properties (Young’s modulus (Tab. 1) and particle size (chapter 2.3)) which is well below the Rayleigh- and Hertz-time [116, 123].

2.2 Geometrical setups of the tableting machines

The details of the force feeder and the paddle wheel shapes of FETTE 1200i (referred as ‘FETTE’, Fette compacting GmbH, Schwarzenbek, Germany) is given in Fig. 1 and more details can be found in [170, 186, 236, 267]. In brief, the system consists of three paddle wheel zones with a dosing wheel on top (green in Fig. 1, DW, either cylindrical (DW-●) or cuboid (DW-■) shaped blades) connected by two holes at the bottom (yellow in Fig. 1) to the below located zones. A counter-clockwise rotating reverse dosing wheel (red in Fig. 1, RW, cuboid shaped blades) and a clockwise rotating filling wheel (pink in Fig. 1, FW, either cylindrical (FW-●) or cuboid (FW-■) shaped blades) are located on the left and right hand side bottom of the force feeder, respectively. The FW and RW are not interlocking with each other, though a small open intersection between the zones allows powder exchange. The system was split into the feeding hopper and the three paddle wheel zones (DW-Z, FW-Z, and RW-Z) for quantitative analysis [170, 186, 236, 267].

The KIKUSUI Virgo tableting machine (referred as ‘KIKUSUI’, Kikusui Seisakusho Ltd., Kyoto, Japan) has two paddle wheels of the same shape (Fig. 1). The left hand side paddle (LHSP) is rotating in counter-clockwise, the right hand side paddle (RHSP) in clockwise direction. Each wheel has 12 blades of a length of 53.0 mm and a cylindrical inner shaft of 45.0 mm radius and 28.0 mm height. The blades height and width are higher at the center (height: 8.4 mm, width: 9.9 mm) and decrease linearly towards the tip (height: 5.1 mm, width: 6.2 mm). The maximum height of the housing is 28 mm (Fig. 1 ‘D’). In the front region of the force feeder involved in die filling, the housing height is decreased to 10 mm (Fig. 1 ‘E’). This results in a blade depth of immersion, defined as the ratio of blade height to powder bed height, of 22% and 35% [209–211, 236, 267]. The blade side face oriented towards the rotation direction through 143° inclination angle which is named as ‘obtuse’ blade rake angle according to impeller blade studies [197, 267]. Both paddle wheels are interlocking. The turret with 18 punch stations and a radius of 20.5 cm rotates in counter-clockwise direction (Fig. 1). Powder is supplied to the force feeder from a feeding hopper which is oval and cylindrical shaped at the bottom and top, respectively. The hopper is located at the back side of the LHSP. The force feeder was split into different sections, namely the LHSP bottom (L-B, pink), LHSP top (L-T, green), RHSP bottom (R-B, red) and RHSP top (R-T, yellow) to facilitate the analysis and it is illustrated in Fig. 5 ($t = 0$ s).

The most distinct geometrical differences between the KIKUSUI and FETTE force feeders are the following:

- Paddle wheels: number of paddle wheels, depth of immersion (confer to [267]), and number, shape, and dimension of blades
- Force feeder housing: height, connection between paddle wheels, volume, and area involved in die filling
- Feeding hopper: volume, shape, location, and connection to paddle wheels

- Turret: diameter, position underneath the force feeder, number of dies, width of arc, and circle of segment length involved in die filling

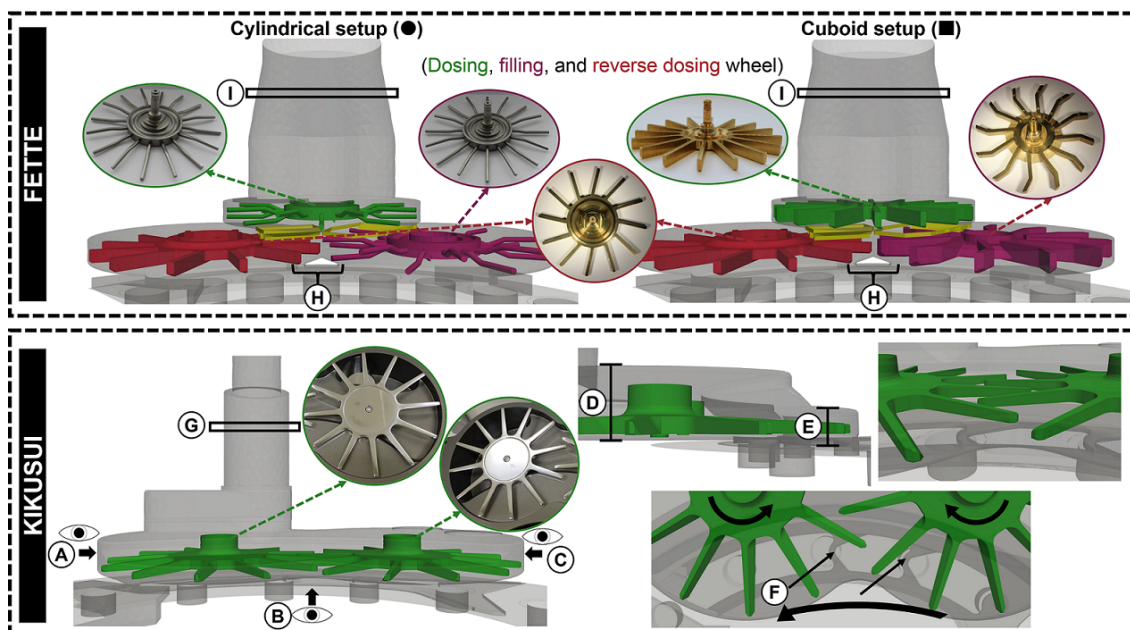


Fig. 1: FETTE (top, cylindrical and cuboid setup) and KIKUSUI (bottom) system illustrations (the images of the paddle wheels in KIKUSUI are shown in bottom view).

2.3 Material properties

A poly-disperse particle size distribution (PSD) consisting of 7 size fractions ($d_{50} = 2107 \mu\text{m}$) is considered in simulations to reflect a direct compression (DC) formulation. Out of those fractions, one size fraction serves as model ‘API’ with a weight fraction of 5% and $1000 \mu\text{m} < x \leq 1129 \mu\text{m}$. Details on the PSD and the material properties are in detail described in our previous studies [170, 186, 236, 267] and given in Tab. 1. The approach of particle size enlargement was considered in other DEM studies, too, though it could provide a general powder flow analysis [41, 93, 94]. The current model cannot represent the influence of very fine particles ($x < 10 \mu\text{m}$) as found in pharmaceutical powders on powder flow issues. The particle shearing in chapter 3.1.2 is related to a potential transformation of particle characteristics (e.g. particle attrition or over lubrication), though the material properties are kept same for the complete computation time, similar as reported by Ketterhagen [41].

2.4 System filling and numerical conditions for high speed tableting

2.4.1 System filling procedure

The procedure for system filling was described in previous studies for FETTE [170, 186, 236, 267] and was performed similarly for KIKUSUI in the current study (details in chapter 3.1.1). The material properties in terms of inter-particle cohesion and particle-wall friction were set to 1.5 MJ/m^3 and 0.30, respectively (Tab. 1). This allows to generate same status quo for different setups in high speed tableting. A similar approach was employed in previous studies [168, 169, 187]. Filling of the system with particles consisted of three steps. It started with the filling of (1) the feeding hopper (until $t = 1.2 \text{ s}$). Afterwards (2) the complete force feeder was filled by slow paddle wheel rotation (at 15 rpm, until $t = 10.2 \text{ s}$). The system filling was completed by (3) one turret rotation (at 10 rpm) and slow

paddle wheel rotation (at 15 rpm, until $t = 16.2$ s) [170, 186, 236, 267]. Supplementary videos of the process support the following description (chapter 5).

Mass distribution

The mass and API content distribution over time were non-uniform in the different sections of the force feeder (confer chapter 2.2), as shown in Fig. 2A & B. Particles were fed from the feeding hopper initially into the LHSP sections causing an increase in the bulk mass in the bottom section (L-B) followed by the top section (L-T). They got then distributed from the LHSP sections by paddle wheel rotation to the RHSP sections until mass steady state was reached after 16.2 s in all sections (Fig. 2A). The final mass of 2145 g was distributed into the feeding hopper (727 g) and into the paddle wheel sections (358 g in L-B, 311 g in L-T, 346 g in R-B, and 327 g in R-T). The remaining mass of 76 g was located in the die filling region between force feeder and turret and in the first filled dies. The feeding hopper contained 31% less mass whereas the paddle wheel zones had twice the mass in KIKUSUI compared to FETTE [170, 236]. This implies that with the existing mass in the paddle wheel sections / zones (KIKUSUI / FETTE) about 254, 128, and 108 dies could be completely filled in KIKUSUI, ● and ■ shaped paddle wheel setups in FETTE, respectively.

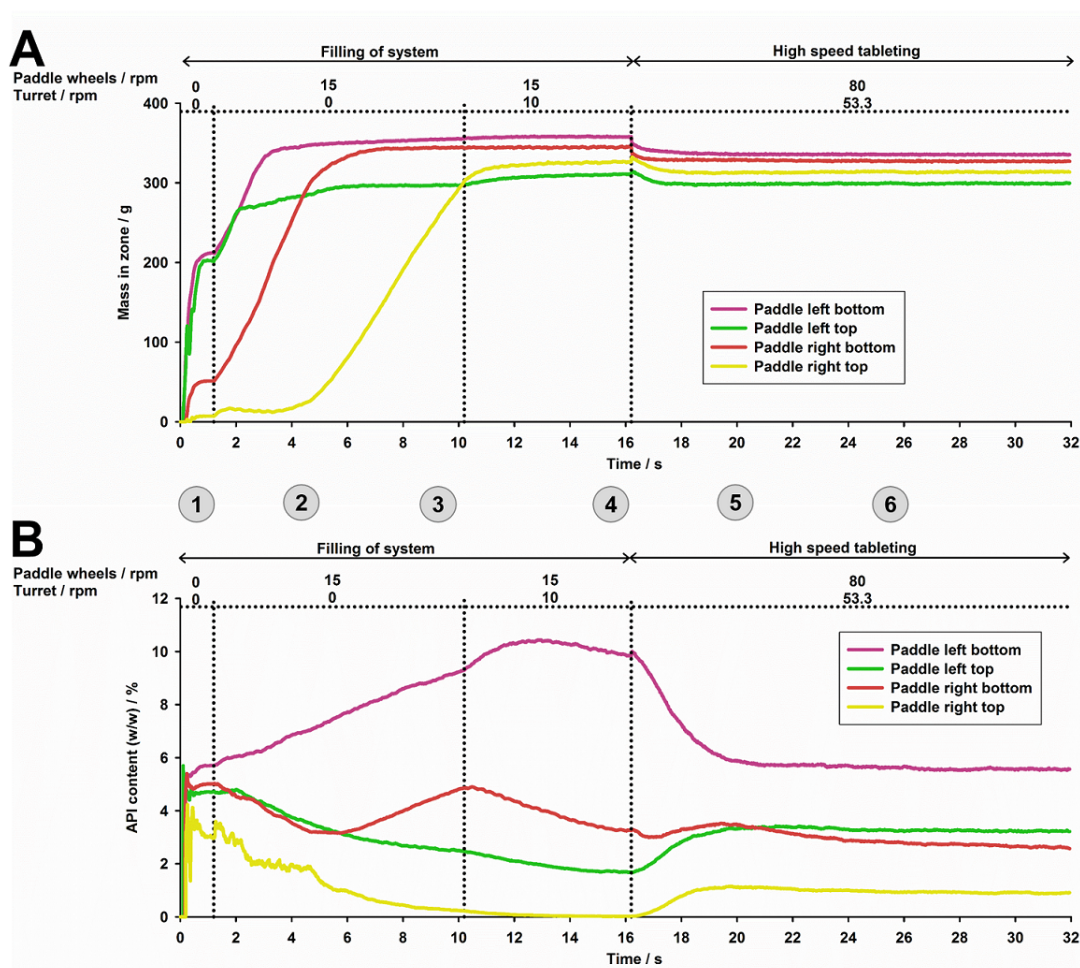


Fig. 2: (A) Mass and (B) API content during system filling and high speed tableting in four sections of the KIKUSUI force feeder (for the color code of the different sections confer to Fig. 3 & 5).

API content distribution

Though the specified API content of the DC model formulation was 5% (w/w) (confer to chapter 2.3), the API contents at the end of system filling ($t = 16.2$ s, Fig. 2B) were 9.8% in L-B, 1.7% in L-T, 3.8% in R-B, and 0.0% in R-T. In Fig. 3 the system is illustrated from different views, i.e. from left hand side (Fig. 1 'A'), front (Fig. 1 'B'), and right hand side (Fig. 1 'C'). The particles are colored by their size and velocity to facilitate the explanation of the API content differences (Fig. 3). The blades of the paddles conveyed solely 22-35% of the powder bed height and only the bottom of the force feeder (chapter 2.2, Fig. 1). The low depth of immersion and the very low paddle wheel rotation speed (15 rpm) led to low particle velocities favoring particle size segregation due to sieving / percolation mechanisms (Fig. 3). These type of mechanisms imply that the finer particles percolated through the larger particle voids to the bottom [181, 195]. These mechanisms have been reported previously for powder mixing by impeller blades [197, 199] and for force feeders [93]. The API particles, considered as fines in the current model and DC formulation ($x \leq 1800$ μm), percolated to the bottom of the L-B and accumulated there to highest extent at the end of system filling (Fig. 2B, $t = 16.2$ s, Fig. 3 '4'). From the L-B the particles got distributed into the R-B (Fig. 2B). Once the fines have started percolating to the feeder bottom (either in the LHSP or RHSP), they hardly appeared in one of the top sections at the end of filling (Fig. 2B and 3). The wave-like API content pattern in the R-B can be explained as follows (Fig. 2B). When the force feeder started to get filled at the beginning ($t < 5.0$ s), predominantly coarse particles could roll directly from the feeding hopper due to trajectory mechanism [195] into the R-B causing an API content (considered as fine particles) decrease. Once the L-B, L-T, and R-B sections were completely filled ($5 \text{ s} < t < 10.2$ s, Fig. 2A), the R-T got filled up and fines percolated / sieved from the same to the bottom (= R-B). This led to a steep API content increase in R-B. Once turret rotation was started at $t = 10.2$ s, the accumulated fines in the R-B discharged into the dies resulting in an API content decrease in R-B (Fig. 2B, $10.2 \text{ s} \leq t \leq 16.2$ s).

After system filling (Fig. 3 '4'), the smaller particles ($x \leq 1800$ μm) are in particular 'trapped' in (1) the bottom front part of the force feeder involved in die filling, (2) the interlocking region of the paddle wheels (more details are given in chapter 3.1.2), and (3) the front face of the rotating blades. Size segregation was quantitatively overestimated compared to reality due to the larger particle sizes considered (chapter 2.3), however the qualitative results are in agreement with literature data [93].

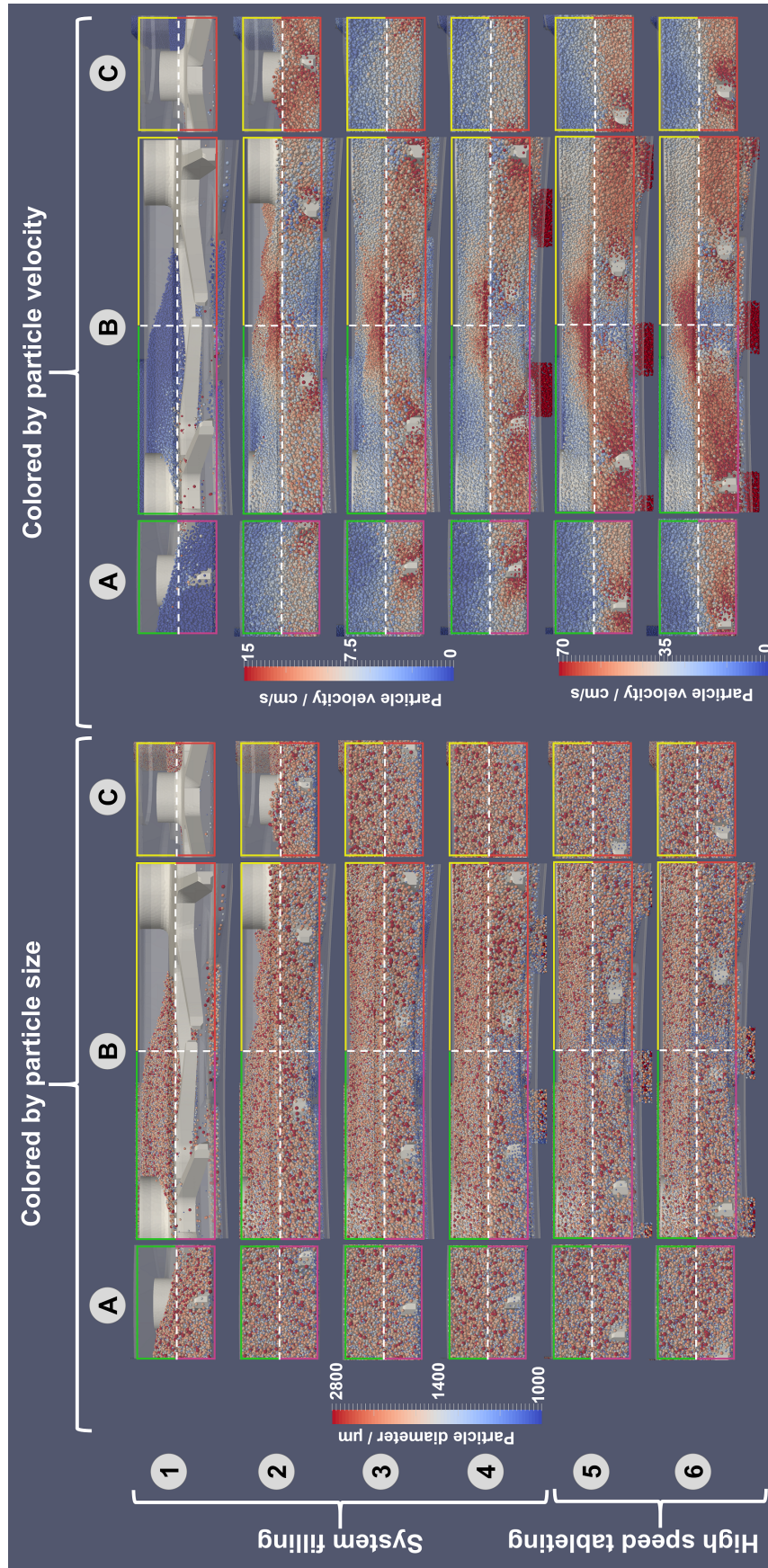


Fig. 3: Different perspectives (confer to Fig. 1) on particles colored by their size (left) and velocity (right) during system filling (time point '1-4' in Fig. 2) and high speed tableting (time point '5 & 6' in Fig. 2).

2.4.2 Numerical setups for high speed tableting

The tablet quality is compared for the two force feeders in chapter 3.2 considering different conditions for high speed tableting. In extension to the previous work (comparison of different paddle wheel shapes in FETTE [267]) additional setups for KIKUSUI were generated. The differences in terms of turret radius (14 cm vs 21 cm) and number of punch stations (24 vs 18) between FETTE and KIKUSUI impede a one-to-one comparison. Different approaches were applied to develop different conditions for comparison.

(1) The first condition corresponds to a high paddle wheel speed and low turret speed in combination with a good powder blend flowability (low inter-particle cohesion and low particle-wall friction, Tab. 1) [267]. For condition 1 either equal process conditions as in FETTE in terms of absolute paddle wheel speed and turret speed (referred as 1K-P) or in terms of mass throughput were developed (referred as 1K-M). For the latter the same number of tablets were produced in time (57600 tablets / hour) at a turret speed of 53.3 rpm keeping the turret to paddle wheel speed ratio of 2/3 as in setup 1K-P.

(2) The second condition was chosen from the previous studies simulating an unfavorable combination of process parameters and a poor powder blend flowability (high inter-particle cohesion and high particle-wall friction, Tab. 1) [186, 267]. Likewise as for condition 1, KIKUSUI setups considering same process conditions (2K-P) and same mass throughput (2K-M) were performed (Tab. 1). For each condition (1 and 2) the tablet quality was compared between the cylindrical (F●) and cuboid (F■) paddle wheel shapes in FETTE (Fig. 1) and the two combinations of process parameters in KIKUSUI (K-P and K-M). Thus for each condition 4 setups were generated (Tab. 1).

Powder flowability for condition 1 and 2 was measured in terms of angle of repose (AOR) and mass flow rate through an orifice (MFR) according to Ph. Eur. [25]. The AOR and MFR resulted in 12.3° and 12.9 g/s for condition 1 and 20.5° and 10.5 g/s for condition 2, respectively. The AOR is lower than found in real DC blends given by the larger particle sizes considered. It was shown in our previous study for the FETTE machine that a low μ_{PW} is providing a high tablet mass and a low tablet mass variation. A low inter-particle cohesion resulted in a slightly higher tablet mass [186].

During high speed tableting in KIKUSUI and FETTE, the randomly mixed DC blend was constantly re-filled into the feeding hopper as mass was discharged into the dies. The same configuration for fill and dosing cam was used. In order to minimize the impact of large particle sizes considered (chapter 2.3) on die filling, a large die diameter was chosen [179]. This way the ratio between die diameter to mean particle diameter is maintained at higher than 14.

A total number of 287,000 and 333,000 particles were in the completely filled systems of FETTE and KIKUSUI, respectively. The computation of a physical time of up to 32 s for one single setup (8 in total, Tab. 1) on a workstation having 72 processors running in parallel took > 4 months. Hence, computation was only performed until mass steady state in high speed tableting measured in terms of constant mass hold up in the force feeder was reached. It comprised the filling of > 232 dies.

Tab. 1: Process conditions and material properties during system filling and high speed tableting (* marked properties are changed between system filling and high speed tableting) [262]. Condition 1 and 2 have same factor combinations as reported in our previous work [186]. F● corresponds to the cylindrical shaped paddle set, F■ to the cuboid shaped paddle wheel set in FETTE. Data written in *italic letters* was reported in our previous work [186]. The KIKUSUI setups K-P and K-M consider same process conditions as in FETTE (F) or same number of tablets filled per time as in FETTE (M), respectively. Best and worst overall CQA desirability for each condition are colored in green and red, respectively.

System filling	Young's modulus / GPa		Condition no.							
	particle-particle ratio / -	particle-wall	1		2		2			
Coefficient of restitution / -	particle-particle	particle-wall	1F●	1F■	1K-P	1K-M	2F●	2F■	2K-P	2K-M
	particle-particle	particle-wall	FETTE	FETTE	KIKUSUI	KIKUSUI	FETTE	FETTE	KIKUSUI	KIKUSUI
Coefficient of friction / -	particle-particle	particle-wall	cylindrical	cuboid	-	-	cylindrical	cuboid	-	-
	particle-particle	particle-wall	40	60	53.3	80	75	30	75	100
Cohesion energy density / CED / MJ/m ³			1.00*		1.00*		1.00*		1.00*	
			1		2		2		2	
Setup symbol			1F●		1F■		1K-P		1K-M	
			FETTE		KIKUSUI		KIKUSUI		KIKUSUI	
Tableting machine			cylindrical		cuboid		cylindrical		cuboid	
			40		60		75		100	
Paddle wheel shape			60		80		30		40	
			60		80		30		40	
Turret speed / rpm			1.0		3.5		3.5		3.5	
			0.25		0.75		0.75		0.75	
Paddle wheel speed / rpm			0.35		0.29		0.19		0.16	
			5.1		5.2		2.7		4.6	
Cohesion energy density (CED) / MJ/m ³			5.1		5.1		2.7		4.6	
			1.1		0.9		14.8		3.2	
Coefficient of friction, particle-wall / -			254.3		266.5		124.1		265.5	
			5.0		5.1		4.6		5.8	
Die filling time underneath force feeder (t_{fill}) / s			100.1		103.3		91.2		115.7	
			12.0		19.3		15.3		26.6	
Mean tablet mass (\bar{m}) / g (CQA)			26.6		44.5		41.0		73.0	
			0.79		0.65		0.15		0.17	
Mean tablet mass variation / % (CQA)			13.1		17.7		8.0		10.1	
			5.2		7.1		5.8		6.2	
Mean API content in dies (w/w) / %			-12.9		-3.7		-28.5		-11.2	
			22.2		18.7		20.9		54.4	
Mean API relative to label claim content (\bar{X}) / %			18.7		49.1		16.6		54.4	
			18.7		49.1		16.6		54.4	
Standard deviation of X (s) / %			18.7		49.1		16.6		54.4	
			18.7		49.1		16.6		54.4	
AV / - (CQA)			18.7		49.1		16.6		54.4	
			18.7		49.1		16.6		54.4	
CQA desirability value / -			18.7		49.1		16.6		54.4	
			18.7		49.1		16.6		54.4	
Mean residence time / s			18.7		49.1		16.6		54.4	
			18.7		49.1		16.6		54.4	
First particles discharged into the dies / s			18.7		49.1		16.6		54.4	
			18.7		49.1		16.6		54.4	
Change of mass hold up / %			18.7		49.1		16.6		54.4	
			18.7		49.1		16.6		54.4	
Remained mass in force feeder after discharge of 630 g in dies / %			18.7		49.1		16.6		54.4	
			18.7		49.1		16.6		54.4	

3 Results and Discussion

First of all, the powder flow pattern in the force feeder of the KIKUSUI tableting machine during high speed tableting is explained (chapter 3.1). It intends to establish a basis for the comparison of the tablet quality obtained in FETTE and KIKUSUI tableting machines for different numerical setups (chapter 3.2). Details on the powder flow in the FETTE tableting machine are reported in our previous studies [170, 186, 236, 267].

3.1 Powder flow in the KIKUSUI tableting machine

In this chapter, the powder flow during high speed tableting in KIKUSUI is exemplarily explained for one setup considering a turret speed of 53.3 rpm, paddle wheel speed of 80 rpm, inter-particle cohesion of 1.0 MJ/m³ CED, and particle-wall coefficient of friction of 0.25 (setup 1K-M, chapter 2.4.1, Tab. 1). The following quantitative and qualitative evaluations are described: mass hold up and particle size segregation in the force feeder, powder flow into the die including content uniformity, and particle trajectories combined with particle residence time in the force feeder. The key metrics for all KIKUSUI setups are provided in Tab. 2 for further reference, though they are not described for the sake of brevity.

Tab. 2: Key metrics during steady state of high speed tableting for KIKUSUI setups

		1K-P	1K-M	2K-P	2K-M
Steady state during high speed tableting / s		9.1-21.0	4.1-15.8	6.1-11.2	5.1-8.4
API content in section / %	L-B	5.8	5.6	6.6	6.5
	L-T	2.7	3.3	2.8	3.0
	R-B	2.3	2.9	1.8	1.7
	R-T	0.4	1.0	0.2	0.2
Mean particle velocity in section / cm/s	L-B	36.5	47.3	16.4	21.4
	L-T	10.8	13.7	5.4	6.8
	R-B	43.7	53.9	18.1	23.6
	R-T	18.9	24.7	10.7	12.6
Mass relative to max. mass of complete blend in die from RHSP / %		98.9	96.1	45.7	61.4
Mass relative to max. mass of API in die from RHSP / %		73.1	75.1	27.5	46.1
Remained mass in zone after discharge of 630 g in dies / %	L-B	10.1	7.9	12.9	11.8
	L-T	10.2	9.9	15.7	14.4
	R-B	11.9	11.0	22.3	24.0
	R-T	31.9	26.1	31.7	34.9

3.1.1 Mass hold up and particle size segregation

Like in system filling, the mass and API content in the different sections of the force feeder for high speed tableting are given in Fig. 2A & B. The mass hold up decreases until equilibrium is reached between the mass discharged into the dies and the mass refilled from the feeding hopper into the paddle wheel sections (Fig. 2A). In comparison to system filling (chapter 2.4.1), the mass hold up in the complete force feeder decreases by 4.9% (Tab. 1 ‘Change of mass hold up’) to 336 g in L-B, 299 g in L-T, 327 g in R-B, and 314 g in R-T. The significant overhead mass in the top sections ensures a sufficiently high mass refill into the bottom sections from where mass is discharged into the dies. Consequently the front part of the force feeder involved in die filling is constantly filled with particles (Fig. 3). Recirculation between inter-blades is diminished as a packed powder bed on top of

the blades is found. As the blade is pushing, a few particles are sliding from one inter-blade zone into the following one as shown in Fig. 3. In contrast, a dominant recirculation phenomenon was found in FETTE [236, 267]. When the blade was pushing into the powder bed, the small free volume above the blade enabled particles to jump over. The minor mass hold up difference between high speed tableting and system filling in KIKUSUI results in a high packing density within the feed frame. It prevents size segregation by the trajectory mechanism [181, 195, 212, 213]. Thus larger particles may not travel along their trajectories, hampered by the low void volume in the inter-blade zones (Fig. 3). In contrast to KIKUSUI, segregation by trajectory mechanism was identified in the paddle wheels zones of the RW and FW-■ in FETTE [236, 267].

3.1.2 Particle velocity and API content distribution

The paddle wheel speed increase from 15 rpm (blade tip speed = 15 cm/s) during system filling to 80 rpm (blade tip speed = 82 cm/s) during high speed tableting leads to a significant particle velocity increase as shown in Fig. 3. The particles at the bottom of the LHSP and RHSP receive highest momentum by contact with the rotating blades and show mean particle velocities of 47.3 cm/s in L-B and 53.9 cm/s in R-B (Tab. 2). In contrast, a clear shear zone between the top and bottom sections develops with relative top to bottom particle velocity differences of 71.0% in the left and 54.1% in the right hand half of the force feeder, respectively. Twice the particle velocity is found in the R-T (24.7 cm/s) compared to the L-T (13.7 cm/s). Particle trajectory analysis (confer below) revealed that the complete powder bulk is agitated in the R-T by momentum transfer from the R-B and is rotating around the RHSP radial axis. In contrast, an off-centered part in the L-T is stationary over the complete discharge time. This gives the explanation for the lower particle velocity in the L-T compared to the R-T (Tab. 2).

The distinct shear zone and the overall higher particle velocities compared to system filling reduce the extent of size segregation by percolation / sieving mechanisms [197, 236]. As a consequence, less fines percolate to the bottom sections compared to system filling. This induces an increase of the API content in the top sections and decrease in the bottom sections, respectively (5.6% L-B, 3.3% L-T, 2.9% R-B, 1.0% R-T during mass steady state ($t = 20.3 - 32.0$ s), Fig. 2B, Tab. 2). The qualitative visualization of the system in Fig. 3 also shows that in the middle, front part of the force feeder (interlocking region, Fig. 3 ‘B’) a small area is found in which the fines accumulate. The blades of the paddle wheels do not overlap in this area resulting in low particle velocities. In particular smaller particles ($x \leq 1800$ μm) cannot follow the opposite particle trajectories attributed to the opposite rotating paddle wheels (Fig. 1) and get trapped in this area. The differences in particle velocities between bottom and top sections imply that the fine particles, which are majorly located in the bottom sections after system filling (Fig. 2B, chapter 2.4.1), are subjected to higher shear forces (higher particle velocities, confer below) compared to the coarse particles in the top sections.

3.1.3 Powder flow into the die

Each die arrives at the force feeder underneath the RHSP as the turret is rotating in counter-clockwise direction. Initially, the die volume is generated by lowering the lower punch up to 1.5 cm ($t = 0.11$ s in Fig. 4), in the region called fill cam. The particles steadily discharge into the die, solely interrupted by two short scrapers at the bottom of the force feeder at $t = 0.085$ s and $t = 0.130$ s (Fig. 1 ‘F’), resulting in 96.1% of maximal mass filled from the RHSP (Fig. 4 ‘A’). The die volume is kept constant as the die is moving underneath the LHSP (Fig. 4 ‘B’). Only 3.9% of the maximal mass in the die comes from the LHSP (Fig. 4 ‘B’). Small particles (diameter < 1800 μm , including API particles), that accumulate in the L-B (confer above and Fig. 2B), can fill up the particle voids in the

die resulting in relative die mass contributions from LHSP up to 33.5% (Fig. 4). After the die has left the force feeder ($t = 0.24$ s in Fig. 4), the lower punch is slightly moved upwards to partly scrape material and to provide a more confined powder bed in the die prior to the powder compaction step (final die height of 1.3 cm, Fig. 4 'C'). The last filled particles, in particular the smaller particles (confer above), are scraped to a higher extent in comparison to the larger particles which entered the die first (Fig. 4). Regional API content differences with a lower one at the bottom and higher one at the top side of the die are found. Differences in PSD over the die height could lead to different powder compaction properties [214–220] constituting a potential risk for tablet capping.

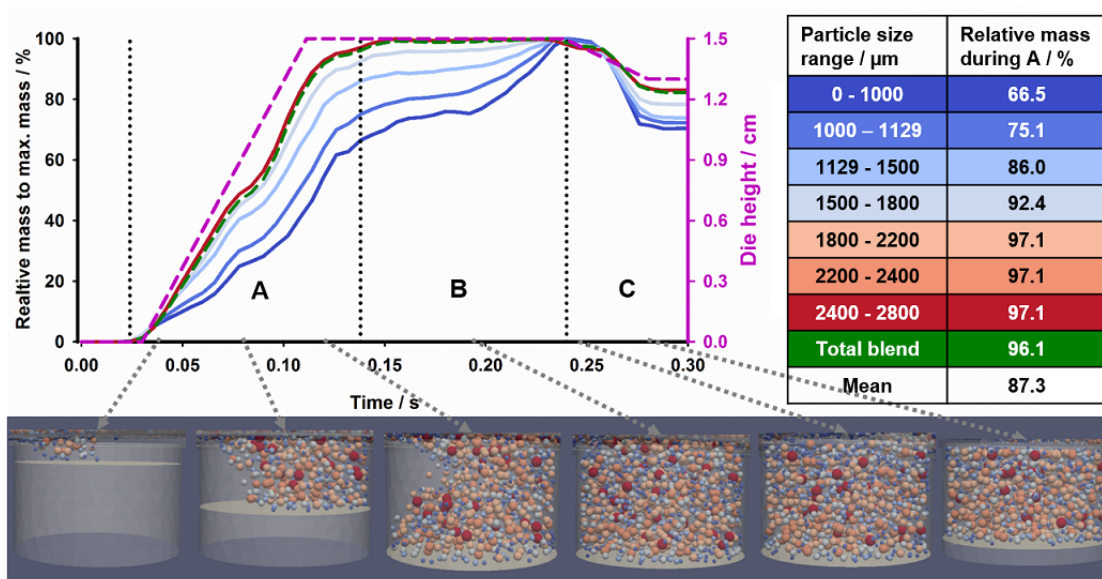


Fig. 4: Mass filled into the die relative to maximal mass per particle size fraction underneath (A) RHSP, (B) LHSP, and (C) dosing cam. Table: Mass relative to max. mass filled from RHSP into the die for different particle size fractions. Bottom: Screenshots of die during filling where particles are colored according to their size (for scale refer to Fig. 3).

A mean tablet mass of 5.13 ± 0.05 g (0.9% RSD) is obtained in 14 rotations of the turret (Tab. 1). This tablet mass is significantly higher than in reality given by the much larger die diameter and the larger particle sizes considered (chapter 2.3 and 2.4).

The final mean API mass is 258.6 ± 41.4 mg (16.0% RSD) corresponding to a mean API content (w/w) of $5.04 \pm 0.78\%$ (15.4% RSD, API mass divided by tablet mass). The API content relative to the label claim content (5% (w/w), chapter 2.3) is $100.4 \pm 16.8\%$ (\bar{X} , Tab. 1, Fig. 9). The initially filled dies show a higher \bar{X} given by the accumulation of fines in the die filling zone and bottom sections of the force feeder during system filling (chapter 3.1.1, Fig. 3 'B', Fig. 9). A rather constant relative API content is found during steady state (Fig. 9). All produced tablets are analyzed for content uniformity (CU) according to Ph. Eur. 2.9.47 [25] via the Acceptance value (AV) defined in Eq. 1 and in detail explained in our previous work [186].

$$AV = |M - \bar{X}| + k * s \quad (1)$$

With

AV acceptance value

M reference value

	if $98.5\% \leq \bar{X} \geq$ then $M = \bar{X}$
	if $98.5\% > \bar{X} \geq$ then $M = 98.5\%$
	if $101.5\% < \bar{X} \geq$ then $M = 101.5\%$
\bar{X}	mean of individual contents (x_1, x_2, \dots, x_n)
k	acceptability constant
	if $n = 10$ then $k = 2.4$
	if $n = 30$ then $k = 2.0$
n	number of samples
s	sample standard deviation

An AV of 37.1 is obtained (Tab. 1) which exceeds the $L1$ and $L2$ criteria to meet CU [25] (more explanation on the calculations and the criteria are provided in [186]). The very high value arises from the high standard deviation of the relative API content (s , Tab. 1). It originates from the large particle sizes considered and the low die volume (chapter 2.3 and 2.4). On average 215 API particles and in total 833 particles are filled into the die, i.e. giving a \bar{X} of 100.4% (Fig. 4 & 6). An increase in API particles by 5% (+10 API particles; i.e. 225 API particles and in total 843 particles) leads to a significant increase in \bar{X} to 105.6%. Hence very little differences in the API particles distribution in the die have a significant effect on CU calculations in the current model. Though the AV is unrealistic, it will be used in section 3.2.2 to unveil general differences between the KIKUSUI and FETTE tableting machine.

3.1.4 Particle trajectories and residence time

The particles are colored by their initial position as high speed tableting is started to visualize the particle trajectories over time (Fig. 5). In addition to the four sections in the force feeder (L-B, L-T, R-B, and R-T), four horizontal zones with a width of 5 mm (white) separated by layers of 22 mm of uncolored particles (blue) are defined in the feeding hopper (Fig. 5). A supplementary video is provided in chapter 5 for visualization. The ratio between colored mass at the beginning and after a discharge of 630 g mass into the dies (at $t = 8.0$ s of high speed tableting, rationale for this mass given in chapter 3.2.4 and in [267]) is calculated in the L-B, L-T, R-B, and R-T (Fig. 5) to estimate the mass throughput in the individual sections. The observations can be summarized as follows:

- A predominant particle mixing from the top into the bottom sections is found (e.g. green colored particles from L-T in L-B at $t = 1.13$ s). The trajectory from top to bottom is consistent with the percolation / sieving size segregation mechanisms described above. The other way round, an interchange between bottom to top sections is solely found in the interlocking region of the LHSP and RHSP given by their opposite rotation directions.
- Particles from the feeding hopper (blue) get distributed first into the LHSP sections before they arrive in the RHSP sections. Solely the right hand half of the hopper is involved in the refilling of the paddle wheel sections given by the counter-clockwise rotation direction of the LHSP. A similar observation was made in the FETTE feeding hopper and the DW-● [236].
- The highest mass turnover in the LHSP sections is found in the radial left and front part. Green colored particles at the central middle/back side remain there stationary over the complete high speed tableting time. This dead zone gives the explanation for the lower mean particle velocity in the L-T compared to the R-T (chapter 3.1.1, Tab. 2).

- Particles from the LHSP sections arrive at the outer back radial part of the RHSP for refilling. The particles in the middle part of the RHSP section do not get interchanged over time but rather get stirred around the radial axis of the RHSP (confer above). On the contrary, a high intermixing and material turnover is found in the outer radial part of the RHSP from where predominantly the particles discharge into the die (Fig. 4) and in which an efficient mass re-fill is required.
- After discharge of 630 g, 7.9%, 9.9%, 11.0%, and 26.1% of initially located mass in L-B, L-T, R-B, and R-T have remained in the same, respectively (Tab. 2). It highlights that highest mass

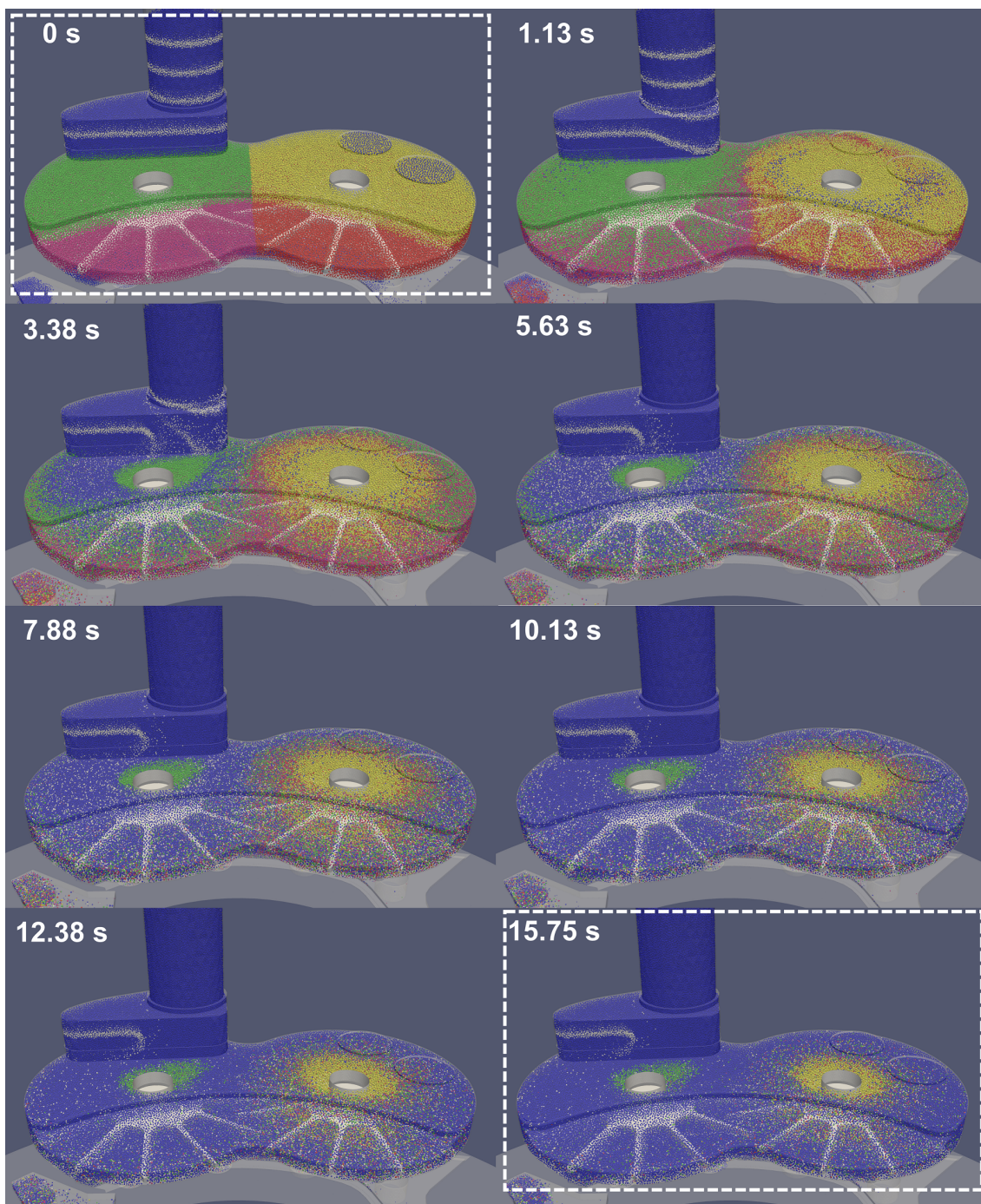


Fig. 5: Qualitative illustration of colored particles distribution at start of ($t = 0$ s) and during high speed tableting.

turnover is found in the LHSP sections which are predominantly refilling the RHSP sections. The low inter-mixing in the center of the RHSP (confer above) is reflected by the high remained mass in the RT (ratio of 26.1%). The second highest ratio of 11.0% is found in the R-B and can be explained by the predominantly radial and non-axial mass turnover.

- The left hand half of the feeding hopper and off-center of the L-T constitute dead zones in the force feeder. Least inter-mixing, though particle movement is found in the middle / central part of the RHSP.

The transport of the material from the feeding hopper through the force feeder into the dies can cause particle shearing. This may lead to an impairment of tablet tensile strength and dissolution [42, 76, 102, 205–208], especially for shear sensitive formulations [110]. Similar to the approach in the previous study [267], the shearing in the force feeder of KIKUSUI is evaluated. The particle velocity and particle residence time in the four sections of the force feeder can serve as a surrogate for particle shearing [267] and are listed in Tab. 2. Even though the particle velocity in the R-T is moderate, the particles are trapped there for the longest time. Out of all sections, a potentially high particle shearing could be found in the R-T. The analysis shows that in practice particles can undergo different shearing depending on their trajectories within the force feeder. It might only provide an estimate for particle shearing though it does not consider exact forces acting on the particles, as proposed by Ketterhagen [41]. In addition, it might oversimplify the actual shear stress as it does not take into account, e.g. particle acceleration, packing density, and relative particle-to-particle velocities found between the bottom and top zones and the interlocking region of the paddle wheels.

Selected particles, initially located in a horizontal slice of 5 mm height and over the complete width of the cylindrical part of the feeding hopper are tracked over high speed tableting time (confer Fig. 1 ‘G’ and Fig. 5 at $t = 0$ s top white colored particle layer). Out of the 20.4 g tracked material, only 58% discharge into the die within 15.8 s of high speed tableting. The particles require at least 5.7 s to travel through the force feeder (Tab. 1) and may rotate several times in the LHSP sections before they get distributed into the RHSP sections and then discharge into the die. Their mean residence time in the force feeder is 13.7 s (Tab. 1) which is consistent with a similar geometrical force feeder setup reported by Mendez et al. [86]. The accumulation of fines at the bottom of the force feeder which is facilitating the discharge into the dies leads to a slightly reduced residence time, i.e. 12.3 s for API particle size fraction.

3.2 Comparison of tablet quality for different tablet machines

Mean tablet mass, tablet mass variation, and content uniformity are, amongst others, considered as critical quality attributes (CQAs, in detail described in our previous study [186]). Those are, in contrast to e.g. tablet tensile strength, measurable with the current DEM model (chapter 2.3). The CQAs are related to different conditions and the two tableting machines, KIKUSUI and FETTE (confer chapter 2.4.2, Tab. 1). All data for FETTE setups (Tab. 1; 1F●, 1F■, 2F●, 2F■) are explained in detail in our previous work [267] and are repeated here for comparison purposes only. Although the conditions differ in terms of process parameters and material attributes, CQAs are mainly related to process condition differences and not material attributes, as reported previously [186, 267]. The KIKUSUI setups in both conditions (1K-P vs 1K-M and 2K-P vs 2K-M, Tab. 1 & 2) could be compared and discussed, but are actually not in the present manuscript for the sake of brevity.

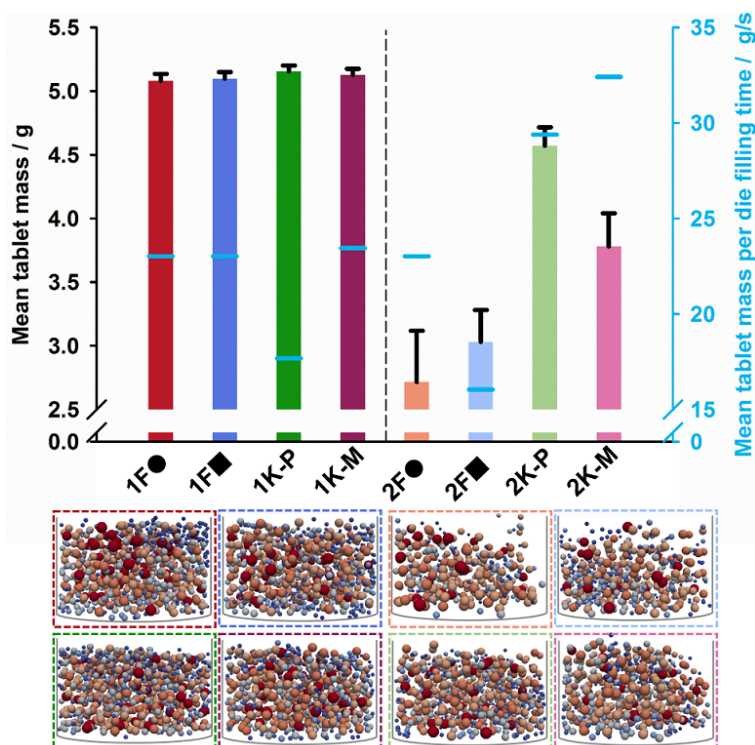


Fig. 6: Mean tablet mass (left y-axis) and mean tablet mass per die filling time (right y-axis) for the different setups. Bottom: Exemplary filled dies for all setups (confer for color code to graph legend). Particles are colored by their size (for scale refer to Fig. 3).

3.2.1 Tablet mass and tablet mass variation

A significant difference in tablet mass is found between the four setups in each condition by one-way ANOVA analysis ($p \leq 0.001$ at $\alpha = 0.05$). All four setups in condition 1 provide similar mean tablet mass, though lowest tablet mass variation (RSD) is found for setup 1K-P (Fig. 6, Tab. 1). Although the length of the die filling segment underneath the force feeder is higher in KIKUSUI (25 cm) compared to FETTE (21 cm), the die filling times at the given turret speeds in condition 1 for KIKUSUI and FETTE setups are sufficiently long to provide complete die filling for all setups (Tab. 1, confer screenshots of dies in Fig. 6).

More distinct differences between KIKUSUI and FETTE force feeders are found at the unfavorable combination of high turret – low paddle wheel speed and low powder flowability (condition 2). All setups show incomplete die filling (qualitative illustration of filled dies in Fig. 6). In real experiments this would entail an adaption of process parameters, though general dependencies related to force feeding capabilities in KIKUSUI and FETTE can be unveiled. The highest tablet mass with lowest tablet mass variation is found for setup 2K-P (Tab. 1). A relatively high mean tablet mass for setup 2K-M is obtained though it has the highest tested tableting speed of 100 rpm (Fig. 6, Tab. 1). Normalization of the mean tablet mass to the die filling time ($\frac{\bar{m}}{t_{fill}}$) allows an easier comparison of the force feeding capability (Tab. 1, lines in Fig. 6, right y-axis). For condition 1, the setups 1F●, 1F■, and 1K-P have similar $\frac{\bar{m}}{t_{fill}}$ whereas it is lower for 1K-M. This one surrogates a lower $\frac{\bar{m}}{t_{fill}}$ though the die is already completely filled and the $\frac{\bar{m}}{t_{fill}}$ is limited by the die volume. Two main explanations can be provided for the significantly higher $\frac{\bar{m}}{t_{fill}}$ for the KIKUSUI setups, 2K-P and 2K-M, compared to the FETTE setups, 2F● and 2F■ in condition 2 (Fig. 6).

First, a sufficiently high powder mass is offered in the front portion of the KIKUSUI force feeder involved in die filling (Fig. 7, 2K-M). This is attributed to (1) the larger force feeder volume in

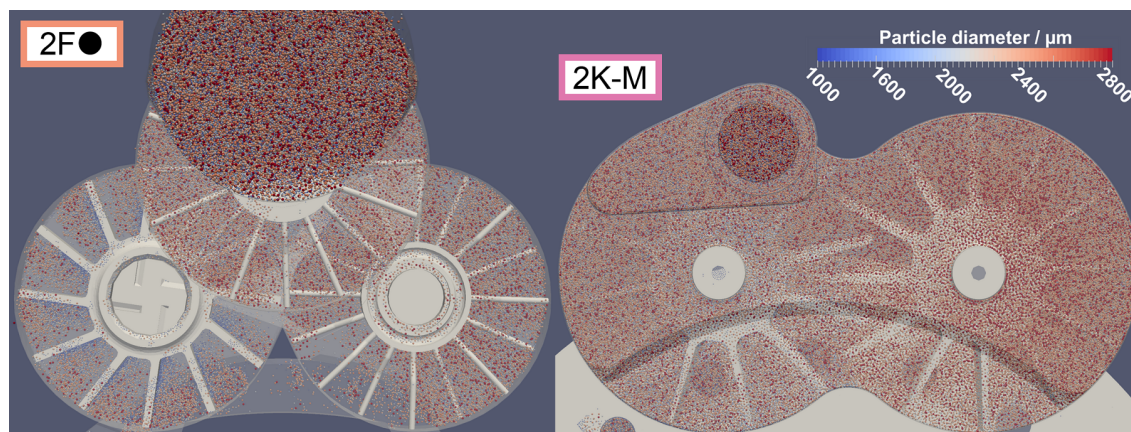


Fig. 7: Top view of force feeders during high speed tableting for FETTE 2F● and KIKUSUI 2K-M setups.

KIKUSUI (2.5-fold higher mass hold up for KIKUSUI compared to FETTE force feeder) and (2) the higher force feeder height allowing a more efficient mass re-filling. The relative difference in force feeder mass hold up between steady state high speed tableting and system filling is significantly lower in KIKUSUI setups compared to FETTE setups (e.g. relative difference of 11% and 30% for 2K-P and 2F●, respectively, Tab. 1). Hence the KIKUSUI force feeder in comparison to the FETTE force feeder is more capable of re-filling the powder that is discharged into the dies.

The second reason for the higher $\frac{\bar{m}}{t_{fill}}$ in KIKUSUI is the interlocking of the paddle wheels (Fig. 1). It ensures that over complete die filling time (Fig. 4 ‘A’ and ‘B’) the blades traverse over the dies. In contrast, an interval of gravity feeding with a reduced mass discharge rate is found between die filling from FW-Z and RW-Z in the FETTE force feeder (Fig. 7, Fig. 1 ‘H’) [170, 186, 236, 267].

A reduced force feeding capability of the KIKUSUI paddle blades would be proposed by studies on mixing by impeller blades. The blades of the KIKUSUI paddle wheels have an ‘obtuse’ orientation of the blade pitch relative to the blade rotation direction [197] (chapter 2.2, Fig. 1) in contrast to a 90° angle in the FW-■ of FETTE [197] (Fig. 1). The reduced blade rake angle of the FETTE FW-■ could direct the particles rather down into the die than just passing over the die holes, as described by Kirsch [268]. However, the force feeder housing geometry in KIKUSUI can overcome the less-favored blade shape and thus result in a higher $\frac{\bar{m}}{t_{fill}}$.

The tablet mass variation (expressed as RSD) is lower in all KIKUSUI compared to FETTE setups (Tab. 1) which can be majorly explained by the higher die fill ratios in KIKUSUI as shown previously [80, 86, 87, 168, 186, 267] and illustrated in the die screenshots in Fig. 6. Furthermore, the higher powder density in the force feeder and on top of the dies ensures a more consistent mass discharge rate into the die in KIKUSUI compared to FETTE (Fig. 7).

3.2.2 Content uniformity

At a given tablet mass and API content in the formulation, the die fill height is adjusted in tablet press settings to obtain the anticipated dose strength in the tablets. For the current study, the same fill and dosing cam settings (chapter 2.4) are used in the model DC formulation with a fixed API content of 5% (w/w) for easier comparison of the force feeder designs and setups although absolute mean tablet mass differs significantly (Fig. 6, Tab. 1).

Relative API content and content variation

The absolute mean API mass (Fig. 8), API content (API mass normalized to \bar{m}), and relative API content to label claim (\bar{X}) are given in Tab. 1. Differences for those measures between the different paddle wheel shapes in FETTE (1F●, 1F■, 2F●, and 2F■) are described in our previous work, i.e. the transfer of the size segregation from the force feeder into the dies [267]. The \bar{X} allows to quantify the size segregation extent of the API size fraction for the different force feeder designs. The DC blend is entered as a random mixture into the feeding hopper (chapter 2.4.2) and may get de-mixed during its trajectory in the force feeder (chapter 3.1.2). All KIKUSUI setups result in an API overdosing ($\bar{X} > 100\%$), which is most significant for setups in condition 2 with 122.9% for 2K-M and 115.7% for 2K-P (Tab. 1). The most distinct \bar{X} trend with a very high API content at the beginning and a correct API content in the later filled dies (die no. > 100) is revealed for setup 2K-M in Fig. 9. The trend is attributed to the changing particle size segregation extent in the force feeder between system filling and steady state high speed tableting (at $t = 4.5$ s, die no. 128; described for setup 1K-M in chapter 3.1.2). The initial change in \bar{X} between the four KIKUSUI setups is majorly related to their (1) mean particle velocity in the different sections (Tab. 2) influencing the extent of size segregation. The lower paddle wheel speeds in condition 2 setups vs. condition 1 setups increase the size segregation extent. By this way a higher API content in L-B for condition 2 setups is resulting (Tab. 2). (2) The second factor is the turret speed as it defines the mean mass relative to the max. mass in the die originating from RHSP (Fig. 4). At higher turret speeds, less mass enters from RHSP and thus allows more mass to be entered from LHSP. This is also true for API mass (Tab. 2). The combination of a higher API content in L-B and a higher API mass contribution from LHSP for condition 2 setups results in higher \bar{X} values in the first filled dies (Fig. 9). An effect of the paddle wheel speed on the size segregation extent and of the turret speed on the particle origin in the dies was also found for the different paddle wheel shapes in the FETTE setups. These observations provided an explanation for the FETTE \bar{X} values (Tab. 1) [267].

By definition of the standard deviation, the high relative API content standard deviation for setup 2K-M ($s = 31.3\%$, Tab. 1) is also linked to the \bar{X} -trend in the filled dies (Fig. 9). Similar as shown for setup 2K-M, the other three KIKUSUI setups produce distinct trends for \bar{X} over time (Fig. 9). The lower heights of the FW-Z and DW-Z in FETTE cause in comparison to KIKUSUI a reduced change of size segregation at different paddle wheel speeds (system filling vs. high speed tableting) [170, 236]. As a result, the trends in \bar{X} are less pronounced in FETTE compared to KIKUSUI and lead to lower s values (Tab. 1).

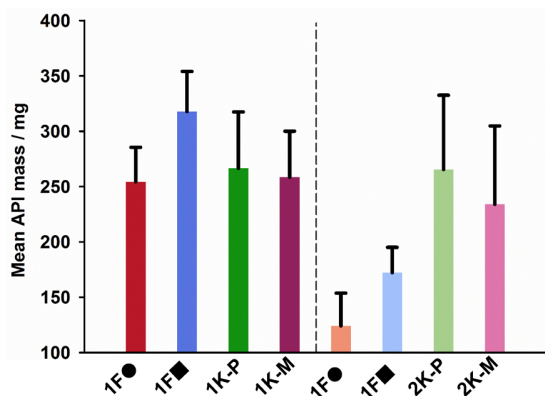


Fig. 8: Mean API mass in the filled dies for different setups.

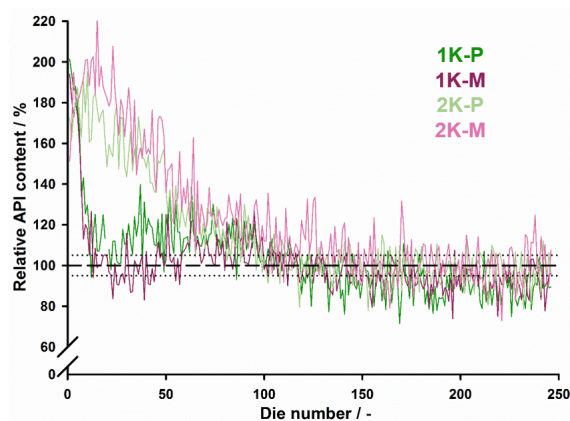


Fig. 9: Relative API content in the filled dies for the four KIKUSUI setups over time.

Acceptance value

All setups show $AV > 25$ according to Ph. Eur. 2.9.47 [25] and Eq. 1 which can be attributed to the very high \bar{X} and s values (Tab. 1, chapter 3.1.2). The very high relative content standard deviation (s) and the distinct false dosing (\bar{X}) in KIKUSUI setups result in higher AV values / lower CU compared to FETTE setups (except for setup 1K-M in condition 1, Tab. 1).

In reality, it is not appropriate to include the first produced tablets into CU analysis, but restricted by computational power (confer chapter 2.4), it was not possible to extend the calculations and to compute a physical time of several minutes or hours of die filling. The setups' different onset times of steady state in high speed tableting (Tab. 2) impede a comparison of \bar{X} and s at a later sampling plan as a different number of samples would have to be included in the statistical analysis.

3.2.3 Combination of CQAs

The three CQAs (tablet mass, tablet mass variation, and AV) are combined in a desirability model to assess the overall tablet quality for each setup (Tab. 1). The CQAs are assigned equal weighing in the calculation of the arithmetic mean with '1' for highest and '0' for lowest desirability [232, 240, 254, 255]. Briefly, a high tablet mass in contrast to a low tablet mass variation and a low AV are desirable (detailed explanation provided in [186]).

The desirability model would suggest to choose the cylindrical shaped paddle wheels in FETTE for condition 1 to obtain highest tablet quality (0.79 for 1F●, Tab. 1). The difference to the 1K-P and 1K-M setups is only minor with 0.65 and 0.72, respectively. The cuboid shaped paddle wheels in FETTE are highly unfavorable for condition 1 (0.32 for 1F■, Tab. 1), nevertheless they provide highest tablet quality for condition 2 (2F■, Tab. 1). The cylindrical shaped paddle wheel setup of FETTE (0.15 for 2F●) and the two KIKUSUI setups (0.17 for 2K-P and 0.13 for 2K-M) reveal lowest tablet quality in condition 2. In other words, depending on the process parameters and material attributes (= condition) a different tableting machine and paddle wheel shape should be considered.

Assigning a different weighing of the three CQAs could suggest other optimal setups. Furthermore, neither of the tableting machines in terms of die filling performs significantly superior / inferior compared to the other one. However, the two force feeders show different challenges when it comes to tablet quality optimization, e.g. the KIKUSUI force feeder might provide a lower CU though at the strength of a higher tablet mass and lower tablet mass variation. The comparison also shows that process transfer from one tableting machine to another one by either choosing same process parameters (K-P) or same productivity (tablets / time, K-M) could significantly change the CQAs. Thus process optimization has to be carefully considered for different tableting machines (and formulations) and adapted for specific force feeder design features. In the future, more different conditions have to be tested to allow a more general advice.

3.2.4 Powder flow in the force feeder

Other tablet quality attributes, such as tablet hardness, friability, and dissolution can be influenced to a small extent by the powder flow pattern in the force feeder, though they are mainly defined by the actual powder compaction. Narang et al. [76] identified e.g. that the 'effect of the force feeder speed on the tensile strength of tablets (...) was much greater than the effect of turret speed at any given force feeder speed'. Those differences for the two force feeders are evaluated, though without performing the actual powder compaction step, the comparison may only serve as an estimate. It can provide an idea for the potential change of powder properties of the material leaving the feed frame relative to the inlet properties [86]. The powder flow is compared in terms of (1) mass throughput and (2) residence time in the force feeder.

(1) Assuming similar cumulative discharged mass into the dies (630 g as this is the minimum mass obtained for setup 2F● after 10 turret revolutions, confer to [267]) a significantly higher mass turnover is found in FETTE compared to KIKUSUI force feeder. On average 20% and 52% of the initial mass in the force feeders have been discharged into the dies over all KIKUSUI and FETTE setups, respectively (ratio of KIKUSUI / FETTE = 2.7, Tab. 1). It can be explained by the 2.5-fold higher mass hold up in the KIKUSUI compared to the FETTE force feeder. The comparison of the KIKUSUI setups with each other in Tab. 2 shows that the higher mass discharge rate from RHSP in condition 1 setups leads to a higher mass turnover in the R-B. In combination with different particle velocities in the setups, which are highest for setup 1K-M (highest paddle wheel speed), the extent of particle shearing especially in different locations of the force feeder varies. Within the different force feeders, different shear zones develop, i.e. in FETTE the bottom of the feeding hopper with the DW-■ [267] and in KIKUSUI the interlocking region of the paddle wheels and the bottom and top of the paddle wheel sections (chapter 3.1.2). Those dissimilar shear effects might be especially critical for shear sensitive formulations and their risk for over lubrication could be assessed prior to tableting by studying the concentration and mixing time of lubricant in a low shear mixer or granulator [207, 269]. The current comparison only provides an idea for high shear zones within the force feeders, though for actual prediction of the shear stress, the forces acting on the particles have to be computed.

(2) Observation no. 1 goes in hand with longer particle residence times in the KIKUSUI compared to the FETTE force feeder (Tab. 1, particles in region 'T' of Fig. 1). The higher force feeder volume in KIKUSUI compared to FETTE leads to a longer trajectory from the feeding hopper through the force feeder into the dies thereby causing a higher residence time. The most significant relative residence time increase of 72% is found for setup 1K-P (17.7 s) compared to 1F■ (10.3 s). Since the current model does not consider the actual powder compaction step, the differences in powder flow in the force feeders, e.g. in terms of residence time, are not included in the desirability model (confer chapter 3.2.3). Particle residence times assessed from numerical simulations could help to adapt or shorten previous blending times.

4 Summary and Conclusion

DEM was employed to evaluate the powder flow for two different force feeders and to relate it to tablet quality. The main design differences between the KIKUSUI Virgo and the FETTE 1200i force feeders are the number of paddle wheels, the force feeder housing in terms of its total volume as well as its geometry, and the position of the feeding hopper. Those differences led to significant changes in the powder flow within the force feeders. The lower depth of immersion of the blades of the KIKUSUI paddle wheels caused an increased particle size segregation extent by percolation / sieving mechanisms. The API particles, considered as fines, accumulated after system filling at the bottom of the force feeder and caused a significant API overdosing in the initially produced tablets. The numerical model allowed an in depth look into the force feeder and unveiled the left hand half of the feeding hopper and the off-centered top part of the left hand half paddle wheel as dead zones. The top part in the right hand half paddle wheel is circulating around the radial axis with hardly any mass exchange. A distinct shear zone was found between the top and bottom sections as the paddle wheels solely rotate in the bottom. Particles in this distinct shear zone might be exposed to higher shear forces with a potential change in their particle properties, e.g. over lubrication or particle attrition.

Two different numerical conditions in terms of process parameters and material attributes were selected to compare the tablet quality obtained by using the KIKUSUI and FETTE force feeders. In addition, different configurations in the paddle wheel shapes (cylindrical or cuboid shaped blades) for the FETTE force feeder were evaluated. The CQAs tablet mass, tablet mass variation, and API content uniformity were computed and included in a desirability model. In general, the KIKUSUI tableting machine was able to produce a higher tablet mass at the same fill and dosing cam configuration. This was given by an increased force feeding capability, e.g. due to a 2.5-fold higher force feeder mass hold up in KIKUSUI compared to FETTE. The higher tablet mass and more consistent mass discharge rate in KIKUSUI implied a lower tablet mass variation. The significant size segregation in the KIKUSUI force feeder resulted in a lower content uniformity compared to FETTE. However, the content uniformity should also be assessed at a later computed time point (> minutes) to exclude the size segregation in the system equilibration phase between system filling and high speed tableting. Depending on the process parameters and material attributes, an optimal selection of the tableting machine / paddle wheel configuration was proposed to obtain an overall improved tablet quality for the CQAs. Neither of the force feeders performed in general significantly superior or inferior, though both force feeder designs revealed distinct tablet quality advantages / disadvantages that could be related to their geometry. In general, the higher mass hold up in the KIKUSUI force feeder compared to the FETTE force feeder caused a significantly higher particle residence time. In combination with e.g. the particle velocity it could provide a first estimate of the shear forces the particles might have experienced through their trajectory in the force feeder. The comparison is a starting point and requires experimental validation.

This study is the first of its kind disclosing the pitfalls and difficulties in process development, especially for process transfer from one to another tableting machine, as shown for the die filling case. An in depth evaluation of the powder flow pattern within tableting machines, e.g. by applying a numerical model, allows an improved process understanding. In addition, the study suggests that process development should be adapted independently for different tableting machines to ensure a consistent tablet quality.

The current model might also be translated to force feeders of similar geometries as found in

KIKUSUI and FETTE. The model does not aim to fully predict the reality as several limitations, especially in terms of particle size, exist. Only two different numerical conditions with regard to process parameters and material attributes were tested, though the analysis adds scientific insight into the die filling process and supports pharmaceutical development. Nevertheless, an experimental validation of the numerical results is indispensable and scope of future work.

5 Supplementary Videos

Illustration of particles filling process in KIKUSUI force feeder (chapter 2.4.1). Particles are colored according to their size (for scale refer to Fig. 3).



Illustration of high speed tableting for setup 1K-M. Particles are colored according to their initial position.



Acknowledgment

The authors would like to thank Thomas Heinrich (Fette compacting GmbH) for providing the CAD files of FETTE. Yasuhiro Suzuki from Daiichi-Sankyo Tokyo is acknowledged for his kind correspondence with Kikusui Seisakusho Ltd and discussion. From Kikusui Seisakusho Ltd. Naoshige Kitamura and Mikio Sugahara are thanked for their technical support and Hiroyuki Matsui for contracting and other work.

4 Overall findings and future perspectives

Pharmaceutical industry is facing a couple of challenges related to the decline of drug approvals and increase of manufacturing costs. In the context of pharmaceutical development and tablet production, it could be shown that mechanistic modeling is capable of improving process understanding thereby decreasing the number of trial and error experiments. In the current study, emphasis was given to the first step in the process of tableting, the die filling. This step is detrimental with respect to the patients' safety as it defines the API content and content uniformity which underlies a tight control asked by the regulators. Classical experiments were combined with statistical tools and high speed camera imaging, and the numerical DEM was joined with 'Quality by Design' methodologies to investigate the powder flow pattern in die filling. Those approaches were used to study both die filling mechanisms, namely gravity filling and force feeding.

An experimental model die filling system made of acrylic glass was developed to discern the powder discharge by gravity from a stationary shoe into a translating die of adjustable speed. A 'flow - no flow' criterion was defined using the powder flowability indicator '*flow function coefficient*' from the ring shear tester. The powder flow patterns of different materials over filling time were unveiled using high speed camera (HSC) imaging. Differences between volume fill ratios from HSC images and mass fill ratios indicated entrapped air / void volume in the die. The differences could be explained by the powder flow patterns of the materials, which were themselves influenced by the particle characteristics such as particle size, particle shape, and cohesive forces. Therefore non-linear least squares regression analysis was utilized to interconnect the volume flow rate with particle size which can then be used to predict volume fill ratios. An exponential decay of the mass fill ratio was found at increasing die speeds which was described with a novel mathematical model. In particular, the decay rate constant represented the relationship of the powder's sensitivity with respect to mass fill ratio at increasing die speeds and was used to define a novel flowability characteristic relevant for die filling. Partial-least squares regression analysis correlated the easily measurable particle size with the decay rate constant, defined as '*Die fill index*' (*DFI*) to quickly estimate a new material's sensitivity to die filling speed.

The model system was predominantly tested for pharmaceutical excipients showing less complexity compared to powder blends (direct compression formulations). Real formulations consist of several excipients and at least one API which individually differ in terms of, e.g. their particle size, particle size distribution, and inter-particle forces. Hence, the applicability of the developed correlations has to be validated for powder mixtures and, if necessary, adapted.

Though the system in its simplicity can be used in early-stage formulation development as only little material is required, the connection between the model die filling system and gravity feeding in rotary tablet presses is still to be established. Different stress levels and flow conditions are found in rotary tablet presses compared to the model die filling system which may influence the powder discharge into the die, e.g. the centrifugal force by turret rotation, the generated partial negative pressure by suction filling, the different geometry of the feeding chute, and the stress exerted from the powder in the blending hopper.

The developed mathematical correlations provide a valuable tool to estimate the powder flowability relevant for die filling. The powder flowability was directly linked with particle size, highlighting the possible effect of particle size enlargement, e.g. by sieving or granulation. Formulation candidates at an early stage may be quickly tested in the model die filling system to establish a preliminary understanding of its powder flowability. For later process optimization, the margin for the potential increase in tableting speed of a more matured formulation may be generated by measuring its sensitivity to die filling speed. In general, a comparison of any formulation with the already tested materials may be helpful to group it into flowability classes and suggests potential levers for optimization.

The DEM, a Lagrangian model, tracks the positions, velocities, and accelerations of each individual particle and offers the opportunity to shed light on highly complex and closed systems. Classical experiments do not allow an in-depth process insight in the context of tableting as die filling units of rotary tablet presses are in general made of steel or anodized aluminum. Different models utilizing the DEM were developed by gradually increasing the complexity of the system to evaluate the powder discharge into the rotating dies of the turret, either by gravity or by force feeding through paddle wheel rotation. Splitting the systems into reasonable sections provided location specific characteristics, namely the relation of powder flow patterns such as particle size segregation mechanisms to design features. In addition to the classical tablet quality attributes which are directly defined by the die filling step (tablet mass, tablet mass variation, and content uniformity), the particle shearing by paddle wheel rotation was indirectly gauged through particle velocity and particle residence time. Hence, the effect of paddle wheel rotation on particle attrition and over-lubrication in the feeding system which could have an impact on tablet hardness, disintegration, and dissolution, was indirectly computed, too.

The numerical model for gravity feeding considered a cylindrical pipe, connected by an inclined chute, and a rectangular box for powder storage. Particles discharged from the rectangular box into the rotating dies of the turret. In the first place, the effect of different process parameters such as turret speed and die diameter, and material properties such as inter-particle cohesion, particle-particle and particle-wall coefficient of friction, and particle-particle and particle-wall coefficient of restitution on die filling of mono-disperse particles was studied by changing one factor at a time and by full factorial designs including selected factors. It provided a basis to evaluate in the second step the powder flow of poly-disperse sized particles for different, previously identified, and die filling influencing, material properties (inter-particle cohesion and coefficient of friction). The model allowed to understand the powder flow pattern from the chute into the feeding box, and the dies and related particle velocity and particle trajectories through particle coloring with particle size segregation mechanisms. Though the geometry of the gravity feeder may seem simple, the detailed analysis showed that the particle rearrangement and in turn size segregation in the feeding box sections were affected by the different sub-processes they are involved in. In addition, high and low shear zones (dead zones) were identified within the gravity feeder and their extent was influenced by material properties, i.e. the coefficient of friction, not by the process condition turret speed.

A material dependent risk assessment showed the impact of material properties on direct (tablet mass, tablet mass variation, and content uniformity) and indirect (tablet hardness and dissolution) tablet quality attributes. Out of all tested material properties, highest and lowest tablet quality could be obtained for formulations with a low and high particle-particle friction, respectively. This study could be a starting point for formulation development guidance as merits and drawbacks of individual

material properties were presented.

An additional process variable compared to gravity feeding, namely the paddle wheel speed comes into play for die filling by force feeding. Two different pilot-scale tableting machines, namely the FETTE 1200i and the KIKUSUI Virgo, were assessed using a model direct compression formulation. The formulation contained an excipient phase of six different particle size fractions and a model API of one size fraction. Micro-mechanical material properties were chosen same for all size fractions and thus powder flowability of the complete blend was assessed by changing uniformly the inter-particle cohesion and the particle-wall coefficient of friction.

The force feeder geometries of the two tableting machines differed in terms of the paddle wheels (number, depth of immersion, shape, and blade dimensions), the force feeder housings (height, connection between paddle wheels, volume, and area involved in die filling), the feeding hoppers (volume, shape, location, and connection to paddle wheels), and the turrets (diameter, position underneath the force feeder, number of dies, width of arc, and circle of segment length involved in die filling). Moreover, for the FETTE 1200i, two different paddle wheel shape configurations were tested.

At first, the powder flow patterns in both tableting machines were described to provide a basic understanding for the material path from the feeding hoppers through the paddle wheel zones into the dies. The DEM allowed to identify force feeder specific shear zones and dead zones. In the three paddled FETTE 1200i force feeder, intriguing powder flow patterns over the width of the feeding hopper were found: If the blades of the dosing wheel located underneath the feeding hopper were cylindrical shaped, only half of the feeding hopper width was involved in refilling whereas the other half remained static (dead zone). In contrast, the higher shear area offered by the cuboid shaped blades of the other dosing wheel transferred while rotation a higher momentum on the particles in the feeding hopper and caused particle circulation in the feeding hopper. Thus, the blade shape of the FETTE 1200i dosing wheel determined the dead zone or the high shear zone in the feeding hopper.

Similar as for the cylindrical shaped dosing wheel configuration in FETTE 1200i, the left hand half of the feeding hopper in the KIKUSUI Virgo tableting machine was unveiled as a dead zone. An additional dead zone in the KIKUSUI Virgo was the off-centered top part of the left hand half paddle wheel zone. Little mass exchange was found in the powder rotating around the radial axis of the right hand half paddle wheel. Another distinct difference between the KIKUSUI Virgo and FETTE 1200i force feeder was the significantly larger housing height and the lower blade depth of immersion of the former. Paddle wheels in the KIKUSUI Virgo rotated solely at the bottom of the force feeder causing a distinct shear zone between the actuating particles in the bottom and the slower moving particles in the top. This comparison shows that in reality the powders may experience different shear forces in the two tableting machines which in turn can result in differing tablet qualities (e.g. dissolution profiles).

The underlying particle size segregation mechanisms for both force feeder types were connected to their corresponding design features. In general, size segregation by sieving / percolation mechanism was found whenever a low momentum was transferred from slowly rotating paddle wheels on the particles. By this mechanism, smaller particles traversed through the powder bed to the bottom, e.g. in the dosing wheel zone in the FETTE 1200i and provoked a different API distribution in the underneath located paddle wheel zones. Though the high powder bed height on top of the paddle wheels and the low void volume in the KIKUSUI Virgo force feeder prevented size segregation by trajectory mechanism, which was found for cuboid shaped FETTE 1200i paddle wheels, it gave rise to a higher sieving / percolation tendency. Mass flow rate analysis into the die connected the size segregation in

the force feeders with content uniformity as well as with over the die-height differences. Similarly as observed in gravity feeding, a higher content of larger particles that were exerted to less shear forces was found at the bottom of the dies.

A screening design of experiments was developed in the ‘Quality by Design’ framework for one paddle wheel configuration of the FETTE 1200i. Based on the understanding from the gravity feeding DEM models, the material properties particle-wall coefficient of friction and inter-particle cohesion, and the influence of the formulation dose strength (API content) were tested for potential critical material attributes. In addition, the process conditions turret speed and paddle wheel speed were included in the experimental design as potential critical process parameters. The DoE allowed to develop linear relationships between the tested factors and the responses tablet mass, tablet mass variation, and content uniformity, which were defined as critical quality attributes, and particle shearing. The provided relationships between process parameters / material attributes and CQAs gave a design space for optimal quality.

The tablet quality obtained using the cylindrical and cuboid shaped paddle wheel configurations in FETTE 1200i as well as the KIKUSUI Virgo force feeder was evaluated utilizing factors combinations which ensued best and worst results in the DoE. Each system came with different strengths and pitfalls with respect to tablet quality that could be explained by their geometrical differences. For example, a higher mass flow rate and lower tablet mass variation at the cost of a lower content uniformity due to a higher size segregation extent was found in the KIKUSUI Virgo. The comparison emphasized the necessity of process development for individual tableting machines and the challenges in process transfer or scale up, though it demonstrated the possibilities in tablet quality improvement by changing the paddle wheel shape or the tableting machine.

The DEM models for gravity and force feeding described the underlying patterns during the system filling and the initial tableting process, though the influence of long-term tableting and feeding hopper emptying were not captured. In addition, more experiments in the DoE and in the tableting machine comparison would have to be performed to identify, e.g. non-linear / higher order factor effects. Other limitations were the required increase in particle size, the simplified particle size distributions, and the idealistic spherical particle shapes, which differ from pharmaceutical powders. Further experiments using simplified systems and a sensitivity analysis would be necessary to identify the effect of those simplifications on the powder flow patterns. Furthermore, a comparison between gravity and force feeding by using the same material (e.g. the model direct compression formulation) could be preformed to evaluate similarities and differences.

Given by the complexity of the tablet presses and the non-transparent nature of their housing, a detailed validation of the numerical results for the powder flow patterns within the feed frames by experiments in the actual tablet presses is unfeasible. However, tablet quality in terms of tablet mass, tablet mass variation, and content uniformity could be tested experimentally. As in reality a higher number of particles (smaller particle size compared to the model formulation) are filled into the die and the feed frames, a lower size segregation extent would be assumed within the feed frames and a lower absolute variation of the result values would be expected. In addition, similar as the experimental model die filling system, experimental systems with a gravity feeder and a one-paddled force feeder have been designed and constructed. In the future, those additional models could be tested with classical pharmaceutical excipients and powder mixtures to identify generally valid conclusions drawn from numerical data.

The current study attained by numerical means an in-depth understanding of the powder flow patterns in different die filling systems and their relation to tablet quality. Given by the strength of in-process particle tracking, the study can serve as a starting point for process development and formulation design. Due to computational limitations, complete prediction of the die filling process and an one-to-one transfer of numerical results to experimental observations were out of scope of the study, yet it provided different levers for process optimization.

On the one hand, the analysis showed that the powder may undergo different particle shearing during its path of the feeding systems. Thus, gravity feeding may be the preferred system for shear sensitive formulations. If force feeding with an active powder transport is necessary, e.g. due to a low powder flowability as shown for some of the materials in the experimental model die filling system, the force feeder type and paddle wheel shape have to be carefully selected. In addition, the combination of paddle wheel speed and turret speed, which define the mass throughput of the powder, plays a crucial role in particle shearing.

The DEM may be suitable to assess the maximal possible turret speed of a product without substantial influence on tablet quality. The required adaption of the paddle wheel speed at maximal turret speed may be estimated without performing a lot of cost intensive experiments. Pharmaceutical development can benefit from simulations by estimating the potential throughput acceleration range and by assessing the production time margin and in return the cost savings.

Furthermore, the study showed that it is worth spending resources in profound material characterization. Although particle properties are tightly connected with each other in reality, the cohesivity and friction of the powder were tested individually in the feeding systems of the numerical models and influenced differently but substantial the tablet quality. Material characterization with respect to particle size, particle size distribution, particle shape, particle surface roughness, dispersive surface energy, and others should be conducted already at an early development stage by analytical methods such as laser diffraction, dynamic image analysis, scanning electron microscopy, and inverse gas chromatography, respectively. Simplified systems such as the model die filling system may be necessary to answer process specific questions.

A comprehensive material characterization can help to gauge problems in die filling and can offer potential solutions, e.g. by changing the grade of an excipient. An appropriate selection of excipients during pharmaceutical development plays a substantial role as procurement costs may later influence commercial manufacturing. Thus interchangeability of excipients with respect to die filling may be considered as early as possible by powder characterization to save raw material costs.

Ideally in future, DEM models could take into account the change in particle properties, e.g. particle attrition, during the powder flow in the feeding system and thus establish the ‘powder history’. Accordingly, the DEM could be combined with the FEM to simulate the compaction of the powder filled in the die into a tablet. Thus a holistic model of the complete tableting process (die filling, powder compaction, and tablet ejection) could be generated instead of independent models of the individual process steps.

As shown in the current studies, mechanistic models are entering step-by-step the pharmaceutical process development and will help to tackle the challenges drug product development is facing.

5 Summary

Pharmaceutical tableting consists of three distinct stages: die filling, powder compaction, and tablet ejection. The first step is crucial with respect to the patient's safety as it defines the content and content uniformity of the active pharmaceutical ingredient(s). Several pre-requisites have to be met to achieve a high content uniformity, such as the lack of segregation during the die filling step and a sufficiently high powder flowability. In rotary tablet presses, the powder is either discharged from a chute by gravity or by force feeding through paddle wheel rotation into the rotating dies of the turret. In reality, nontransparent gravity or force feeders impede a detailed examination of the powder transfer into the dies.

In this work, different experimental and numerical methods were developed to improve process understanding in die filling and to relate powder properties and process parameters with tablet quality attributes.

In the first step, a transparent model die filling system was developed to visualize powder discharge into the die by high speed camera imaging and to discern powder flow patterns, e.g. bulk, nose, and intermittent flow, as described in literature. The powder flow pattern influenced the particle void space within the die and can influence the powder compaction. Entrained air could not escape from the die for very good flowing materials which resulted in a higher volume compared to mass fill ratio. In addition, the flexible speed adjustment of the die translating underneath the powder storage block represented the basis for the development of a novel die filling metric. This metric allowed to quickly assess a material's sensitivity, in terms of die fill ratio, on die speed variations. Several mathematical correlations using easily accessible powder characteristics, such as particle size, were established to estimate the flowability for new materials in die filling. Thus the effect of particle size enlargement on powder flowability improvement for die filling could be quantified.

In addition to the experimental custom designed instrument, a numerical gravity die filling system was developed utilizing the *Discrete element method* (DEM). The DEM tracks each individual particle and thus provides a high level of detail in complex powder handling / transporting systems. Using the DEM, the general powder flow pattern from the feeding chute through the feeding box into the dies was discerned, e.g. the particle rearrangement within the feeding box by shearing of the rotating turret was visualized. Furthermore, the influence of material properties and process parameters on die filling of mono- and poly-disperse particles was studied to generate a starting point for formulation optimization with respect to highest tablet quality. This could be obtained by tuning the material properties to a low particle-particle friction, e.g. by changing the particle morphology to spheres (via spray drying) or by smoothing the particle surface.

Force feeding was studied by numerical means in two pilot-scale tableting machines mainly differing in terms of number of paddle wheels, blade shapes, and housing geometries. The powder transfer from the feeding hoppers through the force feeders, in particular the paddle wheels rotating in different directions, was visualized by the DEM. Thus, the underlying particle size segregation mechanisms of a model direct compression formulation were discerned and related to geometrical properties of the force feeders and to process conditions. Furthermore, dead zones and high shear zones were de-

tected in the feeding hoppers and pose a risk for powder caking or over lubrication of shear sensitive formulations, respectively. A screening design of experiments for one of the tableting machines gave first hints to critical material attributes (powder cohesivity and particle-wall coefficient of friction) and critical process conditions (turret speed and paddle wheel speed) on critical quality attributes (tablet mass, tablet mass variation, and content uniformity). Factor combinations resulting in highest and lowest tablet quality were ascertained. For a limited number of setups, comparative studies were performed for different paddle wheel shapes and a different tableting machine. The comparison emphasized the necessity of an individual process development for different tableting machines and pointed out challenges in technical transfer as the varying geometries provided different strengths and weaknesses when it came to tableting performance. For instance, the KIKUSUI Virgo tableting machine provided at same fill and dosing cam settings a higher tablet mass at a lower tablet mass variation compared to the FETTE 1200i.

The application of different means, such as custom-designed instruments, statistical tools, and DEM, enabled a detailed understanding of powder flow in the tableting machine and its influence on tablet quality. Different levers for process and formulation optimization were presented and could aid pharmaceutical development in the context of the *Quality by design* approach. Those models can serve as a basis for future studies, e.g. the extension of the model die filling system to an experimental custom-designed force feeder, or to additional numerical setups which could, benefiting from computational progress, simulate more realistic material properties as found in real formulations.

6 Summary (German)

Die Herstellung von Tabletten auf schnell-laufenden Rundläuferpressen kann in drei individuelle Schritte untergliedert werden: die Matrizenfüllung, die Pulverkompaktierung und den Tablettenausstoß. Die Matrizenfüllung sorgt für die Sicherheit des Patienten, da sie die Zusammensetzung und Gleichförmigkeit des Wirkstoffes vorgibt. Eine niedrige Entmischungstendenz und eine ausreichende Fließfähigkeit der Formulierung sind Voraussetzungen für eine hohe Gleichförmigkeit des Gehalts. Zwei Matrizenfüll-Mechanismen existieren in Rundläuferpressen. Entweder fällt in Kammerfüllschuhen das Pulver passiv durch den Füllapparat, oder horizontal rotierende Rührflügelräder streichen in Rührwerkschuhen das Pulver aktiv in die Matrizen. Die in der Regel undurchsichtigen Gehäusematerialien verhindern, dass der Pulverfluss in die Matrize von außen beobachtet werden kann.

In der vorliegenden Arbeit wurden experimentelle und numerische Methoden entwickelt, um diesen Prozessschritt besser zu verstehen und um eine Verbindung zwischen Pulvereigenschaften und Prozessparametern und der Tablettenqualität herzustellen.

Im ersten Schritt wurde der Matrizenfüllprozess mit einem transparenten Modell-System visualisiert und unterschiedliche Fließmechanismen mittels einer Hochgeschwindigkeitskamera identifiziert. Der Fließmechanismus beeinflusste den Leerraum zwischen den Partikeln in der Matrize, welcher bei der anschließenden Pulverkompaktierung einen Einfluss spielen kann. So wurde zum Beispiel mehr Füllvolumen als Füllmasse bei sehr gut fließenden Materialien festgestellt, da die eingeschlossene Luft zu wenig Zeit zum Entweichen hatte. Durch die variabel einstellbare Geschwindigkeit der Matrize, die unterhalb des Füllapparates durchfährt, konnte ein neuer Fließfähigkeitsparameter entwickelt werden. Dieser beschreibt die Empfindlichkeit des Materials in Bezug auf den Matrizenfüllgrad und der Matrizingeschwindigkeit. Mathematische Zusammenhänge wurden entwickelt, um einfach zu messende Materialeigenschaften, wie die Partikelgröße, mit der Matrizenfüllung zu korrelieren. Diese können zur Abschätzung der Fließfähigkeit im Kontext des Matrizenfüllprozesses für neue Materialien dienen. Die Korrelationen ermöglichen es auch, den Einfluss der Partikelgrößenzunahme auf die Fließfähigkeit zu messen.

Weiterhin wurde zum Kammerfüllschuh neben dem experimentellen auch ein numerisches Modell mit der *Diskreten Element Methode* (DEM) entwickelt. In der DEM wird jeder einzelne Partikel individuell betrachtet, wodurch komplexe partikuläre Systeme auf Partikelebene aufgelöst werden können. Der Pulvertransport im Kammerfüllschuh - vom Fülltrichter in die Füllbox und schließlich in die rotierenden Matrizen - wurde zunächst mittels der DEM veranschaulicht. Dies beinhaltete beispielsweise das Verschieben der Partikel in der Füllbox durch die Scherwirkung des rotierenden Matrizenstückes. Der Einfluss von verschiedenen Materialeigenschaften und Prozessparametern auf die Matrizenfüllung von mono- und poly-dispersen Partikeln wurde untersucht. Diese Erkenntnisse können zur Formulierungsoptimierung und zur Gewährleistung einer möglichst hohen Tablettenqualität dienen. Diese kann erzielt werden, wenn der Reibungskoeffizient zwischen Partikeln möglichst klein ist, was beispielsweise durch eine Änderung der Partikelmorphologie zu Sphären (durch Sprühtrocknung) oder durch eine Oberflächenglättung der Partikel erreicht werden kann.

Außerdem wurden mittels DEM die Rührwerksfüllschuhe von zwei verschiedenen Tablettenpressen

im Technikumsmaßstab untersucht. Primär unterschieden sich die Füllschuhe in Anzahl und Form der Rührflügel und der Gehäusegeometrie. Für beide Tablettenpressen wurde der Pulverfluss vom Fülltrichter durch die Füllschuhplatte mit den gegenläufig rotierenden Füllrädern in die Matrizen simuliert und visualisiert. Die hohe Prozessauflösung durch DEM erlaubte die Identifizierung von Segregationsmechanismen einer direktverpressbaren Modellformulierung mit unterschiedlichen Partikelgrößen, die auf die geometrischen Eigenschaften der Füllschuhe zurückgeführt wurden. Die festgestellten Totzonen und Bereiche mit hohem Schereintrag in den Fülltrichtern könnten entweder zum Verklumpen oder zur Übersmierung von scherempfindlichen Formulierungen führen. Ein Screening-Versuchsplan für eine Tablettenpresse untersuchte den Einfluss potentiell kritischer Materialeigenschaften (Reibungskoeffizient zwischen Partikel und Geometrie und Kohäsion) und Prozessparametern (Tablettier- und Füllrädergeschwindigkeit) auf kritische Qualitätsmerkmale (Tablettengewicht, und -gewichtsschwankung und Gleichförmigkeit des Gehalts) und ermittelte Faktorkombinationen, die zu optimalen beziehungsweise ungünstigen Tablettenqualitäten führten. Verschiedene Füllräder und ein anderer Rührwerksfüllschuh wurden für eine Auswahl von Faktorkombination miteinander verglichen. Die unterschiedlichen Rührwerksfüllschuhe führten zu verschiedenen Stärken und Schwächen bezogen auf die Tablettenqualität, die sich auf die unterschiedlichen Geometrien zurückführen ließen. Darüber hinaus wurden die Herausforderungen des Prozesstransfers von dem einen auf den anderen Rührwerksfüllschuh demonstriert, die individuelle Prozessentwicklungen auf unterschiedlichen Tablettenpressen erforderlich machen. So erzielte bei gleichen Füll- und Dosierkurven die KIKUSUI Virgo im Vergleich zur FETTE 1200i Tablettenpresse ein höheres mittleres Tablettengewicht bei geringerer Schwankung.

Der Pulverfluss in der Tablettenpresse und dessen Einfluss auf die Tablettenqualität wurden mittels verschiedener Ansätze, beispielsweise eines eigens entwickeltem Experimentalsystem, statistischen Instrumenten und DEM, untersucht. Es wurden verschiedene Möglichkeiten zur Prozess- und Formulierungsoptimierung entwickelt, die die pharmazeutische Entwicklung im Kontext des *Quality by Design* Ansatzes unterstützen können. Die Modelle stellen eine Grundlage für weitere Untersuchungen dar, wie beispielsweise die Erweiterung des Modell-Kammerfüllschuhsystems zu einem Rührwerksfüllschuhsystem oder weiteren numerischen Studien, die in Zukunft durch den technologischen Fortschritt realistischere Materialeigenschaften abbilden könnten.

References

- [1] J. W. Scannell, A. Blanckley, H. Boldon, and B. Warrington. Diagnosing the decline in pharmaceutical r&d efficiency. *Nature Reviews Drug Discovery*, 11:191, 2012.
- [2] *2017 Annual report, Ensuring Safe, Effective, and Affordable Medicines for the American Public*, 2018.
- [3] ICH Q8(R2). Pharmaceutical development. Part I: pharmaceutical development, and. Part II: annex to pharmaceutical development, 2009.
- [4] P. Suresh and P. K. Basu. Improving pharmaceutical product development and manufacturing: Impact on cost of drug development and cost of goods sold of pharmaceuticals. *Journal of Pharmaceutical Innovation*, 3(3):175–187, 2008.
- [5] A. J. Rogers, A. Hashemi, and M. G. Ierapetritou. Modeling of particulate processes for the continuous manufacture of solid-based pharmaceutical dosage forms. *Processes*, 1(2):67–127, 2013.
- [6] K. Plumb. Continuous processing in the pharmaceutical industry: Changing the mind set. *Chemical Engineering Research and Design*, 83(6):730–738, 2005.
- [7] S. L. Lee, T. F. O’Connor, X. Yang, C. N. Cruz, S. Chatterjee, R. D. Madurawe, C. M. V. Moore, L. X. Yu, and J. Woodcock. Modernizing pharmaceutical manufacturing: from batch to continuous production. *Journal of Pharmaceutical Innovation*, 10(3):191–199, 2015.
- [8] G. V. Reklaitis, J. Khinast, and F. Muzzio. Pharmaceutical engineering science—new approaches to pharmaceutical development and manufacturing. *Chemical Engineering Science*, 65(21):iv–vii, 2010.
- [9] P. Basu, G. Joglekar, S. Rai, P. Suresh, and J. Vernon. Analysis of manufacturing costs in pharmaceutical companies. *Journal of Pharmaceutical Innovation*, 3(1):30–40, 2008.
- [10] S. García-Muñoz. Establishing multivariate specifications for incoming materials using data from multiple scales. *Chemometrics and Intelligent Laboratory Systems*, 98(1):51–57, 2009.
- [11] R. Leardi. Experimental design in chemistry: A tutorial. *Analytica Chimica Acta*, 652(1–2):161–172, 2009.
- [12] E. Tomba, P. Facco, F. Bezzo, and M. Barolo. Latent variable modeling to assist the implementation of quality-by-design paradigms in pharmaceutical development and manufacturing: A review. *International Journal of Pharmaceutics*, 457(1):283–297, 2013.
- [13] Food and Drug Administration (FDA). Guidance for industry, framework for innovative pharmaceutical development, manufacturing, and quality assurance, 2004.

- [14] S. K. Wilkinson, S. A. Turnbull, Z. Yan, E. H. Stitt, and M. Marigo. A parametric evaluation of powder flowability using a freeman rheometer through statistical and sensitivity analysis: A discrete element method (DEM) study. *Computers & Chemical Engineering*, 97:161–174, 2017.
- [15] J. Bourquin, H. Schmidli, P. van Hoogevest, and H. Leuenberger. Advantages of artificial neural networks (ANNs) as alternative modelling technique for data sets showing non-linear relationships using data from a galenical study on a solid dosage form. *European Journal of Pharmaceutical Sciences*, 7(1):5–16, 1998.
- [16] R. Jukka and K. Johannes. The future of pharmaceutical manufacturing sciences. *Journal of Pharmaceutical Sciences*, 104(11):3612–3638, 2015.
- [17] A. Rogers and M. Ierapetritou. Challenges and opportunities in modeling pharmaceutical manufacturing processes. *Computers & Chemical Engineering*, 81:32 – 39, 2015.
- [18] D. M. Kremer and B. C. Hancock. Process simulation in the pharmaceutical industry: A review of some basic physical models. *Journal of Pharmaceutical Sciences*, 95(3):517–529, 2006.
- [19] M. Moakher, T. Shinbrot, and F. J. Muzzio. Experimentally validated computations of flow, mixing and segregation of non-cohesive grains in 3d tumbling blenders. *Powder Technology*, 109(1–3):58–71, 2000.
- [20] W. R. Ketterhagen, M. T. am Ende, and B. C. Hancock. Process modeling in the pharmaceutical industry using the discrete element method. *Journal of Pharmaceutical Sciences*, 98(2):442–470, 2009.
- [21] S. Sarkar, R. Mukherjee, and B. Chaudhuri. On the role of forces governing particulate interactions in pharmaceutical systems: A review. *International Journal of Pharmaceutics*, 526:516–537, 2017.
- [22] F. J. Muzzio, T. Shinbrot, and B. J. Glasser. Powder technology in the pharmaceutical industry: the need to catch up fast. *Powder Technology*, 124(1):1–7, 2002.
- [23] H. P. Zhu, Z. Y. Zhou, and A. B. Yu. Discrete particle simulation of particulate systems: Theoretical developments. *Chemical Engineering Science*, 62(13):3378–3396, 2007.
- [24] H. P. Zhu, Z. Y. Zhou, R. Y. Yang, and A. B. Yu. Discrete particle simulation of particulate systems: A review of major applications and findings. *Chemical Engineering Science*, 63(23):5728–5770, 2008.
- [25] Council of Europe. *European Pharmacopoeia*. European Pharmacopoeia, Strasbourg, France, '9.5 edition, 2018.
- [26] B. R. Conway. *Solid Dosage Forms*. John Wiley & Sons, Inc., Cary, North Carolina, 2007.
- [27] *The Top 15 Best-Selling Drugs of 2017, Amid Talk of Curbing Prices, Most Treatments Show Sales Gains*, 2018.
- [28] A. Bauer-Brandl and W. A. Ritschel. *Die Tablette, Handbuch der Entwicklung, Herstellung und Qualitätssicherung*. Cantor-Verlag für Medizin und Naturwissenschaften, Aulendorf, Germany, 3 edition, 2012.

-
- [29] D. Barrasso and R. Ramachandran. Discrete element modeling of solid dosage manufacturing processes. In M. G. Ierapetritou and R. Ramachandran, editors, *Process Simulation and Data Modeling in Solid Oral Drug Development and Manufacture*, pages 105–131. Springer New York, New York, NY, 2016.
- [30] D. O. Potyondy and P. A. Cundall. A bonded-particle model for rock. *International Journal of Rock Mechanics and Mining Sciences*, 41(8):1329–1364, 2004.
- [31] A. V. Potapov and C. S. Campbell. Computer simulation of impact-induced particle breakage. *Powder Technology*, 81(3):207–216, 1994.
- [32] P. Cleary. Modelling comminution devices using DEM. *International Journal for Numerical and Analytical Methods in Geomechanics*, 25(1):83–105, 2001.
- [33] M. J. Metzger and B. J. Glasser. Simulation of the breakage of bonded agglomerates in a ball mill. *Powder Technology*, 237(0):286–302, 2013.
- [34] A. Jafari and V. Saljooghi Nezhad. Employing DEM to study the impact of different parameters on the screening efficiency and mesh wear. *Powder Technology*, 297:126–143, 2016.
- [35] M. Marigo, M. Davies, T. Leadbeater, D. L. Cairns, A. Ingram, and E. H. Stitt. Application of positron emission particle tracking (PEPT) to validate a discrete element method (DEM) model of granular flow and mixing in the turbula mixer. *International Journal of Pharmaceutics*, 446(1–2):46–58, 2013.
- [36] P. E. Arratia, N.-h. Duong, F. J. Muzzio, P. Godbole, and S. Reynolds. A study of the mixing and segregation mechanisms in the bohle tote blender via DEM simulations. *Powder Technology*, 164(1):50–57, 2006.
- [37] P. Kleinebudde. Roll compaction/dry granulation: pharmaceutical applications. *European Journal of Pharmaceutics and Biopharmaceutics*, 58(2):317–326, 2004.
- [38] A. Mazor, L. Orefice, A. Michrafy, A. de Ryck, and J. G. Khinast. A combined DEM & FEM approach for modelling roll compaction process. *Powder Technology*, 2017.
- [39] A. Hassanpour, M. Pasha, L. Susana, N. Rahmanian, A. C. Santomaso, and M. Ghadiri. Analysis of seeded granulation in high shear granulators by discrete element method. *Powder Technology*, 238:50–55, 2013.
- [40] D. K. Kafui and C. Thornton. Fully-3d dem simulation of fluidised bed spray granulation using an exploratory surface energy-based spray zone concept. *Powder Technology*, 184(2):177–188, 2008.
- [41] W. R. Ketterhagen. Simulation of powder flow in a lab-scale tablet press feed frame: Effects of design and operating parameters on measures of tablet quality. *Powder Technology*, 275(0):361–374, 2015.
- [42] J. Wang, H. Wen, and D. Desai. Lubrication in tablet formulations. *European Journal of Pharmaceutics and Biopharmaceutics*, 75(1):1–15, 2010.
- [43] M. Jivraj, L. G. Martini, and C. M. Thomson. An overview of the different excipients useful for the direct compression of tablets. *Pharmaceutical Science & Technology Today*, 3(2):58–63, 2000.
-

- [44] G. Thoorens, F. Krier, B. Leclercq, B. Carlin, and B. Evrard. Microcrystalline cellulose, a direct compression binder in a quality by design environment - a review. *International Journal of Pharmaceutics*, 473(1-2):64–72, 2014.
- [45] K. H. Bauer, K.-H. Frömming, and C. Führer. *Pharmazeutische Technologie*. Wissenschaftliche Verlagsgesellschaft, 10 edition, 2017.
- [46] T. Sinha, R. Bharadwaj, J. S. Curtis, B. C. Hancock, and C. Wassgren. Finite element analysis of pharmaceutical tablet compaction using a density dependent material plasticity model. *Powder Technology*, 202(1–3):46–54, 2010.
- [47] H. Diarra, V. Mazel, V. Busignies, and P. Tchoreloff. FEM simulation of the die compaction of pharmaceutical products Influence of visco-elastic phenomena and comparison with experiments. *International Journal of Pharmaceutics*, 453(2):389–394, 2013.
- [48] G. Toschkoff, S. Just, A. Funke, D. Djuric, K. Knop, P. Kleinebudde, G. Scharrer, and J. G. Khinast. Spray models for discrete element simulations of particle coating processes. *Chemical Engineering Science*, 101(0):603–614, 2013.
- [49] G. Toschkoff and J. G. Khinast. Mathematical modeling of the coating process. *International Journal of Pharmaceutics*, 457(2):407–422, 2013.
- [50] P. Boehling, G. Toschkoff, K. Knop, P. Kleinebudde, S. Just, A. Funke, H. Rehbaum, and J. G. Khinast. Analysis of large-scale tablet coating: Modeling, simulation and experiments. *European Journal of Pharmaceutical Sciences*, 90:14–24, 2016.
- [51] B. Aksu, T. D. Beer, S. Folestad, J. Ketolainen, H. Lindén, J. A. Lopes, M. d. Matas, W. Oostra, J. Rantanen, and M. Weimer. Strategic funding priorities in the pharmaceutical sciences allied to quality by design (QbD) and process analytical technology (PAT). *European Journal of Pharmaceutical Sciences*, 47(2):402–405, 2012.
- [52] K. V. Gernaey, A. E. Cervera-Padrell, and J. M. Woodley. A perspective on PSE in pharmaceutical process development and innovation. *Computers & Chemical Engineering*, 42:15–29, 2012.
- [53] N. Govender, D. N. Wilke, P. Pizette, and R. K. Rajamani. Industrial scale particle simulations on the GPU using the Blaze-DEM Code. In X. Li, Y. Feng, and G. Mustoe, editors, *Proceedings of the 7th International Conference on Discrete Element Methods*, pages 1379–1388. Springer Singapore, 2016.
- [54] C. A. Radeke, B. J. Glasser, and J. G. Khinast. Large-scale powder mixer simulations using massively parallel GPU architectures. *Chemical Engineering Science*, 65(24):6435–6442, 2010.
- [55] J. Xu, H. Qi, X. Fang, L. Lu, W. Ge, X. Wang, M. Xu, F. Chen, X. He, and J. Li. Quasi-real-time simulation of rotating drum using discrete element method with parallel GPU computing. *Particuology*, 9(4):446–450, 2011.
- [56] N. Jiménez-Herrera, G. K. P. Barrios, and L. M. Tavares. Comparison of breakage models in DEM in simulating impact on particle beds. *Advanced Powder Technology*, 29(3):692–706, 2018.
- [57] S. Jackson, I. C. Sinka, and A. C. F. Cocks. The effect of suction during die fill on a rotary tablet press. *European Journal of Pharmaceutics and Biopharmaceutics*, 65(2):253–256, 2007.

-
- [58] H. H. Hausner. Effect of quench sintering on the grain structure of sintered metals. *International Journal of Powder Metallurgy*, 8:159–161, 1972.
- [59] L. Svarovsky. *Powder testing guide*. Published on behalf of the British Materials Handling Board by Elsevier Applied Science, 1987.
- [60] M. Rios. Developments in powder flow testing. *PharmTech*, 30(2):38–49, 2006.
- [61] J. Schwedes. Review on testers for measuring flow properties of bulk solids. *Granular Matter*, 5(1):1–43, 2003.
- [62] D. Schulze. *Powders and Bulk Solids: Behavior, Characterization, Storage and Flow*. Springer, 2003.
- [63] C.-Y. Wu, L. Dihoru, and A. C. F. Cocks. The flow of powder into simple and stepped dies. *Powder Technology*, 134(1–2):24–39, 2003.
- [64] A. Zettler, J. Hilden, M. Koenig, C. Breslin, A. Aburub, M. Allgeier, P. Patel, and B. Mitra. Evaluation of small-scale powder flow characterization tests in the prediction of large-scale process failures. *Journal of Pharmaceutical Innovation*, 11(3):189–199, 2016.
- [65] C. C. Sun. Setting the bar for powder flow properties in successful high speed tableting. *Powder Technology*, 201(1):106–108, 2010.
- [66] M. Capece, K. R. Silva, D. Sunkara, J. Strong, and P. Gao. On the relationship of inter-particle cohesiveness and bulk powder behavior: Flowability of pharmaceutical powders. *International Journal of Pharmaceutics*, 511(1):178–189, 2016.
- [67] M. Capece, R. Ho, J. Strong, and P. Gao. Prediction of powder flow performance using a multi-component granular bond number. *Powder Technology*, 286(Supplement C):561–571, 2015.
- [68] F. Podczeczek and Y. Mia. The influence of particle size and shape on the angle of internal friction and the flow factor of unlubricated and lubricated powders. *International Journal of Pharmaceutics*, 144(2):187–194, 1996.
- [69] H. Hou and C. C. Sun. Quantifying effects of particulate properties on powder flow properties using a ring shear tester. *Journal of Pharmaceutical Sciences*, 97(9):4030–4039, 2008.
- [70] N. Leyva and M. P. Mullarney. Modeling pharmaceutical powder-flow performance using particle-size distribution data. *Pharmaceutical Technology*, 33(3), 2009.
- [71] W. R. Ketterhagen and B. C. Hancock. Optimizing the design of eccentric feed hoppers for tablet presses using DEM. *Computers & Chemical Engineering*, 34(7):1072–1081, 2010.
- [72] N. Kholá and C. Wassgren. Correlations for shear-induced percolation segregation in granular shear flows. *Powder Technology*, 288:441–452, 2016.
- [73] H. J. Venables and J. I. Wells. Powder mixing. *Drug Development and Industrial Pharmacy*, 27(7):599–612, 2001.
- [74] A. D. Rosato, D. L. Blackmore, N. Zhang, and Y. Lan. A perspective on vibration-induced size segregation of granular materials. *Chemical Engineering Science*, 57(2):265–275, 2002.
- [75] P. Tang and V. M. Puri. Percolation segregation model for similar and differing constituents. *Particulate Science and Technology*, 28(4):287–297, 2010.
-

- [76] A. S. Narang, V. M. Rao, H. Guo, J. Lu, and D. S. Desai. Effect of force feeder on tablet strength during compression. *International Journal of Pharmaceutics*, 401(1–2):7–15, 2010.
- [77] I. C. Sinka, J. C. Cunningham, and A. Zavaliangos. Analysis of tablet compaction. II. finite element analysis of density distributions in convex tablets. *Journal of Pharmaceutical Sciences*, 93(8):2040–53, 2004.
- [78] L. C. R. Schneider, I. C. Sinka, and A. C. F. Cocks. Characterisation of the flow behaviour of pharmaceutical powders using a model die–shoe filling system. *Powder Technology*, 173(1):59–71, 2007.
- [79] C.-Y. Wu and A. C. F. Cocks. Numerical and experimental investigations of the flow of powder into a confined space. *Mechanics of Materials*, 38(4):304–324, 2006.
- [80] Y. Yaginuma, Y. Ozeki, M. Kakizawa, S. I. Gomi, and Y. Watanabe. Effects of powder flowability on die-fill properties in rotary compression. *Journal of Drug Delivery Science and Technology*, 17(3):205–210, 2007.
- [81] C.-Y. Wu. DEM simulations of die filling during pharmaceutical tableting. *Particuology*, 6(6):412–418, 2008.
- [82] Y. Guo, C. Y. Wu, K. D. Kafui, and C. Thornton. 3D DEM/CFD analysis of size-induced segregation during die filling. *Powder Technology*, 206(1–2):177–188, 2011.
- [83] E. N. Nwose, C. Pei, and C.-Y. Wu. Modelling die filling with charged particles using dem/cfd. *Particuology*, 10(2):229–235, 2012.
- [84] C.-Y. Wu and Y. Guo. Numerical modelling of suction filling using DEM/CFD. *Chemical Engineering Science*, 73(0):231–238, 2012.
- [85] R. Furukawa, Y. Shiosaka, K. Kadota, K. Takagaki, T. Noguchi, A. Shimosaka, and Y. Shirakawa. Size-induced segregation during pharmaceutical particle die filling assessed by response surface methodology using discrete element method. *Journal of Drug Delivery Science and Technology*, 35:284–293, 2016.
- [86] R. Mendez, F. Muzzio, and C. Velazquez. Study of the effects of feed frames on powder blend properties during the filling of tablet press dies. *Powder Technology*, 200(3):105–116, 2010.
- [87] E. Peeters, T. De Beer, C. Vervaet, and J.-P. Remon. Reduction of tablet weight variability by optimizing paddle speed in the forced feeder of a high-speed rotary tablet press. *Drug Development and Industrial Pharmacy*, 41(4):530–539, 2015.
- [88] W. Grymonpré, V. Vanhoorne, B. Van Snick, B. Blahova Prudilova, F. Detobel, J. P. Remon, T. De Beer, and C. Vervaet. Optimizing feed frame design and tableting process parameters to increase die-filling uniformity on a high-speed rotary tablet press. *International Journal of Pharmaceutics*, 548(1):54–61, 2018.
- [89] M. Duelle, H. Oezcoban, and C. S. Leopold. Investigations on the residence time distribution of a three-chamber feed frame with special focus on its geometric and parametric setups. *Powder Technology*, 331:276–285, 2018.
- [90] R. Mendez, F. J. Muzzio, and C. Velazquez. Powder hydrophobicity and flow properties: Effect of feed frame design and operating parameters. *AIChE Journal*, 58(3):697–706, 2012.

-
- [91] W. Li, L. Bagnol, M. Berman, R. A. Chiarella, and M. Gerber. Applications of NIR in early stage formulation development. Part II. content uniformity evaluation of low dose tablets by principal component analysis. *International Journal of Pharmaceutics*, 380(1):49–54, 2009.
- [92] H. W. Ward, D. O. Blackwood, M. Polizzi, and H. Clarke. Monitoring blend potency in a tablet press feed frame using near infrared spectroscopy. *Journal of Pharmaceutical and Biomedical Analysis*, 80:18–23, 2013.
- [93] D. Mateo-Ortiz, F. J. Muzzio, and R. Mendez. Particle size segregation promoted by powder flow in confined space: The die filling process case. *Powder Technology*, 262:215–222, 2014.
- [94] D. Mateo-Ortiz and R. Mendez. Microdynamic analysis of particle flow in a confined space using DEM: The feed frame case. *Advanced Powder Technology*, 21(4):1597–1606, 2016.
- [95] D. Mateo-Ortiz and R. Méndez. Relationship between residence time distribution and forces applied by paddles on powder attrition during the die filling process. *Powder Technology*, 278:111–117, 2015.
- [96] I. C. Sinka, L. C. R. Schneider, and A. C. F. Cocks. Measurement of the flow properties of powders with special reference to die fill. *International Journal of Pharmaceutics*, 280(1–2):27–38, 2004.
- [97] X. Xie and V. M. Puri. Uniformity of powder die filling using a feed shoe: A review. *Particulate Science and Technology*, 24(4):411–426, 2006.
- [98] I. C. Sinka, F. Motazedian, A. C. F. Cocks, and K. G. Pitt. The effect of processing parameters on pharmaceutical tablet properties. *Powder Technology*, 189(2):276–284, 2009.
- [99] A. Mehrotra, B. Chaudhuri, A. Faqih, M. S. Tomassone, and F. J. Muzzio. A modeling approach for understanding effects of powder flow properties on tablet weight variability. *Powder Technology*, 188(3):295–300, 2009.
- [100] C.-Y. Wu, X. F. Fan, F. Motazedian, J. P. K. Seville, D. J. Parker, and A. C. F. Cocks. Quantitative investigation of powder flow during die filling using positron emission particle tracking. *Proceedings of the Institution of Mechanical Engineers, Part E: Journal of Process Mechanical Engineering*, 224(3):169–175, 2010.
- [101] Y. Guo, C. Y. Wu, K. D. Kafui, and C. Thornton. 3D DEM/CFD analysis of size-induced segregation during die filling. *Powder Technology*, 206(1–2):177–188, 2011.
- [102] R. Mendez, C. Velazquez, and F. J. Muzzio. Effect of feed frame design and operating parameters on powder attrition, particle breakage, and powder properties. *Powder Technology*, 229(0):253–260, 2012.
- [103] C.-Y. Wu, B. Armstrong, and N. Vlachos. Characterization of powder flowability for die filling. *Particulate Science and Technology*, 30(4):378–389, 2012.
- [104] L. A. Mills and I. C. Sinka. Effect of particle size and density on the die fill of powders. *European Journal of Pharmaceutics and Biopharmaceutics*, 84(3):642–652, 2013.
- [105] K. Järvinen, W. Hoehe, M. Järvinen, S. Poutiainen, M. Juuti, and S. Borchert. In-line monitoring of the drug content of powder mixtures and tablets by near-infrared spectroscopy during the continuous direct compression tableting process. *European Journal of Pharmaceutical Sciences*, 48(4):680–688, 2013.
-

- [106] P. R. Wahl, G. Fruhmann, S. Sacher, G. Straka, S. Sowinski, and J. G. Khinast. PAT for tableting: Inline monitoring of API and excipients via NIR spectroscopy. *European Journal of Pharmaceutics and Biopharmaceutics*, 87(2):271–278, 2014.
- [107] D. Mateo-Ortiz, Y. Colon, R. J. Romañach, and R. Méndez. Analysis of powder phenomena inside a fette 3090 feed frame using in-line NIR spectroscopy. *Journal of Pharmaceutical and Biomedical Analysis*, 100:40–49, 2014.
- [108] S. Šašić, D. Blackwood, A. Liu, H. W. Ward, and H. Clarke. Detailed analysis of the online near-infrared spectra of pharmaceutical blend in a rotary tablet press feed frame. *Journal of Pharmaceutical and Biomedical Analysis*, 103:73–79, 2015.
- [109] Y. Tsunazawa, Y. Shigeto, C. Tokoro, and M. Sakai. Numerical simulation of industrial die filling using the discrete element method. *Chemical Engineering Science*, 138:791–809, 2015.
- [110] E. Peeters, V. Vanhoorne, C. Vervaet, and J.-P. Remon. Lubricant sensitivity in function of paddle movement in the forced feeder of a high-speed tablet press. *Drug Development and Industrial Pharmacy*, 42(12), 2016.
- [111] P. Durão, C. Fauteux-Lefebvre, J.-M. Guay, N. Abatzoglou, and R. Gosselin. Using multiple process analytical technology probes to monitor multivitamin blends in a tableting feed frame. *Talanta*, 164:7–15, 2017.
- [112] S. Schiano, L. Chen, and C.-Y. Wu. The effect of dry granulation on flow behaviour of pharmaceutical powders during die filling. *Powder Technology*, 2017.
- [113] F. De Leersnyder, E. Peeters, H. Djalabi, V. Vanhoorne, B. Van Snick, K. Hong, S. Hammond, A. Y. Liu, E. Ziemons, C. Vervaet, and T. De Beer. Development and validation of an in-line NIR spectroscopic method for continuous blend potency determination in the feed frame of a tablet press. *Journal of Pharmaceutical and Biomedical Analysis*, 151:274–283, 2018.
- [114] H. Dalvi, C. Fauteux-Lefebvre, J.-M. Guay, N. Abatzoglou, and R. Gosselin. Concentration monitoring with near infrared chemical imaging in a tableting press. *J. Spectral Imaging*, 7, 2018.
- [115] P. A. Cundall and O. D. L. Strack. A discrete numerical model for granular assemblies. *Geotechniques*, 29(1):47–65, 1979.
- [116] *LIGGGHTS(R)-PUBLIC Documentation, Version 3.X*.
- [117] C. Geuzaine and J.-F. Remacle. Gmsh: A 3-D finite element mesh generator with built-in pre- and post-processing facilities. *International Journal for Numerical Methods in Engineering*, 79(11):1309–1331, 2009.
- [118] U. Ayachit. *The Paraview Guide: A Parallel Visualization Application*. Kitware, 2015.
- [119] A. Di Renzo and F. P. Di Maio. Comparison of contact-force models for the simulation of collisions in DEM-based granular flow codes. *Chemical Engineering Science*, 59(3):525–541, 2004.
- [120] H. Hertz. Über die Berührung fester elastische Körper - on the contact of elastic solids. *Journal für die reine und angewandte Mathematik*, 92:156–171, 1882.

-
- [121] T. Gröger and A. Katterfeld. On the numerical calibration of discrete element models for the simulation of bulk solids. In W. Marquardt and C. Pantelides, editors, *Computer Aided Chemical Engineering*, volume 21, pages 533–538. Elsevier, 2006.
- [122] R. D. Mindlin and H. Deresiewicz. Elastic spheres in contact under varying oblique forces. *Journal of Applied Mechanics*, 20:327–344, 1953.
- [123] C. Kloss, C. Goniva, A. Hager, S. Amberger, and S. Pirker. Models, algorithms and validation for opensource DEM and CFD-DEM. *Progress in Computational Fluid Dynamics*, 12(2/3):140–152, 2012.
- [124] H. C. Hamaker. The London-van der Waals attraction between spherical particles. *Physica*, 4(10):1058–1072, 1937.
- [125] H. Krupp. Particle adhesion theory and experiment. *Advances in Colloid and Interface Science*, 1:111–239, 1967.
- [126] R. A. Fisher. On the capillary forces in an ideal soil; correction of formulae given by w. b. haines. *The Journal of Agricultural Science*, 16(03):492–505, 1926.
- [127] K. L. Johnson, K. Kendall, and A. D. Roberts. *Surface Energy and the Contact of Elastic Solids*, volume 324. 1971.
- [128] B. Govedarica, I. Ilić, R. Šibanc, R. Dreu, and S. Srčić. The use of single particle mechanical properties for predicting the compressibility of pharmaceutical materials. *Powder Technology*, 225(0):43–51, 2012.
- [129] I. Ilić, B. Govedarica, R. Šibanc, R. Dreu, and S. Srčić. Deformation properties of pharmaceutical excipients determined using an in-die and out-die method. *International Journal of Pharmaceutics*, 446(1–2):6–15, 2013.
- [130] L. J. Taylor, D. G. Papadopoulos, P. J. Dunn, A. C. Bentham, J. C. Mitchell, and M. J. Snowden. Mechanical characterisation of powders using nanoindentation. *Powder Technology*, 143–144(0):179–185, 2004.
- [131] V. M. Masterson and X. Cao. Evaluating particle hardness of pharmaceutical solids using AFM nanoindentation. *International Journal of Pharmaceutics*, 362(1–2):163–171, 2008.
- [132] M. Perkins, S. J. Ebbens, S. Hayes, C. J. Roberts, C. E. Madden, S. Y. Luk, and N. Patel. Elastic modulus measurements from individual lactose particles using atomic force microscopy. *International Journal of Pharmaceutics*, 332(1–2):168–175, 2007.
- [133] F. Bassam, P. York, R. C. Rowe, and R. J. Roberts. Young’s modulus of powders used as pharmaceutical excipients. *International Journal of Pharmaceutics*, 64(1):55–60, 1990.
- [134] C. Mangwandi, Y. S. Cheong, M. J. Adams, M. J. Hounslow, and A. D. Salman. The coefficient of restitution of different representative types of granules. *Chemical Engineering Science*, 62(1–2):437–450, 2007.
- [135] R. Liburkin, D. Portnikov, and H. Kalman. Comparing particle breakage in an uniaxial confined compression test to single particle crush tests—model and experimental results. *Powder Technology*, 284:344–354, 2015.
-

- [136] D. Portnikov and H. Kalman. Determination of elastic properties of particles using single particle compression test. *Powder Technology*, 268:244–252, 2014.
- [137] R. J. Roberts, R. C. Rowe, and P. York. The poisson’s ratio of microcrystalline cellulose. *International Journal of Pharmaceutics*, 105(2):177–180, 1994.
- [138] R. Šibanc, T. Kitak, B. Govedarica, S. Srčić, and R. Dreu. Physical properties of pharmaceutical pellets. *Chemical Engineering Science*, 86(0):50–60, 2013.
- [139] L. Wang, W. Zhou, Z. Ding, X. Li, and C. Zhang. Experimental determination of parameter effects on the coefficient of restitution of differently shaped maize in three-dimensions. *Powder Technology*, 284(0):187–194, 2015.
- [140] R. Bharadwaj, C. Smith, and B. C. Hancock. The coefficient of restitution of some pharmaceutical tablets/compacts. *International Journal of Pharmaceutics*, 402(1–2):50–56, 2010.
- [141] S. Antonyuk, S. Heinrich, J. Tomas, N. G. Deen, M. van Buijtenen, and J. A. M. Kuipers. Energy absorption during compression and impact of dry elastic-plastic spherical granules. *Granular Matter*, 12(1):15–47, 2010.
- [142] J. Ai, J.-F. Chen, J. M. Rotter, and J. Y. Ooi. Assessment of rolling resistance models in discrete element simulations. *Powder Technology*, 206(3):269–282, 2011.
- [143] Y. Li, Y. Xu, and C. Thornton. A comparison of discrete element simulations and experiments for ‘sandpiles’ composed of spherical particles. *Powder Technology*, 160(3):219–228, 2005.
- [144] W. R. Ketterhagen, R. Bharadwaj, and B. C. Hancock. The coefficient of rolling resistance (corr) of some pharmaceutical tablets. *International Journal of Pharmaceutics*, 392(1–2):107–110, 2010.
- [145] A. Jensen, K. Fraser, and G. Laird. Improving the precision of discrete element simulations through calibration models. In *Proceedings of the 13th International LS-DYNA Conference, Dearborn, MI, USA.*, 2014.
- [146] M. J. Bunker, C. J. Roberts, M. C. Davies, and M. B. James. A nanoscale study of particle friction in a pharmaceutical system. *International Journal of Pharmaceutics*, 325(1–2):163–171, 2006.
- [147] B. C. Hancock, N. Mojica, K. St.John-Green, J. A. Elliott, and R. Bharadwaj. An investigation into the kinetic (sliding) friction of some tablets and capsules. *International Journal of Pharmaceutics*, 384(1–2):39–45, 2010.
- [148] M. Lohrmann, M. Kappl, H.-J. Butt, N. A. Urbanetz, and B. C. Lippold. Adhesion forces in interactive mixtures for dry powder inhalers – evaluation of a new measuring method. *European Journal of Pharmaceutics and Biopharmaceutics*, 67(2):579–586, 2007.
- [149] M.-J. Colbert, M. Grandbois, and N. Abatzoglou. Identification of inter-particle forces by atomic force microscopy and how they relate to powder rheological properties measured in shearing tests. *Powder Technology*, 284:396–402, 2015.
- [150] T. T. Nguyen, C. Rambanapasi, A. H. de Boer, H. W. Frijlink, P. M. v. D. Ven, J. de Vries, H. J. Bussecher, and K. v. D. V. Maarschalk. A centrifuge method to measure particle cohesion forces to substrate surfaces: The use of a force distribution concept for data interpretation. *International Journal of Pharmaceutics*, 393(1–2):89–96, 2010.

-
- [151] G. R. Salazar-Banda, M. A. Felicetti, J. A. S. Gonçalves, J. R. Coury, and M. L. Aguiar. Determination of the adhesion force between particles and a flat surface, using the centrifuge technique. *Powder Technology*, 173(2):107–117, 2007.
- [152] M. C. Thomas and S. P. Beaudoin. An enhanced centrifuge-based approach to powder characterization: Particle size and Hamaker Constant determination. *Powder Technology*, 2786:412–419, 2015.
- [153] P. Kulvanich and P. J. Stewart. Fundamental considerations in the measurement of adhesional forces between particles using the centrifuge method. *International Journal of Pharmaceutics*, 35(1–2):111–120, 1987.
- [154] U. Zafar, C. Hare, A. Hassanpour, and M. Ghadiri. Drop test: A new method to measure the particle adhesion force. *Powder Technology*, 264(0):236–241, 2014.
- [155] A. Schweiger and I. Zimmermann. A new approach for the measurement of the tensile strength of powders. *Powder Technology*, 101(1):7–15, 1999.
- [156] M. Davies, A. Brindley, X. Chen, M. Marlow, S. W. Doughty, I. Shrubbs, and C. J. Roberts. Characterization of drug particle surface energetics and young’s modulus by atomic force microscopy and inverse gas chromatography. *Pharmaceutical Research*, 22(7):1158–1166, 2005.
- [157] C. J. Coetzee. Review: Calibration of the discrete element method. *Powder Technology*, 310:104–142, 2017.
- [158] L. Bennani, H. Neau, C. Baudry, J. Laviéville, P. Fede, and O. Simonin. Numerical simulation of unsteady dense granular flows with rotating geometries. *Chemical Engineering Research and Design*, 120(Supplement C):333–347, 2017.
- [159] S. C. Thakur, J. Y. Ooi, and H. Ahmadian. Scaling of discrete element model parameters for cohesionless and cohesive solid. *Powder Technology*, 293:130–137, 2016.
- [160] Y. T. Feng, K. Han, R. R. J. Owen, and J. Loughran. On upscaling of discrete element models: similarity principles. *Engineering Computations*, 26(6):599–609, 2009.
- [161] A. Dubey. 3 - powder flow and blending. In P. Pandey and R. Bharadwaj, editors, *Predictive Modeling of Pharmaceutical Unit Operations*, pages 39–69. Woodhead Publishing, 2017.
- [162] A. Hassanpour, H. Tan, A. Bayly, P. Gopalkrishnan, B. Ng, and M. Ghadiri. Analysis of particle motion in a paddle mixer using discrete element method (DEM). *Powder Technology*, 206(1):189–194, 2011.
- [163] M. Paulick, M. Morgeneyer, and A. Kwade. Review on the influence of elastic particle properties on DEM simulation results. *Powder Technology*, 283:66–76, 2015.
- [164] S. Just, G. Toschkoff, A. Funke, D. Djuric, G. Scharrer, J. Khinast, K. Knop, and P. Kleinebudde. Experimental analysis of tablet properties for discrete element modeling of an active coating process. *AAPS PharmSciTech*, 14(1):402–411, 2013.
- [165] K. J. Berger and C. M. Hrenya. Challenges of DEM: II. wide particle size distributions. *Powder Technology*, 264:627–633, 2014.
-

- [166] B. Remy, T. M. Canty, J. G. Khinast, and B. J. Glasser. Experiments and simulations of cohesionless particles with varying roughness in a bladed mixer. *Chemical Engineering Science*, 65(16):4557–4571, 2010.
- [167] M. Marigo and E. H. Stitt. Discrete element method (DEM) for industrial applications: Comments on calibration and validation for the modelling of cylindrical pellets. *KONA Powder and Particle Journal*, 32:236–252, 2015.
- [168] S. R. Gopireddy, C. Hildebrandt, and N. A. Urbanetz. Numerical simulation of powder flow in a pharmaceutical tablet press lab-scale gravity feeder. *Powder Technology*, 302:309–327, 2016.
- [169] C. Hildebrandt, S. R. Gopireddy, R. Scherließ, and N. A. Urbanetz. Simulation of particle size segregation in a pharmaceutical tablet press lab-scale gravity feeder. *Advanced Powder Technology*, 29:765–780, 2018.
- [170] C. Hildebrandt, S. R. Gopireddy, R. Scherließ, and N. A. Urbanetz. Numerical analysis of the die filling process within a pharmaceutical tableting machine. *Chemie Ingenieur Technik*, 9(4):483–492, 2018.
- [171] C. Hildebrandt, S. R. Gopireddy, R. Scherließ, and N. A. Urbanetz. Powder flow within a pharmaceutical tablet press - a DEM analysis. In P. Wriggers, M. Bischoff, E. Oñate, D. Owen, and T. Zohdi, editors, *V International Conference on Particle-based Methods - Fundamentals and Applications*, volume 5, pages 237–248, 2017.
- [172] M. Alian, F. Ein-Mozaffari, and S. R. Upreti. Analysis of the mixing of solid particles in a plowshare mixer via discrete element method (DEM). *Powder Technology*, 274(0):77–87, 2015.
- [173] B. Freireich, R. Kumar, W. Ketterhagen, K. Su, C. Wassgren, and J. A. Zeitler. Comparisons of intra-tablet coating variability using DEM simulations, asymptotic limit models, and experiments. *Chemical Engineering Science*, 131(0):197–212, 2015.
- [174] L. Fries, S. Antonyuk, S. Heinrich, D. Dopfer, and S. Palzer. Collision dynamics in fluidised bed granulators: A DEM-CFD study. *Chemical Engineering Science*, 86(0):108–123, 2013.
- [175] R. Rajamani, S. Rashidi, and N. Dhawan. Advances in discrete element method application to grinding mills. *Mineral Processing and Extractive Metallurgy: 100 Years of Innovation*, pages 117–128, 2014.
- [176] D. Kretz, S. Callau-Monje, M. Hitschler, A. Hien, M. Raedle, and J. Hesser. Discrete element method (DEM) simulation and validation of a screw feeder system. *Powder Technology*, 287:131–138, 2016.
- [177] A. Anand, J. S. Curtis, C. R. Wassgren, B. C. Hancock, and W. R. Ketterhagen. Predicting discharge dynamics of wet cohesive particles from a rectangular hopper using the discrete element method (DEM). *Chemical Engineering Science*, 64(24):5268–5275, 2009.
- [178] H. J. Herrmann and S. Luding. Modeling granular media on the computer. *Continuum Mechanics and Thermodynamics*, 10(4):189–231, 1998.
- [179] W. A. Beverloo, H. A. Leniger, and J. van de Velde. The flow of granular solids through orifices. *Chemical Engineering Science*, 15:260–269, 1961.

-
- [180] V. Boonkanokwong, B. Remy, J. G. Khinast, and B. J. Glasser. The effect of the number of impeller blades on granular flow in a bladed mixer. *Powder Technology*, 302:333–349, 2016.
- [181] P. Tang and V. M. Puri. Methods for minimizing segregation: A review. *Particulate Science and Technology*, 22(4):321–337, 2004.
- [182] J. R. Johanson. Predicting segregation of bimodal particle mixtures using the flow properties of bulk solids. *Pharmaceutical Technology*, 20(5):46–57, 1996.
- [183] C. Hildebrandt, S. R. Gopireddy, A. K. Fritsch, T. Profitlich, R. Scherließ, and N. A. Urbanetz. Evaluation and prediction of powder flowability in pharmaceutical tableting. *Pharmaceutical Development and Technology*, pages 1–13, 2017.
- [184] A. Anand, J. S. Curtis, C. R. Wassgren, B. C. Hancock, and W. R. Ketterhagen. Predicting discharge dynamics from a rectangular hopper using the discrete element method (DEM). *Chemical Engineering Science*, 63(24):5821–5830, 2008.
- [185] D. Antypov, J. A. Elliott, and B. C. Hancock. Effect of particle size on energy dissipation in viscoelastic granular collisions. *Physical Review E*, 84(2), 2011.
- [186] C. Hildebrandt, S. R. Gopireddy, R. Scherließ, and N. A. Urbanetz. Assessment of material and process attributes’ influence on tablet quality using a QbD and DEM combined approach. *Powder Technology*, under review, 2018.
- [187] O. I. Imole, D. Krijgsman, T. Weinhart, V. Magnanimo, B. E. Chávez Montes, M. Ramaioli, and S. Luding. Experiments and discrete element simulation of the dosing of cohesive powders in a simplified geometry. *Powder Technology*, 287:108–120, 2016.
- [188] J. Bridgwater. Mixing of powders and granular materials by mechanical means—a perspective. *Particuology*, 10(4):397–427, 2012.
- [189] R. Hogg. Characterization of relative homogeneity in particulate mixtures. *International Journal of Mineral Processing*, 72(1–4):477–487, 2003.
- [190] R. Hogg. Mixing and segregation in powders: evaluation, mechanisms and processes. *KONA Powder and Particle Journal*, 27:3–17, 2009.
- [191] G. R. Chandratilleke, A. B. Yu, J. Bridgwater, and K. Shinohara. A particle-scale index in the quantification of mixing of particles. *AIChE Journal*, 58(4):1099–1118, 2012.
- [192] P. M. C. Lacey. Developments in the theory of particle mixing. *Journal of Applied Chemistry*, 4(5):257–268, 1954.
- [193] L. Pernenkil and C. L. Cooney. A review on the continuous blending of powders. *Chemical Engineering Science*, 61(2):720–742, 2006.
- [194] M. Cho, P. Dutta, and J. Shim. A non-sampling mixing index for multicomponent mixtures. *Powder Technology*, 319:434–444, 2017.
- [195] J. Mosby, S. R. de Silva, and G. G. Enstad. Segregation of particulate materials - mechanisms and testers. *KONA Powder and Particle Journal*, 14:31–43, 1996. Segregation.
- [196] G. R. Chandratilleke, A. B. Yu, and J. Bridgwater. A DEM study of the mixing of particles induced by a flat blade. *Chemical Engineering Science*, 79:54–74, 2012.
-

- [197] S. L. Conway, A. Lekhal, J. G. Khinast, and B. J. Glasser. Granular flow and segregation in a four-bladed mixer. *Chemical Engineering Science*, 60(24):7091–7107, 2005.
- [198] M. Halidan, G. R. Chandratilleke, S. L. I. Chan, A. B. Yu, and J. Bridgwater. Prediction of the mixing behaviour of binary mixtures of particles in a bladed mixer. *Chemical Engineering Science*, 120:37–48, 2014.
- [199] B. Remy, J. G. Khinast, and B. J. Glasser. Polydisperse granular flows in a bladed mixer: Experiments and simulations of cohesionless spheres. *Chemical Engineering Science*, 66(9):1811–1824, 2011.
- [200] Y. C. Zhou, A. B. Yu, R. L. Stewart, and J. Bridgwater. Microdynamic analysis of the particle flow in a cylindrical bladed mixer. *Chemical Engineering Science*, 59(6):1343–1364, 2004.
- [201] G. R. Chandratilleke, A. B. Yu, R. L. Stewart, and J. Bridgwater. Effects of blade rake angle and gap on particle mixing in a cylindrical mixer. *Powder Technology*, 193(3):303–311, 2009.
- [202] S. Radl, D. Brandl, H. Heimbürg, B. J. Glasser, and J. G. Khinast. Flow and mixing of granular material over a single blade. *Powder Technology*, 226:199–212, 2012.
- [203] M. S. Siraj, S. Radl, B. J. Glasser, and J. G. Khinast. Effect of blade angle and particle size on powder mixing performance in a rectangular box. *Powder Technology*, 211(1):100–113, 2011.
- [204] R. L. Stewart, J. Bridgwater, and D. J. Parker. Granular flow over a flat-bladed stirrer. *Chemical Engineering Science*, 56(14):4257–4271, 2001.
- [205] J. Kushner Iv and F. Moore. Scale-up model describing the impact of lubrication on tablet tensile strength. *International Journal of Pharmaceutics*, 399(1–2):19–30, 2010.
- [206] D. S. Desai, B. A. Rubitski, S. A. Varia, and A. W. Newman. Physical interactions of magnesium stearate with starch-derived disintegrants and their effects on capsule and tablet dissolution. *International Journal of Pharmaceutics*, 91(2–3):217–226, 1993.
- [207] A. C. Shah and A. R. Mlodozieniec. Mechanism of surface lubrication: Influence of duration of lubricant-excipient mixing on processing characteristics of powders and properties of compressed tablets. *Journal of Pharmaceutical Sciences*, 66(10):1377–1382, 1977.
- [208] A. Mehrotra, M. Llusa, A. Faqih, M. Levin, and F. J. Muzzio. Influence of shear intensity and total shear on properties of blends and tablets of lactose and cellulose lubricated with magnesium stearate. *International Journal of Pharmaceutics*, 336(2):284–91, 2007.
- [209] D. F. Bagster and J. Bridgwater. The flow of granular material over a moving blade. *Powder Technology*, 3(1):323–338, 1969.
- [210] D. F. Bagster. The prediction of the force needed to move blades through a bed of cohesionless granules. *Powder Technology*, 3(1):153–162, 1969.
- [211] D. F. Bagster and J. Bridgwater. The measurement of the force needed to move blades through a bed of cohesionless granules. *Powder Technology*, 1(4):189–198, 1967.
- [212] R. A. Carson, J. W. and Royal and D. A. Goodwill. Understanding and eliminating particle segregation problems. *Bulk Solids Handling*, 6:139–144, 1986.

-
- [213] J. R. Johanson. Solids segregation - causes and solutions. *Powder and Bulk Engineering Magazine*, pages 13–19, 1988.
- [214] M. Santl, I. Ilic, F. Vrečer, and S. Baumgartner. A compressibility and compactibility study of real tableting mixtures: the effect of granule particle size. *Acta Pharm*, 62(3):325–40, 2012.
- [215] B. Johansson, F. Nicklasson, and G. Alderborn. Effect of pellet size on degree of deformation and densification during compression and on compactability of microcrystalline cellulose pellets. *International Journal of Pharmaceutics*, 196:35–48, 1998.
- [216] M. Wikberg and G. Alderborn. Compression characteristics of granulated materials. ii evaluation of granule fragmentation during compression by tablet permeability and porosity measurements. *International Journal of Pharmaceutics*, 62:229–241, 1990.
- [217] K. Zuurman, K. A. Riepma, G. K. Bolhuis, H. Vormans, and C. F. Ierk. The relationship between bulk density and compactability of lactose granulations. *International Journal of Pharmaceutics*, 102:1–9, 1994.
- [218] K. A. Riepma, H. Vormans, K. Zuurman, and C. F. Lerk. The effect of dry granulation on the consolidation and compaction of crystalline cellulose. *International Journal of Pharmaceutics*, 97:29–38, 1993.
- [219] A. B. Bangudu, O. F. Akande, and V. T. Adewuyi. The effect of interaction variables on the compaction performance of paracetamol / millet starch tablets. *World Journal of Pharmaceutical Sciences*, 8:87–90, 1991.
- [220] M. Rehula. The effect of granule size on dissolution of drugs from tablets. *Folia Pharmacologica Japonica*, 8:101–107, 1985.
- [221] S. Lakio, S. Siiriä, H. Rääkkönen, S. Airaksinen, T. Närvänen, O. Antikainen, and J. Yliruusi. New insights into segregation during tableting. *International Journal of Pharmaceutics*, 397(1–2):19–26, 2010.
- [222] C. Nyström, G. Alderborn, and M. Duberg. Bonding surface area and bonding mechanism - two important factors for the understanding of powder compactability. *Drug Development & Industrial Pharmacy*, 19:2143–2196, 1993.
- [223] D. Fichtner, A. Rasmuson, and G. Alderborn. Particle size distribution and evolution of tablet structure during and after compaction. *International Journal of Pharmaceutics*, 292:211–225, 2005.
- [224] S. Patel, A. M. Kaushal, and A. K. Bensal. Effect of particle size and compression force on compaction behavior and derived mathematical parameters of compressibility. *Pharmaceutical Research*, pages 111–124, 2007.
- [225] T. Lee and C. S. Kuo. Effect of initial average particle size on tableting: Evaluating predictive tools for crystal engineers and formulators. *Pharmaceutical Technology*, 30, 2006.
- [226] J. A. Hersey, G. Bayraktar, and E. Shotton. The effect of particle size on the strength of sodium chloride tablets. *Journal of Pharmacy and Pharmacology*, 19:24–30, 1967.
- [227] T. Yajima, S. Itai, H. Hayashi, K. Takayama, and T. Nagai. Optimization of size distribution of granules for tablet compression. *Chem Pharm Bull (Tokyo)*, 44(5):1056–1060, 1996.
-

- [228] C. Sun and D. J. W. Grant. Effects of initial particle size on the tableting properties of l-lysine monohydrochloride dihydrate powder. *International Journal of Pharmaceutics*, 215(1):221–228, 2001.
- [229] Y. Gao, F. J. Muzzio, and M. G. Ierapetritou. A review of the residence time distribution (RTD) applications in solid unit operations. *Powder Technology*, 228:416–423, 2012.
- [230] R. Fahmy, R. Kona, R. Dandu, W. Xie, G. Claycamp, and S. W. Hoag. Quality by design I: application of failure mode effect analysis (FMEA) and plackett–burman design of experiments in the identification of ‘main factors’ in the formulation and process design space for roller-compacted Ciprofloxacin Hydrochloride immediate-release tablets. *AAPS PharmSciTech*, 13(4):1243–1254, 2012.
- [231] ICH Q9. Quality risk management, 2005.
- [232] J. Huang, G. Kaul, C. Cai, R. Chatlapalli, P. Hernandez-Abad, K. Ghosh, and A. Nagi. Quality by design case study: An integrated multivariate approach to drug product and process development. *International Journal of Pharmaceutics*, 382(1–2):23–32, 2009.
- [233] G. V. Reklaitis, S. Garcia-Munoz, and C. Seymour. *Comprehensive Quality by Design for Pharmaceutical Product Development and Manufacture*. John Wiley & Sons, 2017.
- [234] D. Suzzi, G. Toschkoff, S. Radl, D. Machold, S. D. Fraser, B. J. Glasser, and J. G. Khinast. DEM simulation of continuous tablet coating: Effects of tablet shape and fill level on inter-tablet coating variability. *Chemical Engineering Science*, 69(1):107–121, 2012.
- [235] S. Adam, D. Suzzi, C. Radeke, and J. G. Khinast. An integrated quality by design (QbD) approach towards design space definition of a blending unit operation by discrete element method (DEM) simulation. *European Journal of Pharmaceutical Sciences*, 42(1–2):106–115, 2011.
- [236] C. Hildebrandt, S. R. Gopireddy, R. Scherließ, and N. A. Urbanetz. Investigation of powder flow within a pharmaceutical tablet press force feeder - a DEM approach. *Powder Technology*, under revision, 2018.
- [237] W. Kleppmann. *Versuchsplanung: Produkte und Prozesse optimieren*. Carl Hanser Verlag GmbH Co KG, 2016.
- [238] B. Singh, N. Kumar R Fau Ahuja, and N. Ahuja. Optimizing drug delivery systems using systematic ‘design of experiments.’ part I: fundamental aspects. *Critical Reviews in Therapeutic Drug Carrier Systems*, 22(1):27–105, 2005.
- [239] M. Andersson, A. Ringberg, and C. Gustafsson. Multivariate methods in tablet formulation suitable for early drug development: Predictive models from a screening design of several linked responses. *Chemometrics and Intelligent Laboratory Systems*, 87(1):125–130, 2007.
- [240] T. Lundstedt, E. Seifert, L. Abramo, B. Thelin, s. Nyström, J. Pettersen, and R. Bergman. Experimental design and optimization. *Chemometrics and Intelligent Laboratory Systems*, 42(1):3–40, 1998.
- [241] G. E. P. Box, W. G. Hunter, and J. S. Hunter. *Statistics for experimenters: an introduction to design, data analysis, and model building*, volume 1. Wiley, New York, 1978.
- [242] SAS Institute. JMP online documentation, 2017.

-
- [243] Y. Vander Heyden, A. Nijhuis, J. Smeyers-Verbeke, B. G. M. Vandeginste, and D. L. Massart. Guidance for robustness/ruggedness tests in method validation. *Journal of Pharmaceutical and Biomedical Analysis*, 24(5):723–753, 2001.
- [244] L. Eriksson, E. Johansson, N. Kettaneh-Wold, C. Wikström, and S. Wold. *Design of experiments - Principles and Applications*. Umetrics Academy, Umea, Sweden, 1 edition, 2000.
- [245] E. C. Harrington. The desirability function. *Industrial Quality Control*, 21(10):494–498, 1965.
- [246] GEA Group. Successful tableting, 2016.
- [247] Z. Li, L. Zhao, X. Lin, L. Shen, and Y. Feng. Direct compaction: An update of materials, trouble-shooting, and application. *International Journal of Pharmaceutics*, 529(1):543–556, 2017.
- [248] B.-J. Lee. *Pharmaceutical Preformulation: Physicochemical Properties of Excipients and Powders and Tablet Characterization*. John Wiley & Sons, Inc., 2007.
- [249] USP. *US Pharmacopeial Convention*. US Pharmacopeial Convention, Rockville, Maryland, 2018.
- [250] m. Holte and M. Horvat. Uniformity of dosage units using large sample sizes. *Pharmaceutical Technology*, 36(10):118–122, 2012.
- [251] B. Remy, J. G. Khinast, and B. J. Glasser. Discrete element simulation of free flowing grains in a four-bladed mixer. *AIChE Journal*, 55(8), 2009.
- [252] B. Remy, B. J. Glasser, and J. G. Khinast. The effect of mixer properties and fill level on granular flow in a bladed mixer. *AIChE Journal*, 56(2):336–353, 2010.
- [253] J. Kushner. Utilizing quantitative certificate of analysis data to assess the amount of excipient lot-to-lot variability sampled during drug product development. *Pharmaceutical Development and Technology*, 18(2):333–342, 2013.
- [254] G. Bolhuis, C. A. A. Duineveld, J. H. de Boer, and P. M. J. Coenegracth. Simultaneous optimization of multiple criteria in tablet formulation: part I. *Pharmaceutical Technology Europe*, 8:42–50, 1995.
- [255] R. H. Myers, D. C. Montgomery, and C. M. Anderson-Cook. *Response surface methodology: process and product optimization using designed experiments*. John Wiley & Sons, 2016.
- [256] D. Schulze and A. Wittmaier. Flow properties of highly dispersed powders at very small consolidation stresses. *Chemical Engineering & Technology*, 26(2):133–137, 2003.
- [257] G. Dau. Measurement of the wall friction angle for bulk solids on different wall materials. *Aufbereitungstechnik*, 24:633–647, 1983.
- [258] N. O. Sierra-Vega, A. Sánchez-Paternina, N. Maldonado, V. Cárdenas, R. J. Románach, and R. Méndez. In line monitoring of the powder flow behavior and drug content in a fette 3090 feed frame at different operating conditions using near infrared spectroscopy. *Journal of Pharmaceutical and Biomedical Analysis*, 154:384–396, 2018.
- [259] M. S. Siraj. Single-blade convective powder mixing: The effect of the blade shape and angle. *Powder Technology*, 267(Supplement C):289–301, 2014.

-
- [260] J. Havlica, K. Jiroukova, T. Travnickova, and M. Kohout. The effect of rotational speed on granular flow in a vertical bladed mixer. *Powder Technology*, 280(Supplement C):180–190, 2015.
- [261] C.-Y. Wu, A. C. F. Cocks, O. T. Gillia, and D. A. Thompson. Experimental and numerical investigations of powder transfer. *Powder Technology*, 138(2–3):216–228, 2003.
- [262] C. Hildebrandt, J. Loerzer, S. R. Gopireddy, and N. Urbanetz. Assessing die filling using high-speed camera imaging. *Chemie Ingenieur Technik*, 90(4):472–482, 2018.
- [263] C. P. Long and J. McQuaid. Strategic approaches to process optimization and scale-up. *Pharmaceutical Technology*, 34(9), 2010.
- [264] European Medicines Agency. Note for guidance, process validation, CPMP/QWP/848/96, 2001.
- [265] C. Bierwisch, T. Kraft, H. Riedel, and M. Moseler. Three-dimensional discrete element models for the granular statics and dynamics of powders in cavity filling. *Journal of the Mechanics and Physics of Solids*, 57(1):10–31, 2009.
- [266] Y. Liu and D. Blackwood. Sample presentation in rotary tablet press feed frame monitoring by near infrared spectroscopy. *American Pharmaceutical Review*, 15(1):1–9, 2012.
- [267] C. Hildebrandt, S. R. Gopireddy, R. Scherließ, and N. A. Urbanetz. A DEM approach to assess the influence of the paddle wheel shape on force feeding during pharmaceutical tableting. *Advanced Powder Technology*, under review, 2018.
- [268] D. Kirsch. Fixing tableting problems. *Pharmaceutical Technology*, 39(5):58–59, 2015.
- [269] N. D. Eddington, M. Ashraf, L. L. Augsburger, J. L. Leslie, M. J. Fossler, L. J. Lesko, V. P. Shah, and G. S. Rekhi. Identification of formulation and manufacturing variables that influence in vitro dissolution and in vivo bioavailability of propranolol hydrochloride tablets. *Pharmaceutical Development and Technology*, 3(4):535–547, 1998.
-

Erklärung nach § 8 der Promotionsordnung

Hiermit erkläre ich gemäß § 8 der Promotionsordnung der Mathematisch-Naturwissenschaftlichen Fakultät der Christian-Albrechts-Universität zu Kiel, dass ich die vorliegende Arbeit, abgesehen von der Beratung durch meinen Betreuer, selbstständig und ohne fremde Hilfe verfasst habe. Weiterhin habe ich keine anderen als die angegebenen Quellen oder Hilfsmittel benutzt und die den benutzten Werken wörtlich oder inhaltlich entnommenen Stellen als solche kenntlich gemacht. Die vorliegende Arbeit ist unter Einhaltung der Regeln guter wissenschaftlicher Praxis entstanden und wurde bei keiner anderen Universität zur Begutachtung eingereicht.

Claudia Hildebrandt

Danksagung

An dieser Stelle möchte ich gerne Allen danken, durch deren Mitwirkung die Promotionszeit für mich zu einer der lehrreichsten, in fachlicher sowie persönlicher Sicht, wurde.

Zunächst möchte ich bei meinen beiden Betreuerinnen, Frau Prof. Dr. Regina Scherließ, meiner Doktormutter, und Frau PD Dr. Nora A. Urbanetz für ihre Hilfe und Unterstützung bedanken. Besonderem Dank gilt Frau Prof. Dr. Scherließ für die freundliche Aufnahme in der Abteilung für pharmazeutische Technologie und Biopharmazie, die meine "praktische" Zeit in Kiel in der Gruppe nicht nur fachlich, sondern auch durch den Kontakt mit vielen "Gleichgesinnten" angenehm in Erinnerung behalten lässt. Frau PD Dr. Urbanetz danke ich zum einen für ihre Ermutigung, Ergebnisse im wissenschaftlichen Umfeld zu präsentieren und zu teilen und zum anderen für ihre Begeisterung an den Ergebnissen und deren Erklärungsfindung.

Dr. Srikanth Gopireddy played a key role in this project as his support was fundamental for me to learn numerical simulations with a pharmaceutical background. He continuously supported the project, helped to set up, run, and analyze the simulations and, in addition, helped to evaluate the results. Besides his scientific support, which is highly appreciated, having him as a colleague made things much easier in difficult project phases! Thank you very much, Srikanth!

Der Daiichi Sankyo Europe GmbH danke ich für die Finanzierung der Doktorarbeit und die Gelegenheit, die Promotionsarbeit im industriellen Umfeld anzufertigen. Neben der finanziellen Unterstützung durch die Daiichi Sankyo Europe GmbH, wirkten auch sehr viele Kollegen in Pfaffenhofen und in Japan an dieser Arbeit mit. Neben den Praktikanten, die zu einem großen Anteil an der Durchführung der Experimente beteiligt waren, möchte ich auch den anderen Kollegen für deren fachliche Unterstützung danken. Die konstruktiven Diskussionen bildeten dabei einen Grundstein, um die numerischen Ergebnisse auch in die Realität bzw. Praxis zu übertragen. Besonderer Dank gilt Herrn Dr. Thomas Profitlich, Frau Dr. Maren Kuhli, Herrn Dr. Wolfgang Bauer und Herrn Dr. Wolfgang Schmid. Das FTI-Team war eine große Stütze während der letzten Monate bei der Anfertigung der Arbeit - danke Maren, Ramona und Christian!

Judith, Mathias, Marie, und alle anderen Kieler Doktoranden und TAs halfen mir beim Zurechtfinden am Lehrstuhl und sorgten dafür, dass ich mich immer willkommen gefühlt habe. Sie gewährten mir nicht nur "Asyl" und sorgten für eine unterhaltsame und schöne Zeit, sondern wurden auch zu einer wichtigen Stütze. Vielen lieben Dank Euch Allen!

Allen meinen Freunden möchte ich für ihre Geduld und Verständnis danken, wenn ich "mal wieder keine Zeit hatte". Ihr habt mich immer unterstützt und aufgebaut - Danke!

Riesen-Dank gilt meinem Freund, Robert. Ohne Deine Unterstützung, Deine Geduld, deine Hilfe und Deinen Optimismus wären die letzten Jahre nicht möglich gewesen. Auf Dich konnte ich immer zählen!

Weiterhin danke ich meiner Familie, meinen Eltern und meiner Schwester, für ihren Rückhalt in allen Lebenslagen und in meiner gesamten Ausbildungszeit!
